UMI University Microfilms International

MICROCOPY RESOLUTION TEST CHART
NATIONAL BUREAU OF STANDARDS
STANDARD REFERENCE MATERIAL 1010a
(ANSI and ISO TEST CHART No. 2)

**University Microfilms Inc.**
300 N. Zeeb Road, Ann Arbor, MI 48106

## INFORMATION TO USERS

This reproduction was made from a copy of a manuscript sent to us for publication and microfilming. While the most advanced technology has been used to photograph and reproduce this manuscript, the quality of the reproduction is heavily dependent upon the quality of the material submitted. Pages in any manuscript may have indistinct print. In all cases the best available copy has been filmed.

The following explanation of techniques is provided to help clarify notations which may appear on this reproduction.

1. Manuscripts may not always be complete. When it is not possible to obtain missing pages, a note appears to indicate this.

2. When copyrighted materials are removed from the manuscript, a note appears to indicate this.

3. Oversize materials (maps, drawings, and charts) are photographed by sectioning the original, beginning at the upper left hand corner and continuing from left to right in equal sections with small overlaps. Each oversize page is also filmed as one exposure and is available, for an additional charge, as a standard 35mm slide or in black and white paper format.*

4. Most photographs reproduce acceptably on positive microfilm or microfiche but lack clarity on xerographic copies made from the microfilm. For an additional charge, all photographs are available in black and white standard 35mm slide format.*

***For more information about black and white slides or enlarged paper reproductions, please contact the Dissertations Customer Services Department.**

UMI University Microfilms International

8613658

Legg, Mark Randall

GEOLOGIC STRUCTURE AND TECTONICS OF THE INNER CONTINENTAL BORDERLAND OFFSHORE NORTHERN BAJA CALIFORNIA, MEXICO

*University of California, Santa Barbara* PH.D. 1985

University
Microfilms
International 300 N. Zeeb Road, Ann Arbor, MI 48106

Copyright 1985

by

Legg, Mark Randall

All Rights Reserved

**PLEASE NOTE:**

In all cases this material has been filmed in the best possible way from the available copy. Problems encountered with this document have been identified here with a check mark ✓.

1. Glossy photographs or pages _____
2. Colored illustrations, paper or print _____
3. Photographs with dark background _____
4. Illustrations are poor copy _____
5. Pages with black marks, not original copy _____
6. Print shows through as there is text on both sides of page _____
7. Indistinct, broken or small print on several pages ✓
8. Print exceeds margin requirements _____
9. Tightly bound copy with print lost in spine _____
10. Computer printout pages with indistinct print ✓
11. Page(s) _____ lacking when material received, and not available from school or author.
12. Page(s) _____ seem to be missing in numbering only as text follows.
13. Two pages numbered _____. Text follows.
14. Curling and wrinkled pages _____
15. Dissertation contains pages with print at a slant, filmed as received _____
16. Other _____

University
Microfilms
International

UNIVERSITY OF CALIFORNIA
Santa Barbara

# Geologic Structure and Tectonics of the Inner Continental Borderland Offshore Northern Baja California, Mexico

A dissertation submitted in partial satisfaction
of the requirements for the degree of

**Doctor of Philosophy**

in

Geological Sciences

by

Mark Randall Legg

Committee in charge:

Professor Ken C. Macdonald, Chairman

Professor Bruce P. Luyendyk

Professor William A. Prothero

Professor Arthur G. Sylvester

December 1985

The dissertation of Mark Randall Legg is approved by:

William A. Prothero Jr.

Bruce P. Luyendyk

Arthur G. Sylvester

Ken C. Macdonald

Committee Chairman

December 1985

December 1985

Copyright by

Mark Randall Legg

1985

Dedicated to

Mary Ellen, Lewis, and Joyce

## ACKNOWLEDGEMENTS

Many individuals and organizations have provided assistance in the completion of this dissertation. I am especially grateful to my co-investigator, Victor Wong, for his help in collecting, analyzing and interpreting the data of this study. We both appreciate the hard-working crew of the R/V Ellen B. Scripps and members of the scientific party: Frank Hubenka, Rick Adair, Ladd El Wardani, Desiree Beaudry, Char Shine Liu and Carl Kuck for their assistance in the primary data collecting cruises for this study. I am also very grateful to Professor Macdonald for his patience and understanding in guiding me through the Ph.D. program at UCSB. Professors Luyendyk, Prothero, Sylvester and Crowell also provided needed assistance, technical discussions and reviews of the dissertation. Dr. Michael P. Kennedy has given me much support and the numerous discussions of Borderland faulting and tectonics that we shared have definitely improved the content of this report. Review of selected parts of the dissertation by Professor Norris was also very helpful.

Many scientists have contributed much additional data which were used in this study. In particular, Bob Tyce, Chris deMoustier, Jacqueline Mammerickx, Tom Shipley, Greg Moore, Dick Hey, Peter Lonsdale, Jeff Fox, Harmon Craig and Ken Macdonald generously donated Sea Beam data from parts of their research cruises which crossed the Inner Borderland. Conventional soundings and seismic reflection data of Dale Krause, Dave Moore, Mike Kennedy and many others at the Scripps

Institution of Oceanography and other institutions provided important information to make this work more complete. Stu Smith and his associates at the SIO Geological Data Center were of invaluable assistance in compiling these data. David Naar and Lynn Abbott helped in preparing the navigation for the Sea Beam plots. Gordon Stewart provided recent seismicity data. Wendy Borst, Teri Gambrel, Heather Sloan and Mike Wightman assisted with the figures. Bob Stevenson, Fran Shepard and Ben Cagle provided much needed moral and scientific support throughout this research.

Funding for various parts of this research, including the author's income, was provided by the National Science Foundation, National Academy of Sciences Arthur L. Day Fund, Office of Naval Research, NOAA Sea Grant Program, California Division of Mines and Geology and the University of California. The government of the Republic of Mexico graciously permitted this research to be conducted within their territorial waters.

Finally, I thank Joyce, my wife, for her assistance with the typing, and most importantly, for her patience and love which helped me through the whole project.

## VITA

| | |
|---|---|
| April 10, 1950-- | Born--Normal, Illinois |
| 1973--B.S. | Florida Institute of Technology |
| 1980--M.S. | University of California, San Diego |
| 1973-1976-- | National Science Foundation Graduate Fellowship |
| 1974-1977-- | Research Assistant, Institute of Geophysics and Planetary Physics |
| 1977-1979-- | Sea Grant Trainee, Scripps Institution of Oceanography |
| 1979-1982-- | Research Assistant, California Division of Mines and Geology |
| 1979-1985-- | Professional Staff, J. H. Wiggins Company, Redondo Beach, CA. |

### Publications


Legg, M.R., D.C. Agnew and R.S. Simons. 1977. Earthquake history and recent seismicity of coastal San Diego County, California, 1800-1976. *in* Kuhn. G. Coastal Zone Geology and Related Sea-Cliff Erosion: San Dieguito River to San Elijo Lagoon, San Diego County, California. San Diego County Board of Supervisors Study #11596-0800-KUHN.

Bradner, H., M.R. Legg and M.S. Reichle. 1978. Sonobuoy measurement of aftershocks of Santa Barbara 13 August 1978 Earthquake. *American Geophysical Union Transactions*. vol. 59, p. 1130.

Legg, M.R. and V.W. Ortega. 1978. New evidence for major faulting in the Inner Borderland off northern Baja California, Mexico. *American Geophysical Union Transactions*. vol. 59, p. 1134.

Agnew, D.C., M.R. Legg and C. Strand. 1979. Earthquake history of San Diego. *in* Abbott, P.L. and W.J. Elliott, editors. Earthquakes and Other Perils - San Diego Region. San Diego Association of Geologists Guidebook. pp. 123-138.

Legg, M.R. and D.C. Agnew. 1979. The 1862 earthquake in San Diego. *in* Abbott, P.L. and W.J. Elliott, editors. Earthquakes and Other Perils - San Diego Region. San Diego Association of Geologists Guidebook. pp. 139-142.

Legg, M.R. and M.P. Kennedy. 1979. Faulting offshore San Diego and northern Baja California. *in* Abbott, P.L. and W.J. Elliott, editors. Earthquakes and Other Perils - San Diego Region. San Diego Association of Geologists Guidebook. pp. 29-46.

Legg, M.R. and V. Wong O. 1979. Faulting and seismic risk offshore southern California (USA) and northern Baja California (Mexico). *in* Proceedings of the Symposium on Human Settlements of the San Andreas Fault System. Tijuana, Mexico. pp. 136-151.

Legg, M.R. and V. Wong O. 1979. Faulting in the Inner Continental Borderland offshore northern Baja California, Mexico. Geological Society of America, *Abstracts with Programs*. vol. 11, p. 464.

Wong, V.O. and M.R. Legg. 1979. Implicaciónes tectónicas de la falla de Agua Blanca en la region de la Bahía de Todos Santos. *in* Proceedings of the 5th Annual Meeting of Centros de Investigaciónes de Baja California y Scripps Institution of Oceanography.

Kennedy, M.P., S.H. Clarke, H.G. Greene and M.R. Legg. 1980. Recency and character of faulting offshore from metropolitan San Diego, California. California Division of Mines and Geology, *Map Sheet #42*. Scale 1:50,000.

Legg, M.R. 1980. Seismicity and Tectonics of the Inner Continental Borderland of Southern California and Northern Baja California, Mexico. Unpublished M.S. Thesis. University of California, San Diego. 60 pp.

Legg, M.R. 1980. Present-day micro-plate tectonics in the Southern California Continental Borderland. *American Geophysical Union Transactions*. vol. 61, p. 1124.

Legg, M.R., R.T. Eguchi and J.H. Wiggins. 1980. National Earthquake Loss Assessment: Sensitivity to Alternative Risk Mapping Procedures. U.S. Geological Survey, *Open-File Report #80-1170. (Contract report)*.

Legg, M.R., R.T. Eguchi and J.H. Wiggins. 1980. U.S. Building Exposure, County Data File - User's Manual. U.S. Geological Survey, *Open-File Report #80-1169*. (Contract report).

Eguchi, R.T., J.M. Hudson, L.L. Philipson, M.R. Legg, C. Taylor and J.H. Wiggins. 1981. Earthquake performance of natural gas distribution systems. *in* Proceedings of the 1981 International Gas Research Conference. Los Angeles, California.

Legg, M.R., R.T. Eguchi, J.H. Wiggins and J.E. Slosson. 1982. Seismic hazard models for the city of Oakland, California. J.H. Wiggins Company *Technical Report #1996-4*. Redondo Beach, California.

Eguchi, R.T., M.R. Legg, C.E. Taylor, L.L. Philipson and J.H. Wiggins. 1983. Earthquake Performance of Water and Natural Gas Supply Systems, Final Report. J.H. Wiggins Company *Technical Report #1996-5*. Redondo Beach, California.

Legg, M.R. and B.P. Luyendyk. 1982. Seabeam survey of an active strike-slip fault in the Southern California Continental Borderland. *American Geophysical Union Transactions*. vol. 63, p. 1107.

Legg, M.R. and J.E. Slosson. 1982. Seismic hazard mapping for lifeline vulnerability analyses. *in* Proceedings of the 3rd International Earthquake Microzonation Conference. Seattle, Washington. pp. 1641-1652.

Legg, M.R. and V. Wong O. 1982. Seismicity, faulting and tectonics of the Inner Continental Borderland offshore northern Baja California, Mexico. Abstract in *American Association of Petroleum Geologists Bulletin*. vol. 66, p. 974.

Legg, M.R., J.E. Slosson and R.T.Eguchi. 1983. Earthquake-induced landslide hazard mapping. *Abstract for* Association of Engineering Geologists 26th Annual Meeting. San Diego, California.

Eguchi, R.T., C.E. Taylor and M.R. Legg. 1983. Earthquake performance of water supply systems. in *Earthquake behaviour and safety of oil and gas storage facilities, buried pipelines and equipment*. ASME, New York City. PVP-vol.77, pp. 406-416.

Legg, M.R. and J.E. Slosson. 1984. Probabilistic approach to earthquake-induced landslide hazard mapping. *in* Proceedings of the Eighth World Conference on Earthquake Engineering. San Francisco, California.

Taylor, C.E., M.R. Legg, J.M. Haber and J.H. Wiggins. 1985. New lifeline multiscenario seismic risk techniques with a model application. *Civil Engineering Systems*. vol. 2, pp. 77-83.

Legg, M.R. 1985. Earthquake epicenters and selected fault plane solutions of the inner-southern California continental margin. Plate 1B. *in* Greene, H.G. and M.P. Kennedy, editors. Geologic map series of the California continental margin. California Division of Mines and Geology. Area 1 of 7, (NOS 1206N-16), Scale 1:250,000.

Legg, M.R. 1985. Earthquake epicenters and selected fault plane solutions of the mid-southern California continental margin. Plate 1B. *in* Greene, H.G. and M.P. Kennedy, editors. Geologic map series of the California continental margin. California Division of Mines and Geology. Area 2 of 7, (NOS 1206N-15), Scale 1:250,000.

Legg, M.R. 1986. Earthquake epicenters and selected fault plane solutions of the outer-southern California continental margin. Plate 1B. *in* Greene, H.G. and M.P. Kennedy, editors. Geologic map series of the California continental margin. California Division of Mines and Geology. Area 3 of 7, (NOS 1306N-19), Scale 1:250,000.

## Fields of Study

**Major Field: Geological Sciences**

Studies in Geophysics: Plate Tectonics and Geomagnetism. Professors Ken C. Macdonald and Bruce P. Luyendyk.

Studies in Geophysics: Reflection Seismology. Professor Bruce P. Luyendyk.

Studies in Geophysics: Earthquake Seismology. Professors William A. Prothero, Hugh Bradner and James N. Brune.

Studies in Geology: Structural Geology and Fault Tectonics. Professors Arthur G. Sylvester, John C. Crowell and Richard H. Sibson.

Studies in Geology: Marine Geology. Professors Francis P. Shepard and Joseph R. Curray.

# ABSTRACT

Geologic Structure and Tectonics of the Inner Continental Borderland
Offshore Northern Baja California, Mexico

by

Mark Randall Legg

The Inner Continental Borderland west of northern Baja California, Mexico, is an active part of the geologically complex Pacific-North American lithospheric plate boundary. To further understand the late Cenozoic tectonic style and evolution of this continental margin plate boundary, it is necessary to study the geologic structure and tectonic style of the California Continental Borderland. This dissertation presents a relatively complete, marine geological study of the Inner Continental Borderland. Detailed bathymetric maps prepared from both conventional single beam, and multi-, narrow-beam (Sea Beam) echo sounding data show that the Inner Borderland is a regionally distinct physiographic province. Numerous tectonic landforms commonly associated with recently-active faults onshore are shown by the detailed, Sea Beam bathymetric charts made along the San Clemente fault. High-resolution, single-channel, seismic reflection profiles also show that the region is crossed by numerous, late Cenozoic faults which are associated with four principal wrench fault zones: (1) San Clemente-San Isidro; (2) San Diego Trough-Bahía Soledad; (3) Coronado Bank-Agua Blanca; (4) Rose Canyon and Descanso-Estero. Estimates of average late Quaternary sedimentation rates, based upon published piston core analyses, and seismic stratigraphy are used to infer late Quaternary ages for fault

activity and submarine canyon/fan development. Right-slip of several kilometers along the major faults is inferred from postulated offset channels and submarine fan/slope apron deposits. The major fault zones are further grouped into two, major wrench fault systems, i.e., San Clemente and Agua Blanca. Each is similar in configuration to the well-known San Andreas and Alpine-Marlborough faults, respectively. Systematic variations in fault character both along strike and at depth in these fault zones are attributed to changes in fault geometry, and/or reorientation of principal strain and inferred stress directions in the region. These variations are inferred to demonstrate that the Inner Borderland is a regionally distinct structural province and that the entire southern California-northern Baja California region may be considered as a broad shear zone associated with transform fault tectonics of Pacific-North American plate interaction.

## Table of Contents


Chapter 1: Introduction and Background ..... 1
Chapter 2: Physiography of the Inner Continental Borderland ..... 11
Introduction ..... 11
Data ..... 13
Navigation and Preparation of Soundings Charts ..... 13
Accuracy and Resolution ..... 19
Discussion ..... 23
Coasts ..... 23
Shelves, Banks, and Ridges ..... 27
Basin and Trough Slopes ..... 43
Tectonic Slopes ..... 44
Depositional and Erosional Slopes ..... 48
Submarine Canyons, Fan Valleys, Gullies and Troughs ..... 50
Basins ..... 62
Submarine Fans and Slope Aprons ..... 66
Conclusions ..... 68
Chapter 3: Seismic Stratigraphy and Quaternary Sedimentation ..... 73
Introduction ..... 73
Seismic Stratigraphic Units ..... 76
Acoustic Basement Units ..... 76
Sedimentary Units ..... 80
Shelf Sediments ..... 83
Slope Deposits ..... 83
Basin Sediments ..... 84
Sedimentation Rates and Chronology ..... 88
Age of the Hemipelagic Unit ..... 92
Age of the Banda Ban Ponded Turbidite ..... 95
Discussion ..... 97

Conclusions ..... 101
Chapter 4: Character and Recency of Faulting ..... 103
Introduction ..... 103
Data ..... 106
Interpretation ..... 110
Character of Faulting ..... 113
San Clemente Fault System ..... 114
Agua Blanca Fault System ..... 123
San Diego Trough-Bahía Soledad Fault Zone ..... 130
Eastern Fault Zones of the Agua Blanca System ..... 138
Recency of Faulting ..... 154
Summary ..... 157
Conclusions ..... 161
Chapter 5: Sea Beam Survey of an Active Strike-Slip Fault ..... 163
Introduction ..... 163
Background - Regional Geology and Tectonic Framework ..... 173
Methods - Narrow Beam Echo Sounding ..... 174
Sea Beam Acoustics ..... 175
Navigation ..... 178
Post-Processing of Sea Beam Data ..... 179
Supplementary Data ..... 181
Tectonic Landforms along Recently Active Faults ..... 181
Discussion ..... 186
Tectonic Landforms along the San Clemente Fault Zone ..... 186
Principal Trace of the San Clemente Fault ..... 186
Branch and Secondary Faults ..... 204
Recency of Faulting in the San Clemente Fault Zone ..... 208
Displacement and Rate of Slip ..... 212
Conclusions ..... 214
Chapter 6: Late Quaternary Sedimentation in North San Clemente Basin and Movement Along the San Clemente Fault ..... 220
Introduction ..... 220
Sediments ..... 220
Acoustic Character ..... 223

Acoustic Horizons and Isopachs ..... 235
Unit 1 Sedimentation Patterns ..... 236
Unit 2 Sedimentation Patterns ..... 250
Bottom Samples ..... 253
Late Quaternary Sedimentation in North San Clemente Basin ..... 256
Origin and Estimated Ages of the Acoustic Horizons ..... 256
Sedimentation Patterns in North San Clemente Basin ..... 259
Depositional ..... 262
Displacement Along the San Clemente Fault ..... 268
Growth Model of a Tectonically Controlled Submarine Fan/Slope Apron and Movement History of the San Clemente Fault ..... 271
Summary and Conclusions ..... 278
Chapter 7: Structural Geology and Tectonics of the Inner Borderland ..... 283
Introduction ..... 283
Geologic Structure of the Inner Borderland ..... 286
San Clemente Fault System ..... 286
Agua Blanca Fault System ..... 296
Offshore Fault Trends and the Inner Borderland Structural Province ..... 301
Fault Geometry and Kinematics ..... 307
Inner Borderland Faults ..... 309
Peninsular Ranges Faults ..... 314
Earthquake Focal Mechanisms ..... 315
Stress Trajectories ..... 317
Conclusions - Inner Borderland Tectonics ..... 324
Baja California Microplate Tectonics ..... 328
References ..... 334
Appendix A ..... 349
Navigation ..... 349
I/O and Program Listings for TRNAV, SMFIX, and HYPRIN ..... 355
Appendix A.1 ..... 366
FORTRAN Program TRNAV used to Compute Ship Position Fixes from Range and Azimuth Data for Shipboard RADAR and Shore-based Transponders. ..... 366

SUBROUTINE INIT(ANT,SGNX,XT,YT,TRFLG) ..... 370
SUBROUTINE NAVIG
(SGNX,XT,YT,NLINE,IDATA,IDAY,MONTH,IYR,ANT)
..... 375
SUBROUTINE BASEL
(XM,YM,DMG,SMG,DEX,DEY,CMG,A12,A21,SGNX,XT,YT)
..... 381
FUNCTION SGN(X) ..... 383
FUNCTION ARCOS(X) ..... 385
Appendix A.2 ..... 387
FORTRAN Program SMFIX used to compute Averaged Ship Positions from a Sequence of Position Fixes during One Minute Time Intervals ..... 387
SUBROUTINE FIXAV
(LT,TNHR,FFLAG,MINT,NFIX,TR1,XLAT,YLON,TFLAG,MINT0,NDAY)
..... 391
SUBROUTINE FIXCM
(FFLAG,NFIX,XLAT,YLON,LT,IHR,MINT0,TR1) ..... 395
SUBROUTINE SUMIT(FFLAG,NFIX,LT,XLAT,YLON) ..... 399
SUBROUTINE NTIME(MONTH,NDAY,TNHR) ..... 401
SUBROUTINE FIXVL(IYR,MINT0,MIN,X0,Y0) ..... 403
Appendix A.3 ..... 405
FORTRAN Subroutine GETFIL to Input Filenames Interactively ..... 405
Appendix A.4 ..... 407
FORTRAN Program HYPRIN to Convert GDC Format Data to SMFIX Input Format ..... 407
Plates in Pocket at End
Plate 1: Bathymetry of the Inner California Continental Borderland
Plate 2: Geomorphology of the Inner California Continental Borderland
Plate 3: Recency and Character of Faulting in the Inner California Continental Borderland
Plate 4: Sea Beam Bathymetry of the San Clemente Fault Zone in North San Clemente Basin
Plate 5: Geomorphology of the San Clemente Fault Zone in North San Clemente Basin

## Table of Tables

Table 1. List of Research Cruises which Provided Data for the Preparation of the Bathymetric and Geologic Maps ..... 14

Table 2. Calculations of Sedimentation Rates and Age of Key Horizons from Piston Core Data ..... 95

Table 3. Tectonic Stress Orientation Indicators in the Inner Continental Borderland and Vicinity ..... 312

Table A.1 - Sample Input File (lun 5) for Program TRNAV ..... 360

Table A.2 - Sample Output File (lun 6) for Program TRNAV ..... 361

Table A.3 - Sample Output File (lun 7) for Program TRNAV ..... 362

Table A.4 - Sample Input File (lun 5) for Program SMFIX ..... 363

Table A.5 - Sample Output File (lun 6) for Program SMFIX ..... 364

Table A.6 - Sample Output File (lun 7) for Program SMFIX ..... 365

## Table of Figures

Figure 1. Map showing the major physiographic provinces of the regions surrounding Baja California and the California Continental Borderland ..... 2

Figure 2. Map showing locations of bathymetric charts prepared for this study ..... 7

Figure 3. Relative navigational accuracy of sounding positions and resolution of bathymetric features ..... 20

Figure 4. Location of selected seismic profiles and Sea Beam swaths shown in this report ..... 24

Figure 5. Airgun profile (Line A-31) crossing the Coronado Shelf and Descanso Plain ..... 28

Figure 6. Airgun seismic profile (Line A-25) across the Descanso Plain and Bahía Descanso ..... 30

Figure 7. Line drawings of airgun profiles extending from the shelf offshore across the southern Descanso Plain ..... 32

Figure 8. Sparker seismic profile (Line B-27) from the Soledad Shelf, southwestward across the Ensenada Trough to Maximinos Knolls ..... 35

Figure 9. Sparker seismic profile (Line B-30'-31-32) across the Descanso Plain southwest of Punta Salsipuedes ..... 37

Figure 10. Airgun seismic profile (Line C) across San Diego Trough and East San Clemente Basin ..... 39

Figure 11. Line drawing of sparker profile (B-3) that obliquely crosses the axis of the San Diego Trough and Descanso Plain ..... 41

Figure 12. Narrow-beam echo sounding profile (Line BONZ-01) from the Coronado Bank to North San Clemente Basin ..... 45

Figure 13. Sea Beam swath across meanders in the Coronado submarine fan valley ..... 54

Figure 14. Long profiles of submarine canyons, fan valleys, and major distributary channels of the Inner Borderland ..... 56

Figure 15. Sea Beam swath showing tectonic sags in the San Isidro Rift Valley ..... 60

Figure 16. Diagram of basin filling sequence proposed by Gorsline and Emery (1959) ..... 64

Figure 17. Sea Beam swath crossing sub-circular depression reminiscent of volcanic craters ..... 71

Figure 18. Map showing the distribution of major, pre-late Cenozoic rock units identified in the Inner Borderland and surrounding regions ..... 78
Figure 19. Map showing the principal late Cenozoic sedimentary units of the Inner Borderland of this study ..... 81
Figure 20. Sediment age versus depth curves for several selected northeast Pacific piston cores ..... 90
Figure 21. Detailed plot of latest Quaternary sedimentation rates for the California Continental Borderland ..... 93
Figure 22. Line drawing of sparker seismic profile (Line B-29) across Bahía Todos Santos ..... 98
Figure 23. Bathymetry of the Inner Continental Borderland west of northern Baja California ..... 104
Figure 24. Tracklines of seismic reflection profiles used for this study and references for additional data included in mapping the regional geology ..... 107
Figure 25. Map showing the principal late Cenozoic faults of the Inner Borderland and adjacent regions of southern California and northern Baja California ..... 115
Figure 26. Line drawings of sparker seismic profiles across the southern part of the study area ..... 118
Figure 27. Histograms of fault strikes for the principal late Cenozoic faults of the San Clemente-San Isidro and San Diego Trough-Bahía Soledad fault zones ..... 121
Figure 28. Airgun profiles (Line C-C') across East San Clemente Basin (Navy Basin) and part of North San Clemente Basin ..... 124
Figure 29. Map comparing portions of San Clemente and San Andreas fault systems at the same scale ..... 128
Figure 30. Line drawing of sparker seismic profile (Line B-1) crossing the shelf and slope region west of Punta Santo Tomás and Punta Banda ..... 132
Figure 31. High-resolution (3.5 kHz) profile across the Bahía Soledad fault zone near Soledad Sea Valley ..... 134
Figure 32. Line drawings of sparker seismic profiles in Bahía Todos Santos showing the Estero fault zone ..... 140
Figure 33a. Magnetic anomaly data of Gonzales (1977) delineate the major faults within Bahía Todos Santos ..... 143
Figure 33b. Gravity anomaly data of Gonzales (1977) ..... 145
Figure 34. Magnetic anomaly profiles of Krause (1965) delineate the

major nearshore fault zones of the Agua Blanca fault system ..... 149

Figure 35. Line drawings of sparker seismic profiles showing transpression along the San Clemente-San Isidro fault zone and transtension(?) along the Coronado Bank-Agua Blanca fault zone ..... 151

Figure 36. Map comparing the Alpine-Marlborough fault system to the Agua Blanca fault system ..... 159

Figure 37. Portion of National Ocean Survey bathymetric contour map showing North San Clemente Basin and surrounding regions ..... 164

Figure 38. Sea Beam bathymetric map of the San Clemente fault zone in the vicinity of Fortymile Bank and North San Clemente Basin ..... 166

Figure 39. Location map of seismic profiles and other detailed figures shown in this study ..... 168

Figure 40. Graph showing relative size of tectonic geomorphic features and the limits of resolution of various marine survey techniques ..... 171

Figure 41. Sea Beam transmit/receive beam geometry ..... 176

Figure 42. Block diagram showing tectonic landforms commonly observed along recently-active, terrestrial (subaerial), strike-slip faults ..... 182

Figure 43. Portion of Sea Beam area shown in detail using the original swath charts, contoured at a 10 m interval ..... 188

Figure 44. High-resolution (3.5 kHz) seismic profiles across the San Clemente fault in North San Clemente Basin ..... 191

Figure 45. Comparison of some pull-apart basins along major, dextral, wrench faults ..... 194

Figure 46. High-resolution (3.5 kHz) seismic profiles across the San Clemente fault zone between Fortymile Bank and North San Clemente Basin (Rift Basin) ..... 196

Figure 47. High-resolution (3.5 kHz) seismic profile across the San Clemente fault zone and the 'shutter ridge' at the base of Fortymile Bank ..... 200

Figure 48. Deep Tow, high-resolution (4 kHz) seismic profiles across the flanks of the 'shutter ridge' ..... 202

Figure 49. High-resolution (3.5 kHz) seismic profiles across the San Clemente fault zone in the North San Clemente Basin region ..... 206

Figure 50. Comparison of the mapped patterns of parts of four major wrench fault zones in California ..... 215

Figure 51. Map showing tracklines of high-resolution seismic data

used in this study ..... 221
Figure 52. Map of acoustic facies along the San Clemente fault zone between Fortymile Bank and North San Clemente Basin ..... 225
Figure 53. Surface ship, high-resolution (3.5 kHz) seismic profiles showing character of acoustic facies ..... 227
Figure 54. Deep Tow high-resolution (4 kHz) seismic profiles showing character of acoustic facies ..... 231
Figure 55. Isopach map of Unit 1, the sediment layer between the seafloor and the middle of the Triplet ..... 237
Figure 56. Deep Tow bottom photographs showing muds with burrows and deep-sea creatures ..... 240
Figure 57. High-resolution (3.5 kHz) seismic profile across Rift Basin showing near surface sedimentary features ..... 248
Figure 58. Isopachs of Unit 2, the sediment layer between the middle of the Triplet and Horizon 2 ..... 251
Figure 59. Comparison of core logs for two piston cores obtained from the North San Clemente Basin ..... 254
Figure 60. Post-Miocene isopach map of Junger and Vedder (1980, personal communication) in the region of North San Clemente Basin ..... 266
Figure 61. Palinspastic reconstructions showing model history of right-slip on the San Clemente fault zone (SCFZ) and growth of Boundary fan/slope apron (BF) ..... 272
Figure 62. High-resolution (3.5 kHz) seismic profile showing upthrusts along transpressive section of the San Clemente-San Isidro fault zone ..... 288
Figure 63. High-resolution (3.5 kHz) seismic profile showing a small graben on the flanks of the bulge associated with the convergent part of the San Clemente-San Isidro fault zone ..... 291
Figure 64. Diagram showing how regional extension combined with fault interaction and vertical movements at the tips of wedges between intersecting strike-slip faults can explain the pattern of faults and seafloor relief in the vicinity of the Ensenada Trough ..... 294
Figure 65. Comparison of the San Andreas and San Clemente fault systems ..... 297
Figure 66. Seismicity of the Inner Borderland (1977-1984) ..... 305
Figure 67. Map showing inferred orientations of horizontal slip vectors for faults in the Inner Borderland and vicinity ..... 310

Figure 68. Map showing inferred orientations of principal stress for the Inner Borderland and vicinity ..... 319
Figure 69. Map showing configuration of postulated microplates or large crustal blocks along the southern California part of the Pacific-North American lithospheric plate boundary ..... 329

# CHAPTER 1
# INTRODUCTION AND BACKGROUND

The North American-Pacific tectonic plate boundary in southern California is a broad, geologically complex zone of shear, including several major, active wrench fault zones. Part of the Cenozoic evolution of this continental margin plate boundary is recorded in the geology of the California Continental Borderland. This evolution includes the collision of the East Pacific Rise with North America, subsequent southward migration of the Rivera ridge-trench-transform fault (RTF) triple junction (and northward migration of the Mendocino triple junction away from the region), and the eventual rifting of the Baja California peninsula from the North American continent (Atwater, 1970). Holocene faulting and modern earthquake activity in this region demonstrate that the California Continental Borderland is a tectonically active part of the present-day North American-Pacific plate boundary. In order to understand the evolution and present-day tectonics of this continental margin boundary, it is necessary to study the tectonic evolution of the California Continental Borderland.

The California Continental Borderland extends from Point Arguello on the north to Bahía Sebastian Vizcaíno (and Cedros Island) on the south (figure 1). Moore (1969) divided the Borderland into five major structural zones. This study focuses on the inner zone. As stated by Moore (1969), "The inner zone of major northwest-trending faults is essentially contained within the region shoreward of the fault paralleling and adjacent to the western side of San Clemente Island." Moore considered his inner zone (Inner Borderland of this study) as an extension of northern Peninsular Ranges structure, however, the present study will show that the Inner Borderland is

Figure 1. Map showing the major physiographic provinces of the regions surrounding Baja California and the California Continental Borderland. Rectangular area indicates the location of this study. Dashed lines are approximate boundaries between the major physiographic provinces. Earlier studies separated the California Continental Borderland into a northern and southern part, separated by the Santo Tomás fault (dashed line trending westward from Pt. Santo Tomás). The northwest-trending dashed line within the Borderland marks the approximate western boundary of the Inner Borderland.

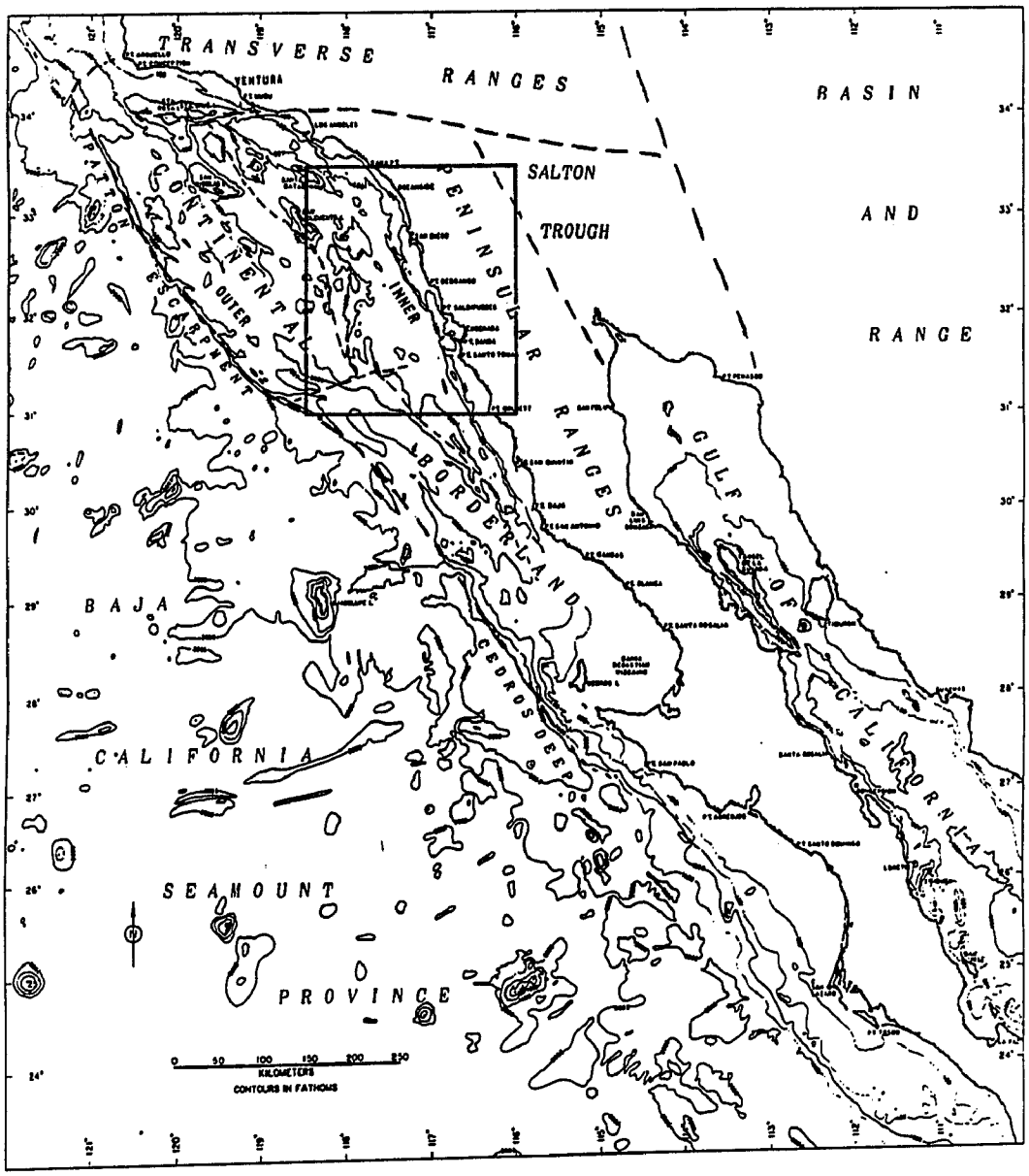
TRANSVERSE
RANGES
VENTURA
BASIN
AND
RANGE
SALTON
TROUGH
PENINSULAR
RANGES
CONTINENTAL
OUTER
INNER
PATTON
ESCARPMENT
BORDERLAND
CEDROS DEEP
GULF OF CALIFORNIA
BAJA
CALIFORNIA
SEAMOUNT
PROVINCE
0 50 100 150 200 250
KILOMETERS
CONTOURS IN FATHOMS

distinct in both physiography and geologic structure. The character of late Cenozoic geologic structure of the Inner Borderland, and its tectonic evolution, are described in the following chapters. Also, the relationship of the Inner Borderland structural province to adjacent regions, and implications of tectonic style and evolution of the Inner Borderland in regard to the San Andreas fault system and the southern California region are examined.

The several chapters of this dissertation have been written so that each stands on its own. It is, therefore, possible for the reader to use chapters of interest independently. However, each chapter holds information of significance to the others and reference among chapters is often made. In general, the ordering of the chapters is believed by the author to present a development of understanding of the offshore geologic structure that is consistent with the scientific method of observations and conclusions. The earlier chapters generally provide a data base and framework important for the interpretations and conclusions derived in subsequent chapters. The order and content of each subsequent chapter is described in the following paragraphs.

Chapter 2 describes the physiography of the region and principal geologic processes responsible for the character and evolution of the prominent seafloor features evident in the detailed bathymetric charts prepared for this study (plate 1). References to selected high-resolution seismic profiles assist in interpretation of the 'geomorphic' character (shown in plate 2) of the seafloor with regard to the internal structure of the near-surface lithology. Also, some mention is made of the detail attained in seafloor topographic maps derived from the recently acquired Scripps Institution of Oceanography 'Sea Beam' (multi- narrow-beam echo sounding) system

and the observation of many seafloor geomorphic features not previously recognized. Sea Beam data are also discussed to a greater extent in subsequent chapters (5 and 6). Data presented in chapter 2 thus provide a basis for developing the interpretations and conclusions of subsequent chapters. Furthermore, the bathymetric maps are used as base maps for the other geological and geophysical maps. An appendix describes the methodology and FORTRAN computer program used to navigate the seismic profiling shiptracks and more accurately locate the numerous soundings used to prepare the bathymetric charts.

Seismic stratigraphy developed for this study is described in chapter 3. This stratigraphy is used to determine the relative timing of late Cenozoic (mostly Quaternary?) tectonic and depositional events. Although originally intended to only provide a basis of estimating the relative age of faulting within the region, it was found that the stratigraphy developed also provides important insights regarding the patterns of sedimentation and the influences of both tectonic activity and eustatic sea level variations. Late Quaternary chronostratigraphic horizons evident in the seismic reflection profiles are mappable throughout most of the major basins within the Inner Borderland. Character of the internal reflections within the seismic sequences defined by these acoustic horizons, and the morphology evident from the bathymetric contours, are used to infer the depositional, structural and erosional(?) processes active in specific areas during Quaternary time. Lithofacies may also be extrapolated from these data. Piston cores in the area (Dunbar, 1981; Emery, 1960) provide data used to estimate the late Quaternary sedimentation rates for turbiditic and hemipelagic deposits of the basins and slopes. These rates are used, along with corrections for sediment compaction, to estimate the absolute ages of 'key' acoustic,

chronostratigraphic horizons. These ages provide constraints on the timing of tectonic activity, as well as submarine canyon/fan depositional system development.

Chapter 4 describes the character and recency of faulting within the Inner Borderland. As previously proposed (Junger, 1976; Legg and Kennedy, 1979), late Cenozoic faulting of the Inner Borderland is predominately associated with major, northwest-trending, dextral, wrench fault zones (plate 3). Two major fault systems, the San Clemente and Agua Blanca, are defined in this study, and the fault zones which delineate these are described. Offset and seismic character of the disrupted reflectors seen in the seismic profiles provide the data necessary to infer the character of faulting both along strike, and locally, at depth, within the major fault zones. Systematic variations in fault character, patterns of faulting, and offsets of geomorphic features are used to infer the primary sense of slip along the major faults. Relative ages of faulting are determined by the stratigraphic levels of the 'youngest' features disrupted by the faulting, based upon the seismic stratigraphy described in the preceding chapter. Moderate penetration airgun and sparker seismic reflection profiles combined with high-resolution, shallow penetration, (3.5 kHz) echo-sounding profiles are used to define relative ages of fault activity. These include four late Cenozoic (Quaternary?) and one older (Tertiary and older?) relative ages.

Chapter 5 describes the geomorphic character, in detail, of the seafloor along a 50 km section of the San Clemente fault zone near Fortymile Bank (figure 2). Detailed 'Sea Beam' bathymetric data provide the main source of information used for the seafloor mapping in this area. Recognition of prominent tectonic landforms, commonly associated with recently-active, strike-slip faults onshore, allows inference

Figure 2. Map showing locations of bathymetric charts prepared for this study. Also shown are locations of U.S. Hydrographic Office navigational charts (H.O. 18765, 21021) which provide additional sounding data for the final charts of this study. A detailed bathymetric chart of North San Clemente Basin, west of Fortymile Bank, prepared from Sea Beam data is presented in chapter 5 of this volume. Other charts outlined in the figure were prepared at large scale as preliminary versions of Plates 1A and 1B. These preliminary charts may be obtained from the author.

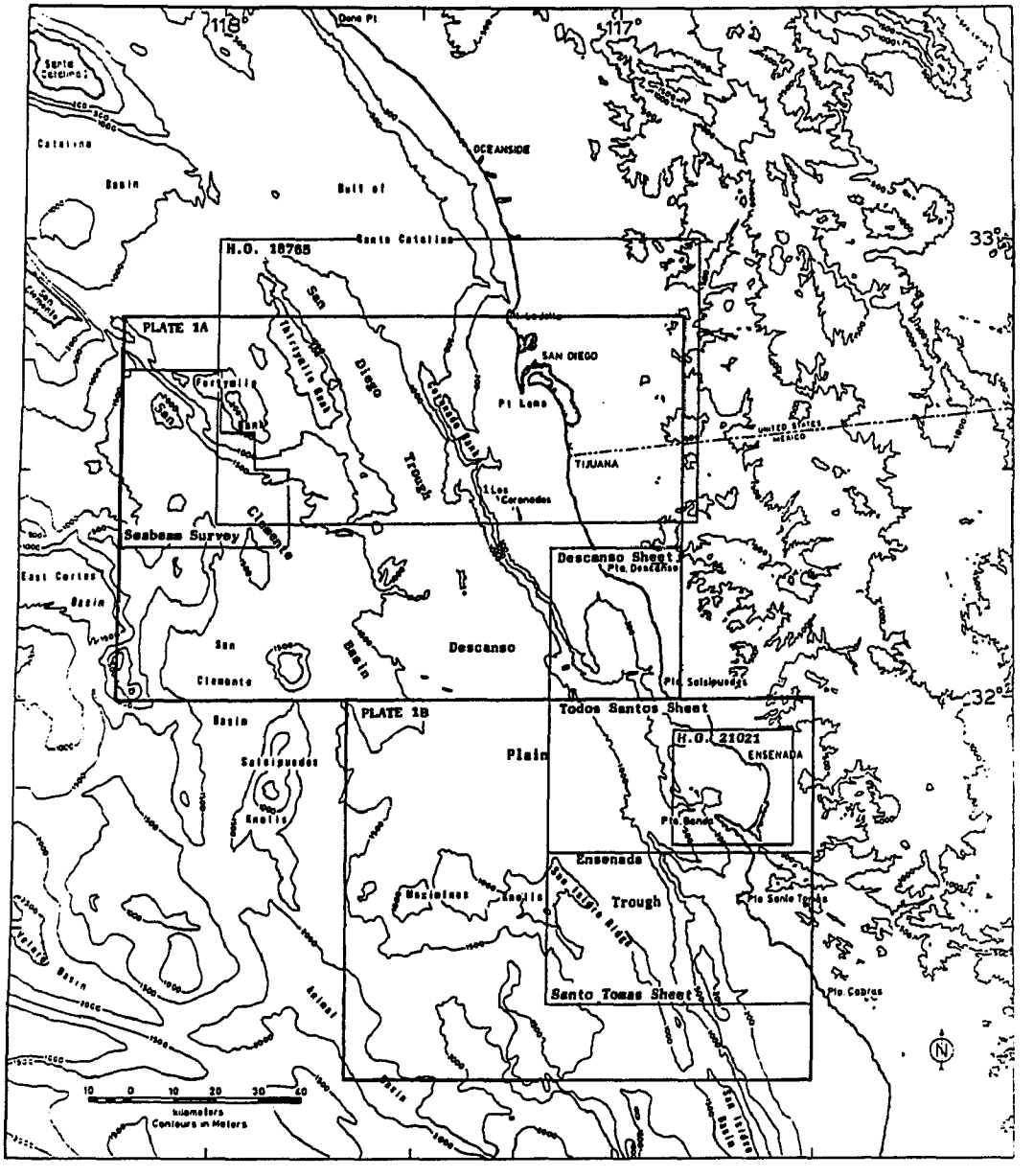
118°
117°
33°
32°
Dana Pt.
Santa Catalina
Catalina
Basin
Gulf of
Santa Catalina
OCEANSIDE
H.O. 18765
PLATE 1A
San
Diego
Trough
Thirtymile Bank
Fortymile
Bank
SAN DIEGO
Pt Loma
TIJUANA
Los Coronados
UNITED STATES
MEXICO
Seabeam Survey
Clemente
East Cortes
Basin
Descanso Sheet
Pta. Descanso
San
Clemente
Basin
Descanso
Pta. Salsipuedes
PLATE 1B
Todos Santos Sheet
H.O. 21021
ENSENADA
Pta. Banda
Plain
Salsipuedes
Knolls
Ensenada
Trough
Maximinos
Knolls
San Isidro Ridge
Pta Santo Tomas
Santo Tomas Sheet
Pta. Cabras
Velero Basin
Animal
Basin
San Isidro Basin
10 0 10 20 30 40
kilometers
Contours in Meters

of the character and recency of faulting along this major submarine fault zone in a region of high seafloor relief. Previous studies (Vedder and others, 1974; Junger, 1976) were unable to map accurately the most significant, active traces of the San Clemente fault, using conventional seismic reflection profiling methods, because of rugged seafloor topography and high relief in this area. Better resolution of seafloor geomorphic features possible with Sea Beam data allow application of tectonic geomorphic principles (as previously accomplished onshore with aerial photographs, for example) to map the recently-active fault traces in this submerged area.

In chapter 6, near bottom geophysical surveys, which include high-resolution, seismic reflection and side-scan SONAR profiles, are used to derive models of the late Quaternary sedimentation of North San Clemente Basin. These data are in the same area as the Sea Beam bathymetric data described in the previous chapter, and so discrimination between tectonic and non-tectonic (sedimentological) geomorphic features mapped by Sea Beam can be made. Piston cores (Emery, 1960) in the basin provide local estimates of the Holocene sedimentation rate, and correlation of prominent acoustic horizons across the area allow extrapolation of sedimentation rates for other parts of the basin. Significant patterns in both thickness (isopachs) and seismic reflection character of the late Quaternary sedimentary units are used to infer the depositional history of the region. Also, rates of movement associated with the San Clemente fault zone are postulated.

The final chapter (7) integrates the data of the preceding chapters and describes the significant implications regarding the tectonic development of the Inner Borderland. The pattern and character of faulting is used to infer orientations of principal strain and stress axes active during late Cenozoic time. These inferences are

examined in light of the predicted North American-Pacific tectonic plate interaction during the same period. Earthquake data which indicate the character of modern tectonism in the area are compared with the geologic data to model the overall late Cenozoic to modern tectonic evolution of the Inner Borderland offshore southern California and northern Baja California. These data suggest microplate tectonics have played an important role in the complex tectonic history of the southern and Baja California region.

# CHAPTER 2

# PHYSIOGRAPHY OF THE INNER CONTINENTAL BORDERLAND

## INTRODUCTION

The California Continental Borderland was first described by Shepard and Emery (1941), who recognized its unique character. Typical continental margins, such as those bordering the north Atlantic, and along the northern California coast, consist of a relatively flat, shallow shelf (of varying width) bounded by a distinct shelf break and slope which leads into the adjoining deep ocean basin. The California Continental Borderland differs and consists of a series of ridges and troughs, lying subparallel to the shoreline, separating the continental land mass from the deep ocean basin. The California Continental Borderland extends from Pt. Arguello on the north to the Vizcaíno Peninsula (and Cedros Island) on the south (figure 1). It is separated from the Pacific Ocean basin on the west by the Patton Escarpment along its northern part, other, less distinct escarpments to the south, and Cedros Deep along its southernmost part. Its eastern boundary is approximately represented by the Pacific shoreline, although borderland physiography extends onshore in places such as the Los Angeles, Ventura, and Vizcaíno basins. Also, the presence of numerous uplifted marine terraces presently onshore, as well as submerged terraces offshore indicate that the position of the shoreline has varied. This study provides data to define the eastern margin of the California Continental Borderland more precisely along its central section.

Krause (1965) divided the Borderland into a northern and southern province, separated by the offshore Santo Tomás fault, located west of Punta Santo Tomás (figure 1). Krause (1965) and Moore (1969) noted that the southern Borderland is generally deeper than the northern Borderland, lacks the prominent Patton escarpment on its western boundary and does not have the flat-topped banks common to the northern province. Doyle and Gorsline (1977) suggested that the southern Borderland is not down-dropped along the Santo Tomás fault (as suggested by Krause, 1965; and Moore, 1969), but rather the entire California Continental Borderland can be represented by a broad, northwest-trending "synclinorium." The present study provides detailed information regarding the transition in physiography from the northern to southern Borderland, across the postulated connection between the offshore Santo Tomás fault (Krause 1965) and the south branch of the Agua Blanca fault located onshore (Allen and others, 1960).

The Inner Borderland is defined herein to be that part of the Continental Borderland landward of the East Santa Cruz basin fault zone (postulated by Howell and others, 1974). As stated by Moore (1969) "The inner zone of major northwest-trending faults is essentially contained within the region shoreward of the fault paralleling and adjacent to the western side of San Clemente Island." Moore considered the Inner Borderland as an extension of northern Peninsular Ranges structure.

This study describes the primary physiographic elements of the Inner Borderland (as defined herein), and demonstrates that the Inner Borderland is a distinct physiographic province. Furthermore, knowledge of the interaction of the fundamental geologic processes which have shaped the geomorphology of the Inner Borderland is developed in this study. This knowledge is important to understanding the late

Cenozoic geological history of the region.

**Data**

Many data were used to compile the detailed bathymetric charts of the Inner Continental Borderland of this study (plate 1). Table 1 lists the oceanographic cruises during which these data were originally collected. In addition to the two high-resolution seismic reflection profiling surveys made by the author (CFAULTS-1 and 2), data from 62 additional Scripps Institution of Oceanography (SIO) and one National Oceanic and Atmospheric Administration (NOAA) cruise collecting conventional echo-sounding data were compiled.* Data from 13 recent SIO Sea Beam cruises which passed through the region are also included in the final chart(s). In addition, finished bathymetric charts of detailed local studies, and nautical charts with soundings of well-surveyed areas in both U.S. and Mexican waters were used. Finally, soundings made by Walton (1954) during his dissertation research in Bahía Todos Santos were re-positioned (using triangulation from his original charts) to recent (and presumably more accurate) charts, and plotted on the soundings charts.

**Navigation and Preparation of Soundings Charts**

Because data collected from numerous different research vessels over a period of several decades were used, significant variation in navigation quality was present in these 'raw' data. In order to compile base charts of the soundings for contouring, with the 'best' possible navigational accuracy, a systematic approach was devised and followed as described below.

---

* These data are available from the SIO Geological Data Center.

Table 1. List of Research Cruises which Provided Data for the Preparation of the Bathymetric and Geologic Maps.

| CRUISE NAME | SHIP | DATES | INSTITUTION[1] | DATA[2] |
|---|---|---|---|---|
| CFAULTS-1 | EB Scripps | 18-25 Jun 78 | SIO | B, RS |
| CFAULTS-2 | EB Scripps | 12-21 Sept 79 | SIO | B, M, RS |
| TODOS SANTOS | HM Smith | 28 Sept - 30 Oct 59 | SIO | B, M |
| SOUTHERN BORDERLANDS | Horizon | 11-14 Dec 59 | SIO | B, M |
| SOUTHERN BORDERLANDS II | Horizon | 16-21 Dec 59 | SIO | B, M |
| SOB-III | SF Baird | 12-19 Feb 60 | SIO | B |
| SOB-IV | SF Baird | 12-15 Mar 60 | SIO | B |
| SOB-V | Orca | 3-9 Aug 60 | SIO | B |
| SOB-VI | Orca | 14-18 Oct 60 | SIO | B |
| FANFARE | SF Baird | 9-20 Jul 59 | SIO | B |
| FANFARE | HM Smith | 6-26 Jul 59 | SIO | B |
| HM SMITH 63 | HM Smith | 22-23 Mar 63 | SIO | B, RS |
| DAVIS 65 | Davis | 11-25 Mar 65 | SIO | B, RS |
| EB SCRIPPS 65 | EB Scripps | 19-20 Oct 65 | SIO | B, RS |
| DAVIS 67-4 | Davis | 5-11 Jan 67 | NEL/SIO | B, RS |
| DAVIS 67-5 | Davis | 3-6 Feb 67 | NEL/SIO | B, RS |
| VERMILION SEA | SF Baird | Feb - Jun 59 | SIO | B |
| VERMILION SEA | Horizon | Feb - Jun 59 | SIO | B |
| SEA DOGS I | EB Scripps | 19 Oct - 11 Nov 76 | SIO/CDMG | RS |
| SEA DOGS III | EB Scripps | Nov - Dec 78 | SIO/CDMG | B, RS |
| CONMCALF | Surveyor | 70 | NOAA | B, M |
| HYPOGENE | Melville | 11 Mar - 21 Apr 72 | SIO | B, M, RS |
| PLEIADES-1 | Melville | 27 Apr - 5 Jun 70 | SIO | B, M |
| GUAYMAS-1 | T Washington | 9-24 Feb 78 | SIO | B, M |
| PIQUERO-1 | T Washington | 9 Dec 63 - 1 Jun 79 | SIO | B, M |
| INDOPAC-1 | T Washington | 23 Mar - 30 Apr 76 | SIO | B, M |

Table 1. List of Research Cruises (continued).

| | | | | |
|---|---|---|---|---|
| SCAN-1 | Argo | 11 Mar - 30 Mar 69 | SIO | B, M, RS |
| SCAN-2 | Argo | 8 Apr - 4 May 69 | SIO | B, M, RS |
| SCAN-5 | Argo | 4 Jul - 4 Aug 69 | SIO | B, M, RS |
| EURYDICE-1 | T Washington | 4 Sep - 15 Sep 74 | SIO | B, M |
| EURYDICE-II | T Washington | 20 Jun - 18 Jul 78 | SIO | B, M |
| NAGA-1 | Stranger | 17 Jun - 28 Jun 59 | SIO | B |
| LUSIAD-1 | Argo | 15 May - 11 Jun 62 | SIO | B, M |
| LUSIAD-8 | Horizon | 21 Jun - 4 Feb 63 | SIO | B |
| RISEPAC-3 | SF Baird | 3 Jan - 5 Feb 62 | SIO | B, M |
| MONSOON-1 | Argo | 26 Aug - 6 Oct 60 | SIO | B, M |
| JAPANYON-5 | SF Baird | 22 Aug - 15 Sep 61 | SIO | B, M |
| ANTIPODE-17 | Melville | 11 Sep - 3 Oct 71 | SIO | B, M |
| GAM-1 | EB Scripps | 1 Nov - 13 Nov 67 | SIO | B, M |
| AMPHITRITE-3 | Argo | 27 Jan - 29 Feb 64 | SIO | B, M |
| DSDP-54 | Glomar Challenger | 29 Apr - 18 Jun 77 | SIO | B, M, RS |
| GAM-II-1 | EB Scripps | 6 Feb - 26 Feb 68 | SIO | B, M |
| COCOTOW-1 | Melville | 26 Aug - 20 Sep 74 | SIO | B, M |
| CØCØTØW-4 | Melville | 20 Nov - 18 Dec 74 | SIO | B, M |
| IGUANA-1 | EB Scripps | 31 Mar - 7 Apr 72 | SIO | B, M, RS |
| IGUANA-5 | EB Scripps | 15 May - 22 May 72 | SIO | B, M, RS |
| SWANSONG-1 | Argo | 5 Sep - 1 Dec 61 | SIO | B, M |
| SIQUEIROS-1 | T Washington | 17 Jun - 11 Jul 74 | SIO | B, M |
| NOVA-1 | Argo | 17 Apr - 16 May 67 | SIO | B, M |
| NOVA-6 | Horizon | 18 Sep - 14 Oct 67 | SIO | B, M |
| NOVA-10 | Argo | 11 Dec - 19 Dec 67 | SIO | B, M |

Table 1. List of Research Cruises (continued).

| | | | | |
|---|---|---|---|---|
| CRUNCH-1 | Oconostota | 28 Jul - 1 Aug 69 | SIO | B, M |
| MARIANNAS-1 | T Washington | | SIO | B, M |
| STYX-1 | A Agassiz | 2 - 26 Apr 68 | SIO | B, M |
| APHRODITE-1 | EB Scripps | 14 - 20 Jul 68 | SIO | B, M |
| BENTHYFACE-1 | Melville | 21 May - 3 Jun 73 | SIO | B, M |
| INDOMED 77-1 | Melville | 24 Sep - 31 Oct 77 | SIO | B, M |
| TRIPOD-1 | Argo | 14 Oct - 10 Nov 66 | SIO | B, M |
| TRIPOD-3 | Argo | 2 Dec - 21 Dec 66 | SIO | B, M |
| CARROUSEL-1 | SF Baird | 13 Jun - 14 Jul 64 | SIO | B, M |
| GAMBUL-1 | EB Scripps | 2 - 15 Oct 68 | SIO | B, M |
| GAMBUL-2 | EB Scripps | 16 Oct - 1 Nov 68 | SIO | B, M |
| FRANCIS DRAKE-1 | Melville | 20 Jan - 14 Feb 75 | SIO | B, M |
| HERM-1 | Oconostota | 15 - 19 Jan 69 | SIO | B, M |
| DOWNWIND-A | Horizon | 21 Oct - 15 Nov 57 | SIO | B |
| PROA-4 | SF Baird | 4 Sep - 3 Oct 62 | SIO | B, M |
| PAPAGAYO-1 | SF Baird | 18 - 29 Jun 65 | SIO | B, M |
| CENT-1 | T Washington | | SIO | B, M |
| ARIES-1A | T Washington | 15 Nov - 2 Dec 70 | SIO | B, M, RS |
| SPRINT-2 | T Washington | 8 - 9 Mar 84 | SIO | B, RS |
| SEABEAM TEST-A | T Washington | 13 Dec 81 | SIO | SB, M |
| CERES-1 | T Washington | 28 - 30 Jun 82 | SIO | SB, DT, M |
| BONANZA-1 | T Washington | 5 - 6 Jun 82 | SIO | SB, M |
| BONANZA-2 | T Washington | 7 - 13 Jun 82 | SIO | SB |
| BONANZA-3 | T Washington | 13 - 19 Jun 82 | SIO | SB |
| SEAMOUNT | T Washington | 17 - 28 Jun 83 | SIO | SB |
| ARIADNE-1 | T Washington | Apr 82 | SIO | SB, M |

Table 1. List of Research Cruises (continued).

| | | | | |
|---|---|---|---|---|
| ARIADNE-3 | T Washington | Oct 82 | SIO | SB, M |
| PASCUA-1 | T Washington | May 83 | SIO | SB, M |
| CERES-2A | T Washington | Jul 82 | SIO | SB, M |
| CERES-4 | T Washington | 82 | SIO | |

1. Institutions - SIO Scripps Institution of Oceanography
   NEL Naval Electronics Laboratory
   CDMG California Division of Mines & Geology
   NOAA National Oceanic and Atmospheric Administration
   USGS United States Geological Survey

2. Data Types - B Bathymetry
   M Magnetic
   RS Reflection Seismic
   SB SeaBeam
   DT Deep Tow

The greatest density of soundings (ship tracks) are in the regions closest to the shoreline and along lines approaching San Diego Bay. Also, much seafloor relief and complex geomorphology is found along the continental slope (between the shelf break and adjacent offshore basin. With this in mind, sounding (and bathymetric contour) charts for these nearshore regions were prepared first, at a relatively large-scale (figure 2). A comparatively well-surveyed chart of Bahía Todos Santos (Ensenada Bay) was recently published by the U.S. Hydrographic office (H.O. #21021, scale 1:35,000), and was used as the base for the first large-scale map. In addition to the soundings shown on the published chart, the additional data (collected by the author, and others at SIO) were added, by plotting the recent, and most accurately navigated (using RADAR transponders) soundings first, followed by successively older cruise data. These older data were adjusted in position to provide good agreement of soundings at line crossings for all the data. Hand contouring of these data produced the first large scale bathymetric chart.

Three areas of the shelf and slope region were then mapped at 1:50,000 scale in a similar fashion (figure 2). The 'master' sounding data for these charts were derived from the most accurately navigated portions of the two reflection profiling surveys conducted by the author. Navigation for these cruises was accomplished using combinations of triangulation on ship to shore-based RADAR transponders, satellite and LORAN-C positioning, and RADAR ranging to landmarks. A discussion of these various navigation techniques is in an Appendix.

The most recently collected bathymetric data, from cruises listed in Table 1, were also navigated with good accuracy (using satellites), and were included as 'master' soundings to the base map. In particular, the recently operational multibeam

'Sea Beam' echo-sounding system aboard the SIO R/V Thomas Washington provided a few detailed computer-contoured swaths of bathymetry that were located using satellite position fixes and provided excellent control lines for the other sounding data. In some cases, minor shifts in these Sea Beam tracks were found to be necessary to provide consistent soundings where Sea Beam swaths crossed.

Digitization of the sounding data from the two, detailed reflection profiling surveys undertaken as a part of this study (CFAULTS 1 and 2) was performed at 5 minute time intervals, (representing a distance of about 1 km at the ship's speed of 6 knots). At significant inflections in the bottom slope, additional soundings were digitized, providing a sampling interval as small as 1 minute (or about 200 m). Sampling intervals for the other bathymetric data (except Sea Beam) varied between 500 m and 5 km, with the majority being about 2 km (5 minutes at 12 knots). The resolution of small features sampled at the short intervals on these two detailed surveys allowed interpolation of bathymetric detail into areas of less frequently sampled sounding lines. Also, more accurate re-location of the poorly navigated data could be accomplished by fitting these data to the 'master' soundings sampled at the more frequent intervals.

**Accuracy and Resolution**

Considering the resolution provided by the sampling intervals and the accuracy of the navigation, the overall accuracy of the sounding positions used in contouring the bathymetric charts is excellent, and the estimated accuracy is shown in figure 3. In general, features as small as 500 m wide, and 10 m high can be distinguished over much of the region. However, identification (recognition) of 'true' shape of features

Figure 3. Relative navigational accuracy of sounding positions and resolution of bathymetric features. Areas of special detailed bathymetric studies, (e.g. Sea Beam, Deep Tow) were continuously navigated using LORAN-C, or acoustic transponders and had close (often overlapping) line spacing. Areas with very good navigation were surveyed using closely-spaced lines and precision, shore-based RADAR transponder navigation, or numerous, high quality satellite position fixes. Areas with good navigation were surveyed using closely-spaced lines, and predominately triangulation to landmarks using RADAR, with occasional, high quality satellite position fixes. Areas with fair navigation were surveyed using more widely-spaced lines, with few reliable RADAR or satellite position fixes and relied upon dead-reckoning in general. Areas with no sounding data for this study were not contoured on Plate 1.

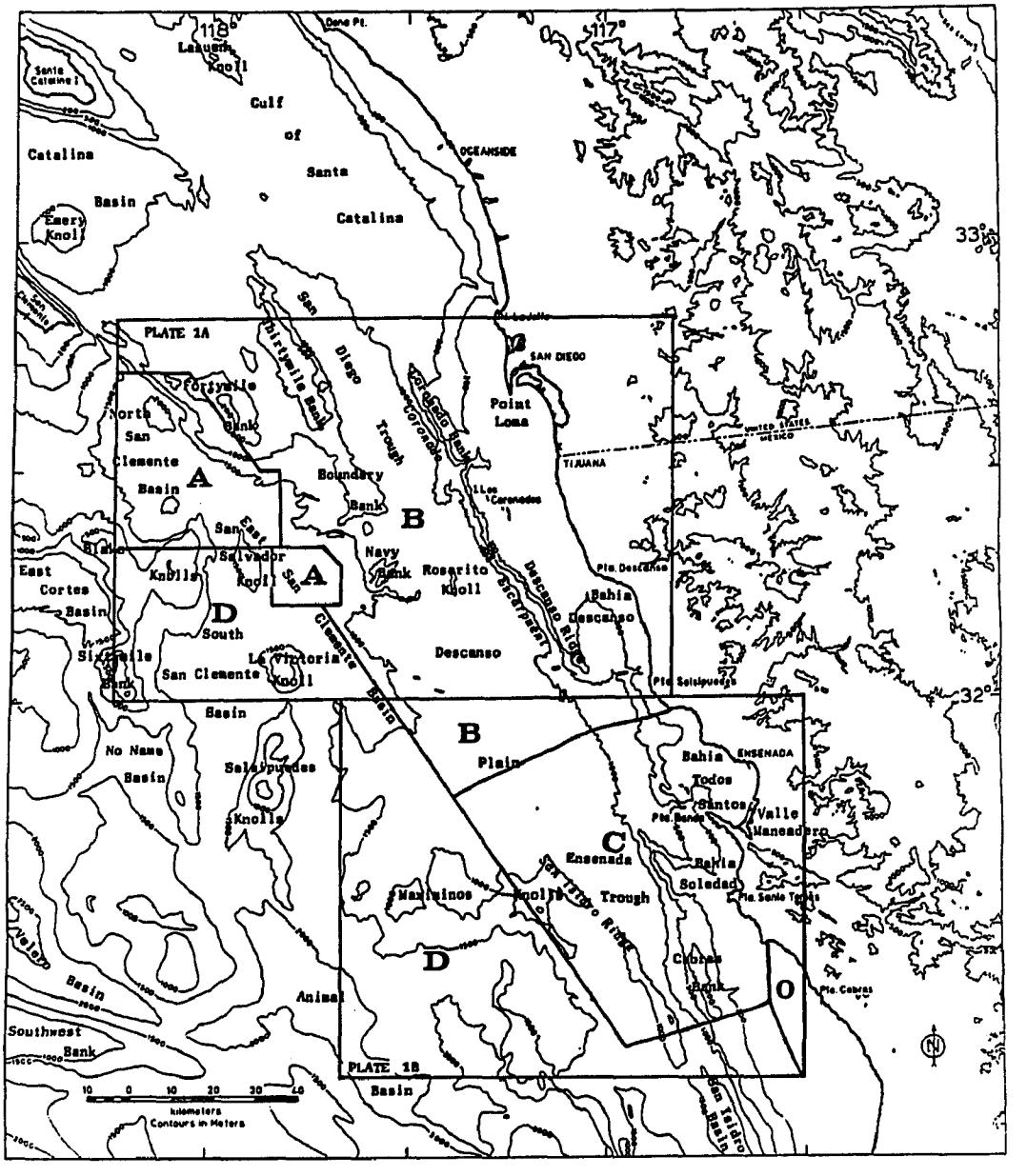


Relative Navigational Accuracy of Sounding Positions and Resolution of Features.

A = Special Study, 50 m in Position, 0.1 - 1 km Resolution in Shape.
B = Very Good Navig, 200 m in Position, 1 - 10 km Resolution in Shape.
C = Good Navigation, 500 m in Position, 5 - 10 km Resolution in Shape.
D = Fair Navigation, 1 km in Position, 10 km Resolution in Shape.
O = No Data, Not Contoured for this Study.

smaller than a few kilometers wide is not likely, except for Sea Beam swaths. Even so, substantially greater resolution of features is apparent in these maps compared to previous maps of the area (cf. Shepard and Emery, 1941; Moore, 1969; Krause, 1965; NOS, 1974). Sea Beam data provide significantly greater resolution of the seafloor topography (about 10-15 m in elevation and 100 m in width for water depths of 1000 m), and more detailed information regarding these data can be found elsewhere (Renard and Allenou, 1979; Desnoes, 1980; chapter 5, this volume).

The large-scale maps, were photographically reduced (both sounding and contour maps) and incorporated into the relevant part of the final bathymetric maps for the entire study area (plate 1). Large scale maps were carefully prepared so that the soundings and contours correctly match adjacent sheets (i.e., some overlap was included between sheets). Sounding data for areas not covered by the large-scale charts were also adjusted to fit the continuations of these data where the ship tracks crossed into the region mapped at large scale. Other soundings were added in the manner described previously for the large-scale charts, with the most accurately navigated data plotted first, followed by successively older, or less-well navigated soundings.

A contour interval of 10 fathoms (assuming a constant sounding velocity of 800 fathoms/second) was used to prepare the final charts. In a few small areas, where detailed bathymetric surveys were previously conducted, the published contour maps of those studies were incorporated directly into the regional chart at the appropriate scale. These detailed studies include those of Normark and others (1979) for Navy fan, chapter 5 (this volume) for North San Clemente Basin, Shepard and Buffington (1968) for La Jolla Fan Valley, and Shepard and Marshall (1975) for parts of

Coronado Fan Valley. Also, the U.S. Hydrographic Office chart No. 18765 (approaches to San Diego Bay) was used as a basis for contouring much of the bathymetry west of San Diego, although numerous recent Sea Beam data crossing this area provide additional detail of interest. The coastline for all of the charts was taken from the appropriate CETENAL (1974-1979) map sheets.

## DISCUSSION

Three fundamental geologic processes are herein considered responsible for the geomorphology (physiography) of the Inner Borderland: (1) tectonic (structural); (2) erosional; and (3) and depositional, including volcanic. All three may occur contemporaneously or any combination may affect the observed character of a particular feature that was shaped originally by one of the other processes. In the following discussion, the principal physiographic elements of the region (as shown in plate 2), are described and the process(es) believed responsible for their morphology are inferred. The bathymetric data provide the primary data for recognition of these features and the processes that shape them, although additional data, such as seismic reflection profiles (figure 4) or bottom samples, are used to provide confirmation of the interpretations when possible. Detailed descriptions of these supplementary data are presented elsewhere (chapters 3 and 4, this volume; Krause, 1961; Moore, 1969; Emery, 1960).

### Coasts

Emery (1960) recognizes two types of shorelines: (1) erosional, and (2) depositional. Such a classification scheme is simple, and distinctions can be accomplished readily from coastal topographic and bathymetric data (Emery, 1960; Shepard, 1963).

Figure 4. Location of selected seismic profiles and Sea Beam swaths shown in this report. Letters and numerals adjacent to track lines identify line numbers of seismic profiles. Identification numbers preceded by SB identify Sea Beam swaths, and the numerals refer to the figure number in the report. Small squares identified with numerals or letters show the locations of high-resolution, 3.5 kHz seismic profiles with reference to the appropriate figure in the report.

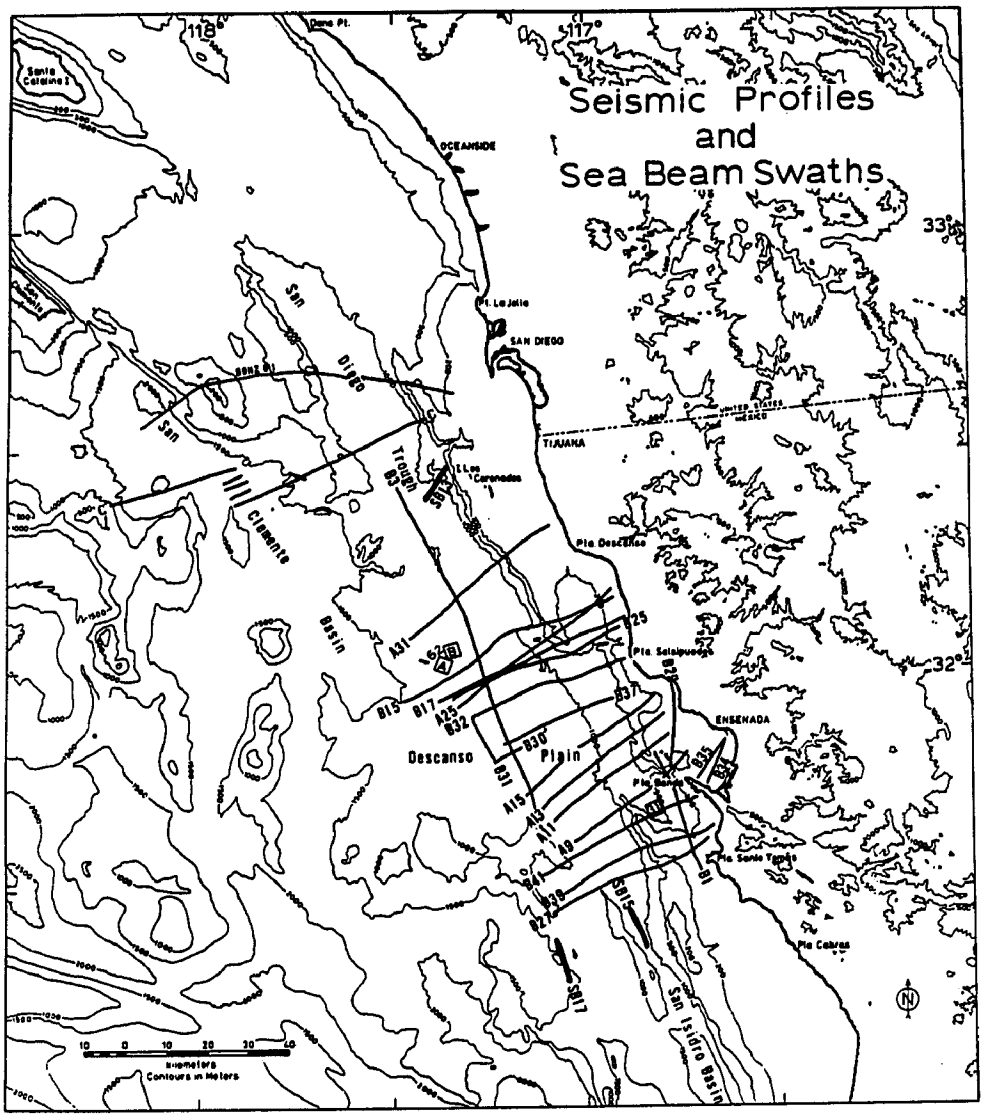
Seismic Profiles
and
Sea Beam Swaths
118°
117°
33°
32°
OCEANSIDE
Pt. La Jolla
SAN DIEGO
TIJUANA
Pte Descanso
Pte Salsipuedes
ENSENADA
Pte Santo Tomas
Pte Colonet
San Diego Trough
San Clemente Basin
Descanso Plain
San Isidro Basin
Kilometers
Contours in Meters

Around the California Continental Borderland Emery (1960) notes that erosional shorelines are either rocky or have (sandy) beaches backed by rocky cliffs. Depositional shorelines have sandy beaches backed by lowlands such as marshes, mud flats, alluvial fans or deltas. Although this simple classification scheme ignores the third geologic process active in shaping the regional physiography, the author finds that tectonic activity is significant in defining the shape of the coast of the Inner Borderland.*

The coastline between San Diego (Point Loma) and Punta San José is dominantly erosional in character (plate 2). Sea cliffs and coastal bluffs are common, including narrow beaches backed by low bluffs that truncate uplifted terraces (Playas Tijuana to La Misión, Gastil and others, 1975), small, pocket beaches (along Punta Banda), and high, steep cliffs that continue beyond the shoreline (Punta Salsipuedes, northeast side of Punta Banda). Large landslides extend into the sea near Punta San Miguel. Quaternary uplift of much of this coast is indicated by the presence of numerous raised marine terraces (Orme, 1974; Ortlieb, 1979), especially along Punta Banda and Punta Santo Tomás. Both highly irregular and relatively straight parts of erosional coastline are found. In some cases, structural control, due to faulting, is implied by long, straight sections of coast such as along the northeast side of Punta Banda and between Tijuana and Punta Descanso. The Agua Blanca fault is known to pass along the northeast side of Punta Banda (Allen and others, 1960; Gastil and others, 1975). Geomagnetic (Krause, 1965) and seismic reflection data (chapter 4, this volume) indicate another fault parallels the coast northwest of Punta Descanso.

---

* Topographic and geologic data used in deriving the coastline classifications described in this section are from the appropriate CETENAL (1974-1979) maps.

The few areas of depositional shoreline are associated with the more significant stream valleys such as at San Diego (Tía Juana and San Diego rivers) and Ensenada (Vallé Manéadero). Structural control and tectonic subsidence for these sediment-filled basins (troughs) are suggested by Kennedy and Welday (1980) for Mission and San Diego Bays, and by Gastil and others, (1975) and Legg and Kennedy (1979) (see also chapter 4, this volume) for the Vallé Manéadero. The supply of sediment from the more significant streams and rivers which enter the sea through these troughs is adequate to form barrier beaches and spits such as the Silver Strand in San Diego and Estero Banda near Ensenada. Other significant coastal embayments may have resulted from tectonic processes, such as Bahía Soledad (Acosta, 1970), but this is not confirmed by the present data. Finally, other small areas of depositional shoreline are associated with smaller streams (La Misión, La Salina), or areas of sand dunes (Cantamar).

**Shelves, Banks, and Ridges**

Depositional, erosional and structural processes have worked together to shape the shelves and banks of the Inner Borderland. The prominent northwest trend of the banks and shelf edges may be a result of the tectonic interaction between the Pacific and North American plates. The flat tops of many banks and the shelves, as well as the numerous submerged terraces, indicate erosional planation of the older rock surfaces during earlier sea level stands, due to eustatic changes or tectonic subsidencc. Seismic reflection data (figures 5, 6 and 7) show that ponding of terrigenous* sediments behind offshore basement ridges has created the wide shelf areas around Islas

---

* Emery and others (1952) describe the seafloor lithology in the region offshore of San Diego.

Figure 5. Airgun seismic profile (Line A-31) crossing the Coronado Shelf and Descanso Plain (see figure 4 for location of profile). Blow down (B.D.) refers to areas where record quality deteriorated because of compressor venting operation. Actual record is compared to line drawing to show the reflection character of acoustic basement and sedimentary sequences. Multiple bubble-pulse oscillations shown by the several strong reflectors in the outgoing pulse (at the top or bottom of the record) make interpretation of these airgun profiles difficult.

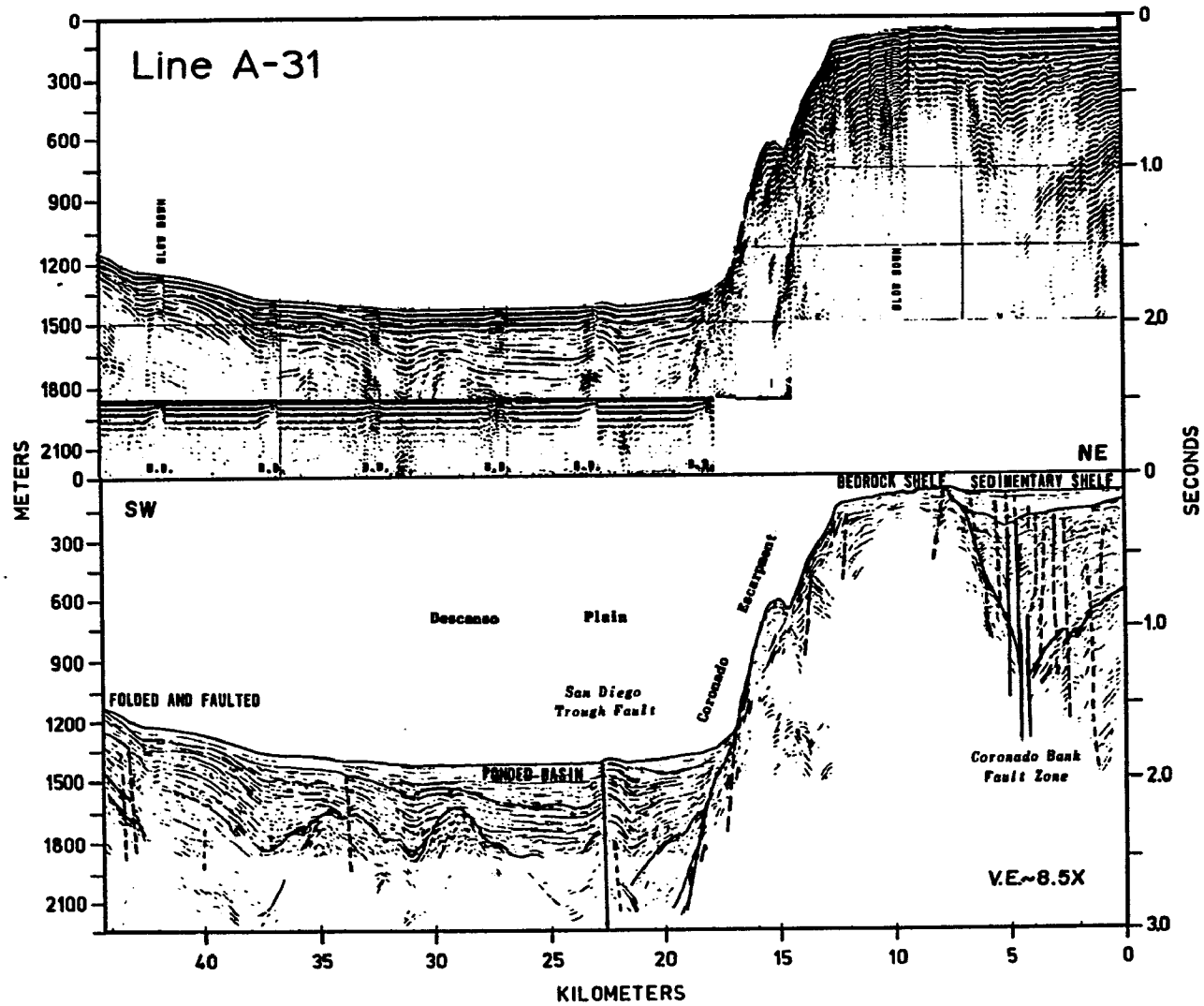
Line A-31
NE
SW
BEDROCK SHELF
SEDIMENTARY SHELF
Descanso
Plain
San Diego
Trough Fault
Coronado
Escarpment
FOLDED AND FAULTED
PONDED BASIN
Coronado Bank
Fault Zone
V.E.~8.5X
METERS
SECONDS
KILOMETERS
0
300
600
900
1200
1500
1800
2100
1.0
2.0
3.0
40
35
30
25
20
15
10
5

Figure 6. Airgun seismic profile (Line A-25) across the Descanso Plain and Bahía Descanso (see figure 4 for location of profile). Comments on previous airgun profile apply to this figure as well. Damming of sediment behind Descanso Ridge is evident. Divergent wrench faulting is shown by the sagging of bedded sediments into the Coronado Bank fault zone. San Clemente fault zone is identified by the trough bisecting the nearly symmetrical fold in the sediments of the Descanso Plain. Transpression is demonstrated by this folding, located where the San Clemente-San Isidro fault zones connect through a large, left (restraining) bend. Increased amplitude of folding with depth shows that the sedimentation is syntectonic. Disruption of the seafloor (evident in 3.5 kHz profile, not shown) implies late Quaternary and possibly Holocene fault movement in this region of active submarine fan deposition.

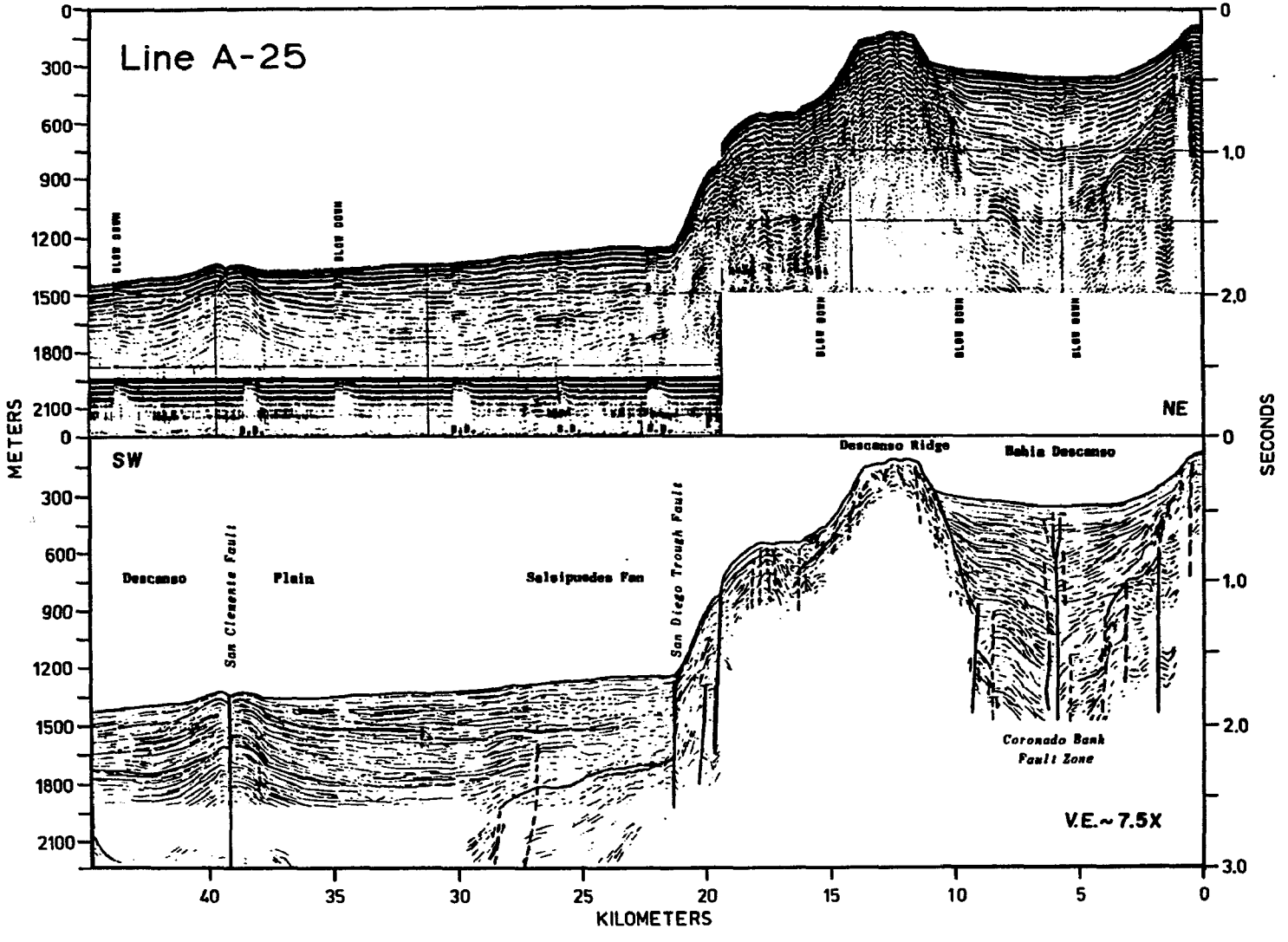
Line A-25
SW
NE
Descanso
San Clemente Fault
Plain
Salsipuedes Fan
San Diego Trough Fault
Descanso Ridge
Bahia Descanso
Coronado Bank
Fault Zone
V.E.~7.5X
METERS
SECONDS
KILOMETERS
0
300
600
900
1200
1500
1800
2100
1.0
2.0
3.0
40
35
30
25
20
15
10
5

Figure 7. Line drawings of airgun profiles extending from the shelf offshore across the southern Descanso Plain (see figure 4 for locations of profiles). Prominent faults and geomorphic features are identified.

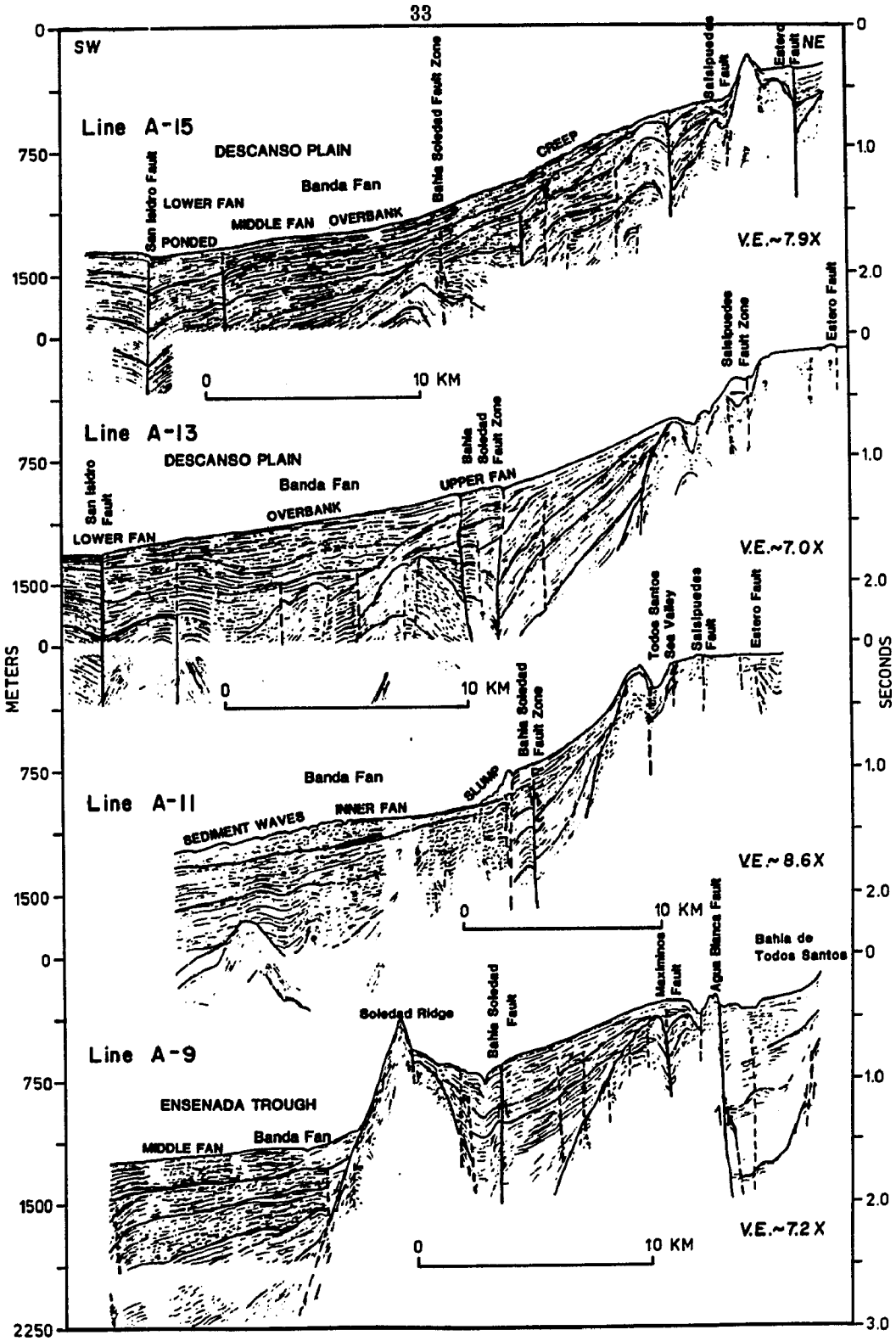
SW
NE
Line A-15
DESCANSO PLAIN
Banda Fan
LOWER FAN
MIDDLE FAN
OVERBANK
PONDED
CREEP
San Isidro Fault
Bahia Soledad Fault Zone
Salsipuedes Fault
Estero Fault
V.E.~7.9X
0
10 KM
Line A-13
DESCANSO PLAIN
Banda Fan
UPPER FAN
OVERBANK
LOWER FAN
San Isidro Fault
Bahia Soledad Fault Zone
Salsipuedes Fault Zone
Estero Fault
V.E.~7.0X
Line A-11
Banda Fan
SLUMP
INNER FAN
SEDIMENT WAVES
Bahia Soledad Fault Zone
Todos Santos Sea Valley
Salsipuedes Fault
Estero Fault
V.E.~8.6X
Line A-9
ENSENADA TROUGH
MIDDLE FAN
Banda Fan
Soledad Ridge
Bahia Soledad Fault
Maximinos Fault
Agua Blanca Fault
Bahia de Todos Santos
V.E.~7.2X
METERS
SECONDS
0
750
1500
2250
1.0
2.0
3.0

Los Coronados, Bahía Todos Santos and possibly the San Isidro Shelf. Thin pockets of sediment filling small basement topographic irregularities also tend to smooth the bank tops and shelf areas.

The banks and shelf closest to the shoreline are generally elongate, trending northwesterly. These nearshore banks are shallow and flat-topped implying that they were beveled during lowered sea levels of Pleistocene time. In some areas, angular unconformities below a thin layer of horizontally stratified surficial deposits are seen in reflection profiles, such as Coronado Bank (figures 5-10), the Descanso shelf and ridge, the shelf north of Islas Todos Santos and the Soledad shelf and ridge. Tectonic influence also may be involved, because the elevations of these nearshore banks and shelves vary along the coast. Similar bevelling of other flat-topped banks is observed farther offshore in the northern Borderland (e.g., Thirtymile, Fortymile, Tanner and Cortes Banks; Emery, 1960; Moore, 1969; Vedder and others, 1974). Internal structure exhibited in seismic reflection profiles shows that some of the northwest-trending ridges and banks are anticlinal (e.g., Coronado Bank, Descanso Ridge, Thirtymile and Fortymile Banks; figure 5, 6 and 7; Vedder and others, 1974), whereas others appear to be fault bounded horsts or tilted fault blocks (Punta Banda and the San Isidro Ridge, figures 7 and 8).

Beyond the continental slope are many peaks of roughly circular or elliptical shape. Many of these peaks are considered to be volcanic in origin. Seismic reflection data (figures 8 and 11) show such peaks to be composed of acoustic basement rock, showing chaotic internal reflectors. Vedder and others (1974) and Junger and Vedder (1980, personal communication) associate such reflection character with volcanic rocks. Samples dredged from some of these peaks include Franciscan-like

Figure 8. Sparker seismic profile (Line B-27) from the Soledad Shelf, southwestward across the Ensenada Trough to Maximinos Knolls (see figure 4 for profile location). These sparker data did not suffer the deterioration of record quality caused by compressor problems and severe, multiple, bubble-pulse oscillations found in the air-gun data (cf. figures 5 and 6). Consequently, several seismic sequences may be identified in the basin sediments, especially where the submarine fans are located. Acoustic facies types interpreted by the author are shown in the stratigraphic key.

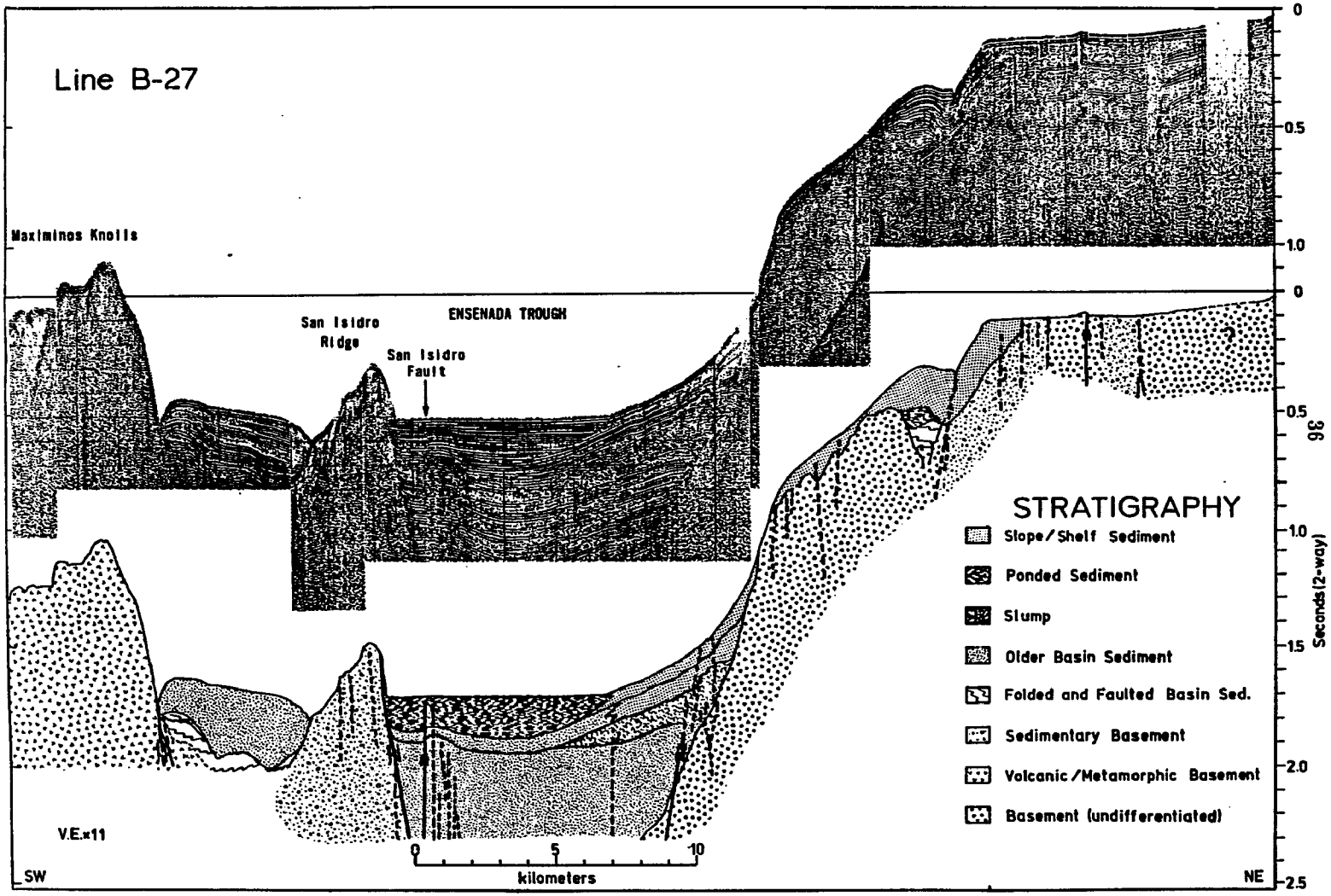
Line B-27
Maximinos Knolls
San Isidro Ridge
ENSENADA TROUGH
San Isidro Fault
STRATIGRAPHY
Slope/Shelf Sediment
Ponded Sediment
Slump
Older Basin Sediment
Folded and Faulted Basin Sed.
Sedimentary Basement
Volcanic/Metamorphic Basement
Basement (undifferentiated)
V.E.x11
SW
NE
0
5
10
kilometers
0
0.5
1.0
0
0.5
1.0
1.5
2.0
2.5
Seconds (2-way)

Figure 9. Sparker seismic profile (Line B-30'-31-32) across the Descanso Plain southwest of Punta Salsipuedes (see figure 4 for profile location). Note the numerous seismic sequences which can be identified in the slope and basin sediments. Two course changes (C/C) are present along this profile. Acoustic facies are identified by name, except for the older slope and basin sediments shown with the same pattern as the sedimentary acoustic basement.

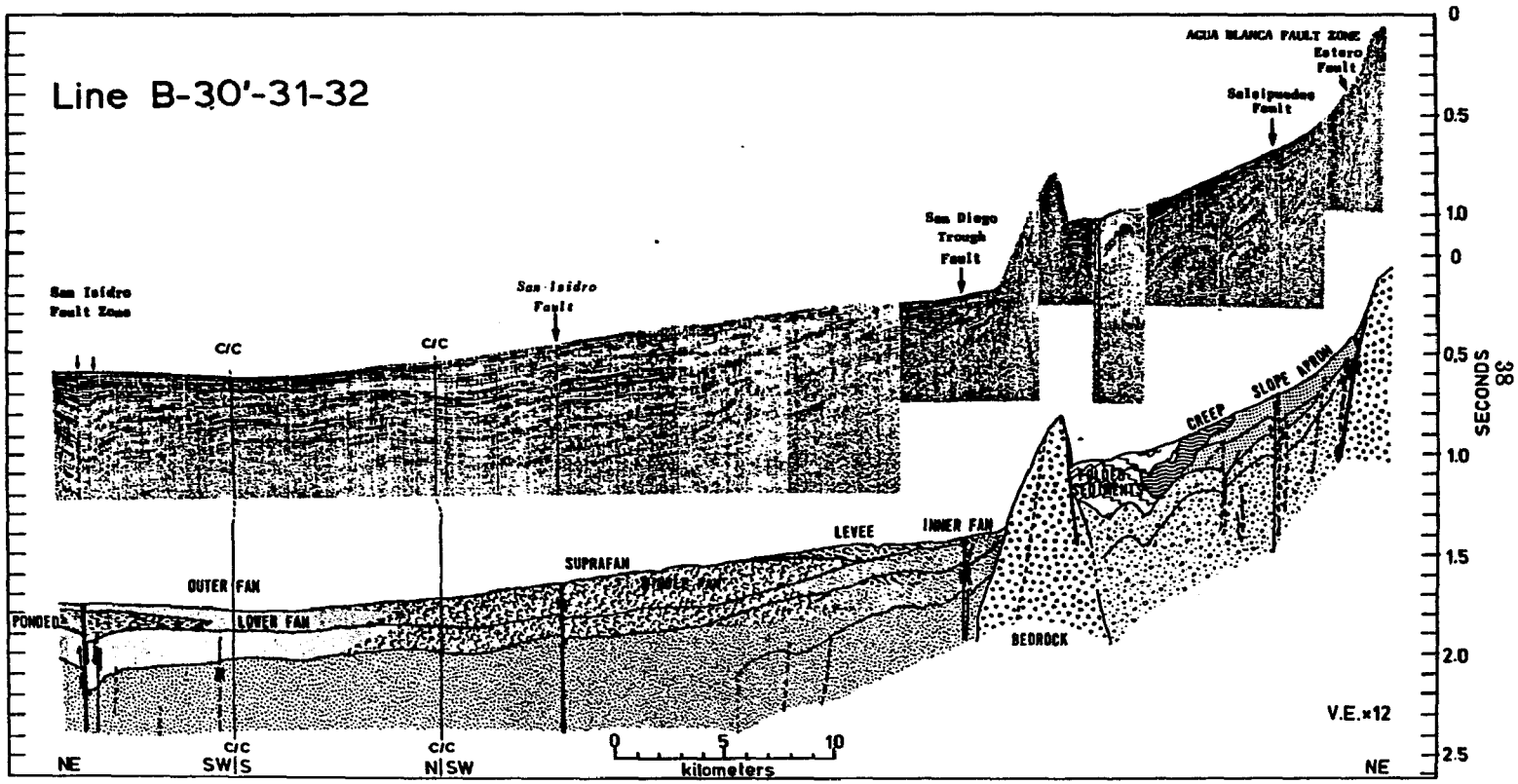
Line B-30'-31-32
AGUA BLANCA FAULT ZONE
Estero Fault
Salsipuedes Fault
San Diego Trough Fault
San Isidro Fault Zone
San Isidro Fault
C/C
C/C
CREEP
SLOPE APRON
LEVEE
INNER FAN
SUPRAFAN
OUTER FAN
LOWER FAN
PONDED
BEDROCK
C/C
C/C
NE
SW|S
N|SW
0
5
10
kilometers
V.E.×12
NE
0
0.5
1.0
0
0.5
1.0
1.5
2.0
2.5
SECONDS

Figure 10. Airgun seismic profile (Line C) across San Diego Trough and East San Clemente Basin (see figure 4 for profile location). Misfiring(?) of airgun is evident as the prominent repetition of bottom reflection about 0.1 second later than the first bottom reflection. Note difference in character between slope and basin sediments and acoustic basement of Boundary Bank. (Profile courtesy of J. Mammerickx and P. Lonsdale).

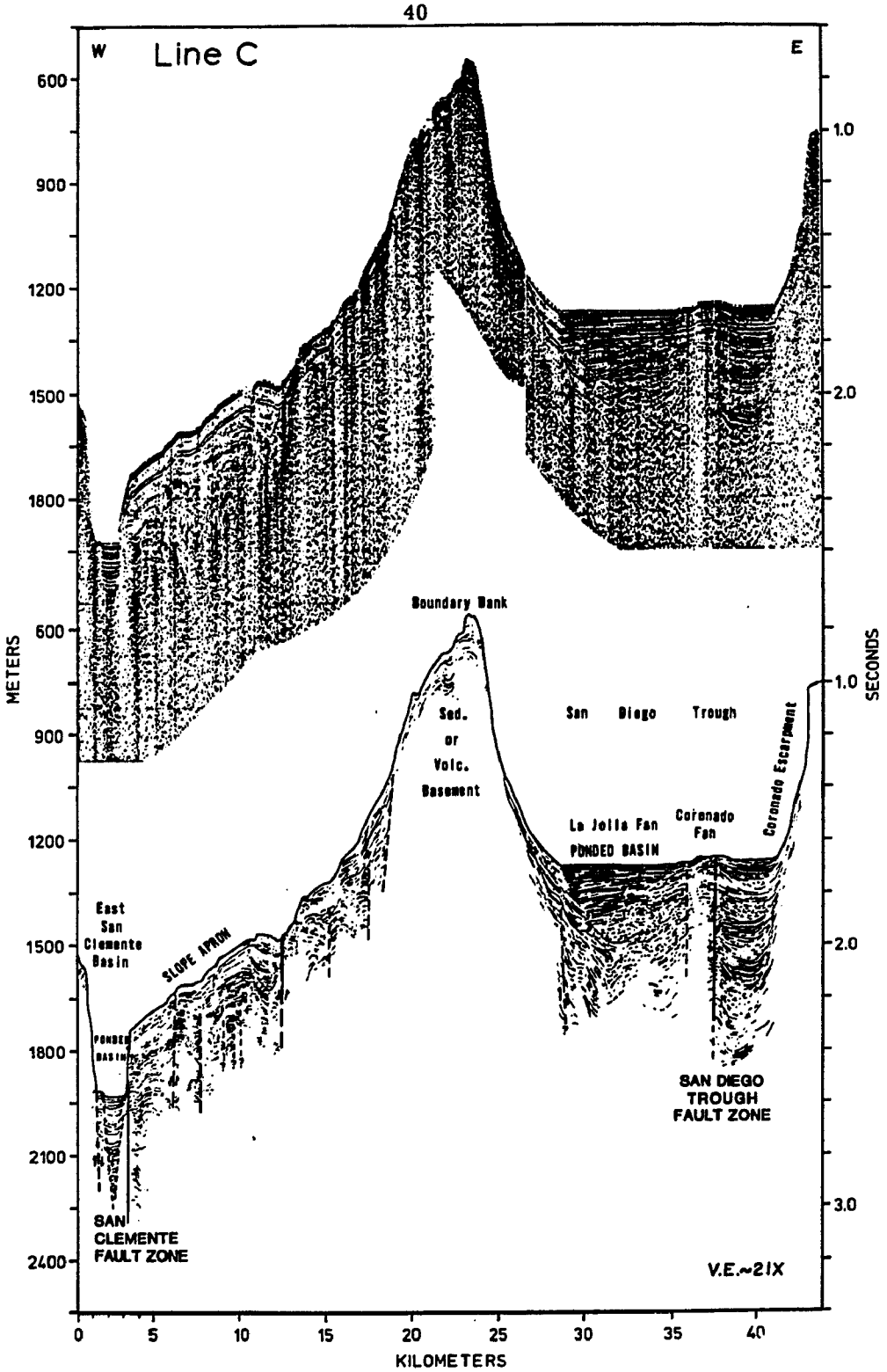
Line C
W
E
METERS
SECONDS
KILOMETERS
Boundary Bank
Sed.
or
Volc.
Basement
San Diego Trough
Coronado Escarpment
La Jolla Fan
PONDED BASIN
Coronado Fan
East
San
Clemente
Basin
SLOPE APRON
PONDED BASIN
SAN DIEGO
TROUGH
FAULT ZONE
SAN
CLEMENTE
FAULT ZONE
V.E.~21X

Figure 11. Line drawing of sparker profile (Line B-3) that obliquely crosses the axis of the San Diego Trough and Descanso Plain (see figure 4 for profile location). Sedimentary units identified include the Descanso and Pelagic (PEL) units described by Smith and Normark (1976). Several seismic sequences in the Banda, Coronado and Salsipuedes fan sediments are delineated. Possible facies changes in the pelagic unit are shown by change in character of reflectors, from relative absence of reflectors to numerous, parallel reflectors shown between the horizons bounding the unit. Total magnetic field intensity anomaly is also shown to point out the correlation of geomagnetic anomaly with acoustic basement of possibly igneous bedrock underlying Rosarito Knoll. Scales of the three sections of magnetic profiles are shifted as shown.

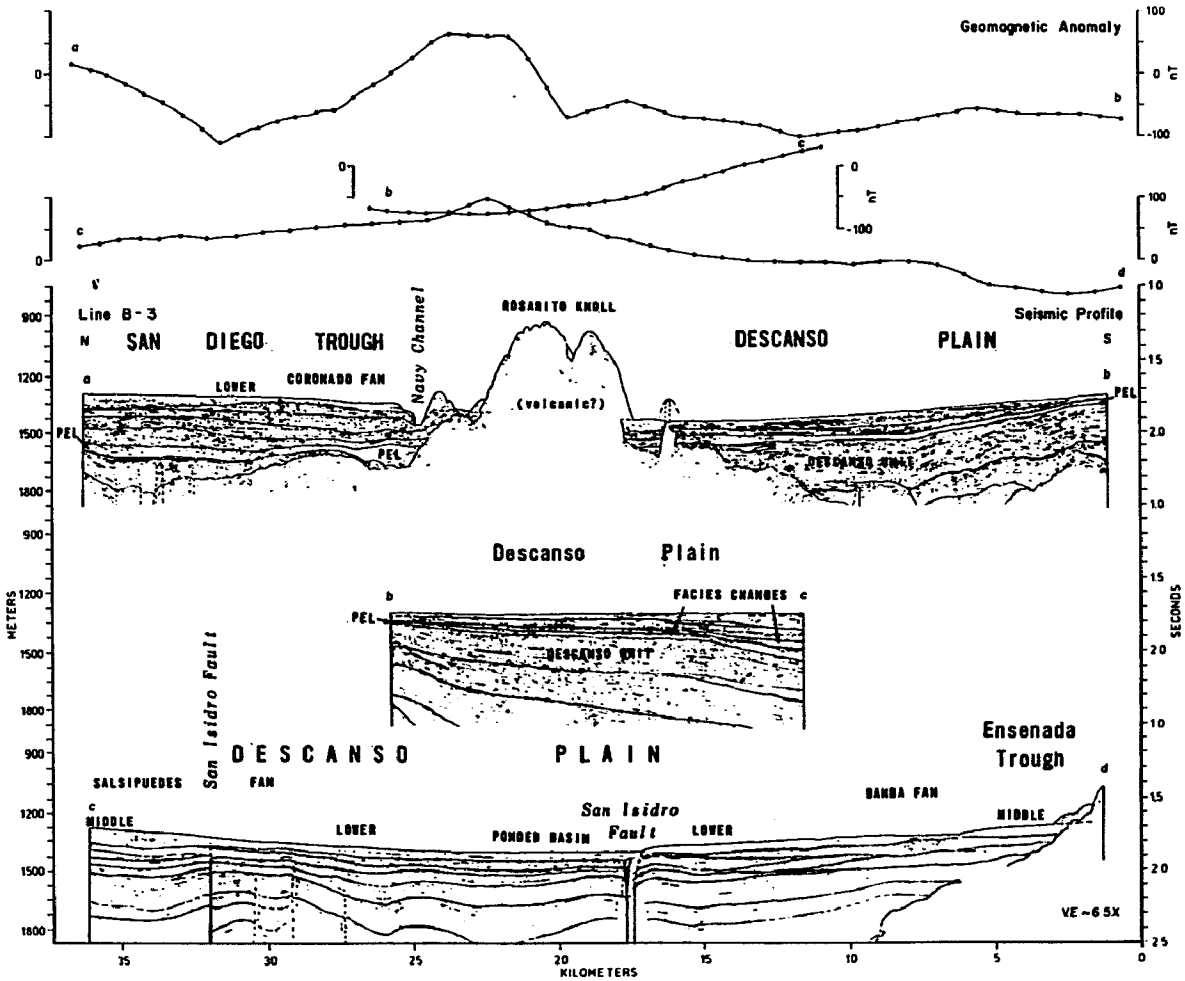
Geomagnetic Anomaly
Line B-3
Seismic Profile
N
S
SAN DIEGO TROUGH
LOWER CORONADO FAN
Navy Channel
ROSARITO KNOLL
(volcanic?)
DESCANSO PLAIN
PEL
Descanso Plain
FACIES CHANGES
DESCANSO PLAIN
San Isidro Fault
SALSIPUEDES FAN
MIDDLE
LOWER
PONDER BASIN
San Isidro Fault
BANDA FAN
Ensenada Trough
VE ~6.5X
METERS
SECONDS
KILOMETERS

blueschist on La Victoria Knoll and hornblende andesitic and dacitic rocks from Navy Bank (Vedder and others, 1974).

A similar small, but prominent elongate peak protrudes through the sediments filling the San Diego Trough (Rosarito Knoll). The author suggests it has a volcanic origin, based on reflection data and a magnetic anomaly coincident with this feature (figure 11). Sea Beam data crossing this feature show the presence of several smaller peaks, which are almost buried by sediments (plate 1). The pronounced north-to-northwest trend of this feature is somewhat oblique to the trend of the San Diego Trough. Volcanic activity associated with divergent wrench faulting, perhaps along a leaky transform fault(?) may have occurred. Another possible explanation is that the feature is a block of basement rock squeezed up between two anastomosing wrench fault strands. Sampling and petrologic analysis (including radiochronology) of rock outcrops from this knoll are necessary to determine the origin of this feature and the timing of possible volcanic(?) activity in this part of the Borderland.

**Basin and Trough Slopes**

The most striking features shown on the bathymetric charts are the slopes which separate the basins from the adjoining shelves, banks, and ridges. These slopes are eye catching, not only because they are steep and delineated by many closely spaced contours, but also because of their remarkable linearity, over significant distances. The slopes can be divided into three categories: (1) long, straight and steep; (2) slightly to moderately curved with gentle inclination; (3) highly irregular, but moderately steep. Slopes of the first group are considered by the author to have been formed by tectonic processes, related to the numerous

northwest-trending faults of the region. Those of the second group include submarine fans, slope aprons and other predominately depositional slope features. The last group includes original tectonic or volcanic slopes significantly modified by erosional and depositional processes.

**Tectonic Slopes**

Long, straight, steep slopes trending predominately toward the northwest in this region have generally been associated with underlying tectonic structure (Shepard and Emery, 1941; Krause, 1965; Moore, 1969). The linearity and overall steepness of such slopes evince their youthful nature. Older slopes are presumed to have large gullies, submarine canyons or slumps that significantly alter their original structural form. Early studies postulated that these slopes were fault scarps, although steep flanks of folds were considered alternate possibilities (Shepard and Emery, 1941). Seismic reflection data have shown that some of these slopes are fault controlled (e.g. Coronado Escarpment, flanks of Boundary Bank, and the San Isidro Ridge, figures 5, 6, 8 and 10; Moore, 1969; chapter 4, this volume), whereas others may be dip slopes (parts of Boundary Bank, Descanso Ridge, and Coronado Escarpment, figures 8 and 10; Vedder and others, 1974). Junger (1976) proposed that folding, associated with convergent wrench faulting in the Borderland, is the primary origin of these dip slopes.

Prominent steps in the Coronado Escarpment and its southward extension may be evidence of subparallel normal faults (figures 5 and 12). Detailed bathymetric (geomorphic) studies using Sea Beam, of the San Clemente fault zone near Fortymile Bank (chapter 5, this volume) show 'hillside' valleys, benches lined with sags or small,

Figure 12. Narrow-beam echo sounding profile (Line BONZ-01, Sea Beam 12 kHz, center beam monitor) from the Coronado Bank across San Diego Trough, Thirtymile Bank and Fortymile Bank to North San Clemente Basin (see figure 4 for location of profile). Narrow beam width of the Sea Beam system allows better resolution of the seafloor configuration in areas of steep slopes and rugged bathymetry. Even so, some slopes shown in the profile are steeper (>45°) than can be resolved by the Sea Beam, for example, at the base of Thirtymile Bank and the Fortymile Escarpment. Such steep slopes are considered fault scarps in this study although erosion along the channel at the base of Thirtymile Bank may have steepened the lower part of that slope.

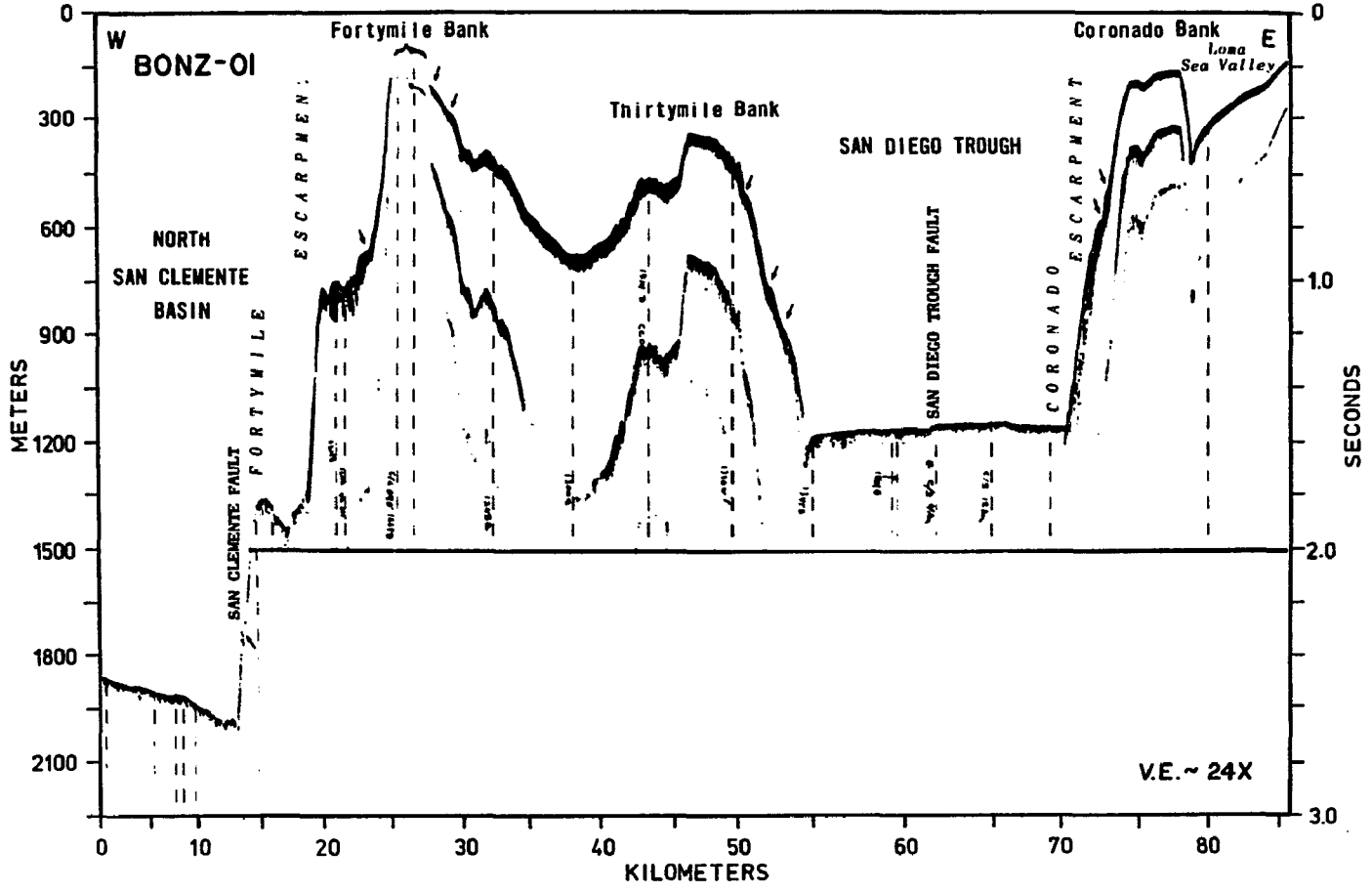
W
BONZ-01
E
Fortymile Bank
Thirtymile Bank
Coronado Bank
Loma Sea Valley
NORTH SAN CLEMENTE BASIN
SAN CLEMENTE FAULT
FORTYMILE ESCARPMENT
SAN DIEGO TROUGH
SAN DIEGO TROUGH FAULT
CORONADO ESCARPMENT
V.E.~ 24X
METERS
SECONDS
KILOMETERS
0
300
600
900
1200
1500
1800
2100
1.0
2.0
3.0
10
20
30
40
50
60
70
80

closed depressions, and other features commonly associated with recently-active faulting. Steps in other straight, steep slopes (such as the Coronado Escarpment) observed at similar depths on several adjacent conventional echo sounding profiles, may be continuous and have possible tectonic origin. Alternatively, they may represent the tops of large-scale slump or slide blocks.

Depressions at the base of the straight, steep slopes were proposed by Shepard and Emery (1941) and Emery (1960) to be additional indications of fault origin for these slopes. Detailed bathymetry contoured from Sea Beam data indeed has shown the presence of linear trenches, troughs, and aligned sags at the base of many of these slopes (chapter 5, this volume) confirming this interpretation for some cases. Other depressions at the base of these escarpments, such as Thirtymile Bank and Coronado (plate 1), are channels associated with submarine fans. Erosion from enhanced bottom currents has also been shown to produce moats around elevated basement features in the deep sea (Johnson and Johnson, 1970).

Although many investigators have inferred fault patterns and continuity from bathymetric data, detailed seismic reflection data reported in chapter 4 (this volume) show that extrapolation of fault continuity between specific escarpments may lead to erroneous conclusions. For example, one may infer that the escarpment west of Punta Santo Tomás was once continuous with, or the equivalent of the Coronado Escarpment to the north. Seismic reflection data show that several northwest-trending, youthful, strike-slip faults separate these two escarpments, and so that an un- known component of strike-slip may have brought these older slopes into approximate alignment. Similarily, the prominent fault scarp along the west side of the Ensenada Trough (east flank of San Isidro Ridge), has been interpreted as the

primary seafloor expression of the San Isidro fault (Moore, 1969), and was inferred to connect with the San Clemente fault to the north (plate 1). The San Clemente fault is marked by the steep, northwest-trending scarp cutting across the low, elliptical ridge near Descanso Plain. Other investigators have postulated that the San Clemente fault connects with the Agua Blanca fault at Punta Banda, based upon the trend of the San Clemente escarpment (eastern flank of San Clemente Island) and Punta Banda. Additional data in support of this interpretation included trends of magnetic anomalies and poorly located earthquake epicenters (Allen and others, 1960; Krause, 1961, 1965; Moore, 1969). Detailed seismic reflection profiling data, however, demonstrate that neither of these interpretations are correct. Instead, the 'active', and relatively continuous traces of the San Clemente - San Isidro fault zone cut through the flat-lying sediments filling the Ensenada Trough and Descanso Plain.

**Depositional and Erosional Slopes**

Curvilinear slopes of more gentle inclination (2° - 10°, 5%-18%) are also evident bordering the basins and ridges in this area. Such slopes are prominent in the area between the Banda and Salsipuedes submarine canyons, and are presumed to result from a combination of depositional and erosional processes. The gentle gradient (~5%) of many of these slopes is similar to that of continental slopes observed on passive margins (Heezen and others, 1959) which have undergone a long history of erosional and depositional processes. Numerous small gullies or swales are apparent on some of these slopes. Evidence of slumping, sliding, or sediment creep is apparent in seismic reflection data (figures 7 and 9; also Kennedy and others, 1985), but these features are generally too small to be accurately mapped with conventional sounding

data (Field and Clarke, 1979). Sea Beam, side-scan sonar or other high resolution sea floor mapping techniques provide better data to identify such features (Prior and Coleman, 1982).

Highly irregular slopes of moderate to steep inclination are widespread in the westernmost parts of the study area. These slopes generally surround the various, roughly equi-dimensional peaks and ridges in this area, some of which protrude above a larger, common elevated base. Both erosional and depositional processes are herein proposed as causes for the irregular shape of these slopes, as various mass wasting processes transport material from the higher to lower levels on these slopes. Hemipelagic deposition tends to smooth irregularities on these slopes as well. Although conventional sounding data cannot resolve the detailed slope morphology, numerous gullies and small canyons are apparent. Where Sea Beam data are available, many small scale features are evident, some may represent small peaks or basement outcrops, others, small channels or closed depressions. Rock samples from peaks in the southwest part of the Maximinos Knolls included Pliocene basalt (Doyle and Gorsline, 1979) isotopically dated at 4 Mya, and so many of these slopes may be underlain by lava flows or volcaniclastic deposits. Seismic reflection data show negligible hemipelagic sediment cover on some of these slopes (figures 8, 9 and 10), and others appear to show exposed, older sedimentary rock (figures 5, 6 and 8). Tectonic movement followed by erosional processes would be responsible for exposing older sedimentary rock on these slopes.

**Submarine Canyons, Fan Valleys, Gullies and Troughs**

Canyons, channels and gullies along the steeper continental slope and flanks of offshore ridges and banks are presumably erosional in origin. Submarine slides, slumps and other slope failure processes are likely causes of these features. Channels on the more gently sloping submarine fan surfaces and between basins may be either depositional, as in elevated fan valley, levee systems, or erosional. Seismic reflection data are necessary to distinguish between the two types, and composite forms have been observed elsewhere (Nelson and Kulm, 1973). The presence of levees, however, is evidence of a depositional channel. Finally, straight, steep-walled channels or valleys paralleling the regional structural trends are considered to be structurally controlled.

Submarine canyons, considered to be primarily erosional in origin, have been the subject of much research and many of those of the California Continental Borderland have been described in detail (Shepard and Emery, 1941; Emery, 1960; Emery and others, 1952; Shepard and Buffington, 1968; Shepard and others, 1969; Shepard and Marshall, 1975; Emery and Shepard, 1945; Shepard and Dill, 1966). Those located offshore of northern Baja California have not received as much attention although Krause (1961, 1965), Moore (1969), and Smith and Normark (1976) described their importance as conduits in the filling of the nearshore basins with turbidites. The detailed bathymetry shown in plate 1, and geomorphology in plate 2, provide a detailed view of the character and morphology of two major, and previously undescribed, submarine canyon/fan systems located in the northern Baja California Borderland. The southernmost canyon heads in Bahía Todos Santos, off the tip of Punta Banda, and is called the Banda Canyon and fan valley (after Moore, 1969). The

second (named herein the Salsipuedes Canyon and fan valley), heads near the coast north of Punta Salsipuedes. Other prominent canyons in the area include Coronado Canyon and fan valley, Navy Channel, La Jolla Canyon and fan valley and the San Clemente Rift Valley. Several other smaller, unnamed submarine valleys and channels of some significance are also present.

Salsipuedes Canyon has two major tributaries at its head, which is typical of submarine canyons offshore California (e.g., La Jolla and Scripps Canyons). Banda Canyon is atypical, having a bowl-shaped head located within a large, coastal embayment (Bahía Todos Santos). This shape may be a result of headward erosion by large-scale slumping and sliding of unconsolidated (or poorly consolidated) sediments. Banda Canyon necks downstream passing through a narrow gorge cut into the older, uplifted bedrock (Alisitos formation?, Gastil and others, 1975) which is subaerially exposed on Punta Banda and Islas Todos Santos .

All of the well-developed submarine canyons in the area show significant sinuosity. Expression of the sinuousity varies from sharp, almost right-angled turns, implying fault or joint control, to smooth meanders, similar to those seen along many rivers. A significant sharp bend in the Banda Canyon just west of Punta Banda may be evidence of four kilometers of right lateral offset associated with a branch of the Agua Blanca fault zone. This canyon offset is aligned with a linear, northwest-trending "fault trough" valley west of Todos Santos Islands (Todos Santos Sea Valley).

A similar sharp bend is apparent in the Salsipuedes Canyon near the head of the upper fan valley (at the base of the continental slope). The canyon makes a sharp, 120° left turn, which is well defined by Sea Beam data which cross this area (plate 1). Other data (Legg and Kennedy, 1979; chapter 4, this volume) demonstrate

that major, northwest-trending faults in this area are right-lateral, strike-slip in character, so the sharp bend in the canyon is not considered to represent fault offset. Instead, structural control of the canyon course through preferential erosion of weaker rock along the fault zone is postulated. Possible 1-2 km offset (dextral) of an older canyon/upper fan valley is shown by the Sea Beam and other detailed bathymetric data just north of this area (plate 1).

Submarine fan valleys and channels may be erosional or depositional in character. All three major fan valleys in the region turn southward (toward the left), and cross the southern part of the fan surface. This phenomenon has been observed for most of the submarine fan valleys in the northern hemisphere (Menard, 1955; Shepard and Emery, 1941; Emery, 1960; She d and Dill, 1966). Menard (1955) attributed this pattern to tilting of the turbidity currents by the Coriolis force so that the right-hand side is thicker, and a higher levee builds up on this side. Later flows would then tend to deviate to the left when encountering the higher levees to the right, and so the main channel would bend to the left as well. The right-hand levees of the upper fan valleys in this area are significantly larger than the left-hand counterparts (figure 9, plate 1). The author (chapter 6, this volume) postulates that right slip on major faults at the head of these fans may also enhance the leftward bending of these upper fan valleys. A rightward shift in the apex of the fan would force the following turbidity currents to deflect to the left, toward the lower part of the fan surface.

Meanders on the La Jolla fan valley were first described by Shepard and Buffington (1967) and recent side-scan sonar data show that meandering submarine fan valleys are common in the California Continental Borderland (Field and others,

1984). One Sea Beam profile (figure 13) crossed well-developed meanders in the upper Coronado Fan Valley. Shepard and Marshall (1969) observed similar meanders at greater depths along the Coronado Fan Valley during submersible dives in this area. The channel thalweg along the meander covered by the Sea Beam data appears to be upwarped for several meters near the 1120 m contour. This upwarp is near the point where the San Diego Trough fault zone crosses the Coronado Fan (chapter 4, this volume). Bottom photographs, core samples and submersible observations provide evidence that the Coronado submarine canyon and fan valley have been relatively inactive since the beginning of the Holocene epoch (Shepard and Marshall, 1969; Emery, 1960; Shepard and Dill, 1966; Moore, 1969). Significant, erosive, turbidity currents or other active submarine canyon/fan valley currents would presumably maintain the steady basinward deepening generally observed along the channels of active submarine canyons (Shepard and Emery, 1941; Emery, 1960). Since the Coronado Canyon heads about 13 km from the shoreline, it is considered relict or inactive, since the time of lowered sea levels during Pleistocene time (Moore, 1969). Therefore, warping of the main channel in the canyon and fan valley is presumably Holocene. Shepard and Marshall (1975) observed similar warping in the Navy Channel during a submersible dive.

Additional evidence of recent tectonic activity affecting these submarine canyons and fan valleys is shown by the longitudinal profiles of the channel axes (figure 14). Although the channel profiles show a generally concave upward curve, which may imply grading, significant inflections or nick points are evident. Emery (1960) discussed the difficulties in identifying real nick points in longitudinal profiles of submarine canyon axes, especially noting the lack of sufficient sounding data or

Figure 13. Sea Beam swath across meanders in the Coronado submarine fan valley (see figure 4 for location of profile). Note how the channel thalweg appears to be slightly upwarped near the 1120 m contour. Sea Beam contour interval is 10 m. Also, note that the right-hand levee (looking downstream) is generally higher than the left-hand levee. (Sea Beam swath courtesy of H. Craig).

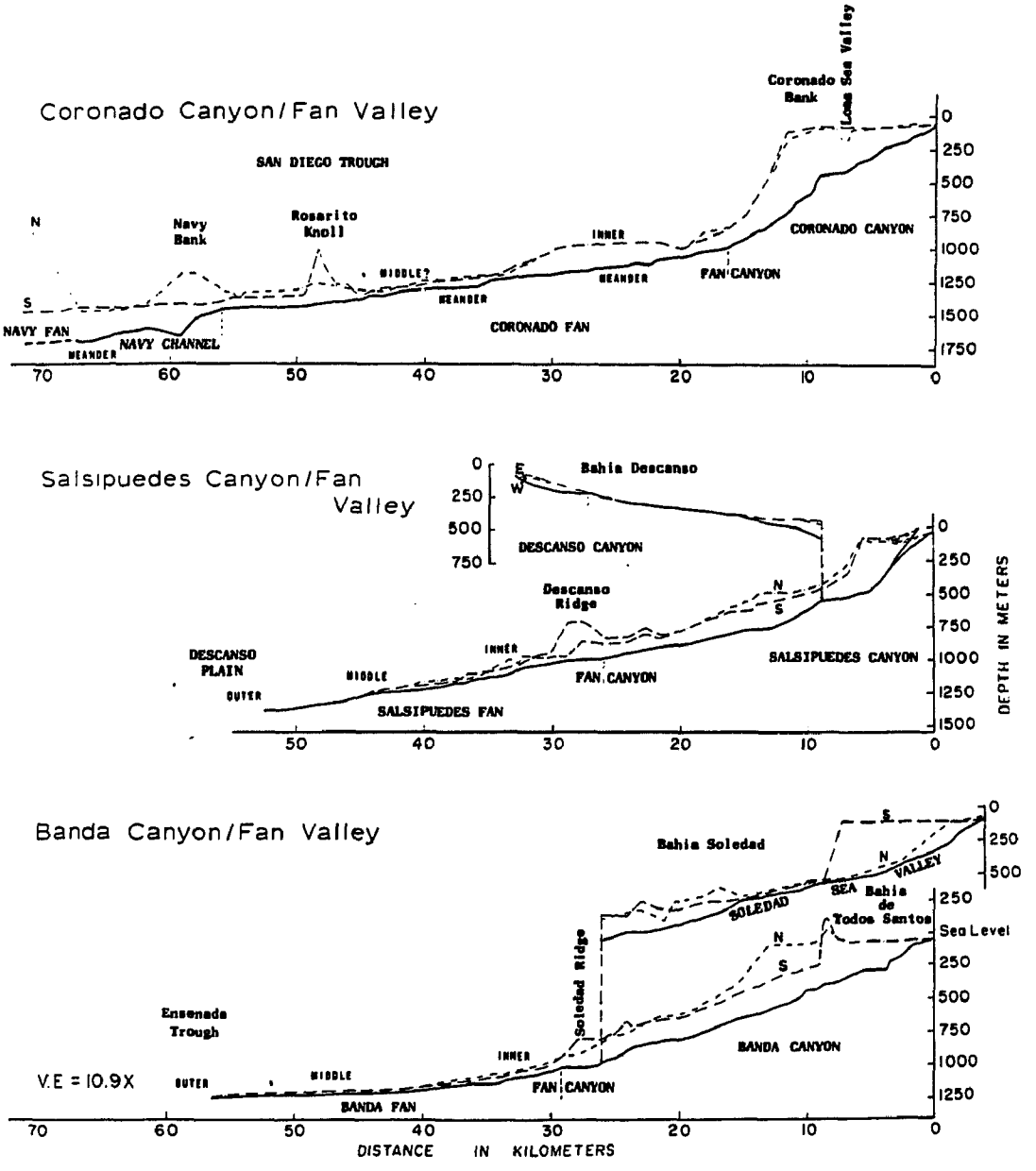
Coronado Canyon/Fan Valley
SAN DIEGO TROUGH
N
S
Navy Bank
Rosarito Knoll
NAVY FAN
MEANDER
NAVY CHANNEL
MIDDLE?
MEANDER
INNER
MEANDER
CORONADO FAN
FAN CANYON
CORONADO CANYON
Coronado Bank
Lost Sea Valley
0
250
500
750
1000
1250
1500
1750
70
60
50
40
30
20
10
0
Salsipuedes Canyon/Fan Valley
Bahia Descanso
E
W
DESCANSO CANYON
Descanso Ridge
N
S
DESCANSO PLAIN
OUTER
MIDDLE
INNER
SALSIPUEDES FAN
FAN CANYON
SALSIPUEDES CANYON
DEPTH IN METERS
Banda Canyon/Fan Valley
Bahia Soledad
S
N
VALLEY
SOLEDAD
SEA
Bahia de Todos Santos
Sea Level
Soledad Ridge
Ensenada Trough
V.E = 10.9X
OUTER
MIDDLE
INNER
BANDA FAN
FAN CANYON
BANDA CANYON
DISTANCE IN KILOMETERS

Figure 14. Long profiles of submarine canyons, fan valleys, and major distributary channels of the Inner Borderland. Solid curves represent the profiles of the channel axes, determined from soundings data of this study. The dashed and dot-dashed curves represent the profile of the adjacent seafloor on the south and north sides, respectively, (east and west sides where the channel has a northerly trend). Major fan divisions and the approximate boundary between submarine canyon and fan valley are also shown. Each profile has the same scale and relative vertical exaggeration.

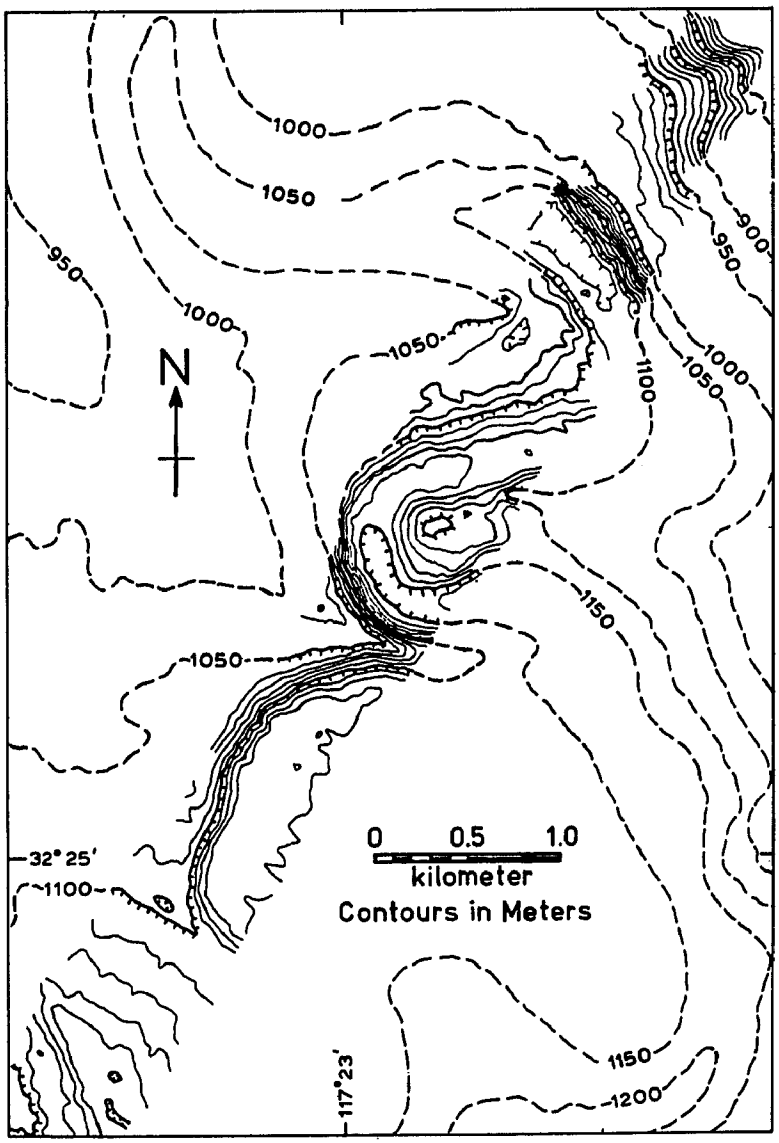
1000
1050
950
1000
1050
N
900
950
1000
1050
1100
1150
1050
0 0.5 1.0
kilometer
Contours in Meters
32° 25'
1100
117°23'
1150
1200

accurate navigation necessary to define the 'true' course and profile of these channels. The data presented herein include a much greater density of soundings than were available to previous investigators (Crowell, 1952; Shepard and Emery, 1941; Emery (1960). Several Sea Beam profiles and submersible dives provide necessary and sufficient data to show the detailed relief along significant stretches of these channels. Therefore, some nick points in the channel profiles are well-defined by the data, and their significance can be discussed regarding submarine canyon origins, and possible tectonic modifications.

A most prominent nick point is apparent along the Coronado Canyon, where it crosses Coronado Bank (figure 14). Shepard and Emery (1941) first noted this steepening and compared it to nick points along land canyons which cross hogbacks. Another similar, but smaller, nick point is evident where the Banda Canyon crosses between Punta Banda and Islas Todos Santos. A second, somewhat larger(?) nick point is observed just west of Punta Banda, and is located just above and east of the sharp, fault-related, right turn in the canyon discussed previously. One other noticeable nick point is located in Bahía Todos Santos, and may be a slump scarp or other unrecognized fault contact. Other smaller, less well-defined nick points seem to occur on the long profiles of these canyons, but lack of dense sounding data make their actual existence uncertain.

Along the channel axes, within the fan valley section, additional small nick points are apparent, in areas where dense soundings from Sea Beam data or submersible observations are available. The most significant of these are associated with meanders along the Coronado Fan Valley and were described previously (Shepard and Marshall, 1975). Nick points apparent in the profiles adjacent to these well-mapped

meander segments may not be real and indicate only that data are inadequate to map accurately the overall meandering course of the channel. Nick points near the fan valley/canyon intersection may be related to changes from depositional to erosional character of the channel, faulting at the base of the continental slope, or to lack of data to define adequately the real channel axis profile at these points. Sea Beam data show a 'real' nick point at the lower end of the fault-controlled(?) left turn in the Salsipuedes Fan Valley. Finally, the nick point marking the Navy Channel/Coronado Fan Valley intersection may be real, demonstrating incision of Navy Channel into the Coronado Fan surface, and a possible change in base level.

Several linear, steep-walled, submarine valleys occur in the area, and these are generally considered to be fault troughs. San Clemente Rift Valley and Loma Sea Valley have been described in detail elsewhere (Shepard and Emery, 1941; Emery, 1960, Shepard and Dill, 1966). A large, deep, 'rift' valley, herein referred to as the San Isidro Rift Valley, connects the Ensenada Trough to the San Isidro Basin (plate 1). Sea Beam data along this trough (figure 15) show several closed depressions interpreted as tectonic sags associated with the dextral, strike-slip San Isidro fault zone which passes through this trough. Also, small hillside benches or terraces appear to flank the sides of the San Isidro Rift Valley, possibly delineating subparallel branch or secondary faults.

Numerous other prominent sea valleys or gullies cross the more gentle slopes which are probably underlain by less well-indurated sedimentary rocks. Some are relatively linear and subparallel to the coast and join other more prominent canyons, such as Soledad and Loma Sea Valley. Others appear to be small submarine canyons with associated small fan or slope apron deposits at their base (e.g., Santo Tomás

Figure 15. Sea Beam swath showing tectonic sags in the San Isidro Rift Valley. Inset cartoon shows how left-stepping, en echelon sags form in a dextral strike-slip fault zone between right-stepping, en echelon fault strands. (Profile location is shown in figure 4). Sea Beam contour interval is 10 m. Other contours drawn from conventional echo sounding profiles (locations shown by tick marks on contours). (Sea Beam profile courtesy of G. Moore and T. Shipley).

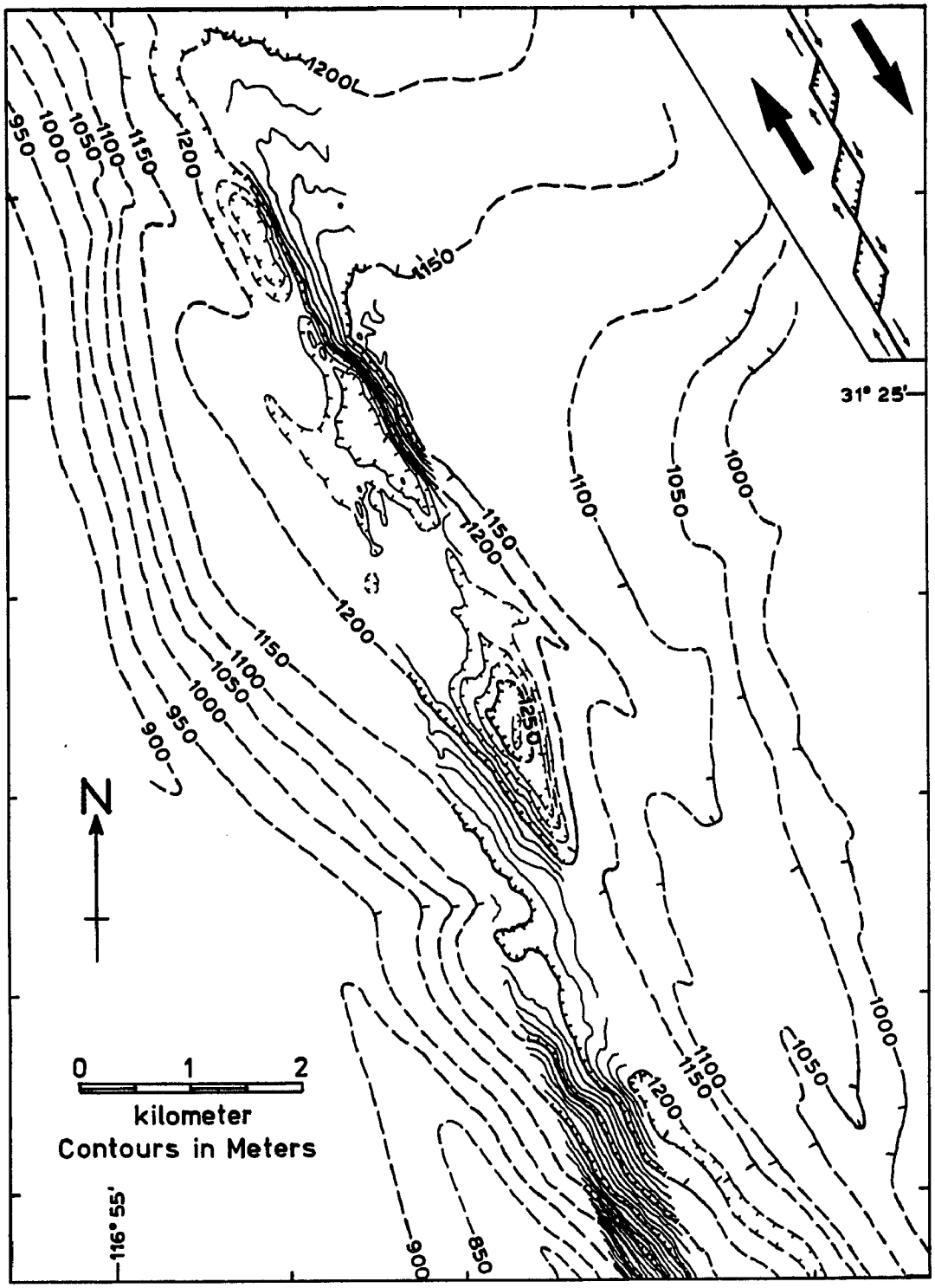
1200
1150
1100
1050
1000
950
900
850
1250
31° 25'
116° 55'
N
0 1 2
kilometer
Contours in Meters

Canyon). Some appear to be minor(?) seafloor channels which link the deeper basins in the area. Lastly, many minor slope gullies cutting across the many slopes of the area are evident. Sounding data are generally inadequate to define accurately the channels of most of these small valleys, and so their lengths and continuity are somewhat uncertain.

**Basins**

The axis of the Inner Borderland is defined by a large, elongate basin: the San Diego Trough, in this area. A second major basin, San Clemente Basin merges with the axial trough in the southern part of the area, forming a large, V-shaped central deep. In detail, both San Clemente Basin and San Diego Trough are composed of several, smaller, closed, flat-floored basins separated by large, relatively smooth and level areas.

All of the basins in this study area are elongate, north- to northwest-trending, and flanked by prominent escarpments on one or more side. Large, roughly circular to elliptical peaks protrude through the relatively flat basin floors, making their overall shape somewhat irregular in some areas. Moore (1969) concluded that Recent turbidites (post-orogenic) partially fill these basins, resulting in their flat floors. Four prominent submarine fans, discussed in the following section, are the major loci of the basin filling sediments. Another, long, narrow basin, adjacent to the coast may have existed in earlier time, but has been filled largely with turbidites and other terrigenous sediments. Remnants of this nearshore 'trough' are seen in this area from Bahía Descanso to Bahía Soledad, and also, south of Punta Santo Tomás. The large, nearshore, submarine ridges, from Coronado Bank to Cabras Bank, have acted as

dams behind which the sediments accumulated. Gorsline and Emery (1959) diagrammed the sequence of offshore basin filling by turbidites (figure 16).

The elongate shape, subparallel to the major, regional structural trends, together with the fault scarps flanking the sides of these basins demonstrate their structural origin. The flat floors and the submarine fans along nearshore parts of these basins are evidence that depositional processes are actively modifying the basin configurations. Seismic reflection profiles (figures 5-11, this volume; Moore, 1969) show that the bedrock floors of the basins are more irregular, and topographic smoothing results from the influx of sediments.

In general, the basin floors progressively deepen to the west and away from the principal continental source of the turbidites as previously described by Gorsline and Emery (1959) and Moore (1969). The deepest basin in the area is North San Clemente Basin. Bathymetric data show that it is almost completely isolated from direct, terrigenous turbidite influx (plate 1), because it is surrounded by ridges and banks, with a deep sill separating it from Navy Fan (chapter 5, this volume).

A deep area between San Isidro Ridge and Animal Basin has an irregular shape with many peaks poking upward through the older(?) sedimentary cover. The deepest parts are elongate, roughly northwest-trending, but the seafloor is somewhat warped compared to the adjacent flat-floored basins. This deep region is herein proposed to have been once connected to the Descanso Plain or Ensenada Trough (or possibly San Isidro Basin?) and received turbidites from the submarine fans in the Descanso Plain. Tectonic movement associated with the San Isidro fault zone then cut off the area by uplift along the San Isidro ridge/escarpment. A low spot, about midway along this escarpment probably marks the area of the former turbidite channel. Seismic

Figure 16. Diagram of basin filling sequence proposed by Gorsline and Emery (1959). Turbidity currents provide the bulk of the fill for the nearshore basins whereas relatively uniform hemipelagic sediments drape over slopes and outer basins, until the nearshore basins fill and turbidites spill over into the outer basins.

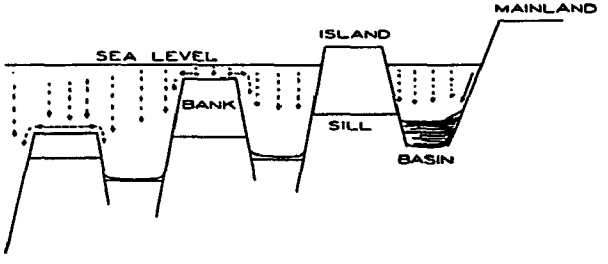


PHASE 1

INNER BASIN FILLING RAPIDLY WITH TURBIDITY CURRENT AND SLUMP SEDIMENTS. OUTER BASINS FILLING SLOWLY WITH ORGANIC AND FINE SUSPENDED LOAD SEDIMENT. BANK TOP SEDIMENT RESIDUAL, FINES WINNOWED OUT.

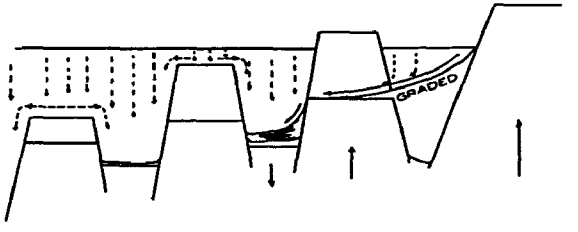


PHASE 3

INNER BASIN SURFACE GRADED AND BYPASSED. MIDDLE BASIN IN PHASE 1. OUTER BASIN AND BANKS AS BEFORE.

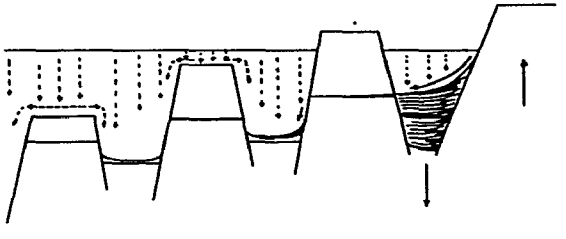

PHASE 2

INNER BASIN FILLED TO SILL. OUTER BASIN AS BEFORE. MIDDLE BASIN BEGINNING PHASE 1.

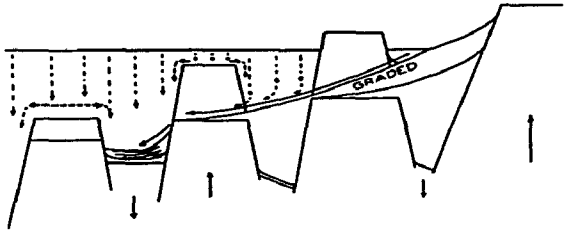


PHASE 4

INNER BASIN FILLING WITH SHALLOW MARINE AND ALLUVIAL SEDIMENTS. MIDDLE BASIN IN PHASE 3. OUTER BASIN IN PHASE 1. BANKS AS BEFORE.

Source: Gorsline and Emery (1959)

reflection profiles show gentle folding of the sediments in this area (figure 8). The absolute age of this tectonic uplift and isolation of the region from turbidity currents has yet to be established. An unknown amount of strike-slip has also occurred since that time, (chapters 4 and 7, this volume). Therefore, the submarine canyon/fan system which supplied the older turbidites to this area is not known with certainty.

**Submarine Fans and Slope Aprons**

The most significant, depositional features in the area are the submarine fans (plate 1); Coronado, Navy, Salsipuedes and Banda fans are the most prominent. The major canyons and fan valleys which conduct the fan sediments (turbidites and so forth) have been described in a previous section, and Coronado and Navy fans have been described in detail elsewhere (Normark and Piper, 1972; Emery, 1960; Normark and others, 1979). Smaller fans, or slope aprons, not well delineated by the bathymetry, but evident in seismic reflection data, are located in Bahía Descanso (Descanso Fan), southern Ensenada Trough (Santo Tomás Fan), and south of Fortymile Bank (Boundary Fan? of chapter 6, this volume). The La Jolla Fan just to the north of this study area has been studied in detail by Shepard and others (1969) and Piper (1970).

The upper (inner fan and middle fan) parts of the major fans are well delineated by the bathymetry, and both Banda and Salsipuedes fans show a classical cone or fan shape. Coronado Fan is somewhat more irregular in outline, whereas the shapes of Navy and La Jolla fans are controlled by the basin margins. The lower (outer fan) parts of the fans coalesce, and seismic reflection data show overlapping and interfingering fan sequences (figure 11; Smith and Normark, 1976; chapter 3, this

volume).

Figures 7, 9 and 11 and plate 2 show the subdivision of the fans based upon their morphology evident in the bathymetric data, and according to the growth model proposed by Normark (1978; also, Normark and Hess, 1980). High-resolution seismic reflection data (3.5 kHz) were used to refine the locations of the fan division boundaries. The upper fan is marked by the prominent fan valley and levee system. Abandoned upper fan valleys are apparent in some cases as discussed previously. The middle fan consists of numerous smaller, leveed, distributary channels (hummocky topography) and the convex upward profile across the fan surface identifies a suprafan in some areas (figure 9). Where detailed data (e.g., Sea Beam, Deep Tow, GLORIA) are available, one relatively, continuous channel apparently is the most recently active, principal distributary channel, continuous with the upper fan valley, whereas other, marginal distributary channels may remain active by receiving overbank flows from turbidity currents (Normark and others, 1979).

As discussed previously, the Salsipuedes Fan Valley is rather sinuous, whereas the Banda Fan Valley is much straighter. Sea Beam data on the Banda Fan confirm this observation. A region (100-150 $km^2$) of large sediment waves is observed on the backside (western) of the large, right-hand levee along the main Banda fan valley (figure 7, plate 2). These waves have amplitudes of from 20 to 40 m and wavelengths between 0.5-2.0 km. A similar, but smaller set of sediment waves is also observed just north of the San Isidro Ridge. Similar waves have been described on the Monterey Fan (Normark and others, 1980) but are not seen on the other fans in this study. Normark and others (1980) propose that, thick, low velocity, sheet flow turbidity currents which spread out after overtopping the main levee at the sharp turn in

the upper fan valley are responsible for the formation of such waves.

All of the lower fans grade into a very smooth, basin plain. Ponding of sediment behind elevated 'bedrock' ridges, scarps and peaks is evident for Banda, La Jolla and part of Navy fans (figures 8 and 10), and has probably occurred at some time for parts of all fans in the region. Turbidites of the Salsipuedes Fan are ponded in the small basin which is being blocked by fault offset of the Banda Fan (figure 11, plate 2). Some of the largest turbidity currents from the Salsipuedes and Navy fans presumably spread out beyond the area of this study, having passed through passes between the knolls and ridges, and out into the more distal basins, including South San Clemente and Animal basins. Seismic reflection data show that predominately hemipelagic sedimentation has occurred most recently in areas such as the southwestern part of East San Clemente Basin (chapter 3, this volume; Smith and Normark, 1976), and between Animal Basin and Ensenada Trough. Tectonic uplift of scarps and folds associated with the active San Clemente - San Isidro fault zone has effectively isolated these areas from more recent turbidite sedimentation.

## CONCLUSIONS

Three fundamental geologic processes have shaped the seafloor of the Inner Borderland. Tectonic processes are most evident and are believed by the author to dominate the overall physiographic style of the region. Erosional and depositional processes are also evident throughout the region, and generally modify the tectonically shaped features. Complex interactions of the three processes working simultaneously result in complicated morphology.

Prominent escarpments and seafloor scarps aligned with the general northwest structural trend of the Californias provide the most dramatic evidence of active tectonics in the area. Elongate ridges and basins subparallel to this structural trend also are evidence of the overall structural control of the regional physiography. Local east-west or north-south trending features, such as South San Clemente Basin and the Maximinos and Salsipuedes Knolls, may exhibit older(?) or secondary tectonic trends.

Submarine canyons and slope gullies are the most obvious features of erosional origin. These features generally cut across the structural grain, although canyon offsets and sharp bends, and linear, fault troughs or rift valleys indicate tectonic or structural control of some erosional features as well. Submarine slumps and slides are probably associated with many slope gullies (Nardin and others, 1979a, 1979b), but detailed, narrow, multi-beam echo-sounding (Sea Beam), side-scan sonar (e.g., Deep Tow or GLORIA), or subbottom (high-resolution seismic) reflection profiles are necessary to confirm the identity of such slope failures. Flat-topped offshore banks and submerged terraces also document erosional truncation of elevated features during Pleistocene and earlier(?) lowered sea levels.

Submarine fans and flat-floored basins are prominent features indicating depositional processes active in the area. Regions of gently to moderately warped deeps and basins evince tectonic modification of older depositional surfaces. Also, youthful fault movements are manifest by low scarps within the basin plains. Channels on the submarine fans may be either depositional or erosional, but levees bordering some channels exhibit depositional effects. Seismic reflection data are again necessary to confirm the origins of many of these features, however.

Some of the more circular or elliptical and cone-shaped peaks are inferred to be volcanic, and Sea Beam data show features resembling craters in some areas (figure 17). Bottom samples support these interpretations in some cases, as do magnetic anomaly patterns and seismic reflection data.

The nearshore shelves result from a combination of erosional truncation of elevated features and sediment ponding behind these offshore 'dams'. Tectonic processes were responsible, in many cases, for initially raising these features above sea level, although eustatic sea level changes have also been significant. All three processes, tectonic, erosional, and depositional, continue to shape the Inner Borderland at present, as shown by periodic filling and deepening of submarine canyon heads (Shepard and Dill, 1966) and the occurrence of numerous earthquakes located within the area (Legg, 1980). Some researchers have proposed a middle to late Miocene origin of the regional physiography (Vedder and others, 1974; Howell and Vedder, 1980), whereas others postulate more recent (Pliocene to Pleistocene) origin (Moore, 1969). These same geologic processes have been continuously shaping and reshaping the Inner Borderland since the East Pacific Rise first impinged upon the the California continental margin.

Figure 17. Sea Beam swath crossing sub-circular depression reminiscent of volcanic craters. Such features may demonstrate that volcanic activity has occurred in this area. (Figure 4 shows the location of this profile). Sea Beam contour interval is 10 m. Other contours are drawn from conventional echo sounding profiles across the region (locations shown by the larger tick marks). (Sea Beam data courtesy of J. Fox).

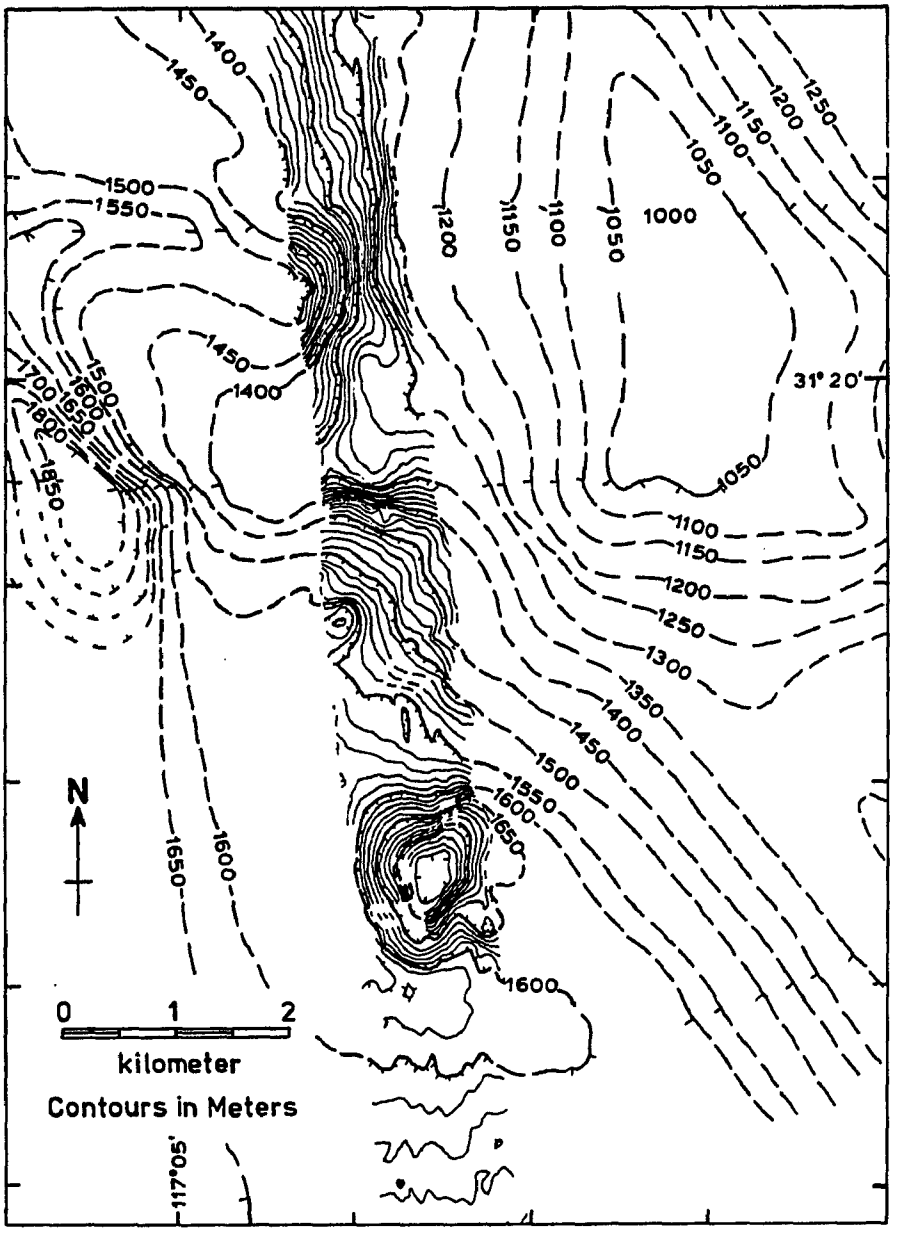
1400
1450
1500
1550
1200
1150
1100
1050
1000
1250
1200
1150
1100
1050
1450
1400
1500
1600
1650
1700
1800
1850
31° 20'
1050
1100
1150
1200
1250
1300
1350
1400
1450
1500
1550
1600
1650
1600
1650
1600
N
0
1
2
kilometer
Contours in Meters
117°05'

# CHAPTER 3

# SEISMIC STRATIGRAPHY AND QUATERNARY SEDIMENTATION

## INTRODUCTION

The California Continental Borderland is a broad continental margin consisting of several subparallel ridges and basins, which separate the California coast from the deep Pacific Ocean basin. Moore (1969) separated the California Continental Borderland into five major zones: (1) northern, Transverse Ranges portion; (2) southern region of northwest-trending structure; (3) central region including an outer fault zone; (4) an inner fault zone; and (5) a broad, folded region between the latter two. This study examines the inner zone (figure 1) and includes part of the southern Borderland. As described elsewhere (Shepard and Emery, 1941; Moore, 1969; chapter 2, this volume), the Inner Borderland is dominated by northwest-trending ridges and basins. The overall steepness and linearity of the slopes and escarpments which flank the ridges and basins are evidence that tectonic activity has shaped the regional physiography. The structure of the Inner Borderland is parallel to that of the San Andreas fault system and is considered to be part of the Pacific - North American tectonic plate boundary (Moore, 1969; Vedder and others, 1974; Legg and Kennedy, 1979; chapter 4, this volume). Models for the tectonic evolution of the California Continental Borderland vary from extension and rifting (Yeats and others, 1974; Yeats, 1976), to right-lateral wrench faulting (Moore, 1969; Howell and others, 1974; Vedder and others, 1974; Crouch, 1979; Legg and Kennedy, 1979), including convergent wrench faulting (Junger, 1976). Clockwise rotation of large crustal blocks in a broad, dextral shear zone, (creating triangular basins) has also been postulated for

the tectonic development of the northernmost parts of the California Continental Borderland (Luyendyk and others, 1980). The author (chapter 4, this volume) demonstrates that right-lateral, wrench faulting dominates the late Cenozoic structure of the Inner Borderland discussed here. Both extension and convergence are locally significant, as is typical of wrench fault systems.

In order to understand the character and history of sedimentation and deformation within the area, it is necessary to develop a regional stratigraphy. In the offshore area, where outcrops have been only sparsely sampled, and even fewer stratigraphic test wells drilled, a working stratigraphy can be developed using seismic reflection data. Two major types of seismic stratigraphic units can be easily recognized on most marine reflection profiles. In general, a well-stratified sedimentary unit overlies a poorly stratified or highly reflective acoustic basement unit. Character of the reflectors within the well-stratified units provides clues regarding the sedimentation processes responsible for deposition of these units (Mitchum and others, 1977; Vail and others, 1977). Correlation of reflection character for both sedimentary and basement units with samples from outcrops, piston cores or drilling have allowed additional inferences about the sedimentary facies or basement rock types in areas with few or no samples.

Moore (1969) defined two litho-orogenic units (pre- and post-orogenic) in the California Continental Borderland based upon their seismic reflection character. Vedder and others (1974), Junger and Wagner (1977) and Junger (1979) combined regional offshore sampling, local onshore and island stratigraphic data and offshore reflection data to develop a more detailed offshore stratigraphy in the area offshore southern California. For the northern part of this study area, Kennedy and others

(1980a,b) defined a simple, two part, Quaternary sedimentary stratigraphy, which overlies acoustic basement of Tertiary and pre-Tertiary age. Smith and Normark (1976) described six sedimentary units in the northwestern part of this study area.

Mitchum and others (1977) define 'sequence' and describe the technique of seismic sequence analysis for use in determination of the depositional history of a region. Acoustic horizons, recognizable by the character of the stratified reflections and their terminations against other sequences, are important for defining the boundaries of each sequence. Also, the character of the reflections and reflector terminations within a sequence are important for understanding the depositional or erosional process which shaped the sequence and provide clues to the lithofacies identification.

The present study utilizes seismic sequence analysis and regional geomorphic data to derive a working stratigraphy for the Inner Borderland west of northern Baja California, Mexico. Recognition of several Quaternary submarine fans from the detailed bathymetric studies of the author (chapter 2, this volume) and of important filled sedimentary basins along parts of the continental shelf allow definition of the major seismic stratigraphic units. Also, distinctive reflection character of other shelf and slope sediments as well as acoustic basement rocks add more stratigraphic units. In a few cases, these deposits can be correlated with the few bottom samples collected in the area by previous investigators. Absolute age estimates of a few, key horizons is attempted using sedimentation rates derived from isotopically dated samples of piston cores obtained in the vicinity. Finally, a brief Quaternary history is described for the region based upon the results of this study, and implications for eustatic sea level changes and tectonic events are discussed.

## SEISMIC STRATIGRAPHIC UNITS

Two major classes of seismic stratigraphic units are easily recognizable on most seismic reflection profiles. In general, a stratified or sedimentary unit overlies an unstratified (or poorly stratified) acoustic basement unit. For this study, these two primary units are subdivided into mappable units, which can be identified based upon their reflection character, geomorphic expression and spatial location, relative to the regional physiography. These units can be correlated along and between adjacent seismic profiles.

### Acoustic Basement Units

Two classes of acoustic basement are recognized in this study: (1) volcanic or metamorphic, and (2) sedimentary. In high-resolution seismic profiles, the volcanic or metamorphic basement rock units show strong reflections, usually with an uneven surface and chaotic or unstratified internal reflections. Locally short, discontinuous, often discordant reflectors are observed within such units, but their general character is an unbedded appearance. An example can be seen in figure 8, (Maximinos Knolls). Doyle and Gorsline (1977) reported 4 Myr old basalt dredged from a peak in this area.

Sedimentary acoustic basement units show some evidence of stratification or bedding below a strong, usually uneven surface which is often unconformable with overlying strata. The bedding within these units is usually significantly deformed, and the strong reflection from the top of such units signifies marked change in acoustic properties between this and overlying deposits. This acoustic impedance change is a result of a significant increase in density and/or seismic velocity possibly exhi-

biting the older, more consolidated nature of the acoustic basement rocks. Alternatively, these may be of a different sediment type, with significantly different porosity, density, or acoustic velocity. Some of these sedimentary basement units correspond to pre-orogenic deposits of Moore (1969) and may correlate with Miocene or older sedimentary rocks observed by Vedder and others (1974) or Kennedy and others (1980a,b).

Although the petrology of these acoustic basement rocks is important in unraveling the geologic history of the Inner Borderland, the high-resolution seismic data of this study do not provide adequate detail to map these units properly. Furthermore, the lack of sufficient bottom samples in the area does not allow proper identification or correlation of such units throughout the area. The regional extent of acoustic basement rock exposures is shown on plate 2, along with the regional geomorphology. Figure 18 crudely shows the distribution of basement rock types mapped in the region, compiled from various sources (Vedder and others, 1974; Gastil and others, 1975; Doyle and Gorsline, 1977; Krause, 1965; Moore and Kennedy, 1970).

Gastil and others (1975) divided the rocks of the Baja California peninsula into three major categories: (1) pre-batholithic, (2) Peninsular Ranges batholith; and (3) post-batholithic. Rocks of the Peninsular Ranges batholith are not known to crop out within the Borderland, except as clasts in younger conglomerates, and so are not discussed in this report. The pre-batholithic rocks found in the vicinity include sedimentary and volcaniclastic rocks of the early Cretaceous Alisitos Formation, for example, Punta Banda and Islas Todos Santos. Offshore Mesozoic basement rocks include Catalina Schist and Franciscan equivalents along Thirtymile Bank and Catalina Island (Vedder and others, 1974). Post-batholithic rocks of late Cretaceous

Figure 18. Map showing the distribution of major, pre-late Cenozoic rock units identified in the Inner Borderland and surrounding regions. These rock types are inferred to represent the major acoustic basement rocks shown on seismic reflection profiles in this study, but their actual distribution within the Inner Borderland is not well-defined at present. Locations of cores and dredges with symbols identifying the principal tock types recovered are also shown along with the sample identification number. Most of the cores shown recovered late Quaternary sediment. Map pattern for Miocene igneous and pre-upper Cretaceous rocks identifies rocks of the Peninsular Ranges batholith onshore in Baja California.

# INNER CONTINENTAL BORDERLAND

## PRE-LATE CENOZOIC ROCKS

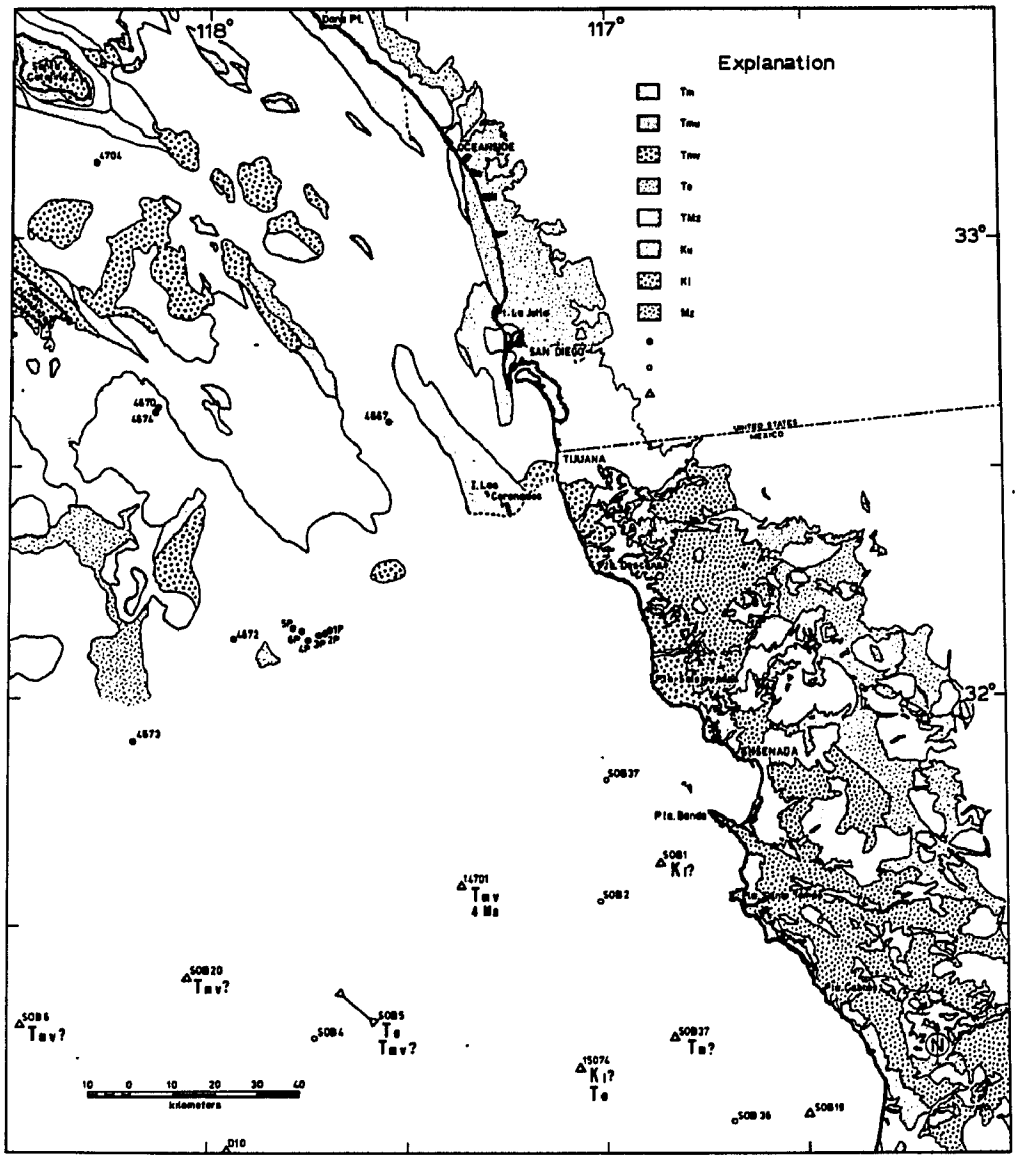

and early Tertiary age are common along the coast (e.g., Rosario and La Jolla formations, Kennedy and Moore, 1971; Kennedy, 1975; Gastil and others, 1975). Offshore such rocks have been found near Point Loma (Moore and Kennedy, 1970), on the Santo Tomás shelf and ridge (Doyle and Gorsline, 1977) and along the northeast flank of Animal Basin (Doyle and Bandy, 1972).

Mid-Cenozoic time was one of extensive volcanism throughout the region (Vedder and others, 1974; Gastil and others, 1975). Volcanic rocks of middle Miocene age have been sampled south of Tijuana (Rosarito Beach Formation, Minch, 1970), and throughout the California Continental Borderland (Vedder and others, 1974). Doyle and Gorsline (1977) found lower Pliocene basalt (ca. 4 Mya) in the vicinity of Maximinos Knolls, and Quaternary volcanic rocks are found on Punta Colinett (Gastil and others, 1975).

Sedimentary rocks of Miocene age are also widespread throughout the Borderland (Vedder and others, 1974), but crop out only along the coast in a few areas. A prominent member of these Miocene units is the San Onofre Breccia and its equivalents found south of Tijuana (Minch, 1970; Stuart, 1974, 1979) and on Islas Los Coronados (Lamb, 1979). Large clasts of Catalina Schist and other Franciscan types imply that a ridge of this Mesozoic basement existed in the Inner Borderland of this area during middle Miocene time (Stuart, 1974, 1979).

**Sedimentary Units**

For this study, the sedimentary seismic stratigraphic units have been subdivided into three broad categories based on their physiographic location: (1) shelf sediments; (2) slope sediments; and (3) basin sediments. Figure 19 shows the approxi-

Figure 19. Map showing the principal late Cenozoic sedimentary units of the Inner Borderland of this study. Diagonal lined patterns generally indicate major basin fills of turbidites supplied by the larger submarine canyon/fan systems. Horizontal lines identify shelf sedimentary units. Stippled patterns are associated with slope aprons or smaller submarine fans. The vertical lines represent the presumably older(?) Descanso unit of Smith and Normark (1976) which underlies much of the central deep area of this study.

# INNER CONTINENTAL BORDERLAND

## PRINCIPAL LATE CENOZOIC SEDIMENTARY UNITS

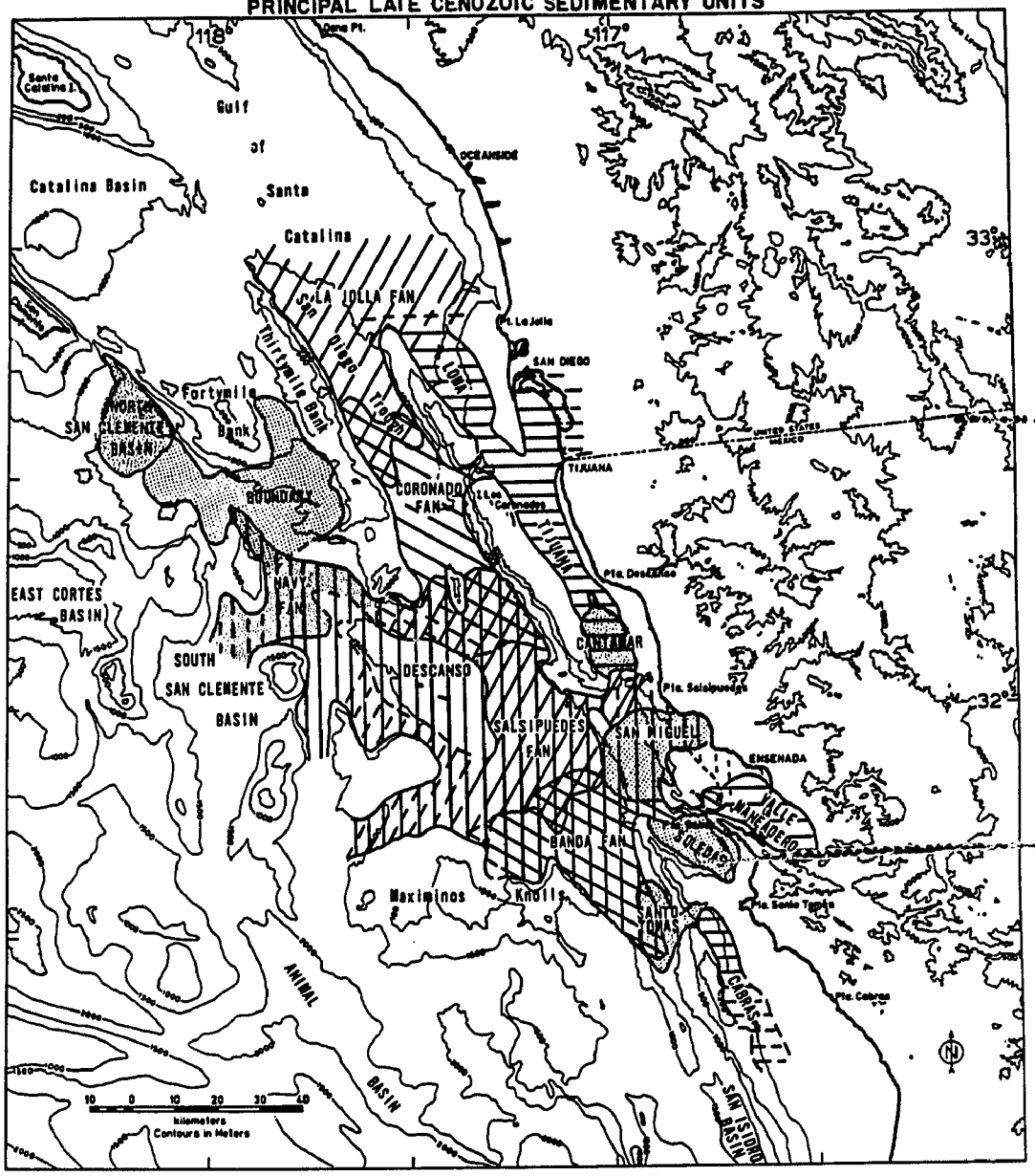

mate distribution of the major late Cenozoic sedimentary units in the Inner Borderland studied herein. Plate 2 also shows the surficial distribution and geomorphic character of these units in more detail.

**Shelf Sediments**

Shelf sediments are separated into two groups for this study. Ponded shelf sediments are generally flat-lying and located shoreward of an offshore acoustic basement rock ridge which has acted as a dam (figure 5). These sediments may grade laterally into the second type of shelf sediments, that is, prograding or cross-bedded units, in a direction sub-parallel to the coastline and offshore ridges.

The prograding deposits are found along the shelves bordered by more gentle slopes. These deposits grade laterally into upper slope deposits in most cases (figure 8). Shelf deposits of this type are along Loma Sea Valley, Bahía Descanso, off Punta San Miguel and in Bahía Soledad. These deposits are the lateral equivalent of their associated slope deposits. The shelf break, an easily identifiable topographic feature, provides the demarcation between shelf and slope deposits.

**Slope Deposits**

An important feature of slope deposits is the common presence of disrupted bedding, such as chaotic and crenulated reflectors, characteristic of slumping, creep or other slope movements (figures 8 and 9). In many cases, slope deposits are relatively transparent, acoustically, and reflection profiles show fewer, or less distinct internal reflectors than nearby basin deposits (figures 8 and 10). Acoustic transparency of sediments is considered to be evidence of dominantly hemipelagic sedimentation (Smith and Normark, 1976), whereas well-bedded deposits with distinct,

continuous, parallel internal reflectors in the nearby basins are interpreted as turbidites (Moore, 1969; Smith and Normark, 1976). On slopes near submarine canyons, overbank deposits from large turbidity currents may produce more regular, well-defined internal reflectors within the slope units. Similarly, prograding shelf deposits tend to show more distinct, closely spaced reflectors than do slopes more isolated from direct shelf sediment influx. Further study with bottom sampling is needed to correlate reflection character with sediment type for these sediments. Reflection data of this study clearly show more than one distinctive type of slope deposit. Also, different acoustic systems can show somewhat different reflection character for the same type of deposit (cf. figures 4, 5, 8, 9 and 10)

**Basin Sediments**

The basin deposits within the California Continental Borderland have been studied by numerous investigators. Moore (1969) determined that most of the sediments in the Borderland basins are turbidites. Gorsline and Emery (1959) diagrammed the sequence of Borderland basin filling by turbidites from the continental landmass seaward (figure 16). Moore (1969) noted that most of the post-orogenic sediments in the outer Borderland basins are relatively thin covers of hemipelagic muds, showing the isolation of these basins from the bottom flowing turbidity currents. He found that inner basins have relatively thicker post-orogenic deposits of turbidites. Smith and Normark (1976) described six sedimentary units within the San Diego Trough and East San Clemente Basin using seismic reflection data. This study expands their work to a larger area, and recognizes additional submarine fan deposits. Seismic sequence analysis as described by Mitchum and others (1977) and Sangree and Wid-

mier (1977) is also used in the present study, and the reader is referred to these papers for detailed discussion of the technique and its terminology.

Using seismic reflection data, basin deposits of the Inner Borderland can be grouped into five distinct classes: (1) middle and upper fan deposits; (2) lower fan and gently sloping basin plain turbidites(?); (3) ponded basin plain turbidites; (4) older, deformed basin turbidites(?); and (5) hemipelagic deposits. Correlations of shallow piston, gravity and box core data with high-resolution seismic reflection data (3.5 kHz) have shown that the depth of acoustic penetration "is a function of the relative amount of sand or coarser material in the near-surface sediments;" for turbidites (Normark and others, 1979). Normark and others (1979) also noted that areas of submarine fans underlain by predominately muddy sediments commonly showed continuous, multiple reflectors and significantly greater acoustic penetration than areas underlain by sandier sediments.

Upper fan deposits are characterized by fan valley and levee complexes (Normark, 1974). Middle fan deposits show hummocky topography on surface echo-sounding data (Normark, 1970, 1974), attributed to numerous small distributary channels. Figure 9 shows that upper and middle fan seismic sequences are distinguished by several strong reflectors, with uneven surfaces, separated by relatively transparent intervals, with few, discontinuous, internal reflectors. Separation between upper and middle fan deposits at the seafloor can be accomplished using geomorphic criteria (plate 2), but is more difficult in older, buried fan deposits. Normark and others (1979) relate the strong bottom reflections and lack of coherent internal reflectors in high-resolution, seismic profiles, to the presence of sands in the upper and middle fan deposits. They also find that overbank sediments show more coherent reflectors than

the channels and depositional lobes, indicative of the well-bedded muds of these deposits.

Middle fan deposits grade into the lower fan and gently sloping basin plain deposits as seen in figure 9. Lower fan and basin deposits are recognized in seismic profiles by the presence of multiple, parallel to sub-parallel reflectors. The undulations seen in figure 9, are a result of gentle folding associated with the tectonically-active San Clemente fault zone. Even where gently folded, these deposits show sub-parallel reflectors and generally do not appear to be truncated against other horizons, except at structural discontinuities.

Ponded, basin plain turbidites(?) are easily recognized by their sub-horizontal, even, parallel, bedded reflectors, which show definite onlap against older basin deposits (figure 8). Again, the deposits shown in the figure are disrupted by youthful fault movement as along the San Isidro fault zone. Examination of the regional bathymetry (plate 1) shows the seafloor is extremely flat in the areas of these ponded basin deposits (gradient $<$ 1:1000). Krause (1961) reports muds with interbedded sand and silt in a gravity core (SOB-2) taken near the ponded deposits shown in figure 8, confirming their turbidite nature. Similar deposits are in North San Clemente Basin and are discussed in detail elsewhere (chapter 6, this volume).

Older basin deposits are generally recognized by two criteria, deformation and stratigraphic superposition. These deposits are more deformed than the younger basin deposits described above. For example, in figure 8 the older basin deposits west of the San Isidro Ridge show both folding and possibly tilting, if they were originally deposited sub-horizontally. Other older basin deposits can be recognized below prominent unconformities at the base of the younger fan and basin deposits. For

example, the ponded basin unit in the Ensenada Trough overlies a gently curved, possibly folded or draped, older basin deposit (figure 8). The Descanso unit of Smith and Normark (1976) is another example of older basin deposits in the area (figure 11).

The last seismic stratigraphic unit to be discussed is the hemipelagic unit. Smith and Normark (1976) showed an acoustically transparent layer within the sediments of the region. They presumed this to be a layer of hemipelagic muds, deposited in areas which had become isolated from direct turbidite influx. This same unit ( PEL in figure 11) can be traced for significant distances throughout the Inner Borderland and provides an excellent chronostratigraphic marker horizon. The unit extends to the seafloor southeast of Navy Fan (figure 2 of Smith and Normark, 1976), where six piston cores were taken (Normark and Piper, 1972). These cores showed a predominance of hemipelagic muds, although there were significant sand and silt layers in those cores located closest to Navy Fan (Normark and Piper, 1972). One of those cores (6P) was studied in detail by Dunbar (1981) and is discussed in the next section. The presence of some layers of fine sand and micaceous mud in all of these cores is an indication that occasional, large turbidity currents are able to surmount the topographic barriers nearby and provide turbidites to these areas. One other important characteristic of hemipelagic deposits is their 'draped' appearance, showing relatively uniform thickness over gentle topography (figure 11; figure 2 of Smith and Normark, 1976).

## SEDIMENTATION RATES AND CHRONOLOGY

With few bottom samples and only one stratigraphic test well (La Jolla Mohole site, Moore, 1964, 1969; Inman and Goldberg, 1963; Hamilton, 1964) in the area, establishment of absolute age of key stratigraphic horizons is difficult. However, the presence of well-defined marker horizons ( **PEL** in figure 11, base of the ponded unit in figure 8), warrants an attempt to estimate the absolute ages of these units. Moore (1969) postulated that the post-orogenic sediments in the Borderland are less than about one million years old, although continuous deformation in the area up to the present makes definition of post-orogenic difficult in some cases. Vedder and others (1974), Junger and Wagner (1977) and Junger (1979) generally consider the younger basin fills of the California Continental Borderland to be post-middle Miocene in age.

Dunbar (1981) performed detailed analyses, including radiocarbon dating and isotopic analyses of piston cores obtained from East San Clemente Basin (also described by Normark and Piper, 1972). One core (**6P**) was found to have an essentially complete record of late Pleistocene to Holocene sedimentation and contained few sand layers, which might indicate rapid variation in sedimentation rates, and possible erosion of underlying beds. This core was used by Dunbar (1981) to study the sedimentation during the last glacial/interglacial transition. Because this core was taken from an area where the hemipelagic layer extends to the surface (see Smith and Normark, 1976; figure 2, line L), an estimate of the average, late Quaternary sedimentation rate based upon this core will allow estimation of the age of the base of the hemipelagic layer.

Sample depth versus absolute age for this core (6P) is plotted in figure 20. Also plotted are depth versus radiocarbon or oxygen isotope ages for several other cores obtained in the California Continental Borderland, and offshore western Oregon. The data selected for this plot are from cores in outer basins of these borderlands, or at least parts of nearshore basins, where insignificant sandy turbidite accumulation has occurred during latest Quaternary time (Emery, 1960; Heath and others, 1976; Kulm and Scheidegger, 1979; Dunbar, 1981).

The most significant feature of the data plotted in figure 20 is the distinct change in sedimentation rate, shown by the slope change for the curves at about 12,000 to 15,000 years B.P. This corresponds with the end of the Wisconsin glaciation. All of the other cores, except for the deep-sea, Gorda Ridge core, show this decrease in sedimentation at about the same time.*

Some of the apparent variability in time of onset for this event may be due to differences in age of the top part of the cores. Emery (1960) and Dunbar (1981) have noted a significant bias in radiocarbon age of seafloor sediments, which may be associated with sediment mixing by benthic organisms, as indicated by thousand year old ages of surficial sediments. It is therefore, necessary to correct ages in the cores by the surface sediment age. Alternatively, time intervals between dated sections of the cores can be used directly to estimate sedimentation rates.

The sedimentation curves shown in figure 20 are remarkably parallel to each other (except for core 6910-2 ). Because the deep-sea (Gorda Ridge, core 6910-2 ) data are also parallel to the Holocene sedimentation data for the other cores, it is

---

* The age resolution is about ±500-1000 years for the radiocarbon dating techniques used.

Figure 20. Sediment age versus depth curves for several selected northeast Pacific piston cores. These curves are used to estimate the late Quaternary sedimentation rates in the region. All data, except for the Gorda Ridge data, are from borderland basins or basins along the continental margin. See the references listed for more detailed descriptions of the cores. Symbols locate the average depth and estimated age for the core samples. The long bars for core 4P represent estimated age limits, based upon *Foraminifera* data. Lines connecting data points are meant to show samples from the same core and possible variations in sedimentation rate. A late Quaternary average sedimentation rate, based upon DSDP data from a slope basin off the Oregon coast, is also shown (Kulm and Scheidegger, 1979).

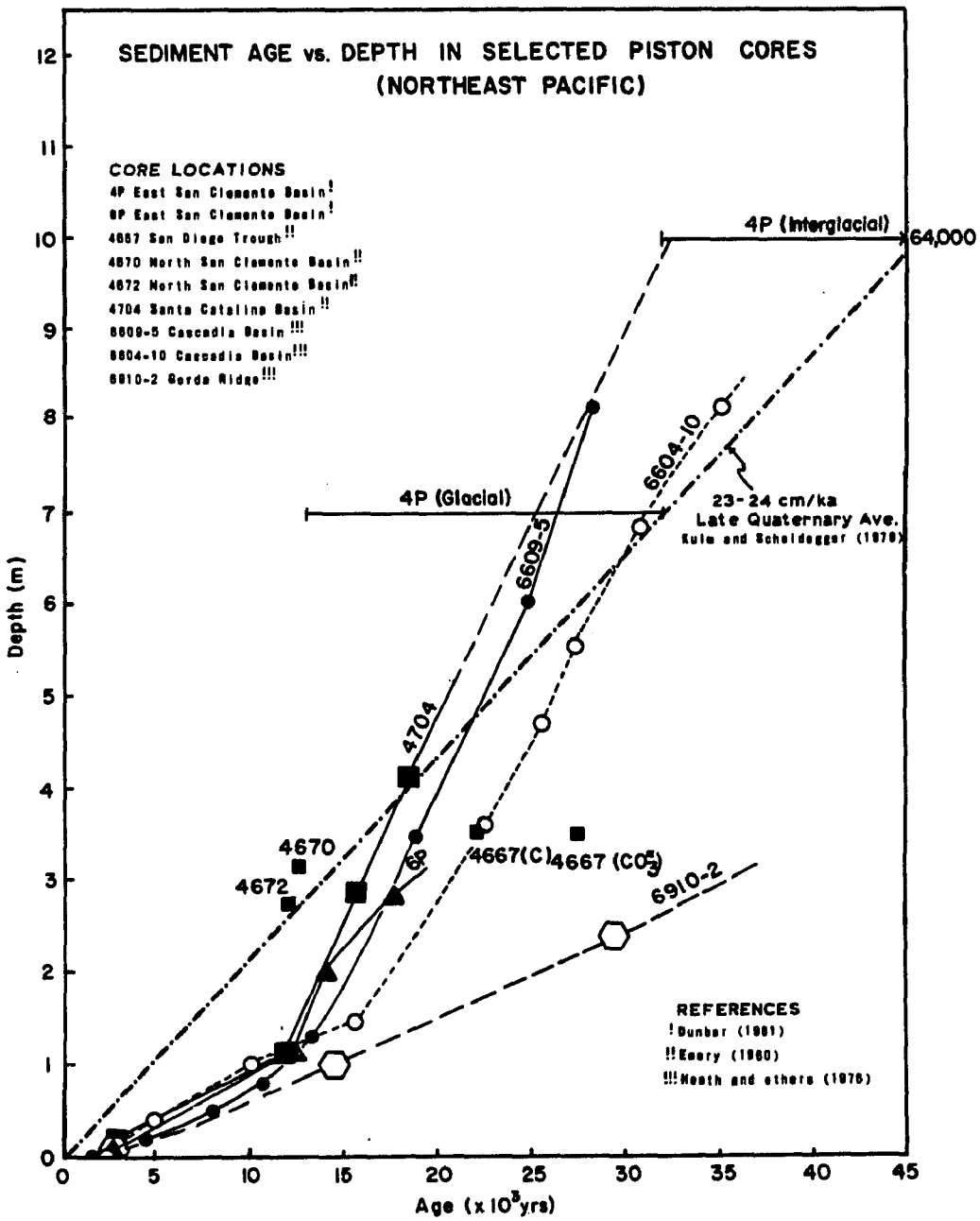
SEDIMENT AGE vs. DEPTH IN SELECTED PISTON CORES
(NORTHEAST PACIFIC)
CORE LOCATIONS
4P East San Clemente Basin!
8P East San Clemente Basin!
4667 San Diego Trough!!
4670 North San Clemente Basin!!
4672 North San Clemente Basin!!
4704 Santa Catalina Basin!!
6609-5 Cascadia Basin!!!
6604-10 Cascadia Basin!!!
6910-2 Gorda Ridge!!!
4P (Interglacial)
64,000
4P (Glacial)
23-24 cm/ka
Late Quaternary Ave.
Kulm and Scheidegger (1978)
6604-10
6609-5
4704
4670
4672
62
4667(C)
4667 (CO3)
6910-2
REFERENCES
!Dunbar (1981)
!!Emery (1960)
!!!Heath and others (1976)
Depth (m)
Age (x 10³yrs)
0
1
2
3
4
5
6
7
8
9
10
11
12
0
5
10
15
20
25
30
35
40
45

reasonable to conclude that the Holocene sedimentation in these areas has been dominated by hemipelagic deposition, consistent with the assumption of Smith and Normark (1976) for the acoustically transparent layer. The higher rates during the Pleistocene epoch may result from more frequent influx of sediments from large turbidity currents that are able to surmount the nearby topographic barriers and reach these more isolated basins. Alternatively, hemipelagic sedimentation in these basins located nearer to the coast than the Gorda Ridge core location, may be significantly higher during the times of lowered sea level.

**Age of the Hemipelagic Unit**

In order to estimate the overall age of the hemipelagic layer (PEL) observed in the seismic profiles, an average late Quaternary sedimentation rate for this part of San Clemente Basin must be determined. Figure 21 shows an enlarged view of the age versus depth data for the California Continental Borderland cores. Table 2 shows the data used to compute the average sedimentation rates and absolute age for the East San Clemente Basin hemipelagic layer near core 6P. An average rate of $18 \pm 2$ cm/ka is used to compute the age of the hemipelagic unit. Because this rate is dominated by the lower, Holocene sedimentation rate, it represents a lower bound estimate of the long-term average, late Quaternary rate. It is comparable to, but significantly lower than, the average rate determined by Kulm and Scheidegger (1979) for a basin offshore Oregon (23-24 cm/ka) over a 300,000 - 400,000 year interval.

Besides estimating an average sedimentation rate, it is also necessary to compute observed sediment thicknesses from travel-time data on the seismic profiles. Correction of these thicknesses for compaction is also necessary to get an accurate

Figure 21. Detailed plot of latest Quaternary sedimentation rates for the California Continental Borderland. Symbols are as described in figure 20. Open symbol for the Santa Catalina Basin data indicates the intersection of the projections of the lines between the data plotted for shallower and deeper samples in the cores. Dashed line represents the estimated average late Quaternary sedimentation rate used in this study and is based upon the data for core 6P.

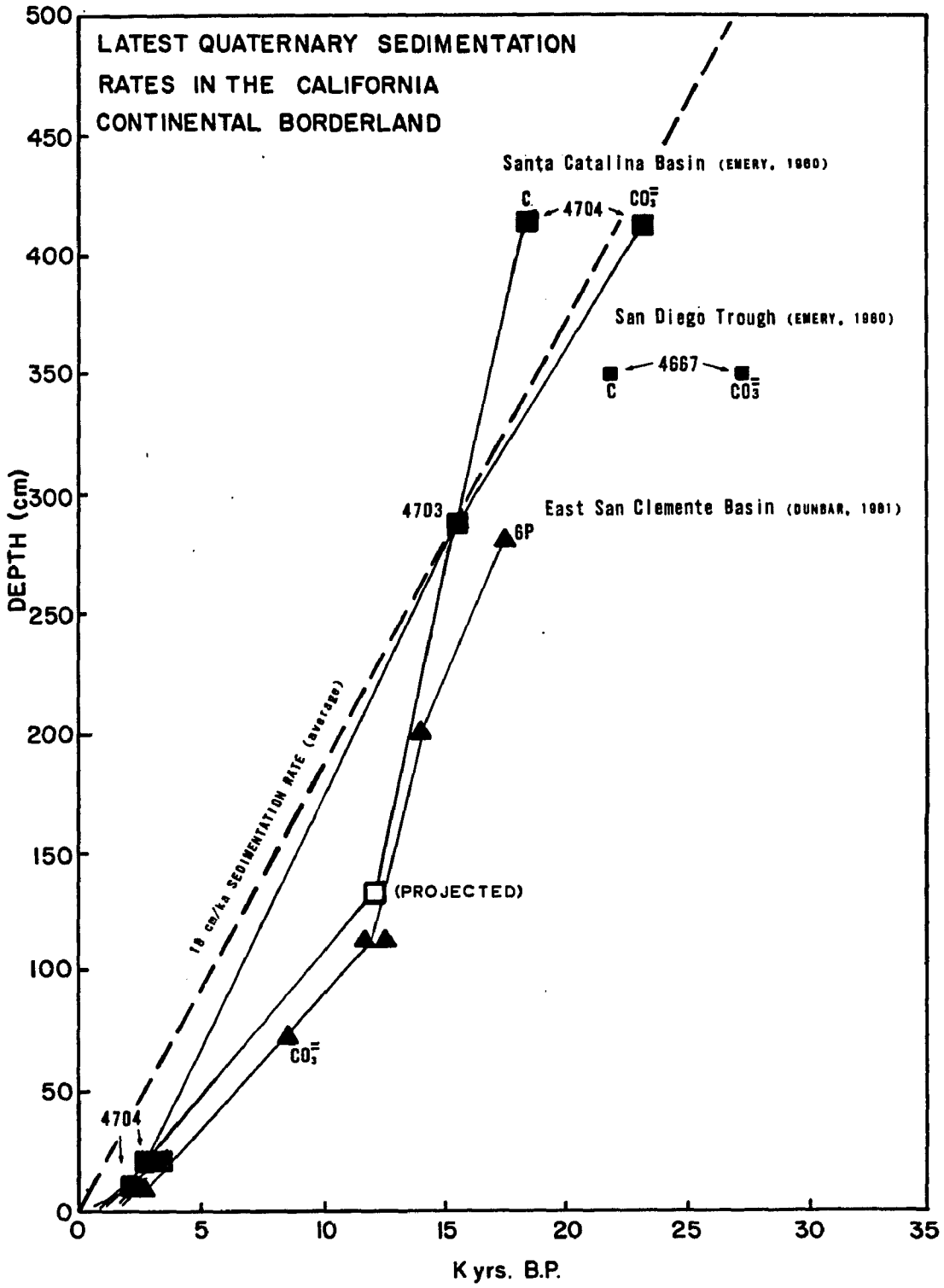
LATEST QUATERNARY SEDIMENTATION
RATES IN THE CALIFORNIA
CONTINENTAL BORDERLAND
Santa Catalina Basin (EMERY, 1960)
C
4704
$CO_3^=$
San Diego Trough (EMERY, 1960)
4667
C
$CO_3^=$
East San Clemente Basin (DUNBAR, 1981)
4703
GP
(PROJECTED)
$CO_3^=$
4704
18 cm/ka SEDIMENTATION RATE (average)
DEPTH (cm)
Kyrs. B.P.
0
50
100
150
200
250
300
350
400
450
500
0
5
10
15
20
25
30
35

estimate of absolute age. Moore (1969), using wide-angle seismic reflection data from San Clemente Basin, reports an interval velocity of 1.5 km/sec for the upper 0.1 seconds of sediments observed. Using this value for interval velocity, and the procedure outlined by Moore (1969) for compaction corrections, an uncompacted thickness for the hemipelagic layer is computed (Table 2). Using the computed sediment thickness and the average rate of sedimentation, an age of 470$\pm$60 ka is calculated for the bottom of the hemipelagic layer. Since the sedimentation rate is a lower bound estimate, the calculated age probably represents a maximum. Smith and Normark (1976) estimated the age of this unit as 200 ka using a sedimentation rate of 30 cm/ka (after Emery, 1960). Their age estimate probably represents a minimum, because they used a significantly higher sedimentation rate and did not correct for compaction. Clearly, the base of the hemipelagic unit, and its correlative conformity which can be mapped throughout the area, is a late Quaternary horizon.

**Age of the Banda Fan Ponded Turbidite**

One other significant marker horizon for which an absolute age was estimated is that delineated by the lap outs at the base of the ponded turbidites of the Banda Fan in the Ensenada Trough. As seen in figure 8, a relatively transparent (acoustically) layer of slope sediments grades laterally into and under the ponded unit. The age of the base of this slope unit serves to date the base of the ponded unit. Assuming these slope deposits are predominately hemipelagic muds with insignificant turbidite influx, a sedimentation rate of 11$\pm$1 cm/ka is used, the Holocene rate for core 6P. Because these are slope deposits and lie at significantly shallower depths than the largest turbidity currents from the Banda Fan can reach, the author believes this

Table 2. Calculations of Sedimentation Rates and Age of Key Horizons from Piston Core Data.

Table 2. Calculations of sedimentation rates and age of key horizons from piston core data.

East San Clemente Basin

| Core 6P* | | | Hemipelagic Layer | | | |
|---|---|---|---|---|---|---|
| Depth (cm.) | $^{14}C$ Age (ka.) | Rate (cm/ka) | Thickness(sec) | Thickness(m-comp)!! | Thickness(m-unc) | Age(ka.) |
| 5-14 | 2.77 ! | | 0.080 | 60. | 84. | 470±60 |
| 100-125 | 11.85±0.50 | 11±1 | | | | |
| 190-210 | 14.00±0.90 | 48±12 | | | | |
| 270-295 | 17.59±0.70 | 23±7 | | | | |
| | | | | Banda Fan Ponded Turbidite (Slope Deposit) | | |
| | | | 0.067 | 50. | 70. | 640±60 |
| Average | | 18±2 | | | | |

Formula for computing uncompacted thicknesses (after Moore, 1969; Hamilton, 1959)

$$H_o = H_f \frac{1 - n_f}{1 - n_o}$$

where:

$H_o$ = uncompacted thickness of sediments

$H_f$ = compacted thickness of sediments (observed value)

$n_o$ = initial porosity of sediments (75% for clayey silts**)

$n_f$ = median value of porosity of compacted sediments (65% for clayey silts with 50-60 m $H_f$**)

*After Dunbar (1981)

!Robert Dunbar, personal communication

**After Moore (1969)

!!An interval velocity of 1.5 km/sec (2-way) was used to compute thicknesses at these shallow levels(Moore, 1969)

slow rate is appropriate for a late Quaternary average. Kulm and Scheidegger (1979) determined upper continental slope sedimentation rates between 10 and 14 cm/ka for the late Quaternary off the Oregon coast. Following the same procedure as described above and shown in Table 2, an estimated age for the base of the ponded unit in the Ensenada Trough is found to be 640±60 ka. Considering the low sedimentation rate, this estimate is also probably an upper bound.

## DISCUSSION

The marked unconformity below the ponded turbidites of the Banda Fan identifies a significant change in deposition during late Pleistocene time. In fact, this horizon may indicate the time of formation of the Banda Fan when the Banda submarine canyon breached the basement rock ridge between Punta Banda and Islas Todos Santos, thus pirating the terrigenous sediments of Valle Maneadero from an older canyon/fan system offshore Punta San Miguel. The bowl-shaped head of Banda Canyon within Bahía Todos Santos, possibly resulting from slumping into the Banda Canyon of unconsolidated deposits ponded behind the Punta Banda - Todos Santos Ridge, is consistent with this hypothesis. Prior to the breaching of this basement ridge, sediments from rivers and streams in the Valle Maneadero and Ensenada area were deposited on the shelf, in Bahía Todos Santos, and reached the deeper, offshore basin through an older submarine canyon west of Punta San Miguel. A buried channel is evident in the shelf sediments in this area (figure 22), and poorly defined canyons are noticeable in the bathymetry across the slope to the west (plates 1 and 2).

Although Punta Banda and Islas Todos Santos have been uplifted throughout the Pleistocene epoch, evident from the numerous uplifted marine terraces, timing for

Figure 22. Line drawing of sparker seismic profile (Line B-29) across Bahía Todos Santos (see figure 4 for location). Different acoustic facies identified are interpreted based upon character of the reflectors. Prominent buried channel may mark former conduit through which sediments of Valle Manéadero and Bahía Todos Santos passed to the deeper offshore basins.

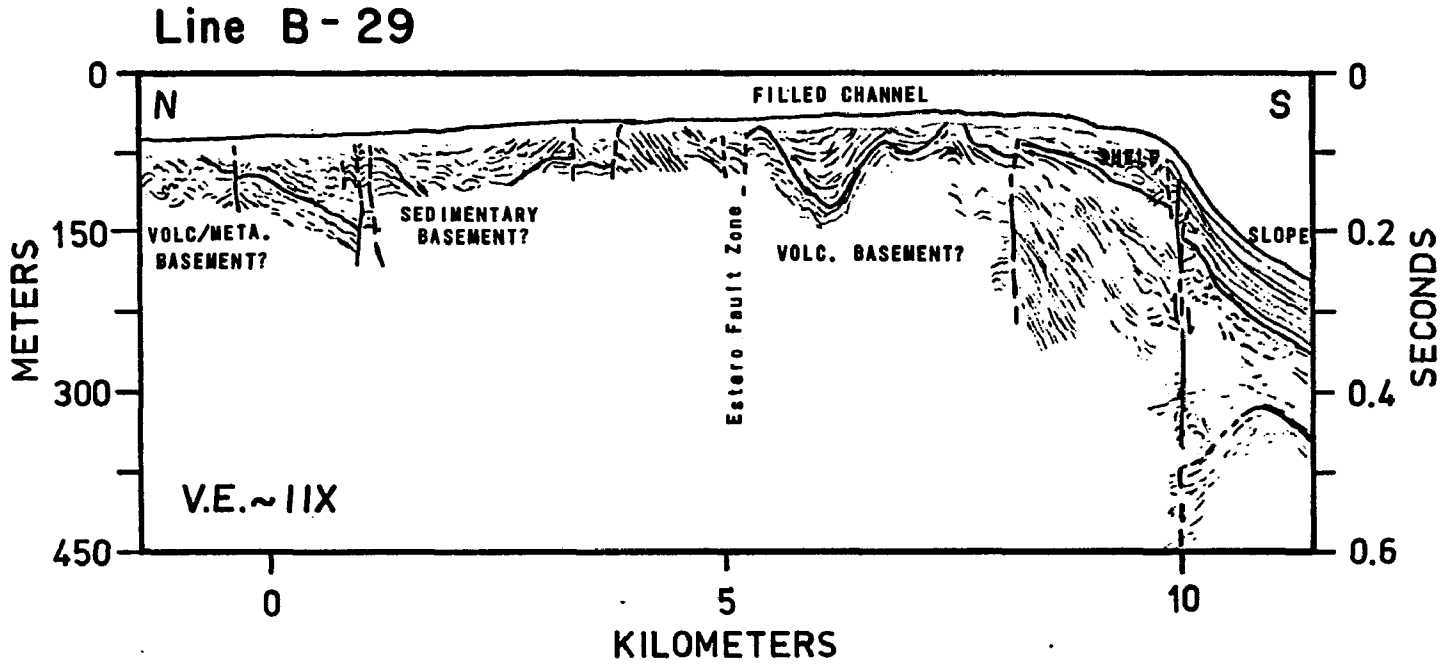
Line B-29
N
S
FILLED CHANNEL
SHELF
SLOPE
VOLC/META. BASEMENT?
SEDIMENTARY BASEMENT?
Estero Fault Zone
VOLC. BASEMENT?
V.E.~11X
METERS
0
150
300
450
SECONDS
0
0.2
0.4
0.6
0
5
10
KILOMETERS

the breach by the Banda Canyon probably correlates with a relative high, sea level stand. Continued erosion by turbidity and/or traction currents within the canyon have since been able to maintain the active channel through the basement ridge even though tectonic uplift of this area has continued.* Tectonic activity may also have had an effect in breaching the ridge, and enhanced erosion of the sheared rocks of the Agua Blanca fault zone probably contributed to the canyon downcutting in this particular location. Farre and others (1983) have described a similar model of headward erosion for the evolution of submarine canyons.

Salsipuedes Fan (figure 9) overlies conformably the older Descanso Fan unit of Smith and Normark (1976). The hemipelagic unit (PEL) is not recognizable in figure 9. A change in acoustic character, possibly signifying progradation of the more proximal fan facies over older basin deposits is apparent in figure 11. The older Descanso unit may be a distal equivalent of the early Salsipuedes Fan, or of the older, now inactive(?) fan off Punta San Miguel discussed above. Based upon the preceding discussion, however, it probably predates the Banda Fan.

The widespread hemipelagic unit represents an extended interval without significant turbidite influx in parts of the San Diego Trough and San Clemente Basin. Both Coronado and Navy submarine fans overlie this unit, (Smith and Normark, 1976; also figure 11), and it is proposed here that the Coronado Canyon has a similar history of development as that discussed previously for the Banda Canyon. Prior to breaching of Coronado Bank by the Coronado Canyon, terrigenous sediments from the San Diego and Tía Juana Rivers ponded behind Coronado Bank and reached the

---

* It is also possible that strike-slip along the Agua Blanca fault zone has occurred in the area (chapter 4, this volume).

San Diego Trough via Loma Sea Valley and La Jolla Fan. Some of these sediments may have been transported southward by longshore drift, to the small canyon in Bahía Descanso (Descanso Canyon) to reach the Salsipuedes Fan. Timing of the breaching of Coronado Bank by Coronado Canyon and abandonment(?) of Loma Sea Valley as a major, active canyon are marked by the age of the upper boundary of the hemipelagic unit below the oldest Coronado Fan deposits. As noted by Smith and Normark (1976), the absence of the hemipelagic unit farther north in the San Diego Trough shows that the La Jolla Canyon and Fan have been active relatively continuously throughout Quaternary time. Smith and Normark (1976), Normark and Piper (1972) and Normark and others, (1979) discuss the history of Navy Fan in more detail.

## CONCLUSIONS

It is evident from the data presented here and elsewhere (Moore, 1969; Normark and Piper, 1972; Smith and Normark, 1976) that sedimentation patterns and rates of deposition have undergone significant variations during late Cenozoic time in the California Continental Borderland. The older basin fills may have accumulated relatively slowly with occasional turbidite influxes separated by long intervals of hemipelagic deposition. As outlined by Gorsline and Emery (1959), the nearshore basins were the first to fill, at least to sill depth. Direct avenues of turbidite transport to parts of the adjacent offshore basins (San Diego Trough, Descanso Plain, and East San Clemente Basin) were available, however. Major fault zones, including the Rose Canyon and the Agua Blanca, provided gaps in the nearshore ridge and bank system for the major submarine canyons to pass.

During late Pleistocene time, new submarine canyons breached the nearshore ridges, and new submarine fans formed, increasing the influx of turbidites to the offshore basins. These breaches are probably related to eustatic sea level changes, and more accurate dating of the prominent unconformities underlying these younger fan deposits may allow their correlation with uplifted marine terraces onshore. Tectonic activity may also have had significant influence on the formation of these new canyon/fan systems. Enhanced erosion along sheared rocks of the major fault zones provided easy avenues for canyon headward(?) erosion. Tectonic activity also created additional topographic barriers, so that (East) San Clemente Basin became further isolated from all but the largest, less frequent turbidity currents. The openning of Navy Channel when San Diego Trough filled to sill depth provided a new avenue for turbidite influx to East San Clemente Basin (Normark and Piper, 1972).

The seismic stratigraphy developed for this study demonstrates the complex interaction between tectonics, eustasy, and sedimentation processes in the late Quaternary filling of the basins of the Inner Borderland offshore of northern Baja California, Mexico. Earlier tectonic activity which formed the major ridges and basins of the California Continental Borderland had a profound impact on the late Cenozoic sedimentation history. Continuing tectonic activity coupled with episodic (quasi-periodic?) eustatic sea level fluctuations has produced a complex post-orogenic(?) depositional history. Further research in the area may unravel more of the details of the sedimentation patterns and lead to increased understanding of the geological history of this continental margin and tectonic plate boundary. Results from this research are of value to understanding resource potential of this and similar continental margins.

# CHAPTER 4

# CHARACTER AND RECENCY OF FAULTING

## Introduction

The characteristic basin and ridge physiography of the California Continental Borderland has long been attributed to faulting and structural control. Lawson (1893), Smith (1898) and Shepard and Emery (1941) recognized the steep, curvilinear slopes bounding the major islands and ridges and proposed their fault origins. Within the Borderland, Moore (1969) described an "inner zone of major northwest-trending faults", which he considered an offshore extension of northern Peninsular Ranges structure.

The present study involves a detailed investigation of the geologic structure of the Inner Borderland, for the region lying approximately between the U.S./Mexico international border and Punta Colinett, along the Baja California Coast (figure 23). This area includes the postulated boundary between the northern and southern Borderland, delineated by the offshore Santo Tomás fault and its previously inferred connection with the southern branch of the Agua Blanca fault onshore (Krause, 1965).

Because the principal structural trend of the California Borderland is subparallel to the San Andreas fault system, the region is considered to be a part of the Pacific-North American tectonic plate boundary (Moore, 1969; Crowell, 1974; Blake and others, 1980; Howell and others, 1950; Legg and Kennedy, 1979). Miocene extension and rifting has been proposed by some to account for the major Borderland physiography (Yeats and others, 1974; Blake and others, 1978, Yeats, 1976). Others have postulated ridge and basin formation due to anastomizing fault strands in a broad

Figure 23. Bathymetry of the Inner Continental Borderland west of northern Baja California. Contour interval offshore is 100 m, and onshore, 500 m. Bathymetric data were compiled from various sources including plate 1 of this study (chapter 2, this volume), Moore, (1969) and the National Ocean Survey (1974) bathymetric charts of the region offshore southern California (NOS charts 1206N-15, -16).

# INNER CONTINENTAL BORDERLAND

## BATHYMETRY

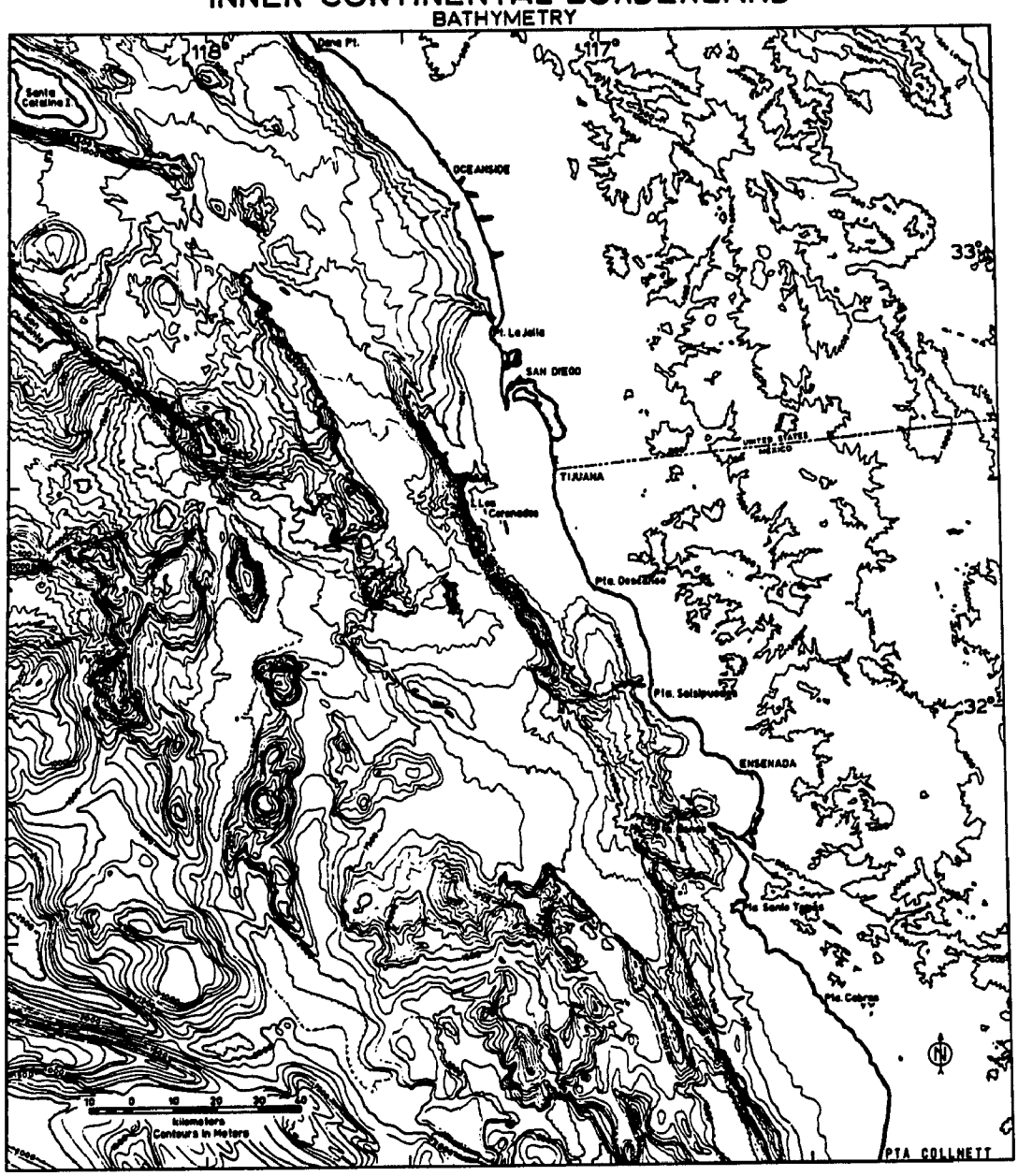

zone of transform faulting (Crowell, 1974, Howell and others, 1980). Wrench faulting has been recognized in the area (Wilcox and others, 1973; Harding, 1973; Greene and others, 1979; Crouch, 1981), and Junger (1976) proposed that convergent, right-lateral, wrench faulting between "deep seated mini-plates" accounts for the primary structural character of the entire southern California part of the Borderland. Preliminary investigation of marine geophysical data in the area of this study allowed southward extension of Junger's hypothesis to include the region offshore of northwestern Baja California (Legg and Ortega, 1978; Legg and Wong, 1979; Legg and Kennedy, 1979).

The principal objectives of this study are to determine (1) the location and extent of deformation associated with the major fault zones in the area offshore of northern Baja California (figure 23); (2) the character of the faulting associated with these zones and their structural relationships; and (3) the recency of movement along each of these faults. A subsequent report (chapter 7, this volume) discusses the tectonic implications of these faults in relation to the regional tectonic framework.

## DATA

The principal data for the present study were collected by the author during two marine geophysical cruises (CFAULTS 1 and 2) during September, 1978 and July, 1979 aboard the Scripps Institution of Oceanography Research Vessel Ellen B. Scripps. Over 3,000 km of sub-bottom, seismic reflection profiles were obtained during these cruises (Figure 24). Both high-resolution, shallow penetration and medium-resolution, deep penetration seismic systems were used, in order to delineate more precisely the significant shallow geological structure. Table 1 lists the cruise

Figure 24. Tracklines of seismic reflection profiles used for this study and references for additional data included in mapping the regional geology. Data from cruise tracks labelled CFAULTS-1 and -2 were obtained by the author and are available from the SIO Geological Data Center. Data from cruise tracks offshore San Diego were obtained by Mike Kennedy and can be obtained from the California Division of Mines and Geology. Data from other cruises shown were obtained by Moore (1969) and are also available at the SIO Geological Data Center.

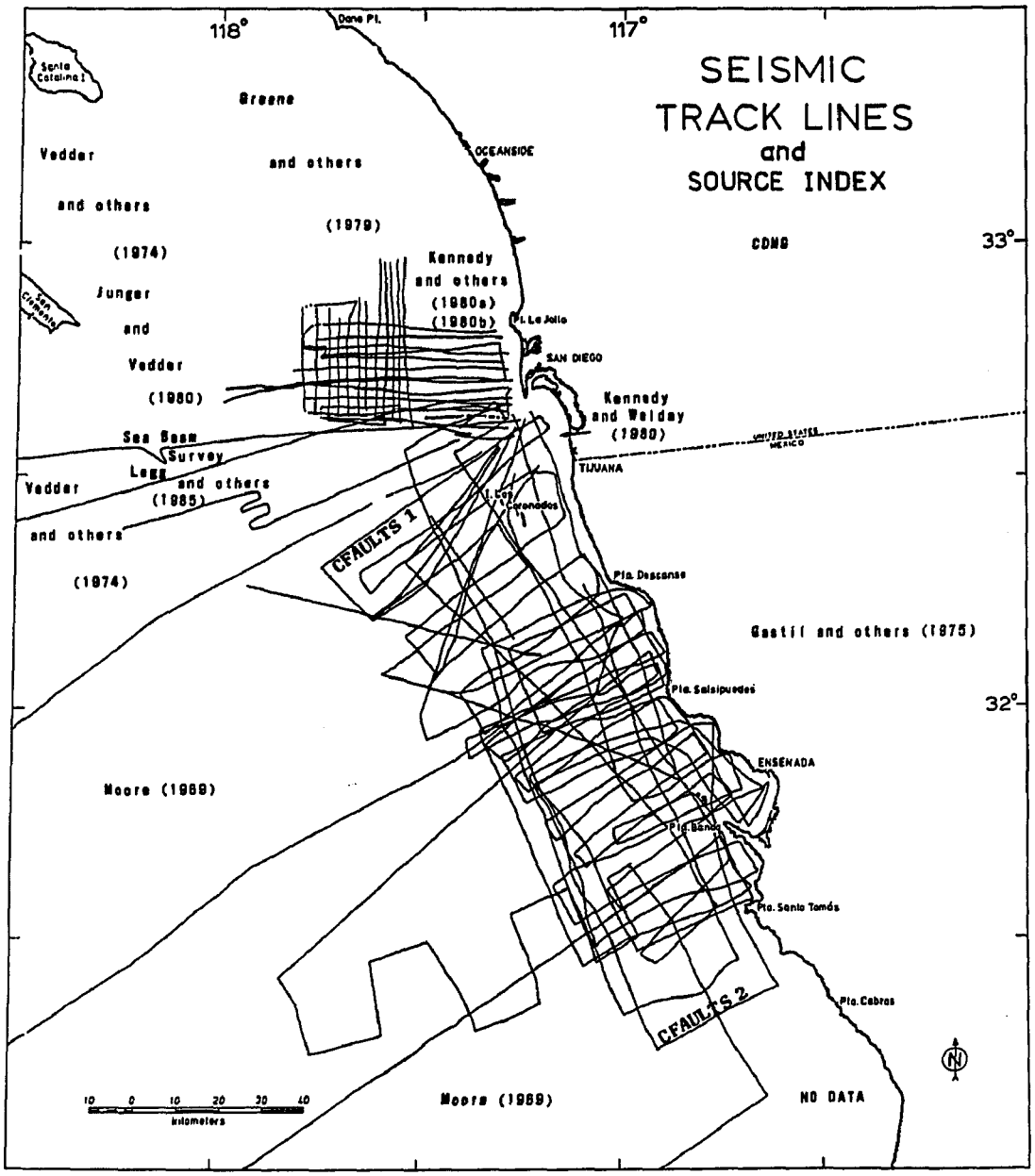
SEISMIC
TRACK LINES
and
SOURCE INDEX
118°
117°
33°
32°
Dana Pt.
Santa Catalina I.
San Clemente I.
Greene
and others
(1979)
Vedder
and others
(1974)
Junger
and
Vedder
(1980)
Sea Beam
Survey
Legg
and others
(1985)
Vedder
and others
(1974)
Moore (1989)
OCEANSIDE
Kennedy
and others
(1980a)
(1980b)
Pt. La Jolla
SAN DIEGO
Kennedy
and Welday
(1980)
CDMG
UNITED STATES
MEXICO
TIJUANA
I. Los Coronados
CFAULTS 1
Pta. Descanso
Gastil and others (1975)
Pta. Salsipuedes
ENSENADA
Pta. Banda
Pta. Santo Tomás
Pta. Cabras
CFAULTS 2
Moore (1989)
NO DATA
10 0 10 20 30 40
kilometers

information and types of data acquired which were used for this study. Seismic equipment employed included a 3.5 kHz echo-sounder, a 30 kJ sparker system (filtered between 63-160 Hz), and a small (5-10 cu. in.) air gun (filtered between 25-150 Hz). Because a large compressor was used, relative to the chamber capacity of the airgun, we had to 'blow-down' the compressor every 30 minutes, resulting in a characteristic, short-lived degeneration of the record quality (see for example, figures 5 and 6).

Navigation for these cruises involved combinations of satellite fixes, RADAR ranging, LORAN-C, precision RADAR transponder ranging, and dead reckoning. The final navigation track plots (shot point maps) were compiled ashore following the cruises using the best navigated lines, either good satellite fixes or precision transponder navigation, for control. The other lines were then adjusted so that the bathymetric soundings matched at line crossings. The procedure is described in more detail elsewhere (chapter 2, this volume, and the Appendix) and was also used to prepare the bathymetric charts used as base maps in this study (plates 1 and 3). Relative position accuracy varied from $\pm 30$ m where transponders were used, to $\pm 500$ m in areas where only RADAR fixes to distant shore points could be made.

Spacing between seismic profiles was generally close (5-10 km) and in areas of special interest, very close ($\sim$500 m). Kennedy and others (1980) found such close spacing is necesssary for detailed correlation of structure between adjacent profiles. A few areas on the perimeter of the study were profiled at significantly wider line spacing, and so detailed correlations were not possible, although bathymetric data based upon more closely spaced soundings allowed interpolation of geologic structure between the seismic profiles. Two significant gaps in detailed seismic data are

present, however, due to insufficient density of seismic profiles crossing these regions. Both lie approximately along the U.S. - Mexico border, one near shore, where equipment problems prevented acquisition of good data on the few crossings of the area, and the second, along the southern end of Thirtymile and Fortymile banks, where older data of Moore (1969) may exist but have not been incorporated into this study. These border gaps are also a result of failure to achieve significant overlap between research cruises conducted by scientists working on opposite sides of the international border.

Other data used in the study include the high-resolution seismic reflection data collected by Mike Kennedy (California Division of Mines and Geology, personal communication) for detailed studies of faulting offshore San Diego (Kennedy and others, 1980a,b; Kennedy and Welday,1980). Also, some of Dave Moore's data from his earlier studies of the California Continental Borderland (Moore, 1969) were used to fill important gaps. Finally, Sea Beam studies of part of the San Clemente fault zone (chapter 5, this volume) including a few high-resolution seismic profiles in that area were also used.

## INTERPRETATION

Several excellent texts on the interpretation of seismic data are available (Sheriff, 1978; Dobrin, 1976; Waters, 1981). Therefore, a brief discussion is presented of only a few of the most important points relevant to the interpretation of the seismic data as used herein for the preparation of the structural maps (plate 3). Detailed explanation, including several excellent examples of seismic reflection interpretations, and of the geologic map symbols used in this study and for the entire

California continental margin is presented by Kennedy and others (1985).

In general, faults are recognized by termination or offset of sub-bottom reflectors in the seismic profiles. Distinct offsets, truncations, or changes in dip of these reflectors mark a well-defined fault. Inferred faults are located where the termination of reflectors is less distinct and may involve bending of the reflectors or changes in seismic reflection character across "an obscure, seismically-disturbed zone" (Kennedy and others 1985). Questionable faults are mapped where the interruption of sub-bottom seismic reflectors is obscure, but that continuation of a better defined fault into the region on the profile in question is likely. Also, some of the more prominent topographic lineaments, marked by steep slopes or scarps are mapped as questionable faults; inferred faults if one or more seismic profile(s) crossing the slope shows a fault. Finally, tectonic geomorphic principles described in chapter 5 (this volume) were used to map the principal, recently(?)-active fault traces in the areas of the Sea Beam precision bathymetric data.

Folds were identified by flexures in the sub-bottom reflectors. Because of the large vertical exaggeration present in the seismic data, what appear to be moderate or even tight folds are, in fact, quite gentle. Most of the folds observed within the basin sediments in the area are very gentle, and would be imperceptible but for the vertical exaggeration. Some are definitely related to tectonic movements, whereas others are interpreted to be related to sediment draping over basement topography. Differential compaction is also possible for some of the more gentle folds observed in the basin sediments, especially where significant variability exists in sedimentation from submarine fan turbidite influx to hemipelagic.

Fault character can be generally determined by the type of offset observed in the reflection profiles, secondary structures and the overall fault pattern, in both vertical and map views. Dip separation is most easily identified on seismic profiles, because all sub-bottom reflectors show the same sense of offset but often of varying amount. Because of the large vertical exaggeration present in the data used in this study, many faults show vertical dips, and so normal versus reverse separation must often be determined by other means. Fault drag apparent in reflectors abutting the fault is most useful. Reverse drag is typically seen associated with normal fault offset in the California Continental Borderland (Moore, 1969). Also, small grabens between subparallel fault traces imply normal fault offsets. Strike-slip faults, common to the area, show variable sense of reflector offset and drag, both along strike on adjacent profiles and within the same profile at various depths.

Many of the major faults in the area show evidence of oblique slip in that the offset character shows significant dip-separation on individual profiles, whereas the sense of the offset changes along strike. Divergent wrench faulting or normal oblique strike-slip is characterized by inverted (negative) flower structure (also called chevron-shaped dilational synclines) in seismic profiles (Harding, 1983, 1985; Bally, 1983). Monoclinal downwarping of sub-bottom reflectors into the main fault zone is the most easily recognized feature of this type in the high-resolution data of this study (figures 7 and 9). The large vertical exaggeration, and relatively shallow penetration of these data preclude identification of convergence of the near surface fault traces with depth. Convergent wrench faults or reverse oblique strike-slip faults are characterized by palm tree or positive flower structure in seismic profiles, (Harding, 1983, 1985; Bally, 1983). Upwarping of the sub-bottom reflectors into prominent

folds, which lie subparallel to the fault trend, and upthrusts (reverse faults which steepen with depth, Sylvester and Smith, 1976; Wilcox and others, 1973; Harding, 1973; Lowell, 1972) are common along these convergent wrench faults, (figure 6).

Simple, parallel wrench faults or pure strike-slip faults show variable apparent reflector offsets with depth in seismic profiles and are often marked by simple, single, throughgoing fault traces in this area (figure 9). Also, as observed by geologists on land, major strike-slip faults have near vertical dips and so cut relatively straight paths across topography, (note the prominent rift valleys and other lineations in the bathymetry, plates 1,3,4 and 5).

## CHARACTER OF FAULTING

The faulting of the Inner Borderland of southern California and northern Baja California is characterized by northwest-trending, right-lateral wrench faults (Junger, 1976; Legg and Ortega, 1978; Legg and Wong, 1979; Legg and Kennedy, 1979; Greene and others, 1979; Kennedy and others, 1980a,b). Data of this study confirm this conclusion and allow a more detailed interpretation of the nature of the major wrench fault zones which dominate the regional structure. Significant variations of structural style along strike and at depths for these fault zones is apparent from the data presented in this section.

As initially proposed by Junger (1976) and extended by Legg and Ortega (1978) and Legg and Kennedy (1979), the late Cenozoic faulting of the Inner Borderland can be divided into four major wrench fault zones. These are: (1) Santa Cruz - San Clemente - San Isidro; (2) San Pedro - San Diego Trough - Bahía Soledad; (3) Palos Verdes Hills - Coronado Bank - Agua Blanca; and (4) Newport - Inglewood - Rose

Canyon - Vallecitos - San Miguel fault zones. As shown in figure 25, the second zone of Legg and Kennedy (1979) has been renamed from Maximinos to Bahía Soledad fault zone. More detailed mapping shows connection of the Bahía Soledad fault to the southern branch of the Agua Blanca fault near Punta Santo Tomás, whereas the Maximinos fault is subparallel to Punta Banda and more closely related spatially and structurally(?) to the Agua Blanca - Coronado Bank fault zone. The faulting in this area is, however, very complex, and both, possibly all of the *innermost* fault zones link with the major transpeninsular (trans-Baja) Agua Blanca fault. Thus, two major fault systems (subsystems of the San Andreas fault system of Crowell, 1962) are apparent, i.e., the San Clemente and Agua Blanca. The following sections discuss some of the more important details of each of these fault zones.

## SAN CLEMENTE FAULT SYSTEM

The San Clemente fault system extends completely across the region of this study and perhaps for a considerable distance beyond at both ends (Moore, 1969; Junger, 1976; Junger and Vedder, 1980, personal communication; Vedder and others, 1974). As shown in plate 3 and figure 25, it is delineated by a narrow, <5 km wide, continuous zone of faulting across the entire length of this study area, (figures 8 and 9) and beyond for a distance in excess of 300 km. As such, it represents the most significant, active late Cenozoic structural feature in the California Continental Borderland. In fact, as a major fault zone, it ranks third, in overall length, for all of California's faults, following the San Andreas and the San Gregorio-Hosgri fault zones. Its southward extent is unknown, but it clearly does *not* link with the Agua Blanca fault as postulated by many previous investigators (Allen and others, 1960;

Figure 25. Map showing the principal late Cenozoic faults of the Inner Borderland and adjacent regions of southern California and northern Baja California. The offshore faults have been divided into two major fault systems: San Clemente and Agua Blanca. Both are principally right-slip in character, although dip-slip is locally important in many areas. (See figure 24 for principal data sources used to delineate the major faults outside the area of the detailed seismic reflection profiling surveys of this study).

# INNER CONTINENTAL BORDERLAND
## PRINCIPAL LATE CENOZOIC FAULTS

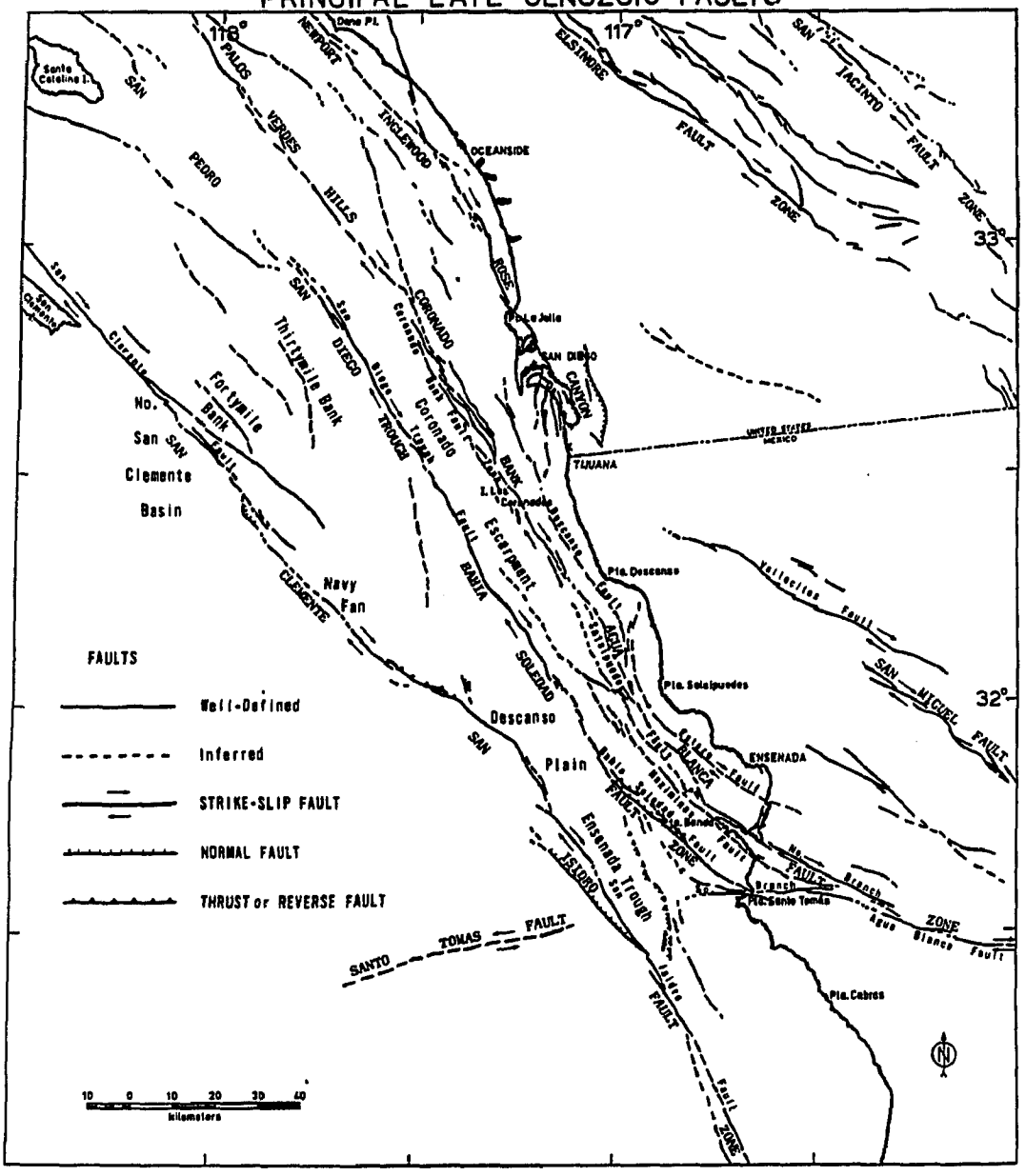

Krause, 1965; Moore, 1969).

Detailed mapping from the seismic reflection data of this study show that the San Clemente fault system is a right-lateral, wrench fault system, as first proposed by Shepard and Emery, (1941). Abundant evidence supporting this conclusion was found by this study, and some of the more striking examples are discussed below. As seen in seismic profiles, sub-bottom reflectors and the seafloor itself show variable offset along strike and within the same profile at depth. No overall, systematic sense of vertical offset or dip-separation is exhibited (figures 6-11 and 26). A major, sinistral bend occurs in association with many features that indicate local north-south convergence, including folding and reverse faulting (upthrusts, see e.g., figure 62, chapter 7, this volume). A small, north-trending graben indicating east-west extension is also present (figure 63, chapter 7, this volume). Tectonic or drag(?) folds along the fault zone, where crossed by enough seismic profiles to determine their orientation, trend approximately east-west, although they are subparallel to the main fault trace in the region of the major left bend. All these features demonstrate the dextral (oblique) strike-slip character of the fault zone.

In other areas, where the main fault trends more northerly (right bend), negative flower tree structure is shown (figures 6,9 and 26) characteristic of divergent, right-lateral wrenching. Also, at right steps in the main fault trace, pull-apart basins are located, such as in parts of North and East San Clemente basins, (chapter 5, this volume).

Significant branch and secondary faults are present, and some are continuous for tens of kilometers. Most prominent are those near Fortymile Bank (Junger fault) and along the western edge of the Ensenada Trough. Both are delineated by

Figure 26. Line drawings of sparker seismic profiles across the southern pare of the study area (see figure 4 for profile locations). Major fault zones are well exhibited by disrupted reflectors. San Isidro fault zone displays inverted (negative) flower structure typical of divergent wrench faults.

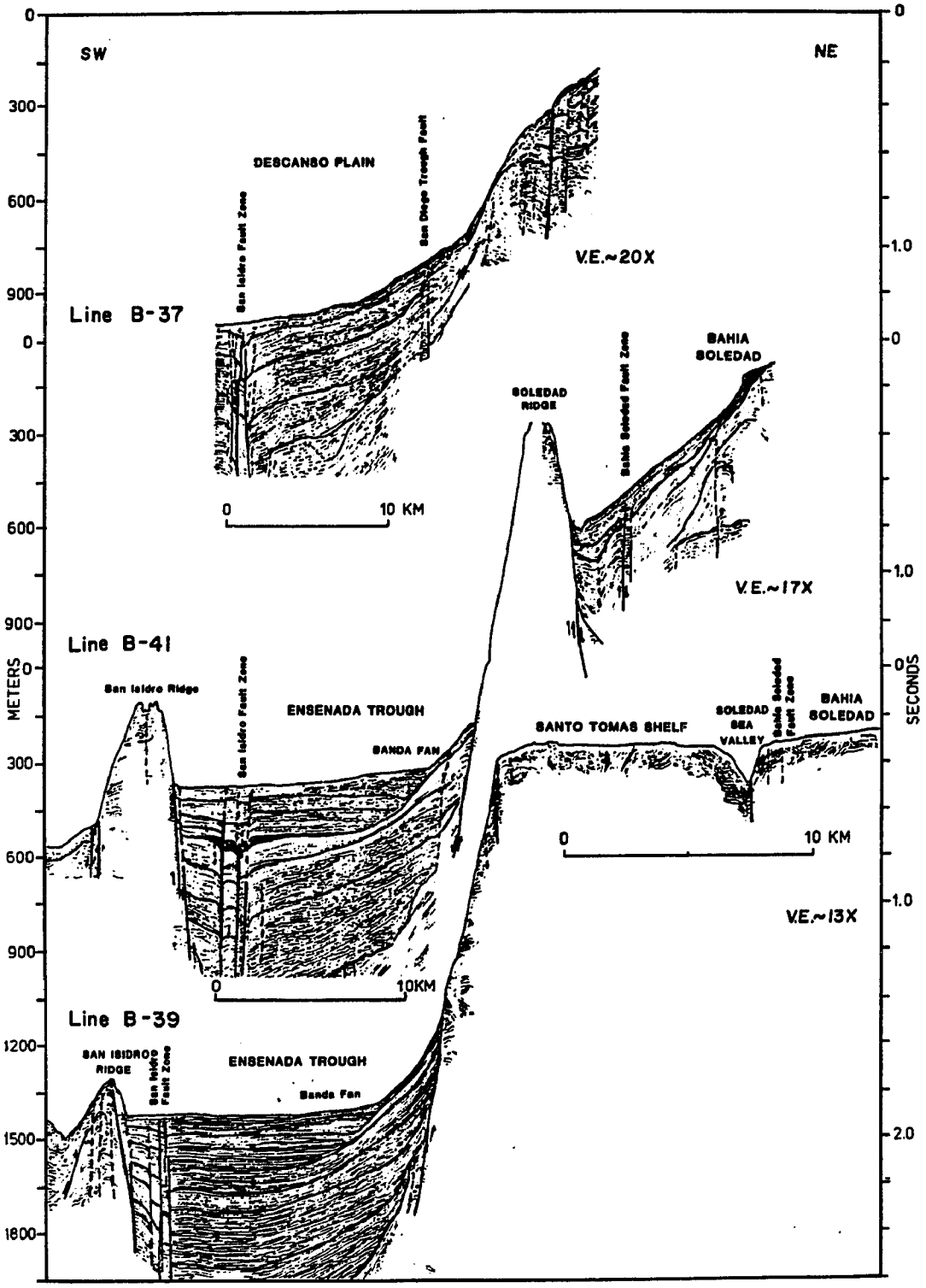
SW
NE
DESCANSO PLAIN
San Isidro Fault Zone
San Diego Trough Fault
V.E.~20X
Line B-37
0
10 KM
SOLEDAD RIDGE
Bahia Soledad Fault Zone
BAHIA SOLEDAD
V.E.~17X
Line B-41
San Isidro Ridge
ENSENADA TROUGH
BANDA FAN
SANTO TOMAS SHELF
SOLEDAD SEA VALLEY
BAHIA SOLEDAD
V.E.~13X
10KM
Line B-39
SAN ISIDRO RIDGE
ENSENADA TROUGH
Banda Fan
METERS
SECONDS
0
300
600
900
1200
1500
1800
1.0
2.0

prominent, linear scarps, reaching elevations of a few hundred to over 1000 meters. Such large scarps imply that significant dip-separation may be associated with these faults. Drag, possibly indicative of normal (oblique?) slip is apparent in the well-bedded reflectors of the Banda Fan, where they abut the fault along the southwest edge of the Ensenada Trough (figure 8).

The Santo Tomás fault (Krause, 1965; Moore, 1969) does not cut the sediments filling the Ensenada Trough and is either truncated and possibly offset or dies out before reaching the San Clemente - San Isidro fault zone. Therefore, it does not connect, and possibly never has connected with the southern branch of the Agua Blanca fault at Punta Santo Tomás. The present data are not adequate to identify conclusively possible offset parts of the Santo Tomas fault along the eastern side of the San Isidro fault zone.

Nothwithstanding the somewhat sinuous nature of the main fault traces of the San Clemente - San Isidro fault zone, a general, systematic difference in average strike of the underlying wrench fault is exhibited by the data (plate 3, figure 25). As shown in figures 25 and 27, the average strike of the main fault traces in the southern (San Isidro fault) area are approximately N30°W. In the northern region (San Clemente fault), the main fault trend is about N40°W. More westerly trending faults of the major left bend link the northern and southern parts of the fault zone. Close inspection of the fault character in the southern regions shows that main fault traces trending about N30°W are transtensile, with several subparallel traces and negative flower structure in seismic profiles (figures 6, 9 and 26). The traces trending about N40°W are simple, single, linear traces and interpreted as pure(?) strike-slip faults. A few, short, transpressive main fault segments, which trend more westerly than

Figure 27. Histograms of fault strikes for the principal late Cenozoic faults of the San Clemente-San Isidro and San Diego Trough-Bahía Soledad fault zones. Data are plotted at 5° increments for the percentage of faults, based upon the length of each fault segment with a specified strike, proportional to the total length of faults of a given type. Only faults estimated to be Quaternary in age and defined by two or more seismic profiles are included. The average strike of fault segments for each group is shown by the number at the base of the histograms. Also, the predicted azimuth of transforms in the Pacific-North American plate boundary for each region is shown by the dashed line (with the value at its base, after Minster and Jordan, 1978). Overall faults lengths for each region varied from 125 km to 282 km. Lengths for each type within a region varied from 9.5 km to 126 km, and main faults always had at least 48 km total lengths. Resolution of fault segment lengths is as small as 0.5 km, although most segments were longer than 1 km.

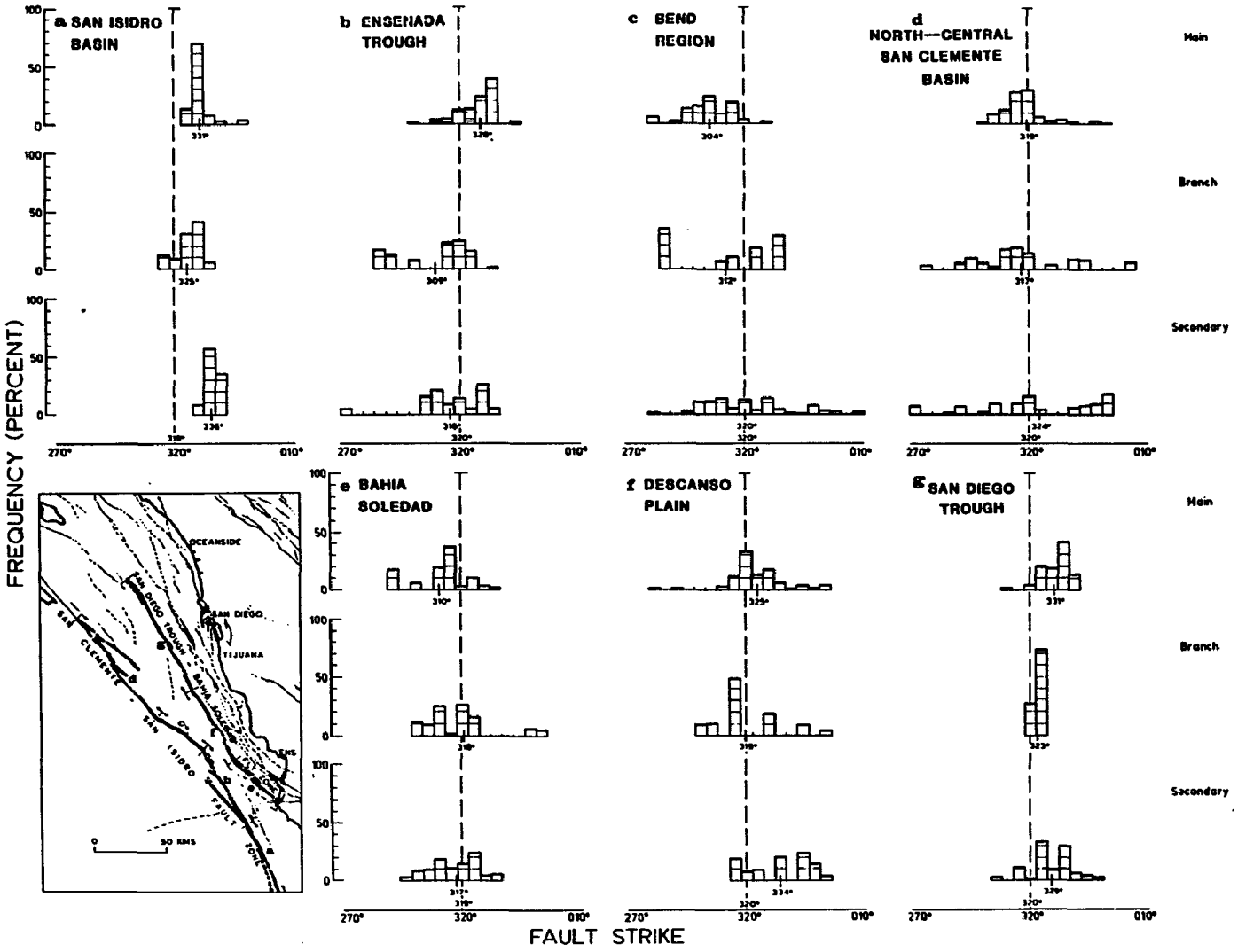
a SAN ISIDRO BASIN
b ENSENADA TROUGH
c BEND REGION
d NORTH—CENTRAL SAN CLEMENTE BASIN
e BAHIA SOLEDAD
f DESCANSO PLAIN
g SAN DIEGO TROUGH
Main
Branch
Secondary
FREQUENCY (PERCENT)
FAULT STRIKE
270°
320°
010°
OCEANSIDE
SAN DIEGO
TIJUANA
SAN CLEMENTE
SAN ISIDORO
FAULT ZONE
50 KMS

N40°W are present in the southern region (figure 8), but the divergent (transtensile) segments are predominant.

Seismic data are not as plentiful along the San Clemente fault segment, but the available data, including the precision Sea Beam bathymetry (chapter 5, this volume) show a relatively narrow, (and simple?) main fault zone. Although negative flower structure typical of the transtensile fault segments of the San Isidro fault are not apparent along the San Clemente fault, pull-apart(?) basins associated with right steps in the main fault trace are evident. A major right step occurs in the vicinity of Navy fan, north of the major left bend. Seismic profiles (figures 10 and 28) across the northernmost segment of this major right step show the principal, near vertical fault trace is along the northwest side of the basin, and a relatively shallow-dipping, normal fault is along the southwest margin. The ponded turbidites of Navy Fan (Normark and others, 1979) lie within a narrow graben between these two fault traces. The strike of this graben, and the main trace of the San Clemente fault, is slightly more north-trending, (N37°W) than the adjacent fault scarps to the north (strike $\simeq$ N41°W). This pull-apart basin configuration, lying north of a major transpressive, left bend of the main fault trace is very similar to the Ridge Basin (Crowell, 1954, 1974, 1975) between the San Gabriel and San Andreas faults (figure 29).

## AGUA BLANCA FAULT SYSTEM

The eastern half of the Inner Borderland structure is pervasively sheared by a complex set of northwest-trending fault zones. For the most part, the major fault zones of this region are subparallel to the continental slope, yet all of these major fault zones are linked at their southeastern ends by the Agua Blanca fault. Because

Figure 28. Airgun profiles (Line C-C') across East San Clemente Basin (Navy Basin) and part of North San Clemente Basin (see figure 4 for location of profiles). Line drawing interpretations show the principal faults of the San Clemente fault zone in this region. See figure 10 for additional information and continuation of profile to the east. (Seismic profile courtesy of J. Mammerickx and P. Lonsdale).

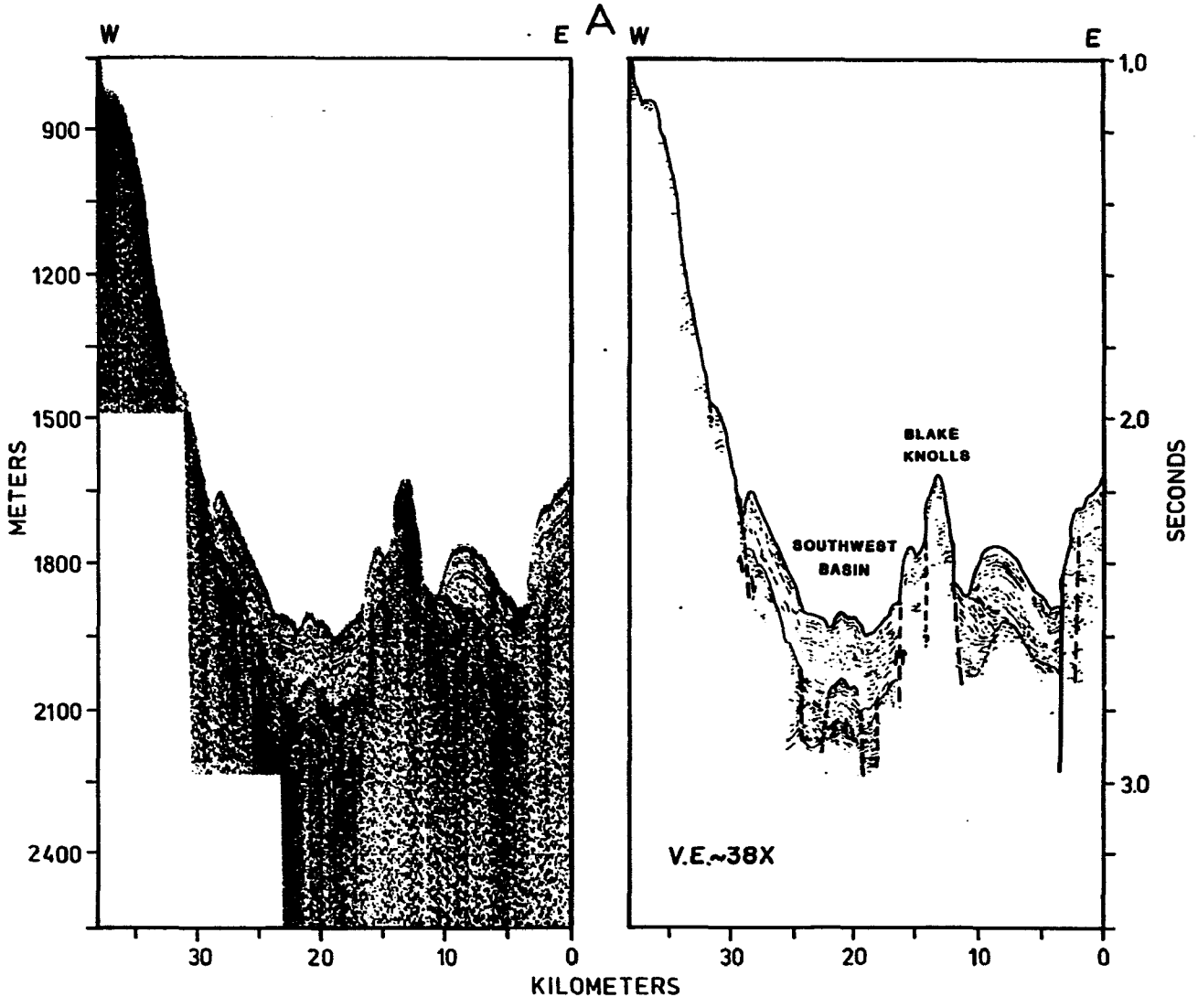
A
W
E
W
E
METERS
900
1200
1500
1800
2100
2400
SECONDS
1.0
2.0
3.0
BLAKE
KNOLLS
SOUTHWEST
BASIN
V.E.~38X
30
20
10
0
30
20
10
0
KILOMETERS

Figure 28. Airgun profiles (Line C-C', Continued).

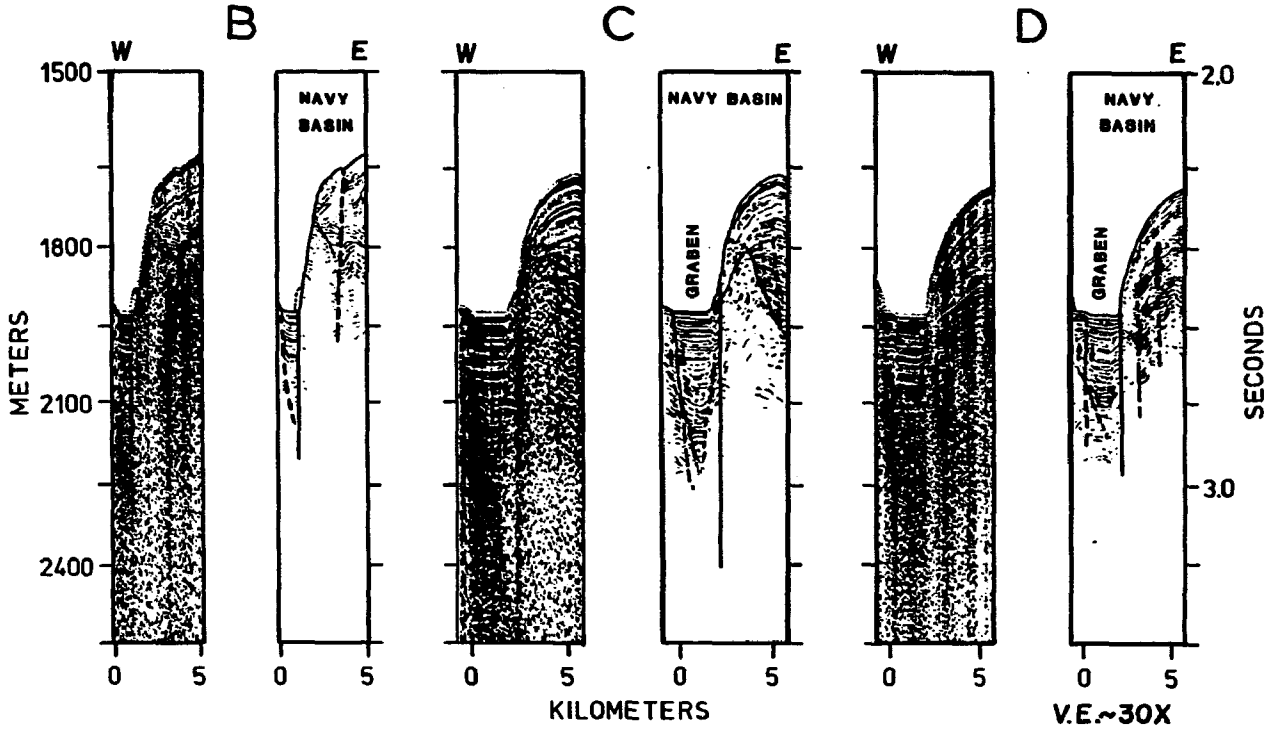
B
C
D
W
E
NAVY BASIN
GRABEN
METERS
1500
1800
2100
2400
SECONDS
2.0
3.0
0
5
KILOMETERS
V.E.~30X

Figure 29. Map comparing portions of San Clemente and San Andreas fault systems at the same scale. Note the similar geometry of the East San Clemente and Ridge basins relative to the left-bending parts of the San Clemente-San Isidro and San Andreas-San Gabriel fault zones. Also, note the position of tectonic uplift, shown by wiggly lines along the San Clemente-San Isidro fault zone and by the San Gabriel mountains along the San Andreas-San Gabriel fault zone. Elevated regions of bedrock are shown by the tick patterns; basin sediments by stippling.

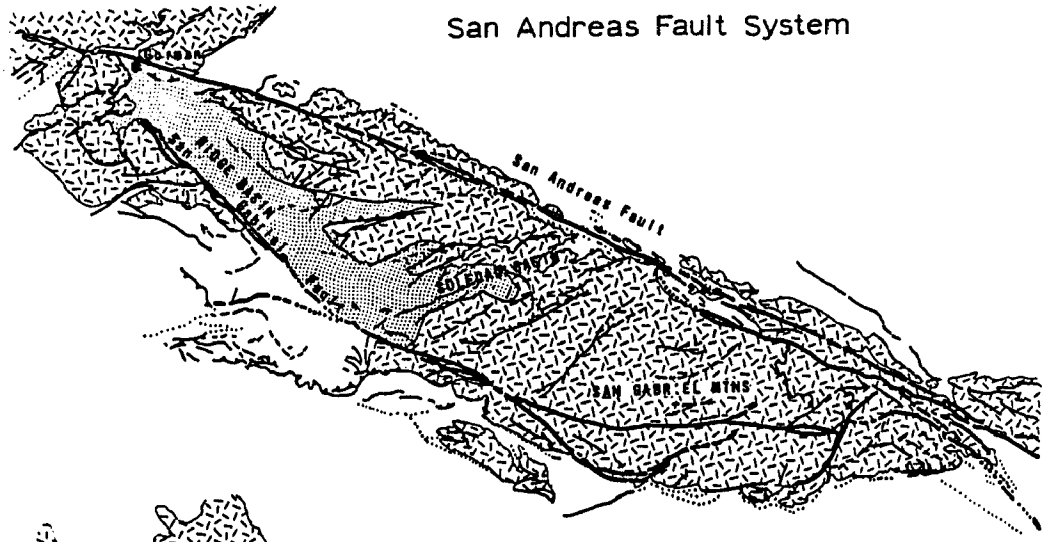
San Andreas Fault System
San Andreas Fault
SAN GABRIEL MTNS

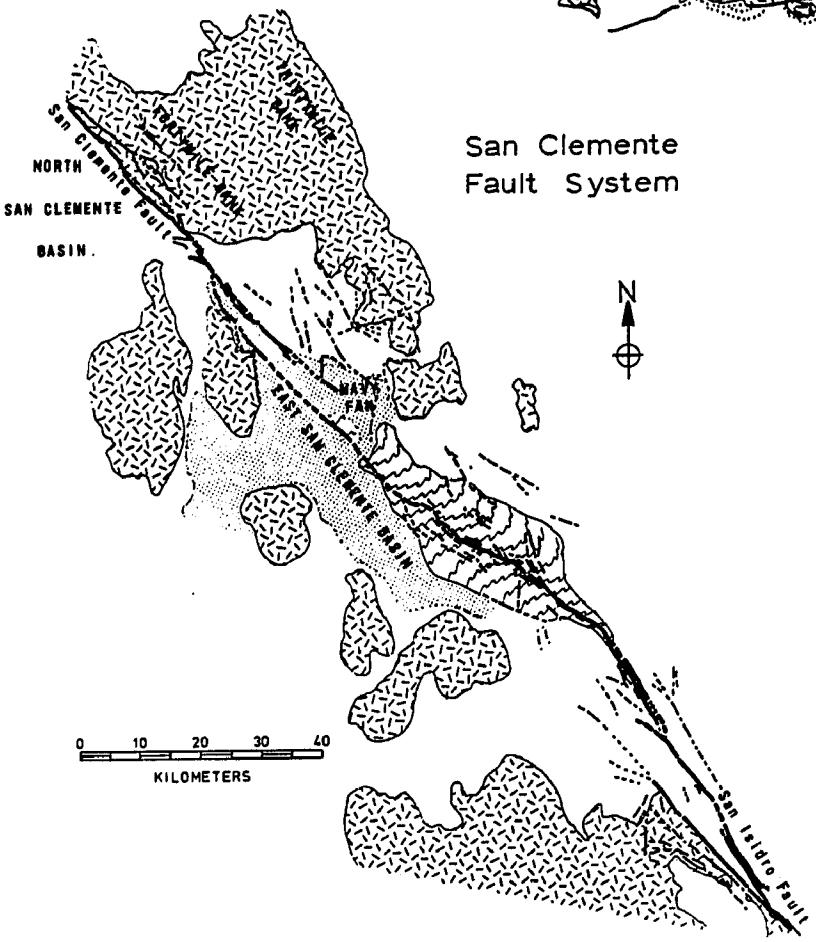
San Clemente
Fault System
NORTH
SAN CLEMENTE
BASIN.
San Clemente Fault
N
0 10 20 30 40
KILOMETERS
San Isidro Fault

the Agua Blanca fault crosses the Baja California peninsula along a trend significantly transverse to the regional structure and Peninsular Ranges physiography, details of the change in character and strike of the offshore faults as they connect with the transpeninsular fault provide important and interesting clues regarding the regional tectonics.

The offshore Agua Blanca fault system is subdivided into three major wrench fault zones. The complexity of faulting implies significant interaction and interconnections between adjacent fault zones, so that identification of the principal fault zones may be obscure in some parts of the area.

**San Diego Trough–Bahía Soledad Fault Zone**

The westernmost fault zone is the San Pedro - San Diego Trough - Bahía Soledad fault zone which had previously been inferred to connect with the Maximinos fault zone south of Punta Banda (Legg and Ortega, 1978; Legg and Kennedy, 1979). This fault zone represents the westernmost major fault to splay off Agua Blanca fault. The southern branch of the Agua Blanca fault does not extend into the Ensenada Trough and apparently dies out near the shelf edge (plate 3). Although apparent left-lateral slip is implied by the offset of the shelf edge, (plates 1 and 3; Krause,1965) it is herein proposed that right oblique slip characterizes the south branch of the Agua Blanca fault. This conclusion is based upon the following reasons: (1) offset of shoreline and formation of Bahía Soledad; (2) secondary structures including faults and folds just south of the main fault show orientations consistent with dextral shear on the main east-trending fault; (3) the axes of the offshore Soledad Ridge and Cabras Bank appear to be offset in a right lateral sense, assuming

they were once continuous; (4) the Bahía Soledad fault is a dextral, oblique reverse-slip fault as described below; and (5) an earthquake, of somewhat inexact location, in the vicinity of Punta Santo Tomás had first motions consistent with dextral strike-slip on an east-trending fault (Legg, 1980). Allen and others (1960) give additional evidence implying dextral slip on the south branch of the Agua Blanca fault, and Acosta (1970) and Orme (1974) have evidence for significant dip-slip in this area. A seismic profile crossing this fault also shows significant dip-separation (figure 30). The present data, however, are inadequate to demonstrate the sense, or amount, of lateral shear on this fault conclusively.

The Bahía Soledad fault zone splays off the southern branch of the Agua Blanca fault in the vicinity of Bahía Soledad (plate 3) and veers northwestward for almost 50 km to the base of the continental slope and the head of the Banda submarine fan. Where this fault and associated secondary faults cut the slope sediment, a consistent southwest-side-up displacement is observed (figures 7, 26 and 31). A small, drag(?) fold on the upthrown side implies that these are reverse, oblique-slip faults. The vertical exaggeration of the seismic data preclude determination of dip, so these are presently interpreted to be steeply dipping or vertical faults. The overall linearity of the fault trace is consistent with this interpretation for the Bahía Soledad fault, and its convergent character identifies it as a right-lateral, oblique, reverse-slip fault. The vertical offset exhibited in the sediments is small, however, the strike-slip may be significantly greater. Except for complex folding and a few minor faults south of Punta Banda, the slope sediments in the vicinity of the Bahía Soledad fault zone are relatively undeformed. This character implies that the Bahía Soledad wrench fault is only slightly convergent, and dominated by strike-slip. Clay cake models of conver-

Figure 30. Line drawing of sparker seismic profile (Line B-1) crossing the shelf and slope region west of Punta Santo Tomás and Punta Banda (see figure 4 for profile location). Prominent magnetic anomaly and seafloor displacement are associated with the major south branch of the Agua Blanca fault, south of the Soledad Sea Valley. Geomagnetic anomaly (based upon total field intensity) data points are shown by the dots, and a smooth curve has been hand drawn through these points to emphasize their trend.

Line B-1

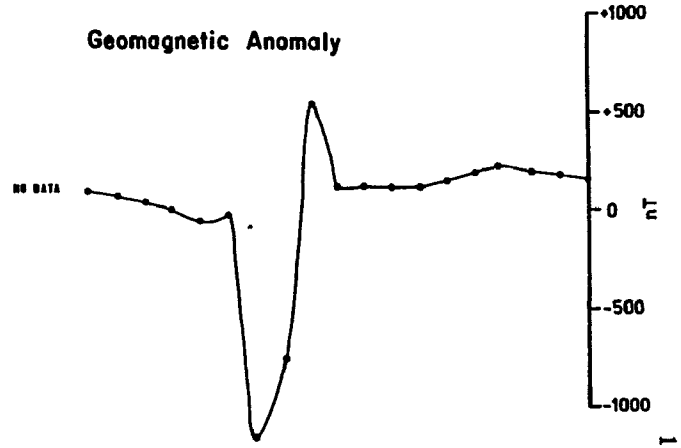


Seismic Profile

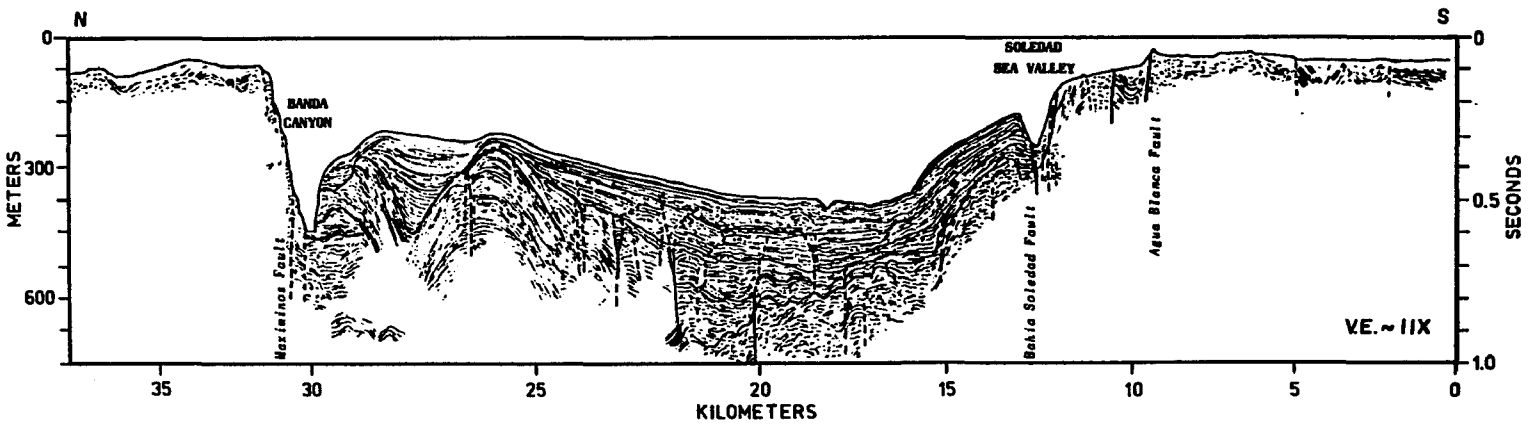

Figure 31. High-resolution (3.5 kHz) profile across the Bahía Soledad fault zone near Soledad Sea Valley (see figure 4 for profile location). Near surface sediments, and possibly the seafloor, are disrupted demonstrating that late Quaternary, possibly Holocene, fault movements have occurred.

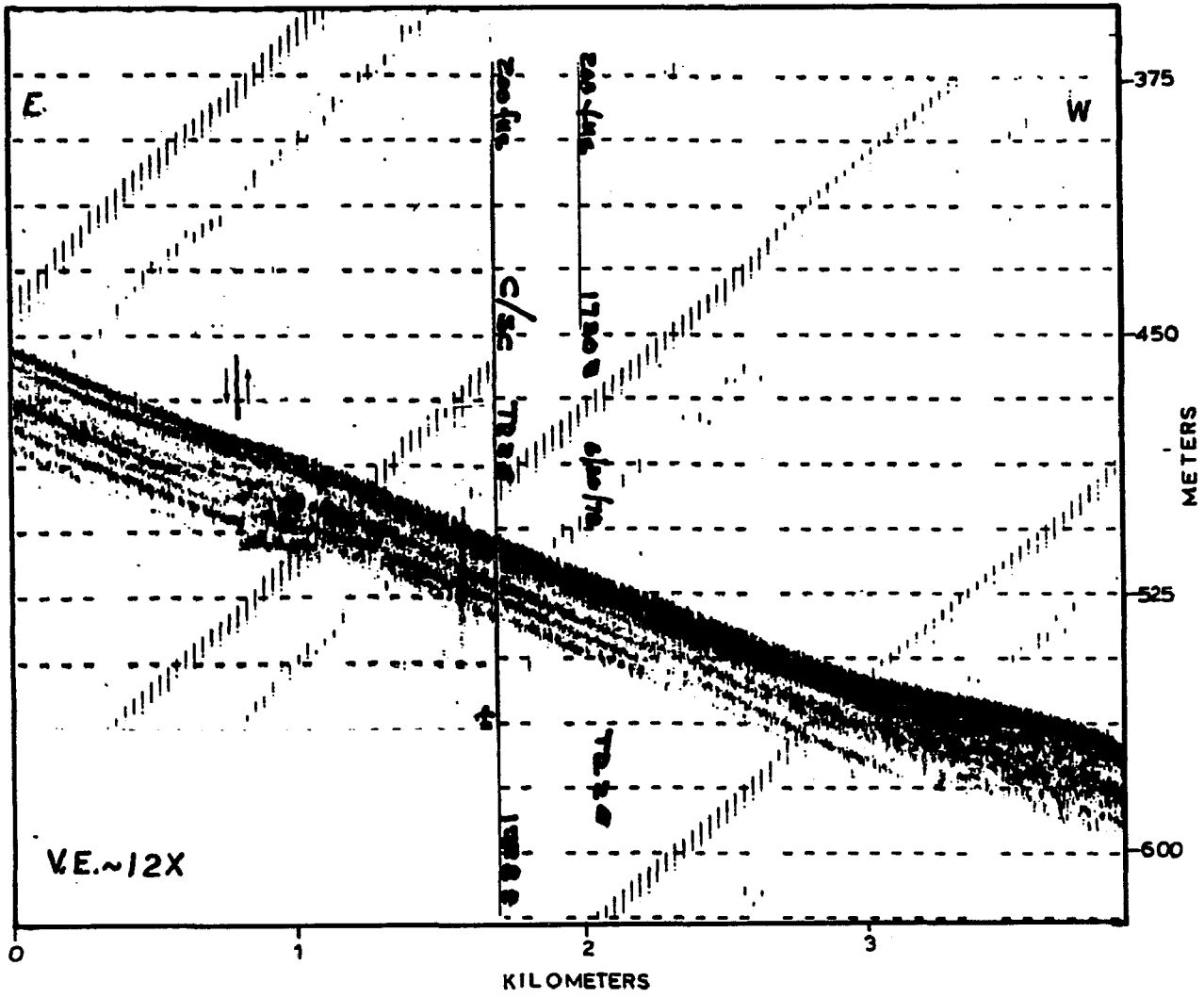
E
W
V.E.~12X
375
450
525
600
METERS
0
1
2
3
KILOMETERS

gent, and simple, parallel wrench faults show early development of an echelon anticlines over the sediment covered fault, (Wilcox and others, 1973, Junger, 1976). The relatively long and continuous, linear main trace of the Bahía Soledad fault is characteristic of a well-developed wrench fault, but the absence of significant folds and secondary structures seems anomalous. Perhaps such secondary structures are present, but too small to be delineated with the available data.

At the base of the continental slope, the Bahía Soledad fault zone turns more northerly, subparallel to the slope, and merges with the San Diego Trough fault zone. The geology and structure are complex in this area which marks a major salient into the steeper continental slope marked by the Coronado and related escarpments. The main fault trace is difficult to define in this region, and in fact, the fault zone may be characterized by several, short, discontinuous, en echelon and subparallel fault segments. A significant, northwest-trending normal(?) fault, delineated by the base of the Soledad Ridge escarpment, intersects the Bahía Soledad fault from the south.

From the head of the Salsipuedes submarine fan to the northern edge of this study area, the San Diego Trough fault zone is conspicuous in seismic profiles. The main fault marks the contact between the Quaternary sediments of the Descanso Plain and the uplifted acoustic basement rocks of a prominent westward protruding block along the southwestern end of the Descanso Ridge. A second major fault trace cuts through the saddle between the block and the ridge and is inferred to link the San Diego Trough fault with other significant faults in the offshore Agua Blanca fault zone, such as the Maximinos fault zone. Farther north, the San Diego Trough fault is delineated by seafloor scarps facing alternate directions along strike. Sinuosity in the main fault trace results in local areas of transpression, marked by folding and

reverse faulting along left bends (figure 5), and transtension, marked by the typical negative flower structure along right bends.

The fault zone becomes somewhat more complex in the vicinity of the Coronado submarine fan where an uplifted block of acoustic basement was inferred to affect the growth of the fan (Moore, 1969; Shepard and Dill, 1966). Transpression is locally exhibited along the San Diego Trough fault in this area (Smith and Normark, 1976). This is apparent from the folding in the sediments adjacent to the fault, (figure 10).

The overall trend of the San Diego Trough fault zone is about N30°W (figure 27). The fault zone is relatively straight, and continuous for over 100 km in the area of this study. The fault zone is considered herein to be underlain by a through-going, parallel wrench fault. The narrowness and overall continuity of the fault zone, and the presence of only short local transpressive or transtensile segments along strike in roughly equal proportions, support this interpretation.

The fact that the fault zone is closely parallel to the axis of the San Diego Trough and its bounding escarpments (along Thirtymile and Coronado banks) implies that the fault zone is directly related to the formation of the structural trough. This trough formation, however, is considered to have resulted from an earlier tectonic regime of slightly different stress orientation when the San Diego Trough fault zone had a more divergent character. The lack of the characteristic negative flower structure, typical of divergent wrenching, except locally along the San Diego Trough fault, shows it is a parallel rather than divergent wrench fault at the present. Also, fault drag is not evident in the younger sediments of the San Diego Trough along its flanking escarpments. Instead, these sediments appear to buttress against the Coronado and Thirtymile Bank escarpments (Kennedy and others, 1980; Greene and others,

1979; Moore, 1969) indicating lack of tectonic deepening of this basin for the present tectonic regime.

**Eastern Fault Zones of the Agua Blanca System**

The easternmost offshore fault zones in the area of this study include the Palos Verdes Hills - Coronado Bank - Agua Blanca and the Newport - Inglewood - Rose Canyon (Vallecitos-San Miguel?) fault zones. The Newport - Inglewood and Rose Canyon fault zones are described in more detail by others (Harding, 1973; Yeats, 1973; Moore, 1972; Moore and Kennedy, 1975; Kennedy and others, 1980a,b; Kennedy and Welday, 1980). These are considered right-lateral wrench fault zones and are characterized by relatively short (10 km), discontinuous, en echelon and subparallel fault traces. Harding (1973) describes the en echelon folds associated with the Newport-Inglewood fault zone, and Kennedy and others, (1980a,b) describe the formation of alternating structural highs and lows associated with gentle S-shaped bends along the Rose Canyon fault zone.

In the southern part of this study area, several major splays of the Agua Blanca fault have been mapped branching toward the northwest, off the major transpeninsular segment (Gastil and others, 1975; Allen and others, 1960; CETENAL, 1974-1979). The prominent northern branch (Allen and others, 1960) has been considered the principal, active trace of the Agua Blanca fault (Legg and Kennedy, 1979). However, as seen in plate 3 and figure 25, two other significant faults, the Maximinos and the Estero faults are also prominent. Gonzalez and Suarez (1984) decribed an earthquake swarm which was apparently associated with the Estero fault. The Maximinos fault appears to trend northwestward, along the southeast side of Punta Banda and not

directly into the Bahía Soledad - San Diego Trough fault zone as previously inferred by Legg and Kennedy (1979). It is inferred herein to step leftward near the Islas Todos Santos and pass through the Todos Santos Sea Valley. The region between the Maximinos and Bahía Soledad faults is structurally complex, and the interpretation shown in plate 3 may differ significantly from reality. A set of prominent southwest(?)-trending folds is evident along the southwest side of Punta Banda (figure 30).

The northern branch of the Agua Blanca fault is marked by the steeply dipping contact between the uplifted Punta Banda basement rock ridge and the sediments of Valle Manéadero which extends northwestward into the southern part of Bahía Todos Santos (figure 7). This fault makes a sharp bend toward the north, and passes the east side of Islas Todos Santos, along a steep, submarine escarpment. Farther north, acoustic basement rock outcrops mark its trace in the northwest part of Bahía Todos Santos. Gastil and others, 1975 considered the Valle Manéadero to be a half-graben, bounded by the Agua Blanca fault along Punta Banda.

The Estero branch of the Agua Blanca fault named herein trends northwesterly offshore from the northern end of Estero Banda. The onshore trace of the fault, if it exists, has not been mapped to date, however, a large scarp cutting across the northern edge of Valle Manéadero may be related to this fault. Armiego and Suárez (1981) also proposed the existence of this branch of the Agua Blanca fault based upon aerial photographs.

The Estero fault is evident in high-resolution seismic profiles within Bahía Todos Santos as a region of folded and truncated near-surface sub-bottom reflectors (figure 32). In the shallow water of the bay, multiple bottom reflectors disrupt the

Figure 32. Line drawings of sparker seismic profiles in Bahía Todos Santos showing the Estero fault zone (see figure 4 for profile locations).

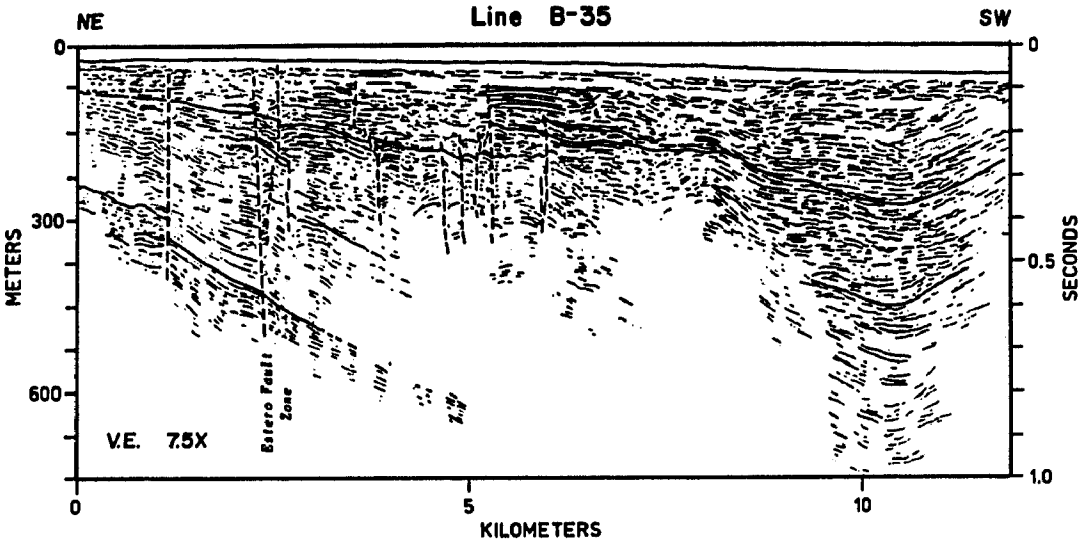
NE
Line B-35
SW
0
300
600
METERS
0
0.5
1.0
SECONDS
Estero Fault Zone
V.E. 7.5X
0
5
10
KILOMETERS

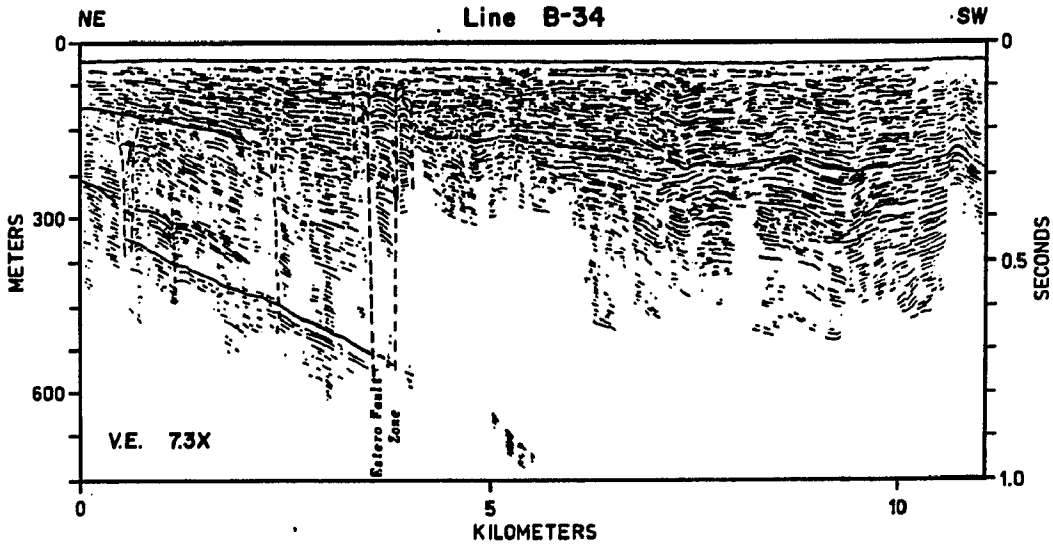
NE
Line B-34
SW
0
300
600
METERS
0
0.5
1.0
SECONDS
Estero Fault Zone
V.E. 7.3X
0
5
10
KILOMETERS

sub-bottom returns and make interpretation difficult. Further evidence for the existence of this fault, however is provided by the magnetic data of Gonzalez (1977). As seen in figure 33, a pronounced steep gradient in the magnetic anomalies is aligned over the fault trace as mapped from the seismic data of this study. Gonzalez originally interpreted the major structure within the bay to be a northeast-trending normal fault, with uplifted acoustic basement on the northern side of Bahía Todos Santos (see e.g. Legg and Kennedy, 1979). Such a fault is present, but in fact trends more east-west, lying between the two principal branches of the Agua Blanca fault within the bay. This presumably older fault is truncated by the more recently active northwest-trending traces of the Agua Blanca fault. The geology of Bahía Todos Santos is considerably more complex than previously suspected, and the configuration of uplifted basement blocks and their bounding faults deserve detailed future investigation. Such studies may provide important data regarding offsets along the major, active traces of the Agua Blanca fault in the offshore area.

The complexity of the offshore continuation of the Agua Blanca fault zone continues northwestward, as far as Bahía Descanso. Structual interpretation of seismic profiles is made more difficult in this area, because of complex bathymetry due to the numerous blocks of acoustic basement rock which protrude above the surrounding gullied slopes and major submarine canyons (plates 1 and 3). Many of these blocks may represent slivers of basement rocks caught between the many anastomosing, en echelon and subparallel fault strands cutting through the area. In some areas, prominent traces of the through-going major branches of the Agua Blanca fault zone can be followed for several kilometers using the seismic profiles. Detailed seafloor topographic mapping using Sea Beam or side-scan sonar systems would provide data to

Figure 33a. Magnetic anomaly data of Gonzales (1977) delineate the major faults within Bahia Todos Santos. Principal fault traces as mapped in this study using seismic reflection data have been superimposed onto Gonzalez' original anomaly contour maps.

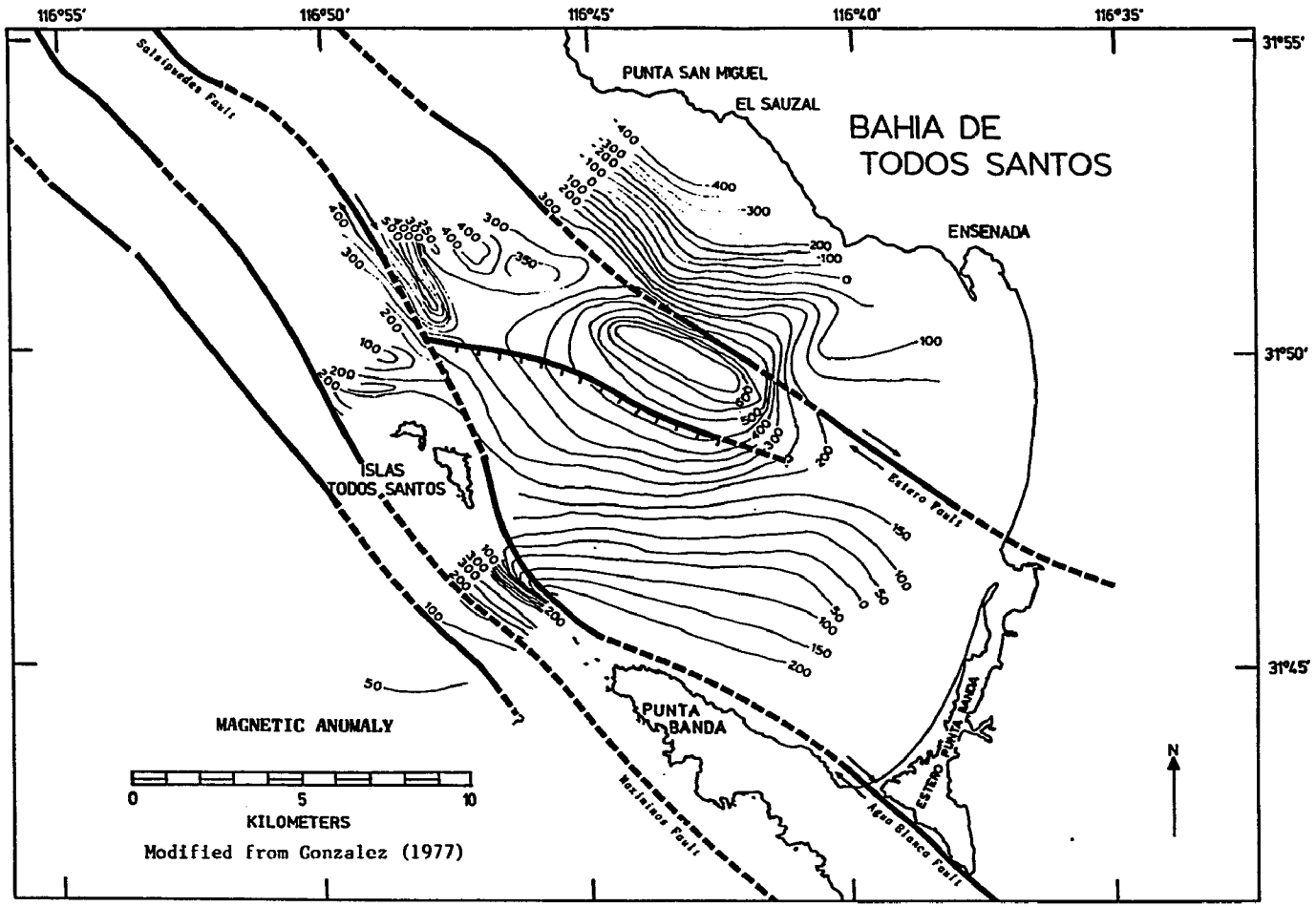


Modified from Gonzalez (1977)

Figure 33b. Gravity anomaly data of Gonzalez (1977). Same comments apply as in the preceding figure.

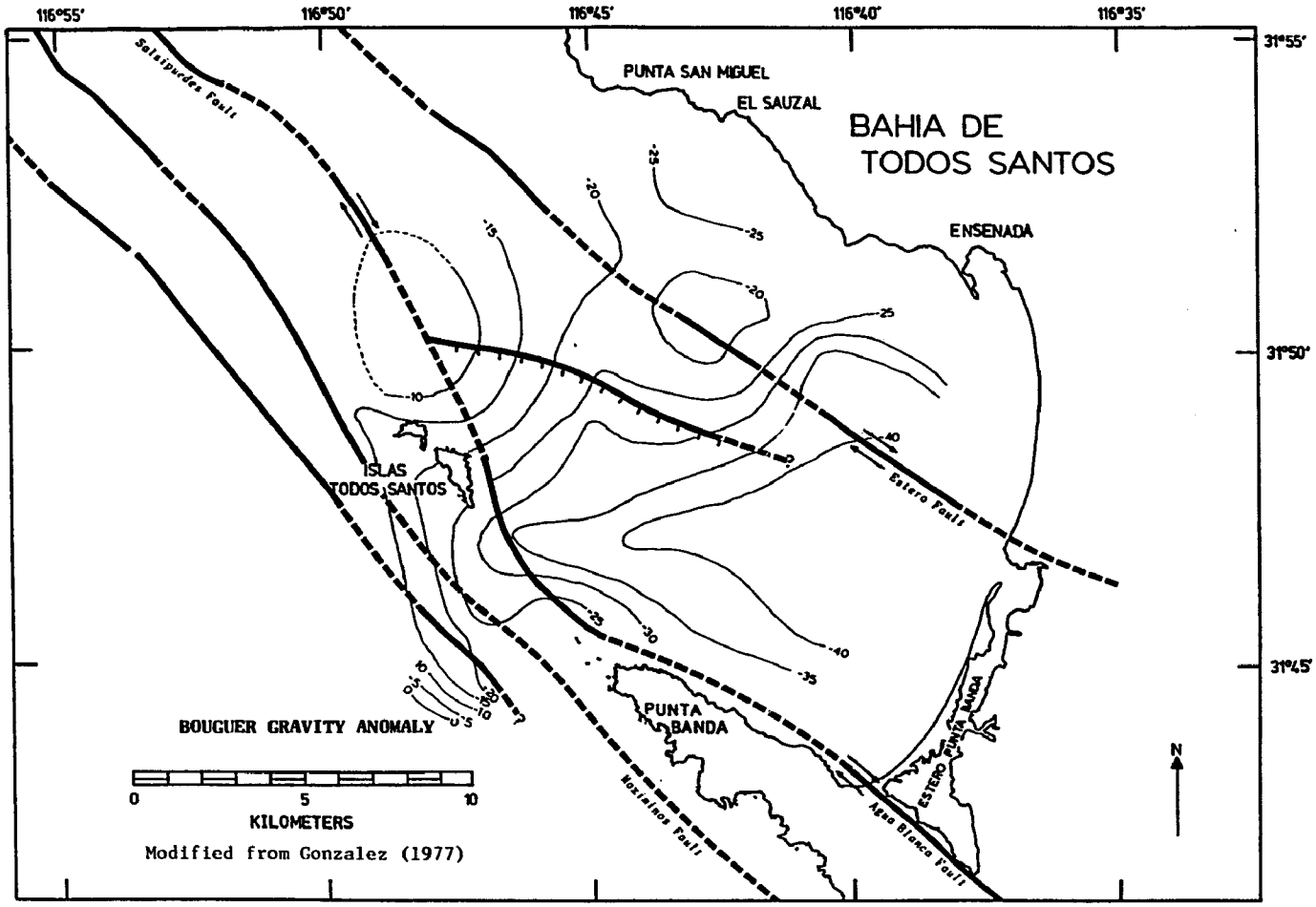


Modified from Gonzalez (1977)

better map the fault traces in this area.

Right slip for major faults of the offshore continuation of the Agua Blanca fault zone is inferred for this region based upon offset of the Banda Submarine Canyon (Maximinos branch), and a composite focal mechanism of earthquakes in Bahía Todos Santos reported by Gonzalez and Suarez (1981) for the Estero branch. Allen and others (1960) describe right-lateral offsets in stream channels along the north side of Punta Banda where the northern branch of the Agua Blanca fault passes. In the area offshore Punta Salsipuedes, southwest side up fault traces, which offset the seafloor locally (figure 9), are inferred to demonstrate right-lateral, oblique reverse-slip. Minor folds with axes lying subparallel to the fault traces in this area, support this interpretation.

From Bahía Descanso to the international border, the Coronado Bank - Agua Blanca fault zone may be somewhat less complex. The more easily identifiable fault traces of the Coronado Bank fault zone are characterized by two or more subparallel faults lying near the axis of the sediment filled basin between the Coronado Bank-Descanso Ridge and the coastline. These fault traces show evidence of divergent wrenching, such as negative flower structures in seismic profiles crossing the area (figure 5). At depth, this fault zone may juxtapose two different basement rock types, but the acoustic basement lithology at depth is unknown in this area. Other branches of the Coronado Bank fault zone lie along the eastern edge of the acoustic basement high which forms the Descanso Ridge and shelf. The easternmost zone of faulting, Descanso fault zone, possibly a continuation of the Estero fault zone, lies along the continental slope directly west of the mainland. This fault zone is interpreted to be composed of left-stepping, en echelon faults, with a few significant branches trending

northeasterly toward the coast. North of Punta Descanso, this fault zone is not accurately traced due to lack of good quality seismic data in the shallow, nearshore area. Magnetic data of Krause (1965) delineate the continuation of a nearshore fault zone, as well as the Coronado Bank fault zone all the way to Point Loma (figure 34).

The general character of the Coronado Bank fault zone within Bahía Descanso is that of a wrench fault. Again, the negative flower structure (chevron-shaped dilational synclines) observed in the seismic profiles indicate divergent wrenching, (figures 5 and 6). These faults generally do not displace the seafloor surface in this region. Other profiles show minor folding between the two principal fault traces (figure 35, line B-15) and changes in character of the apparent fault drag along strike. Line spacing between good quality seismic profiles, however, are inadequate to allow detailed mapping of the fault zone in this area as was accomplished for the San Clemente - San Isidro fault zone, discussed above, or the Coronado Bank fault zone offshore San Diego (Kennedy and others, 1980). The region around Islas Los Coronados unfortunately has few good data, and so the interpretations are rather uncertain there.

North of the international border and offshore San Diego, the faulting has been described in detail elsewhere (Kennedy and others, 1980a,b; Kennedy and Welday, 1980), but a brief summary of the structure in this region is presented here. "The Coronado Bank fault zone,..., is characterized by a series of both left- and right-stepping en echelon, mostly northwest-trending, subparallel faults" (Kennedy and others, 1980b). Seafloor relief is present along much of its length in this area, and most of the faults extend to within a few meters of the seafloor. The Coronado Bank fault zone offshore from San Diego can be divided into two parts, one lying adjacent to the

Figure 34. Magnetic anomaly profiles of Krause (1965) delineate the major nearshore fault zones of the Agua Blanca fault system.

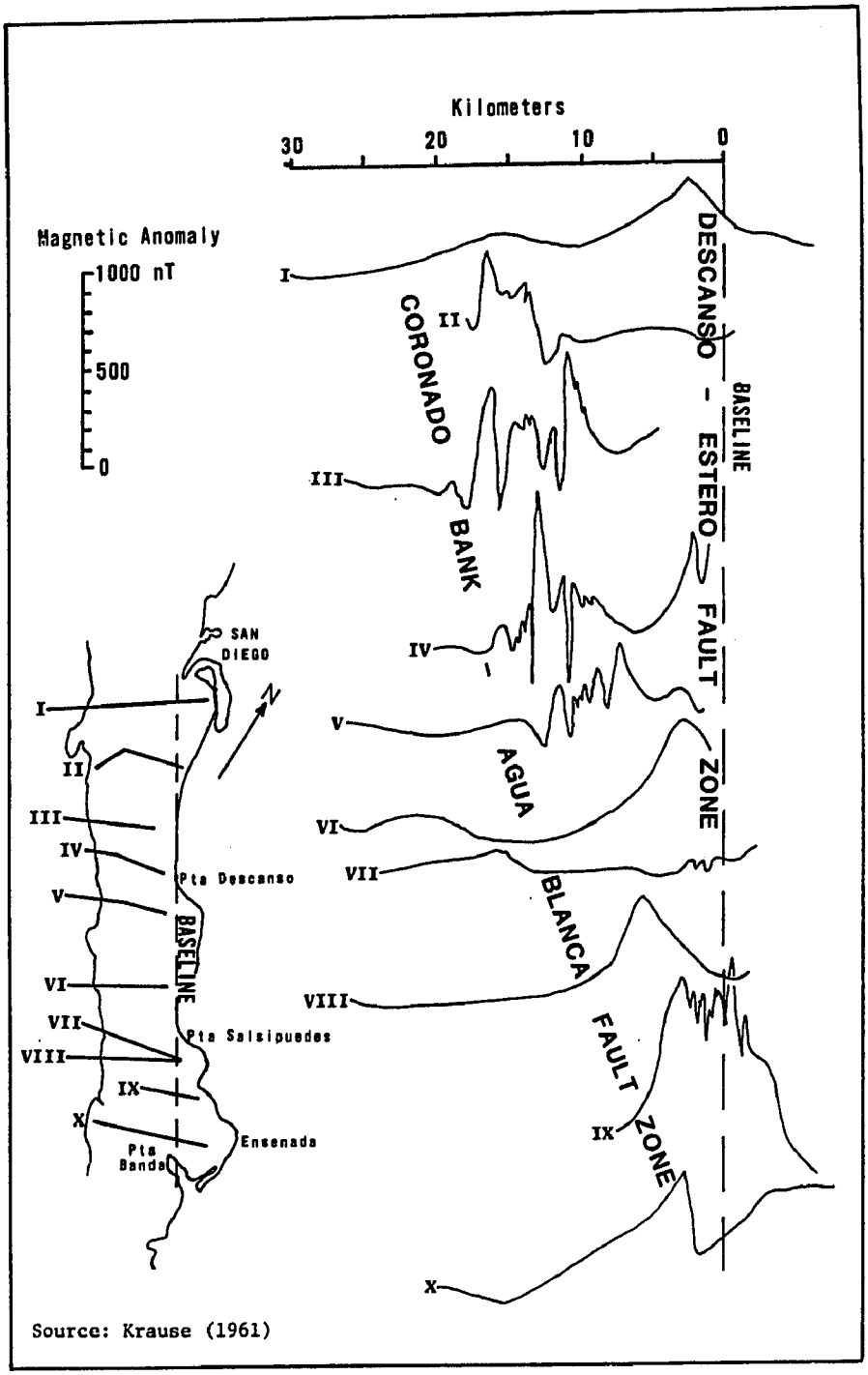


Source: Krause (1961)

Figure 35. Line drawings of sparker seismic profiles showing transpression along the San Clemente-San Isidro fault zone and transtension(?) along the Coronado Bank-Agua Blanca fault zone. (See figure 4 for profile locations). Several seismic sequences may be delineated in the basin sediments, but absolute ages of these units have not been determined.

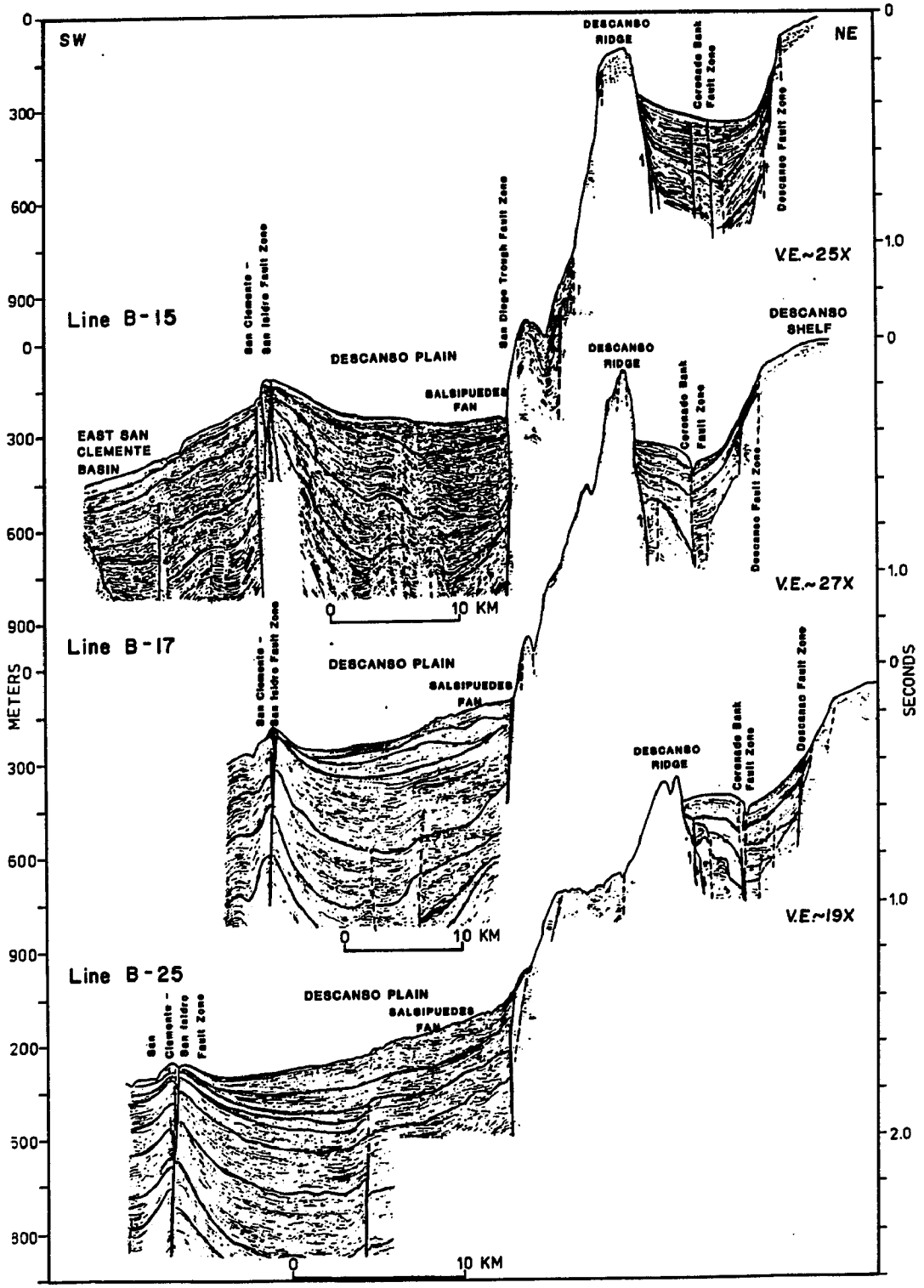
SW
NE
Line B-15
Line B-17
Line B-25
DESCANSO RIDGE
DESCANSO SHELF
DESCANSO PLAIN
SALSIPUEDES FAN
EAST SAN CLEMENTE BASIN
San Clemente - San Isidro Fault Zone
San Diego Trough Fault Zone
Coronado Bank Fault Zone
Descanso Fault Zone
V.E.~25X
V.E.~27X
V.E.~19X
0
10 KM
METERS
SECONDS
0
300
600
900
200
500
800
1.0
2.0

eastern flank of Coronado Bank, the second along the eastern side of Loma Sea Valley. The eastern fault zone is marked by two discrete faults, spaced about 500 m apart, similar to the fault zone within parts of Bahía Descanso.

The Rose Canyon fault zone is also characterized by left- and right-stepping en echelon faults, and has been divided into four sub-zones (Kennedy and others, 1980a). The westernmost lies mostly within older acoustic basement rocks and consists of relatively short, discontinuous segments. The La Jolla graben, through which the La Jolla submarine canyon passes, is formed by one central subzone of faulting. This zone also consists of short, discontinuous segments which displace surfical sediments and the seafloor in places. The nearshore subzone lies east of La Jolla submarine canyon and trends northwesterly from the coast, consisting of "discontinuous, subparallel, en echelon breaks similar to those observed onshore in the Rose Canyon fault zone" (Kennedy and others, 1980a). The fourth subzone of short, generally northeast-trending faults, although prominent onshore is not evident in offshore seismic profiles. Gentle S-shaped curvature of the main faults through the San Diego area, associated with alternating tectonic highs and lows, is proposed to indicate alternating zones of convergence and extension in a predominately right-lateral, wrench fault zone (Kennedy and others, 1980a).

Lastly, a prominent, northwest-trending fault lying a few kilometers southwest of Point Loma may represent an extension of the Descanso-Estero fault zone from offshore Punta Descanso. This fault apparently ends west of the tip of Point Loma, but an anticline extends northwestward along this same trend for a few kilometers. This fault may be related to the Rose Canyon fault zone but its significance is little understood at present. The numerous faults to the east, in the San Diego Bay and

offshore bight, may be a result of a major right step in the Rose Canyon fault zone. The San Diego Bay and offshore bight could be a large pull-apart basin associated with this right-step, appropriate for dextral wrench faulting.

The southward continuation of this prominent offshore fault zone cannot be accurately mapped with the present data, although magnetic profiles (figure 34, Krause, 1965) imply such continuation. The complexity of the faulting in this area is further demonstrated by the prominent north and northeast-trending faulting shown by Gastil and others (1975) onshore south of Tijuana. This complexity may be related to the convergence of the offshore Descanso-Estero Fault Zone with the onshore Rose Canyon and Vallecitos - San Miguel fault zones. The northeast trending graben is consistent with antithetic faulting in a right-lateral wrench fault zone.

## RECENCY OF FAULTING

Without substantial bottom sampling or drilling in the offshore region of this study, age of the faulted sediments and rocks can only be estimated using the acoustic character evident in the reflection profiles. The author (chapter 3, this volume) discusses the seismic stratigraphy devised for this area in some detail. A brief explanation of this stratigraphy and the symbols used to display the inferred age of faulting or folding is presented in this section.

As seen in plate 3, five different seismic-stratigraphic ages for faulting are defined for this study. The youngest age of the faulting is determined based upon the youngest stratigraphic unit for which offset is observed in the seismic profiles. In areas where the seafloor is offset (symbol shown on bar on relatively down-dropped side of fault), the minimum age of faulting may be considerably younger than the

offset strata, especially where older, acoustic basement is exposed.

Faults which offset the seafloor, or reach within a few meters of the seafloor (as observed on 3.5 kHz records) in basin sediments, are inferred to be Holocene in age. Emery and Bray (1962), Emery (1960), and Dunbar (1981) found that the Holocene - Pleistocene boundary was approximately three meters deep in the sediments of San Clemente Basin, San Diego Trough and Santa Catalina Basin. In areas of the most recent turbidite deposition from active submarine fans, there may be a significantly greater thickness of Holocene deposits. On the slopes and shelves, a thin layer of acoustically transparent material (observed on the 3.5 kHz records) is also inferred to be Holocene in age, as suggested by Kennedy and others (1980a,b) and Moore (1972).

The author (chapter 3, this volume) describes prominent acoustic horizons within the basin sediments of the area, and using sedimentation rates derived from isotopically dated samples from piston cores within the area, computes a late Pleistocene age (<700 ky.B.P.) for these horizons. Two of these horizons are evident in figures 8 and 11. Faults which offset strata above these horizons, but do not reach the seafloor are labelled late Quaternary as shown by the symbol in plate 3. Also, faults which are delineated by steep, seafloor escarpments that juxtapose older acoustic basement against basin sediments of late Quaternary age are inferred to be late Quaternary if evidence of fault drag in the young sediments abutting the fault is apparent (figure 8). If such evidence is absent, the fault is labelled late Tertiary - Quaternary, undifferentiated (e.g. Thirtymile Bank fault, figure 10). Near surface sediments along the more gentle slopes, slope aprons and the small fan in Bahía Descanso are also inferred to be late Quaternary in age.

Faults which do not cut these prominent late Quaternary horizons within the basin sediments, or do not reach within a few tens of meters of the seafloor in the sub-horizontal, well-bedded strata of the more gentle slopes, slope aprons, and nearshore embayments are labelled as Pleistocene faults. These faults extend above the acoustic basement into the overlying well-bedded strata, however.

In areas presently removed from direct turbidite influx, via submarine canyon/fan systems of the continental slope, late Tertiary-Quaternary undifferentiated age is assigned. Such deposits include the older(?), gently folded and tilted strata west of the San Isidro Ridge, slope deposits along the flanks of Thirtymile, Fortymile, Navy and Boundary banks and other, 'outer basin' sediments. Deepest strata, well-bedded but not acoustic basement within the major nearshore basins (San Diego Trough, Descanso Plain, and Ensenada Trough), are also considered late Tertiary-Quaternary undifferentiated in age. Flat lying, well bedded, presumably poorly consolidated (?) sediments ponded between the offshore ridges and the coast including the Coronado shelf and Bahía Todos Santos, are likewise, inferred to be late Tertiary-Quaternary in age.

Acoustic basement rocks are considered to be Tertiary or older. Outcrops of acoustic basement rock sampled in the area include Miocene sedimentary, volcaniclastic and igneous rocks (San Onofre Breccia, San Clemente Island volcanic rocks, Vedder and others, 1974); Mesozoic metamorphic rocks, (Catalina Schist), late Cretaceous sedimentary and volcanic rocks of the Rosario group, (Kennedy, 1975; Gastil and others, 1975), and Eocene rocks of La Jolla and Poway Groups (Kennedy, 1975). Pliocene rocks in the area are known from outcrops in the San Diego area (San Diego Group, Kennedy, 1975) but are not delineated in the offshore area for this study.

Other prominent acoustic horizons recognized in the offshore area may correlate with Plio-Pleistocene unconformities or disconformities, but the present data are inadequate to define such stratigraphic markers properly.

Finally, a simple, but crude, distinction between older and younger folds was made for this study. Younger folds, symbolized by the arrows, are in the well-bedded strata of the basins, slope aprons and some 'ponded' shelf sediments, such as Bahía Descanso. Older folds lie in acoustic basement units or the older, deeper sedimentary deposits of the nearshore shelf, as in offshore Tijuana. Significant overlap in ages of some of these folds may be present, but as a first approximation the distinction is believed valid for this study. Also, most(?) of the folds in acoustic basement rocks are much tighter than those of the young sediments, and with the vertical exaggeration present in the seismic data used for this study, many of these could not be accurately mapped on plate 3. In addition, deeper structure, below the penetration of the seismic profiles used for this study (>1-2 seconds) could not be identified.

## SUMMARY

Faults in the Inner Continental Borderland are divided into two major subsystems of the Pacific - North American tectonic plate boundary and the San Andreas fault system. The San Clemente fault system (Santa Cruz - San Clemente - San Isidro fault zones) in many ways resembles the larger San Andreas fault zone (figure 29 and 65, chapter 7, this volume). A major left bend, is associated with a transversely oriented folded and uplifted region analogous to the Transverse Ranges of perhaps an earlier era. Directly north of this bend is an elevated basement ridge, which may correspond to the Sierra Nevada. A major right step at the northern end of the fault

which curves through the bend has formed a pull-apart basin, analogous to Ridge Basin of Miocene age. South of the bend, the more northerly-trending San Isidro fault zone exhibits extensile character, similar to faulting within the Salton Trough. Although significant differences exist between the San Andreas and San Clemente fault zones, the similarities are striking enough to hint at common origins. More detailed study of the character and evolution of the San Clemente fault system may lead to significant insights regarding the tectonic evolution of the San Andreas fault system, and *vice versa*. Significant differences in the fault zones may be related to the different scales involved, different basement lithology and rheology, or different lithospheric/crustal dynamics.

The Agua Blanca fault system is significantly more complex that the San Clemente fault system. Three major wrench fault zones can be delineated in the Inner Borderland segments of the Agua Blanca fault system. Each of these major faults merges into the transpeninsular, Agua Blanca fault. This situation is analogous to the Alpine fault system in New Zealand which splays into the several Marlborough faults (figure 36; Freund, 1974). The transition from the more westerly-trending Baja California, Peninsular Ranges faults to the more northerly-trending, Borderland faults occurs within a relatively short distance (10-20 km). This transition region marks the structural and physiographic boundary between the Peninsular Ranges and the California Continental Borderland and may locate a significant basement boundary as suggested for the Newport - Inglewood fault zone (Barrows, 1974). Data of this study are inadequate to describe the basement lithology across the offshore region, however.

Figure 36. Map comparing the Alpine-Marlborough fault system to the Agua Blanca fault system. Note the different scales used in order to emphasize the similarities in the mapped fault patterns. Also, New Zealand has been reoriented so that the faults of the two fault systems appear sub-parallel on the figure.

Alpine-Marlborough Fault System
New Zealand

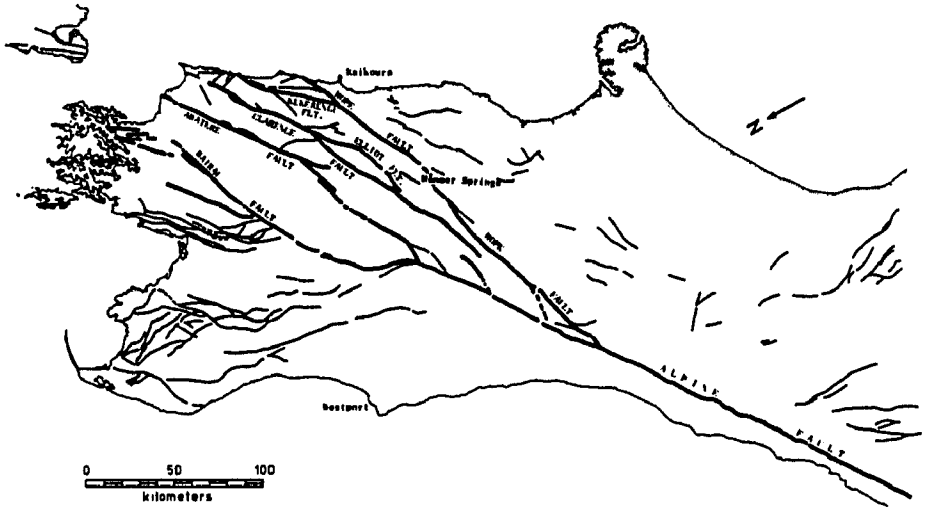


Agua Blanca Fault System
Baja California

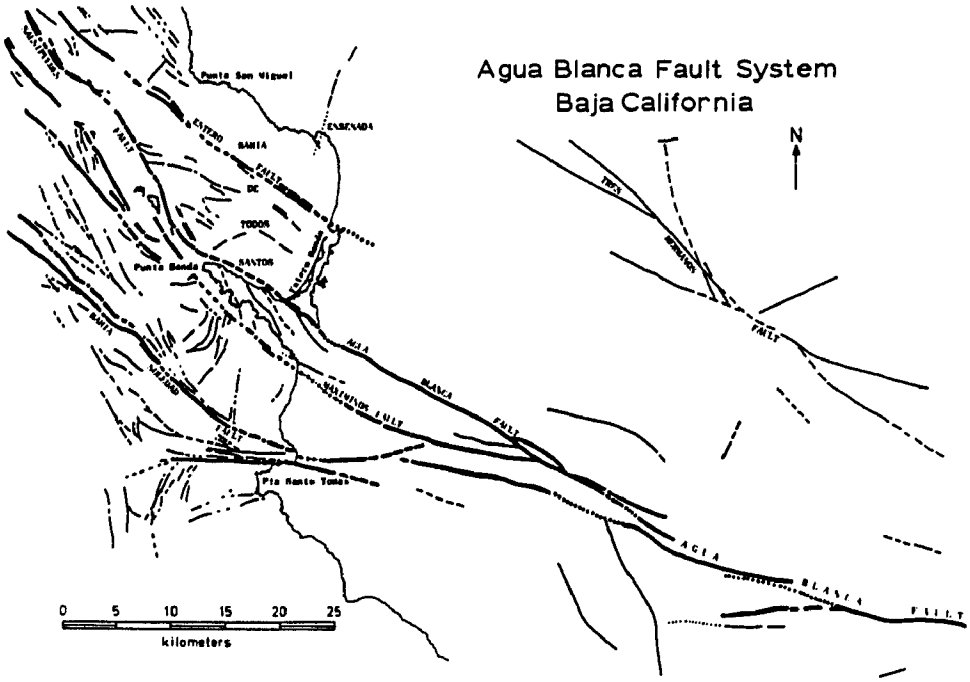

Although most of the individual fault traces are relatively short and discontinuous within the Agua Blanca fault system, several significant exceptions are apparent. The San Diego Trough and Bahía Soledad faults both are shown to be straight and continuous for lengths of several tens of kilometers (plate 3). Likewise, the Agua Blanca fault from Punta Banda eastward across Baja California is relatively straight and continuous. The complexity of both structure and bathymetry throughout much of the offshore parts of the Agua Blanca fault system makes accurate delineation of the many fault traces more difficult in this area.

Finally, the offshore, Santo Tomás fault (Krause, 1965; Moore, 1969) does not connect with the south branch of the Agua Blanca fault but is truncated by the San Isidro fault zone. The overall tectonic significance and detailed character of this important Borderland fault remain to be determined.

## CONCLUSIONS

Several important conclusions regarding the structural style and recency of faulting within the Inner Borderland can be made based upon the data discussed in the preceding sections. In general, the structural style of the region is that of dextral, parallel, wrench faulting, although locally, regions of convergent or divergent wrenching are present. The overall trend of the principal fault traces and presumably the underlying 'master' wrench faults in the Inner Borderland (N30°-40°W) are distinct from those of the Peninsular Ranges. On this basis, I conclude that the Inner Borderland is a distinct structural and physiographic province. The systematic association of dilational structure where principal fault traces step or bend to the right, and convergent structure at left bends or steps, conclusively demonstrate the right

slip nature of these faults. Additionally, dextral offset of submarine fan facies, submarine canyon channels, and other topographic features is apparent in some places.

Age of faulting as determined in this study, varies from Mesozoic(?) to modern. Most of the faults observed within the basins are late Cenozoic in age, and differentiation based upon a simple seismic stratigraphy divides these into four age groups. A fifth group includes older(?) faults in acoustic basement rocks. Principal fault traces of each of the major wrench fault zones show evidence of late Quaternary (<700 ka) to Holocene movement (including seafloor offsets). Several of the branch and secondary faults associated with these zones are inferred to be older, because they are apparently buried by the younger basin sediments. Major faults along the basin margins, which juxtapose acoustic basement rocks against Quaternary sediments, in some areas show evidence of Quaternary movement, (such as drag folds in the Quaternary deposits, whereas others are inferred to be older because the younger deposits appear to be undisturbed in seismic profiles). Age of faulting in areas of acoustic basement outcrops cannot be determined precisely, but continuation of some of these fault traces into younger basin sediments implies late Cenozoic to Quaternary movement.

# CHAPTER 5

# SEA BEAM SURVEY OF AN ACTIVE STRIKE—SLIP FAULT

## INTRODUCTION

Seafloor topographic mapping was one of the first methods used to identify major structural features covered by the oceans. Recognition of the Mid-Atlantic Ridge and other mid-ocean ridges helped investigators to formulate the basic ideas of continental drift and seafloor spreading. Offshore of southern California, Shepard and Emery (1941) used bathymetric maps to infer that the ridge and basin topography is structurally controlled. Major northwest-trending faults, similar to those observed on land nearby, were concluded to be delineated by long, linear, steep, escarpments which bound the major offshore ridge and island blocks. For example, the San Clemente fault is delineated by the prominent escarpment along the eastern flank of San Clemente Island (figure 37).

More recent oceanographic studies have used seismic reflection profiles to map offshore geologic structure, identifying faults by the offset of acoustic reflectors (e.g., Moore, 1969; Ridlon, 1969; Vedder and others, 1974). The seismic reflection method is well-suited to map sub-bottom structure in areas of low relief and gentle slopes ($<15^{\circ}$). In rugged areas, however, because of the relatively wide beam width of these acoustic systems, sub-bottom features, and in many instances, the bottom reflection itself (directly beneath the ship) are not recorded, or are masked by acoustic reflections from adjacent topography.

Figure 37. Portion of National Ocean Survey bathymetric contour map showing North San Clemente Basin and surrounding regions. Rectangle outlines region of detailed Sea Beam bathymetric survey. Note differences between shapes of prominent seafloor features mapped from the conventional echo sounding data (NOS charts, this figure) and the detailed Sea Beam, multi- narrow-beam, echo sounding data (figure 38, plate 4). Parts of NOS (1974) charts 1206N-15 and -16 are shown.

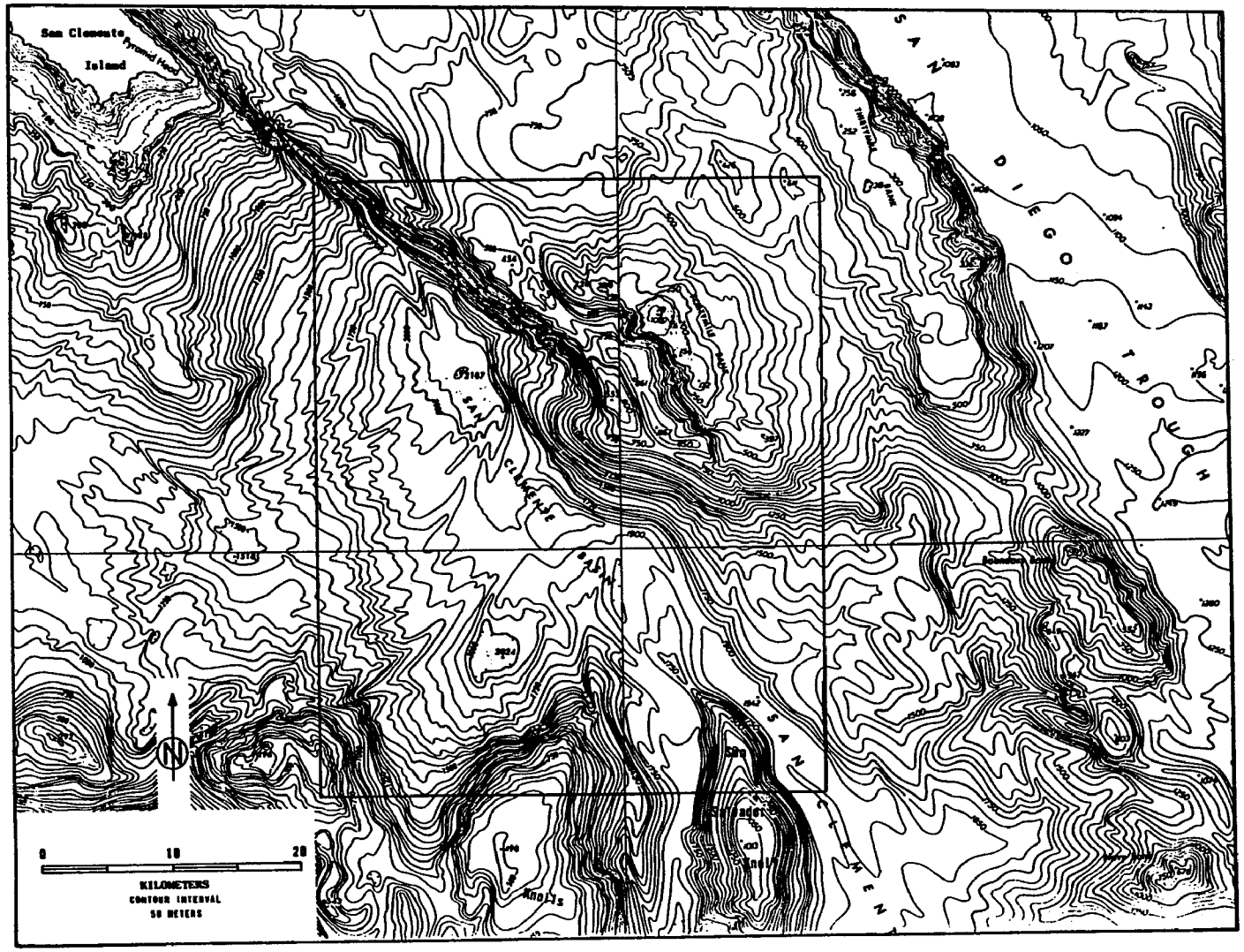
San Clemente
Island
Pyramid Head
SAN DIEGO TROUGH
SAN CLEMENTE BASIN
SAN CLEMENTE
Knolls
0
10
20
KILOMETERS
CONTOUR INTERVAL
50 METERS

Figure 38. Sea Beam bathymetric map of the San Clemente fault zone in the vicinity of Fortymile Bank and North San Clemente Basin. Areas of closely spaced contours (20 m contour interval) identify Sea Beam swath coverage. Contours shown by dashed lines are extrapolated beyond the areas of Sea Beam coverage. Tick marks point in the downslope direction. Some contours have been deleted in areas of very steep slopes to improve map legibility (see plate 4 for complete contour map of region).

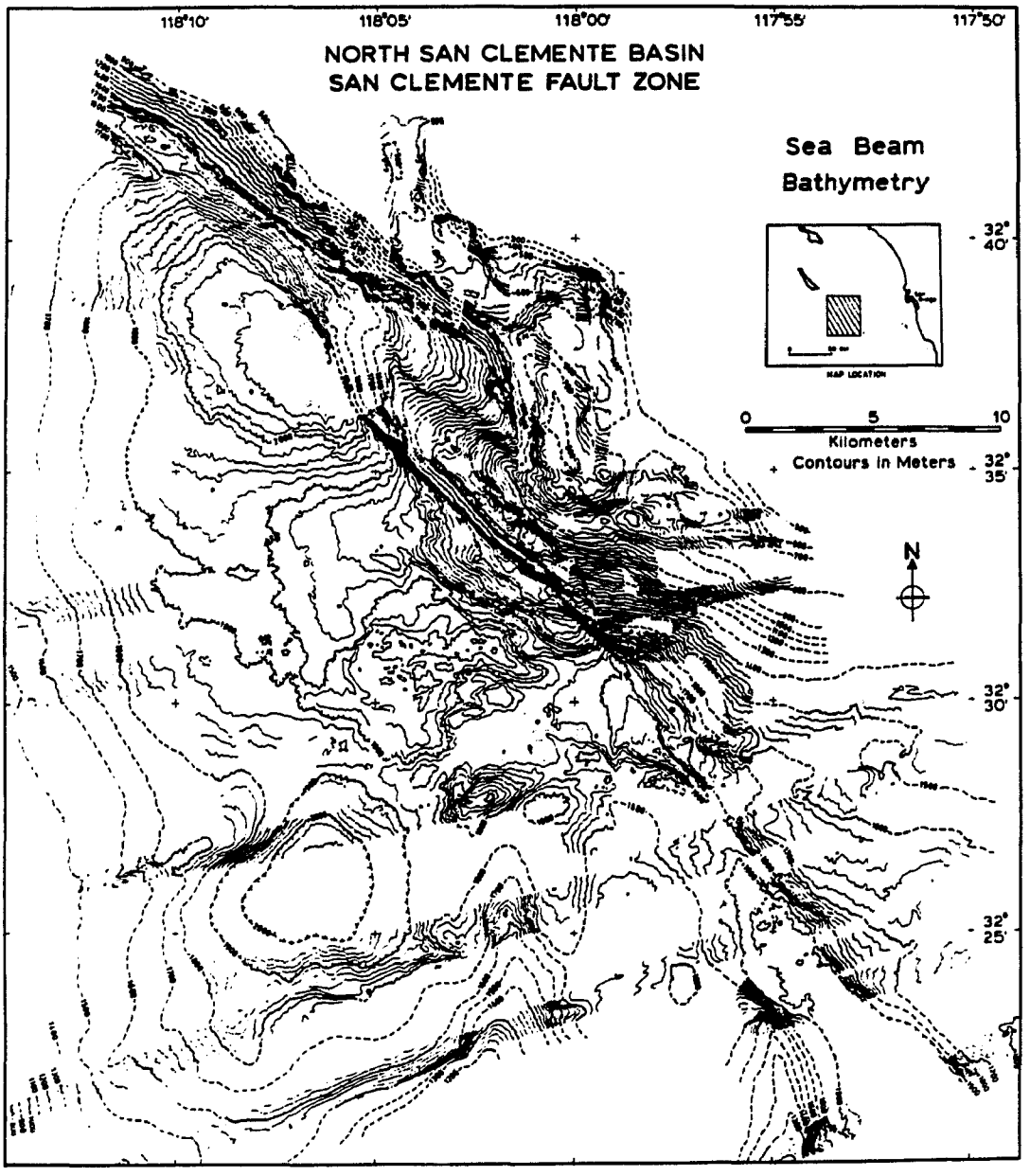
118°10'
118°05'
118°00'
117°55'
117°50'
NORTH SAN CLEMENTE BASIN
SAN CLEMENTE FAULT ZONE
Sea Beam
Bathymetry
32° 40'
0 5 10
Kilometers
Contours in Meters
32° 35'
N
32° 30'
32° 25'

Figure 39. Location map of seismic profiles and other detailed figures shown in this study. Figure numbers are identified for location of each figure with respect to the regional bathymetry. Names given to prominent bathymetric features are also shown.

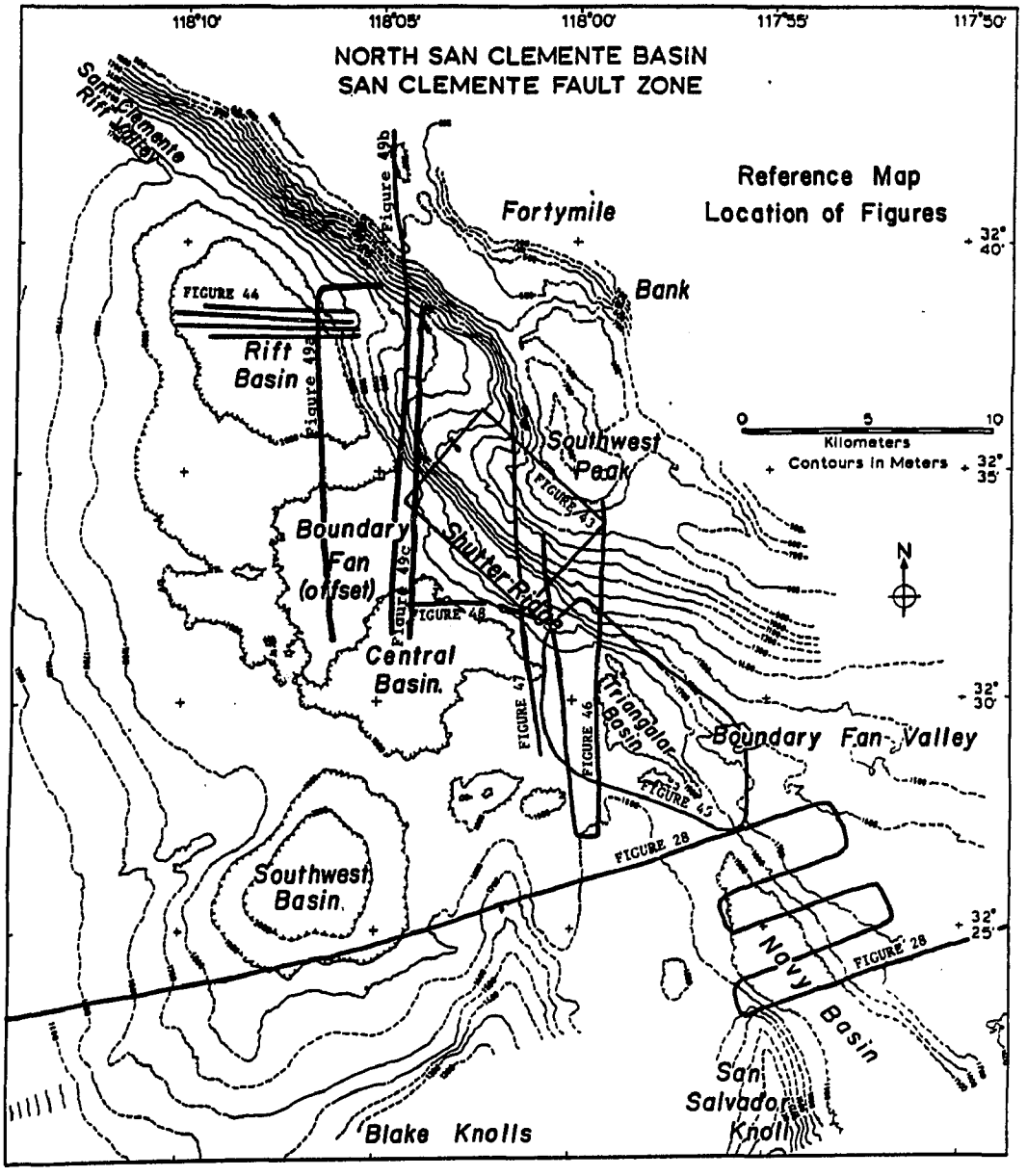
118°10'
118°05'
118°00'
117°55'
117°50'
NORTH SAN CLEMENTE BASIN
SAN CLEMENTE FAULT ZONE
San Clemente Rift Valley
Reference Map
Location of Figures
Fortymile
Bank
32° 40'
FIGURE 44
Rift Basin
Figure 49a
Figure 49b
Figure 49c
Southwest Peak
FIGURE 43
0 5 10
Kilometers
Contours in Meters
32° 35'
Boundary Fan (offset)
Shutter Ridge
FIGURE 48
Central Basin
FIGURE 47
FIGURE 46
Triangular Basin
FIGURE 45
Boundary Fan Valley
32° 30'
FIGURE 28
Southwest Basin
32° 25'
Navy Basin
San Salvador Knoll
Blake Knolls
N

Marine geologists use detailed maps of the bathymetry to infer fault connections between seismic profiles. In areas of abundant sounding data, bathymetric contours delineate many features of possible tectonic origin. Structural geologists in land-based studies have recognized many geomorphic features which are characteristic of recently-active faulting. These features recognized from aerial and satellite photographs, RADAR and other remote sensing imagery, and reconnaissance field work have been used for many years to map the recently-active traces of major faults. Unfortunately, the limitations of conventional echo-sounding methods, such as the broad beam width of the sounding system, poor navigation, and lack of numerous closely-spaced soundings precluded recognition of all but the largest of such geomorphic features in the submarine environment. Detailed high-resolution, precisely navigated, near bottom studies including Deep Tow have provided detail necessary to map seafloor features accurately on a scale more appropriate for identification of tectonic landforms (figure 40; cf. Normark and others, 1979). More recently, a multibeam, narrow-beam, echo-sounding system, Sea Beam has become available to oceanographers, allowing accurate and more precise mapping of seafloor topography over large areas. Several short, test cruises using the recently operational Sea Beam aboard the Scripps Institution of Oceanography R/V Thomas Washington were conducted in the California Continental Borderland offshore San Diego. This paper describes the detailed investigation, using Sea Beam, of a 50 km length of the San Clemente fault zone in a region of rugged topography (figures 37 and 38). Additional marine geophysical data, including high-resolution seismic reflection profiles and near bottom (Deep Tow) data were used to assist in the interpretations of the seafloor structure.

Figure 40. Graph showing relative size of tectonic geomorphic features and the limits of resolution of various marine survey techniques (modified from Normark and others, 1979).

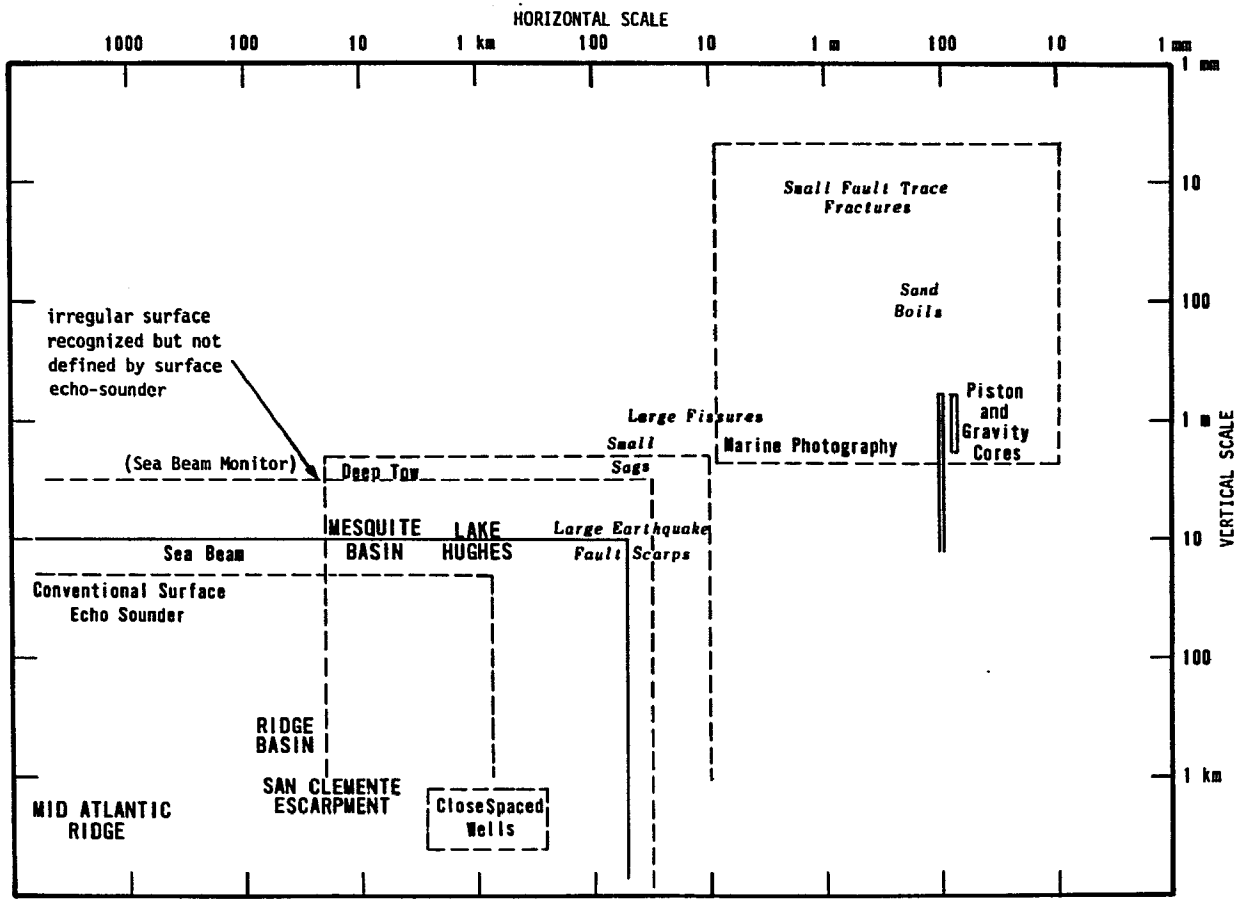
HORIZONTAL SCALE
1000
100
10
1 km
100
10
1 m
100
10
1 mm
VERTICAL SCALE
1 mm
10
100
1 m
10
100
1 km
Small Fault Trace Fractures
Sand Boils
Piston and Gravity Cores
Large Fissures
Small Sags
Marine Photography
irregular surface recognized but not defined by surface echo-sounder
(Sea Beam Monitor)
Deep Tow
MESQUITE BASIN
LAKE HUGHES
Large Earthquake Fault Scarps
Sea Beam
Conventional Surface Echo Sounder
RIDGE BASIN
SAN CLEMENTE ESCARPMENT
CloseSpaced Wells
MID ATLANTIC RIDGE

**BACKGROUND – Regional Geology and Tectonic Framework**

The late Cenozoic tectonic history of the southern California region has been dominated by interaction between the Pacific and North American tectonic plates (Atwater, 1970). The San Andreas fault system (Crowell, 1962) consists of several major, northwest-trending, dextral wrench fault zones, and forms the broad, continental transform fault boundary between the Pacific and North American plates. This broad transform fault boundary is inferred to extend offshore and include major northwest-trending faults such as the San Clemente fault (Legg and Kennedy, 1979). Although some have proposed that Miocene east-west extension and block faulting account for Borderland structure and physiography (Yeats, 1976), right-lateral wrenching along major northwest-trending shear zones has been recognized for many late Cenozoic structures within the Borderland (Crouch, 1981; Junger, 1976; Legg and Kennedy, 1979; Greene and others, 1979; chapter 4, this volume).

Relative displacements of once continuous features across major Borderland fault zones have not been accurately determined to date, although many hypotheses of significant lateral slip have been proposed. Most proponents of large lateral displacements maintain these occurred during Miocene time (Howell and others, 1974; Howell, 1976; Yeats, 1976; Kies and Abbott, 1983; Crouch, 1979) citing offset of geologic markers such as the Eocene conglomeratic suite found in the San Diego area and offshore on the northern Channel Islands.

Estimates of late Cenozoic, that is, post Miocene, displacement on Borderland faults have generally been small (Junger, 1976; Junger and Vedder, 1980 personal communication). Some have postulated that a significant proportion (20% - 33%) of the overall relative plate motion is taken up on offshore faults (Anderson, 1979; Weldon

and Sieh (1985). Shepard and Emery (1941) first proposed 40 km (25 miles) of right-slip along the San Clemente fault by restoring Fortymile Bank to a position adjacent to San Clemente Island. Kennedy and others (1980) postulated 2.5 km of right-slip on the offshore Rose Canyon fault zone, realigning the axes of the La Jolla and Scripps submarine canyons. Legg and Kennedy (1979) and the author (chapter 7, this volume) have proposed dextral offsets of a few kilometers for other submarine canyons which cross the major fault zones of the Inner Continental Borderland.

Recognition of characteristic linear geomorphic features such as channels, which are offset across active submarine fault zones, may provide additional indicators of lateral slip in the Borderland. Truncated end points of linear features offset by lateral slip on faults provide true 'piercing points' from which the amount and sense of strike-slip can be accurately(?) determined. Age determinations of the offset features then allows estimation of the slip rate on the faults in question. Sieh (1978, 1984), Sieh and Jahns (1984) and Weldon and Sieh (1985) have had much success in mapping offset geomorphic features across the San Andreas fault in southern California, and estimating the late Quaternary slip for this major subaerial fault zone. Accurate, detailed bathymetric maps of *submarine* fault zones may provide information to identify similar geomorphic features offset across submarine fault zones.

**METHODS – Narrow Beam Echo Sounding**

Resolution of small scale seafloor features ('mesotopography' as defined by Normark and others, 1979) has been accomplished in past studies through the use of expensive near-bottom surveys over small areas, or with the few narrow-beam echo sounders then available (figure 40). More recently, side-scan SONAR, towed at rela-

tively shallow depths has been useful in mapping seafloor morphology over large areas (e.g. GLORIA, Searle, 1976; Field and others, 1984; Sea MARC, Batiza and others, 1984). Sea Beam has recently proven very useful in compiling detailed bathymetric maps allowing identification of geomorphic features associated with many seafloor processes (Renard and Allenou, 1979; Macdonald and others, 1984; Mammerickx, 1984; Batiza and others, 1984). With its narrow beam width, the Sea Beam system is very useful in detailed mapping of rugged seafloor topography, and many interesting features, including offset spreading centers, submarine canyons and channels, seamount craters and calderas, and submarine landslides have been observed.

**Sea Beam Acoustics***

Sea Beam generates, in near real time, contour maps of the seafloor while the ship is underway, using a multibeam, narrow beam echo-sounder (12 kHz) and an echo processor. The Sea Beam transmit/receive beam geometry is shown in figure 41. The transmitted beam pattern spans 54° athwartships by 2 2/3° in the fore-and-aft direction. The transmitted beam pattern spans 54° athwartships by 2 2/3° in the fore-and-aft direction. This beam is pitch stabilized to within 10° of vertical projection. Beam forming by the Sea Beam system results in a receiving beam pattern approximated by 16 adjacent rectangles, 2 2/3° by 20°. The resulting acoustic energy received at the ship comes from the intersection of the transmit and receive beam patterns as shown in figure 41.

Resolution of seafloor topography is related to the area insonified by each beam 'footprint' and is a function of the overall water depth beneath the ship. For 1000 m

---

* A more detailed description of the Sea Beam system is given by Renard and Allenou (1979).

Figure 41. Sea Beam transmit/receive beam geometry. Transmit beam pattern is narrow (2 2/3°) in the fore-and-aft direction, and sixteen long, narrow receive beam patterns are formed by the echo processor receiver array.

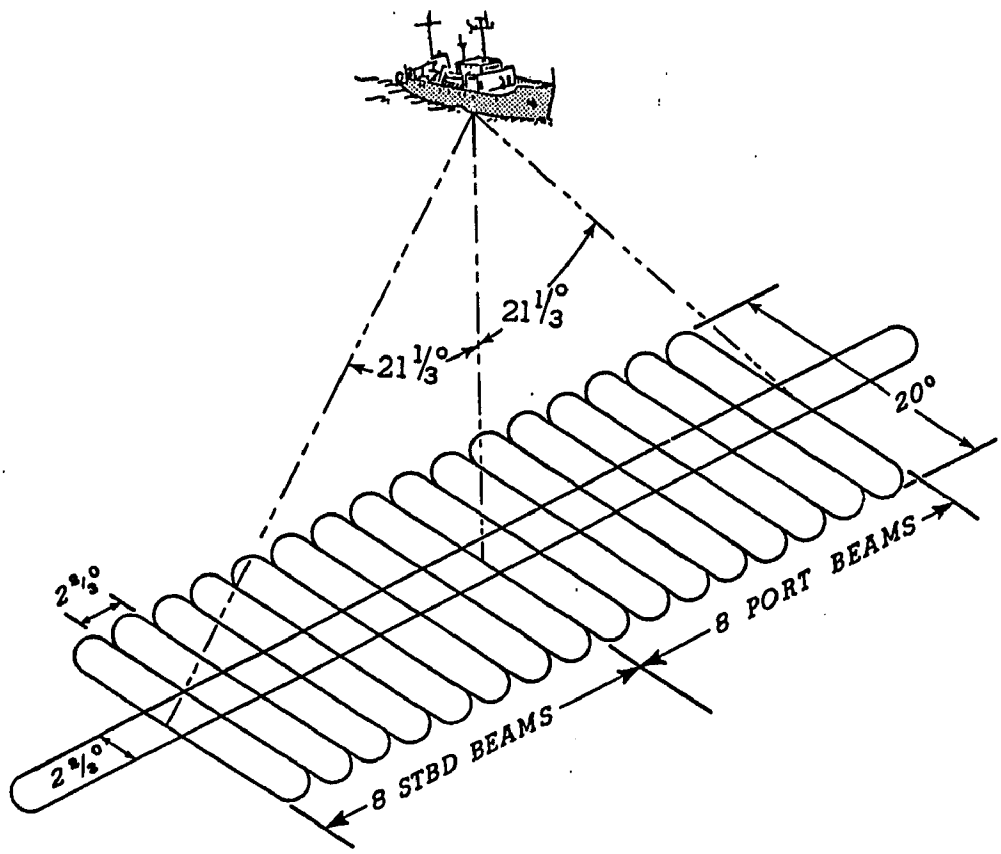
21 1/3°
21 1/3°
20°
2 2/3°
2 2/3°
8 PORT BEAMS
8 STBD BEAMS

of water depth, a footprint approximately 50 m square is covered by each beam. Renard and Allenou (1979) found a mean accuracy for all beams of about 10-15 m for the recorded depth. The center beam is monitored on an analog recorder (Universal Graphic Recorder), and the accuracy of the monitor beam depth is within 2-3 m.

**Navigation**

Because the swath width covered by each Sea Beam 'ping cycle' is depth dependent (up to 80% of the overall depth), accurate navigation of the ship becomes extremely important in relatively shallow areas so that slight overlap of swaths is achieved for correlation of adjacent swaths. For depths of from 1 to 2 km, as in this study, line spacing of about 1 km is desireable.

Several different Sea Beam test cruises collected the data used in this study; consequently, different navigational systems were used, and accuracies varied accordingly. A large part of the area was surveyed using LORAN-C radionavigation with fixes every 21 seconds, combined with occasional satellite and RADAR positions. Systematic error present in the LORAN-C data was corrected using the best available satellite fixes in the area. Error ellipses for satellite fixes were generally smaller than 0.2 nautical miles on a side. In addition to the systematic error in the LORAN navigation, a random error in position of about $\pm 0.3$ nautical mile in latitude and $\pm 0.05$ nautical mile in longitude was observed. This 'jitter' was removed by low-pass filtering of the data. The uncorrected data showed significant mismatch of contours between adjacent lines, whereas the smoothed data showed excellent fit, with alignment of contours between overlapping adjacent swaths. Further navigational refinement was accomplished in the post-processing stage by matching contours from

swaths on adjacent and crossing ship tracks.

Some data used in the present study had relatively poor navigation. At times, the redundant LORAN data were not available to allow the smoothing process to be applied. For these other cruises, occasional LORAN fixes were obtained along with infrequent satellite and RADAR positions. For long, straight cruise tracks, the few available data were adequate to locate each line approximately, and final positioning was accomplished in the post-processing stage, matching the depth contours to those of the more accurately navigated areas.

**Post-Processing of Sea Beam Data**

Even with the 'best' possible navigation, contours plotted from the raw Sea Beam data on overlapping or intersecting lines often do not match exactly. In some instances, features appear on tracks crossing structure in one direction, but are absent on data collected at right angles. Also, because of the discrete sampling of the bathymetric data, the depth points sampled on overlapping or intersecting lines will, in general, not be in exactly the same positions. When the Sea Beam contouring programs are applied to data on the different tracks, different contour shapes may result, especially in areas of low relief. Various post-processing techniques are applied to the Sea Beam and navigational data so that accurate bathymetric charts can be prepared in the desired format (cf. Desnoes, 1980; Edwards and others, 1984). Minimum distortion of features, and matching of contours in shape and position between overlapping swaths on the final plots is the desired result of the post-processing procedures.

Increased accuracy of the Sea Beam contours is obtained through smoothing by averaging over several 'ping cycles' (Desnoes, 1980). The real-time contouring does not involve this smoothing, and so more detail is apparent in the contours. This apparent detail is often not real, especially in flat or smooth areas, the contours shown resulting from noise in the system or due to poor side-lobe rejection of a strong bottom return, and sometimes from interference of other acoustic signals such as the 3.5 kHz echo-sounder. Five cycle averaging was used in this study, because at a survey speed of 9 knots, in water depths of 1-2 km from 3-6 ping cycles were obtained for each area the size of the Sea Beam footprint.

Preliminary contour plots of the various Sea Beam cruise data were prepared at 50 m contour intervals. Swath matching of these data then allowed repositioning of the data to prepare more accurate final charts. Using the best navigated data as a base, the other data were adjusted to fit matching contours on adjacent and crossing swaths. When a relatively satisfying fit between the various Sea Beam plots was achieved at the 50 m contour interval plots of these data at 10 m and 20 m contour intervals were prepared. The final bathymetric chart (plate 4, figure 38) was hand-drawn from these plots, and overlain on a light table so that a 'best' fit of contours was achieved.

The final chart is consistent with the overall 10-15 m accuracy of Sea Beam data as reported by Renard and Allenou (1979). Sufficient detail to delineate major geomorphic features as well as adequate smoothing to improve overall accuracy of the data is provided by the 20 m contour interval. Real time contouring at 5-10 m contour intervals was accomplished for most of the region. These raw data are useful in showing details of features not apparent at the larger contour interval, providing one

considers overall resolution of the system and compares data from intersecting swaths.

Overall accuracy of the final map is estimated to be better than 500 m in geographic position and better than 200 m in relative position over most of the area. Depth accuracy is approximately 10-15 m as mentioned above. Features as small as 50-100 m are resolved, although the shape of these small features is not resolved. Many small features apparent in the flat areas may not be real, although, some minor relief in these areas is apparent from the center beam (12 kHz monitor) data.

**Supplementary Data**

Additional data were collected during the cruises which provided the Sea Beam data for this study. High-resolution seismic reflection data including airgun and 3.5 kHz sources, Deep Tow side-scan SONAR, shallow penetration seismic and near bottom magnetometer data, and surface total magnetic field intensity data were collected over various parts of the study area. These additional data provide constraints on the structural and tectonic interpretations made from the bathymetric data using geomorphic principles. Descriptions of the nature and theory regarding these other data types are published elsewhere (Moore, 1969; Spiess and Tyce, 1973).

## TECTONIC LANDFORMS ALONG RECENTLY ACTIVE FAULTS

Landforms produced along active strike-slip faults are shown in figure 42. Detailed description of the various tectonic and non-tectonic landforms associated with active faults are discussed elsewhere (Lawson, 1908; Slemmons, 1977; Patterson, 1979; Davis, 1982). For the present study, a brief description of the method used to identify tectonic landforms from detailed Sea Beam bathymetric contour plots

Figure 42. Block diagram showing tectonic landforms commonly observed along recently-active, terrestrial (subaerial), strike-slip faults. Many of these features may be observed along the *submarine* San Clemente fault in the area of this study.

## BLOCK DIAGRAM SHOWING LANDFORMS PRODUCED ALONG RECENTLY ACTIVE FAULTS

A. SCARP
B. FACETED RIDGE
C. LINEAR TRENCH
D. LINEAR VALLEY
E. LINEAR RIDGE
F. SHUTTER RIDGE
G. NOTCH
H. HILLSIDE VALLEY
I. BENCH
J. OFFSET CHANNEL
K. SPRING
L. DEFLECTED CHANNEL
M. OFFSET RIDGE
N. DEPRESSION (SAG POND)
O. DEPRESSION (BASIN)
P. PONDED SEDIMENT

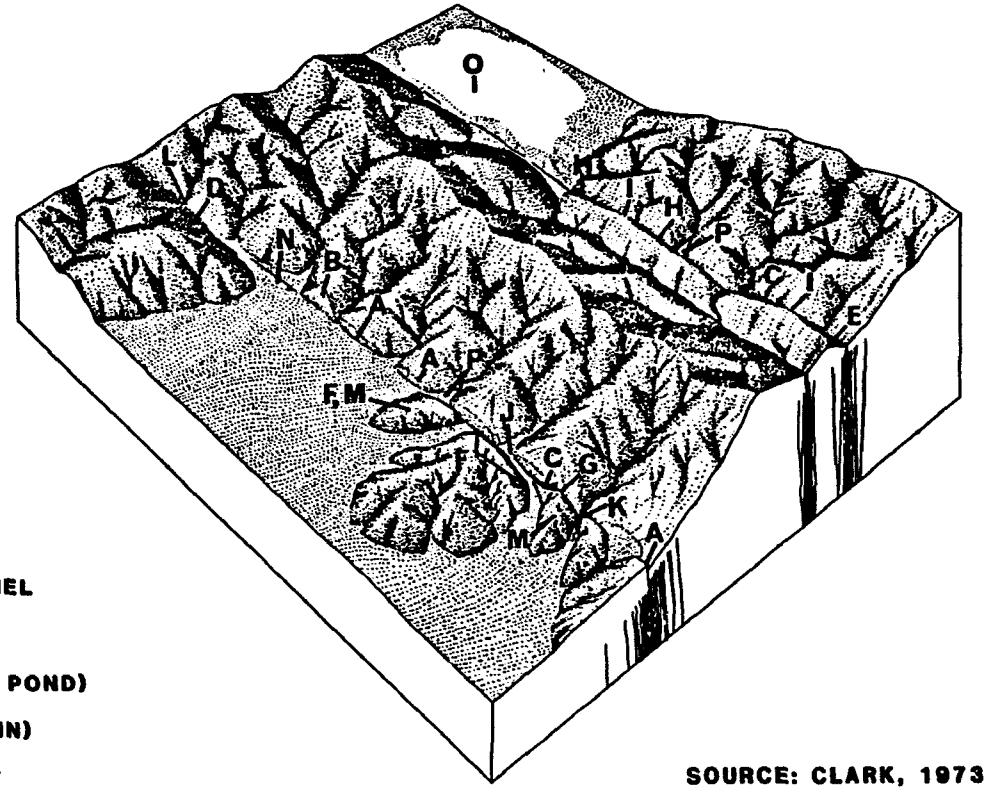


SOURCE: CLARK, 1973

follows.

Resolution of seafloor topographic features with Sea Beam data limits one to the identification of the major geomorphic features along active faults. Minor features, commonly formed during single tectonic events, such as fissures, small scarps and fault traces, have been identified on the seafloor by other means, such as Deep Tow and bottom photography. Major features, as shown in figure 42, should be recognizable on Sea Beam contour charts. Land based studies rely upon the geomorphic features to identify, trace and characterize active faults (Slemmons, 1977). These features are often first recognized from aerial including low sun angle and satellite photographs, side-looking RADAR or field reconnaissance. Later field work is necessary to confirm fault identifications made from remote imagery.

Field work on the seafloor is very difficult, of course, and expensive, although remote sensing provided by Sea Beam, seismic reflection profiling, and other methods are readily accomplished. The combination of various marine geological and geophysical data may provide enough information to verify interpretations made from bathymetric data alone. For this study, the principal criterion used for recognizing tectonic landforms is the identification of numerous seafloor features resembling those shown in figure 42. The alignment of numerous characteristic 'tectonic landforms' may provide convincing evidence of an active fault zone.

Lineaments are among the most common features observed in remote imagery of active fault zones. On the seafloor, lineaments include strongly linear features such as scarps, trenches and troughs, valleys and ridges, and the large escarpments alluded to in previous sections. Other seafloor lineaments include alignments of smaller, or more irregular features such as depressions or sags, saddles, notches,

linear channel segments, and sediment wave crests and troughs. Additional data, such as seismic reflection profiles which show offset sub-bottom reflectors, are desireable to confirm tectonic origins for seafloor lineaments. In the absence of such supportive data, the presence of numerous characteristic landforms along the principal lineaments observed may identify active tectonic features.

Tectonic and other geomorphic landforms interpreted from the Sea Beam data of this study are shown on plate 5. Scarps inferred to be tectonic in origin are very straight and generally steep, with lengths from several hundred to thousands of meters. Scarps of non-tectonic or uncertain origin are generally curved. Compound scarps, showing more than one principal slope gradient, are identified on plate 5, and may represent different episodes of tectonic activity, tectonic scarp modification by other geomorphic processes, or multiple, subparallel active fault strands in the region. Slump or slide scarps are arcuate in plan view, and have downslope bulges where the slide mass came to rest. Faults identified from seismic reflection profiles are identified with a special symbol astride the fault if the seafloor is not displaced, or attached to a bar on the relatively downthrown side of the fault where the seafloor is offset. The recency of faulting inferred from the seismic data is shown by the type of symbol. The author, (chapter 4, this volume) provides a more detailed description of the seismic stratigraphy used to infer age of faulting in the Inner Continental Borderland of southern California. Most of the features plotted on plate 5 were, however, identified solely from the Sea Beam bathymetric chart (plate 4).

# DISCUSSION

## TECTONIC LANDFORMS ALONG THE SAN CLEMENTE FAULT ZONE

The San Clemente fault zone separates the elevated basement structure of Fortymile Bank from the deep, irregularly-shaped North San Clemente Basin. Numerous scarps, linear ridges, valleys and trenches, aligned depressions, and larger fault-bounded basins delineate the recently-active fault traces (plates 4 and 5). Secondary tectonic and non-tectonic landforms are useful in determining the character of faulting and possibly imply lateral offsets. High-resolution seismic profiles assist in defining tectonic origins of seafloor features as well as recency of fault activity in the area.

### Principal Trace of the San Clemente Fault

The principal trace* of the San Clemente fault in the study area consists of three continuous, relatively straight northwest-trending segments separated by distinct steps or bends (plate 5). In the central segment, the principal fault trace lies near the base of the major escarpment which forms the northeastern boundary of North San Clemente Basin. This escarpment is composed of numerous subparallel scarps throughout the study area. Straight, steep scarps, up to 15 km long and 1000 m high are the most prominent features associated with the principal fault trace. The great height and composite nature of some of these scarps probably represents many episodes of movement, over an extended period of time or along subparallel traces within the main fault zone. Landslide or other gravity controlled scarps are

---

* The principal fault trace is the major, throughgoing fault which has experienced most of the displacement in the zone.

generally concave, and some scarps with this character are also observed in the area (figure 43).

The fault traces are inferred to lie along the base of the *steepest* part of individual scarps and not at the base of possible talus or debris slopes.* In some cases, aligned depressions or linear trenches at the base of the scarps mark the fault trace. Shepard and Emery (1941) also found depressions at the bases of many of the escarpments they mapped in the California Continental Borderland. The small closed depressions observed along the scarps are herein inferred to be of two kinds: (1) true sags as found along terrestrial wrench faults; (2) unfilled depressions surrounded by slides and slumps filling a small hillside valley. True tectonic sags are interpreted in this study to be at small releasing bends or en echelon offsets along the strike-slip fault trace. Depressions of the second kind are found aligned along a wide ($\simeq$1 km) tectonic bench or partially filled hillside valley shown in figure 43. Several features interpreted to be submarine slides or slumps are observed surrounding some of the depressions along this bench.

Other mesotopography characteristic of strike-slip fault origin for these scarps include linear troughs, small tectonic benches, aligned mounds, pressure ridges or push-ups, and pronounced, linear changes in slope gradient (figure 43).

Significant variability in the height and steepness of the scarps exists. Much of this variation may be ascribed to differences in surficial lithology as well as relative scarp age. The steepest, and highest scarps are found in the areas where acoustic

---

* On land, the fault trace is usually found near the middle of the individual scarp, and if the scarp profile is similar to that of an error function (Hanks, 1984), the base of the steepest slope corresponds with the inflection point where the fault trace is located.

Figure 43. Portion of Sea Beam area shown in detail using the original swath charts, contoured at a 10 m interval. Many tectonic landforms similar to those shown in figure 42 are identified. Also, the inferred principal trace of the San Clemente fault is delineated by the dashed line. Sags are shown by shading. (See figure 39 for location of figure).

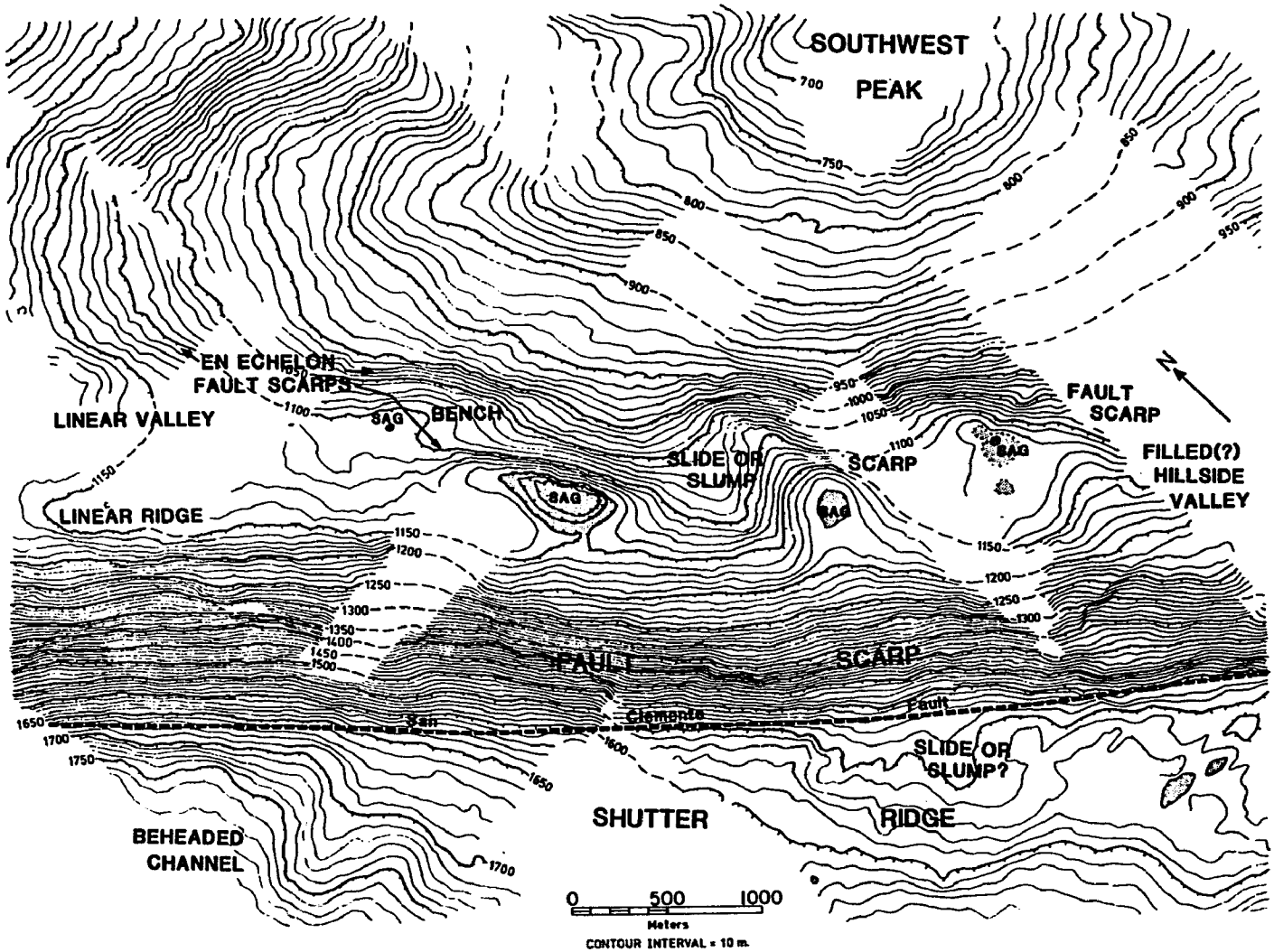


NORTH SAN CLEMENTE BASIN

basement, and hence older and well-indurated rock, is exposed (figure 49; cf. figure 51, chapter 6, this volume). Where younger sedimentary deposits are observed, scarps are much lower, both in elevation and steepness (figures 28 and 44, but are still generally straight.

The northern segment of the principal San Clemente fault trace is not marked by large scarps in the study area. Instead, it enters the region along the axis of the San Clemente Rift Valley, marked by a scarp on its southwestern flank and a broad terrace on its northeastern flank. From the San Clemente Rift Valley toward the southeast, the principal fault trace is identified in the Sea Beam data by the break in slope at the edge of the 'Rift Basin'. The Rift Basin is the deepest, large, closed depression within North San Clemente Basin. A major branch fault splits off the San Clemente fault within the San Clemente Rift Valley and is discussed later. High-resolution seismic profiles show the surficial sediments of the Rift Basin have been dragged where they abut the main fault (figure 44).

The overall trend of the principal trace is noticeably straight, cutting directly across topography typical of a steeply dipping, nearly vertical fault surface. Although significant dip-slip is implied by the height of the escarpments, the overall straightness of the principal fault zone across the entire mapped area is more typical of a strike-slip fault. By contrast, in mountainous areas, major normal fault zones are delineated by more complex, less linear, often zig-zag fault patterns than strike-slip fault zones (Slemmons, 1977). Exceptions are the long, straight, steep escarpments bounding the inner graben on mid-ocean ridges, such as the Mid-Atlantic Ridge.

Figure 44. High-resolution (3.5 kHz) seismic profiles across the San Clemente fault in North San Clemente Basin (see figure 39 for profile locations). Arrow identifies location of San Clemente fault trace. Note disruption and possible fault drag in the near surface sediments along the fault.

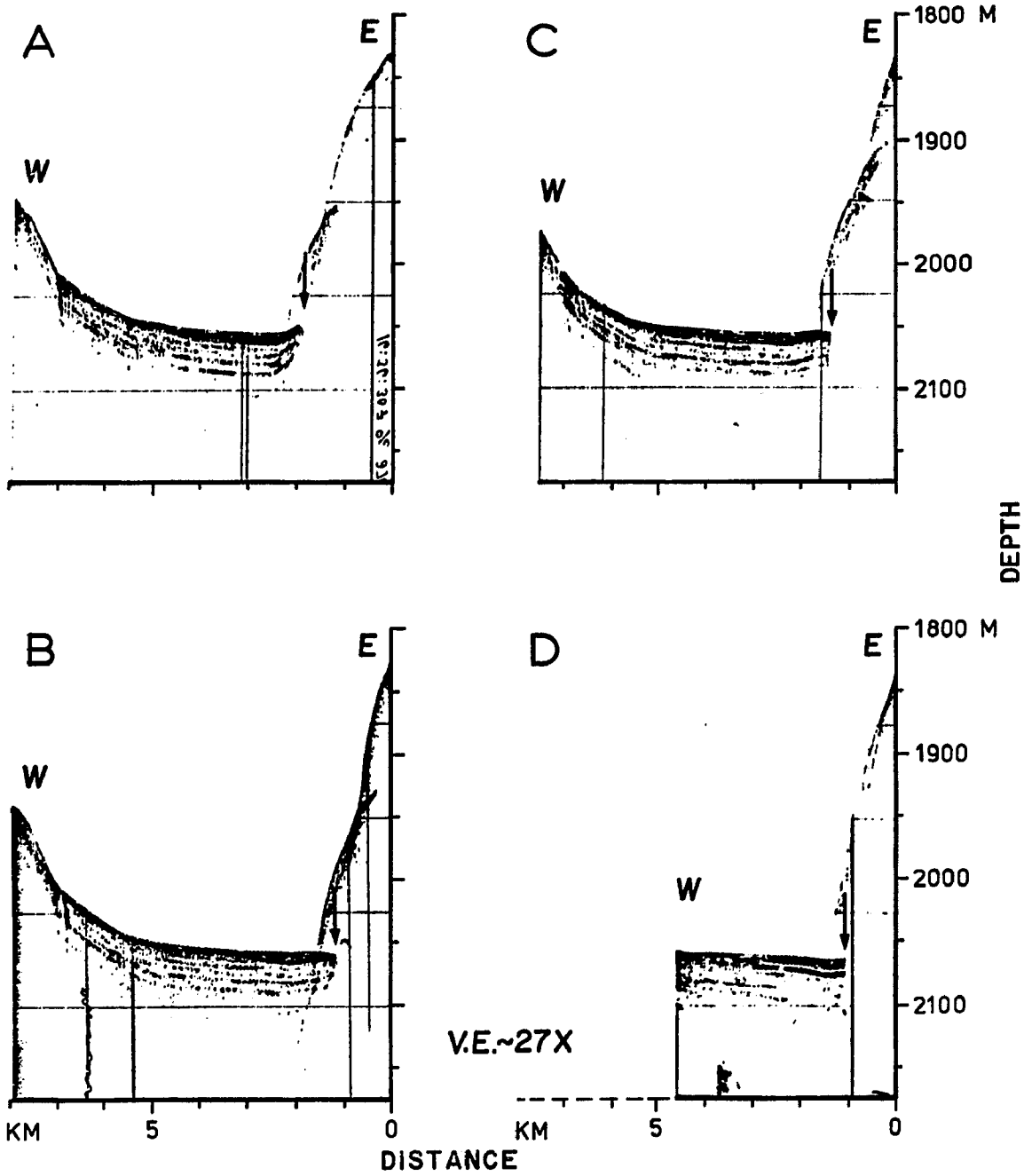
A
W
E
B
W
E
C
W
E
D
W
E
1800 M
1900
2000
2100
DEPTH
V.E.~27X
KM
5
0
KM
5
0
DISTANCE

Two significant right steps or double bends along the principal fault trace are responsible for slight sinuousity in the overall trend. Large depressions or basins are associated with each of these junctions between principal fault segments. Pull-apart origin in a right-slip fault zone is proposed by the author for these basins. Unlike the 'idealized' pull-apart basin described by Crowell (1974), topography and seismic cross-sections show these basins are half grabens or trap-door structures, bounded on one side by the major fault scarp and monoclinal structure on the opposite side (figure 46). Crowell (1976) and Junger (1976) described similar basins in the Borderland. The significant thickening of the sediments in the Rift Basin, as well as the aligned sags, adjacent to the right-bending fault scarp (releasing double bend) demonstrate basin growth has continued throughout late Quaternary time.

Topography is suggestive of a slightly more complicated development of 'Triangular Basin'. The scarp along its southern boundary may be associated with local folding and possibly, reverse faulting associated with a left-bending branch fault. Alternatively, dip-slip associated with the ending of a predominantly strike-slip fault segment which bounds a pull-apart at a right step between en echelon fault strands may also explain this feature. Freund (1971) calls such features 'termination bulges' and shows several examples along the Hope fault in New Zealand. Similar features are observed at the northern end of the Imperial fault in southern California (Mesquite Basin, Sharp and others, 1982; figure 45). Two low scarps separated by a small bench or terrace along the northeast margin may delineate sub-parallel fault traces, or show that possible large-scale slumping of the relatively unconsolidated sediments into the basin has occurred. A small closed depression or sag is located on this terrace, aligned with the principal San Clemente fault trace to the northwest.

Figure 45. Comparison of some pull-apart basins along major, dextral, wrench faults. Shaded area identifies depression associated with pull-apart. Features possibly associated with termination bulges are shown by the other, textured pattern as labelled. (a) Mesquite Basin lies at the northern end of the Imperial fault, a major segment of the San Andreas fault system south of the Salton Sea; (b) Hanmer Plains lie along the Hope fault zone (HFZ) in New Zealand. (c) Triangular Basin lies along the San Clemente fault zone (SCFZ) in the area of this study (North San Clemente Basin). Other tectonic features are also identified. All three pull-aparts shown are associated with right-steps (releasing bends) in dextral wrench faults.

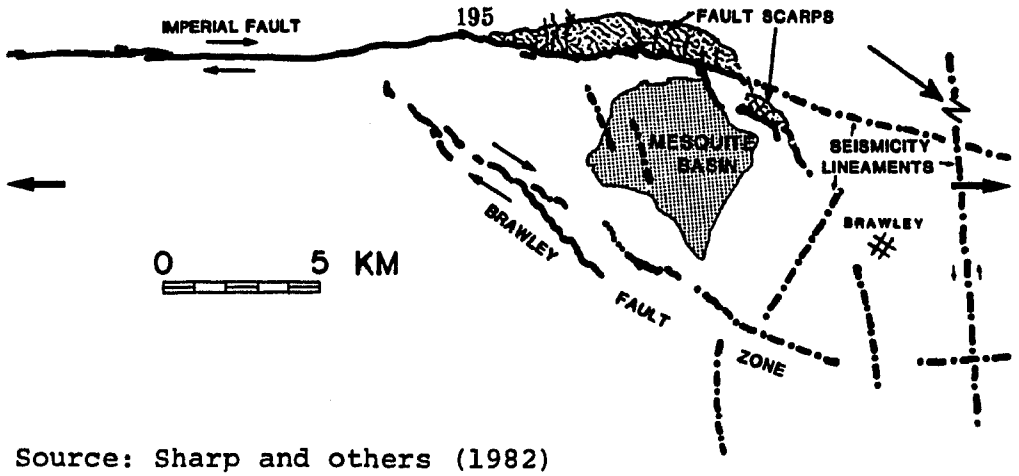


Source: Sharp and others (1982)

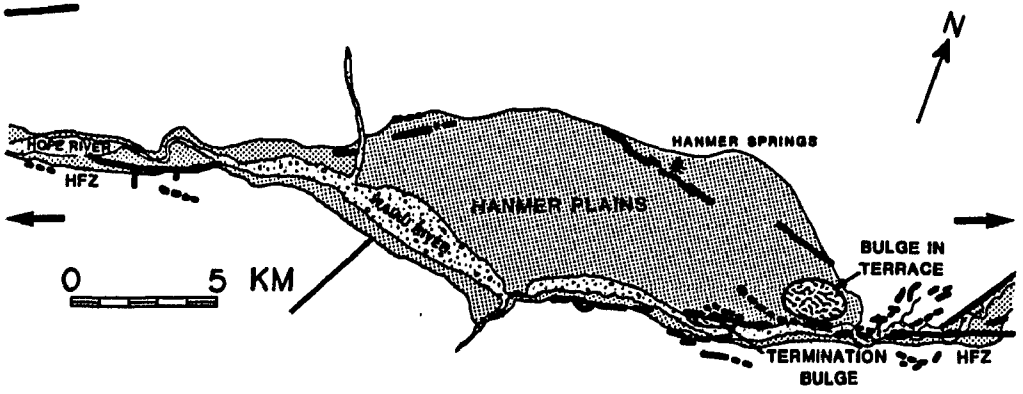


Source: Freund (1971)

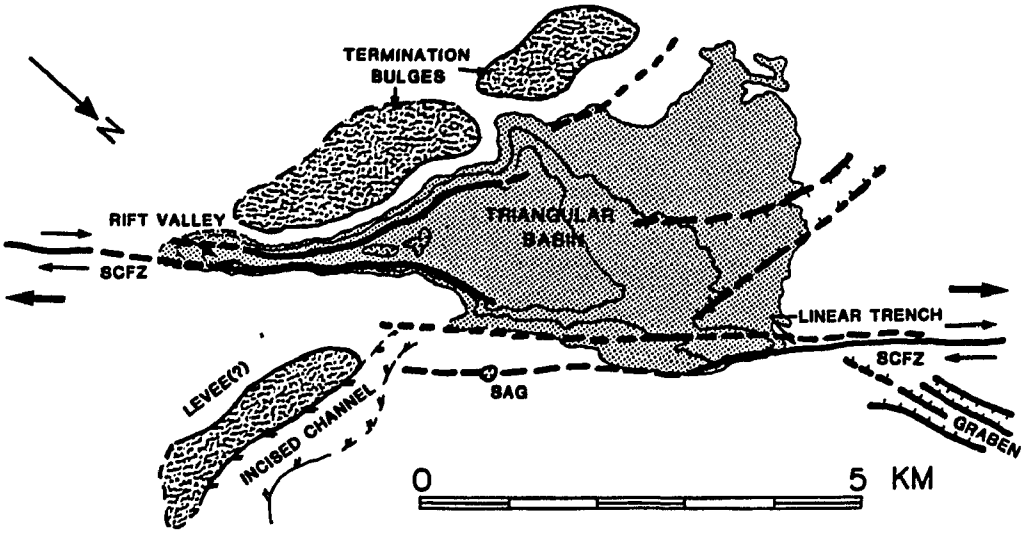

Figure 46. High-resolution (3.5 kHz) seismic profiles across the San Clemente fault zone between Fortymile Bank and North San Clemente Basin (Rift Basin). Arrows identify locations of fault traces. (See figure 39 for profile locations).

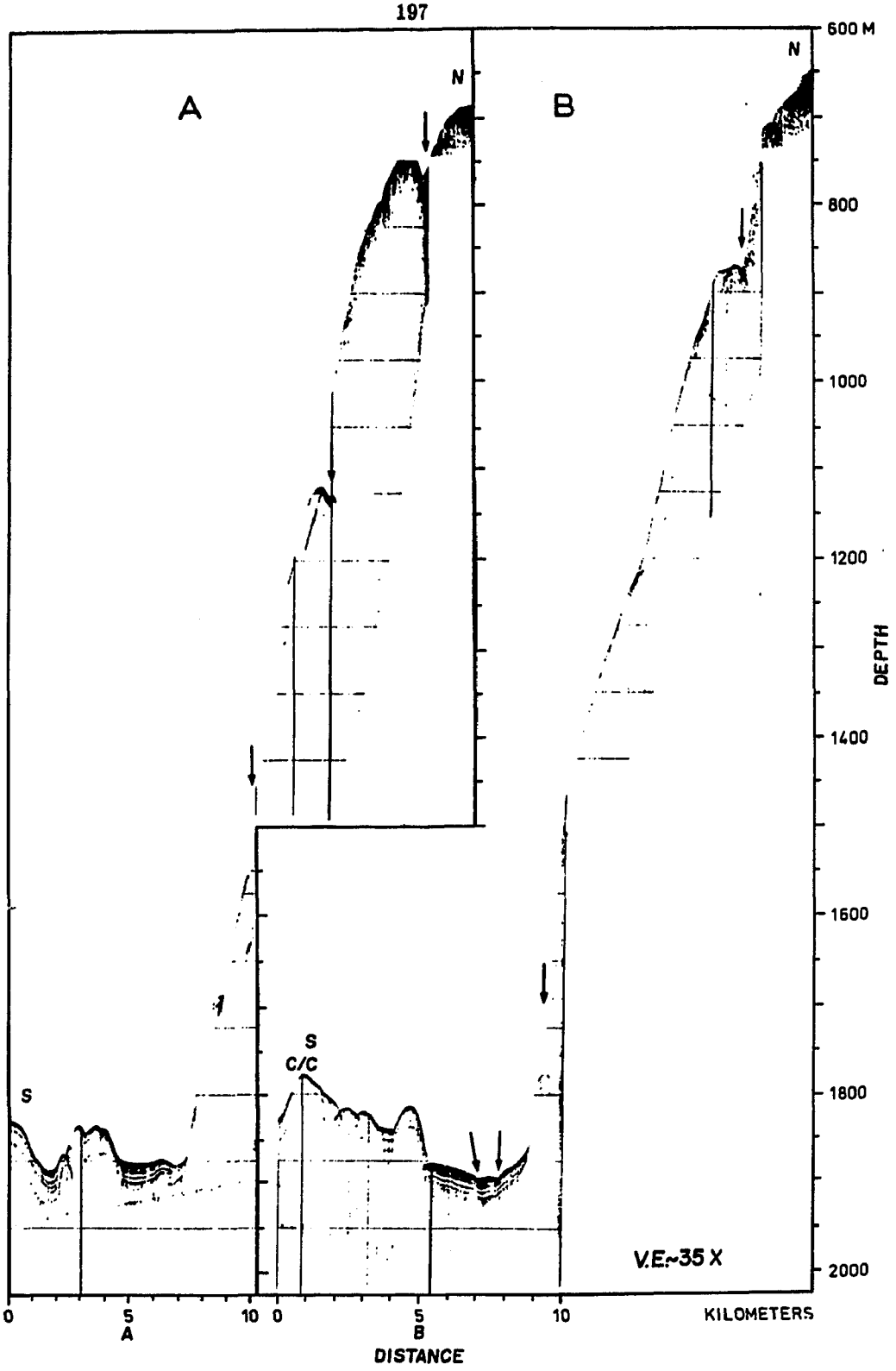
A
B
N
N
S
S
C/C
600 M
800
1000
1200
1400
1600
1800
2000
DEPTH
V.E.~35 X
0
5
10
0
5
10
KILOMETERS
A
B
DISTANCE

The western margin has a gentle slope into the basin with no topographic evidence for faulting. A small 'keystone' graben is apparent on one 3.5 kHz profile crossing this western margin (figure 46), but other high-resolution seismic data necessary to confirm structural interpretations of the basin and its margins are not presently available.

The southern, principal San Clemente fault segment forms the northeastern margin of the elongate 'Navy Basin'. The fault passes through a narrow rift valley at the northwest end of Navy Basin and is marked by the scarps which form the northeast edge of the basin. Seismic reflection profiles (figure 28) show the fault clearly. In some places, fault drag is evident in the relatively flat-lying sediments of the basin. Navy Basin corresponds to the '1868 Basin' of Normark and Piper (1972), which they found filled with ponded turbidites from nearby Navy Fan.

Scarps along the northeast flank of San Salvador Knoll and along the San Clemente fault mark the two long sides of this basin. Normal drag is shown within the ponded turbidites adjacent to the San Clemente fault (figure 28). A second, steeply-dipping fault with normal separation displaces the ponded turbidites a few hundred meters away from the base of San Salvador Knoll on the west side of Navy Basin. These relations imply that the northwest part of Navy Basin is a recently active graben that has formed between basement of the structural block northeast of the San Clemente fault and that of San Salvador Knoll to the southwest. The buried acoustic basement flank of San Salvador Knoll dips northeastward until it is truncated by the more steeply dipping San Clemente fault surface. Slightly divergent, dextral, strike-slip along the San Clemente fault would cause formation of the graben within the young, ponded sediments. The strike of this segment of the San Clemente

fault trends (5°-10°) more northerly than the other two principal fault segments mapped in this study. Other data (chapter 4, this volume) show that Navy Basin and East San Clemente Basin form an elongate pull-apart between major, right-stepping, en echelon traces of the San Clemente fault.

In general, the principal trace of the San Clemente fault in the study area separates elevated basement or other structure along the northeast from the basin areas to the southwest. Beyond the area of this study, the opposite is true for many tens of kilometers along the fault. The most famous example is the northeast-facing escarpment along San Clemente Island. In other places where elevated structures are along both sides of the fault, a narrow rift valley is present. Examples of the latter situation include the large San Clemente Rift Valley at the northwest corner of this study area and the smaller rift valley separating Triangular Basin from Navy Basin.

A small, elevated 'acoustic' basement structure, apparent in the central part of the study area, abuts the San Clemente fault at the base of a prominent scarp. No rift or other valley separates this feature from the elevated flank of Fortymile Bank, although a linear trench marks the principal fault trace at the southeastern corner of this feature, and a large sag lies near its center. This feature is proposed herein to be a shutter ridge, formed by strike-slip displacement of an elevated basement (bedrock?) structure cut by the fault. Ponding of sediment behind the ridge may be partly responsible for the relatively flat surface topping the shutter ridge adjacent to the fault scarp (figure 47). Deep Tow 4 kHz data show that erosion of tilted sedimentary deposits has occurred along the flanks of this feature (figure 48), demonstrating that older sedimentary deposits may constitute at least part of the acoustic basement of this feature. The steep slopes of this feature prevent significant acoustic

Figure 47. High-resolution (3.5 kHz) seismic profile across the San Clemente fault zone and the 'shutter ridge' at the base of Fortymile Bank (see figure 39 for profile location). Other features shown on the bathymetric map (figure 43) are identified for reference.

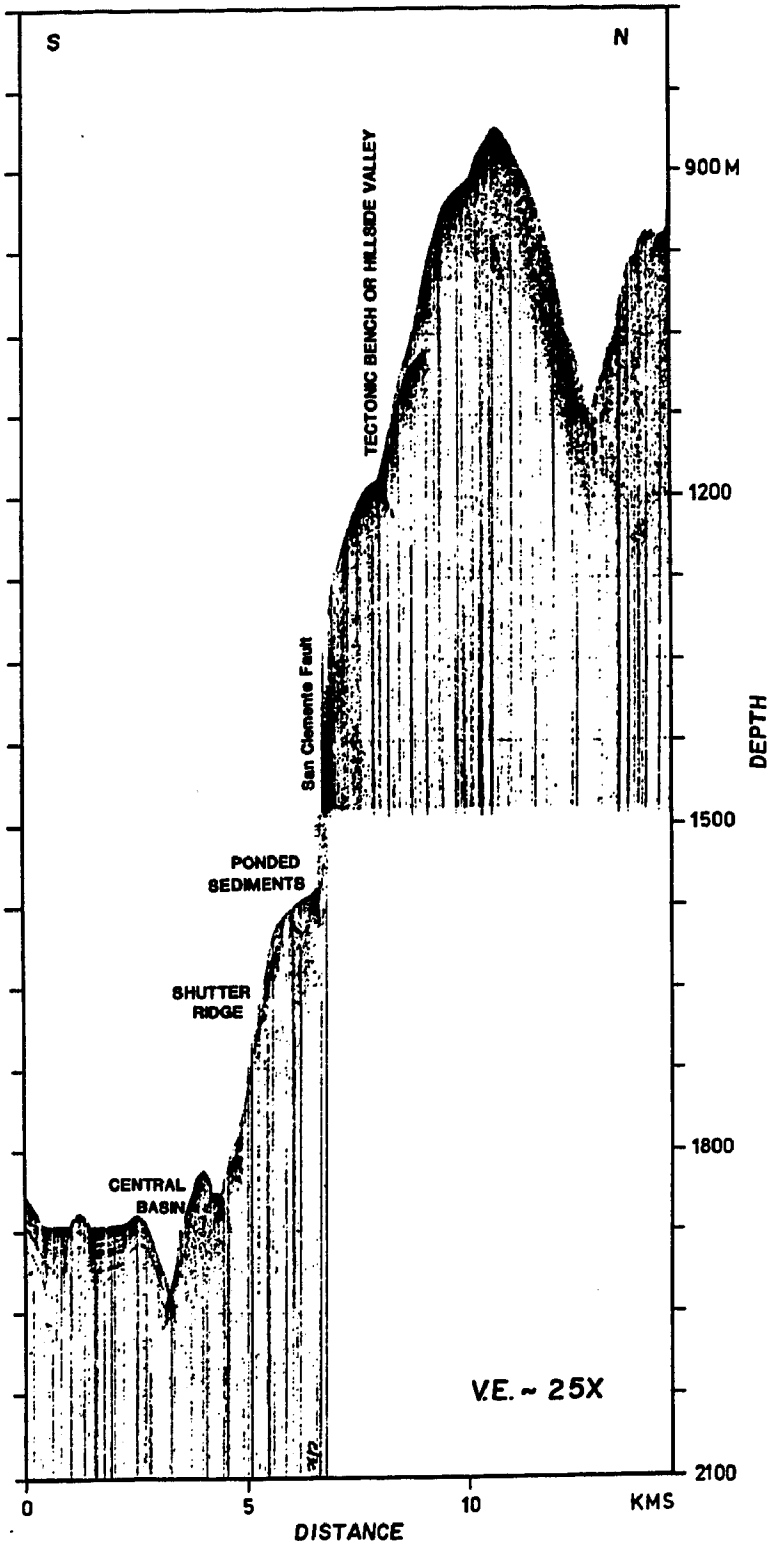
S
N
TECTONIC BENCH OR HILLSIDE VALLEY
San Clemente Fault
PONDED SEDIMENTS
SHUTTER RIDGE
CENTRAL BASIN
V.E. ~ 25X
900 M
1200
1500
1800
2100
DEPTH
0
5
10
KMS
DISTANCE

Figure 48. Deep Tow, high-resolution (4 kHz) seismic profiles across the flanks of the 'shutter ridge' (see figure 39 for profile locations). Poor quality of these records make interpretation difficult, although beds truncated at the seafloor are apparent in some places, along inferred channels.

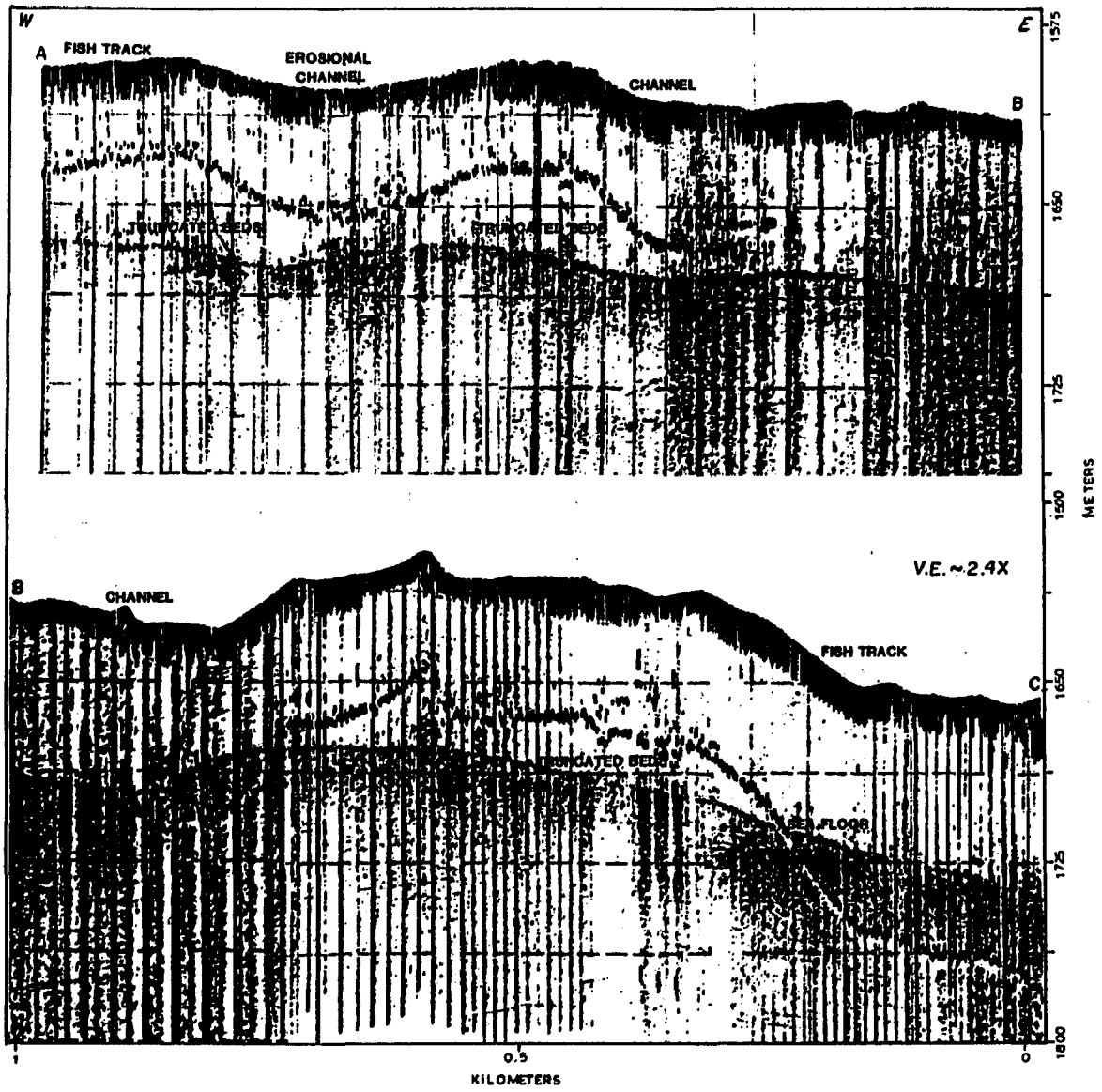
W
E
A
FISH TRACK
EROSIONAL
CHANNEL
CHANNEL
B
TRUNCATED BEDS
TRUNCATED BEDS
1575
1650
1725
1800
METERS
V.E. ~2.4X
B
CHANNEL
FISH TRACK
C
TRUNCATED BEDS
SEA FLOOR
1650
1725
1800
1
0.5
0
KILOMETERS

penetration with the surface ship 3.5 kHz system, although some evidence of bedded deposits is exhibited (figure 47). The author (chapter 6, this volume) suggests that lateral movement of this shutter ridge along the San Clemente fault has controlled late Cenozoic sedimentation patterns in North San Clemente Basin. Detailed study of these sedimentation patterns may, therefore, provide a displacement history for this fault.

**Branch and Secondary Faults**

In addition to the principal fault trace, numerous branch and secondary fault traces can be identified with the Sea Beam and high-resolution seismic data. These fault traces are most easily recognized by linear, steep scarps of variable length, and in a few instances, by offset reflectors in seismic profiles.

The most prominent branch fault (hereinafter referred to as the Junger fault*) is marked by the large (over 1000 m high) scarp in the northern half of the study area. This fault joins the main fault in the San Clemente Rift Valley, just beyond the northwest corner of this study area. In places, sags are aligned at the base of this scarp. The fault can be easily traced for more than 12 km along the straight, northwest-trending part of the scarp.

A more complicated pattern of faulting is inferred by the author in the central area of the study, where this large scarp curves sharply to a more northerly trend. Several small scarps, aligned sub-parallel to the main fault, and en echelon to each other in a left-stepping pattern, flank the northeast margin of a northwest-trending

---

* The author informally refers to this fault as the Junger fault, named after Arne Junger who spent many years studying the San Clemente fault zone.

linear ridge. Seismic data show offset sub-bottom reflectors at the top of the scarps (figure 49), and acoustic basement is truncated at the base of the scarps.

Another significant secondary fault is delineated by aligned sags and scarps along a northwest-trending terrace or tectonic bench located above the shutter ridge. The author infers that this secondary fault ends at a small, north-trending fault scarp (or graben) which may connect to the principal fault trace at the southern end of the shutter ridge. The north-south trend of the graben-like feature is consistent with local east-west extension in a northwest-trending, right-lateral, shear zone. The northern end of this secondary fault may connect with the en echelon faults described previously, or with another branch from the main fault delineated by a small tectonic bench near the southern end of Rift Basin (figure 38). Alternatively, it may end within the linear ridge just north of the sags shown in Figure 43.

Additional secondary faults are apparent along the flanks of Fortymile Bank. Most of these are delineated by straight, steep scarps, and aligned or linear depressions. Some of these correspond to faults mapped by U.S. Geological Survey scientists using moderate to deep penetration seismic reflection data (Vedder and others, 1974; Junger and Vedder, 1980 personal communication; Greene and others, 1985). The abundant gaps in the Sea Beam data of this study on the elevated parts of Fortymile Bank preclude more detailed interpretation of these faults. Numerous scarps of probable non-tectonic origin are also apparent in this area as well and have been mapped accordingly (plates 4 and 5).

Other secondary faults, associated with the San Clemente fault zone are present in the gentle slopes northeast of Navy Basin. These faults are not readily apparent in the Sea Beam contours, although line spacing is too wide to provide overlap of

Figure 49. High-resolution (3.5 kHz) seismic profiles acorss the San Clemente fault zone in the North San Clemente Basin region (see figure 39 for profile locations). Arrows identify locations of fault traces.

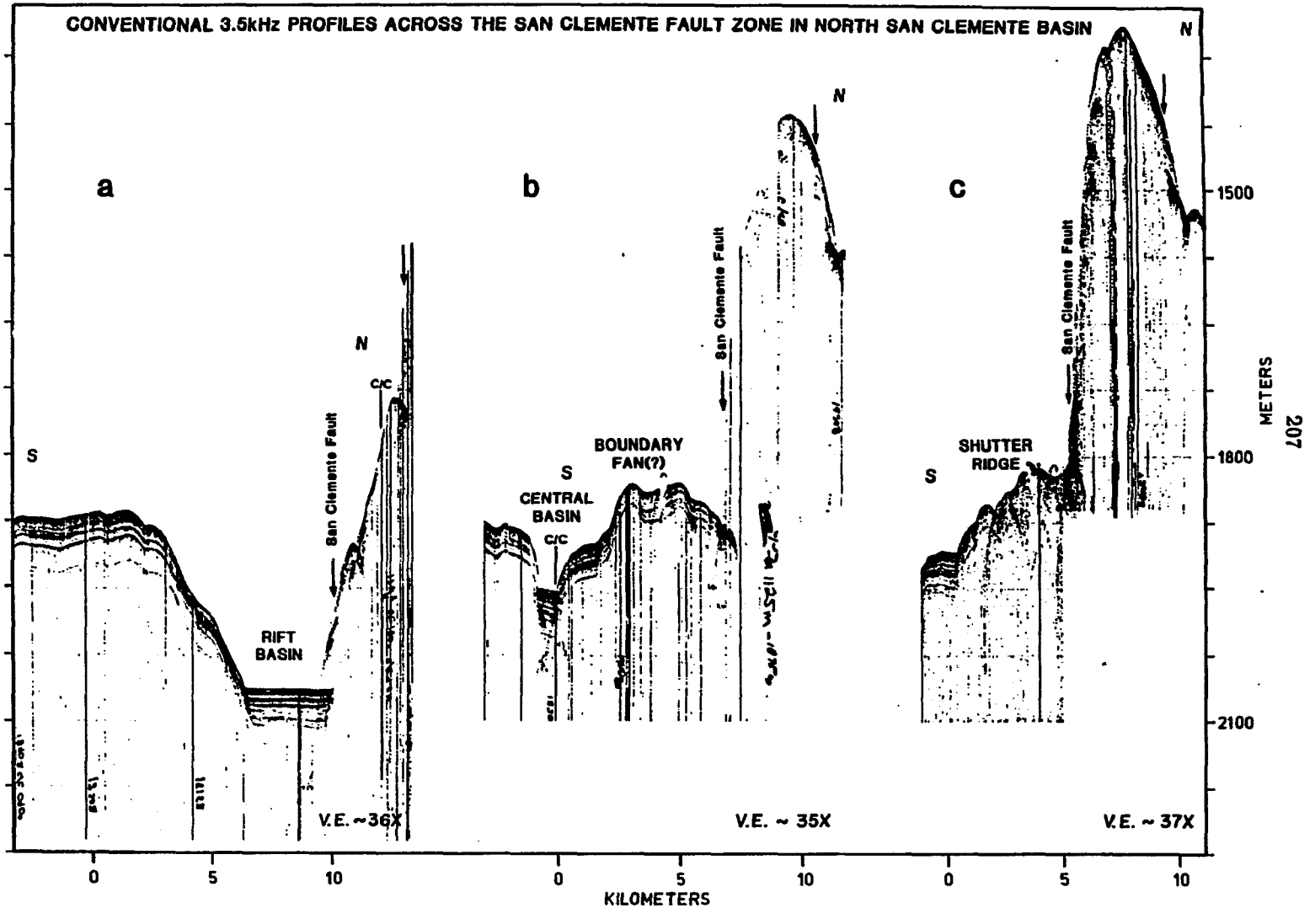
CONVENTIONAL 3.5kHz PROFILES ACROSS THE SAN CLEMENTE FAULT ZONE IN NORTH SAN CLEMENTE BASIN
a
b
c
S
N
C/C
RIFT BASIN
San Clemente Fault
CENTRAL BASIN
BOUNDARY FAN(?)
SHUTTER RIDGE
V.E. ~36X
V.E. ~ 35X
V.E. ~ 37X
1500
1800
2100
METERS
0
5
10
KILOMETERS

adjacent swaths. The airgun profiles (figure 10 and 28) provide the most significant evidence for the existence and locations of these faults. The complex structure in these profiles and their limited number, however, do not allow accurate mapping of these faults in the present study. Where these faults are shown on the tectonic geomorphology map (plate 5), strike was inferred from topographic contours in the Sea Beam plot. The author has mapped the faults in this area in more detail elsewhere (chapter 4, this volume).

**Recency of Faulting in the San Clemente Fault Zone**

Abundant evidence of late Quaternary movement of faults within the study area is shown by the Sea Beam and high-resolution seismic reflection data. First, numerous geomorphic features commonly associated with active strike-slip faults (figure 42, plate 5) may imply that late Quaternary activity has occurred. Because erosion of deep submarine topography may be relatively slow in general, and Holocene sedimentation rates in the region vary from 0 to 35 cm/1000 yrs (chapter 3, this volume; Emery and Bray, 1962), use of geomorphic criteria may not demonstrate Holocene fault movement. Locally, submarine mass-wasting processes may rapidly obscure primary tectonic relief, however. Scarp heights and slope gradients correlate with lithology, the highest and steepest scarps being associated with the acoustic basement materials. The presence of low scarps in youthful sedimentary deposits may be evidence of late Quaternary and possibly Holocene activity. Aligned sags in the late Quaternary-Holocene deposits of Rift Basin provide better evidence of late Quaternary, possibly Holocene fault movement than do the tectonic landforms found in the older sedimentary deposits or basement rock. These small depressions would

be rapidly filled by sediments, and therefore continued tectonic activity is required to maintain them.

Second, offset or disruption of key stratigraphic horizons in sedimentary deposits in the region also may signify late Quaternary to Holocene fault activity. Unfortunately, from the available, high-resolution seismic reflection data, prominent acoustic horizons cannot be correlated across the principal fault traces. The character of the deposits adjacent and across the large, steep fault scarps cannot be adequately defined with surface ship data as stated previously, and we have no Deep Tow profiles across the main fault trace(s).

In the area of somewhat more gentle slopes where the main fault trace crosses Rift Basin into San Clemente Rift Valley, conventional 3.5 kHz profiles provide the best available evidence for late Quaternary, possibly Holocene fault movements. Several profiles which cross the fault in this area show weak evidence of fault drag in late Quaternary and Holocene sediments which abut the fault (figure 44). The noticeable thickening of the sediments between prominent horizons adjacent to the fault, observed in the southernmost profile (figure 44) may demonstrate continued basin subsidence associated with late Quaternary fault movements. Late Quaternary to Holocene activity of both the main fault and the secondary fault forming the graben in Navy Basin is inferred from offset reflectors and drag features seen in the airgun profiles crossing that area (figure 10 and 28).

For near bottom and high-resolution seismic data, a significant thickness of layered Holocene deposits would be desireable to show displaced Holocene deposits. Turbidite sediments of Navy Fan may provide such a setting, yet Normark and others (1979) found no compelling evidence for Holocene faulting within the area they

surveyed using Deep Tow. Numerous linear features were observed on the fan surface, but these were attributed to depositional or erosional processes associated with normal fan growth. Sub-bottom reflectors in the Navy Fan area crossed by the San Clemente fault are discontinuous, and fault offsets cannot be identified with certainty.

Submersible observations of the seafloor in other areas of the Borderland where young faults have been interpreted to break the seafloor (based upon high-resolution seismic reflection data), showed that extensive bioturbation of the upper sediments would obscure all but the most recent seafloor displacements (Kennedy and others, 1985b). Lonsdale (1979) observed very steep slopes ($\simeq 60^{\circ}$) on a scarp cutting the southern edge of Navy Fan during submersible dives. He also observed mounds of barite deposits associated with hydrothermal vents along the San Clemente fault.

Seismologic data provide a third type of evidence indicating Holocene fault movements. Numerous earthquakes have occurred along the trend of the San Clemente fault zone (Hileman and others, 1974; Legg, 1980; figure 66, chapter 7, this volume), but most of these are not located with sufficient accuracy to correlate with specific fault traces. Several moderate-sized events (magnitude 4.0-4.7) have occurred somewhat to the east of the main traces of the San Clemente fault, being located between Fortymile and Thirtymile Banks. A large earthquake (magnitude 5.9) was located at the southern tip of San Clemente Island, near San Clemente Rift Valley. These events demonstrate present-day activity of faults within the San Clemente fault zone.

Earthquake focal mechanisms determined using first motions recorded on seismograms for several earthquakes in the Fortymile Bank area are not consistent with dextral strike-slip on northwest-trending fault planes, (Legg, 1980). Instead, left-lateral motion on north- to northwest-trending fault planes or right-lateral slip on the conjugate fault planes was observed. This tectonic complexity has yet to be resolved. Elsewhere along the San Clemente fault zone, focal mechanisms of earthquakes are consistent with the character of faulting (right-slip on northwest-trending fault planes) inferred from the geological data. Some extension across the fault is indicated by mechanisms showing right-lateral, oblique normal slip on the northwest-trending focal planes of some of these earthquakes.

Timing of the initiation of movement along the San Clemente fault zone cannot be adequately determined with the data of this study. The author infers that movement has been continuous throughout Quaternary time, as evidenced by progressively greater deformation of the more deeply buried strata in seismic reflection profiles (figures 10, 28 and 44). Also, the abundance of geomorphic features related to recently-active faulting observed on the elevated basement flanks of Fortymile Bank, compared to the absence of such features in the younger, sediment covered basin areas implies that fault activity commenced prior to deposition of the uppermost sediments found in the basin area. Middle Miocene timing of fault development associated with the formation of many of the present-day banks and ridges in the Borderland was proposed by others (Vedder and others, 1974; Junger, 1976; Junger and Vedder, personal communication). Howell and others (1974) have postulated a long history of movement, involving significant displacements (up to 180 kilometers) on an East Santa Cruz Basin fault zone. This postulated fault zone may be ancestral to the

present-day San Clemente fault zone or to the Santa Cruz-San Clemente-San Isidro fault zone of Legg and Kennedy, (1979).

**Displacement and Rate of Slip**

The most difficult task of marine geoscientists attempting to study offshore faulting is to quantify displacements and rate of slip for faults covered with thousands of meters of sea water. Vertical offsets are relatively easy to estimate, because seismic reflection profiles offer a suitable approximation of geological cross-sections, when properly interpreted. Age of key horizons is more difficult to obtain, although bottom sampling of outcrops, core data and drilling provide necessary data at some cost, however. Strike-slip is much more difficult to determine, and recognition of 'valid' piercing points under the sea is not readily accomplished. Distinctive linear submarine features such as channels, lava and debris flows, fold axes along specific horizons, canyons and fan valleys, and characteristic magnetic anomaly patterns may provide such piercing points. The latter features have proven most useful in estimating offsets and slip rates of major oceanic transforms (Heirtzler and others, 1968). Sea Beam data provide detailed information on shape and continuity of seafloor mesotopography, and therefore, should be useful in attempts to determine components of strike-slip along major offshore faults.

Dip-slip along parts of the San Clemente fault can be estimated from the thickening of the ponded sediments along the fault in Rift Basin. From ten to fifteen meters of relative thickening is evident in the seismic profiles, within the upper 60 meters of sediment penetrated by 3.5 kHz data (figure 44). Assuming a constant sedimentation rate of 30* cm/1000 yrs (Emery and Bray, 1962) for this part of the basin,

---

* The sedimentation rate may have been significantly greater during the glacial and marine transgression stages of the Pleistocene (Dunbar, 1981; chapter 3, this volume).

and correcting for compaction (see chapter 3, this volume; Moore, 1969), a dip-slip component of fault movement can be estimated. Values of from 20 to 25 m of deepening, over an interval of about 200,000 years yields a dip-slip rate of about 0.1 mm/yr for this part of the fault. Similar rates for the uplift of terraces on nearby San Clemente Island have been measured (Muhs and others, 1979) Muhs, 1983). In as much as the structural pattern typifies predominately strike-slip, the overall slip rate for the San Clemente fault may be at least an order of magnitude greater.

Several topographic features which may be offset by the fault are apparent in the area. The shutter ridge may be offset from another elevated basement structure not yet identified, but presumably located on the northeast side of the fault elsewhere along strike. A channel appears to be offset a few kilometers in a dextral sense, by the fault near Triangular Basin. Close inspection of the 3.5 kHz data do not show evidence extending the channel leading into 'Central Basin' across Triangular Basin to the fault. Instead, isopach maps (Figures 55 and 58, chapter 6, this volume) show a partially buried channel, shown by topography and thicker sediment accumulation along the channel axis, located south of Central Basin. This feature may be offset between 1.7 and 2.3 km from an existing channel incised into the low scarps on the southeast side of Triangular Basin. The author (chapter 6, this volume) also notes that the low, broad elevated area between Rift Basin and Central Basin has a shape roughly similar to a small submarine fan. The apex of this postulated fan, which appears to have a leveed(?) channel, is offset between 7 and 10 km from possible ancient channels (upper fan valley?) located on the opposite side of the fault. Based upon late Quaternary sedimentation rates for the area, and the estimated ages of some prominent acoustic horizons (chapter 6, this volume), the author proposes that

an average late Quaternary slip rate of 1-10 mm/yr provides an order-of-magnitude estimate for the San Clemente fault zone near Fortymile Bank.

None of the strike-slip displacements postulated above has been confirmed to date. Carefully located bottom samples, detailed high-resolution seismic reflection surveys and near bottom studies are necessary to provide additional data which may document timing and amount of any postulated fault offsets.

## CONCLUSIONS

Sea Beam provides important data which can be used to map recently active fault traces in regions of rugged seafloor topography with high relief. Numerous tectonic landforms similar to those observed along active terrestrial strike-slip faults are apparent in Sea Beam contour plots of the San Clemente fault zone near Fortymile Bank and San Clemente Basin. Major scarps, from tens to hundreds of meters high and hundreds to thousands of meters in length; closed depressions such as tectonic sags and small basins; and linear topography such as ridges, valleys, troughs, trenches, and other aligned depressions are the most common tectonic landforms observed along the San Clemente fault zone. Sedimentary and other non-tectonic(?) structural features on the seafloor can be recognized from the Sea Beam contours, but additional data such as high-resolution, surface ship and near bottom, seismic reflection data, bottom samples and photographs are necessary to verify the interpretations of the seafloor geomorphology.

Sea Beam and other data used in this study show that the San Clemente fault zone, in this area, is a fully-developed, right-lateral wrench fault (figure 50). Long, straight scarps mark the principal displacement fault, which is essentially continuous

Figure 50. Comparison of the mapped patterns of parts of four major dextral wrench fault zones in California. Stippling delineates areas of elevated bedrock or older sediments. Similarity in fault patterns, including continuity of principal fault segments and narrowness of the main fault zones are characteristics of well-developed wrench faults (Wilcox and others, 1973). All fault zones shown are mapped at the same scale.

Newport - Inglewood

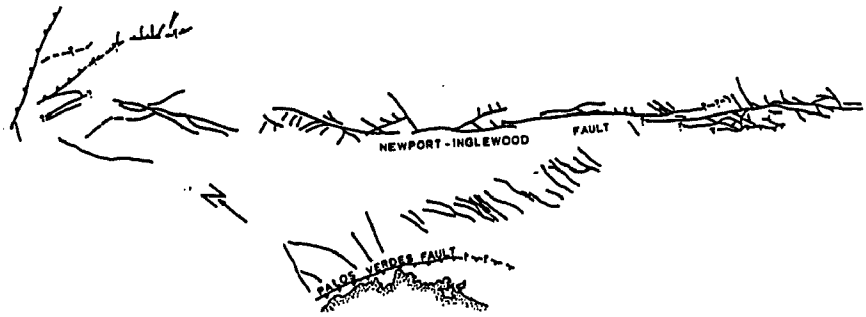


San Jacinto

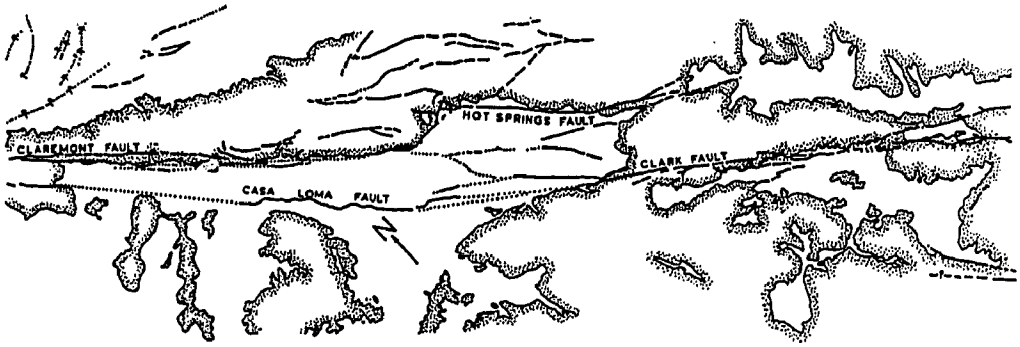


Hayward

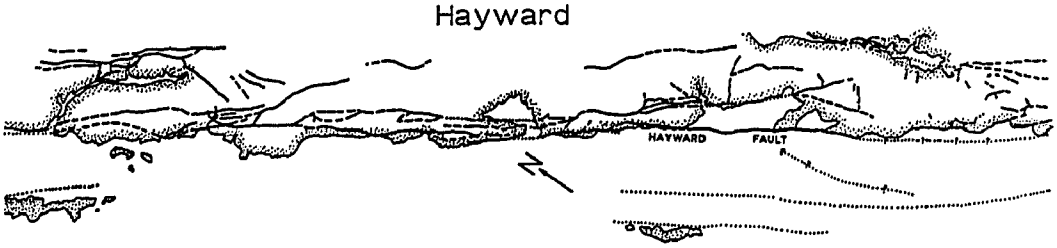


San Clemente

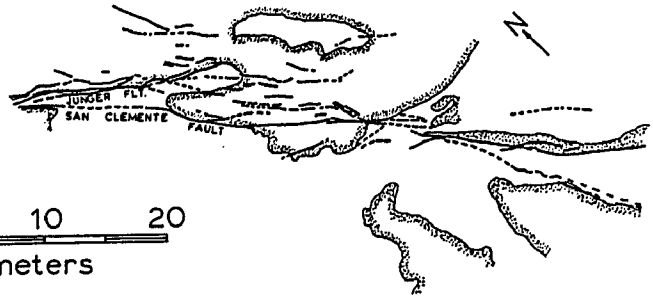


5 0 10 20
kilometers

along the 50 km section mapped in this study. Some sinuosity of the principal fault trace is evident as two significant, right, en echelon, fault steps or releasing double bends. Tectonic pull-apart basins, with trap-door or half graben configuration are at these bends, demonstrating the dextral strike-slip character of the fault. Numerous sub-parallel branch and secondary fault traces are delineated by scarps and other lineaments apparent in the older deposits of the uplifted acoustic basement flanks of Fortymile Bank. Few tectonic landforms are observed in the recent sediments of the basin areas away from the principal fault trace. A significant exception is the graben formed in the young, ponded turbidites of Navy Basin, indicative of an extensional component of strain across this more northerly trending section of the San Clemente fault. Other data (chapter 4, this volume) imply that Navy Basin is also a pull-apart between offset, en echelon fault strands.

The principal, active trace of the San Clemente fault lies at the base of the major scarps separating Fortymile Bank from North San Clemente Basin. Previous investigators (Moore, 1969; Vedder and others, 1974) were unable to map this fault accurately from seismic reflection profiles because of the steep topography, and instead showed major fault traces closer to the crest of Fortymile Bank. One of these, the Junger fault, is a major branch fault which connects to the main fault in the San Clemente Rift Valley, and it follows the base of a thousand meter high scarp and separates Fortymile Bank from a linear, northwest-trending ridge adjacent to the Rift Basin. The Junger fault is difficult to follow with the bathymetric data toward the southeast, where it crosses the southwest corner of Fortymile Bank along a discontinuous series of scarps and aligned depressions. Other significant secondary faults lie subparallel to the principal fault trace and are apparent as long, straight,

northwest-trending scarps and aligned depressions which cross a bench on the southwest flank of Fortymile Bank.

Sedimentary and other apparently nontectonic features are useful to determine recency of faulting and possible displacements. Thickening of late Quaternary to Holocene ponded turbidites and evidence of drag in these sediments adjacent to the main fault trace are used to infer that movement occurred during late Quaternary and probably Holocene time. Postulated right-lateral offsets of features include partially buried channels (1.7-2.3 km), a shutter ridge (unknown displacement), and a possible small submarine fan or slope apron deposit (7-10 km). Age and character of these features are not yet confirmed by careful bottom sampling or detailed high-resolution seismic surveys. Approximate ages of some of these features based upon sedimentation rates and isopachs are used by the author to propose a late Quaternary average slip rate of 1-10 mm/yr for the San Clemente fault.

Seismologic data show that numerous earthquakes have occurred along the trend of the San Clemente fault zone. Focal mechanisms of the larger events in the Fortymile Bank and San Clemente Island area, however, are *not* consistent with the geologic evidence for right-slip on northwest-trending fault planes. Tectonic complexity in the Fortymile Bank area demonstrated by the occurrence of these 'backwards' earthquakes may be associated with numerous scarps and other tectonic landforms evident in the Sea Beam bathymetric chart of the area (plates 4 and 5).

Additional work is necessary to identify real piercing points offset by the San Clemente fault in this and other areas so that reliable estimates of late Quaternary slip can be made. A program of carefully located bottom sampling and possibly drilling, coupled with additional, accurately navigated Sea Beam and high-resolution,

moderate penetration seismic reflection surveys would be most desireable. The San Clemente fault is considered by the author to be the most significant, active fault in offshore southern California, and a slip rate of several millimeters per year would be of significant interest from both an earthquake hazards and tectonic viewpoints. It is important, therefore, to investigate the seafloor geology and tectonic activity of this area more fully.

# CHAPTER 6
# LATE QUATERNARY SEDIMENTATION IN NORTH SAN CLEMENTE BASIN AND MOVEMENT ALONG THE SAN CLEMENTE FAULT

## INTRODUCTION

### Sediments

A detailed examination of the sedimentation patterns in the Sea Beam survey area provides additional insight into the character and recency of the tectonic activity. The 3.5 kHz surface ship and Deep Tow 4 kHz data allow interpretations of the sedimentation rates and processes active for the most recent geological past as recorded in the upper 50-100 m of sediment. Airgun data over a part of the area allows investigation of a significantly greater thickness of sediments. Contouring isopachs of different sedimentation intervals separated by prominent acoustic horizons in the seismic data allow interpretation of relative rates of sedimentation as well as insights into mode of sedimentation, direction of transport, and possible tectonic effects. For the present study, detailed examination of sedimentation patterns is restricted to the deep areas where relief is low, and abundant, high quality seismic data from both Deep Tow 4 kHz and surface ship 3.5 kHz systems are available (figure 51). Correlation of sediment 'acoustic character' and seafloor morphology also provide insights regarding the seafloor geomorphology and possible lateral fault offsets.

Figure 51. Map showing tracklines of high-resolution seismic data used in this study. Numbers identify sections of seismic profiles reproduced as figures in the report. Bathymetry is from the detailed Sea Beam study of the area (chapter 5, this volume).

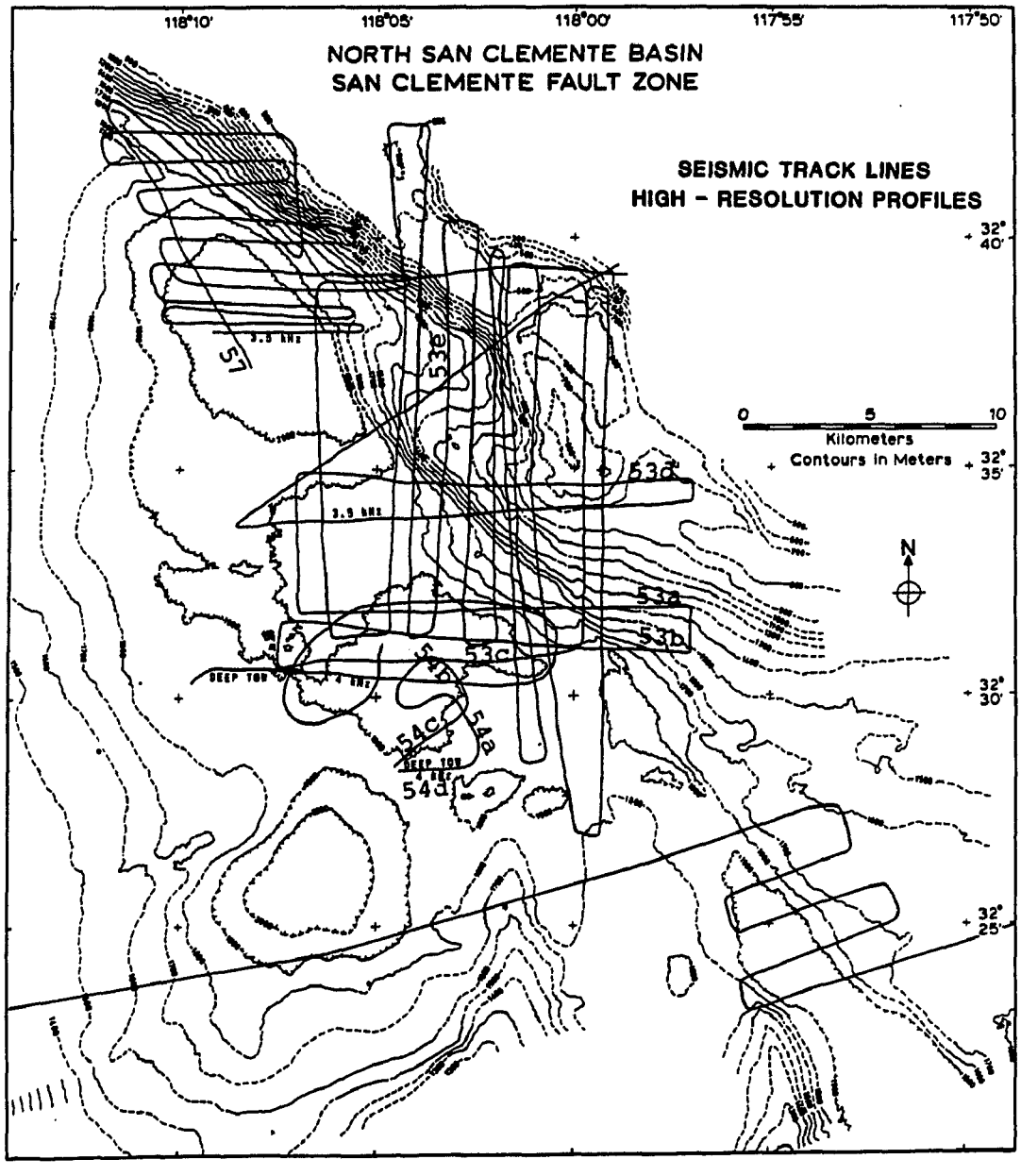
118°10'
118°05'
118°00'
117°55'
117°50'
NORTH SAN CLEMENTE BASIN
SAN CLEMENTE FAULT ZONE
SEISMIC TRACK LINES
HIGH - RESOLUTION PROFILES
32° 40'
32° 35'
32° 30'
32° 25'
0
5
10
Kilometers
Contours in Meters
N
57
53e
53d
53a
53b
53c
54c
54a
54d
3.5 kHz
DEEP TOW
4 kHz

**Acoustic Character**

Depth of penetration and character of internal reflectors provide qualitative estimates of surficial sediment types, (grain-size and mode of emplacement). Hamilton (1970) showed that reflectivity and attenuation of high-frequency acoustic waves in marine sediments is directly correlated with grain size, sands being more reflective and attenuative than clays. Many other investigators have found that depth of acoustic penetration for high-resolution seismic systems is an indicator of the relative amount of sand or coarser materials in the near surface deposits (Normark and Piper, 1972; Damuth, 1975; Normark and others, 1979).

In submarine fan areas, Normark and others (1979) and Damuth (1980) found that muddy sediments show multiple internal reflectors with good continuity and acoustic penetration of several tens of meters. Coarser grained silt, sand and gravel generally showed "distinct, continuous sharp bottom echoes with no apparent sub-bottom reflectors" according to Damuth (1975). Kennedy and others (1980) and Moore (1957) describe a near surface, acoustically transparent unit as unconsolidated, possibly Holocene, sediment. A uniformly deposited layer of water-saturated, unconsolidated hemipelagic mud would be expected to have this acoustically transparent character. Finally, acoustic basement in the high-resolution seismic profiles is recognized by distinct seafloor reflectors with a prolonged return. In some cases, sub-bottom reflectors can be identified in areas of older sedimentary rock, the relative age and basement character being inferred from the strength of the echo and by its prolonged reverberation.

With the above observations in mind, the author has mapped five acoustic facies (figure 52) which are inferred to be representative of the seafloor lithology and sediments: (1) areas showing distinct, multiple, closely-spaced (<5 meters) continuous, conformable, parallel reflectors, and onlap character at the edges of generally flat-floored basins, with acoustic penetration in excess of 20 m; (2) areas showing distinct, multiple, continuous, parallel reflectors that are more widely spaced (>5 m) and show draped appearance over gentle topography, with acoustic penetration in excess of 20 m; (3) areas showing few distinct, parallel reflectors separated by relatively wide (>10 m), 'acoustically transparent' zones, with acoustic penetration in excess of 20 meters; (4) areas showing distinct seafloor reflections with prolonged return, and some sub-bottom reflections; and (5) areas showing strong, diffuse seafloor reflections with very prolonged return and no sub-bottom reflections. Examples of these acoustic facies are shown in figures 53 and 54 for the two high-resolution seismic systems used in this study. Sediments mapped as units 1-3 are inferred to be predominately mud, the more closely-spaced parallel reflectors possibly identifying turbidites and the few, widely-spaced reflectors identifying predominately hemipelagic sediments. The few cores available from North San Clemente Basin support this interpretation, showing predominately green mud, with few, thin sandy layers within the upper few meters of sediment (Emery and Rittenberg, 1952; Emery, 1960; Emery and Bray, 1962).

Acoustic facies 4 and 5 are considered acoustic basement types in this study, although areas underlain by coarse-grained sediments may also be included in facies 4. Areas mapped as facies 4 or 5 may include small pockets or thin deposits of acoustically transparent material overlying the acoustic basement. In areas of steep

Figure 52. Map of acoustic facies along the San Clemente fault zone between Fortymile Bank and North San Clemente Basin. See figure 51 for the location of high-resolution seismic tracklines used to identify the acoustic facies.

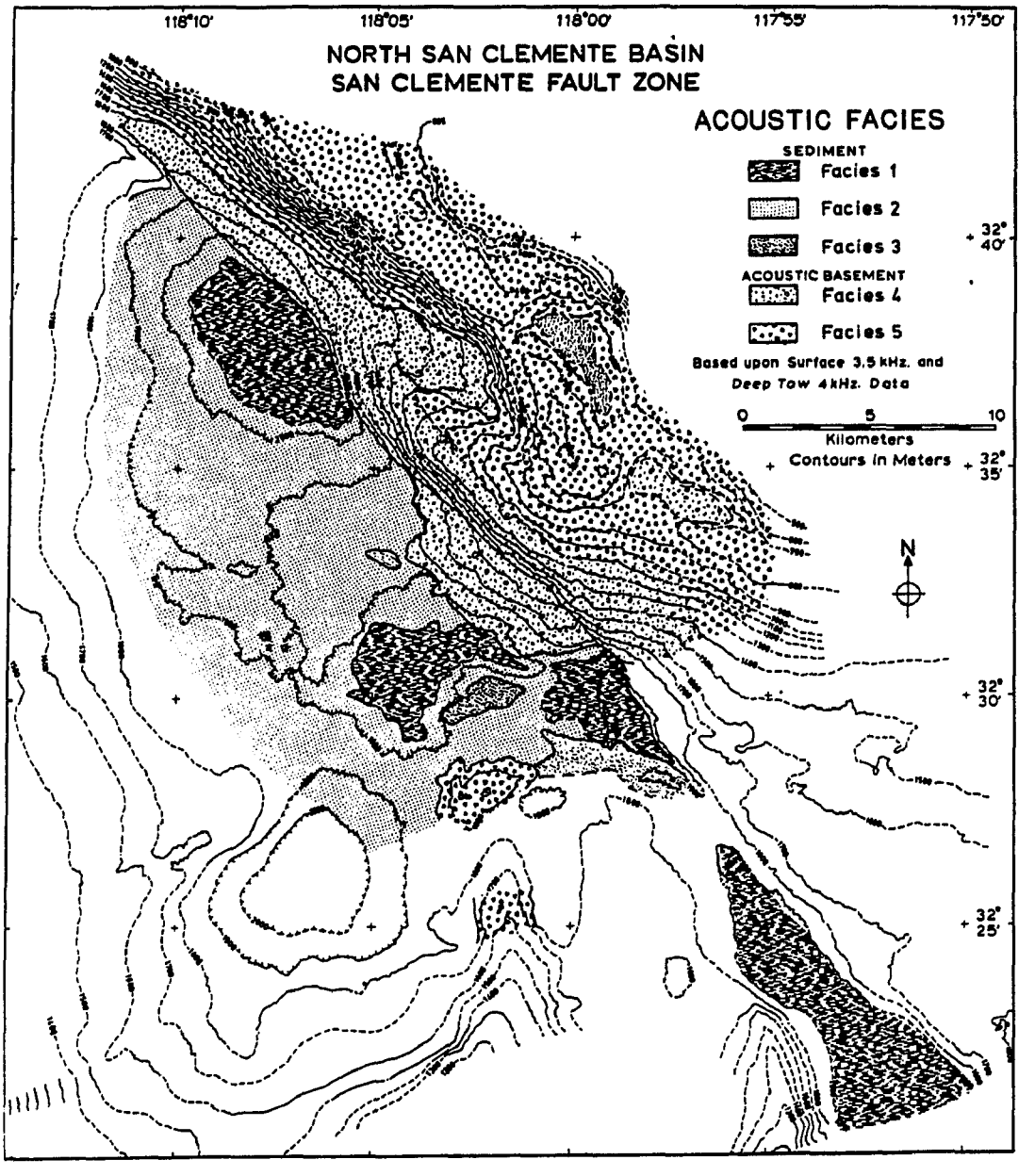
118°10'
118°05'
118°00'
117°55'
117°50'
NORTH SAN CLEMENTE BASIN
SAN CLEMENTE FAULT ZONE
ACOUSTIC FACIES
SEDIMENT
Facies 1
Facies 2
Facies 3
ACOUSTIC BASEMENT
Facies 4
Facies 5
Based upon Surface 3.5 kHz. and
Deep Tow 4 kHz. Data
0
5
10
Kilometers
Contours in Meters
32° 40'
32° 35'
32° 30'
32° 25'
N

Figure 53. Surface ship, high-resolution (3.5 kHz) seismic profiles showing character of acoustic facies (see figure 51 for location of profiles). Prominent acoustic horizons (Triplet and Horizon 2) have also been identified in the basin sediments.

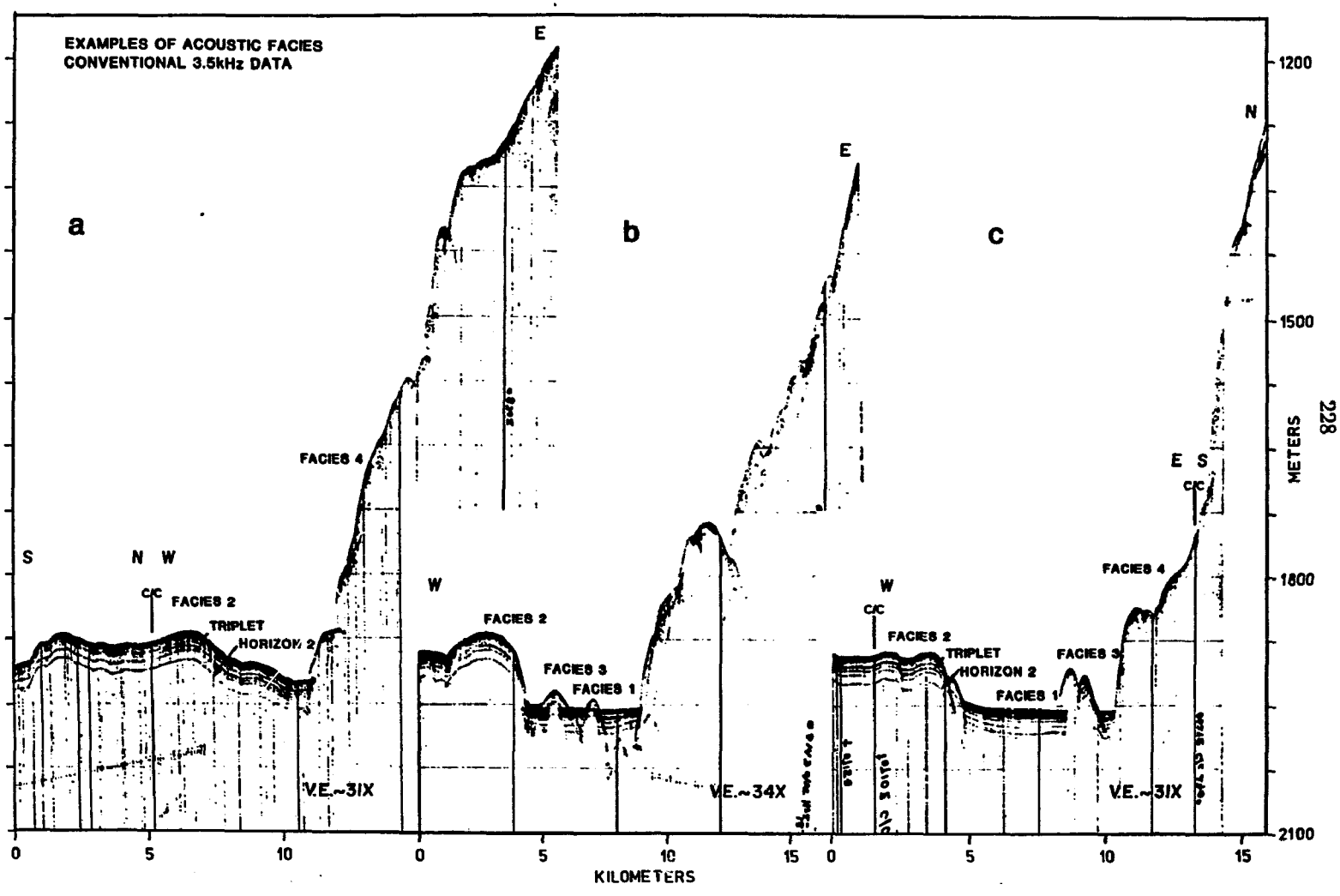
EXAMPLES OF ACOUSTIC FACIES
CONVENTIONAL 3.5kHz DATA
a
b
c
S
N
W
E
C/C
FACIES 2
TRIPLET
HORIZON 2
FACIES 4
FACIES 3
FACIES 1
V.E.~31X
V.E.~34X
V.E.~31X
1200
1500
1800
2100
METERS
0
5
10
15
KILOMETERS

Figure 53. Surface ship, high-resolution (3.5 kHz) profiles showing acoustic facies. (Continued).

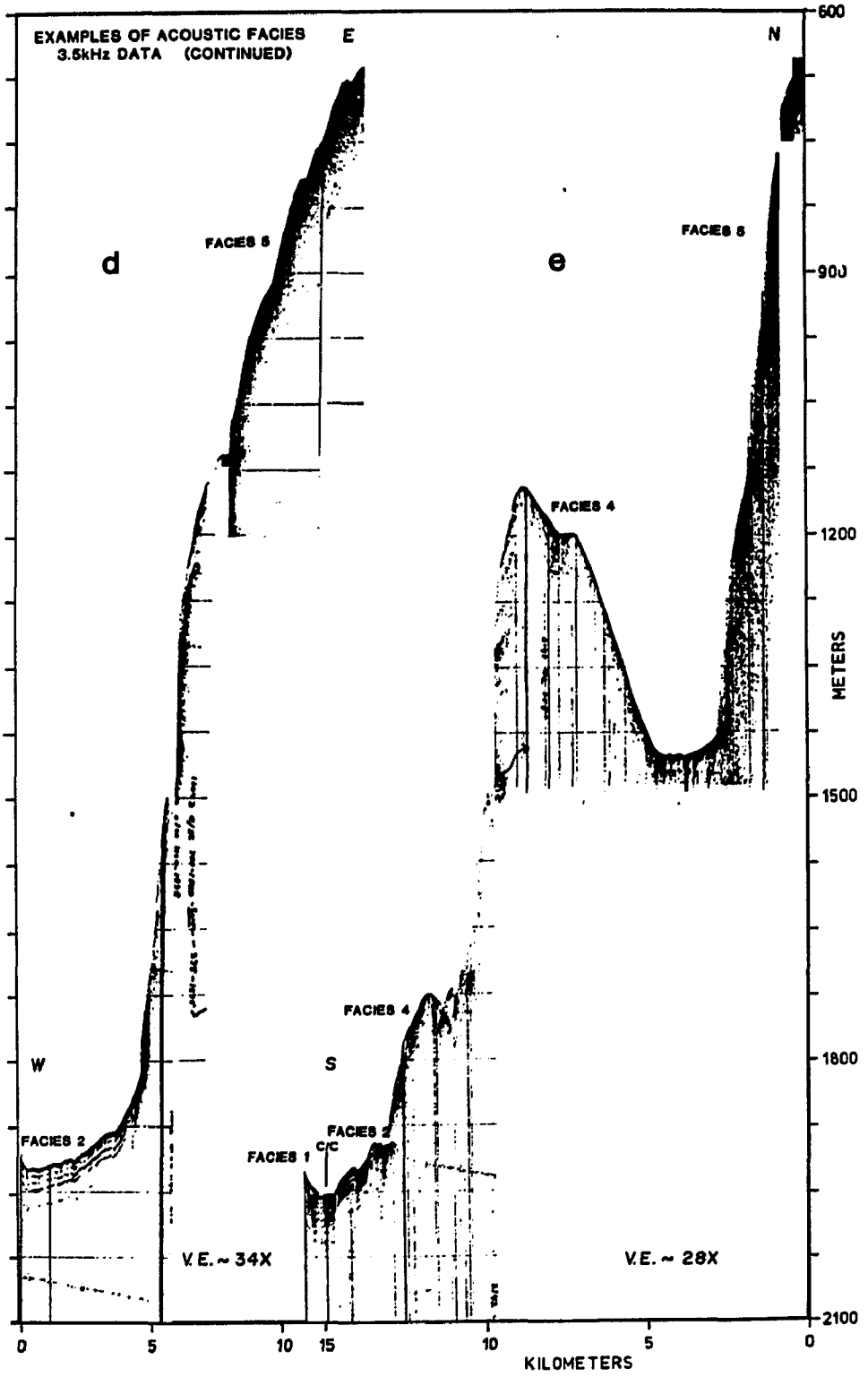
EXAMPLES OF ACOUSTIC FACIES
3.5kHz DATA (CONTINUED)
E
N
d
e
FACIES 5
FACIES 5
FACIES 4
FACIES 4
FACIES 2
FACIES 1
FACIES 2
C/C
W
S
V.E. ~ 34X
V.E. ~ 28X
600
900
1200
1500
1800
2100
METERS
0
5
10
15
10
5
0
KILOMETERS

Figure 54. Deep Tow high-resolution (4 kHz) seismic profiles showing character of acoustic facies (see figure 51 for location of profiles). Prominent acoustic horizons (Triplet and Horizon 2) have also been identified in the basin sediments.

EXAMPLES OF ACOUSTIC FACIES ~ DEEP TOW 4kHz Profiling System

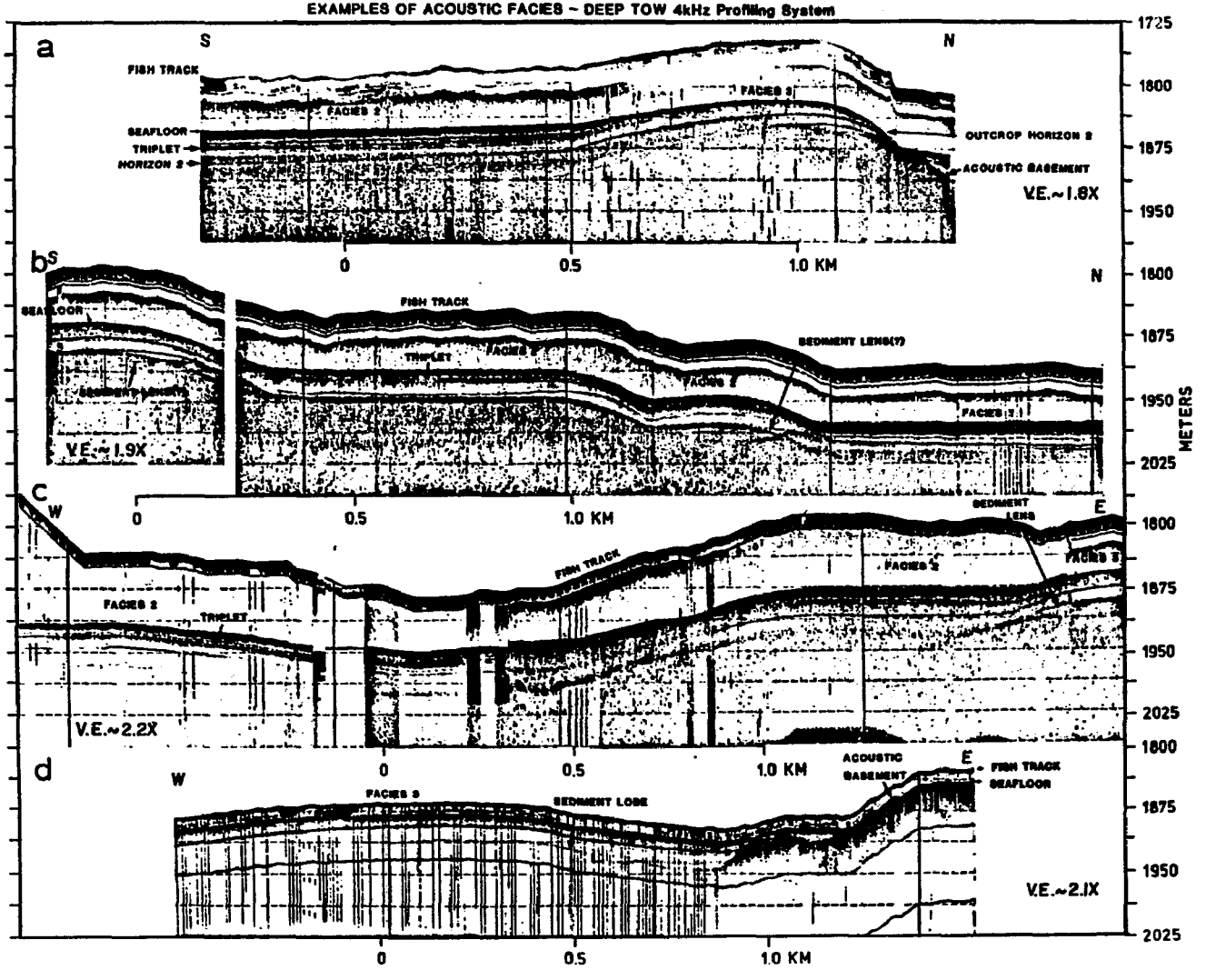

topography (slopes >15°), it is difficult to distinguish between facies 4 and 5 with surface ship data, and so these areas are generally mapped as facies 5 when data are inadequate to allow a distinction. Care must be exercised, therefore, in inferring significant lithologic variations across the many fault scarps observed in this area based solely upon the surface ship 3.5 kHz data.

Two major seafloor lithologic divisions are apparent from the acoustic facies map (figure 52): (1) areas underlain by acoustic basement, and (2) areas of significant sedimentary cover. The entire mapped area is divided roughly in half by these two zones. Acoustic basement facies are in the northeast, where Fortymile Bank, an area of significant relief is located. Sedimentary facies are present in the west and south, where North San Clemente Basin is located, a deep area of low relief. Scattered outcrops of acoustic basement are located where steep-sided peaks protrude through the sedimentary cover of the basin area. A gently sloping region of sedimentary facies is located in the southeast part of the map, although few high-resolution seismic data are available in this area to delineate its boundaries more accurately.

Although the seafloor of Fortymile Bank is generally underlain by acoustic basement facies, some pockets of sedimentary fill are locally present filling some of the deeper holes (figure 52). Some parts of Fortymile Bank are underlain by sedimentary rock. Samples from the crest and flanks of Fortymile Bank include both Miocene sedimentary and volcanic rocks of undetermined(?) age (Vedder and others, 1974). Junger and Vedder (1980, personal communication) infer that Mesozoic basement rocks are along the lower parts of Fortymile Escarpment.

Sediments in the basin areas are grouped into the three acoustic facies described above. In as much as these three facies all show significant acoustic penetration, and continuous, parallel reflectors, predominately very fine-grained deposits such as clay or silty-clay are likely to underlie these areas. Smith and Normark (1972), Normark and others (1979), and Damuth (1975, 1980) have correlated such reflection character with relative absence of coarse-grained (silt/sand/gravel sized), bedded sediment in piston cores.

The deepest basins tend to be flat-floored and filled with facies 1 (figure 52). The onlap evident on seismic profiles crossing the edges of these basins (figures 53 and 54) imply that these deposits are ponded turbidites, similar to those observed in the nearby Navy Fan basin plains (Normark and others, 1979; Normark and Piper, 1972). Facies 2 is found in relatively flat areas which are elevated slightly above the ponded basins, including the large area of gentle relief between the two larger ponded basins in the center of the mapped area. Facies 3 is located in small patches, mostly along the crests of the higher, rounded peaks in the southern basin area. Facies 3 is most easily recognized on Deep Tow 4 kHz profiles (figure 54). Facies 2 grades laterally into facies 3, and layers between prominent reflectors either pinch out or thin appreciably leaving few reflectors visible in facies 3 seismic profiles (figure 54). Facies 1 generally onlaps facies 2 in the study area, although some prominent acoustic horizons can be traced continuously through all three 'sedimentary' acoustic facies described above (figure 54).

**Acoustic Horisons and Isopachs**

Of the prominent acoustic horizons apparent in the surface 3.5 kHz and Deep Tow 4 kHz data, two are relatively continuous, and hence, mappable throughout most of the basin area studied. The first is most easily recognized as consisting of a 'triplet' of evenly spaced, parallel reflectors which appear continuously over most of the area (figures 53 and 54). In following this triplet throughout the region, additional parallel reflectors become apparent or disappear between the three primary reflectors. In some areas one or another of the primary reflectors becomes obscure, although at least two of the three can be followed continuously for several kilometers. The middle reflector of this triplet is the most continuous and easily followed throughout the study area, and so it was selected as one horizon for mapping the near surface sediment isopachs.

A second prominent reflector observed throughout most of the basin area is evident from 10 to 20 m (at 1500 m/sec acoustic velocity) below and mostly parallel to the base of the triplet (figure 54). This reflector is generally observed as a single, distinct and strong reflector, although in a few places, a second, less prominent reflector lies parallel and within 5 meters to the primary reflector. The more prominent reflector is used as the second horizon in the isopach studies.

Other prominent reflectors lying somewhat deeper, but mostly parallel to the two described above, are also apparent and continuous for several kilometers on seismic profiles across North San Clemente Basin. These reflectors, however, generally lie too deep below the seafloor, in the flat floored basin deeps to be seen with the high-resolution seismic systems used in this study. Therefore, these other reflectors were not used for mapping additional isopachs.

Reflectors present in narrow band width (band limited), high-resolution, seismic profiles are not always images of specific subsurface discontinuities. Mayer (1979a,b; 1980) showed that multiple reflectors can be acoustic interference patterns, resulting from many, thin layers of varying acoustic impedance. Although some or all of the reflectors used as acoustic horizons in this study may be of such nature, the author believes they still represent correlatable horizons and uses them as such, because their overall continuity across the region supports this interpretation. Furthermore, the author assumes these horizons are isochrons and can therefore measure the spatial variability in sedimentation rates throughout the area. Additional data, including numerous long piston cores throughout the area are needed to test these hypotheses.

**Unit 1 Sedimentation Patterns**

Isopachs for Unit 1, showing the thickness in meters between the seafloor and the middle reflector of the triplet are shown in figure 55. A contour interval of five meters was used. The resolution of the 3.5 kHz and Deep Tow 4 kHz data is about 1-2 meters in sediment thickness. An interval velocity of 1500 m/sec was used to compute sediment thickness based upon sediment velocity studies of Hamilton and others (1974) in this part of North San Clemente Basin. Emery and Bray (1962) report a late Quaternary to Holocene sedimentation rate of 30* cm/1000 yrs for North San Clemente Basin, based upon a piston core from the location shown in the isopach maps. Because the thickness of Unit 1 at this location is approximately 30 m, the contour values shown for this map can also be used to indicate average sedimentation rates, (in cm/1000 years), for the latest Quaternary, assuming this average is

---

* The late Quaternary sedimentation rate may have been substantially greater during glacial and marine transgression stages (Dunbar, 1981; chapter 3, this volume).

Figure 55. Isopach map of Unit 1, the sediment layer between the seafloor and the middle of the Triplet. Thicknesses are in meters using an interval velocity of 1500 m/sec (Hamilton and others, 1974) and are not corrected for compaction. Tracklines of seismic data used to contour these isopachs are shown in figure 51. Dot shows location of piston cores described in the text.

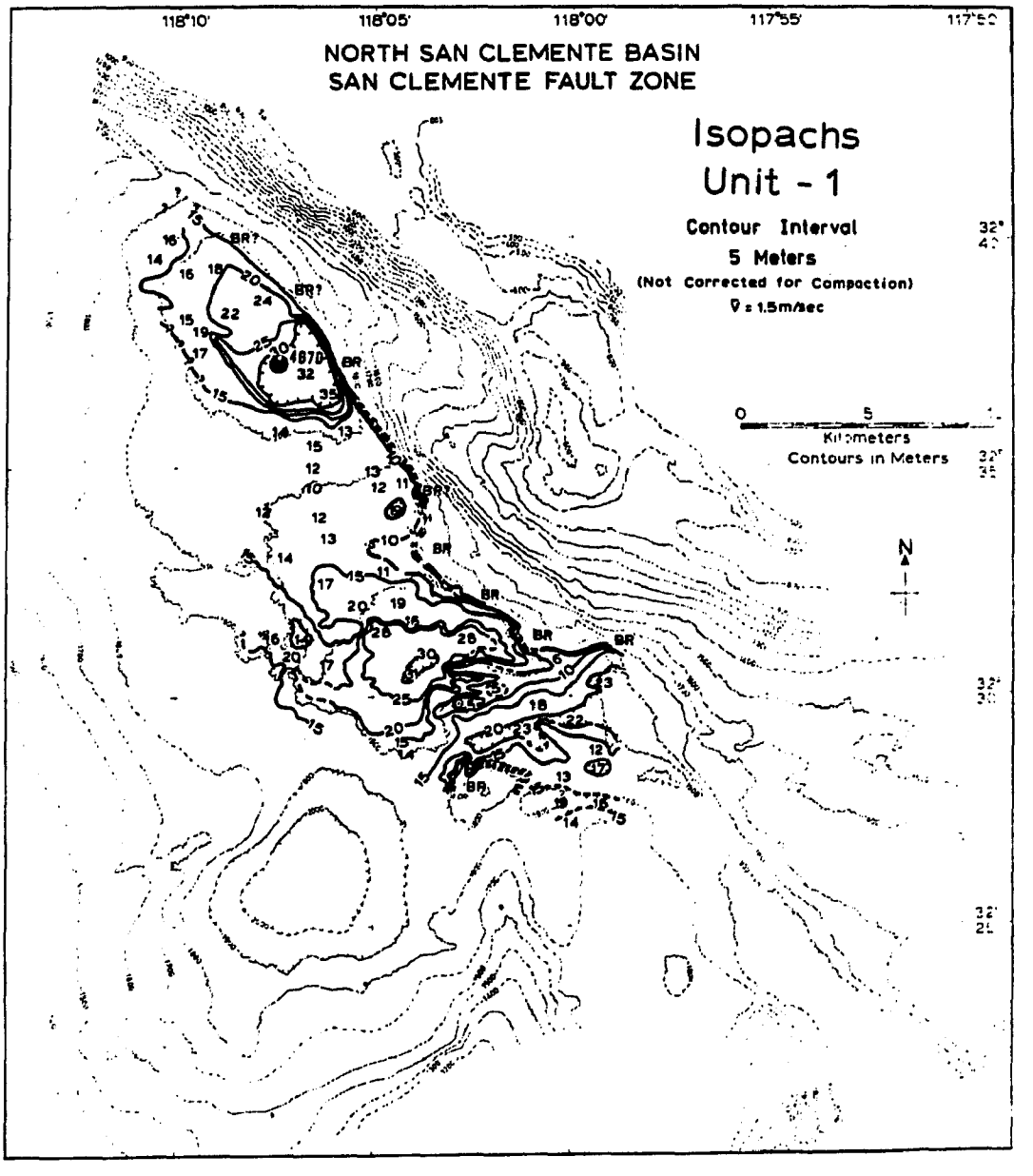
118°10'
118°05'
118°00'
117°55'
NORTH SAN CLEMENTE BASIN
SAN CLEMENTE FAULT ZONE
Isopachs
Unit - 1
Contour Interval
5 Meters
(Not Corrected for Compaction)
V̄ = 1.5m/sec
0
5
Kilometers
Contours in Meters
N

relatively constant throughout the time represented by the interval between Horizon 1 and the present seafloor.

The spatial patterns of sediment thickness and sedimentation rate shown for Unit 1 are roughly correlated with topography. The deepest, enclosed basins show the highest rates and thickness, whereas the highest topographic peaks have significantly less sediment cover. This is consistent with predominately turbidite ponding within basins and predominately hemipelagic sedimentation over elevated regions. Also, downslope transport through mass-wasting and other processes, resulting in redistribution of sediment from the high areas to the low, may have occurred. The absence of disturbed sediments in these relatively flat-lying sediments, however, implies that such effects are minor, except where locally evident. Reworking by bottom currents may also have occurred in the past, but bottom photographs showing numerous, neutrally buoyant organisms, and a surface layer of fine mud show that significant bottom currents are absent over most of the basin (figure 56). The significant variability in sediment thickness and hence sedimentation rates over some of the elevated regions reveals that draping of hemipelagic sediment is not uniform, and other sediment sources may be locally significant.

Over the central, low, broad ridge between Rift and Central basins, the sediment thickness and sedimentation rates are fairly uniform, over wide areas. On this basis, the author infers that predominately hemipelagic deposition occurred during this period over that area. A significant trend of thickening towards the south also implies that some turbidite or other bottom flowing contribution from a southerly or southeasterly source is likely. Locally thin sediment cover is found over low, topographic peaks, where bottom flowing turbidites are less likely to reach, and locally

Figure 56. Deep Tow bottom photograph showing muds with burrows and deep-sea creatures. Scale is approximately the same for each photograph. Absence of current marks and presence of numerous benthic organisms, burrows and trails imply that bottom currents are generally low in this area. (Photo courtesy of R. Tyce and C. deMoustier).

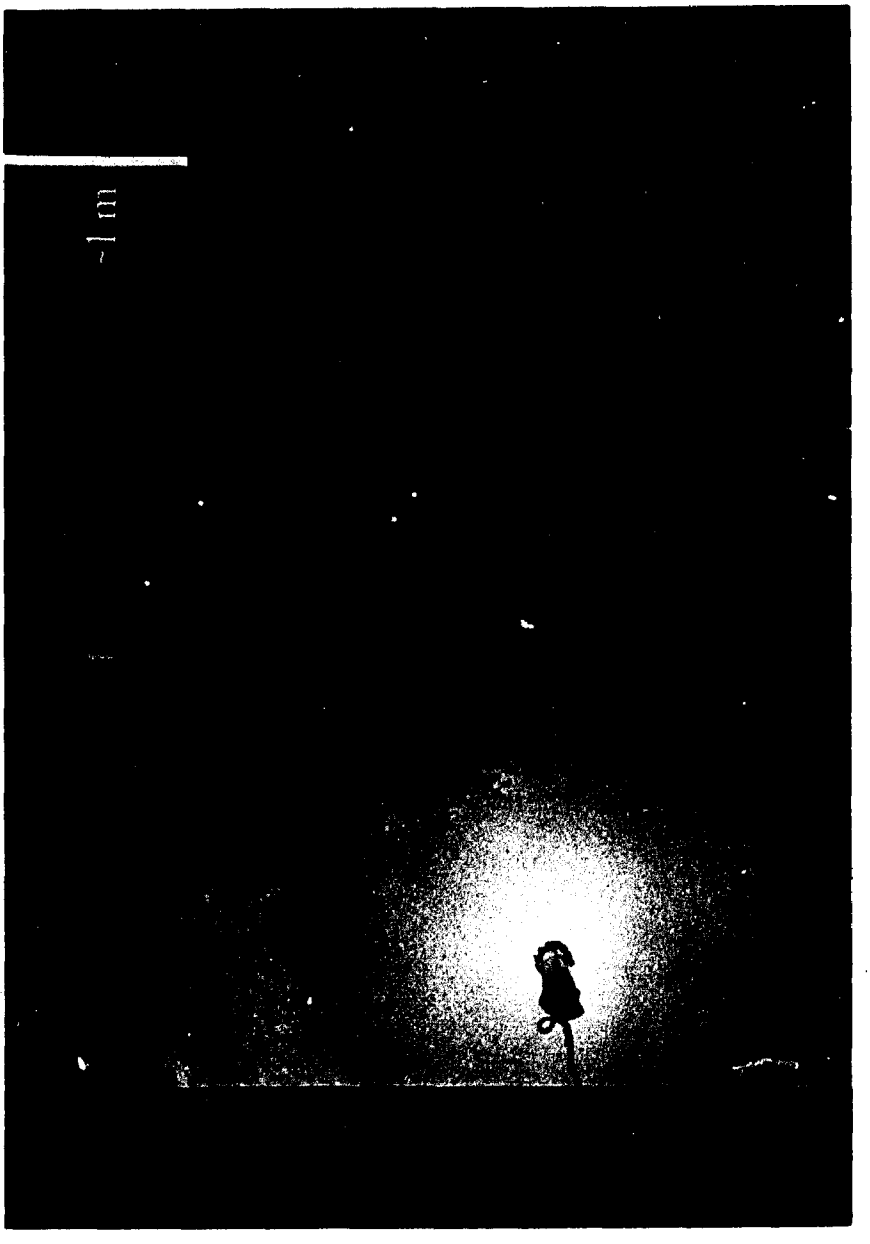
1m

Figure 56. Deep Tow Bottom Photographs (Continued).

Figure 56. Deep Tow Bottom Photographs (Continued).

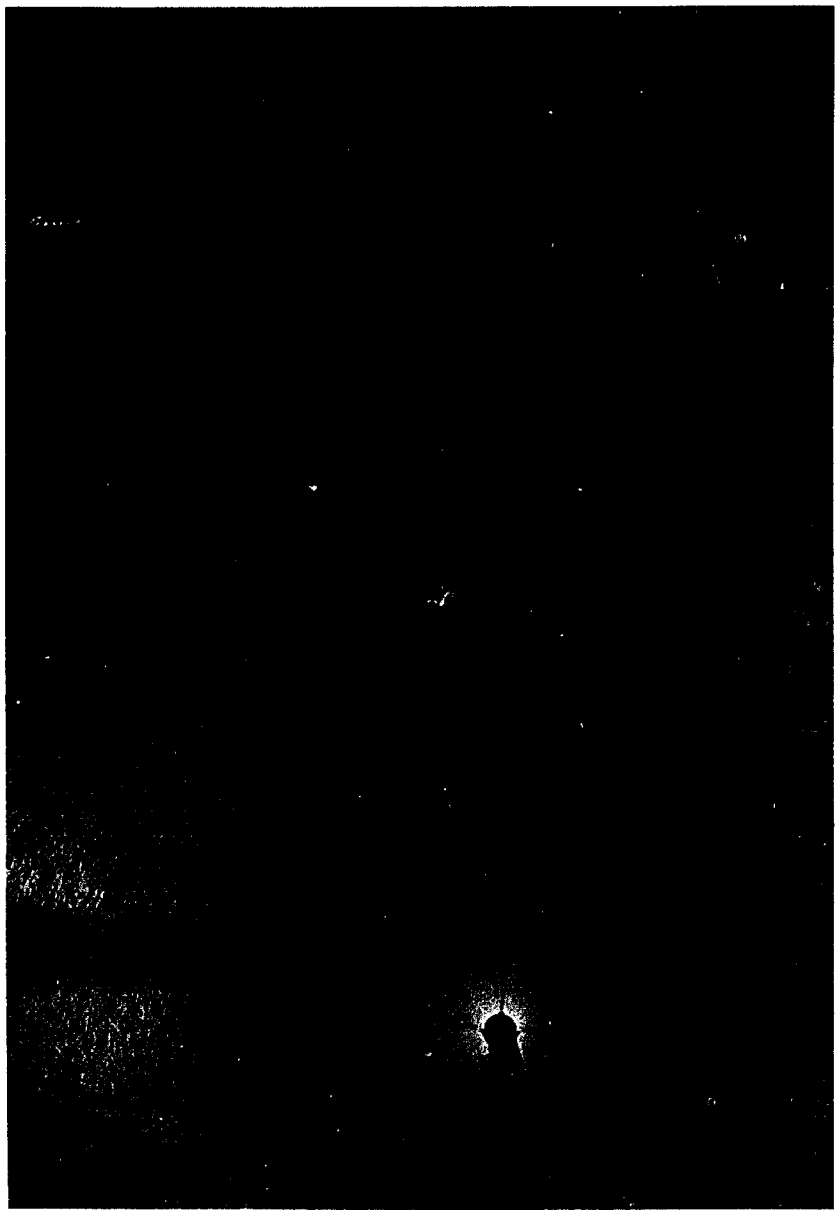

thick areas represent filled, former depressions of the ancient seafloor. Enhanced current flow due to the Bernoulli effect over and around the topographic peaks may also inhibit sedimentation in these areas (Johnson and Johnson, 1970).

A similar, relatively flat, elevated region at the south edge of the mapped isopachs shows greater variability in sedimentation. This region is bounded by topographic ridges along its northern and southern margins, which have relatively thin sediment cover, and in places, exposed acoustic basement (figure 54d). The smooth, relatively flat tops of the low ridges along the southern edges of Central Basin show a thin layer of almost acoustically transparent sediment above Horizon 1 (figure 54). Horizon 1 is very faint as well, implying that almost 'pure' hemipelagic deposition has occurred at this spot, although some erosion or overbank turbidite deposition may occur sporadically. South of this ridge, an elongated, west-trending region of relatively thicker sediments is observed. This pattern follows the topographically deepest parts of the area and may delineate a channel being filled by turbidites or other bottom following sediment flows. At the southwestern end of this channel, a topographic high is found, which also shows sediment thickening between horizons (figure 54d). The significance of this feature is discussed in more detail in a later section.

The deeper, enclosed basins show the greatest sediment thicknesses. These are also the regions where onlap against the basin margins of the numerous, closely-spaced, multiple, parallel reflectors within the basin (facies 1), is observed in high-resolution seismic profiles. Such data are inferred by the author to identify ponded turbidites filling these basins. In general, the deepest parts of the basins are also the locations of the thickest deposits, although these basins have relatively flat horizontal

floors. The deepest part of Central Basin is approximately in the center of the basin, whereas the northern Rift Basin is deepest adjacent to the fault scarp along its northeastern margin. The thickening of sediments of this basin adjacent to the fault scarp as well as the present topographic low in the same area may demonstrate that this basin has continued to deepen, slightly faster than sediments can fill it (to a horizontal level).

Rift Basin is separated into two halves by the northeast-trending 25 m isopach. The deeper, more thickly sedimented southeastern part has a small, but consistent trend of topographic deepening and sediment thickening toward the fault bounded northeast margin. The author proposes that this is the more recent, tectonically-active part of the basin. The northwestern half has a more uniform sediment thickness and depth, although a narrow, trough of somewhat deeper bathymetry and thicker sediments, aligned along the base of the fault scarp, may represent local tectonic deepening (or filling of an older channel?). An east-trending tongue of thin sediments near the northwest margin of this basin may be interpreted as a relative thinner sediment cover over an ancient submarine slump or debris flow deposit. The 3.5 kHz profiles show a region of thickening and disruption (back tilting) of internal reflectors in this region (figure 57) which is consistent with the buried slump interpretation. The deeper isopachs (Unit 2) show thickening in this area along this trend.

The 3.5 kHz data show only thin, isolated pockets of youthful sediment lying above acoustic basement on the scarps and elevated parts of Fortymile Bank. Deep Tow 4 kHz data across the 'shutter ridge' between the main fault scarp and North San Clemente Basin in the central mapped area also show only isolated patches of

Figure 57. High-resolution (3.5 kHz) seismic profile across Rift Basin showing near surface sedimentary features. Note the two major course changes (C/C) along the profile (see figure 51 for profile location).

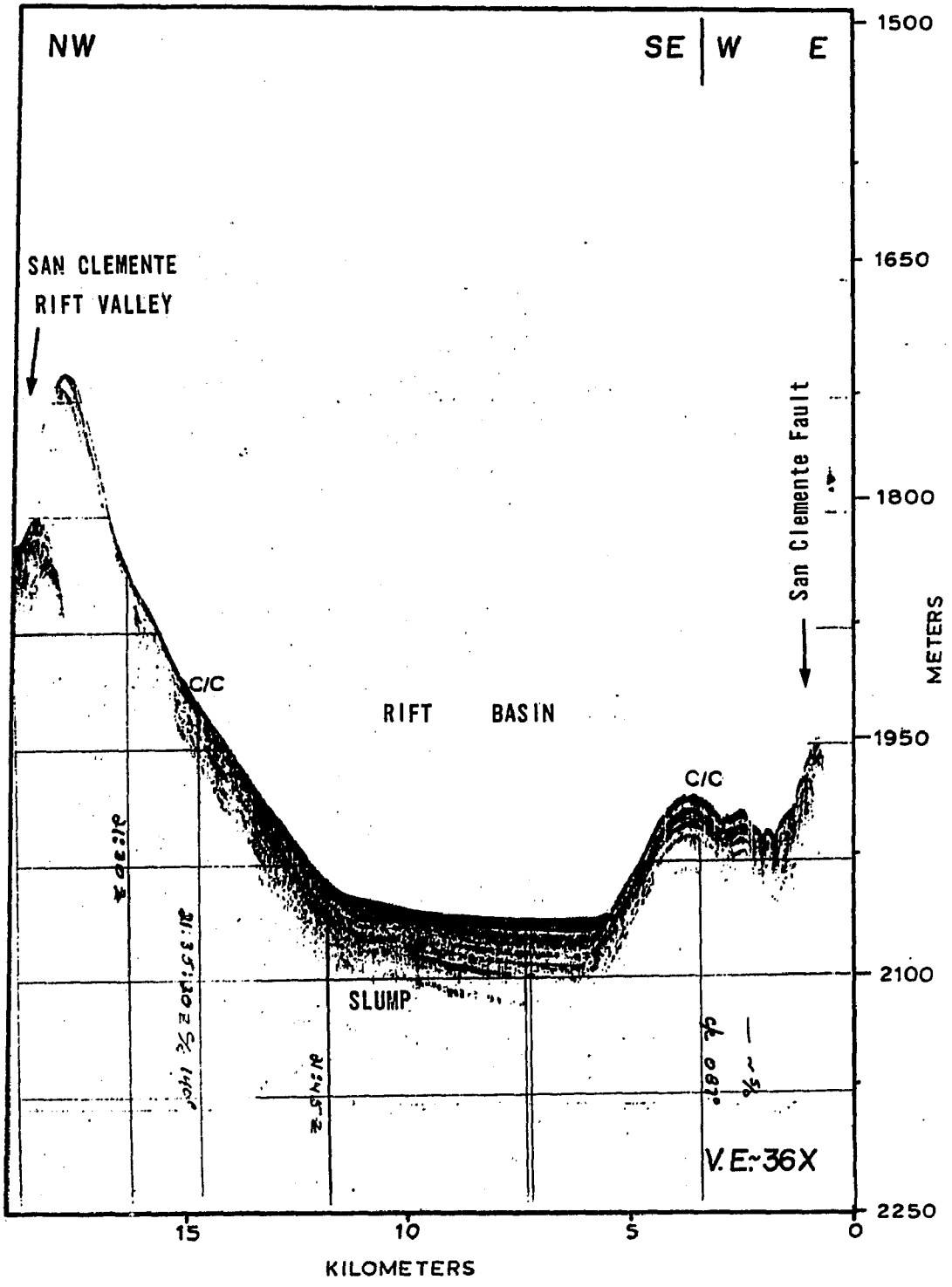
NW
SE | W
E
SAN CLEMENTE
RIFT VALLEY
C/C
RIFT BASIN
C/C
SLUMP
San Clemente Fault
V.E.~36X
1500
1650
1800
1950
2100
2250
METERS
15
10
5
0
KILOMETERS

thin, acoustically transparent sediment lying over acoustic basement and older sedimentary deposits which themselves show erosional truncations at the surface. These areas of negligible sediment cover have, therefore, undergone significant periods of either erosion or non-deposition, because no significant layer (>5 m) of hemipelagic drape is apparent. Perhaps significant tidal or other bottom currents have inhibited deposition on these slopes. Current ripples observed by Moore (1969) during a submersible dive into San Clemente Rift Valley showed that significant bottom currents have occurred locally, during the recent past. Even so, Lonsdale (1979) reports that the steep slopes of a scarp along the San Clemente fault near Navy Fan are covered by silty mud, and no outcrops were visible although acoustic profiles indicated truncated beds of layered sediment.

**Unit 2 Sedimentation Patterns**

Isopachs of Unit 2, sediments between the middle triplet acoustic horizon, and the second prominent horizon discussed previously, show patterns spatially similar to the overlaying Unit 1 deposits (figure 58). Basins show thickest sediments whereas elevated regions show less, and steepest slopes generally have no recent sediment cover. A broad area of relatively uniform thickness is apparent over the central area where the broad, low ridge is located. As in Unit 1, Unit 2 sediments here also thicken uniformly toward the south, and local pockets of thicker sediments are apparent. These locally thicker areas are roughly coincident with shallow, surface channels in some cases (along the east edge of the low ridge) and may represent channel filling by bottom following sediment flows such as turbidites or mudflows. A similar elongate, west-trending thick sediment area is located along the southern part of

Figure 58. Isopachs of Unit 2, the sediment layer between the middle of the Triplet and Horizon 2. See figure 55 for additional information.

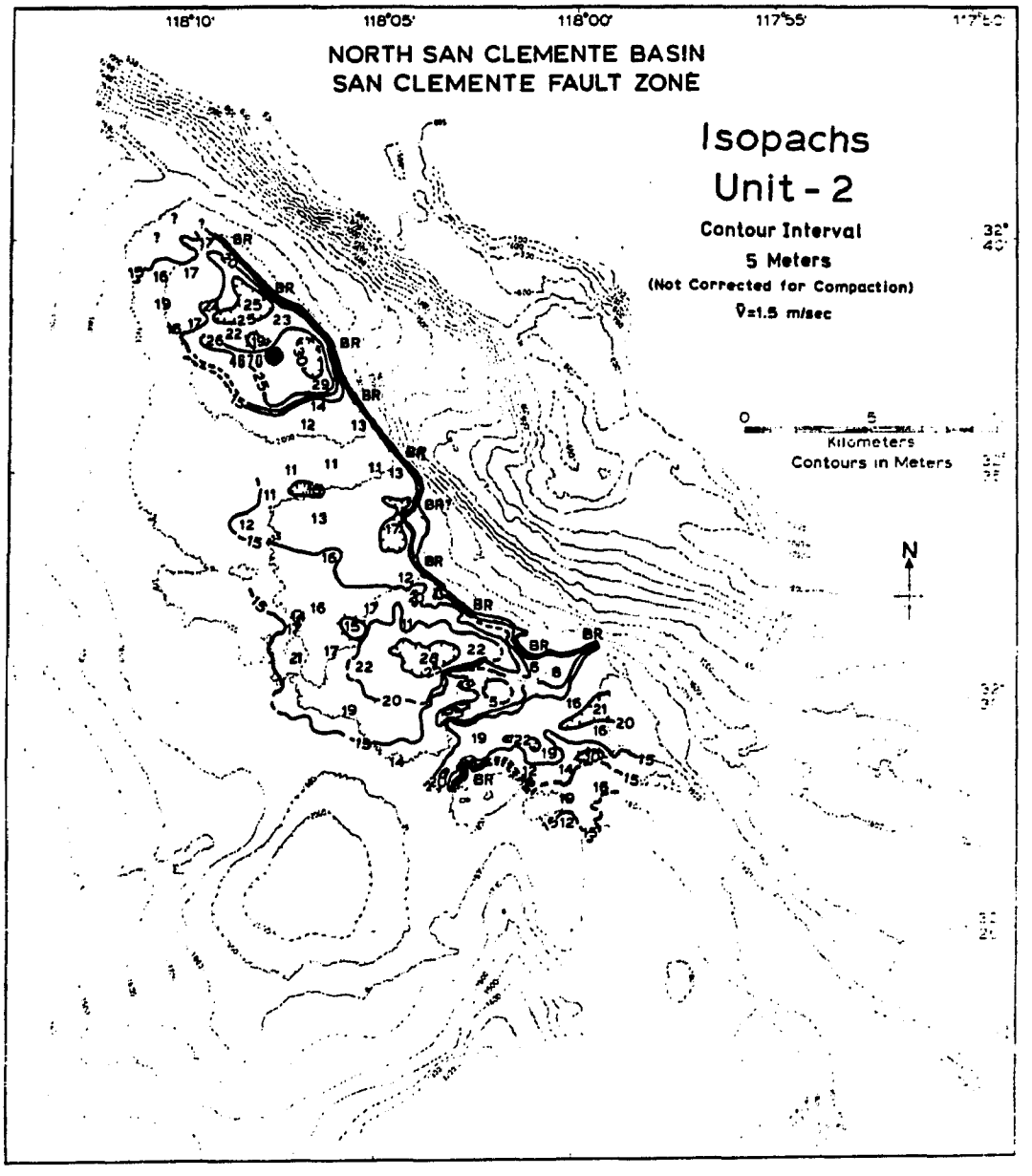
118°10'
118°05'
118°00'
117°55'
NORTH SAN CLEMENTE BASIN
SAN CLEMENTE FAULT ZONE
Isopachs
Unit - 2
Contour Interval
5 Meters
(Not Corrected for Compaction)
V=1.5 m/sec
0
5
Kilometers
Contours in Meters
N
BR

the region between the low ridges in the ancient channel described previously. The low, elongate ridges again have relatively thin, acoustically transparent sediment layers between the major horizons, whereas in the deeper regions, high-resolution seismic data show other continuous, parallel reflectors between these major horizons. An exception is at the end of the southern, elongate channel where a thick 'lobe' of sediments is associated with a topographic mound (figure 54d).

Sediment thicknesses in Central Basin are again greatest at the center, and thin uniformly toward the margins. Rift Basin is shown to have two areas of thicker sediments separated by a northeast-trending ridge of thinner sediments. The southern half of the basin has thickest sediments adjacent to the fault flanking the eastern margin. The northern half seems to have the thicker sediments aligned along two trends, one northwestward, parallel to the fault and the other, east-trending, subparallel to the ridge of thin sediments. A thick lobe of sediment along the western margin of the basin is inferred to represent a local debris flow or slump deposit.

**Bottom Samples**

Two piston cores from North San Clemente Basin have been studied previously in some detail (Emery and Rittenberg, 1952; Crouch, 1952; Orr, Emery and Grady, 1958; Emery, 1960; Emery and Bray, 1962). Both were located in the deepest parts of North San Clemente Basin and sampled about three meters of sediment. Figure 59 shows a comparison of the two cores as described by these investigators, including the median grain size and *Foraminifera* data (Crouch, 1952), of core 1984. The most significant features of these two cores, relevant to the present study, is that both contain sand layers. Grading bedding above the sand layers is implied by the

Figure 59. Comparison of core logs for two piston cores obtained from the North San Clemente Basin (after Emery and Rittenberg, 1952; Crouch, 1952; and Orr and others, 1958). Sediment type, microfauna and median grain size are shown at several intervals for core 1984. Sediment type and radiocarbon age are shown for core 4670.

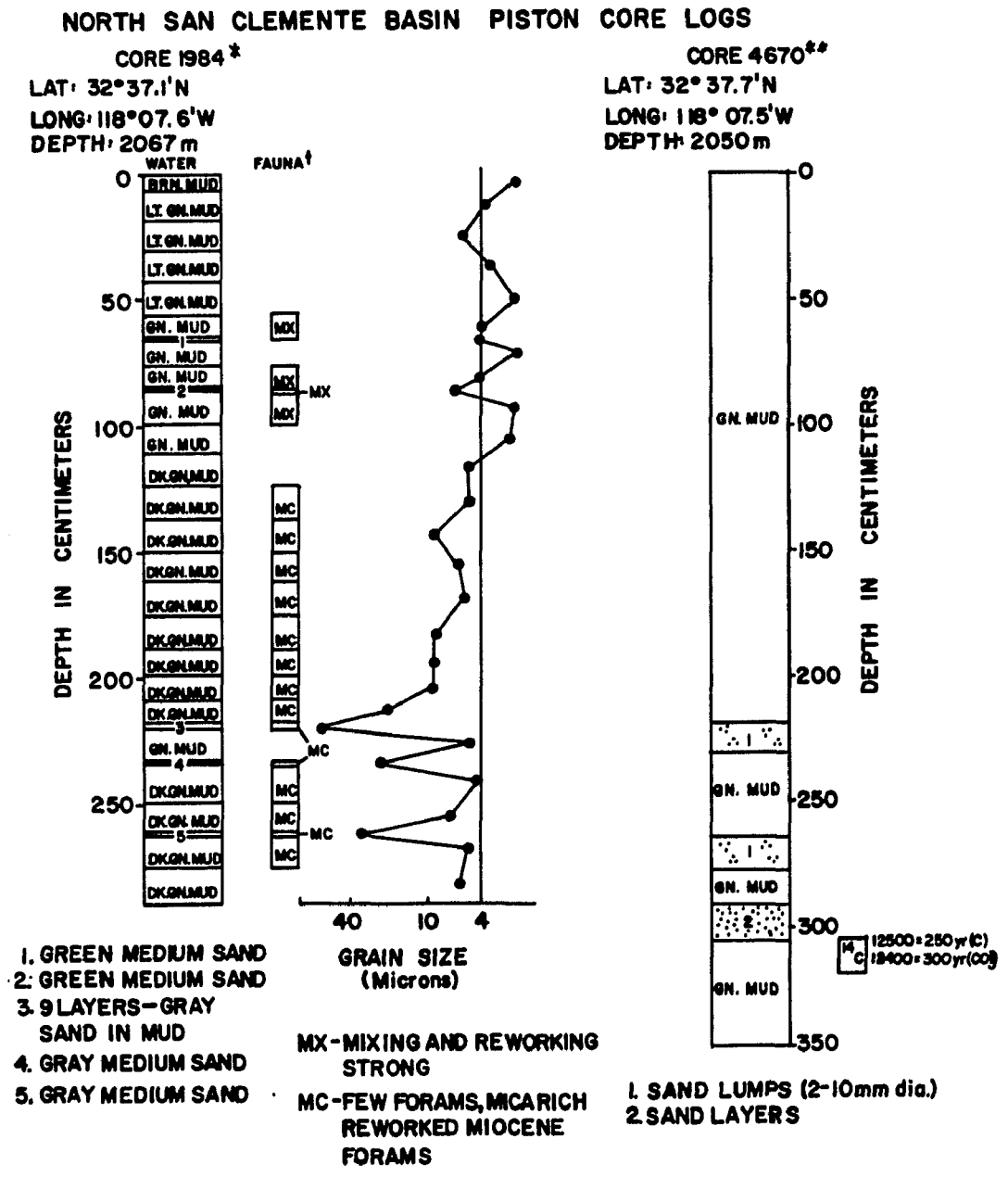


1. GREEN MEDIUM SAND
2. GREEN MEDIUM SAND
3. 9 LAYERS—GRAY SAND IN MUD
4. GRAY MEDIUM SAND
5. GRAY MEDIUM SAND

MX-MIXING AND REWORKING STRONG

MC-FEW FORAMS, MICA RICH REWORKED MIOCENE FORAMS

1. SAND LUMPS (2-10mm dia.)
2. SAND LAYERS

*EMERY AND RITTENBERG (1952)

†CROUCH (1952)

**ORR, EMERY AND GRADY (1958)

grain size profile for core 1984. Crouch (1952) notes that reworked Miocene *Foraminifera* were present throughout this core, and abundant mica was present in its relatively barren, lower half. These data demonstrate that turbidity currents have provided a significant amount of the late Quaternary sediment in this basin. Emery and Rittenberg (1952) propose that these turbidity currents are of local origin, coming from the offshore banks, in this case, San Clemente Island or Fortymile Bank.

## LATE QUATERNARY SEDIMENTATION IN NORTH SAN CLEMENTE BASIN

### Origin and Estimated Ages of the Acoustic Horizons

Horizon 1 is represented by the middle reflector of a series which is most commonly observed as a triplet. In following these reflectors along the different reflection profiles, the basic character, as a triplet, is generally unchanging, allowing identification of this sequence over most of the survey area. Details of this pattern, however, are observed to change, with intermediate reflectors appearing and disappearing, and in some cases, one or another of the main triplet reflectors disappears. The spacing between the triplet reflectors also varies, generally being widest in the low-lying areas. This reflector behavior is similar to the observations made by Mayer (1980) using synthetic seismograms with a real reflection coefficient log from the equatorial Pacific. In his experiments, various strong reflectors, representing an acoustic interference pattern from the many closely spaced, weakly reflecting interfaces of the seafloor sediments, changed character, faded and disappeared as the layer thicknesses incrementally increased. Most of these reflectors did not mark specific lithologic boundaries, although the entire pattern resulted from the closely-

spaced layers of varying acoustic properties.

The author proposes that the triplet observed over much of the survey area is also such an interference pattern resulting from a specific sequence of thin sedimentary units of varying acoustic properties. Thin graded turbidite beds interlayered with hemipelagic sediments would be one likely sedimentary sequence having this character. Alternatively, variability in hemipelagic sedimentation caused by climatic changes could also produce such a thin, layered sequence.

An approximate age for the unit is estimated by applying the average Holocene sedimentation rate determined by Emery (1960). Examination of the 3.5 kHz data in North San Clemente Basin where the dated core was obtained, and at the appropriate water depth of the core because some navigational errors are likely, the three prominent reflectors of the triplet are at depths of 17, 23, and 32 m, using the 1500 m/sec interval velocity of Hamilton and others (1974). Using a method described by Moore (1969) these depths are corrected for compaction, yielding 20, 28, and 38 m, and approximate ages computed using the average sedimentation rate. Ages of 64,000, 92,000, and 126,000 years B.P. are obtained, showing that sediments in the middle of the triplet (Horizon 1) are about 100,000 years old. The approximate age of the bottom of the triplet is very close to that of a major glacial stage boundary, predicted from oxygen isotope data (Shackleton and Opdyke, 1976; Broecker and van Donk, 1970). An age of 128,000 years B.P. was estimated for this boundary by Shackleton and Opdyke (1973, 1976) assuming a constant sedimentation rate at their western equatorial Pacific core site. The uplifted Nestor marine terrace in the San Diego area also has a similar age (Kern, 1977; Lajoie and others, 1979). Other uplifted terraces on San Clemente Island appear to be correlative as well (Muhs, 1979).

Unlike the triplet, Horizon 2 is a relatively strong, distinct, single reflector throughout the survey area. The intensity of this reflection decreases significantly only where it is more deeply buried, such as under the ponded basin turbidites, yet this reflector remains apparent as a distinct horizon. Furthermore, over the crests of the low ridges in the southern part of the survey area, this horizon remains as a strong, distinct reflector while the triplet fades to imperceptibility on the Deep Tow 4 kHz records (figure 54). Because of the strong, continuous character of this reflector, the author asserts that it represents a significant discontinuity in the sediment column, and possibly a disconformity. It seems to outcrop along the flank of the low, west-trending ridge on the south margin of Central Basin (figure 54a) and, therefore, could be sampled by submersible or other well-located sampling device.

Following the procedure described previously, the age of this horizon is estimated as approximately 220,000 yrs B.P. Again, this is close to a major stage boundary estimated at 251,000 years B.P. (Shackleton and Opdyke, 1976; Broecker and van Donk, 1970). Uplifted marine terraces of similar age are recognized from San Onofre to Newport Beach on the mainland (Lajoie and others, 1979), and on the Palos Verdes Hills (Muhs and Rosholt, 1984).

Significant temporal changes in sedimentation patterns or rates may be associated with these horizons. Dunbar (1981) found that terrigenous sedimentation rates increased significantly on the margin of South San Clemente Basin during the Pleistocene-Holocene deglaciation. He estimated that the deglaciation event lasted about 3000 years using oxygen and carbon isotope ratios in *Formaminifera* from a piston core taken in that area. Normark and Piper (1972) concluded that Navy Fan formed by relatively rapid sedimentation during glacial periods when sea level was

lowered and the Coronado submarine canyon was active. The sedimentation declined significantly during interglacial periods of high sea level. Data in this study show significant spatial variability in late Quaternary sedimentation rates. The coincident ages among the acoustic horizons and known Pleistocene sea-level events, as shown by the uplifted marine terraces, may be of real significance, implying that significant changes in sedimentation patterns occurred in association with these eustatic sea level changes. The ancient, possibly accelerated, coastal erosion evident from the elevated marine terraces may be directly correlated to more rapid deposition in the offshore basins, evident as acoustic horizons. These acoustic horizons may be associated with enhanced turbidite deposition.

**Sedimentation Patterns in North San Clemente Basin**

The spatial patterns of sedimentation can be inferred from the data discussed above, and a sedimentation model for the area proposed. The deeper basins have the thickest accumulations of sediment representing the highest average rates of deposition. Ponding of sediment, sand beds and reworked microfauna of Miocene to Recent age observed in piston core samples demonstrate sediment influx by turbidity currents in North San Clemente Basin. San Clemente Rift Valley was proposed by Ridlon (1969) to be a major conduit for influx of such sediment from the San Clemente Island area. Other sources may have been more important in the southern part of the survey area. North San Clemente Basin turbidites may be of identifiably different composition or character than turbidites derived from a direct continental source, such as via Coronado submarine canyon to Navy Fan.

The elevated areas of low relief surrounding the deeper basins have relatively slower rates of deposition shown by thinning of sequences between prominent acoustic horizons. The low relative sedimentation rates, general acoustic transparency between major horizons, and significant acoustic penetration achieved in high-resolution seismic profiles over the highest of these low ridges (figure 54) imply to the author that predominately hemipelagic sedimentation is occurring in those places. The relatively uniform isopach values and sedimentation rates over the broad, low ridge between Rift and Central basins imply that this area has also received a drape of predominately hemipelagic sediments during late Quaternary time.

Values of sedimentation rates and isopachs intermediate between those of the rapidly filling ponded basins and thinly covered, higher elevated ridge tops, coupled with the presence of distinctive sequences of continuous, parallel reflectors seen in acoustic profiles may signify that some layered sediment sequences are present in these low, elevated areas. The southward increase of sediment thickness in the central area is possible evidence of a northward flow of some sort contributing additional sediments to this area. This flow has generally either been unable to overtop the 1850 m bathymetric contour and deposit sediments, or occasional erosion of these elevated areas has reduced the overall sedimentation rate to the observed low values on the ridge tops.

At some time in the past, however, rapid deposition along some of these low ridges occurred formed the thick deposits observed in the Deep Tow 4 kHz profiles (figures 54). Thus, these ridges are herein considered to be depositional in origin and their lobate shape is similar to that of depositional lobes observed on submarine fans (Normark and others, 1979). Alternatively, they may represent mudflow lobes which

reached the area from the steep slopes flanking the basin. One lobe is at the end of a former, partially filled channel delineated by the west-trending, elongate thickening of isopachs for both Units 1 and 2 (figures 55 and 58). Deep Tow 4 kHz data crossing this lobe show greater local deposition to have occurred prior to the deposition of Horizon 2 (figure 54d), although the relative thickening of Unit 2, (and even Unit 1) over this ridge may imply that some process of enhanced sedimentation has continued to occur at this place, although at a slower rate. This pattern of sedimentation is consistent with deposition of a sediment lobe at the end of a leveed channel. Lateral migration of the channel occurs subsequently, and overbank deposition on top of the old lobe forms a levee for the new channel.

Sea Beam and high-resolution seismic reflection profiles are used by to the author to propose an interesting progression of this postulated lobe to levee and channel migration pattern. The low ridges along the southern margin of Central Basin are herein postulated to be depositional lobe/channel levees. The northern lobe shows a possible episode of increased deposition prior to the deposition of Unit 2, and in fact, significantly earlier than the deposition of the westernmost lobe discussed above. The Deep Tow data show a thick lens of sediment below a prominent acoustic horizon approximately 10 m below Horizon 2 (figure 54). Acoustic basement is evident below this, limiting the acoustic penetration over this ridge. The 3.5 kHz data over the same ridge do not record such a prolonged echo from this acoustic basement horizon as is commonly observed where bedrock is exposed (figure 47). It is, therefore, possible that this may be a coarse-grained sediment horizon rather than a bedrock horizon. Coarse-grained sediments in the area may imply that submarine fan-like turbidite deposition has occurred. A small outcrop of this horizon is

apparent from the Deep Tow 4 kHz profiles (figure 54). The apparent sediment lens above this horizon may be the final episode of lobe deposition on this feature before channel migration occurred.

**Depositional History**

The acoustic stratigraphy and bathymetry are used by the author to propose the following model of the depositional history in this area. First, a major sediment lobe was deposited at the southeast end of Central Basin. Subsequent turbidity currents flowing through the channel leading to this first lobe were unable to overtop this lobe, and were therefore diverted around it (cf., fan growth model of Normark and others, 1979). Although the deeper basin to the north provided a good site for subsequent deposition, for some reason, the channel migrated to the south. Menard (1955) postulated that such southward (leftward) migration of deep-sea fan valleys was due to a thickening of the right side of turbidity currents under the influence of the Coriolis force forming higher levees on this side in the northern hemisphere. The author postulates that right-slip along the San Clemente fault may also have contributed to southward channel migration, that is, the main source channel, across the fault, moves relatively southeastward during the fault movements.

Additional, coarse-grained(?) sediment lobes were deposited at the ends of the migrating channel when large turbidity currents swept through. Overbank deposition continued to build the northern levees until these reached a height that such flows could not reach their tops. These overbank flows continued to fill Central Basin with muddy, interchannel turbidites, while the more coarse-grained, basal sediment flows of the turbidity currents built additional lobes at the end of the channels. The last

lobe to be deposited, at least according to the author's data, is the westernmost, although a channel continues to the south into an area where no data were available. This 'suprafan-like' building process was shut off, however, when the Triangular Basin pull-apart formed and deepened, trapping the subsequent coarse-grained sediments coming from the postulated upper fan valley to the east.

Sea Beam data show a well-incised channel lying to the east of Triangular Basin. This channel is a good candidate for the postulated upper fan valley which controlled the suprafan growth postulated above. A possible levee along the south side of this channel is present, but the northern wall is not elevated above the surrounding slopes. Therefore, the author infers that the present channel is erosional, and not depositional. Subsidence of the pull-apart would lower the base level for this channel and, therefore, initiate downcutting of the older, perhaps originally depositional channel. Other channels and possibly leveed valleys across this slope area are shown by the Sea Beam data but the one described above presently lies closest to the postulated channel-levee-lobe system west of the San Clemente fault.

This channel system may also have provided occasional large turbidite flows that reached the broad, low ridge area between Rift and Central basins. The postulated levees are breached in two places, as shown by the bathymetric data. The available Deep Tow 4 kHz data crossing these 'breached' areas, however, do not show erosional truncations of any reflectors within the upper 40 to 50 m of resolvable data (including Horizons 1, 2 and a third approximately twice as deep as #2). Erosional truncation of reflectors is indicated in the Deep Tow high-resolution profiles crossing the northern edge of these levees (figure 54a).

Timing of the large turbidity currents may be indicated by the prominent acoustic horizons, if these horizons do, in fact, represent periods of enhanced turbidite influx. The similarity between the estimated ages of these horizons and known, major eustatic sea level changes also may demonstrate an interesting correspondence between the sedimentation patterns and these eustatic events.* Alternatively, enhanced tectonic activity may have triggered numerous large slope failures, on the nearby escarpments, which reached the basin as mudflows or turbidity currents.

Extending the depositional model proposed above, the author proposes that the low, broad ridge separating Central and Rift basins is an older, presently inactive suprafan complex. This feature is convex upward in radial profiles, characteristic of suprafans (Normark, 1970; Normark and others, 1979). A leveed channel is apparent at the eastern, and topographically highest edge of the broad ridge. Other smaller channels are apparent across the surface, although the resolution of the Sea Beam system does not allow accurate mapping of those smaller than about 100 m wide or less than 10 m deep. A larger, southeast-trending channel follows the base of the steep, basement ridge (shutter ridge) flanking the east side of the proposed suprafan deposit. Southward projecting topographic highs, with lobate form project from this channel into Central Basin.

The overall shape of this proposed suprafan also makes a right-angle bend southward and forms the western margin of Central Basin. Southward migration of leveed fan valleys forming southward-bending submarine fans is commonly observed along the west coast of North America (Menard, 1955). Deep penetration seismic

---

* Note that the elevated banks, Fortymile and Boundary, presently lie below wave base, and so, would only be susceptible to enhanced erosion during periods of lowered sea level, when they would be affected by wave or possibly subaerial erosion.

reflection data of Junger and Vedder (1980, personal communication) indicate post-Miocene undeformed or post-orogenic sediments are buttressed against a buried, near surface, northwest-trending fault along the western margin of this feature. Deflection of turbidity currents or mudflows flowing down the postulated fan surface by a scarp associated with this fault could also be responsible for this bend in the 'fan' shape. Later deposition could cover the scarp, with overbank deposits forming another levee, while the channel continued to be diverted southward. Finally, since active fan deposition on this surface ceased, a thick, predominately hemipelagic drape now overlies the old suprafan surface. As discussed previously, some bottom flowing sediments, presumably large turbidity currents or mudflows from nearby slope failures would cause more rapid deposition in the former channels.

Although the existence of the proposed buried suprafan is not yet confirmed, data of Junger and Vedder (1980, personal communication) are consistent with the model proposed. Their post-Miocene sediment isopach map (figure 60) shows the regional depositional pattern for a significantly longer period than the two late Quaternary maps presented herein. The overall sedimentation pattern shown by their map is roughly similar to that described herein with the locus of deposition in the deepest basins, especially the Rift Basin. Structural control of sedimentation is also shown, by buttressing of thick sediment fill against faults, and basement folds. The thick pocket of sediment at the western edge of Central Basin and buried fan implies that a deep hole has almost been filled by the postulated fan sediments, leaving only Central Basin as a remnant. The thinning of these sediments toward the northeast, in an upslope direction may show that the postulated suprafan built outward onto a westward dipping older, basement slope, which may outcrop as the

Figure 60. Post-Miocene isopach map of Junger and Vedder (1980, personal communication) in the region of North San Clemente Basin. Only a few deep penetration seismic profiles cross this region and so details in the shape of the isopachs are somewhat speculative. Circles and dots identify sample localities, and the age of the sampled material is identifies by an appropriate symbol (see Vedder and others, 1974, for explanation of map symbols). Bathymetry shown is from the NOS (1974) charts 1206N-15 and -16.

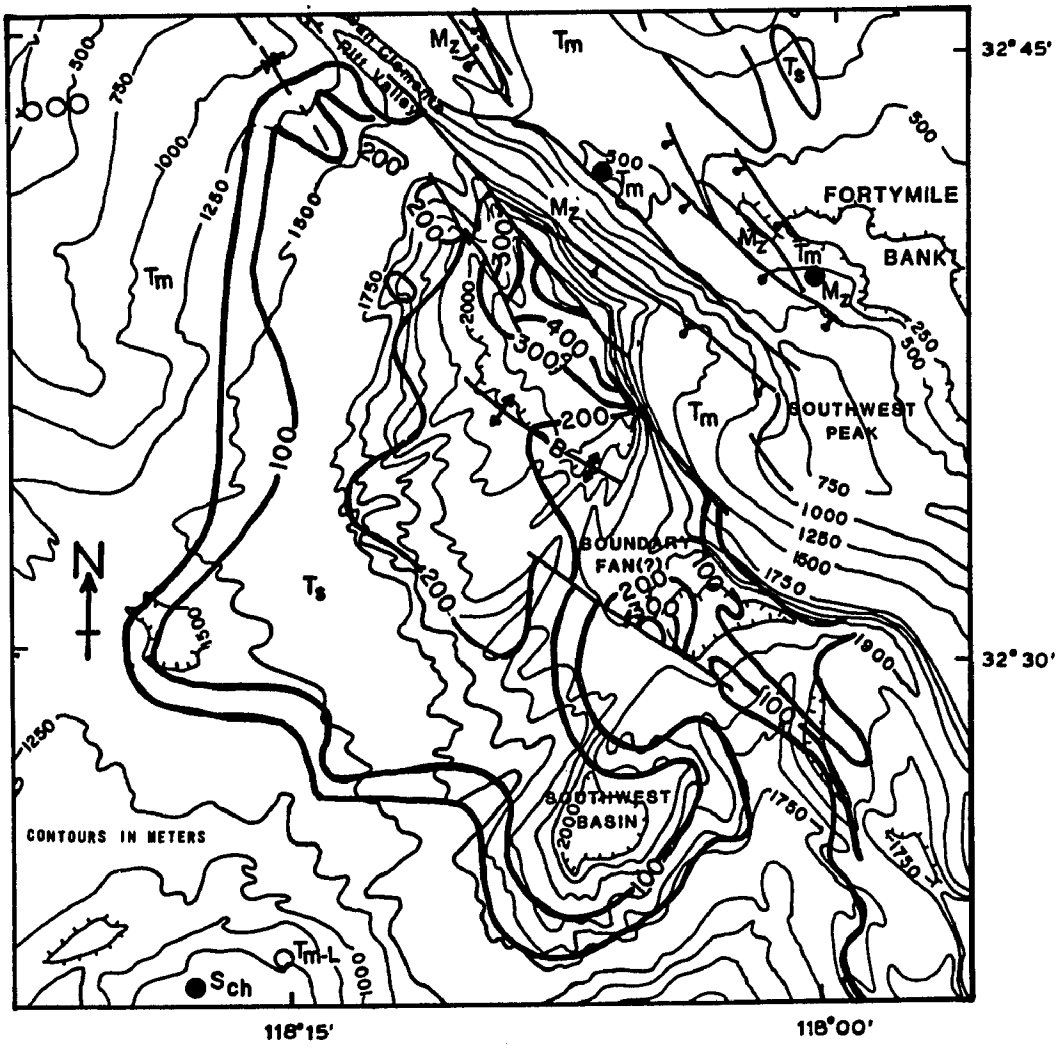
32°45'
32°30'
118°15'
118°00'
FORTYMILE
BANK
SOUTHWEST
PEAK
BOUNDARY
FAN(?)
SOUTHWEST
BASIN
CONTOURS IN METERS
N
Mz
Tm
Ts
Sch
Tm-L

shutter ridge. This feature may be truncated to the southwest against the buried, northwest-trending fault which has dammed the westward flowing fan turbidites. Although these deposits are considered post-Miocene by Junger and Vedder (1980, personal communication), if the average sedimentation rate reported by Emery (1960) were valid for this entire interval of sedimentation, then the bulk of these deposits could be Pleistocene in age.

**Displacement Along the San Clemente Fault**

If the above model of submarine fan growth and subsequent isolation has validity, then some important conclusions regarding the tectonic movement history of the San Clemente fault can be derived. Because the present position of the old upper suprafan channel now abuts the acoustic basement scarp of the San Clemente fault, it must have been displaced from its original source, that is, from the upper fan valley. San Clemente Island and Fortymile Bank are located to the north and west of the proposed suprafan, and so no likely upper fan valley candidates may be found for many tens of kilometers to the northwest, along the fault.

To the southeast, the incised channel lying east of the San Clemente fault and the Triangular Basin pull-apart, however, may be the ancestral upper fan valley. If these channels were once continuous, then they provide a valid piercing point, and a right-lateral offset of about 10 km is exhibited. Because considerable time has elapsed since the proposed suprafan was active, one may not expect its former upper fan valley to still be topographically displayed at present. In fact, the blocking of the old upper fan valley by the shutter ridge would cause a major shift in the active channel, possibly filling the old channel with deposits from subsequent turbidity currents

dammed by the shutter ridge. Some of these ponded sediments may have been carried along with the shutter ridge during later fault movement and now underlie the relatively flat top of this ridge along its central segments.

The last possible place for the old suprafan channel, upper fan valley to connect before being blocked by the shutter ridge is at the southern edge of Fortymile Bank, where the bedrock-sediment contact is located. High-resolution seismic data from this study do not cross this area, and so one can only estimate this contact based upon the bathymetry. Since the abandoned channel abuts the fault scarp at the level of the 1700 m contour, the approximate basement contact is selected at the point where the 1700 m contour curves eastward, away from the fault scarp. This location also lies along a northeast-trending lineament formed by a sharp bend in the bathymetric contours, from east-trending to south-trending, seen in the Sea Beam data (plate 4). In as much as this would be the closest the extinct upper fan valley could be to the offset suprafan valley, a minimum right-lateral displacement of about seven kilometers is indicated.

The age of the proposed inactive upper suprafan valley is unknown, as yet, so that a reliable slip rate cannot be determined from the available data. A minimum age can be estimated, however, by assuming a constant, average, late Quaternary sedimentation rate over the inactive suprafan. All of the acoustic reflectors shown in the 3.5 kHz data are parallel to each other, characteristic of a primarily hemipelagic drape overlying an uneven lower horizon. Using the previously determined ages for the triplet and Horizon 2, and correcting for compaction, the thickness of sediment overlying the lowermost reflector above the postulated suprafan (64 increased to 89.6 m), an age for this deepest horizon can be estimated. The values determined vary

from 428 to 586 ka, depending on which shallower horizon is used for a reference age.

Using 0.5 Mya as a rough estimate for the minimum age of the last suprafan deposition and a minimum offset of seven kilometers, an upper bound of 14 mm/yr for the slip rate on the San Clemente fault is obtained. This value is an order-of-magnitude greater than any previous estimate of slip rate for this fault (Bird, 1982). Other estimates for the lateral slip can be obtained from the offset of the other 'hypothetical' depositional lobe/channel systems south of Central Basin which have been displaced smaller amounts. The northern lobe/levee is covered by a relatively thin layer of hemipelagic(?) sediments. An age of 412 to 540 ka is estimated for the acoustic horizon atop the sediment lens which is interpreted to represent the last major sediment lobe deposition. The westernmost and youngest postulated lobe shows 10% to 20% thickening between Horizon 2 and the triplet, implying that active suprafan(?) deposition occurred as recently as 126 to 222 ka. The northernmost and westernmost, older, buried channels which connected these lobe/levee systems to the upper fan valley, which is now present as a well-incised channel on the northeast side of the Triangular Basin pull-apart, are offset 2.3 km and 1.7 km, respectively. Thus, rough slip rate estimates of 4.6-5.6 mm/yr and 7.7-13.5 mm/yr, respectively, are determined from these data.

The slip rate estimates are based upon many assumptions which are speculative at present. The rate of sedimentation in the area has been shown to vary by up to an order-of-magnitude, both spatially and temporally, in the region during late Quaternary time. The postulated suprafan depositional lobes and channel levees need to be sampled to determine their true character. Lastly, the postulated upper fan, with its leveed valley and slopes also must be sampled, and additional high-resolution seismic

profiles from these areas, not available for the present study, need to be collected. Then, data correlating fan valleys, distributary channels, lobes and levees may be found, and reliable tectonic slip rates determined.

**Growth Model of a Tectonically Controlled Submarine Fan/Slope Apron and Movement History of the San Clemente Fault**

Based upon the preceding discussion, a simple model of late Quaternary movement on the San Clemente fault and growth of a sediment starved(?) submarine fan* can be constructed (figure 61). In the first stage, Boundary Fan was young, and formed directly across the San Clemente fault. In the early part of this stage, the fan valley emptied directly into Rift Basin (figure 61a). While this basin deepened continuously, due to tectonic movement on the San Clemente fault zone, it formed a laterally restricted, deep hole into which fan turbidites became ponded, and a well-developed fan morphology was unable to form. Later in this stage, as the shutter ridge continued its northwestward movement along the San Clemente fault, Boundary Fan built outward and southwestward across the northern flank of the shutter ridge forming the suprafan (figure 61b). The pronounced left, southward hook of this fan resulted from a combination of construction of large fan valley levees on the northern side of the channel, because of the Coriolis effect (Menard, 1955), dextral strike-slip fault movements, and damming of these deposits by the now buried fault scarp on the western side of Rift Basin (Junger and Vedder, 1980, personal communication; figure 60). The last major turbidite deposition on this suprafan occurred just prior to the blocking of the upper fan valley by the shutter ridge.

---

* Hereinafter this feature is referred to as the Boundary Fan, located west of Boundary Bank, straddling the U.S./Mexico border.

Figure 61. Palinspastic reconstructions showing model history of right-slip on the San Clemente fault zone (SCFZ) and growth of Boundary fan/slope apron (BF). San Clemente Island (SCI), the shutter ridge (SR), Blake and San Salvador Knolls, and Triangular Basin (TB) are all identified, and delineated approximately from the Sea Beam and other bathymetric contours. See text for explanation of details of growth and displacement history.

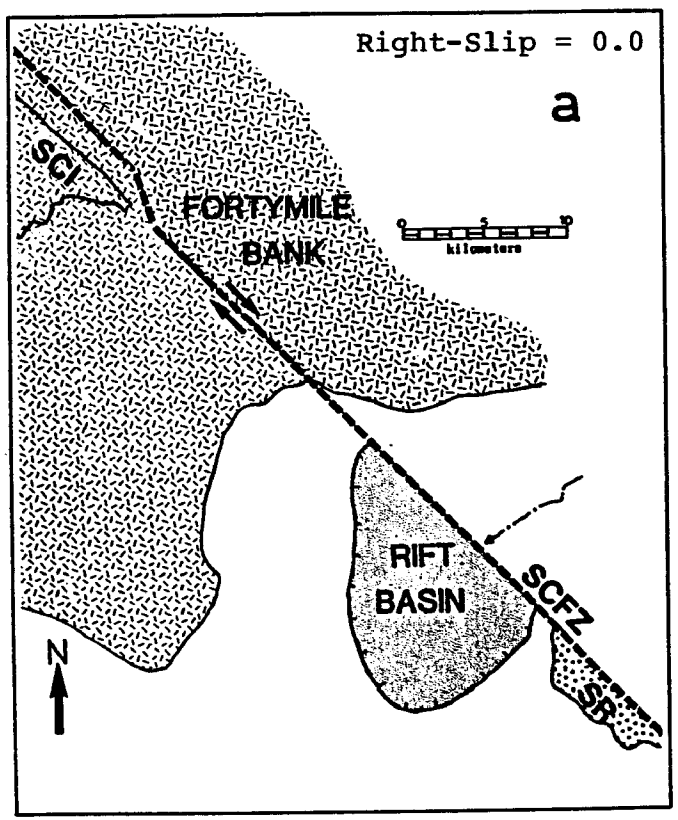
Right-Slip = 0.0
a
SCI
FORTYMILE
BANK
kilometers
RIFT
BASIN
SCFZ
SR
N

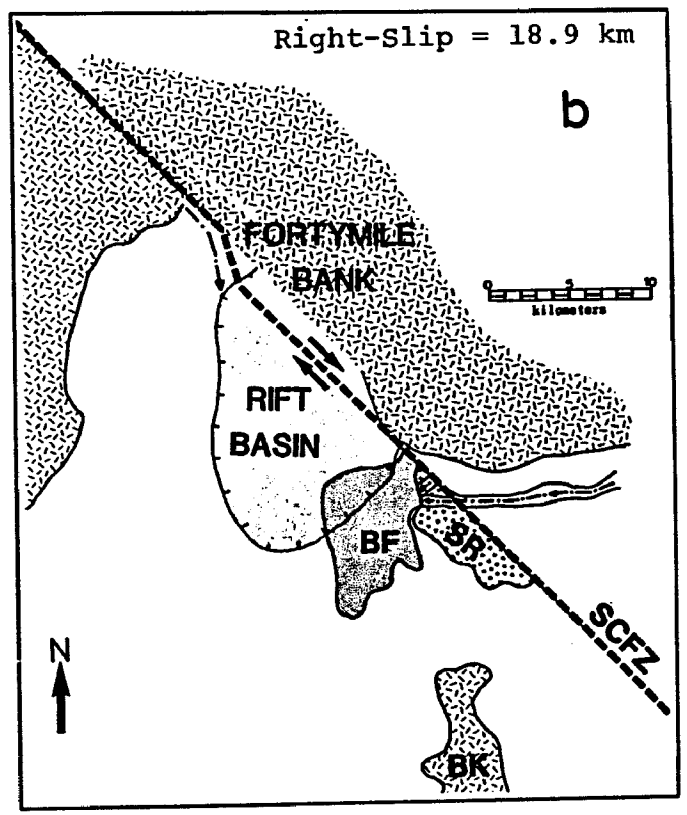
Right-Slip = 18.9 km
b
FORTYMILE
BANK
kilometers
RIFT
BASIN
BF
SR
SCFZ
BK
N

Figure 61. Palinspastic reconstructions (Continued).

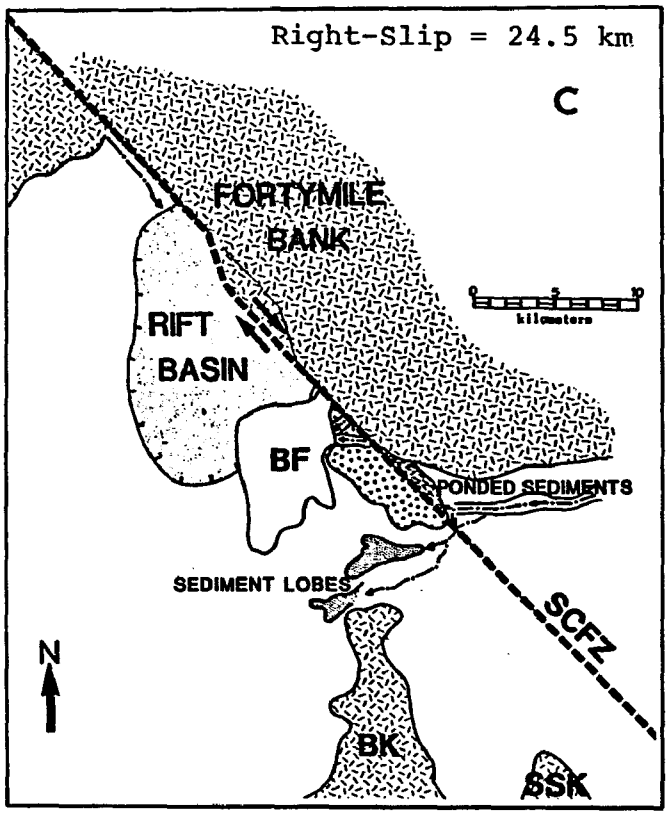
Right-Slip = 24.5 km
c
FORTYMILE
BANK
RIFT
BASIN
BF
PONDED SEDIMENTS
SEDIMENT LOBES
SCFZ
N
BK
SSK

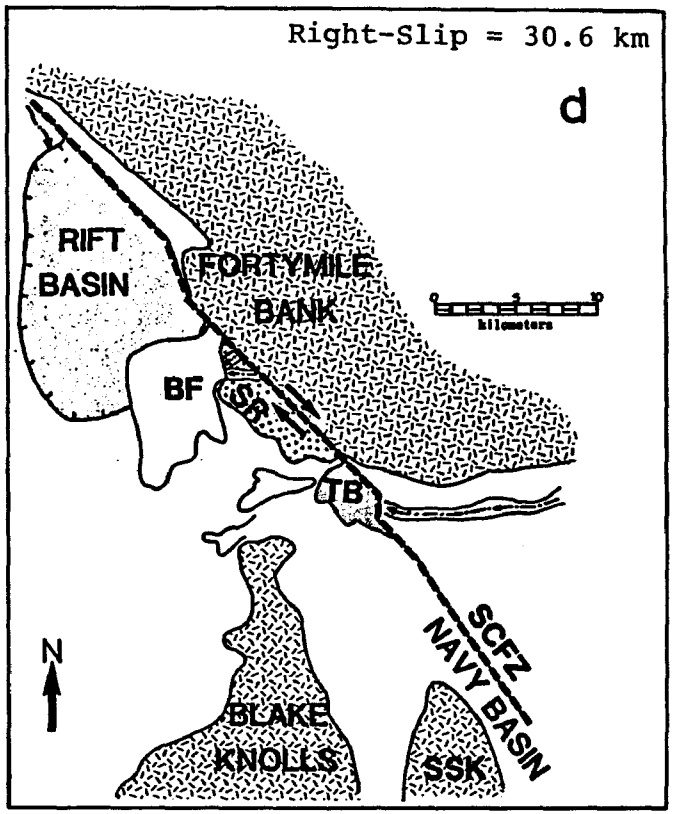
Right-Slip = 30.6 km
d
RIFT
BASIN
FORTYMILE
BANK
BF
SR
TB
SCFZ
NAVY BASIN
N
BLAKE
KNOLLS
SSK

During the second stage, the shutter ridge blocked off the northernmost upper fan valley, diverting the active fan valley around the southeast end of the shutter ridge (figure 61c). Ponding of sediments in the old valley behind the shutter ridge occured. A new suprafan began to form at this time within the deeper area south of the shutter ridge. This basin was restricted, however, to the south by the Blake and San Salvador knolls. The Coriolis effect and the right-slip along the San Clemente fault again caused higher, better developed levees to form along the north side of the fan distributary channels which extended westward across this region. The shutter ridge and these levees blocked direct fan growth into the region southwest of the shutter ridge, and so Central Basin is being slowly filled today by hemipelagic, and possibly turbidite overbank deposition.

In the latter part of the second stage, the western lobe was deposited, and the gradient across the suprafan surface flattened. The levees and depositional lobes, plus the other elevated features to the south almost encircled the suprafan area, so that the northern levees became breached by turbidity currents allowing increased deposition in Central Basin. The timing of this breaching is not constrained by the available data and may have occurred before deposition of the western lobe, or later during the final stage.

In the final stage, the Triangular Basin pull-apart formed, and deepened to a level where coarser sediments flowing down the upper fan valley were trapped when they entered the basin (figure 61d). The finer-grained, or more energetic parts of the turbidity currents were able to flow beyond the pull-apart, and either cross the northern levee breaches into Central Basin, or travel farther west, and south into other, adjoining basins. The upper fan valley became incised into the fan surface due to the

lowering of its base level by the deepening pull-apart basin. Other lateral shifts in the upper fan valley may have occurred, turning more southward to deposit sediments into the northern end of Navy Basin. The data available for this study show that a prominent seafloor scarp along the San Clemente fault has not been incised by such a channel leading into this area (plate 4).

Meanwhile, hemipelagic deposits draped relatively evenly over the elevated parts of the formerly active suprafan. These hemipelagic deposits are occasionally interbedded with sediments from large turbidity currents which surmount the low relief of the entire North San Clemente Basin. Slumps and other slope failures also contributed to the basin sedimentation, although apparently at a much lower overall rate, except locally, than the turbidites or hemipelagic deposits. Bottom currents either eroded, scoured or inhibited deposition, as shown by the lack of youthful sediments over acoustic basement in some areas, notably the steeper slopes and higher elevations of Fortymile Bank.

San Clemente Rift Valley was a second major conduit of turbidites to Rift Basin throughout late Quaternary time, and a poorly developed fan may exist at its mouth. No well-defined leveed fan valley is apparent in either the seismic profiles or bathymetric contours. Cores from Rift Basin (Emery, 1960; Emery and Rittenberg, 1952; Emery and Bray, 1962) show that turbidites have been deposited within the area during Holocene time.

## SUMMARY AND CONCLUSIONS

Sea Beam data are most useful for identifying the shapes as well as size of many interesting seafloor features. Additional data, such as high-resolution seismic profiles, bottom samples, Deep Tow side-scan sonar and shallow penetration acoustic reflection profiles were used in this study to establish the character of mesotopography interpreted from the Sea Beam data. As more studies using Sea Beam coupled with these additional data sources are accomplished, characteristic shapes and patterns of seafloor mesotopography may be better correlated with specific seafloor geomorphic processes such as tectonic activity or sedimentation processes. In some cases, careful bottom sampling is still necessary to test hypotheses made regarding some of the significant features.

Non-tectonic features recognized in the study area include channels, some with levees, small basins and other closed depressions, slides and slumps, terraces both depositional and erosional, basement outcrops and other peaks, and postulated submarine fan ('suprafan') depositional lobes. Submarine channels may be depositional or erosional in nature, and high-resolution seismic data have been most useful in identifying the character of many channels. In as much as depositional channels, such as deep-sea fan, upper fan valleys are usually elevated above the surrounding slopes, Sea Beam data are adequate to identify such features. Similarily, incised channels lie below the adjacent seafloor.

Two types of basins were observed in this study: (1) tectonically formed; (2) depositionally formed. The tectonically formed basins, such as Rift, Triangular and Navy basins are bounded, on at least one side, by prominent fault scarps. The thickest sediment accumulations, as shown by high-resolution seismic data, are adjacent

to the faults, and not necessarily centered in the topographic depression. The flat floors of these basins, and onlap observed in seismic profiles, are characteristic of ponded sediment fill, probably turbidites. In some cases, small closed depressions at the edges of these basins, are aligned with the inferred fault trace and are believed to be tectonic sags. Other relief around the margins of these basins includes sediment slump or debris flow masses and lobes, small-leveed channels, and other mesotopography not resolvable with Sea Beam.

One large non-tectonic basin, Central Basin, was examined in this study. It was apparently formed by depositional processes. The basin developed where sedimentation was restricted, whereas high rates of sedimentation from turbidite influx on the surrounding sides enclosed Central Basin. Most recently, ponding of overbank or basin plain(?) turbidites are filling the deeper Central Basin more rapidly than the surrounding areas of low relief. If these sources of turbidites are cutoff by continued fault offset, this basin will remain at its topographically lower position as the entire area receives a slow, relatively uniform drape of hemipelagic sediments. Modification of this sedimentation pattern may occur due to other bottom currents, or slope failure sedimentation processes.

Elevated features of low, gentle relief were also observed, and hypotheses for their origins were presented based upon the Sea Beam and high-resolution seismic data. The lobate shape of some of these features and their proximity or association with modern and buried channels implied to the author that these are depositional features associated with growth of a submarine fan or debris flow slope apron(?). The Normark (1974) fan model was used to develop this hypothesis because Navy Fan (Normark and others, 1979; Smith and Normark, 1972) is located within 50 km of our

survey area. In this model, the convex-upward suprafan surface, composed of coarse-grained sediment (sand?) depositional lobes are interpreted to underlie at present a drape of late Quaternary hemipelagic sediments. The most recent of these lobes may be identified by thickening of an acoustic (sedimentary) unit between prominent acoustic horizons. This thickening is proposed to represent more rapid accumulation of sediments, locally, at the end of a partially filled, leveed channel. The resulting elevation of the seafloor at this depositional lobe caused a lateral shift of the channel, so that subsequent deposition occurred at the end of the new channel.

If this sequence of deposition occurs over an extended period of time, a large, convex upward, suprafan develops which heads at a major, upper fan valley, distributary system. The broad, low ridge between Rift Basin and Central Basin is interpreted to be an inactive suprafan, which has been cutoff from its upper fan valley, turbidite source by 7 to 10 km of right-slip across the San Clemente fault. A drape of hemipelagic sediments at least 50 to 100 m thick now covers this feature, so that sampling with standard piston corers would not penetrate the postulated suprafan deposits. The truncated upper fan valley at the head of this feature, however, may have been kept clear of hemipelagic deposits by bottom currents focused at the base of the San Clemente fault scarp, so that carefully positioned piston cores could sample these deposits. Deeper penetration, high-resolution seismic reflection profiles may also provide data useful in establishing the identity of this feature.

Both surface ship 3.5 kHz and Deep Tow 4 kHz seismic reflection data were used to map sediment thicknesses (isopachs) between the seafloor and two prominent acoustic horizons. Although the actual nature of these acoustic horizons in the sediment column is not yet known, their lateral continuity over hundreds of square

kilometers supports the author's assumption that they are isochrons. The lateral variability of the sediment thicknesses shown by these maps show significant spatial variations in sedimentation during late Quaternary time, and correlations of sediment thickness (sedimentation rate) with bathymetry and seafloor morphology support several conclusions made by the author regarding the modes of sedimentation active in the different areas.

The thickest accumulations, and hence greatest sedimentation rates, are generally located in the deeper basins and other depressions. Also, the flat basin floor and presence of multiple, continuous, closely-spaced parallel reflectors which lap onto the basin margin seen in acoustic profiles, are evidence of sediment ponding within the basin. Based on these observations, the author proposes that a substantial part of the basin sediments are turbidites. Piston cores from Rift Basin are in agreement with this hypothesis. The ridges with low, gentle relief have relatively thinner accumulations of young sediments, whereas the higher elevations and steepest slopes are relatively uncovered by young sediments. Deposition of a relatively uniform drape of hemipelagic sediments covers most of the low ridges, although some larger turbidity currents add overbank(?) or levee deposits to some of these features, giving them intermediate sediment thicknesses and sedimentation rates. Bottom currents may have kept the steep slopes and higher elevations of Fortymile Bank relatively clear of young sediments.

The acoustic horizons themselves, may represent measureable episodes of enhanced deposition. Their estimated ages, assuming a constant, average, late Quaternary sedimentation rate for Rift Basin, are similar to major Pleistocene interstadials determined from deep-ocean piston cores. Dunbar (1981) found

enhanced sedimentation during the glacial/interglacial marine transgression at the beginning of Holocene time, for nearby South San Clemente Basin. Prominent acoustic horizons evident in the high-resolution seismic profiles may correlate with similar eustatic sea level events of the Pleistocene epoch. Future work to investigate these features may provide better methods for determining sedimentation rates and absolute ages of acoustic horizons for marine geological studies without requiring expensive seafloor drilling.

# CHAPTER 7

# STRUCTURAL GEOLOGY AND TECTONICS OF THE INNER BORDERLAND

## INTRODUCTION

The California Continental Borderland is geologically a complicated part of the broad boundary between the North American and Pacific tectonic plates. This study describes the structural geology of the inner part of the California Continental Borderland, from Santa Catalina Island to Punta Colinett (figure 1) and the post late Miocene tectonic style of deformation for this region. Implications regarding present day tectonic activity of the region, based upon studies of the local earthquake activity (Legg, 1980) are also included for comparison with the geological data. Finally, constraints imposed upon numerous models already proposed for the late Cenozoic tectonic evolution of the California Continental Borderland and the Pacific-North American plate boundary are discussed.

The Inner Borderland,* of this study, and described by Moore (1969), "is essentially contained within the region shoreward of the fault paralleling and adjacent to the western side of San Clemente Island". Although Moore (1969) considered the Inner Borderland as an extension of Peninsular Ranges structure, data presented by the author, (chapters 2 and 4, this volume) demonstrate that the Inner Borderland is a distinct physiographic and structural province. The primary structural and physiographic character of the Inner Continental Borderland consists of several sub-parallel

---

* In this study, California Continental Borderland refers to the entire region from Pt. Conception to the Viscaïno Peninsula. Inner Borderland refers to the inner part of the California Continental Borderland, as defined by Moore (1969) and the author (chapter 2, this volume) for this study.

ridges, banks, islands and troughs which trend northwesterly, sub-parallel to the coastline and the Pacific-North American plate boundary. Previous investigations of the geology of this region recognized this character and proposed its tectonic origins, relating the steep, roughly linear escarpments to faulting (Shepard and Emery, 1941; Krause, 1965).

The tectonic evolution of the California Continental Borderland was complicated, progressing from a convergent plate boundary with the subduction of the Farallon plate on its western side, to the modern strike-slip tectonics of the San Andreas fault system, which represents the transform fault boundary between North America and the Pacific (Atwater, 1970). The transition between the subduction and transform fault tectonics involved the passage of the Rivera ridge-trench-fault triple junction and the Mendocino fault-fault-trench triple junctions past or possibly through the California Continental Borderland during middle Tertiary time (Atwater, 1970). Postulated instabilities of the Rivera triple junction as it migrated southward are inferred to account for much of the geological complexity of the California Continental Borderland (McKenzie and Morgan, 1969; Dickinson and Snyder, 1979). Blake and others (1978) also relate the timing of offshore basin formation in the California Continental Borderland to the passage of the triple junction. They proposed that progressively younger basin formation occurred to the south and east.

Other models of the tectonic evolution of the California Continental Borderland include complex reorganization of elongate basement blocks or slivers in a right-lateral shear couple and clockwise rotation, as indicated by paleomagnetic data, of these blocks in the Transverse Ranges and vicinity, (Luyendyk and others, 1980; Crouch, 1979). Large scale horizontal movements involving dextral strike-slip along

major northwest trending fault zones (Howell, 1974, Crouch, 1978) or oblique(?) normal slip associated with east-west extension (Yeats, 1976) have also been postulated. Another proposed model involves convergent wrench faulting along deep seated shear zones separating relatively intact, crustal 'miniplates' (Junger, 1976).

Post-Miocene tectonics of the Inner Borderland are generally considered to involve wrench faulting along several prominent, northwest-trending shear zones, (Harding, 1973; Junger, 1976; Nardin and Henyey, 1977; Greene and others, 1979; Legg and Kennedy, 1979) and clockwise rotation of Santa Cataline Island (Luyendyk and others, 1980). Estimates of late Quaternary strike-slip rates across California Continental Borderland faults range from a few millimeters per year (Yeats, 1973; Kennedy, 1975; Bird and Rosenstock 1984; Jordan and others, 1985) to a significant fraction (20-30% or 10-20 mm/yr) of the overall Pacific-North American relative plate motion (Anderson, 1979; Weldon and Sieh, 1985). Few measurements of strike-slip offsets on Inner Borderland faults are available owing to the obvious difficult of confirming real piercing points on sumbarine faults. Furthermore, detailed mapping of geologic structures over large areas of the California Continental Borderland, especially to the south, offshore of Mexico, have yet to be accomplished, so that many active tectonic features which play an important part in the regional tectonic history are yet unrecognized.

Howell and Vedder (1981) describe four terranes of contrasting stratigraphic succession across the northern half of the California Continental Borderland, two of which are located in the area of this study. They consider that basement rocks of Franciscan-like assemblages underlying the western terrane are juxtaposed against crystalline(?) basement rocks of the Peninsular Ranges underlying the eastern terrane

along an undefined structural discontinuity within the Inner Borderland. The ancestral Newport-Inglewood fault zone has been proposed to form one part of this terrane boundary (Howell and Vedder, 1981). Other faults, mapped for this study, may mark this terrane boundary to the south.

## GEOLOGIC STRUCTURE OF THE INNER BORDERLAND

Detailed marine geophysical surveys of the Inner Borderland west of northern Baja California demonstrate that the region is underlain by two, major, northwest-trending, right-lateral wrench fault systems: (1) San Clemente; and (2) Agua Blanca (figure 25, plate 3, chapter 4, this volume). These fault systems are delineated by one or more relatively long and continuous, narrow, primary wrench fault zone. High-resolution and moderate penetration seismic profiles show that these fault zones displace late Quaternary submarine fan and basin deposits, and unconsolidated surficial deposits of the continental shelf and slopes (chapter 4, this volume). Seafloor relief is evident along most parts of these fault zones including scarps from a few to over 1000 m high. Dextral shear is indicated by local convergence, expressed as folding and upthrusts in association with left bends or more westerly-trending fault segments, and divergence expressed as sagging and pull-apart basin formation along more northerly trending or right-stepping, en echelon, principal fault traces.

### San Clemente Fault System

The San Clemente fault system lies along the western part of the Inner Borderland and is delineated by the San Clemente-San Isidro fault zones. Together, these form a long (>300 km), narrow (<5-10 km), continuous zone of faulting, linked through a major left bending, 'transpressive' fault segment. This divergent wrench

fault character is expressed in seismic profiles as 'negative flower' structure (figures 7, 9 and 26; Harding, 1985) and in map view as a zone of subparallel, branching and anastomosing, fault traces flanked by monoclinal flexures which dip in toward the fault zone. In some areas, small apparent grabens are between major fault strands (figure 9). En echelon sags between right-stepping en echelon fault traces are also shown in detailed seafloor topographic (Sea Beam) data (figure 15, chapter 2, this volume). Locally, the San Isidro fault zone is delineated by single, linear fault traces, which strike N40°W and juxtapose dissimilar acoustic stratigraphic successions (figures 9 and 27). These segments are interpreted as parallel wrench faults showing pure strike-slip. Also, short ($\simeq$5km) left-bends in the principal fault trace along the San Isidro fault zone are convergent, as shown by the folding and uplift of originally flat-lying sediments across and adjacent to the principal fault traces (figure 8).

The central, 'transpressive', left-bending segment of the San Clemente-San Isidro fault zone is marked by a broad zone of folding and reverse faulting. Upthrusts(?) displace the seafloor adjacent to the large, seafloor scarp associated with the main fault trace (figure 62). Folds are oriented subparallel to the principal fault trace in this area, and the intensity of folding and secondary faulting increases both toward the center of the bend, and with depth in the seismic section (figures 6, 7, and 35). Although the uplift associated with the convergence is roughly symmetrical at the southeast end of the bend, it is markedly asymmetrical toward the northwest, with the northeast side rising up and presumably over(?) the southwest side (figure 35, line B-15). This asymmetry may result from the tectonic transport from the south of relatively flat-lying turbidites. The deposits on the northeast side of the bend are relatively stationary, with respect to the bend, and would suffer more relative

Figure 62. High-resolution (3.5 kHz) seismic profile showing upthrusts along the transpressive section of the San Clemente-San Isidro fault zone (see figure 4 for location).

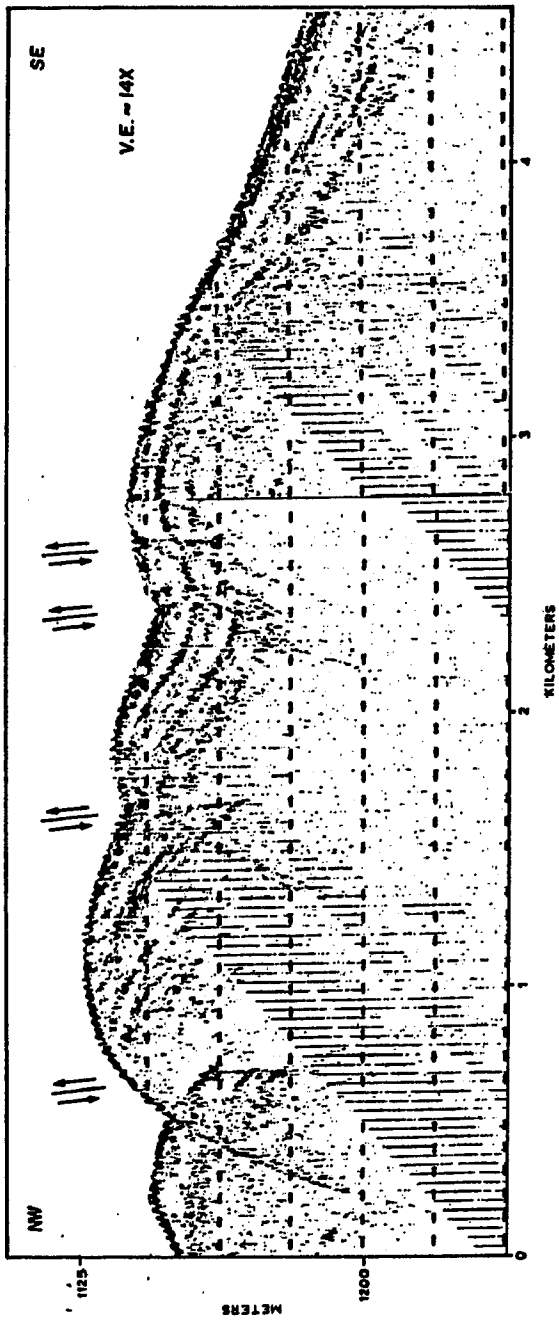
NW
SE
V.E. ~ 14X
1125
1200
METERS
0
1
2
3
4
KILOMETERS

shortening (because they are always in the region of convergence). Turbidites on the southwest side of the bend may initially have been deposited in basins along the extensile, San Isidro fault zone, and experience shortening only when they are tectonically moved into the bend region. Other factors, perhaps including dissimilar basement rocks juxtaposed across the fault, may also be relevant in developing the asymmetry. A small, shallow, north-trending graben along the eastern side of the transpressive 'bulge' may show the local directions of principal strain (figure 63).

The northern section, the San Clemente fault zone, is delineated by a set of N35°-40° W-trending, generally right-stepping, en echelon fault traces (figures 25 and 27). A major, right step in the vicinity of Navy Fan (figure 25) is associated with a long, narrow graben in which turbidites of Navy Fan have been ponded (figure 10; also, Normark and others, 1979). Across this graben the southwestern fault changes from a high angle, predominately strike-slip fault showing little vertical separation to a relatively low angle ($\simeq$45° dip to the northeast), predominately dip-slip fault. The low angle fault is interpreted to merge at depth into the near vertical, northeastern fault trace (figures 10 and 28, chapter 4, this volume). Sea Beam data show that the northeastern fault is marked by prominent scarps in both bedrock and unconsolidated(?) slope deposits (plates 4 and 5). The southwestern flank is the San Salvador Knoll.

At each right step, or small change in fault strike, small basins are formed, representing pull-apart origin in a dextral wrench fault zone. Unlike the Navy Fan pull-apart graben described previously, these other small pull-apart basins, including North San Clemente Basin, are interpreted to be half grabens or trap door structures, bounded by a high-angle fault on their northeastern sides, and by monoclinal

Figure 63. High-resolution (3.5 kHz) seismic profile showing a small graben on the flanks of the bulge associated with the convergent part of the San Clemente-San Isidro fault zone (see figure 4 for profile location).

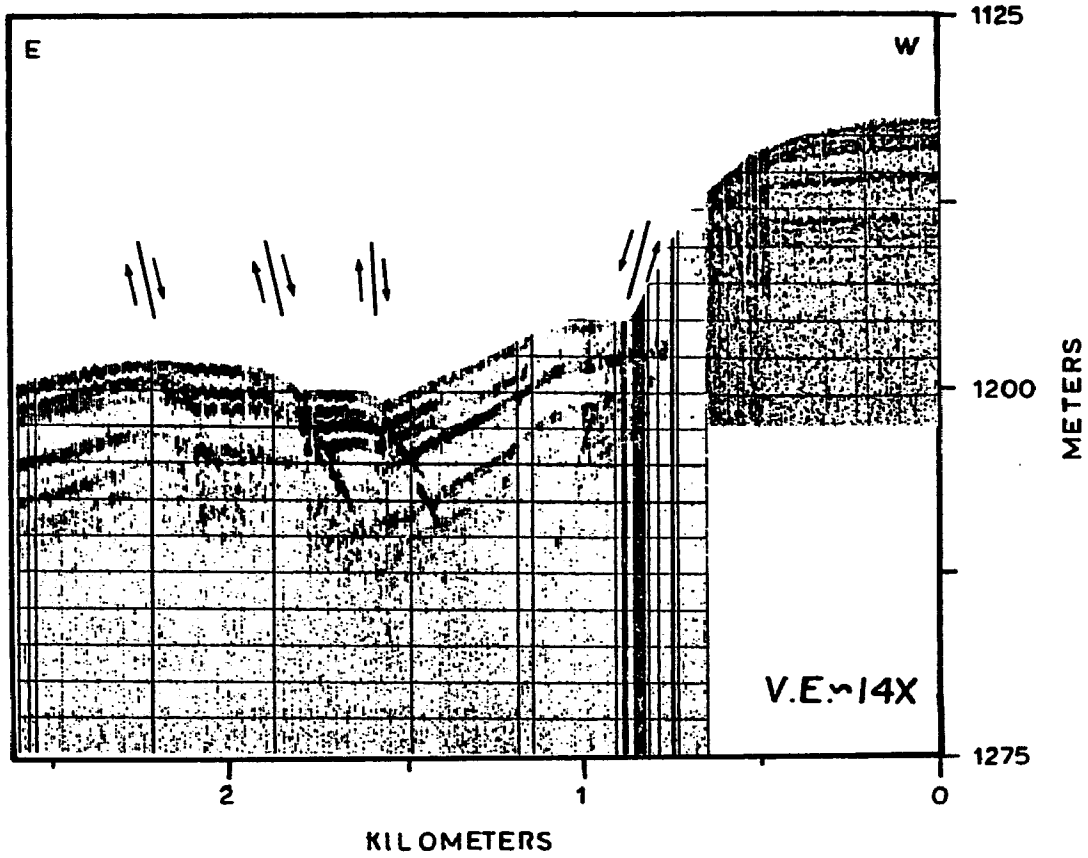
E
W
1125
1200
1275
METERS
V.E.~14X
2
1
0
KILOMETERS

downwarping of the basin sediments into the fault zone, on the southwestern side so that the thickest deposits are adjacent to the fault (figures 44, 55, 58 and 60). No en echelon fault overlap is evident from the Sea Beam contours or high-resolution seismic profiles at these right steps.

Major branch faults are associated with both the northern and southern sections of the San Clemente fault system. The Junger fault diverges (plate 4, chapter 5, this volume) from the San Clemente fault in the vicinity of the San Clemente Rift Valley and trends southeastward across the flanks of Fortymile Bank. It is marked by an 1100 m high scarp which forms the southwest flank of Fortymile Bank, and so is probably associated with significant dip-slip. Seismic profiles across these steep ($>35^{\circ}$-$45^{\circ}$) slopes are unable to resolve the sub-bottom structure adjacent to the fault and, in fact, are not able to resolve the seafloor along the slope.

To the south, another long ($\simeq$50km), straight, branch fault, delineated by a major scarp, bounds San Isidro Ridge and merges with the San Isidro fault at the end of the San Isidro Rift Valley. Fault drag apparent in the flat-lying, ponded turbidites of the Ensenada Trough, (figures 8 and 26) adjacent to this fault, implies that normal fault movements have occurred. Also, the San Isidro Ridge is inferred to be a westward tilted fault block. Continued movement throughout late Quaternary time is evident by the increasing amount of drag within the ponded sediments of the Ensenada Trough. Interaction between these faults is consistent with Crowell's (1974) interpretation of fault wedge tip kinematics, modified by the regional east-west extension across the Ensenada Trough associated with divergent wrench faulting on the San Isidro fault (figure 64).

Figure 64. Diagram showing how regional extension combined with fault interaction and vertical movements at the tips of wedges between intersecting strike-slip faults can explain the fault pattern and seafloor relief in the vicinity of the Ensenada Trough (modified from Crowell, 1974). Hachures delineate regions of elevated seafloor. The regional extension is a result of divergent wrench faulting along the San Isidro fault zone.

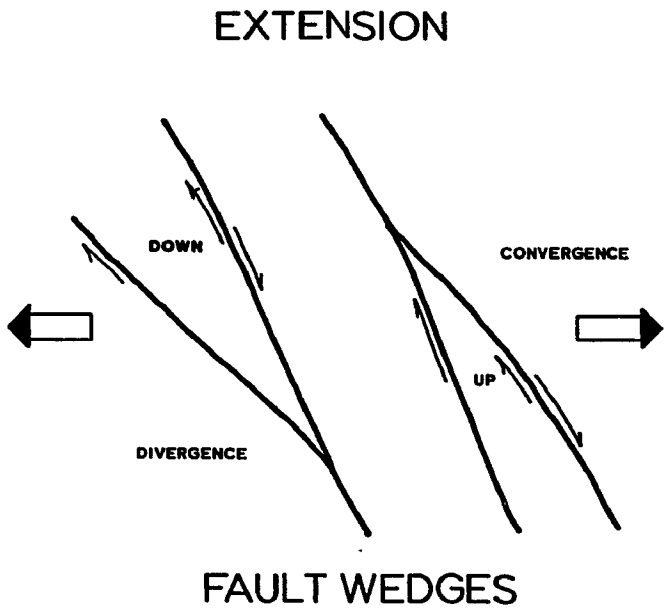
EXTENSION
DOWN
CONVERGENCE
UP
DIVERGENCE
FAULT WEDGES

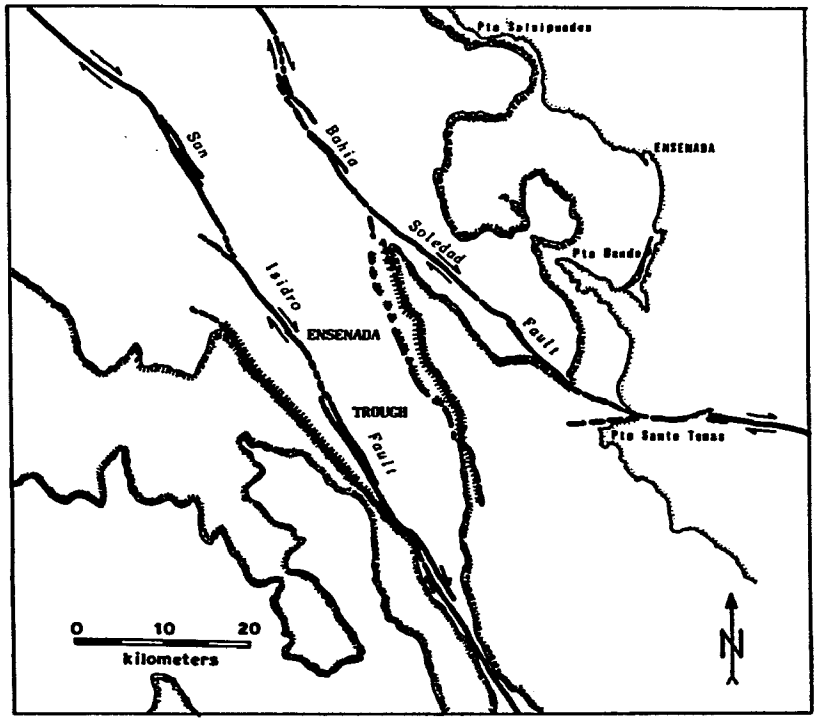
Pta Salsipuedes
ENSENADA
Pta Banda
Pta Santo Tomas
San
Isidro
Fault
Bahia
Soledad
Fault
ENSENADA
TROUGH
Fault
0
10
20
kilometers
N

Overall, the offshore San Clemente fault system is remarkably similar to the San Andreas fault system (figure 65). Both are long and continuous, and the main zone of faulting is confined to a narrow band only a few kilometers wide. Both consist of major, roughly linear northern and southern fault segments which are linked by a major, convergent, left bend (restraining bend) in the fault zone. The large right step of the San Clemente fault and associated Navy Fan pull-apart basin, located north of the major left bend in the fault, is similar to the San Gabriel fault and the Ridge Basin during an earlier, phase of activity on the San Andreas fault system. The similarity between these two major, active fault systems implies that additional detailed study of one fault zone may lead to important insights regarding the tectonic development of the other.

**Agua Blanca Fault System**

The Agua Blanca fault system is a complex zone of northwest- trending dextral shear, delineated by three or more, subparallel, principal, wrench fault zones. The westernmost, San Diego Trough-Bahía Soledad fault zone, in the area of this study, consists of relatively long and continuous ($\simeq$50km), through-going fault traces which cut the Quaternary sediments and locally the seafloor of the nearshore basin trough. The main trace of the southern, Bahía Soledad fault, trends approximately N50°W (figure 25 and 27, plate 3) and the consistent up-to-the-southwest offset coupled with a small fold implies that some convergence on this predominately strike-slip fault has occurred (figures 7, 26 and 31). The San Diego Trough fault, however, trends more northerly (N30°W) and is interpreted to be a parallel wrench fault in general, although locally, at small fault bends or en echelon offsets, minor vertical components

Figure 65. Comparison of the San Andreas and San Clemente fault systems. The pattern of faulting for both systems is similar, and many major physiographic features surrounding these fault systems have similar configurations, too. For example, the position of the Sierra Nevada, a region of thickened crust is roughly similar to that of the Thirtymile, Boundary and Navy Banks in relation to the major left bends in the fault systems. Also, the Salton Trough and the Ensenada Trough are regions of active subsidence due to regional extension associated with divergent wrench faulting at somewhat different scales. Note the difference in the scale for each fault system (for a comparison at the same scale, see figure 29).

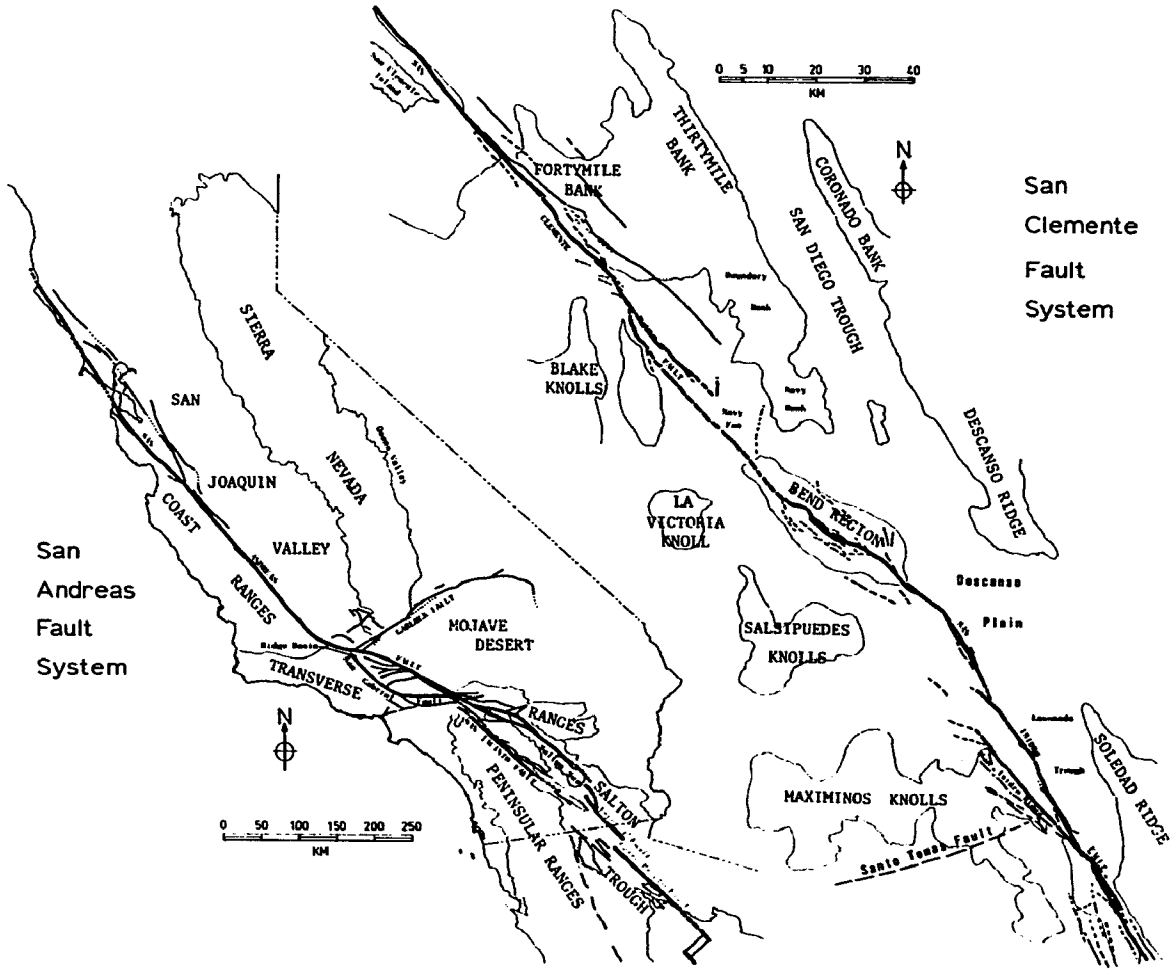
San Clemente Fault System
San Andreas Fault System
FORTYMILE BANK
THIRTYMILE BANK
CORONADO BANK
SAN DIEGO TROUGH
DESCANSO RIDGE
BLAKE KNOLLS
LA VICTORIA KNOLL
BEND TECTONIC
SALSIPUEDES KNOLLS
MAXIMINOS KNOLLS
SOLEDAD RIDGE
Descanso Plain
Santa Tonia Fault
SIERRA NEVADA
SAN JOAQUIN VALLEY
COAST RANGES
TRANSVERSE RANGES
MOJAVE DESERT
PENINSULAR RANGES
SALTON TROUGH
N
0 5 10 20 30 40
KM
0 50 100 150 200 250
KM

of movement are evident. The San Diego Trough fault lies along the axis of the San Diego Trough and is generally marked by a single main fault trace in seismic profiles (figure 10, also cf. Moore, 1969, plate 8).

The Coronado Bank-Agua Blanca fault zone is more complicated than the fault zones described above. Numerous discontinuous, subparallel, right- and left-stepping, en echelon and anastomosing fault segments, often associated with significant structural relief, mark this central fault zone of the Agua Blanca system (figure 25). This fault zone disrupts presumed late Quaternary and possibly Holocene sediments of the shelf and nearshore slopes including the seafloor in places (Legg and Kennedy, 1979; Kennedy and others, 1980). Typically, two or more, subparallel, principal fault traces are observed in seismic profiles along the Coronado Bank fault zone (figures 5, 6 and 35 also cf. Kennedy and others, 1980), and numerous minor branch and secondary faults can also be seen. The Agua Blanca fault (north branch of Allen and others, 1960) passes offshore along the north side of Punta Banda where it marks the steeply dipping contact between basement rocks of the peninsula, Islas Todos Santos, and the thick fill of sediments in Valle Maneadero and Bahía Todos Santos. Numerous elevated marine terraces on Punta Banda, Islas Todos Santos, and around Punta Santo Tomás imply that substantial uplift has occurred along these coastal sections of the Agua Blanca fault system. The Agua Blanca fault makes a sharp turn from its N60°-65°W strike along Punta Banda to a more northerly (N25°-35°W) strike east of Islas Todos Santos (figure 25, plate 3). The fault zone is rather complex from Bahía Todos Santos to Loma Sea Valley, and two or more main fault traces are mapped; one lies along the east flank of the flat-topped and almost buried Descanso Ridge and Coronado Shelf, and the second lies along the axis of the sediment filled

trough between the Coronado Bank-Descanso Ridge and the mainland (figure 25, plate 3).

Nearshore zones of faulting, marked by the Newport-Inglewood-Rose Canyon fault zone to the north, and by the Descanso-Estero fault zone to the south, trend subparallel to the coast and pass onshore near San Diego and Ensenada, respectively. The southern, Descanso-Estero fault zone is inadequately defined by the few nearshore seismic profiles obtained across its trace, but generally is shown near the coastal shelf break, which has been buried from Punta Descanso to Point Loma. Numerous north-trending faults in the San Diego Bay and offshore bight may be associated with fault interaction in a right-stepping, en echelon fashion between the Rose Canyon and Descanso fault zones. Additional tectonic complexity in the San Diego-Tijuana area is possible, as a result of the impingement of the northwest-trending San Miguel-Vallecitos fault zone into this area, which has been inferred to connect at depth with the Rose Canyon fault zone (Legg and Kennedy, 1979, Brune and others, 1979). Right-lateral shear is proposed to account for the alternating structural lows (Mission and San Diego Bays) and highs (Mount Soledad and Point Loma) along the broadly sinuous trace of the Rose Canyon fault zone through the San Diego area (Kennedy and others, 1980; Kennedy and Welday, 1980). Right-lateral offsets of submarine canyons (La Jolla, Coronado, Banda and Salispuedes) are also inferred to be a result of movement along fault zones of the Agua Blanca system.

In the vicinity of Ensenada and Punta Bunda, the pattern of faults of the Agua Blanca system resembles that of the Alpine-Marlborough fault zones in New Zealand (figure 36). The overall pattern is that of a single, narrow, primary fault zone, that is transpeninsular Agua Blanca or Alpine, which branches into several splays that trend

obliquely from the main fault trace. The main fault along its principal trend eventually dies out with slip being transferred to the other faults (Freund, 1974). In New Zealand, a change in tectonic movement, such that oblique convergence on the Alpine fault is accomodated by strike-slip on the Marlborough fault system has been inferred to explain the fault configuration (Arabasz and Robinson, 1976). In Baja California, however, the transpeninsular Agua Blanca fault is not known to be associated with significant oblique slip (Allen and others, 1960), and the offshore faults of the Agua Blanca system also generally are interpreted herein to be parallel wrench faults. The large structural relief along parts of the Agua Blanca fault system may however, imply that episodes of significant oblique- or dip-slip occurred. In particular, structural relief where the Agua Blanca fault system passes offshore near Ensenada is presumably related to the change in fault orientations or ending of fault segments with predominately strike-slip, similar to the northern end of the Imperial fault. Alternatively, vertical movements associated with fault interaction between en echelon or subparallel fault strands may cause this relief (e.g. figure 64).

## OFFSHORE FAULT TRENDS AND THE INNER BORDERLAND STRUCTURAL PROVINCE

As seen in figure 25 and plate 3, the north to northwest trends of the Inner Borderland faults are distinctly different from those of the Peninsular Ranges. For this reason, the author concludes that the Inner Borderland is a distinct structural province as previously inferred by others including Gastil and others (1975). These fault trends fall into two main groups, one about N30°W and the other about N40°W (figures 25 and 27). The eastern and southern fault zones including the San Diego

Trough, Coronado Bank and San Isidro have the N30°W trends. The westernmost, including the San Clemente fault zone has a N40°W trend. Both offshore trends are at least 10° more northerly than the trends of the nearby fault zones in the Peninsular Ranges. Several possible explanations for these different fault trends may be proposed.

Kamerling (1984) postulated that the change in fault trends from N22°W along the Patton Escarpment to N50°W along Peninsular Ranges faults showed that the orientation of faulting rotated 28° counterclockwise as the locus of faulting along the North American continental margin shifted from west to east. Data described above showing that the easternmost faults of the Inner Borderland have a more northerly trend than those to the west is inconsistent with Kamerling's (1984) model. Alternatively, the easternmost faults of the Inner Borderland, with the more northerly trends, may have rotated 10° clockwise, relative to the San Clemente fault zone, in a manner similar to that proposed by Luyendyk and others (1980) for the northern Channel Islands including Santa Catalina. Kamerling (1984) points out that San Clemente Island, and the other southern Channel Islands, except for Catalina, show no significant rotation based upon paleomagnetic data.

Another plausible explanation is that both sets of fault trends formed contemporaneously under the same tectonic regime, that is, dextral wrench faulting along an underlying trend subparallel to the Pacific-North American plate boundary. The differing strikes would then be inferred to show the different types of shears observed in wrench faulting experiments (cf. Tchalenko, 1970; Wilcox and others, 1973; Bartlett and others, 1981). For example, the N30°W-trending faults may be considered synthetic Riedel or R shears, and the N40°W-trending faults, either P or

principal displacement (Y) shears. Because the orientation of transforms predicted for present-day Pacific and North American lithospheric plate interaction is N40°W at this location (Minster and Jordan, 1978), the author considers that the San Clemente fault zone, with its N40°W trend, exhibits the modern trend of wrench faulting, and the more northerly-trending fault zones exhibit synthetic shear along older, pre-existing fault trends. These other fault zones, such as the San Diego Trough, Coronado Bank and San Isidro, are not considered Riedel shears in a larger wrench fault zone because each exhibits the character of a fully developed wrench fault on its own. This character is best demonstrated by the relatively long, straight, narrow and continuous nature of the principal or main fault traces (figures 25 and 27). Furthermore, the branch and secondary faults of each major zone shows orientations consistent with the Riedel and other secondary shears observed during wrench fault experiments (figure 27; Tchalenko, 1970; Wilcox and others, 1973; Bartlett and others, 1981).

Two additional possible explanations for the two distinct fault zone orientations evident in the Inner Borderland are proposed here: (1) two different ages of faulting, with reactivation of older faults along a trend of favorable orientation for the newer shear direction; (2) differences in shear angle due to differences in crustal rheology or possibly different levels of faulting such as lithospheric versus upper crustal. Arguments presented here in favor of the first explanation include the observation that the N30°W trend of the Inner Borderland faults is parallel to the axes of the nearshore basins and troughs (chapter 4, this volume). Thus, these physiographic and tectonic features may have similar origins. Furthermore, the N30°W trend is also parallel to the line of Santillán and Barrera (1930) described by Gastil and others

(1975) as the hinge line between emergent Peninsular Ranges and submerged California Continental Borderland physiography during late Cretaceous time. Also, the principal structural trend of the prebatholithic rocks of the Baja California peninsula is N30°W (Allen and others, 1960; Gastil and others, 1975).

Moore (1969) considered that the major northwest-trending fault zones were formed during middle Miocene time and reactivated in Pliocene and Pleistocene time. Considering how remarkably parallel this N30°W trend is to the older, late Cretaceous and even prebatholithic structural trends, over large distances (possibly reaching half of the length of Baja California), the author proposes that these nearshore fault zones are reactivated along ancient, possibly Mesozoic structural discontinuities. The N30°W trend is very close to the present-day transform direction, and therefore such reactivation is reasonable. The San Clemente fault zone, with its N40°W trend, is considered a younger system, and does seem to cross-cut some of the more northerly trends (figures 23 and 25), although this fault system is diverted along the N30°W-trending San Isidro fault zone to the south. The divergent wrench fault character of the San Isidro fault zone is consistent with the younger, more westerly-trending slip direction of the present-day plate boundary.

Lastly, different levels of faulting may be involved, such as lithospheric-scale, plate boundary faulting or shallow, upper-crustal, block faulting. The eastern, more northerly-trending faults are possibly associated with relatively shallow, upper-crustal faulting over an unidentified detachment surface. The author proposes that the divergence between the trend of epicenters along the Coronado Bank fault zone and the mapped fault traces (figure 66) is possible evidence for such a detachment. Also, the complexity of faulting within the Agua Blanca fault system may be evidence

Figure 66. Seismicity of the Inner Borderland. Only epicenters for earthquakes with $M_L \geq 2.5$ have been plotted in order to present a more homogeneous sampling of activity throughout the region. The principal, late Cenozoic faults are also shown for comparison with trends in earthquake locations. The greatly expanded southern California seismograph network allows recording and location of the epicenters for most events with $M_L \geq 2.5$ in the southern California area. The accuracy of the locations is generally poor in the offshore region, although relative locations are more reliable so that spatial trends in seismicity may be of real significance. Data are from the Caltech seismological laboratory (plot courtesy of G. Stewart).

SEISMICITY 1977-1984 NEARSHORE SAN DIEGO

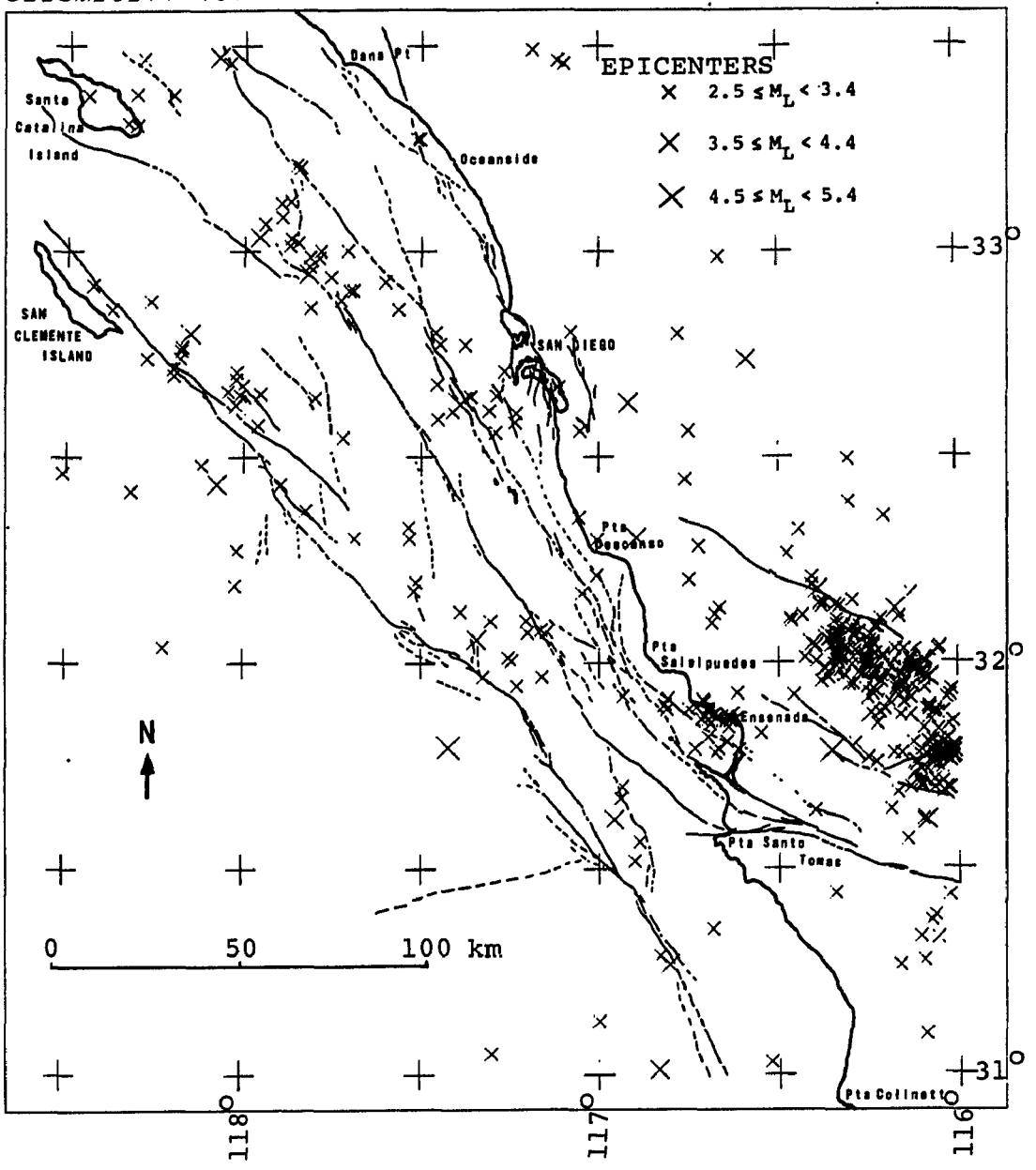

of the disaggregation of the upper crust in a broad, but shallow shear zone. Numerous detachment faults have been described throughout the southern California region (Yeats, 1983) and the abundant evidence of ancient subduction along the California continental margin (Howell and others, 1980; Howell and Vedder, 1981) are consistent with such an interpretation.

The author proposes that the San Clemente fault system may be a lithospheric fault, delineating the boundary between tectonic plates or microplates. The relatively simple, narrow, long, straight and continuous character of the San Clemente-San Isidro fault zones, compared to the Agua Blanca fault system, is more typical of major transform fault systems. Also, the trend of seismicity associated with the San Clemente fault system seems to follow more closely the mapped fault traces than does the Coronado Bank trend (Figure 66) although the epicenters are poorly located. The data regarding all of the above hypotheses regarding the origin and development of fault trends in the Inner Borderland are presently inconclusive, so that no single model or combination of models can be presented as fact.

**Fault Geometry And Kinematics**

Data and assumptions regarding fault geometry and character are used to provide criteria which define kinematic models of the complicated North American - Pacific tectonic plate boundary. Several kinematic models of the tectonic deformation within the California part of the plate boundary have been proposed (Anderson, 1979; McKenzie and Jackson, 1983; Bird and Rosenstock, 1984; Minster and Jordan, 1984). Differing conclusions regarding the relative importance of California Continental Borderland faults in contributing to the overall plate motion have been put

forward. The data of the present study are used by the author to provide additional constraints on possible models for the late Cenozoic, mostly Quaternary regional tectonics.

The first simplifying assumption considered in this, and also the previous studies (Anderson, 1979; McKenzie and Jackson, 1983; Bird and Rosenstock, 1984; Minster and Jordan, 1984) is that of a two dimensional geometry. In the present study, plane geometry is a reasonable assumption for small areas such as southern California and the Inner Borderland. Fault movement in this simple, two dimensional model is defined by the horizontal projection of the slip vector (hereafter referred to as the slip vector), and vertical movements are considered unimportant. As shown by the data described above, the major Inner Borderland faults are strike-slip in character, and vertical movements, although locally significant, are not generally important. Regional vertical movements associated with the large scale divergent or convergent wrench faulting will not be considered in the present study although they may be important. The major wrench faults of this study are assumed to be vertical, and so the slip vector is parallel to the fault strike. Orientations of slip vectors for the oblique-slip fault zones are determined from local segments of faults that are determined to be 'parallel' or 'pure' strike-slip in character (chapter 4, this volume). A block tectonic model is considered, assuming the deformation to be localized along the major fault zones, and the intervening areas considered as rigid blocks. McKenzie and Jackson (1983) have considered models of distributed shear, and some of their conclusions relevant to the present study are also considered. The thickness of the blocks is not considered important in the simple plane geometry model herein, although Bird and Rosenstock (1984) propose a model with block thicknesses

substantially thinner than the overall thickness of the lithosphere in most places.

Magnitudes of the slip vectors are not generally known for the submerged faults of the Inner Borderland. Previous studies (Anderson, 1979; Bird and Rosenstock, 1984; Minster and Jordan, 1984, Jordan and others, 1985; Weldon and Sieh, 1985) have proposed widely varying estimates of late Quaternary slip rates for faults offshore of southern California. Values ranging from negligible ($\simeq$1-2 mm/yr) to significant (10-20 mm/yr, or 20% - 33% of the overall North American-Pacific relative plate motion) have been estimated. Even without knowing the magnitudes of the slip vectors on the principal offshore faults, important conclusions regarding the kinematics of plate boundary or microplate(?) tectonics within the Inner Borderland and the southern California region can be made using the more readily determined slip vector orientations. In addition, using reasonable assumptions regarding crustal fault rheology, for example, friction coefficients and failure criteria, it is possible to develop useful conclusions about the stress field within the plate boundary zone of deformation.

**Inner Borderland Faults**

Systematic variations in the orientations of the slip vectors for the major Inner Borderland fault zones are shown in figure 67 and Table 3. In general, slip along the San Clemente fault system is determined to be N40°W, parallel to the predicted relative plate motion vector for the Pacific-North American plate interaction in this area (Minster and Jordan, 1978). Slip vectors for other fault zones in the Inner Borderland and the Peninsular Ranges are observed to deviate significantly from the predicted direction of relative plate motion. In particular, the San Diego Trough

Figure 67. Map showing inferred orientations of horizontal slip vectors for faults in the Inner Borderland and vicinity. Data used to infer these slip vector orientations are listed in Table 3. The direction of movement of the block on the northwest side of the fault is shown, and is expected to be subparallel to the direction of relative movement of the Pacific lithospheric plate with respect to North America (i.e., $\simeq$N40°W in this region according to Minster and Jordan, 1978).

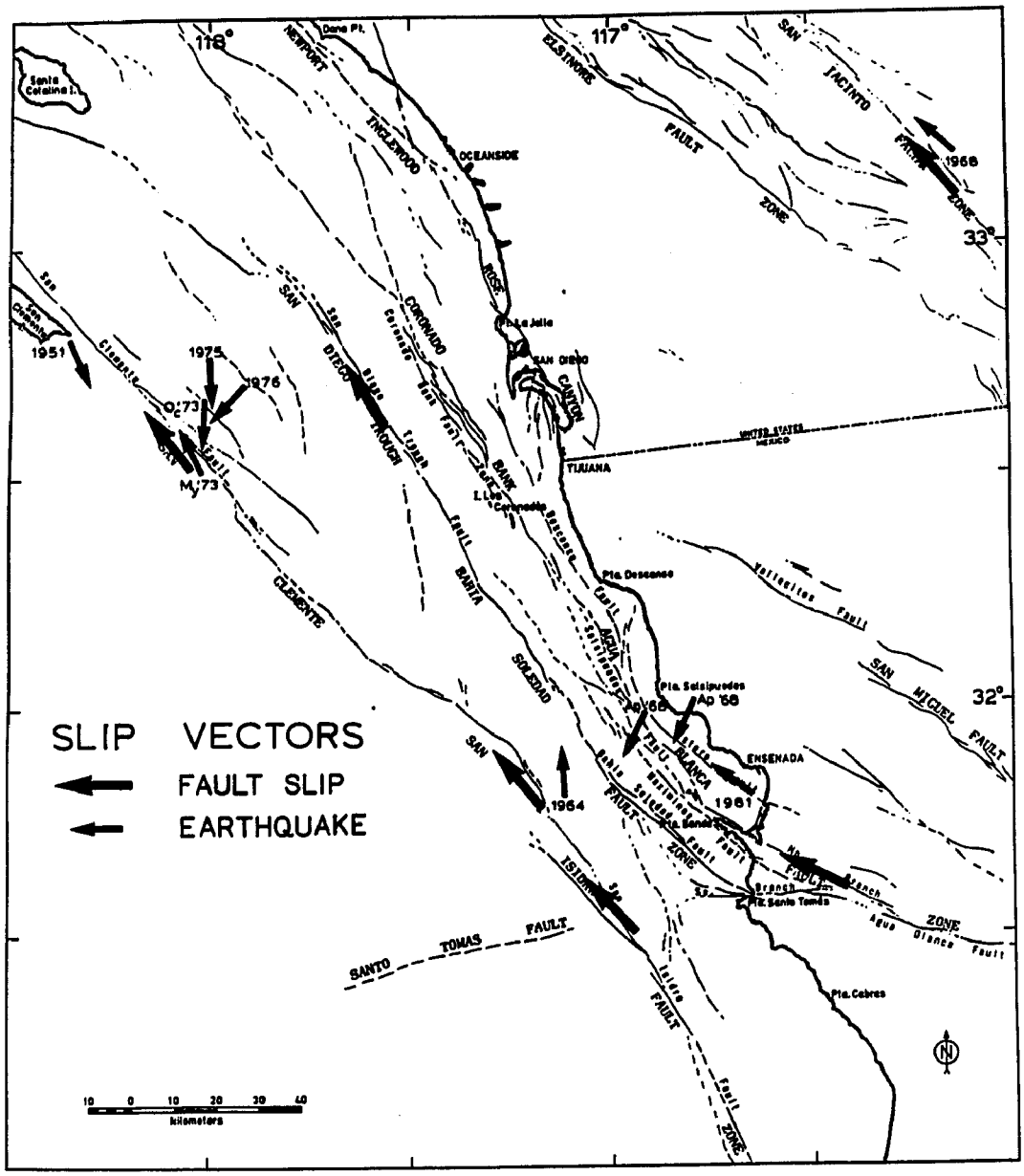
SLIP VECTORS
FAULT SLIP
EARTHQUAKE
118°
117°
33°
32°
Santa Catalina I.
Dana Pt.
NEWPORT
INGLEWOOD
ELSINORE
FAULT
ZONE
SAN
JACINTO
FAULT
ZONE
1968
OCEANSIDE
ROSE
CORONADO
BANK
CANYON
Pt. La Jolla
SAN DIEGO
TIJUANA
UNITED STATES
MEXICO
SAN
DIEGO
TROUGH
BAHIA
SOLEDAD
CLEMENTE
1951
1975
1976
O'73
M'73
Pta. Descanso
Vallecitos Fault
SAN
MIGUEL
FAULT
Pta. Salsipuedes
Ap '68
ENSENADA
1961
1964
SAN
ISIDRO
FAULT
ZONE
Pta. Santo Tomás
Agua Blanca Fault
SANTO
TOMAS
FAULT
Pta. Cabras
10 0 10 20 30 40
Kilometers

Table 3. Tectonic stress orientation indicators in the Inner Continental Borderland and vicinity.

| Site No. | Location | Slip Vector[1] | Stress Regime[2] | Principal Stress[3] | Type of Indicator[4] | Comments | Reference |
|---|---|---|---|---|---|---|---|
| 1 | 33° 11.4' N<br>116° 07.7' W | N48°W<br>Dextral | Strike-Slip | $S_1$ = N18°W<br>$S_3$ = N72°E | Earthquake Focal Mechanism | Borrego Mtn.<br>9 April 1968 | Allen & Nordquist (1972) |
| 2 | 33° 10' N<br>116° 09' W | N30° -40°W<br>Dextral | Strike-Slip | $S_1$=N00°-10°W<br>$S_3$=N80°-90°E | Fault Slip (EQ) | Borrego Mtn.<br>9 April 1968 | Clark (1972) |
| 3 | 33° 59.5' N<br>116° 55.0' W | S25° -31°W<br>Sinistral | Strike-Slip<br>(Obl. Normal) | $S_1$=N01°-05°W<br>$S_3$=S85°-89°W | Earthquake Focal Mechanism | Pta. Salispuedes<br>10 April 1968 | Legg (1980) |
| 4 | 31° 56.3' N<br>116° 53.0' W | S27½°W<br>Sinistral | Strike-Slip<br>(Obl. Normal) | $S_1$ = N03°W<br>$S_3$ = S87°W | Earthquake Focal Mechanism | Pta. Salispuedes<br>10 April 1968 | Legg (1980) |
| 5 | 32° 06.7' N<br>116° 46.9' W | S27°W<br>Sinistral | Strike-Slip<br>(Obl. Normal) | $S_1$ = N03°W<br>$S_3$ = S87°W | Earthquake Focal Mechanism | Pta. Salispuedes<br>23 April 1968 | Legg (1980) |
| 6 | 31° 45' N<br>115° 55' W | N60°W<br>Dextral | Strike-Slip<br>(Oblique?) | $S_1$ = N10°W<br>$S_3$ = N80°E | Fault Slip (EQ) | San Miguel<br>Feb. 1956 | Shor & Roberts (1958) |
| 7 | 31° 45' N<br>115° 55' W | N69°W<br>Dextral | Strike-Slip | $S_1$ = N59°W<br>$S_3$ = N48°E | Earthquake Focal Mechanism | San Miguel<br>Feb. 1956 | Hodgson & Stevens (1969?) |
| 8 | 31° 47' N<br>116° 40' W | N52°W<br>Dextral | Strike-Slip | $S_1$ = N21°W<br>$S_3$ = N67°E | Composite EQ Focal Mechanism | Bahia Todos Santos 1981 | Gonzalez & Suarez (1984) |
| 9 | 31° 37' N<br>116° 27' W | N63°W<br>Dextral | Strike-Slip | $S_1$ = N33°W<br>$S_3$ = N57°E | Fault Strike | Agua Blanca<br>(V. Maneadero) | Allen & al. (1960) |
| 10 | 32° 02' N<br>117° 22' W | | Extension<br>(Local in SS) | $S_1$ =N05±10°W<br>$S_3$ =N85±10°E | Graben | San Clemente-<br>San Isidro F.Z. | Legg (1985) |
| 11 | 32° 35' N<br>118° 00' W | | Extension<br>(Local in SS) | $S_1$ = N15±2°E<br>$S_3$ = N75±2°E | Graben | San Clemente<br>Fault Zone | Legg & al. (1985) |
| 12 | 32° 12' N<br>117° 27' W | | Compression<br>(Local in SS?) | $S_1$ = N78°W<br>$S_3$ = N12°E | Young Folds | San Clemente<br>Fault Zone | Legg (1985) |
| 13 | 32° 32' N<br>118° 04' W | N27°W<br>Dextral | Strike-Slip<br>(Obl. Normal) | $S_1$ =N05-07°E<br>$S_3$ =N85-87°W | Earthquake Focal Mechanism | Fortymile Bank<br>26 May 1973 | Legg (1980) |
| 14 | 32° 41' W<br>118° 05' W | N00-06°E<br>Sinistral | Strike-Slip | $S_1$ =N21-35°W<br>$S_3$ =N56-66°E | Earthquake Focal Mechanism | Fortymile Bank<br>28 Oct. 1973 | Legg (1980) |

Table 3. (Continued)

| Site No. | Location | Slip Vector[1] | Stress Regime[2] | Principal Stress[3] | Type of Indicator[4] | Comments | Reference |
|---|---|---|---|---|---|---|---|
| 15 | 32° 45' N<br>117° 59.9' W | N04°W<br>Sinistral | Strike-Slip | $S_1$ = N34°W<br>$S_3$ = N57°E | Earthquake Focal Mechanism | Fortymile Bank<br>12 Jan. 1975 | Legg (1980) |
| 16 | 32° 43' N<br>117° 55' W | N80°-90°W<br>46°E-40°S | Extension<br>Normal Oblique | $S_1$ =N49-55°W<br>$S_3$ =N37-40°E | Earthquake Focal Mechanism | Fortymile Bank<br>18 Oct. 1976 | Legg (1980) |
| 17 | 32° 49' N<br>118° 21' W | N20°-26°W<br>Sinistral | Strike-Slip<br>(Obl. Normal?) | $S_1$ = N53°W<br>$S_3$ =N34-36°W | Earthquake Focal Mechanism | San Clemente Isl.<br>26 Dec. 1964 | Legg (1980) |
| 18 | 31° 49' N<br>117° 07' W | N02-04°W<br>Dextral | Strike-Slip<br>(Obl. Normal?) | $S_1$ =N24-30°E<br>$S_3$ =N67-80°W | Earthquake Focal Mechanism | Decanso Plain<br>22 Dec. 1964 | Legg (1980) |
| 19 | 31° 28' N<br>116° 03' W | N65° -70°W<br>Dextral | Strike-Slip | $S_1$ =N35-40°W<br>$S_3$ =N20-25°E | Fault Strike | Agua Blanca<br>(U. Agua Blanca) | Allen & al.(1960) |
| 20 | 32° 30' N<br>117° 34' W | N29°W<br>Dextral | Strike-Slip | $S_1$ = N01°E<br>$S_3$ = N89°W | Fault Strike | San Diego Trough Fault | Legg (1985) |
| 21 | 32° 34' N<br>118° 02' W | N40°W<br>Dextral | Strike-Slip | $S_1$ = N10°W<br>$S_3$ = N80°E | Fault Strike | San Clemente Fault<br>No. San Clemente Basin | Legg and others, (1985) |
| 22 | 11° 33' N<br>117° 00' W | N41°W<br>Dextral | Strike-Slip | $S_1$ = N11°W<br>$S_3$ = N79°E | Fault Strike | San Isidro Fault<br>Ensenada Trough | Legg (1985) |
| 23 | 31° 98' N<br>117° 11' W | N41°W<br>Dextral | Strike-Slip | $S_1$ = N11°W<br>$S_3$ = N79°E | Fault Strike | San Isidro Fault<br>Decanso Plain | Legg (1985) |

1. Slip vector inferred from fault slip data for earthquakes or known fault plane orientations. (Horizontal component)
2. Stress regime inferred from type of stress regime indicator, e.g. strike-slip fault, or small graben are local indicators of the type of stress regime.
3. Maximum principal stress ($S_1$) is inferred to be oriented 30° from the local slip vector, for strike-slip faults, and parallel to the trends of small grabens, normal to the trend of young folds. The horizontal component is shown above, and in the region, where wrench faulting dominates the tectonics, the maximum and minimum stress vectors are approximately horizontal.
4. Geophysical or geological observation which provides an indication of the stress orientations. For this study, primarily fault slip data from earthquakes, earthquake focal mechanisms (body-wave), fault character and orientation and geologically youthful fold axes are used to infer the principal stress orientations.

fault zone exhibits simple shear along a N30°W trend. The San Isidro fault zone the south also has an overall trend of N30°W, but is clearly divergent, and N40°W is the strike of the parallel wrench fault segments and therefore, the orientation of the slip vector for this zone. Thus, there is a 10° clockwise rotation of the simple shear slip vector, from south to north, and from west to east, across the Inner Borderland. Oblique convergence across the Inner Borderland fault zones of similar trends to the north (for example, San Pedro, Palos Verdes Hills, and Newport-Inglewood; Harding, 1973; Bulka and Teng, 1979; Fischer and others, 1977; Junger, 1976; Junger and Wagner, 1977; Teng, 1985) implies that this clockwise reorientation of slip and presumably strain and stress(?) axes occurs as far north as the Transverse Ranges. Also, the fault patterns to the north, approaching the Transverse Ranges, seems to become more complex with more diverse orientations (figures 25 and 69).

**Peninsular Ranges Faults**

Onshore, the orientations of the slip vectors of the major Peninsular Ranges fault zones, including the Agua Blanca, San Miguel, Vallecitos, Elsinore and San Jacinto are more westerly (N45°-70°W) than those of the Inner Borderland (figures 25 and 69). The transition from Peninsular Ranges to Inner Borderland fault strikes occurs in a very narrow belt along the coast which marks, the boundary between these two structural provinces. Slip data for the major Peninsular Ranges faults show that predominately strike-slip has occurred (Allen and others, 1960; Clark, 1972; Sharp, 1972; Kennedy, 1977), although oblique slip is evident where systematic vertical offsets have been observed (Shor and Roberts, 1958). The general clockwise reorientation of the slip vectors towards the north is also apparent for these Peninsular

Ranges faults, as the southernmost, Agua Blanca fault has a N60°-65°W strike onshore, whereas to the north, Elsinore and Coyote Creek faults strike N45°-50°W (figure 25).

**Earthquake Focal Mechanisms**

Earthquake focal mechanisms provide instantaneous measures of the slip vector orientations for faulting within the Inner Borderland. In the simple model considered here, the horizontal projection of the slip vector, computed from earthquake body-wave first motions is used to infer the orientation of horizontal slip for several small to moderate earthquakes ($M_L$ = 4-6) that occurred in the Inner Borderland (figure 67; Table 4; cf. figures 9, 10 and 12, Legg, 1980). Of the two possible fault plane solutions shown by first motion diagrams, the one containing the slip vector is constrained to be subparallel to aftershock seismicity trends or observed fault slip for earthquakes occurring onshore. Most of the offshore events, however have few well-located after shocks, and so the fault plane chosen is the one subparallel to the most prominent mapped fault traces in the area. Although these earthquake slip vectors are generally subparallel to the mapped fault traces, for example, Borrego Mountain, 1968, and Bahía Todos Santos, 1981, significant deviations are notable in the offshore area.

The events near Punta Salsipuedes are part of a small earthquake swarm. Although the slip directions seem anomalous, these mechanisms are consistent with sinistral, oblique, normal-slip on antithetic shears in a complex zone of northwest oriented, dextral wrench faulting. The alternate focal plane solution (N60°W) is subparallel to the fault trends of the major Peninsular Ranges faults but has a more westerly orientation than the mapped faults at the coast.

The 22 December 1964 earthquake has a slip vector oriented almost north-south and may be associated with the small, en echelon, right step in the San Isidro fault zone near the epicenter. The focal mechanism for this event is relatively well-constrained, although the epicenter is not well-located. The P-wave first motion diagram showed almost pure strike-slip on a near vertical fault plane (Legg, 1980).

An important group of earthquakes with unexpected slip vectors are those located near San Clemente Island and Fortymile Bank (figure 67). As described by Legg (1980), these earthquakes showed first motions that were *not* consistent with right-lateral, strike-slip on northwest-oriented fault planes. Instead, left-slip on north- to northwest-trending, steeply-dipping faults or right-slip on east-west trending conjugate fault planes were exhibited. These focal mechanisms are well-constrained for the largest ($M_L$=5.9, 26 December 1951) and the more recent ($M_L$=4.7, 12 January 1975) earthquakes in this area (Legg, 1980). Other events with focal mechanisms consistent with San Andreas fault system tectonics (26 May 1973 and 13 February 1952 - not shown) imply that the region of anomalous slip lies between the southern tip of San Clemente Island and the southern flank of Fortymile Bank. Unfortunately, data necessary for detailed mapping of the geologic structure of the Fortymile Bank region were not available for this study, so that association of these earthquakes with specific, possibly anomalous(?) geologic structure is not possible at the present time. The few prominent faults which have been mapped in the area are generally northwest-trending (figure 25, plates 3 and 5). Furthermore, the geologic data show that right-slip has been the dominent mode of deformation along the San Clemente fault in this area during late Quaternary time (chapter 5, this volume). This apparent contradiction between geologic and seismologic data may be evidence

of local complexity of short duration(?) in the tectonics of the Inner Borderland. Alternatively, a new pattern of movement, such as incipient clockwise rotation of a small microplate or large crustal block delineated by the region of earthquake epicenters with anomalous focal mechanisms may be developing. Additional data are needed to explain the source of this complexity.

**Stress Trajectories**

Anderson (1951) discussed the formation of faults based upon Mohr and Coulomb failure criteria, and prescribed the orientation of the predicted fault planes and slip directions in relation to the principal stress directions. Since the earth's surface is largely traction free, he inferred that one principal stress would be vertical, and the other two lie in the horizontal plane for shallow crustal faults. In strike-slip regimes, the intermediate principal stress is vertical, and the major and minor stress axes are horizontal. The angle between the strike of the vertical fault plane and the maximum principal stress axis is less than 45°.

Although the Anderson fault theory describes failure of intact, homogeneous material, it is also useful for determining the most favorable orientations for slip on pre-existing faults within a given stress regime. For the simple, two-dimensional model of this study, horizontal stress trajectories, are inferred from the fault orientations and earthquake slip vectors. Local deviations of these trajectories from a homogeneous stress field are identified and explained in terms of fault character and geometry where possible. Systematic regional deflections of stress orientations are also described and explanations for these variations are proposed based upon the regional tectonic framework. Unexplained variations in the principal stress orienta-

tions identify areas where additional data are especially needed to develop better models of the regional tectonics.

Geological indicators of the principal strain and inferred stress directions are based upon the sense of slip on faults and the orientation of secondary features such as folds or extension fractures. For this study, only latest Cenozoic, mainly Quaternary, features are considered, because the regional stress field is likely to have undergone substantial changes throughout the complex Cenozoic tectonic development of the region (Atwater, 1970; Crouch, 1979; Luyendyk and others, 1980). Slip directions for the pure strike-slip faults in the area are the major features used to infer the regional average stress orientations at the resolution and scale of this study.

Numerous observations have shown that the maximum principal stress is oriented approximately 30° to the strike of the fault plane for strike-slip faults (Moody and Hill, 1956). Although heterogeneity in the upper crustal rheology is likely, it is assumed herein, as a first approximation, that the shear resistance of all late Cenozoic faults in the region is the same. Thus the maximum principal stress axes plotted (figure 68) are at an angle of 30° to the slip direction for the pure strike-slip faults. A test of these inferred stress orientations is provided by small, secondary structures located near the faults in the area.

A small, shallow graben displaces the seafloor near the major left bend of the San Clemente-San Isidro fault zone (figure 63, plate 3). The axis of this extensional feature has a N05°W trend which is close to the N10°W trend of the inferred maximum principal stress axis for the main fault traces of the San Clemente fault system. The slight misalignment of these two inferred principal stress directions may be due to local stress reorientation associated with fault interaction between the two

Figure 68. Map showing inferred orientations of principal stress for the Inner Borderland and vicinity. The Anderson (1951) criteria of failure is assumed, with a shear angle of 30° (i.e., the angle between the maximum principal stress and the fault plane). Data used to derive these orientations are listed in Table 3.

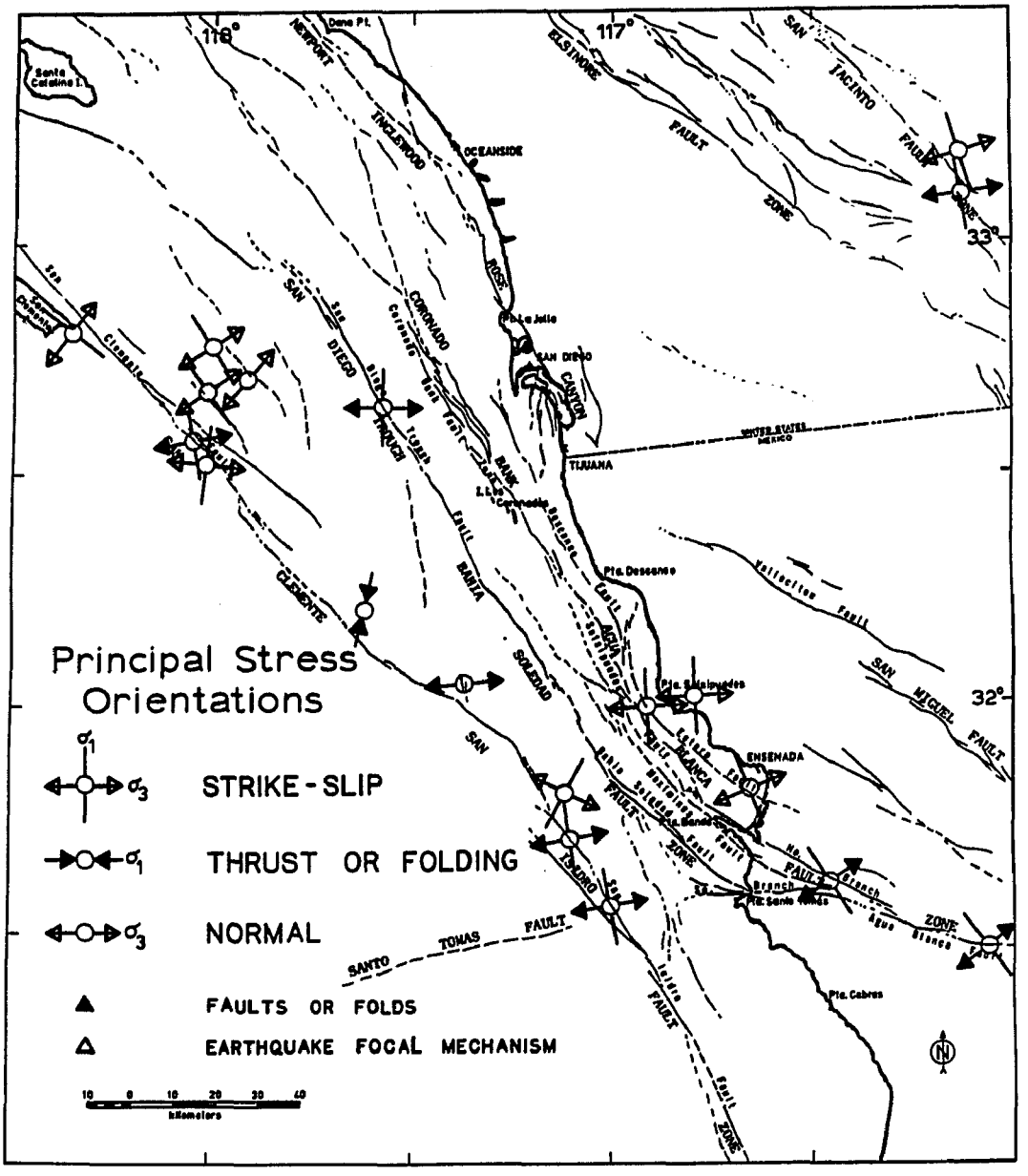
Principal Stress Orientations
STRIKE-SLIP
THRUST OR FOLDING
NORMAL
FAULTS OR FOLDS
EARTHQUAKE FOCAL MECHANISM
118°
117°
33°
32°
Dana Pt.
Santa Catalina I.
NEWPORT
INGLEWOOD
OCEANSIDE
ELSINORE
FAULT
ZONE
SAN
JACINTO
FAULT
ZONE
CORONADO
BANK
SAN DIEGO
CANYON
TIJUANA
UNITED STATES
MEXICO
Pta. Descanso
Valleciton Fault
SAN
MIGUEL
FAULT
ENSEMADA
SAN
ISIDRO
FAULT
ZONE
SANTO
TOMAS
FAULT
Pta. Cabras
Agua Blanca Fault
ZONE
kilometers

major, offset linear segments of the San Clemente fault system. Segall and Pollard (1980), however, show that a 10° *counterclockwise* rotation of the stress axes is expected at left steps of en echelon, dextral, strike-slip faults. Alternatively, the small graben may be related to gravity sliding of the surficial sediments down the flank of the broad uplift associated with the left bend. The latter possibility is unlikely because the graben trends obliquely to the gentle (<5%) slope gradient in this area. Also, no evidence of slope movement is observed on seismic reflection profiles adjacent to the feature. The assumed 30° angle between the maximum principal stress axis and the fault plane may be incorrect, and an angle of 45° would yield consistent orientations of stress trajectories according to the static theory described by Segall and Pollard (1980).

Another small graben on the lower, southwest flank of Fortymile Bank has a N15°W trend, (plate 5) which is also within 5° of the inferred maximum principal stress orientation for the main trace of the nearby San Clemente fault. This graben is in presumably older, acoustic basement rocks of Fortymile Bank and so may be associated with older fault movements. Its prominent geomorphic expression, however, implies that it has a relatively youthful age. Other complications regarding the stress orientations near Fortymile Bank are discussed subsequently.

Lastly, a series of young, east-west trending folds located between Navy Bank and the left bend in the San Clemente-San Isidro fault zone (plate 3) indicates a N10° - 15°E orientation of the maximum principal stress axis in this area. The 25° - 25° misalignment of the inferred stress axes for this feature may be evidence of stress reorientation associated with convergence between the fault bend and Navy Bank. Southward termination of the northeastern branch of the San Clemente fault

along the southern end of the Navy Fan pull-apart may also be involved (chapter 4, this volume).

Principal stress orientations based upon the earthquake focal mechanisms and slip vectors discussed previously are generally consistent with the geologically determined estimates. The maximum principal stress, inferred to be oriented at 30° to the slip vector in the extensional quadrant of the focal sphere, is roughly north-south. The choice of the antithetic slip vector for the Salsipuedes earthquake swarm provides principal stress orientations more consistent with the other offshore data. The alternate slip vector (N60°W), however, is consistent with the Peninsular Ranges fault movements.

The 22 December 1964 earthquake shows a clockwise deflection of the stress axes relative to the other fault segments. Segall and Pollard (1980) report clockwise deflection ($\simeq$15°) of the principal stress axes in the vicinity of right steps and pull-aparts of en echelon, dextral wrench faults. Thus, this earthquake may be associated with the small pull-apart basin discussed previously.

Inferred principal stress orientations for the Agua Blanca fault system show a systematic clockwise rotation from the transpeninsular, Agua Blanca fault northward to the San Diego Trough and perhaps the Transverse Ranges. It is not certain whether this rotation is sudden, occurring at the coastal boundary between Peninsular Ranges and Inner Borderland structure, or occurs more gradually across the region. Additional data are needed to provide a regionally more continuous measure of these stress orientations along the Agua Blanca fault system, especially for the Coronado Bank, Rose Canyon and Bahía Soledad fault zones, and to the north toward the San Pedro basin and Palos Verdes peninsula. As discussed previously, oblique

convergence on the northernmost fault zones of the Agua Blanca system is consistent with stress reorientation all the way to the Transverse Ranges. Therefore, the author proposes that north-south directed compression across the Transverse Ranges may be responsible for systematic reorientation of the principal stress trajectories across the Inner Borderland and southern California.

Orientations of the inferred principal stress directions along the San Clemente fault system (N10°W) are consistent along strike, except for the region of anomalous earthquakes around Fortymile Bank. As discussed previously, slip vectors for these earthquakes are opposite to what is expected for the area based upon regional tectonics and the geological and geomorphological evidence for faulting along the San Clemente fault. Because the earthquakes involved are among the largest recorded in the California Continental Borderland, they must be considered when attempting to evaluate the present day tectonic processes occurring in the area.*

As shown by the inferred stress orientations, only a 45° counterclockwise deflection of the stress trajectories is associated with the anomalous events. Until more detailed mapping of the geologic structure in the Fortymile Bank area is accomplished, it is not possible to determine if these earthquakes represent a short-lived phenomenon associated with the instantaneous kinematics and/or dynamics of the San Clemente fault system, or whether an ongoing, complex, microplate tectonic deformation is underway. For example, Luyendyk and others (1980) proposed that clockwise rotation of long, narrow, crustal blocks in a broad zone of dextral shear occurred during middle to late Miocene time, based upon paleomagnetic data.

---

* Small earthquakes are often observed to have focal mechanisms of widely different character in a small area, possibly due to local stress reorientations following other activity, and probably due to breaking of asperities or inhomogeneities near faults.

Interestingly, their model predicts left slip on initially north- to northeast-trending faults, (cf. Luyendyk and others, 1980, figure 3a), which subsequently rotate clockwise into a more east-west trend. The inferred fault planes of the anomalous Fortymile Bank earthquakes have a north to northeast strike, and so incipient rotation of a small microplate or fault block may be occurring. The slip vector (N20°-26°W) of the larger, San Clemente Island earthquake is not as well explained by this mechanism.

## CONCLUSIONS - INNER BORDERLAND TECTONICS

Notwithstanding the decades of research into the marine geology and tectonics of the California Continental Borderland, lack of accurate, detailed bathymetric and geologic maps for much of the region has hindered understanding of the geologic history and tectonic evolution of this important part of the modern Pacific-North American tectonic plate boundary. The present study, a more complete compilation of geological and geophysical data for the Inner Borderland south of the international border than previously available, improves the understanding of the late Cenozoic tectonics of the region. Several conclusions derived in this study are relevant to this understanding.

The late Cenozoic geologic structure of the Inner Borderland is dominated by two, major, northwest-trending, dextral wrench fault systems, the San Clemente and the Agua Blanca (figure 25). The character of faulting throughout these fault systems provides important constraints on models of the late Cenozoic tectonics of the region.

The overall pattern of the San Clemente fault system to the west resembles that of the larger San Andreas fault system onshore. Two, long, roughly linear, principal

fault segments, San Clemente and San Isidro fault zones, are linked by a major, transpressive, left-bending, fault segment, much as the northern and southern San Andreas faults are linked through the 'big bend' in the Transverse Ranges. The southern, San Isidro part of the offshore system is divergent, as are the Salton Trough and Gulf of California along the southern San Andreas fault system. The northern parts of both fault systems seem to be mostly pure strike-slip in character. Based upon these similarities, additional insights regarding the tectonic history and development of one fault system may be derived through close study of the other.

The nearshore Agua Blanca fault system is substantially more complicated than the San Clemente fault system, and consists of three or more, subparallel, northwest-trending, dextral, wrench fault zones. The westernmost of these, San Diego Trough-Bahía Soledad fault zone, is the most continuous, delineated by one or two relatively straight, primary fault traces that seem to continue uninterrupted for lengths as great as 40-50 km. The central fault zone, Coronado Bank-Agua Blanca fault zone, is generally delineated by two or three, subparallel, en echelon and branching, discontinuous fault segments that are generally only 10-20 km in length. A nearshore zone of faulting, not well delineated by the present study, lies subparallel to the coast, and consists of the Newport-Inglewood- Rose Canyon fault zone to the north, and the Descanso-Estero fault zone to the south. Where adequate data exist, this nearshore zone also seems to consist of numerous, discontinuous, subparallel, en echelon fault strands of limited length. The author proposes that these two nearshore zones interact, through a major right step in the San Diego area, forming the San Diego Bay and offshore bight structural low as a large pull-apart basin or sag. All of the major faults of the Agua Blanca system are interpreted to be right-slip in

character, although large structural relief associated with these fault zones indicates oblique slip may be important, at least locally.

The marked change in strike of the faults in the Agua Blanca system, where they pass offshore, shows that the Inner Borderland is a distinct structural province and not part of the Peninsular Ranges. The geometry of the Agua Blanca system in the Bahía Todos Santos area resembles that of the Alpine-Marlborough fault zones in New Zealand. Arabasz and Robinson (1976) relate the change in fault strike between the Alpine and Marlborough faults to a change in direction of relative plate movement. Alternatively, a change in the direction of relative plate motion may be responsible for the change in fault trends (Scholz, 1977; Kamerling, 1984).

The northwest-trending ridge and basin physiography of the Inner Borderland is also distinctive. Close alignment between the Inner Borderland faults and the axes of the ridges and troughs implies either common origins or reactivation of the younger faults on old, pre-existing structural trends. The overall strike of the Inner Borderland fault zones (N30°W) is parallel to the principal, pre-batholithic structural trends of the Baja California peninsula, and therefore, may indicate reactivation along older, perhaps Mesozoic structural features. Data regarding these speculations are, at present, inconclusive.

Within the Inner Borderland, slip vectors and inferred principal stress orientations for the major faults show systematic variations. The San Clemente fault system generally shows right-slip oriented N40°W, which is parallel to the predicted vector of relative motion between the Pacific and North American tectonic plates in southern California. The southern San Isidro fault zone, trends more northerly (N30°W) and is generally characterized by divergent wrench faulting, consistent with

the overall plate motion. This divergence is also manifest as continued late Quaternary subsidence of the Ensenada Trough. Earthquakes with unexpected focal mechanisms around San Clemente Island and Fortymile Bank demonstrate, as yet unexplained complexity in the present day tectonics of the region.

Even though the fault zones of the offshore, Agua Blanca fault system trend more northerly than the San Clemente system or the plate motion vector, they are not divergent at least for late Quaternary time, but instead, appear to be parallel wrench faults. This feature is well expressed by the San Diego Trough fault, which is relatively long and straight, and lies along the axis of the nearshore San Diego Trough. Farther north, convergence is reported across the Newport-Inglewood, Palos Verdes Hills and other major wrench faults of the Inner Borderland (Junger, 1976; Bulka and Teng, 1977; Teng, 1985). Based upon these observations, the author proposes that clockwise reorientation of principal strain and stress axes results from the major left bend in the San Andreas fault and convergence across the Transverse Ranges. In as much as the San Diego Trough fault is coaxial with the nearshore San Diego Trough, the author proposes that this fault zone was divergent during an earlier period of activity, and resulted in the opening and subsidence of the San Diego Trough. Such divergent wrenching is presently occurring within the Ensenada Trough along the San Isidro fault zone and possibly along the Coronado Bank fault zone closer to the coast (chapter 4, this volume). Others have proposed convergence in a dextral wrench fault environment as a mechanism to form the ridges bounding the San Diego Trough, but this study finds no evidence of late Quaternary convergence across the major faults within the vicinity, except locally, at small bends in the fault traces. Recognition of the earlier sense and timing of movement along the San Diego

Trough and related faults could provide important insights regarding the tectonic development of the Inner Borderland and possibly the surrounding portions of the Pacific-North American plate boundary. If the author's hypothesis is valid, that convergence in the 'big bend' region of the San Andreas fault and Transverse Ranges have affected the tectonic style of the Inner Borderland, then observable changes in Inner Borderland tectonic development may be correlated to changes in the tectonic development of the San Andreas fault and the Transverse Ranges. This postulated overprint of Transverse Ranges tectonic style on the northern California Continental Borderland has probably complicated the study of California Continental Borderland tectonics. Even though such an effect may not be present, this study has shown that the late Quaternary tectonic style of the Inner Borderland south of the international border has important differences from the area to the north.

**Baja California Microplate Tectonics**

In as much as the San Clemente fault system extends an undetermined distance southward west of Baja California, and modern seismicity also occurs in the Inner Borderland west of the peninsula, late Quaternary slip has been occurring between Baja California and the Pacific tectonic plate. Therefore, Baja California may be considered a microplate which has been detached from North America but is not welded to the Pacific plate (figure 69). The idea is not new, and the recognition of other active faults west of Baja California (for example, Tosco-Abreojos fault of Spencer and Normark, 1979) has led others to similar hypotheses. From the present study, a major 'microplate boundary' transform fault zone, that is, the San Clemente fault system, has been better defined. Its southward extent is unknown, at present,

Figure 69. Map showing configuration of postulated microplates or large crustal blocks along the southern California part of the Pacific-North American lithospheric plate boundary. The principal fault zones bounding the large crustal blocks or microplates are shown by heavy lines. Other faults are shown by lighter lines.

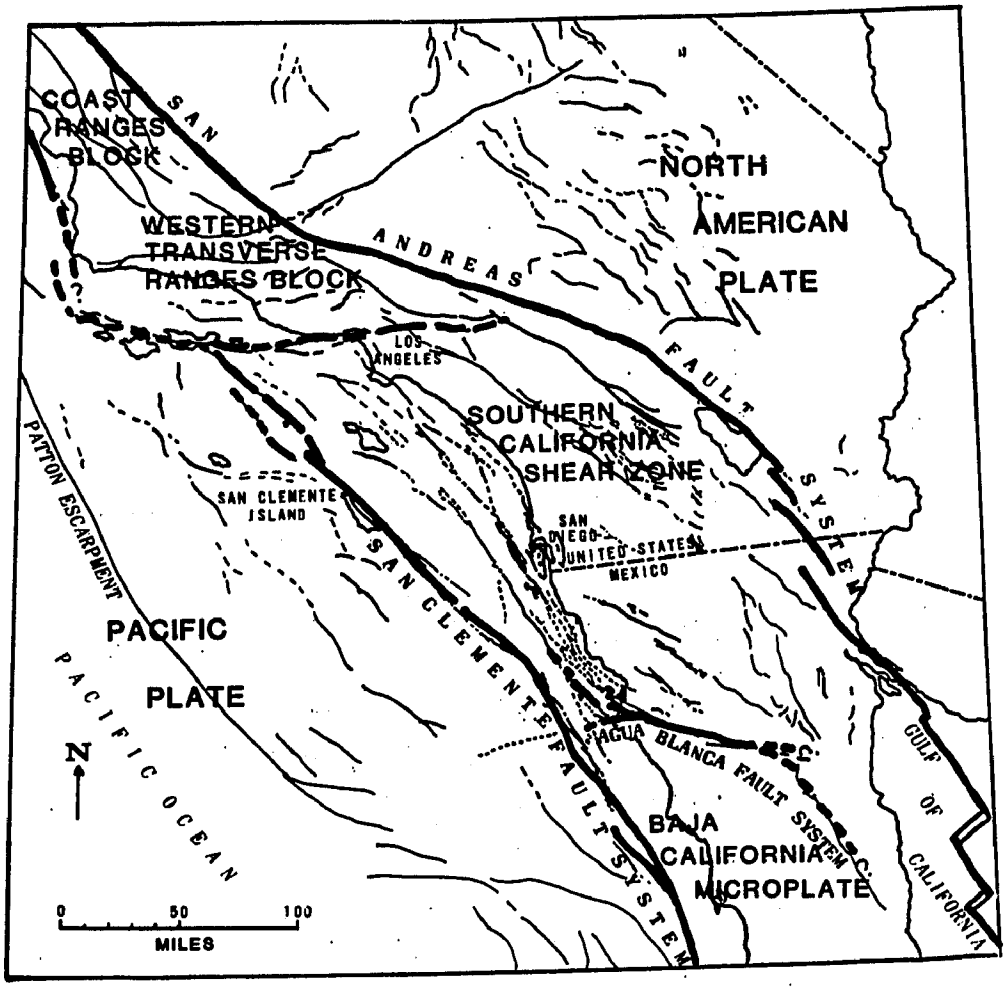
COAST RANGES BLOCK
SAN ANDREAS FAULT SYSTEM
WESTERN TRANSVERSE RANGES BLOCK
NORTH AMERICAN PLATE
LOS ANGELES
SOUTHERN CALIFORNIA SHEAR ZONE
SAN CLEMENTE ISLAND
SAN DIEGO
UNITED STATES
MEXICO
PATTON ESCARPMENT
PACIFIC PLATE
PACIFIC OCEAN
SAN CLEMENTE FAULT SYSTEM
AGUA BLANCA FAULT SYSTEM
BAJA CALIFORNIA MICROPLATE
GULF OF CALIFORNIA
N
0 50 100
MILES

and to the author's knowledge, no important, Quaternary, transpeninsular faults have been mapped south of the Agua Blanca fault. Such faults have been postulated (Normark and Curray, 1968; Rusnak and others, 1964), but other data (Colletta and others, 1981; Angelier and others, 1981) show that the Baja California peninsula has acted as a relatively rigid block for the past few million years.

On the other hand, the southern California area, extended southward to the Agua Blanca fault, has not behaved as a single, rigid block during post-Miocene time as is evident from the numerous, active fault zones which cut across the region. Rigid plate tectonic theory is not applicable to the complex zone of deformation within a major plate boundary such as that in southern California. Several investigators (Bird and Piper, 1980; Bird and Rosenstock, 1984) have invoked microplate tectonics to explain the deformation of the southern C 'ifornia region, and sophisticated finite-element models have been developed to simulate the regional kinematics. Block tectonic models developed by Bird and Rosenstock (1984) were useful in describing the kinematics of the southern California region, but unknown slip rates on the offshore faults were assumed to be minor in the absence of data to the contrary. Also in their model, the San Clemente fault system was truncated by the Agua Blanca fault system, so motion between the Pacific and Baja California was not considered to the south. Others have implied that a large proportion of the overall Pacific-North American relative plate motion is occurring offshore in southern California (Anderson, 1979; Weldon and Sieh, 1985), whereas Jordan and others (1984) limit this offshore slip to a minor amount.

Lastly, the oblique trend of the San Andreas fault relative to the predicted plate motion direction led Minster and Jordan (1984) to conclude that convergence should be occurring along the offshore fault trends. Such convergence is *not* evident in the Quaternary geologic structure of the Inner Borderland from the San Diego Trough southward, although convergent wrench faulting has been reported to the north (Crouch and others, 1984; Junger, 1976). Thus, the postulated effect of Transverse Ranges tectonics upon the southern California region may be limited to the region north of the Agua Blanca fault.

The author proposes that the bend in the San Andreas fault and Transverse Ranges convergence may have caused the 'breaking up' of the northern end of the Baja California microplate. The southern California area would thus be considered a broad zone of dextral shear, distributed over the several active faults cutting across the region. As shown by McKenzie and Jackson (1983), instability of distributed shear zones with several strike-slip faults leads to either reconfiguration of the fault pattern, or to concentration of slip on one of the boundary faults. They postulated that this effect might explain the concentration of slip along the San Andreas fault in California. Their model considered shear zones with uniformly distributed slip, and so the extrapolation to more heterogeneous shear zones may allow additional primary strike-slip fault zones to be simultaneously active at comparable slip rates. Alternatively, reconfiguration of the shear zone, through microplate tectonics or block rotations may be an ongoing process.

Future research effort should be directed at reliable determination of the slip rates and displacement histories for the offshore faults. Such data will permit better understanding and modelling of the kinematics of a complicated, continental

transform plate boundary. Such a boundary may be the locus of the large scale tectonic erosion and accretion of 'exotic terranes' which have been inferred along the western North American Cordillera (Saleeby, 1983).

## REFERENCES


Acosta, M.C. 1970. Upper Cretaceous geology of the Bahía Soledad - Punta China area. in *Pacific Slope Geology of Northern Baja California and Adjacent Alta California*. Pacific Sections, AAPG and SEPM, p. 30-36.

Allen, C.R., Silver, L.T. and Stehli, F.G. 1960. The Agua Blanca fault - a major transverse structure of northern Baja California, Mexico. *Geol. Soc. America, Bulletin*. vol. 71, p. 357-482.

Anderson, E.M. 1951. *The Dynamics of Faulting and Dyke Formation, with Applications to Britain*. 2nd Edition. Edinburgh, Oliver and Boyd. 206 pp.

Anderson, J.G. 1979. Estimating the seismicity from geologic structure for seismic risk studies. *Seismological Soc. America, Bulletin*. vol. 69, p. 135-158.

Angelier, J., Colletta, B., Chorowicz, J., Ortlieb, L. and Rangin, C. 1981. Fault tectonics of the Baja California peninsula and the opening of the Sea of Cortez, Mexico. *Jour. Structural Geology*. vol. 3, p. 347-357.

Arabasz, W.J. and Robinson, R. 1976. Microseismicity and geologic structure in the northern South Island, New Zealand. *New Zealand Jour. Geology and Geophysics*. vol. 19, p. 569-601.

Armiego, R. and Suarez, F. 1981. Neotectonics of northern Baja California. Geological Soc. America, *Abstracts with Programs*. vol. 13, p. 42.

Atwater, T. 1970. Implications of plate tectonics for the Cenozoic tectonic evolution of western North America. *Geological Soc. America, Bulletin*. vol. 81, p. 3515-3536.

Bally, A.W. 1983. *Seismic Expression of Structural Styles –A Picture and Work Atlas*. AAPG Studies in Geology 15, 3 volumes.

Bartlett, W.L., M. Friedman and J.M. Logan. 1981. Experimental folding and faulting of rocks under confining pressure: Part IX. Wrench faults in limestone layers. *Tectonophysics*. vol. 79, p. 255-277.

Barrows, A.G. 1974. A review of the geology and earthquake history of the Newport-Inglewood structural zone, southern California. California Div. Mines and Geology, *Special Report 114*. 155 pp.

Batiza, R., Fornari, D.J., Vanko, D.A. and Lonsdale, P. 1984. Craters, calderas, and hyaloclastites on young Pacific seamounts. *Jour. Geophysical Research*. vol. 89, p. 8371-8390.

Bird, P. and Piper, K. 1980. Plane-stress finite-element models of tectonic flow in southern California. *Physics Earth and Planetary Interiors*. vol. 21, p. 158-175.

Bird, P. and Rosenstock, R.W. 1984. Kinematics of present crust and mantle flow in southern California. *Geological Soc. America, Bulletin*. vol. 95, p. 946-957.

Blake, M.C., Jr., Campbell, R.H., Dibblee, T.W., Jr., Howell, D.G., Nilsen, T.H., Normark, W.R., Vedder, J.G. and Silver, E.A. 1978. Neogene basin formation in relation to plate-tectonic evolution of San Andreas fault system, California. *American Assoc. Petroleum Geologists Bulletin*. vol. 62, p. 344-372.

Bowditch, N. 1984. *American Practical Navigator*. Defense Mapping Agency Hydrographic/Topographic Center. Publication No. 9. Washington, D.C. 2 volumes, 1114 pp., 961 pp.

Bowen, A.J., Normark, W.R. and Piper, D.J.W. 1984. Modelling turbidity currents on Navy submarine fan, California Continental Borderland. *Sedimentology*. vol. 31, p. 169-185.

Broecker, W.S. and van Donk, J. 1970. Insolation changes, ice volumes and the $O^{18}$ record in deep-sea sediments. *Rev. Geophysics and Space Physics*. vol. 8, p. 169-198.

Brune, J.N., Simons, R.S., Rebollar, C. and Reyes, A. 1979. Seismicity and faulting in northern Baja California. in Abbott, P.L. and Elliott, W.J., editors. *Earthquakes and other perils – San Diego Region*. San Diego Association of Geologists Guidebook, p. 83-100.

Buffington, E.C. 1964. Structural control and precision bathymetry of La Jolla submarine canyon, California. *Marine Geology*. vol. 1, p. 44-58.

Buika, J.A. and Teng, T.L. 1979. A seismicity study for portions of the Los Angeles Basin, Santa Monica Basin and Santa Monica Mountains, California. Univ. Southern California, Geophysical Lab. *Tech. Report No. 79–9*. 191 pp.

CETENAL (Comision de Estudios del Territorio Nacional). 1974-1979. Cartas geologicas de Estados Unidos Mexicanos. Cartas topograficos de Estados Unidos Mexicanos. Mexico City, Mexico. Scale 1:50,000.

Clark, M.M. 1973. Map showing recently active breaks along the Garlock and associated faults, California. U.S. Geological Survey. *Misc. Geologic Investigations. Map I–741*. Scale 1:24,000.

Clarke, S.H., H.G. Greene, M.P. Kennedy and J.G. Vedder. 1985. Geologic map of the Inner - Southern California Continental Margin. Area 1 of 7 (NOS 1206N-16). in California Div. Mines and Geology. *Geologic Map Series of the California Continental Margin*. (in press). Scale 1:250,000.

Colletta, B., J. Angelier, J. Chorowicz, C. Rangin and L. Ortlieb. 1981. Faulting pattern in the peninsula of Baja California, Mexico. Geological Soc. America. *Abstracts with Programs*. vol. 11, p. 50.

Crouch, J.K. 1979a. Neogene tectonic evolution of the western Transverse Ranges and the California Continental Borderland. *Geological Soc. America, Bulletin*. vol. 90, p. 338-345.

Crouch, J.K. 1979b. Marine geology and tectonic evolution of the northwestern margin of the California Continental Borderland. Ph.D. dissertation. Scripps Inst. Oceanography.

Crouch, J.K. 1981. Northwest margin of the California Continental Borderland: marine geology and tectonic evolution. *American Assoc. Petroleum Geologists, Bulletin*. vol. 65, p. 191-218.

Crouch, J.K., Bachman, S.B. and Shay, J.T. 1984. Post-Miocene compressional tectonics along the central California margin. in Crouch, J.K. and Bachman, S.B., editors. *Tectonics and sedimentation along the California margin*. Pacific Section, Soc. Econ. Paleo. Mineralogists. p. 37-54.

Crouch, R.W. 1952. Significance of temperature on Foraminifera from deep basins off southern California coast. *American Assoc. Petroleum Geologists, Bulletin.* vol. 36, p. 807-843.

Crowell, J.C. 1952. Submarine canyons bordering central and southern California. *Jour. Geology.* vol. 60, p. 58-83.

Crowell, J.C. 1954. Geology of the Ridge basin area, Los Angeles and Ventura counties, California. California Div. Mines and Geology. *Bulletin 170. Map Sheet 7.*

Crowell, J.C. 1962. Displacement along the San Andreas fault, California. Geological Soc. America. *Special Paper No. 71* 61 pp.

Crowell, J.C. 1974a. Sedimentation along the San Andreas fault, California. in *Modern and Ancient Geosynclinal Sedimentation.* Soc. Econ. Paleo. Mineralogists, Special Publication 19. p. 292-303.

Crowell, J.C. 1974b. Origin of late Cenozoic basins in southern California. in *Tectonics and Sedimentation.* Soc. Econ. Paleo. Mineralogists, Special Publication 22. p. 190-204.

Crowell, J.C. 1975. The San Gabriel fault and Ridge Basin, southern California. in Crowell, J.C., editor, *The San Andreas fault in southern California.* California Div. Mines and Geology, Special Report No. 118. p. 208-219.

Crowell, J.C. 1976. Implications of crustal stretching and shortening of coastal Ventura Basin, California. in Howell, D.G., editor. *Aspects of the Geological History of the California Continental Borderland.* Pacific Section, AAPG. Misc. Publication 24. p.365-379.

Damuth, J.E. 1975. Echo character of the western equatorial Atlantic floor and its relationship to the dispersal and distribution of terrigenous sediments. *Marine Geology.* vol. 18, p. 17-45.

Damuth, J.E. 1980. Use of high-frequency (3.5 kHz - 12 kHz) echograms in the study of near-bottom sedimentation processes in the deep-sea: a review. *Marine Geology* vol. 38, p. 51-75.

Davidson, G. 1897. The submerged valleys of the coast of California, U.S.A. and of Lower California, Mexico. *Proc. California Acad. Sciences, 3rd Series.* vol. 1, no. 2 (Geology), p. 74-102.

Davis, T.L. 1983. Late Cenozoic structure and tectonic history of the western 'Big Bend' of the San Andreas fault and adjacent San Emigdio Mountains. Unpublished Ph.D. dissertation. Univ. California, Santa Barbara. 580 pp.

Desnoes, Y. 1980. Off-line contouring of the data from the multibeam Sea Beam. *Inter. Hydrographic Review.* vol. 57, p. 55-76.

Diblee, T.W., Jr. 1977. Strike-Slip tectonics of the San Andreas fault and its role in Cenozoic basin evolvement. in, *Late Mesozoic Sedimentation and Tectonics in California.* San Joaquin Geol. Society. p. 26-38.

Dickinson, W.R. and Snyder, W.S. 1979. Geometry of triple junctions related to San Andreas transform. *Jour. Geophysical Research.* vol. 84, p. 561-572.

Dobrin, M.B. 1976. *Introduction to Geophysical Prospecting.* 3rd Edition. McGraw-Hill, New York. 630 pp.

Doyle, L.J. and Bandy, O.L. 1972. Southern Continental Borderland, Baja California: Its tectonic and environmental development. *Geological Soc. America, Bulletin.* vol. 83, p. 3785-3794.

Doyle, L.J. and Gorsline, D.S. 1977. Marine geology of Baja California Continental Borderland, Mexico. *American Assoc. Petroleum Geologists, Bulletin.* vol. 61, p. 903-917.

Dunbar, R.B. 1981. Sedimentation and the history of upwelling and climate in high fertility areas of the northeastern Pacific Ocean. Ph.D. dissertation. Scripps Inst. Oceanography.

Edwards, M.H., Arvidson, R.E. and Guinness, E.A. 1984. Digital image processing of Seabeam bathymetric data for structural studies of seamounts near the East Pacific Rise. *Jour. Geophysical Research.* vol. 89, p. 11,108-11,116.

Emery, K.O. 1960. *The Sea Off Southern California.* John Wiley and Sons, New York.

Emery, K.O. and Bray, E.E. 1962. Radiocarbon dating of California basin sediments. *American Assoc. Petroleum Geologists, Bulletin.* vol. 46, p. 1839-1856.

Emery, K.O., Butcher, W.S., Gould, H.R. and Shepard, F.P. 1952. Submarine geology off San Diego, California. *Jour. Geology.* vol. 60, p. 511-548.

Emery, K.O. and Rittenberg, S.G. 1952. Early diagenesis of California basin sediments in relation to origin of oil. *American Assoc. Petroleum Geologists, Bulletin.* vol. 36, p. 735-806.

Emery, K.O. and Shepard, F.P. 1945. Lithology of the seafloor off southern California. *Geological Soc. America, Bulletin.* vol. 56, p. 431-478.

Farre, J.A., McGregor, B.A., Ryan, W.B.F. and Robb, J.M. 1983. Breaching the shelf break: Passage from youthful to mature phase in submarine canyon evolution. in Stanley, D.J. and Moore, G.T., editors. *The Shelf Break: Critical Interface on Continental Margins.* Soc. Econ. Paleo. and Mineralogists, Special Publication 33. p. 25-39.

Field, M.E. and Clarke, S.H., Jr. 1979. Small-scale slumps and slides and their significance for basin slope processes, southern California Borderland. in Doyle, L.J. and Pilkey, O.H., editors. *Geology of Continental Slopes.* Soc. Econ. Paleo. Mineralogists, Special Publication 27. p. 223-230.

Field, M.E., Edwards, B.D., Kenyon, N., Somers, M. and Hey, R.N. 1984. Volcanic and depositional patterns on the seafloor off southern California as seen by GLORIA side-scan sonar. *American Geophys. Union Transactions.* vol. 65, p. 1083.

Fischer, P.J., Parker, J. and Farnsworth, R. 1977. Beta platform site evaluations. California State Univ., Northridge. *Marine Studies 77-2.*

Freund, R. 1971. The Hope fault - A strike-slip fault in New Zealand. *N. Z. Geological Survey Bulletin.* n.s. 86. 49 pp.

Freund, R. 1974. Kinematics of transform and transcurrent faults. *Tectonophysics*. vol. 21, p. 93-134.

Friedman, M.E., Whitcomb, J.H., Allen, C.R. and Hileman, J.A. 1976. Seismicity of the southern California region 1 January, 1972 to 31 December, 1974. California Inst. Technology, Div. Geological and Planetary Sciences. *Contribution No. 2734*.

Gastil, R.G., Phillips, R.P. and Allison, E.C. 1975. Reconnaissance geology of the state of Baja California. Geological Soc. America. *Memoir No. 140*. 170 pp.

Gonzalez, J.J. and Suarez, F. 1984. Geological and seismic evidence of a new branch of the Agua Blanca fault. *Geophysical Research Letters*. vol. 11, p. 42-45.

Gonzalez S., A. 1977. Anomalías gravimétricas y magnéticas de la Bahía de Todos los Santos. Professional Thesis. Ciencias Marinas, UABC. Ensenada, Mexico. 52 pp.

Gorsline, D.S. and Emery, K.O. 1959. Turbidity-current deposits in San Pedro and Santa Monica basins off southern California. *Geological Soc. America, Bulletin*. vol. 70, p. 270-290.

Greene, H.G., Bailey, K.A., Clarke, S.H., Ziony, J.I. and Kennedy, M.P. 1979. Implications of fault patterns of the inner California Continental Borderland between San Pedro and San Diego. in Abbott, P.L. and Elliott, W.J., editors. *Earthquakes and other perils: San Diego region*. San Diego Assoc. Geologists Guidebook. p. 21-27.

Hamilton, E.L. 1964. Consolidation characteristics and related properties of sediments from experimental Mohole (Guadalupe site). *Jour. Geophysical Research*. vol. 69, p. 4257-4269.

Hamilton, E.L. 1970. Sound velocity and related properties of marine sediments, North Pacific. *Jour. Geophysical Research*. vol. 75, p. 4423-4446.

Hamilton, E.L., Moore, D.G., Buffington, E.C., Sherrer, P.L. and Curray, J.R. 1974. Sediment velocities from sonobuoys: Bay of Bengal, Bering Sea, Japan Sea, and North Pacific. *Jour. Geophysical Research*. vol. 79, p. 2653-2668.

Hanks, T.C., R.C. Bucknam, K.R. Lajoie, and R.E. Wallace. 1984. Modification of wave-cut and faulting-controlled landforms. *Jour. Geophysical Research*. vol. 89, p. 5771-5790.

Harding, T.P. 1973. Newport-Inglewood trend, California - an example of wrench style deformation. *American Assoc. Petroleum Geologists, Bulletin*. vol. 57, p. 97-116.

Harding, T.P. 1983. Divergent wrench fault and negative flower structure, Andaman Sea. in Bally, A.W., editor. *Seismic Expression of Structural Styles – A Picture and Work Atlas*. AAPG Studies in Geology 15. vol. 3, p. 4.2-1 to 4.2-8.

Harding, T.P. 1985. Seismic characteristics and identification of negative flower structures, positive flower structures, and positive structural inversion. *American Assoc. Petroleum Geologists, Bulletin*. vol. 69, p. 582-600.

Heath, G.R., Moore, T.C., Jr. and Dauphin, J.P. 1976. Late Quaternary accumulation rates of opal, quartz, organic carbon, and calcium carbonate in the Cascadia Basin area, northeast Pacific. Geological Soc. America. *Memoir 145*. p. 393-409.

Heezen, B.C., Tharp, M. and Ewing, M. 1959. The floors of the oceans: 1. The North Atlantic. Geological Soc. America. *Special Paper No. 65*. 122 pp.

Heirtzler, J.R., G.O. Dickson, E.M. Herron, W.C. Pitman, III and X. LePichon. 1968. Marine magnetic anomalies, geomagnetic field reversals, and motions of the ocean floor and continents. *Jour. Geophysical Research*. vol. 73, p. 2119-2136.

Hileman, J.A., Allen, C.R. and Nordquist, J.M. 1973. Seismicity of the southern California region, 1 January, 1932 to 31 December, 1972. California Inst. Technology, Div. Geological and Planetary Sciences. *Contribution No. 2385*.

Howell, D.G. 1976. A model to accommodate 1000 kilometers of right-slip, Neogene displacement in the southern California area. in Howell, D.G., editor. *Aspects of the geologic history of the California Continental Borderland*. Pacific Section, AAPG. Misc. Publication 24. p. 530-540.

Howell, D.G., Crouch, J.K., Greene, H.G., McCulloch, D.S. and Vedder, J.G. 1980. Basin development along the late Mesozoic and Cainozoic California margin: a plate tectonic margin of subduction, oblique subduction and transform tectonics. in Ballance, P.F. and Reading, H.G. *Sedimentation in Oblique-Slip Mobile Zones*. Inter. Assoc. Sedimentologists. Special Publication No. 4. p. 43-62.

Howell, D.G. and Link, M.H. 1983. Eocene conglomerate sedimentology and basin analysis, San Diego and the southern California Borderland. *Jour. Sedimentary Petrology*. vol. 49, p. 517-540.

Howell, D.G., Stuart, C.J., Platt, J.P. and Hill, D.J. 1974. Possible strike-slip faulting in the southern California Borderland. *Geology*. vol. 2, p. 93-98. Reply. *Geology*. vol. 3, p. 3-4.

Howell, D.G. and Vedder, J.G. 1981. Structural implications of stratigraphic discontinuities across the southern California Borderland. in Ernst, W.G., editor. *The Geotectonic Development of California, Rubey Volume 1*. Prentice-Hall, Englewood Cliffs, New Jersey. p. 535-558.

Inman, D.L. and Goldberg, E.D. 1963. Petrogenesis and depositional rates of sediments from the experimental Mohole drilling off La Jolla, California. *American Geophys. Union, Transactions*. vol. 44, p. 68-69.

Johnson, D.A. and Johnson, T.C. 1970. Sediment redistribution by bottom currents in the central Pacific. *Deep-Sea Research*. vol. 17, p. 157-169.

Jordan, T.H., Minster, J.B., Christodoulidis, D.C. and Smith, D.E. 1985. Constraints on western U.S. deformation from satellite LASER ranging. *Science*. (in press).

Junger, A. 1976a. Offshore structure between Santa Cruz and Santa Rosa Islands. in Howell, D.G., editor. *Aspects of the Geological History of the California Continental Borderland. Pacific Section, AAPG. Misc. Publication 24. p. 418-426.*

Junger, A. 1976. Tectonics of the southern California Borderland. in Howell, D.G., editor. *Aspects of the geological history of the California Continental Borderland*. Pacific Section, AAPG. Misc. Publication 24. p. 486-498.

Junger, A. 1979. Geology of the northern Channel Islands platform, California Continental Borderland. U.S. Geological Survey. *Misc. Field Studies Map MF-991*. Scale 1:250,000.

Junger, A. and Vedder, J.G. 1980. Geologic map of Catalina Basin and adjoining ridges, southern California Borderland. (personal communication). Map Scale 1:250,000.

Junger, A. and Wagner, H.C. 1977. Geology of the Santa Monica and San Pedro Basins, California Continental Borderland. U.S. Geological Survey. *Misc. Field Studies Map MF-820*. 10 pp. Map Scale 1:250,000.

Kamerling, M. 1984. Paleomagnetically constrained tectonic reconstruction of the southern California continental borderland. Am. Assoc. Petrol. Geol. *Abstracts with Programs*. Pacific Section. p. 80.

Kamerling, M.J. and B.P. Luyendyk. 1979. Tectonic rotations of the Santa Monica Mountains region, western Transverse Ranges, California, suggested by paleomagnetic vectors. *Geol. Soc. America, Bulletin*. vol. 90, p. 331-337.

Kamerling, M.J. and B.P. Luyendyk. 1985. Paleomagnetism and Neogene tectonics of the northern Channel Islands, California. *Jour. Geophysical Research*. (in press).

Kennedy, M.P. 1975. Geology of the San Diego metropolitan area, California. Section A - western San Diego metropolitan area. California Div. Mines and Geology. *Bulletin 200*. p. 1-39.

Kennedy. M.P. 1977. Recency and character of faulting along the Elsinore fault zone in southern Riverside County, California. California Div. Mines and Geology. *Special Report 131*. 12 pp. Map Scale 1:24,000.

Kennedy, M.P., Clarke, S.H., Greene, H.G. and Legg, M.R. 1980a. Recency and character of faulting offshore metropolitan San Diego, California. California Div. Mines and Geology. *Map Sheet 42*. Scale 1:50,000.

Kennedy, M.P., S.H. Clarke, H.G. Greene and P.F. Lonsdale. 1985. Observations from DSRV Alvin of Quaternary faulting in the southern California continental margin. U.S. Geological Survey, *Open-File Report, No. OF85-0039*. 26 pp.

Kennedy, M.P., Greene, H.G., Clarke, S.H. and Bailey, K.A. 1980b. Recency and character of faulting offshore metropolitan San Diego, California. California Div. Mines and Geology. *Map Sheet 41*. Scale 1:50,000.

Kennedy, M.P., H.G. Greene, and S.H. Clarke. 1985. Atlas of geologic features, stratigraphy, and bibliography from the California continental margin. California Div. Mines and Geology Bulletin. (in press).

Kennedy, M.P. and Moore, G.W. 1971. Stratigraphic relations of upper Cretaceous and Eocene formations, San Diego coastal area, California. *American Assoc. Petroleum Geologists, Bulletin*. vol. 55, p. 709-722.

Kennedy, M.P. and Welday, E. 1980. Recency and character of faulting offshore metropolitan San Diego, California. California Div. Mines and Geology. *Map Sheet 40*. Scale 1:50,000.

Kern, J.P. 1977. Origin and history of upper Pleistocene marine terraces, San Diego, California. *Geological Soc. America, Bulletin*. vol. 88, p. 1553-1566.

Kies, R.P and Abbott, P.L. 1983. Rhyolite clast populations and tectonics in the California Continental Borderland. *Jour. Sedimentary Petrology*. vol. 53, p. 461-475.

Krause, D.C. 1961. Geology of the southern Continental Borderland west of Baja California, Mexico. Ph.D. dissertation. Scripps Inst. Oceanography. 205 pp.

Krause, D.C. 1965. Tectonics, bathymetry, and geomagnetism of the southern Continental Borderland west of Baja California, Mexico. *Geological Soc. America, Bulletin*. vol. 76, p. 617-650.

Kulm, L.D. and Scheidegger, K.F. 1979. Quaternary sedimentation on the tectonically active Oregon continental slope. in Doyle, L.J. and Pilkey, O.H., editors. *Geology of Continental Slopes*. Soc. Econ. Paleo. Mineralogists Special Publication 27. p. 247-263.

Lajoie, K.R., Kern, J.P., Wehmiller, J.F., Kennedy, G.L., Mathieson, S.A., Sarna-Wojcicki, A.M., Yerkes, R.F. and McCrory, P.F. 1979. Quaternary marine shorelines and crustal deformation, San Diego to Santa Barbara, California. in Abbott, P.L., editor. *Geological excursions in the southern California area*. San Diego Assoc. Geologists Guidebook. p. 3-15.

Lamb, T.N. 1979. Geology of the Coronado Islands, northwestern Baja California, Mexico. in Stuart, C.J., editor. *Miocene lithofacies and depositional environments, coastal California and northwestern Baja California*. Pacific Section, SEPM Guidebook. p. 119-138.

Lawson, A.C. 1893. Post-Pliocene diastrophism of the coast of southern California. *California Univ. Dept. Geology Bulletin* vol. 1, p. 115-160.

Lawson, A.C., and others. 1908. The California earthquake of April 18, 1906, Report of the State Earthquake Investigation Commission. Carnegie Inst. Washington, D.C. 2 volumes and atlas. 451 pp.

Legg, M.R. 1980. Seismicity and tectonics of the inner Continental Borderland of southern California and northern Baja California, Mexico. M.S. Thesis. Scripps Inst. Oceanography. 60 pp.

Legg, M.R. and Kennedy, M.P. 1979. Faulting offshore San Diego and northern Baja California. in Abbott, P.L. and Elliott, W.J., editors. *Earthquakes and other perils – San Diego region*. San Diego Assoc. Geologists Guidebook. p. 29-46.

Legg, M.R. and Ortega, V.W. 1978. New evidence for major faulting in the inner Borderland off northern Baja California, Mexico. *American Geophys. Union Transactions*. vol 59, p. 1134.

Legg, M.R. and Wong O., V. 1979. Faulting in the inner Continental Borderland offshore northern Baja California, Mexico. Geological Soc. America. *Abstracts with Programs*. vol. 11, p. 464.

Lonsdale, P. 1979. A deep-sea hydrothermal site on a strike-slip fault. *Nature*. vol. 281, p. 531-534.

Lowell, J.D. 1972. Spitsbergen Tertiary orogenic belt and the Spitsbergen fracture zone. *Geological Soc. America, Bulletin*. vol. 83, p. 3091-3102.

Luyendyk, B.P., Kamerling, M.J. and Terres, R. 1980. Geometric model for Neogene crustal rotations in southern California. *Geological Soc. America, Bulletin*. vol. 91, p. 211-217.

Macdonald, K., Sempere, J.C. and Fox, P.J. 1984. East Pacific Rise from Siqueiros to Orozco fracture zones: Along strike continuity of axial neovolcanic zone and structure and evolution of overlapping spreading centers. *Jour. Geophysical Research*. vol. 89, p. 6049-6069.

Mammerickx, J. 1984. The morphology of propagating spreading centers: new and old. *Jour. Geophysical Research*. vol. 89, p. 1817-1828.

Mann, P., Hempton, M.R., Bradley, D.C. and Burke, K. 1983. Development of pull-apart basins. *Jour. Geology*. vol. 91, p. 529-554.

Mayer L. 1979a. The origin of fine scale acoustic stratigraphy in deep-sea carbonates. *Jour. Geophysical Research*. vol. 84, p. 6177-6184.

Mayer, L.A. 1979b. Deep sea carbonates: acoustic, physical, and stratigraphic properties. *Jour. Sedimentary Petrology*. vol. 49, p. 819-836.

Mayer, L.A. 1980. Deep-sea carbonates: physical property relationships and the origin of high-frequency acoustic reflections. *Marine Geology*. vol. 38, p. 165-183.

McKenzie, D. and Jackson, J. 1983. The relationship between strain rates, crustal thickening, palaeomagnetism, finite strain and fault movements within a deforming zone. *Earth Planetary Science Letters*. vol. 65, p. 182-202.

McKenzie, D.P. and Morgan, W.J. 1969. Evolution of triple junctions. *Nature*. vol. 224, p. 125-133.

Menard, H.W., Jr. 1955. Deep-sea channels, topography and sedimentation. *American Assoc. Petroleum Geologists, Bulletin*. vol. 39, p. 236-255.

Minch, J.A. 1970. The Miocene of northwestern Baja California, Mexico. in *Pacific slope geology of northern Baja California and adjacent Alta California*. Pacific Sections, AAPG, SEPM and SEG Guidebook. p. 100-102.

Minster, J.B. and Jordan, T.H. 1978. Present-day plate motions. *Jour. Geophysical Research*. vol. 83, p. 5331-5334.

Minster, J.B. and Jordan, T.H. 1984. Vector constraints on Quaternary deformation of the western United States east and west of the San Andreas fault. in Crouch, J.K. and Bachman, S.B., editors. *Tectonics and sedimentation along the California margin*. Pacific Section, Soc. Econ. Paleo. Mineralogists. p. 1-16.

Mitchum, R.M., Jr., Vail, P.R. and Thompson, S., III. 1977. The depositional sequence as a basic unit for stratigraphic analysis. in Payton, C.E., editor. *Seismic Stratigraphy – applications to hydrocarbon exploration*. AAPG Memoir No. 26. p. 53-62.

Mitchum, R.M., Jr., Vail, P.R. and Sangree, J.B. 1977. Stratigraphic interpretation of seismic reflection patterns in depositional sequences. in Payton, C.E., editor. *Seismic Stratigraphy – applications to hydrocarbon exploration.* AAPG Memoir No. 26. p. 117-134.

Moody, J.D. and Hill, M.J. 1956. Wrench fault tectonics. *Geological Soc. America, Bulletin.* vol. 67, p. 1207-1246.

Moore, D.G. 1957. Acoustic sounding of Quaternary marine sediment off Point Loma, California. U.S. Naval Electronics Laboratory. *Research Report 815.* 17 pp.

Moore, D.G. 1964. Shear strength and related properties of sediments from experimental Mohole (Guadalupe site). *Jour. Geophysical Research.* vol. 69, p. 4271-4291.

Moore, D.G. 1969. Reflection profiling studies of the California Continental Borderland: structure and Quaternary turbidite basins. Geological Soc. America. *Special Paper 107.* 142 pp.

Moore, G.W. 1972. Offshore extension of the Rose Canyon fault, San Diego, California. in *U.S. Geological Survey Paper 800–C.* p. 113-116.

Moore, G.W. and Kennedy, M.P. 1970. Coastal geology of the California-Baja California border area. in *Pacific slope geology of northern Baja California and adjacent Alta California.* Pacific Sections, AAPG, SEPM and SEG Guidebook. p. 4-9.

Moore, G.W. and Kennedy, M.P. 1975. Quaternary faults at San Diego Bay, California. *U.S. Geological Survey, Jour. Research.* vol. 3, p. 589-595.

Muhs, D.R. 1979. Marine terrace age assignments, uplift rates and sea level events on San Clemente Island, California. Geological Soc. America. *Abstracts with Programs.* vol. 11, p. 484.

Muhs, D.R. 1983. Quaternary sea-level events on northern San Clemente Island, California. *Quaternary Research.* vol. 20, p. 322-341.

Muhs, D.R. and Rosholt, J.N. 1984. Age of marine terraces on the Palos Verdes Hills, California, by amino acid and uranium trend dating. Geological Soc. America. *Abstracts with Programs.* vol. 16, p. 603.

Nardin, T.R., Edwards, B.D. and Gorsline, D.S. 1979. Santa Cruz Basin, California Borderland: Dominance of slope processes in basin sedimentation. in Doyle, L.J. and Pilkey, O.H., editors. *Geology of Continental Slopes.* Soc. Econ. Paleo. Mineralogists, Special Publication 27. p. 209-221.

Nardin, T.R., Hein, F.J., Gorsline, D.S. and Edwards, B.D. 1979. A review of mass movement processes, sediment and acoustic characteristics, and contrasts in slope and base-of-slope systems versus canyon-fan-basin floor systems. in Doyle, L.J. and Pilkey, O.H., editors. *Geology of Continental Slopes.* Soc. Econ. Paleo. Mineralogists, Special Publication 27. p. 61-73.

Nardin, T.R. and Henyey, T.L. 1978. Pliocene-Pleistocene diastrophism of the Santa Monica and San Pedro shelves, California Continental Borderland. *American Assoc. Petroleum Geologists, Bulletin.* vol. 62, p. 247-272.

NOS (National Ocean Survey). 1974. Bathymetric Map of the California Continental Borderland. Sheets 1206N-15 and -16. Scale 1:250,000.

Nelson, C.H. and Kulm, L.D. 1973. Submarine fans and channels. in *Turbidites and deep water sedimentation.* Pacific Section, SEPM Short Course. Anaheim, California. p. 39-78.

Normark, W.R. 1970. Growth patterns of deep-sea fans. *American Assoc. Petroleum Geologists, Bulletin.* vol. 54, p. 2178-2195.

Normark, W.R. 1974. Submarine canyons and fan valleys. in Dott, R.H. and Shaver, R.H., editors. *Modern and Ancient Geosynclinal Sedimentation.* Soc. Econ. Paleo. Mineralogists, Special Publication 19. p. 56-68.

Normark, W.R. 1978. Fan valleys, channels and depositional lobes on modern submarine fans: characters for recognition of sandy turbidite environments. *American Assoc. Petroleum Geologists, Bulletin.* vol. 62, p. 912-931.

Normark, W.R. and J.R. Curray. 1968. Geology and structure of the tip of Baja California, Mexico. *Geol. Soc. America, Bulletin.* vol. 79, p. 1589-1600.

Normark, W.R. and G.R. Hess. 1980. Quaternary growth patterns of California submarine fans. in *Quaternary depositional environments of the Pacific coast.* Pacific Section, SEPM. Pacific Coast Paleogeography Symposium No. 4. p. 201-210.

Normark, W.R., Hess, G.R., Stow, D.A.V. and Bowen, A.J. 1980. Sediment waves on the Monterey Fan levee: a preliminary physical interpretation. *Marine Geology.* vol. 37, p. 1-18.

Normark, W.R. and Piper, D.J.W. 1972. Sediments and growth pattern of Navy deep-sea fan, San Clemente basin, California Borderland. *Jour. Geology.* vol. 80, p. 198-223.

Normark, W.R., Piper, D.J.W. and Hess, G.R. 1979. Distributary channels, sand lobes and mesotopography of Navy Submarine Fan, California Borderland, with applications to ancient fan sediments. *Sedimentology.* vol. 26, p. 749-774.

Orme, A.R. 1974. Quaternary deformation of marine terraces between Ensenada and El Rosario, Baja California, Mexico. in *Geology of Peninsular California.* Pacific Sections, AAPG, SEPM, and SEG Guidebook. p. 67-79.

Orr, W.L., Emery, K.O. and Grady J.R. 1958. Preservation of chlorophyll derivatives in sediments off southern California. *American Assoc. Petroleum Geologists, Bulletin.* vol. 42, p. 925-962.

Ortlieb, L. 1979. Quaternary shorelines around Baja California peninsula, Mexico: Neotectonic implications. Geological Soc. America. *Abstracts with Programs.* vol. 11, p. 490.

Ortlieb, L. 1981. Pleistocene interglacial high stands of sea level in the Gulf of California, Mexico. Geological Soc. America. *Abstracts with Programs.* vol. 13, p. 99.

Patterson, R.H. 1979. Tectonic geomorphology and neotectonics of the Santa Cruz Island fault, Santa Barbara County, California. Unpublished M.A. Thesis. Univ. California, Santa Barbara. 141 pp.

Piper, D.J.W. 1970. Transport and deposition of Holocene sediment on La Jolla deep sea fan, California. *Marine Geology*. vol. 8, p. 211-227.

Prior, D.B. and Coleman, J.M. 1982. Active slides and flows in underconsolidated marine sediments on the slopes of the Mississippi Delta. in Saxov, S. and Nieuwenhuis, J.K. *Marine Slides and Other Mass Movements*. NATO Marine Science Series No. 6. Plenum.

Renard, V. and Allenou, J.P. 1979. Sea Beam, multi-beam echo-sounding in "Jean Charcot". *Inter. Hydrographic Review*. vol. 56, p. 35-67.

Ridlon, J.B. 1969. San Clemente Island Rocksite Project: Offshore geology, Part 2, Reconnaissance survey around the island. Naval Undersea Research and Development Center. San Diego, California.

Rusnak, G.A., R.L. Fisher and F.P. Shepard. 1964. Bathymetry and faults of Gulf of California. in, van Andel, Tj. H. and G.G. Shor, Jr., editors. *Marine Geology of the Gulf of California – A Symposium*. AAPG Memoir No. 3, p 59-75.

Saleeby, J. 1983. Ocean floor accretion and volcanoplutonic arc evolution of the Mesozoic Sierra Nevada. in Ernst, W.G., editor. *The Geotectonic Development of California. Rubey Volume 1*. Prentice-Hall, Englewood Cliffs, New Jersey. p. 132-181.

Sangree, J.B. and Widmier, J.M. 1977. Seismic interpretation of clastic depositional facies. in Payton, C.E., editor. *Seismic Stratigraphy – applications to hydrocarbon exploration*. AAPG Memoir No. 26. p. 165-184.

Santillán, M. y Barrera, T. 1930. Las posibilidades petroliferas en la costa occidental de la Baja California, entre los paralelos 30 y 32 de latitud norte. *Mexico Inst. Geologia Anales*. vol. 5, p. 1-37.

Scholz, C.H. 1977 Transform faults systems of California and New Zealand: Similarities in their tectonic and seismic styles. *J. Geol. Soc. London*. vol. 133, p. 215-229.

Segall, P. and Pollard, D.D. 1980. Mechanics of discontinuous faults. *Jour. Geophysical Research*. vol. 85, p. 4337-4350.

Shackleton, N.J. and Opdyke, N.D. 1973. Oxygen isotope and paleomagnetic stratigraphy of equatorial Pacific core V23-238: oxygen isotope temperatures and ice volumes on a $10^5$ and $10^6$ year time scale. *Quaternary Research*. vol. 3, p. 39-55.

Shackleton, N.J. and Opdyke, N.D. 1976. Oxygen-isotope and paleomagnetic stratigraphy of Pacific core V28-239 late Pliocene to latest Pleistocene. in, Cline, R.M. and J.D.Hays, editors. *Investigation of Late Quaternary Paleoceanoraphy and Paleoclimatology*. Geological Society America, Memoir 145. p. 449-464.

Sharp, R.V. 1972. Map showing recently active breaks along the San Jacinto fault zone between the San Bernardino area and Borrego Valley, California. U.S. Geological Survey. *Misc. Geol. Invest. Map I–675*. Scale 1:24,000.

Sharp, R.V., Lienkaemper, J.J., Bonilla, M.G., Burke, D.B., Fox, B.F., Herd, D.G., Miller, D.M., Morton, D.M., Ponti, D.J., Rymer, M.J., Tinsley, J.C., Yount, J.C., Kahle, J.E., Hart, E.W. and Sieh, K.E. 1982. Surface faulting in the central Imperial Valley. in *The Imperial Valley, California, earthquake of October 15, 1979*. U.S. Geological Survey Prof. Paper 1254. p. 119-143, plate 1.

Shepard, F.P. 1963. *Submarine Geology*. 2nd Edition. Harper and Row, New York. 557 pp.

Shepard, F.P. and Buffington, E.C. 1968. La Jolla submarine fan-valley. *Marine Geology*. vol. 6, p. 107-143.

Shepard, F.P. and Dill, R.F. 1966. *Submarine Canyons and Other Sea Valleys*. Rand McNally and Company, Chicago. 381 pp.

Shepard, F.P., Dill, R.F. and von Rad, U. 1969. Physiography and sedimentary processes of La Jolla submarine fan and fan-valley. *American Assoc. Petroleum Geologists, Bulletin*. vol. 53, p. 390-420.

Shepard, F.P. and Emery, K.O. 1941. Submarine topography off the southern California coast - canyons and tectonic interpretation. Geological Soc. America. *Special Paper No. 31*. 171 pp.

Shepard, F.P. and Marshall, N.F. 1975. Dives into outer Coronado Canyon system. *Marine Geology*. vol. 18, p. 313-323.

Sheriff, R.E. 1978. *A First Course in Geophysical Exploration and Interpretation*. Inter. Human Res. Development Corp. Boston, Mass. 313 pp.

Shor, G.G., Jr. and Roberts, E. 1958. San Miguel, Baja California Norte, earthquakes of February, 1956: A field report. *Seismological Soc. America, Bulletin*. vol. 48, p. 101-116.

Sieh, K.E. 1978. Slip along the San Andreas fault associated with the great 1857 earthquake. *Seismological Soc. America, Bulletin*. vol. 68, p. 1421-1428.

Sieh, K.E. 1984. Lateral offsets and revised dates of large pre-historic earthquakes at Pallett Creek, southern California. *Jour. Geophysical Research*. vol. 89, p. 7641-7670.

Sieh, K.E. and Jahns, R.H. 1984. Holocene activity of the San Andreas fault at Wallace Creek, California. *Geological Soc. America, Bulletin*. vol. 95, p. 883-896.

Slemmons, D.B. 1977. Faults and Earthquake Magnitude. Report 6 of: State of the Art for Assessing Earthquake Hazards in the United States. U.S. Army Corps of Engineers. *Misc. Paper S-73-1*. 129 pp.

Smith, D.L. and Normark, W.R. 1976. Deformation and patterns of sedimentation, south San Clemente Basin, California Borderland. *Marine Geology*. vol. 22, p. 175-188.

Smith, W.S.T. 1898. A geological sketch of San Clemente Island. U.S. Geological Survey. *18th Annual Report*. Part 2. p. 465-496.

Spencer, J.E. and Normark, W.R. 1979. Tosco-Abreojos fault zone: A Neogene transform plate boundary within the Pacific margin of southern Baja California, Mexico. *Geology*. vol. 7, p. 554-557.

Spiess, F.N. and Tyce, R.C. 1973. Marine Physical Laboratory Deep Tow instrumentation system. Scripps Inst. Oceanography. *Reference 73–4.*

Stuart, C.J. 1974. The San Onofre Breccia in northwestern Baja California and its regional tectonic implications. in *Geology of Peninsular California.* Pacific Sections, AAPG, SEPM, and SEG Guidebook. p. 80-90.

Stuart, C.J. 1979. Lithofacies and origin of the San Onofre Breccia, coastal southern California. in Stuart, C.J., editor. *Miocene lithofacies and depositional environments, coastal California and northwestern Baja California.* Pacific Section, SEPM Guidebook. p. 25-42.

Sylvester, A.G. and Smith, R.R. 1976. Tectonic transpression and basement-controlled deformation in San Andreas fault zone, Salton Trough, California. *American Assoc. Petroleum Geologists, Bulletin.* vol. 60, p. 2081-2102.

Tchalenko, J.S. 1970. Similarities between shear zones of different magnitudes. *Geol. Soc. America, Bulletin.* vol. 81, p. 1625-1640.

Teng, L. S. 1985. Seismic stratigraphic study of the California Continental Borderland basins: Structure, stratigraphy and sedimentation. Ph.D. dissertation. Univ. Southern California.

Vail, P.R., Todd, R.G. and Sangree, J.B. 1977. Chronostratigraphic significance of seismic reflections. in Payton, C.E., editor. *Seismic Stratigraphy – applications to hydrocarbon exploration.* AAPG Memoir No. 26. p. 99-116.

Vedder, J.G., Beyer, L.A., Junger, A., Moore, G.W., Roberts, A.E., Taylor, J.C. and Wagner, H.C. 1974. Preliminary report on the geology of the Continental Borderland of southern California. U.S. Geological Survey. *Misc. Field Studies Map MF–624.* Scale 1:500,000.

Vedder, J.G. and D.G. Howell. 1980. Topographic evolution of the southern California Borderland during late Cenozoic time. in, Power, D.M. editor. *The California Islands: Proceedings of a Multidisciplinary Symposium.* Santa Barbara Museum of Natural History. p. 7-31.

Walton, W.R. 1954. Ecology of living benthonic Foraminifera, Todos Santos Bay, California. Ph.D. dissertation. Scripps Inst. Oceanography.

Waters, K.H. 1981. *Reflection Seismology: a tool for energy resource exploration.* 2nd Edition. John Wiley and Sons, New York. 453 pp.

Weldon, R.J., II and Sieh, K.E. 1985. Holocene rate of slip and tentative recurrence interval for large earthquakes on the San Andreas fault, Cajon Pass, southern California. *Geological Soc. America, Bulletin.* vol. 96, p. 793-812.

Wilcox, R.E., Harding, T.P. and Seely, D.R. 1973. Basic wrench tectonics. *American Assoc. Petroleum Geologists, Bulletin.* vol. 57, p. 74-96.

Woodford, A.O., Schoellhamer, J.E., Vedder, J.G. and Yerkes, R.F. 1954. Geology of the Los Angeles Basin. in Jahns, R.H., editor. *Geology of Southern California.* California Div. Mines and Geology. Bulletin 170. Part 5. p. 65-81.

Yeats, R.S. 1973. Newport-Inglewood fault zone, Los Angeles Basin, California. *American Assoc. Petroleum Geologists, Bulletin.* vol. 57, p. 117-135.

Yeats, R.S. 1976. Extension *versus* strike-slip origin of the southern California Borderland. in Howell, D.G., editor. *Aspects of the geological history of the California Continental Borderland.* American Assoc. Petroleum Geologists. Misc. Publication 24. p. 455-485.

Yeats, R.S., Cole, M.R., Merschat, W.R. and Parsley, R.M. 1974. Poway fan and submarine cone and rifting of the inner southern California Borderland. *Geological Soc. America, Bulletin.* vol. 85, p. 293-302.

Yeats, R.S. 1983. Large-scale Quaternary detachments in Ventura Basin, southern California. *Jour. Geophysical Research.* vol. 88, p. 569-584.

# APPENDIX A

## NAVIGATION

Accurate navigation is crucial for mapping submarine features such as bathymetry or geologic structure. The smaller the features to be mapped, the more precise the navigation must be in order to locate such features on the maps. For studies such as the one presented here, accurate positioning of fault crossings is necessary to determine fault continuity and fault strike; important data for tectonic analyses. Sea Beam studies also need precise, accurate navigation in shallow regions (<2000 m) so that minimum overlap between adjacent swaths is obtained, and contours can be matched between swaths without excessive interpolation.

Many navigation systems and techniques have been developed throughout history. More recently, sophisticated electronic systems using satellites or radionavigation, including LORAN and OMEGA, compute absolute position and provide measures of latitude and longitude directly to the user. The discussion of such systems is beyond the scope of this work and they are not further described here. Several good texts on nautical techniques, including navigation, are available, (for example, Bowditch, 1958), and the reader should consult these for additional information.

Another less sophisticated method of navigation uses two or more ranges or azimuths to fixed landmarks and computes geographic position by triangulation. This method is the primary technique used for this study and will be discussed below. Improved accuracy over the earlier navigator's ability to locate himself using this method is accomplished with RADAR, that is electronic distance (and azimuth)

determination by measuring the transit time of electromagnetic waves reflected off of landmarks or other objects. Greater accuracy and increased range of operation are accomplished by use of active transponders, that is electronic devices that respond to the incident RADAR signal by emitting their own RADAR signal, which can be encoded with other information. The transit time is measured electronically with reference to very accurate clocks, so that the range can be calculated to within a few meters. Absolute geographic position can then be calculated using triangulation, for two or more ranges, or range/azimuth pairs, providing that the geographic position of the landmark is known. Real-time shipboard navigation is often accomplished by the triangulation method, using RADAR ranging to shore-based landmarks that are shown on nautical charts. For the present study, additional navigational accuracy was obtained in some areas by RADAR ranging to fixed shore-based transponders. These fixed transponders do not suffer the position errors introduced by uncertainty in the actual location of the natural landmarks which reflect the incident RADAR beam.

A Motorola Mini-Ranger* RADAR transponder system was used for the present study. The configuration of the system used in this study included four shore-based transponders and one shipboard transmit/receive system. The shipboard system simultaneously interrogates two of the shore-based transponders and computes the range to each. These date are displayed on the shipboard console and also printed onto a paper tape. A precise clock provides the time of each fix to the nearest second. The rate of interrogation can be adjusted as can the transponders being interrogated. When in range of at least one transponder, several ranges can be calculated each minute. Two ranges are required to compute the ship's position unless

---

* Registered Trademark

other data, such as azimuth to the landmark can be provided.

For the typical research cruises such as those conducted for the present study, thousands of such ranges will be determined. Consequently, thousands of position fixes must be computed, and so, the FORTRAN computer programs described in the following pages were developed.

The overall process of navigation, that is locating the ship tracks and position with respect to geographic coordinates and standard time, involved four major steps in this study. First, absolute positions as a function of time, for each and every valid range or range/azimuth pair is computed by the program TRNAV. Second, these fixes are smoothed, that is averaged, using the program SMFIX for times when numerous fixes are computed. Third, additional smoothing of the shiptrack is accomplished by plotting the data using standard software developed at the Scripps Institution of Oceanography Geological Data Center (GDC).* Fourth, final editing and position mapping is accomplished by hand adjusting ship tracks using the bathymetric data so that soundings (or Sea Beam contours) match at line crossings. This appendix describes the programs used for the first two steps. The last step was discussed in chapter 2 of this volume.

TRNAV computes the position, that is latitude and longitude of the ship at the time of each RADAR range or range/azimuth measurement using triangulation. Exactly two data, either ranges to two different landmarks or transponders or the range and azimuth to one landmark are used for each fix calculation. If several data are available for any one time, several position estimations (fixes) can be computed

---

* Contact Stu Smith at the SIO Geological Data Center for information regarding these programs.

using combinations of data pairs, and the result averaged using the second program, SMFIX.

For simplicity, a flat-earth is assumed. This approximation introduces insignificant errors for the small area covered by this study. A Mercator projection is used, so that each latitude, longitude coordinate pair can be transformed into a rectangular Cartesian coordinate pair. To ensure accuracy, the transformation uses the Clarke spheroid of 1866 (see Bowditch, 1958) to compute the factors for converting distance in degrees latitude or longitude into meters for the rectangular grid. This spheroid approximation of the geoid is used to produce most of the nautical charts used in North American waters, and is therefore appropriate for this study. A right-handed, Cartesian coordinate system is derived with the abcissa (x-axis) directed to the north and the ordinate (y-axis) to the west. The origin of this grid is the average geographic position of the entire set of landmarks and transponder sites input to the program. The position of each landmark is then converted from geographic coordinates into the grid coordinates for the triangular procedure. Also, baseline matrices, that is the baseline distances and azimuths between each possible pair of landmarks is computed and stored for use in the triangulation.

Ship positions (or fixes) are computed using triangulation and the trigonometric 'law of cosines' with the known ranges, baseline distances and azimuths. If ranges to only two landmarks are used, there is an uncertainty as to which side of the baseline the correct position is located. This uncertainty is usually eliminated because the coast approximately marks the baseline, and so the offshore position is the correct one. Where island landmarks are used or large coastal embayments are located, a baseline crossing is possible, that is positions on either side of the baseline are

possible. The program automatically selects the north, or west side for the position. The alternate position can be selected by setting the flag IBASE = 1 in the input data. For positions near to the baseline, fixes on both sides may be computed, and the user selects the 'best' position.

Occasionally, for positions near the baseline, because of inaccuracies in the range measurements or positions of the landmarks, the data will not converge to a real position. When the program recognizes this situation, the message 'DOES NOT CONVERGE' is printed to the output file. The user can then check the ranges, landmark coordinates or adjacent fixes to obtain a good fix for such times. In some cases, the data are bad, due to spurious noise signals or incorrect data recording. Such errors are generally easily identifiable. The data are edited as necessary, and the final version run through TRNAV to obtain a list of positions and times. The program has been designed to allow future incorporation of algorithms to compute estimates of the error in calculated position when range or other errors can be input.

Output from TRNAV includes a regular print file, which lists positions, times and messages, such as 'BASELINE CROSSING', or 'DOES NOT CONVERGE', and messages to the terminal, if the job is run interactively. Also, optional data files for use with other programs such as SMFIX, HYPERMAP, or the SIO-GDC plotting programs can be generated by specifying non-zero values of the parameter IDATA in the input file. IDATA = 1 yields an output file in GDC format, that is degrees and decimal minutes, with west <u>negative.</u> IDATA = 2 yields data suitable for HYPERMAP or SMFIX, that is decimal degrees, with west <u>negative.</u> Specific details of the input/output data for TRNAV will be discussed later.

SMFIX computes average positions for times that have numerous range or azimuth pairs. In order to use SMFIX, the time of each fix must be different, and input chronologically. Otherwise, error messages will result, and smoothed fixes are not computed. This program is especially useful for combining transponder fixes, obtained several times each minute, into one average position interpolated to the exact minute in time. Average speed-made-good (SMG) and course-made-good (CMG) are also computed that prove useful in editing the data, identifying anomalous speeds or courses. SMFIX is also useful for computing average positions for times with three or more range/azimuth data from the conventional RADAR. It must be emphasized that the times for these fixes must be arbitrarily set to different values, usually by adding one or more second to each so that an average will be computed, and the error condition 'SAME TIME' averted. Of course, the computed SMG and CMG are invalid in such situations.

The average position is computed using linear regression, that is, least squares analysis. Regression analyses for both 'x' and 'y' positions as a function of time are done, and the computed functions of position versus time used to determine the ship position at the exact minute. The program automatically selects only times up to 30 seconds before or 29 seconds after the exact minute for computation of each average fix. Statistics are also presented for averages derived from three or more fixes, and appropriate messages for one or two point fixes are also listed.

Output from SMFIX includes both the full print file with fixes, statistics and messages, and the file in proper format for the GDC programs, except that west longitude is listed as positive, and must be changed before use in the GDC plotting routines. Details of the input/output values for SMFIX are discussed susequently.

**I/O and Program Listings for TRNAV, SMFIX, and HYPRIN**

Sample input and output files for programs TRNAV and SMFIX are shown in Tables A.1 - A.6. The program listings for both TRNAV and SMFIX are also presented as Appendices A.1 and A.2. Subroutine GETFIL, necessary for both TRNAV and SMFIX, is listed in Appendix A.3 (courtesy of Don Altman). Program HYPRIN converts GDC formatted data (degrees and decimal minutes) into HYPER-MAP or SMFIX input format (decimal degrees) is listed in Appendix A.4. Numerous comment cards have been incorporated into the these listings to aid in the understanding of the logic and variable identification. All of these programs were written and compiled on the SIO Prime 500 computer, and can be run either interactively, or as 'phantoms'. Details of the SIO operating system can be obtained at the computer center at the Institute of Geophysics and Planetary Physics in La Jolla.

Input for TRNAV is from two main sources, the user's terminal (or command file) and data file, logical unit number (lun) 5. The program prompts the user for the name of the input file which is internally known as lun 5. Similar prompts for the names of the output files are also provided. Subroutine GETFIL provides this interactive logic.

A sample input file (lun 5) for TRNAV is shown in Table A.1. The first line has an integer '1', and a title (up to 60 characters permitted). The integer '1' is the value of IDATA used for this test run of TRNAV, and sets the program to output a file in GDC format (as lun 7). A zero entry here would suppress this secondary output file, and a value of 2 would create a file in HYPERMAP or SMFIX format instead of the GDC format. The program will prompt the user to enter the appropriate 6 character

names for all input and output files. The prompt calls the GDC (or HYPERMAP/SMFIX) output file 'OUTDAT', whereas the standard files, lun 5 and lun 6, are called 'INPUT' and 'OUTPUT', respectively. The user can respond with any valid 6 character name for these files.

The second line of data lists the number of transponders (8 in the example shown), shipboard antenna height (meters), and the value of the optional parameter IRITE. The number of transponders listed must correspond exactly with the number of transponder or RADAR landmarks used and listed in the following cards. The shipboard antenna height is used to correct slant ranges to horizontal ranges, and assumes that both the conventional shipboard RADAR and transponder system antennae are at the same elevation. The parameter IRITE, if set equal to 1 will list additional information, including the input data, to the user's terminal (lun 1).

The next 8 lines give the transponder/RADAR landmark position data. First the code TRNS for transponders or RADR for RADAR landmarks is listed, followed by the two-digit code number. These code numbers must be in sequential order, as shown, with no gaps. The next values are the latitude and longitude of the site, with both north and west positive. The site elevation (meters) follows. The next decimal value lists the estimated error of the site position, in decimal minutes of latitude (approximately in nautical miles). These estimated error values are not used in the present version of the program. The last 28 columns are for a name or description of the site.

The card following the site position data is a 'day header' card. The date, that is day, month and year, of the following navigational data are listed. The 400 in the example corresponds to the line number (which is arbitrary in the present version)

and the 67 specifies the heading. The last number (6.0) is the ship speed in knots. These last three values are used only for the user's information.

The next series of cards represents the actual fix data. First, the time in hours, minutes and seconds is listed, followed by the two site codes and ranges. Note that both RADAR and transponder sites can be used, and a RADAR range and azimuth may be specified. The RADAR ranges are in nautical miles. The transponder ranges are in meters. The azimuths are in degrees true (0° to 360°). The code number with each site code must exactly correspond with the appropriate site code listed in the site coordinates input list.

At the end of a day's set of fix data, a blank card, shown here as 6 zeroes, must be placed. One blank card specifies the end of a day. A second (or subsequent) day's set of data would follow the blank card in the same sequence as that shown for the 18 September 1979 in the example, that is a day header card would follow one blank card, and the range/azimuth data afterwards. Two blank cards signifies the end of the input data file, and signals the program to complete execution and exit.

Table A.2 shows a sample TRNAV output file (lun 6) for the input file shown in Table A.1. The first line gives the parameter IDATA followed by the title. A day header line follows. Headings for the output data are given for each day and/or new page of output. Most variables are self-explanatory. XM and YM are the grid coordinates, in meters, of the fix points. XER and YER are two estimates of the position error, which in the present version should be zero and represent the difference between the X and Y position computed using each of the two sites as the reference site. SMG and CMG are the average speed and course-made-good since the previous fix. These values can be useful in editing the data.

Table A.3 shows a sample TRNAV output file (lun 7) in GDC format. Note that latitude and longitude are in degrees and decimal minutes, with north positive and west negative. The date and time (hours and minutes only) precede the coordinates, and the type of fix is at the end. This file would result from specification of the input parameter IDATA = 1.

Table A.4 represents a sample input file (lun 5) for the program SMFIX. This file would also be an output file (lun 7) for TRNAV with the option IDATA = 2. The coordinates are here listed in decimal degrees, with west negative again. Such a file is also appropriate for use with the HYPERMAP plotting program available at SIO. Note also that the full times (hours, minutes and seconds) are given.

Table A.5 is a sample output file (lun 6) for the program SMFIX. The date and average time, to the nearest minute of the fix are listed in the first three columns. The average or rather estimated position, in decimal degrees, for the ship at the minute specified is listed next, with west negative. The type of fix is followed by the statistics including the regression coefficients, '$r_x$' and '$r_y$', the standard deviations (in meters or seconds as appropriate) $\sigma_x$, $\sigma_y$, and $\sigma_t$ for the least squares analysis of the position. The next two columns list the average speed and course-made-good during the minute averaged. The last column is the number of fix points used in the regression analysis. For the special cases of only one or two fixes, appropriate messages are listed and no statistics given. Remember that SMG and CMG for RADAR fix averages are usually bogus in this program. At the end, if all goes well, the note 'FINIS' is written.

Table A.6 is the sample output file (lun 7) for SMFIX in GDC format, except that longitude is positive for west. This helps to differentiate this file from the output file for TRNAV, since both are in degrees and decimal minutes and show time only by hours and minutes. Remember that SMFIX may have averaged several seconds worth of data to get one average fix for the minute specified, whereas TRNAV would show several, possibly different fixes for the same minute of time listed in the GDC formatted output file. Again, 'FINIS' indicates the program ran to completion successfully.

**Table A.1 — Sample Input File (lun 5) for Program TRNAV.**

```
1  TRANSPONDER NAVIGATION TEST CASE  30 APR 82
   8     10.    00
  TRNS01  31.4820   116.4774     95.        0.1        S. TODOS SANTOS ISL.
  TRNS02  32.1641   117.0138    115.        0.1        PUNTA DESCANSO
  TRNS03  32.0811   116.5323     60.        0.1        PLAZA SANTA MARIA
  TRNS04  31.5398   116.4495     45.        0.1        PUNTA SAN  MIGUEL
  RADR05  32.1615   117.0165     10.        0.1        PUNTA DESCANSO(RADAR)
  RADR06  32.0204   116.5314     10.        0.1        NORTH POINT
  RADR07  31.5862   116.5000     10.        0.1        EL PESCADERO(SOUTH POINT)
  RADR08  31.4858   116.4848     10.        0.1        N. TODOS SANTOS ISL.
 18 09 79  400  67.     6.0
073000    RADR08    3.4        AZIM08  33.5        0
140000    RADR07   24.0        RADR08  24.6        0
150000    RADR06   18.3        RADR05  24.0        0
150500    RADR06   18.3        RADR05  24.0        1
163756    TRNS03 25430.        TRNS02 34627.       0
164157    TRNS03 24335.        TRNS02 34555.       0
165319    TRNS03 22834.        TRNS02 34077.       0
171713    TRNS03 18980.        TRNS01 27373.       0
172351    TRNS03 17926.        TRNS01 27076.       0
172952    TRNS03 17050.        TRNS01 26788.       0
000000
000000
```

**Table A.2 — Sample Output File (lun 6) for Program TRNAV.**

1 TRANSPONDER NAVIGATION TEST CASE 30 APR 82

18 9 79 LINE 400 COURSE 67. SPEED 6.0

| 0 GMT | TRANS | RANGE | TRANS | RANGE | XM | YM | XER | YER | LATITUDE | LONGITUDE | SMG | CMG |
|---|---|---|---|---|---|---|---|---|---|---|---|---|
| 733 0 | RADR 8 | 6297. | AZIM 8 | 34. | -29147. | -6439. | 0. | 0. | 31 45.738N | 116 48.477W | 0.0 | 0. |
| 14 0 0 | RADR 7 | 44448. | RADR 8 | 45559. | -17594. | 38682. | 0. | 0. | 31 51.990N | 117 17.134W | 3.9 | 284. |
| 15 0 0 | RADR 6 | 33892. | RADR 5 | 44448. | -14016. | 31293. | -0. | -0. | 31 53.926N | 117 12.442W | 4.4 | 64. |
| BASELINE CROSSING | | | | | | | | | | | | |
| 15 5 0 | RADR 6 | 33892. | RADR 5 | 44448. | 16961. | -28988. | -0. | -0. | 32 10.687N | 116 34.156W | 3439 | 63. |
| 163756 | TRNS 3 | 25430. | TRNS 2 | 34627. | -6860. | 17879. | -0. | -0. | 31 57.798N | 117 3.922W | 18.3 | =117 |
| 164157 | TRNS 3 | 24335. | TRNS 2 | 34555. | -6951. | 16059. | -0. | -0. | 31 57.748N | 117 2.767W | 14.7 | 93. |
| 165319 | TRNS 3 | 22834. | TRNS 2 | 34077. | -6542. | 14090. | -0. | -0. | 31 57.970N | 117 1.515W | 5.7 | 78. |
| 171713 | TRNS 3 | 18980. | TRNS 1 | 27373. | -4183. | 10631. | 0. | 0. | 31 59.247N | 116 59.319W | 5.7 | 56. |
| 172351 | TRNS 3 | 17926. | TRNS 1 | 27076. | -3608. | 9500. | 0. | 0. | 31 59.557N | 116 58.601W | 6.2 | 63. |
| 172952 | TRNS 3 | 17050. | TRNS 1 | 26788. | -3157. | 8456. | 0. | 0. | 31 59.801N | 116 57.937W | 6.1 | 67. |

**Table A.3 — Sample Output File (lun 7) for Program TRNAV.**

```
18  9 1979      730  31 45.74-116 48.48        RADR
18  9 1979    14 0   31 51.99-117 17.13        RADR
18  9 1979    15 0   31 53.93-117 12.44        RADR
18  9 1979    15 5   32 10.69-116 34.16        RADR
18  9 1979    1637   31 57.80-117  3.92        TRNS
18  9 1979    1641   31 57.75-117  2.77        TRNS
18  9 1979    1653   31 57.97-117  1.52        TRNS
18  9 1979    1717   31 59.25-116 59.32        TRNS
18  9 1979    1723   31 59.56-116 58.60        TRNS
18  9 1979    1729   31 59.80-116 57.94        TRNS
```

**Table A.4 — Sample Input File (lun 5) for Program SMFIX.**

```
13 979   95613   32.03774-117.28152    TRNS
13 979   95614   32.03772-117.28160    TRNS
13 979   95757   32.02723-117.28954    TRNS
13 979   95958   32.02889-117.28975    TRNS
13 979   10 612  32.03778-117.29216    TRNS
13 979   10 645  32.03811-117.29211    TRNS
13 979   10 650  32.03905-117.29242    TRNS
13 979   10 714  32.03906-117.29243    TRNS
13 979   10 742  32.03981-117.29262    TRNS
```

**Table A.5 — Sample Output File (lun 6) for Program SMFIX.**

| IDAY | IYEAR | MON | LT(1,2) | X0 | Y0 | TR1 | RX | RY | SIGX | SIGY | SIGT | SMG | CMG | NFIX |
|---|---|---|---|---|---|---|---|---|---|---|---|---|---|---|
| 14 | 979 | | 645 | 31.94126 | -116.96339 | TRNS | 1.007279 | 1.075706 | 0.000021 | 0.000028 | 1.527525 | 4.155 | 338.404 | 3 |
| 14 | 979 | | 652 | 31.93161 | -116.95919 | TRNS | 1.014185 | 0.755929 | 0.000020 | 0.000018 | 1.527525 | 2.232 | 319.474 | 3 |
| 14 | 979 | | 657 | 31.92781 | -116.96332 | TRNS | 0.000 | 45.000 | TWO POINTS | | | | | |
| 15 | 979 | | 022 | 32.03713 | -117.31596 | TRNS | 0.928954 | 0.862478 | 0.000219 | 0.000106 | 5.567764 | 5.169 | 51.635 | 3 |
| 15 | 979 | | 025 | 32.04112 | -117.31721 | TRNS | SINGLE FIX INPUT | | | | | | | |
| 15 | 979 | | 028 | 32.04169 | -117.31740 | TRNS | 0.000 | 103.241 | TWO POINTS | | | | | |
| | | | | | | FINIS | | | | | | | | |

**Table A.6 — Sample Output File (lun 7) for Program SMFIX.**

```
14   9 1979      645  31 56.48 116 57.80          TRNS
14   9 1979      652  31 55.90 118 57.55          TRNS
14   9 1979      657  31 55.67 116 57.80          TRNS
15   9 1979      022  32  2.23 117 18.96          TRNS
15   9 1979      025  32  2.47 117 19.03          TRNS
15   9 1979      026  32  2.50 117 19.04          TRNS
                                                  FINIS
```

# APPENDIX A.1

## FORTRAN Program TRNAV used to Compute Ship Position Fixes from Range and Azimuth Data for Shipboard RADAR and Shore-based Transponders.

```
(0001)  C       PROGRAM  TRNAV (INPUT,OUTPUT,TAPE5=INPUT,TAPE6=OUTPUT)
(0002)  C
(0003)  C  THIS PROGRAM COMPUTES POSITIONS FROM RANGES TO 2 TRANSPONDERS OR RADAR RANGES
(0004)  C
(0005)          DOUBLE PRECISION  B(50,50),R2,R1,PI,RAD,FLAT,FLON,XT(50),YT(50)
(0006)          COMMON /PMAP/ OLAT,OLON,FLAT,FLON,RAD,PI
(0007)          COMMON /TRANS/ B,PSI(50,50),XPOR(50,50),XLAT(50),YLON(50)
(0008)          COMMON /REGRES/ X0,Y0,DMG0,CMG0,SMG0,CCFLAG,T0
(0009)          COMMON /POSIT/ X1,X2,Y1,Y2,R1,R2,N1,N2,TR1,TR2,GMT
(0010)          COMMON /FILES/  NAMLEN
(0011)          INTEGER DUTNAM(40),DATNAM(40)
(0012)          DIMENSION  TITLE(15),SGNX(50,50)
(0013)          DIMENSION INNAM (40)
(0014)          LOGICAL  CCFLAG
(0015)          DATA  X0,Y0,T0,DMG0,SMG0,CMG0,TRFLG,CCFLAG /2*0.0,-1.,4*0.,.TRUE./
(0016)          DATA  PI /3.141592653589793/
(0017)          DATA  B,PSI,XPOR /5750*0.0/
(0018)          DATA  SGNX /2500*1./
(0019)          CALL GETFIL ('INPUT ',6,INNAM)
(0020)          CALL GETFIL ('OUTPUT',6,OUTNAM)
(0021)          CALL CONTRL (1,INNAM,5)
(0022)          READ (5,402) IDATA,TITLE
(0023)    402   FORMAT (I2,15A4)
(0024)          WRITE (1,404) TITLE,IDATA
(0025)    404   FORMAT (1X,15A4,5X,'IDATA =',I2)
(0026)          CALL INIT (ANT,SGNX,XT,YT,TRFLG)
(0027)          IF (TRFLG.EQ.1) GO TO 9999
(0028)          CALL CONTRL (2,OUTNAM,6)
(0029)  C**** IDATA IS OPTION TO WRITE OUTPUT FILE FOR GUC PLOTTING ROUTINES, IDATA = 1,
(0030)  C**** WRITE NAVIGATION OUTPUT TO FILE07
(0031)  C****
(0032)          IF (IDATA.GE.1) CALL GETFIL('OUTDAT',6,DATNAM)
(0033)          IF (IDATA.GE.1) CALL CONTRL(2,DATNAM,7)
(0034)     40   CONTINUE
(0035)  C  READ LINE DATA, DAY, MONTH, YEAR
(0036)          READ (5,400) IDAY,MONTH,IYEAR,LINE,COURSE,SPEED
(0037)    400   FORMAT (3(1X,I2),2X,I3,1X,F5.0,F5.1)
(0038)          IF (IDAY.EQ.0)  GO TO 9999
(0039)          CMG0 = COURSE
(0040)          SMG0 = SPEED
(0041)     43   NLINE = 0
(0042)          WRITE (6,401) (TITLE(I),I=1,15),IDAY,MONTH,IYEAR,LINE,COURSE,SPEED
(0043)    401   FORMAT (1H1,1X,15A4//3(1X,I2),2X,4HLINE,I4,5X,7HCOURSE ,F5.0,3X,
(0044)         16HSPEED ,F5.1)
(0045)          WRITE (6,403)
(0046)    403   FORMAT (1H0,2X,2HGMT,5X,5HTRANS,3X,5HRANGE,7X,5HTRANS,2X,5HRANGE,
(0047)         16X,2HXM,8X,2HYM,7X,3HXER,7X,3HYER,6X,8HLATITUDE,3X,9HLONGITUDE,3X,
(0048)         23HSMG,1X,3HCMG,6X,3HDMG)
(0049)     45   IF (NLINE .GE. 60)  GO TO 40
(0050)          IYR = IYEAR + 1900
(0051)          CALL NAVIG (SGNX,XT,YT,NLINE,IDATA,IDAY,MONTH,IYR,ANT)
(0052)          IF (TR1.EQ.'    ') GO TO 40
(0053)          NLINE = NLINE + 1
(0054)          GO TO 45
(0055)   9999   CALL CONTRL (4,INNAM,5)
(0056)          WRITE (6,1099)
(0057)          CALL CONTRL (4,OUTNAM,6)
(0058)          IF (IDATA .GE. 1) WRITE (7,1099)
```

```
(0059)   1099 FORMAT (10X,'FINIS')
(0060)        IF (IDATA.GE.1) CALL CONTRL (4,DATNAM,7)
(0061)        CALL EXIT
(0062)        END
PROGRAM SIZE:   PROCEDURE - 001050    LINKAGE - 012774    STACK - 000044
```

```
ANT     R LINKAGE  013352   0026A  0051A
B       D /TRANS/  000000   0005S  0007S  0017I
CCFLAG  L /REGRES/ 000012   0008S  0014S  0015I
CMGE    R /REGRES/ 000006   0008S  0015I  0039M
CONTRL  R EXTERNAL 000000   0021   0028   0033   0055   0057   0060
COURSE  R LINKAGE  013356   0036M  0039   0042
DATNAM  I LINKAGE  012266   0011S  0032A  0033A  0060A
DMGO    R /REGRES/ 000004   0008S  0015I
EXIT    R EXTERNAL 000000   0061
FLAT    D /PMAP/   000004   0005S  0006S
FLON    D /PMAP/   000010   0005S  0006S
GETFIL  R EXTERNAL 000000   0019   0020   0032
GMT     R /POSIT/  000026   0009S
I       I LINKAGE  000414   0042M
IDATA   I LINKAGE  000403   0022M  0024   0032   0033   0051A  0058   0060
IDAY    I LINKAGE  000407   0036M  0038   0042   0051A
INIT    I EXTERNAL 000000   0026
INNAM   I LINKAGE  012336   0013S  0019A  0021A  0055A
IYEAR   I LINKAGE  000411   0036M  0042   0050
IYR     I LINKAGE  000417   0050M  0051A
LINE    I LINKAGE  000412   0036M  0042
MONTH   I LINKAGE  000410   0036M  0042   0051A
N1      I /POSIT/  000020   0009S
N2      I /POSIT/  000021   0009S
NAMLEN  I /FILES/  000000   0013S
NAVIG   I EXTERNAL 000000   0051
NLINE   I LINKAGE  000413   0041M  0049   0051A  0053M
OLAT    R /PMAP/   000000   0006S
OLON    R /PMAP/   000002   0006S
OUTNAM  I LINKAGE  012406   0011S  0020A  0028A  0057A
PI      D /PMAP/   000020   0005S  0006S  0016I
PSI     R /TRANS/  023420   0007S  0017I
R1      D /POSIT/  000010   0005S  0009S
R2      D /POSIT/  000014   0005S  0009S
RAD     D /PMAP/   000014   0005S  0006S
SGNX    R LINKAGE  000456   0012S  0018I  0026A  0051A
SMGO    R /REGRES/ 000010   0008S  0015I  0040M
SPEED   R LINKAGE  013360   0036M  0040   0042
TO      R /REGRES/ 000013   0008S  0015I
TITLE   R LINKAGE  012456   0012S  0022M  0024   0042
TR1     R /POSIT/  000022   0009S  0052
TR2     R /POSIT/  000024   0009S
TRFLG   R LINKAGE  000454   0015I  0026A  0027
X0      R /REGRES/ 000000   0008S  0015I
X1      R /POSIT/  000000   0009S
X2      R /POSIT/  000002   0009S
XLAT    R /TRANS/  040164   0007S
XPDR    R /TRANS/  035230   0007S  0017I
XT      D LINKAGE  012514   0005S  0026A  0051A
Y0      R /REGRES/ 000002   0008S  0015I
Y1      R /POSIT/  000004   0009S
Y2      R /POSIT/  000006   0009S
YLON    R /TRANS/  040330   0007S
YT      D LINKAGE  013024   0005S  0026A  0051A

$1099              000775   0056   0058   0059D
$4[illegible]      000227   0034D  0052
$4[illegible]      000305   0036   0037D
```

```
$401                 000452   0042   0043D
$402                 000060   0022   0023D
$403                 000531   0045   0046D
$404                 000114   0024   0025D
$43                  000346   0041D  0049
$45                  000645   0049D  0054
$9999                000724   0027   0038   0055D

0000 ERRORS [<.MAIN.>FTN-REV18.1]
```

## SUBROUTINE INIT(ANT,SGNX,XT,YT,TRFLG)

```
      SUBROUTINE  INIT (ANT,SGNX,XT,YT,TRFLG)
C
C  THIS ROUTINE READS TRANSPONDER DATA, SETS UP X,Y COORDINATES, AND COMPUTES
C  BASELINE ARRAY FOR TRANSPONDER NETWORK
C
      DOUBLE PRECISION  B(50,50),DXIJ,DYIJ,DXJI,DYJI,AXIJ,AYIJ,XT(50),
     2 YT(50), FLAT,FLON,RAD,PI
      COMMON /PMAP/ OLAT,OLON,FLAT,FLON,RAD,PI
      COMMON /TRANS/ B,PSI(50,50),XPDR(15,50),XLAT(50),YLON(50)
      DIMENSION  SGNX(50,50)
      PARAMETER   (A0=111132.09,A1=566.05,A2=1.25,A3=0.002,B0=111415.13,
     *            B1=94.55,B2=0.12)
      DATA  RAD /1.7453292519943330-02/
      DECDG(X) = IFIX(X) + (X - IFIX(X))/.6
      OLAT = 0.0
      OLON = 0.0
      READ (5,100)N,ANT,NOPRT
  100 FORMAT (I5,F10.0,I2)
      WRITE (1,104) N,ANT,NOPRT
  104 FORMAT (3X,I5,F10.0,5X,'NOPRT =',I2)
C  NOPRT IS AN OPTION TO SUPPRESS OUTPUT OF BASELINE MATRICES (NOPRT.GE.1)
C  ASSUMES RADAR AND TRANSPONDER RECEIVER ANTENNA ARE AT SAME HEIGHT ANT(M)
      IF (N.GT.50)  WRITE (1,105) N
  105 FORMAT (1H0,5X,'TOO MANY TRANSPONDERS, N =',I5)
      IF (N.GT.50) GO TO 19
      DO 10 I=1,N
      READ (5,101) (XPDR(K,I),K=1,13)
  101 FORMAT (2X,A4,F2.0,2X,4F10.0,2X,7A4)
C  XPDR IS THE ARRAY OF TRANSPONDER POSITION DATA
C  XPDR (1,2)= NAME OF TRANSPONDER (E.G., TRNS01 OR RADR10, 6 CHARACTERS ONLY)
C  XPDR (3)  = LATITUDE OF TRANSPONDER  (DD.MMMMM = DEGREES.DECIMAL MINUTES,N=+)
C  XPDR (4)  = LONGITUDE OF TRANSPONDER  (AS ABOVE, W=+)
C  XPDR (5)  = HEIGHT (ELEVATION) OF TRANSPONDER  (METERS)
C  XPDR (6)  = ERROR IN TRANSPONDER POSITION  (DECIMAL MINUTES, LATITUDE)
C  XPDR (14)  = X POSITION OF TRANSPONDER (TO BE COMPUTED)
C  XPDR (15)  = Y POSITION OF TRANSPONDER (TO BE COMPUTED)
C  XPDR (7-13)= NAME OF TRANSPONDER SITE (28 CHARACTERS POSSIBLE)
C
      XLAT(I) = DECDG (XPDR(3,I)) * RAD
      YLON(I) = DECDG (XPDR(4,I)) * RAD
      OLAT = (OLAT + XLAT(I))/N)
      OLON = (OLON + YLON(I)/N)
   10 CONTINUE
C  COMPUTE METERS PER DEGREE CONVERSION FACTORS USING THE CLARKE SPHEROID (1866)
      FLAT = A0 - A1*COS(2.*OLAT) + A2*COS(4.*OLAT) - A3*COS(6.*OLAT)
      FLON = B0*COS(OLAT) - B1*COS(3.*OLAT) + B2*COS(5.*OLAT)
      DO 11 I=1,N
      XT(I) = (XLAT(I) - OLAT)*FLAT/RAD                                 XTMETERS
      YT(I) = (YLON(I) - OLON)*FLON/RAD                                 YTMETERS
      XPDR(14,I) = XT(I)
      XPDR(15,I) = YT(I)
   11 CONTINUE
      DO 12 I=1,N
      DO 12 J=1,I
      IF (I.EQ.J) GO TO 12
      DXIJ = XT(I) - XT(J)                                              DELTA XT
      DYIJ = YT(I) - YT(J)                                              DELTA YT
      DXJI = -DXIJ
```

```
      DYJI = -DYIJ
      SGNX(I,J) = SGN(DXIJ)
      SGNX(J,I) = -SGNX(I,J)
      B(I,J) = DSQRT (DXIJ**2 + DYIJ**2)                                BASELINE
      B(J,I) = B(I,J)
      AXIJ = DABS(DXIJ)
      AYIJ = DABS(DYIJ)
      IF (DYIJ.EQ.0.)  GO TO 13
      SNPSI = SGN (DYIJ*DXIJ)
      PSI(I,J) = SNPSI*DATAN2(AYIJ,AXIJ)
      GO TO 14
   13 PSI(I,J) = 0.
   14 PSI(J,I) = -PSI(I,J)
C  B(I,J) IS THE BASELINE DISTANCE MATRIX, I.E. DISTANCE BETWEEN XPDRS I AND J
C  PSI(I,J) IS THE AZIMUTH ALONG B(I,J) FROM XPDR I TO XPDR J
   12 CONTINUE
      XOLAT = OLAT/RAD
      YOLON = OLON/RAD
      WRITE(1,106) XOLAT,YOLON,FLAT,FLON
  106 FORMAT(10X,*OLAT = *,F10.5,5X,*OLON = *,F10.5,5X,*FLAT = *,
     2 F10.2,5X,*FLON = *,F10.2)
      WRITE (1,102) ((XPDR(K,I),K=1,6),XT(I),YT(I),(XPDR(K,I),K=7,13),
     1I=1,N)
  102 FORMAT (4X,4HXPDR,4X,8HLATITUDE,2X,9HLONGITUDE,2X,6HHEIGHT,4X,
     15HERROR,7X,6HX-COOR,9X,6HY-COOR//(1X,A4,F3.0,2X,2F10.3,F10.5,
     *F10.5,2F15.1,7X,7A4))
      IF (NOPRT.GE.1)  GO TO 16
C****
C     OUTPUT OF BASELINE DISTANCE AND ANGLE MATRICES
C     OUTPUT SUPPRESSED IF NOPRT .GE. 1
C****
      J0 = 1
      JC = 0
  111 JC = JC + 1
      JC10 = 10*JC
      JM = N
      IF (N.GT.JC10) JM = JC10
      WRITE (1,1031) (J,J=J0,JM)
      DO 15 I=1,N
   15 WRITE (1,103) I,(B(I,J),J=J0,JM)
      IF (N.GT.JM) GO TO 110
      GO TO 121
  110 J0 = J0 + 10
      GO TO 111
  121 J0 = 1
      JC = 0
  122 JC = JC + 1
      JC10 = 10*JC
      JM = N
      IF (N.GT.JC10) JM = JC10
      WRITE (1,1032) (J,J=J0,JM)
      DO 151 I=1,N
  151 WRITE (1,103) I,(PSI(I,J),J=J0,JM)
      IF (N.GT.JM) GO TO 123
      RETURN
  123 J0 = J0 + 10
      GO TO 122
 1031 FORMAT(1H1,5X,*BASELINE DISTANCE MATRIX (METERS)*//* I *, J*,4X,I2,
```

```
(0179)          *9(9X,I2)/)
(0180)    103   FORMAT(1X,I2,3X,10(1PE11.4))
(0181)    1032  FORMAT(1H1,5X,'BASELINE ANGLE MATRIX (RADIANS)'//' I , J',4X,I2,
(0182)          *9(9X,I2)/)
(0183)     16   CONTINUE
(0184)          RETURN
(0185)     19   IRFLG = 1.
(0186)          RETURN
(0187)          END
PROGRAM SIZE:   PROCEDURE = 002442     LINKAGE = 000172     STACK = 000106
```

| | | | | | | | | | | |
|---|---|---|---|---|---|---|---|---|---|---|
| A0 | R | PARAMETER | | 0073S | 0107 | | | | | |
| A1 | R | PARAMETER | | 0073S | 0107 | | | | | |
| A2 | R | PARAMETER | | 0073S | 0107 | | | | | |
| A3 | R | PARAMETER | | 0073S | 0107 | | | | | |
| ANT | R | ARGUMENT | 000046 | 0063S | 0079M | 0081 | | | | |
| AXIJ | D | LINKAGE | 000544 | 0068S | 0126M | 0130A | | | | |
| AYIJ | D | LINKAGE | 000552 | 0068S | 0127M | 0130A | | | | |
| B | D | /TRANS/ | 000000 | 0068S | 0071S | 0124M | 0125M | 0160 | | |
| B0 | R | PARAMETER | | 0073S | 0108 | | | | | |
| B1 | R | PARAMETER | | 0073S | 0108 | | | | | |
| B2 | R | PARAMETER | | 0073S | 0108 | | | | | |
| COS | R | EXTERNAL | 000000 | 0107 | 0108 | | | | | |
| COSSX | R | EXTERNAL | 000000 | 0108 | 0109 | | | | | |
| DABS | D | EXTERNAL | 000000 | 0126 | 0127 | | | | | |
| DATAN2 | D | EXTERNAL | 000000 | 0130 | | | | | | |
| DECDG | R | | 000000 | 0076I | 0101 | 0102 | | | | |
| DSQRSX | D | EXTERNAL | 000000 | 0125 | | | | | | |
| DSQRT | D | EXTERNAL | 000000 | 0124 | | | | | | |
| DXIJ | D | LINKAGE | 000516 | 0068S | 0118M | 0120 | 0122A | 0124 | 0126A | 0129 |
| DXJI | D | LINKAGE | 000526 | 0068S | 0120M | | | | | |
| DYIJ | D | LINKAGE | 000522 | 0068S | 0119M | 0121 | 0124 | 0127A | 0128 | 0129 |
| DYJI | D | LINKAGE | 000532 | 0068S | 0121M | | | | | |
| FLAT | D | /PMAP/ | 000004 | 0068S | 0070S | 0107M | 0110 | 0139 | | |
| FLON | D | /PMAP/ | 000010 | 0068S | 0070S | 0108M | 0111 | 0139 | | |
| I | I | LINKAGE | 000406 | 0088M | 0089 | 0101 | 0102 | 0103 | 0104 | 0109M |
| | | | | 0110 | 0111 | 0112 | 0113 | 0115M | 0116 | 0117 |
| | | | | 0118 | 0119 | 0122 | 0123 | 0124 | 0125 | 0130 |
| | | | | 0132 | 0133 | 0142M | 0159M | 0160 | 0172M | 0173 |
| IFIX | I | EXTERNAL | 000000 | 0076 | | | | | | |
| INIT | I | | 000000 | 0063S | | | | | | |
| J | I | LINKAGE | 000413 | 0116M | 0117 | 0118 | 0119 | 0122 | 0123 | 0124 |
| | | | | 0125 | 0130 | 0132 | 0133 | 0158M | 0160M | 0171M |
| | | | | 0173M | | | | | | |
| JB | I | LINKAGE | 000420 | 0152M | 0158 | 0160 | 0163M | 0165M | 0171 | 0173 |
| | | | | 0176M | | | | | | |
| JC | I | LINKAGE | 000421 | 0153M | 0154M | 0155 | 0166M | 0167M | 0168 | |
| JCIC | I | LINKAGE | 000422 | 0155M | 0157 | 0168M | 0170 | | | |
| JM | I | LINKAGE | 000424 | 0156M | 0157M | 0158 | 0160 | 0161 | 0169M | 0170M |
| | | | | 0171 | 0173 | 0174 | | | | |
| K | I | LINKAGE | 000407 | 0089M | 0142M | | | | | |
| N | I | LINKAGE | 000401 | 0079M | 0081 | 0085 | 0087 | 0088 | 0103 | 0104 |
| | | | | 0109 | 0115 | 0142 | 0156 | 0157 | 0159 | 0161 |
| | | | | 0169 | 0170 | 0172 | 0174 | | | |
| NOPRT | I | LINKAGE | 000402 | 0079M | 0081 | 0147 | | | | |
| OLAT | R | /PMAP/ | 000000 | 0070S | 0077M | 0103M | 0107 | 0108A | 0110 | 0137 |
| OLON | R | /PMAP/ | 000002 | 0070S | 0078M | 0104M | 0111 | 0138 | | |
| PI | D | /PMAP/ | 000020 | 0068S | 0070S | | | | | |
| PSI | R | /TRANS/ | 023420 | 0071S | 0130M | 0132M | 0133M | 0173 | | |
| RAD | D | /PMAP/ | 000014 | 0068S | 0070S | 0075I | 0101 | 0102 | 0110 | 0111 |
| | | | | 0137 | 0138 | | | | | |
| SGN | R | EXTERNAL | 000000 | 0122 | 0129 | | | | | |
| SGNX | R | ARGUMENT | 000031 | 0063S | 0072S | 0122M | 0123M | | | |
| SNPSI | R | LINKAGE | 000556 | 0129M | 0130 | | | | | |
| TRFLG | R | ARGUMENT | 000062 | 0063S | 0185M | | | | | |
| X | R | | 000000 | 0076 | | | | | | |
| XLAT | R | /TRANS/ | 040164 | 0071S | 0101M | 0103 | 0110 | | | |
| XOLAT | R | LINKAGE | 000564 | 0137M | 0139 | | | | | |
| XPOP | R | /TRANS/ | 000220 | 0071S | 0089M | 0101A | 0102A | 0112M | 0113M | 0142 |

```
XT      D ARGUMENT 000054   0063S  0068S  0110M  0112   0118   0142
YLON    R /TRANS/  040330   0071S  0102M  0104   0111
YOLON   R LINKAGE  000566   0138M  0139
YT      D ARGUMENT 000057   0063S  0068S  0111M  0113   0119   0142

$10                000436   0088   0105D
$100               000067   0079   0080D
$101               000301   0089   0090D
$102               001571   0142   0144D
$103               002310   0160   0173   0180D
$1031              002243   0158   0178D
$1032              002325   0171   0181D
$104               000133   0081   0082D
$105               000200   0085   0086D
$106               001363   0139   0140D
$11                000711   0109   0114D
$110               002057   0161   0163D
$111               001715   0154D  0164
$12                001265   0115   0116   0117   0136D
$121               002065   0162   0165D
$122               002073   0167D  0177
$123               002235   0174   0176D
$13                001230   0128   0132D
$14                001243   0131   0133D
$15                001772   0159   0160D
$151               002150   0172   0173D
$16                002371   0147   0183D
$19                002374   0087   0185D

0000 ERRORS [<INIT  >FTN-REV18.10
```

# SUBROUTINE NAVIG(SGNX,XT,YT,NLINE,IDATA,IDAY,MONTH,ITY,ANT)

```
      SUBROUTINE NAVIG (SGNX,XT,YT,NLINE,IDATA,IDAY,MONTH,IYR,ANT)
C
C  THIS ROUTINE COMPUTES THE SHIP POSITION AT TIME GMT USING TWO TRANSPONDERS TO
C  FIX THE LOCATION
C
      DOUBLE PRECISION  B(50,50),PI,RAD,FLAT,FLON,R1,R2,XT(50),YT(50)
      COMMON /POSIT/ X1,X2,Y1,Y2,R1,R2,N1,N2,TR1,TR2,GMT
      COMMON /REGRES/  X0,Y0,DMG0,CMG0,SMG0,CCFLAG,T0
      COMMON /PMAP/  OLAT,OLON,FLAT,FLON,RAD,PI
      COMMON /TRANS/ B,PSI(50,50),XPDR(15,50),XLAT(50),YLON(50)
      DIMENSION  LT(3),SGNX(50,50)
      LOGICAL  CCFLAG
      DATA  PHI /360./
      XFLAG = 1000000.
      IYEAR = IYR - 1900
      READ (5,200) (LT(I),I=1,3),TR1,N1,R1,TR2,N2,R2,IBASE
  200 FORMAT (3I2,3X,A4,I2,F10.0,4X,A4,I2,F10.0,4X,I1)
      IF (TR1.EQ.'    ')  RETURN
      IF (TR2.EQ.4HAZIM)  GO TO 37
      IF (N1 .EQ. N2)  GO TO 78
   37 CONTINUE
C  CHANGE TIME FROM HHMMSS TO DECIMAL HOURS (HH.0000)
      DECS = LT(3)/60.
      DECM = LT(2) + DECS
      GMT = LT(1) + DECM/60.
      TST = T0
      IF (GMT .EQ. TST) GO TO 79
C  DETERMINE WHAT TRANSPONDER IS USED   N1 = NO. OF 1ST XPDR, N2 = NO. OF 2ND
C  TEST FOR ZERO RANGES
      IF (R1.LE.0.0) GO TO 75
C  TEST FOR SAME TIME AS LAST FIX
      IF (TR1.EQ.4HTRNS) GO TO 30
C  FOR RADAR FIXES, COMPUTE ERROR AND CONVERT NAUTICAL MILES TO METERS
      R1 = R1*1852.
      AER1 = R1*RAD
      EPS1 = R1*0.01
C  TEST FOR ZERO RANGES, AZIMUTH, ETC.
   30 IF (TR2.EQ.4HAZIM) GO TO 35
      IF (R2.LE.0.0) GO TO 75
      IF (TR2.EQ.4HTRNS) GO TO 31
      R2 = R2*1852.
      AER2 = R2*RAD
      EPS2 = R2*0.01
   31 R1 = DSQRT(R1**2 + (XPDR(5,N1) - ANT)**2)
      R2 = DSQRT(R2**2 + (XPDR(5,N2) - ANT)**2)
      Z12 = (R1**2 + B(N1,N2)**2 - R2**2)/(2.*R1*B(N1,N2))
      Z21 = (R2**2 + B(N2,N1)**2 - R1**2)/(2.*R2*B(N2,N1))
      IF (Z12 .GT. 1.0)  GO TO 77
      IF (Z21 .GT. 1.0)  GO TO 77
      A12 = ARCOS (Z12)
      A21 = ARCOS (Z21)
      IF (IBASE.EQ.1) GO TO 33
      THETA1 = A12 - PSI(N1,N2)*SGNX(N1,N2)
      THETA2 = A21 - PSI(N2,N1)*SGNX(N2,N1)
      X1 = XT(N1) + SGNX(N2,N1)*R1*COS(THETA1)
      X2 = XT(N2) - SGNX(N2,N1)*R2*COS(THETA2)
      Y1 = YT(N1) + R1*SIN(THETA1)
      Y2 = YT(N2) + R2*SIN(THETA2)
```

```
(0246)          GO TO 36
(0247)   C
(0248)   C  COMPUTE POSITION FOR RANGE R1, AZIMUTH R2 (RADAR FIX)
(0249)   C
(0250)     35   R1 = DSQRT(R1**2 + (XPDR(5,N1) - ANT)**2)
(0251)          THETA = PI - R2*RAD
(0252)          X1 = XT(N1) + R1*COS(THETA)
(0253)          X2 = X1
(0254)          Y1 = YT(N1) + R1*SIN(THETA)
(0255)          Y2 = Y1
(0256)   C
(0257)   C  A12 AND A21 ARE THE ANGLES ENCLOSED BY THE BASELINE AND R1, R2 RESPECTIVELY
(0258)   C  THETA1,2 ARE THE ANGLES (AZIMUTHS) OF THE VECTORS FROM THE TRANSPONDER TO THE
(0259)   C  FIX POSITION
(0260)   C  X,Y ARE THE COORDINATES OF THE FIX POSITIONS, 1 FROM TRNS01, 2 FROM TRNS02
(0261)     36   XM = (X1 + X2)*0.5
(0262)          YM = (Y1 + Y2)*0.5
(0263)          IF (CCFLAG) GO TO 34
(0264)          DMG = SQRT((XM-X0)**2 + (YM-Y0)**2) / 1852.
(0265)          SMG = DMG/(GMT - T0)
(0266)          DEX = XM - X0
(0267)          DEY = YM - Y0
(0268)          IF (DEX .EQ. 0.)  XFLAG = 0.0
(0269)          IF (DEY .EQ. XFLAG) GO TO 76
(0270)          IF (DEY.LT.0.) PHI = 0.
(0271)          CMG = PHI - (ATAN2(DEY,DEX))/RAD
(0272)   C
(0273)   C  DMG = DISTANCE MADE GOOD, SMG = SPEED MADE GOOD, CMG = COURSE MADE GOOD
(0274)   C
(0275)          GO TO 34
(0276)     33   CALL BASEL (XM,YM,DMG,SMG,DEX,DEY,CMG,A12,A21,SGNX,XT,YT)
(0277)          NLINE = NLINE + 1
(0278)     34   CONTINUE
(0279)   C PLATM, PLONM ARE THE LATITUDE AND LONGITUDE OF THE POSITION IN DECIMAL DEGREES
(0280)   C   LATM, LONM DEGREES LATITUDE, LONGITUDE
(0281)   C  PAMN, POMN  MINUTES LATITUDE, LONGITUDE  (DECIMAL)
(0282)   C
(0283)          PLATM = XM/FLAT + OLAT/RAD
(0284)          LATM = IFIX (PLATM)
(0285)          PLONM = YM/FLON + OLON/RAD
(0286)          LONM = IFIX (PLONM)
(0287)          PAMNM = (PLATM - LATM)*60.
(0288)          POMNM = (PLONM - LONM)*60.
(0289)          ELAT = X2 - X1
(0290)          ELON = Y2 - Y1
(0291)          NLON = -LONM
(0292)          PLON = -PLONM
(0293)   C**** NLON IS NEGATIVE OF DEGREES LONG FOR GDC OUTPUT
(0294)   C**** PLON IS NEGATIVE DECIMAL DEGREES FOR HYPERMAP INPUT
(0295)   C
(0296)   C  BEGIN OUTPUT OF POSITION DATA
(0297)   C
(0298)          WRITE (6,201) (LT(I),I=1,3),TR1,N1,R1,TR2,N2,R2,XM,YM,ELAT,ELON,
(0299)         1LATM,PAMNM,LONM,POMNM,SMG,CMG,DMGO
(0300)     201  FORMAT (1H ,3I2,2X,A4,I2,F10.0,4X,A4,I2,5F10.0,1X,I2,1X,F6.3,2HN ,
(0301)         1I3,1X,F6.3,2HW ,F4.1,1X,F4.0,2X,F10.3)
(0302)   C**** OUTPUT OF GDC POSITION DATA TO FILE07, OPTIONAL FOR IDATA.EQ.1
(0303)   C**** OUTPUT OF HYPERMAP INPUT DATA TO FILE07, OPTIONAL FOR IDATA.EQ.2
```

```
(0304)        IF (IDATA.EQ.1) WRITE (7,202) IDAY,MONTH,IYR,(LT(I),I=1,2),LATM,
(0305)       * PAMNM,NLON,POMNM,TR1
(0306)        IF (IDATA.EQ.2) WRITE (7,203) IDAY,MONTH,IYEAR,(LT(I),I=1,3),
(0307)       * PLATM,PLON,TR1
(0308)   202  FORMAT (3I2,I3,I5,6X,2I2,2(I4,F6.2),12X,A4)
(0309)   203  FORMAT (3I2,2X,3I2,1X,2F10.5,5X,A4)
(0310)        X0 = XM
(0311)        Y0 = YM
(0312)        TC = GMT
(0313)        CCFLAG = .FALSE.
(0314)        DMG0 = DMG0 + DMG
(0315)        RETURN
(0316)    75  WRITE (6,275) (LT(I),I=1,3),TR1,N1,R1,TR2,N2,R2
(0317)   275  FORMAT (11X,'ZERO RANGE',4X,3I2,2(4X,A4,I2,F10.0))
(0318)        RETURN
(0319)    76  WRITE (6,276) (LT(I),I=1,3),TR1,N1,R1,TR2,N2,R2
(0320)   276  FORMAT (1H ,13HSAME POSITION,4X,3I2,2(4X,A4,I2,F10.0))
(0321)        RETURN
(0322)    77  WRITE (6,277) (LT(I),I=1,3),TR1,N1,R1,TR2,N2,R2
(0323)   277  FORMAT (1H ,39HDOES NOT CONVERGE  COS GREATER THAN 1.0,4X,3I2,
(0324)       12(4X,A4,I2,F10.0))
(0325)        RETURN
(0326)    78  WRITE (6,278) (LT(I),I=1,3),TR1,N1,R1,TR2,N2,R2
(0327)   278  FORMAT (1H ,16HSAME TRANSPONDER,4X,3I2,2(4X,A4,I2,F10.0))
(0328)        RETURN
(0329)    79  WRITE (6,279) (LT(I),I=1,3), TR1,N1,R1,TR2,N2,R2
(0330)   279  FORMAT (1H ,9HSAME TIME,4X,3I2,2(4X,A4,I2,F10.0))
(0331)        RETURN
(0332)        END
PROGRAM SIZE:   PROCEDURE - 003464    LINKAGE - 000266    STACK - 000122
```

| | | | | | | | | | | |
|---|---|---|---|---|---|---|---|---|---|---|
| A12 | R | LINKAGE | 000546 | 0237M | 0240 | 0276A | | | | |
| A21 | R | LINKAGE | 000552 | 0238M | 0241 | 0276A | | | | |
| AER1 | R | LINKAGE | 000522 | 0222M | | | | | | |
| AER2 | R | LINKAGE | 000530 | 0229M | | | | | | |
| ANT | R | ARGUMENT | 000074 | 0188S | 0231 | 0232 | 0250 | | | |
| ARCOS | R | EXTERNAL | 000000 | 0237 | 0238 | | | | | |
| ATAN2 | R | EXTERNAL | 000000 | 0271 | | | | | | |
| B | D | /TRANS/ | 000000 | 0193S | 0197S | 0233 | 0234 | | | |
| BASEL | R | EXTERNAL | 000000 | 0276 | | | | | | |
| CCFLAG | L | /REGRES/ | 000012 | 0195S | 0199S | 0263 | 0313M | | | |
| CMG | R | LINKAGE | 000626 | 0271M | 0276A | 0298 | | | | |
| CMGO | R | /REGRES/ | 000006 | 0195S | | | | | | |
| COS | R | EXTERNAL | 000000 | 0242 | 0243 | 0252 | | | | |
| COS$X | I | EXTERNAL | 000000 | 0243 | 0244 | 0253 | | | | |
| DECM | R | LINKAGE | 000512 | 0211M | 0212 | | | | | |
| DFCS | R | LINKAGE | 000510 | 0210M | 0211 | | | | | |
| DFX | R | LINKAGE | 000622 | 0266M | 0268 | 0271A | 0276A | | | |
| DFY | R | LINKAGE | 000624 | 0267M | 0269 | 0270 | 0271A | 0276A | | |
| DMG | R | LINKAGE | 000610 | 0264M | 0265 | 0276A | 0314 | | | |
| DMGO | R | /REGRES/ | 000004 | 0195S | 0298 | 0314M | | | | |
| DSQR$X | D | EXTERNAL | 000000 | 0232 | 0233 | 0251 | | | | |
| DSQRT | D | EXTERNAL | 000000 | 0231 | 0232 | 0250 | | | | |
| ELAT | R | LINKAGE | 000654 | 0289M | 0298 | | | | | |
| ELON | R | LINKAGE | 000656 | 0290M | 0298 | | | | | |
| EPS1 | R | LINKAGE | 000526 | 0223M | | | | | | |
| EPS2 | R | LINKAGE | 000532 | 0230M | | | | | | |
| FLAT | D | /PMAP/ | 000004 | 0193S | 0196S | 0283 | | | | |
| FLON | D | /PMAP/ | 000010 | 0193S | 0196S | 0285 | | | | |
| GMT | R | /POSIT/ | 000026 | 0194S | 0212M | 0214 | 0265 | 0312 | | |
| I | I | LINKAGE | 000403 | 0203M | 0298M | 0304M | 0306M | 0316M | 0319M | 0322M |
| | | | | 0326M | 0329M | | | | | |
| IBASE | I | LINKAGE | 000404 | 0203M | 0239 | | | | | |
| IDATA | I | ARGUMENT | 000000 | 0188S | 0304 | 0306 | | | | |
| IDAY | I | ARGUMENT | 000063 | 0188S | 0304 | 0306 | | | | |
| IFIX | I | EXTERNAL | 000000 | 0284 | 0286 | | | | | |
| IYEAR | I | LINKAGE | 000400 | 0202M | 0306 | | | | | |
| IYR | I | ARGUMENT | 000071 | 0188S | 0292 | 0304 | | | | |
| LATM | I | LINKAGE | 000415 | 0284M | 0287 | 0298 | 0304 | | | |
| LONM | I | LINKAGE | 000416 | 0286M | 0288 | 0291 | 0298 | | | |
| LT | I | LINKAGE | 000454 | 0198S | 0203M | 0210 | 0211 | 0212 | 0298 | 0304 |
| | | | | 0306 | 0316 | 0319 | 0322 | 0326 | 0329 | |
| MONTH | I | ARGUMENT | 000066 | 0188S | 0304 | 0306 | | | | |
| N1 | I | /POSIT/ | 000020 | 0194S | 0203M | 0207 | 0231 | 0233 | 0234 | 0240 |
| | | | | 0241 | 0242 | 0243 | 0244 | 0250 | 0252 | 0254 |
| | | | | 0298 | 0316 | 0319 | 0322 | 0326 | 0329 | |
| N2 | I | /POSIT/ | 000021 | 0194S | 0203M | 0207 | 0232 | 0233 | 0234 | 0240 |
| | | | | 0241 | 0242 | 0243 | 0245 | 0298 | 0316 | 0319 |
| | | | | 0322 | 0326 | 0329 | | | | |
| NAVIG | I | | 000000 | 0188S | | | | | | |
| NLINE | I | ARGUMENT | 000055 | 0188S | 0277M | | | | | |
| NLON | I | LINKAGE | 000417 | 0291M | 0304 | | | | | |
| OLAT | R | /PMAP/ | 000000 | 0196S | 0283 | | | | | |
| OLON | R | /PMAP/ | 000002 | 0196S | 0285 | | | | | |
| PAMNM | R | LINKAGE | 000650 | 0287M | 0298 | 0304 | | | | |
| PHI | R | LINKAGE | 000452 | 0202I | 0270M | 0271 | | | | |
| PI | D | /PMAP/ | 000020 | 0193S | 0196S | 0251 | | | | |
| PLATM | R | LINKAGE | 000634 | 0285M | 0284 | 0287 | 0306 | | | |
| PLON | R | LINKAGE | 000660 | 0292M | 0306 | | | | | |

| | | | | | | | | | | |
|---|---|---|---|---|---|---|---|---|---|---|
| PLONM | R | LINKAGE | 000642 | 0285M | 0286 | 0288 | 0292 | | | |
| POMNM | R | LINKAGE | 000652 | 0288M | 0298 | 0304 | | | | |
| PSI | R | /TRANS/ | 023420 | 0197S | 0240 | 0241 | | | | |
| R1 | D | /POSIT/ | 000010 | 0193S | 0194S | 0203M | 0217 | 0221M | 0222 | 0223 |
| | | | | 0231M | 0233 | 0234 | 0242 | 0244 | 0253M | 0252 |
| | | | | 0254 | 0298 | 0316 | 0319 | 0322 | 0326 | 0329 |
| R2 | D | /POSIT/ | 000014 | 0193S | 0194S | 0203M | 0226 | 0228M | 0229 | 0230 |
| | | | | 0232M | 0233 | 0234 | 0243 | 0245 | 0251 | 0298 |
| | | | | 0316 | 0319 | 0322 | 0326 | 0329 | | |
| RAD | D | /PMAP/ | 000014 | 0193S | 0196S | 0222 | 0229 | 0251 | 0271 | 0283 |
| | | | | 0285 | | | | | | |
| SGNX | R | ARGUMENT | 000044 | 0188S | 0198S | 0240 | 0241 | 0242 | 0243 | 0276A |
| SIN | R | EXTERNAL | 000000 | 0244 | 0245 | 0254 | | | | |
| SIN$X | I | EXTERNAL | 000000 | 0245 | 0246 | 0255 | | | | |
| SMG | R | LINKAGE | 000620 | 0265M | 0276A | 0298 | | | | |
| SMGD | R | /REGRES/ | 000210 | 0195S | | | | | | |
| SQRT | R | EXTERNAL | 000000 | 0264 | | | | | | |
| SQRT$X | R | EXTERNAL | 000000 | 0265 | | | | | | |
| TD | R | /REGRES/ | 000013 | 0195S | 0213 | 0265 | 0312M | | | |
| THETA | R | LINKAGE | 000576 | 0251M | 0252A | 0254A | | | | |
| THETA1 | R | LINKAGE | 000554 | 0240M | 0242A | 0244A | | | | |
| THETA2 | R | LINKAGE | 000560 | 0241M | 0243A | 0245A | | | | |
| TR1 | R | /POSIT/ | 000022 | 0194S | 0203M | 0205 | 0219 | 0298 | 0304 | 0306 |
| | | | | 0316 | 0319 | 0322 | 0326 | 0329 | | |
| TR2 | R | /POSIT/ | 000024 | 0194S | 0203M | 0206 | 0225 | 0227 | 0298 | 0316 |
| | | | | 0319 | 0322 | 0326 | 0329 | | | |
| TST | R | LINKAGE | 000516 | 0213M | 0214 | | | | | |
| X0 | R | /REGRES/ | 000000 | 0195S | 0264 | 0266 | 0310M | | | |
| X1 | R | /POSIT/ | 000000 | 0194S | 0242M | 0252M | 0253 | 0261 | 0289 | |
| X2 | R | /POSIT/ | 000002 | 0194S | 0243M | 0253M | 0261 | 0289 | | |
| XFLAG | R | LINKAGE | 000460 | 0201M | 0268M | 0269 | | | | |
| XLAT | R | /TRANS/ | 040164 | 0197S | | | | | | |
| XM | R | LINKAGE | 000602 | 0261M | 0264 | 0266 | 0276A | 0283 | 0298 | 0310 |
| XPOR | R | /TRANS/ | 035230 | 0197S | 0231 | 0232 | 0250 | | | |
| XT | D | ARGUMENT | 000047 | 0188S | 0193S | 0242 | 0243 | 0252 | 0276A | |
| Y0 | R | /REGRES/ | 000002 | 0195S | 0264 | 0267 | 0311M | | | |
| Y1 | R | /POSIT/ | 000004 | 0194S | 0244M | 0254M | 0255 | 0262 | 0290 | |
| Y2 | R | /POSIT/ | 000006 | 0194S | 0245M | 0255M | 0262 | 0290 | | |
| YLON | R | /TRANS/ | 040330 | 0197S | | | | | | |
| YM | R | LINKAGE | 000604 | 0262M | 0264 | 0267 | 0276A | 0285 | 0298 | 0311 |
| YT | D | ARGUMENT | 000052 | 0188S | 0193S | 0244 | 0245 | 0254 | 0276A | |
| Z12 | R | LINKAGE | 000540 | 0233M | 0235 | 0237A | | | | |
| Z21 | R | LINKAGE | 000544 | 0234M | 0236 | 0238A | | | | |
| $200 | | | 000121 | 0203 | 0204D | | | | | |
| $201 | | | 002065 | 0298 | 0300D | | | | | |
| $202 | | | 002400 | 0304 | 0308D | | | | | |
| $203 | | | 002425 | 0306 | 0309D | | | | | |
| $275 | | | 002601 | 0315 | 0317D | | | | | |
| $276 | | | 002733 | 0319 | 0320D | | | | | |
| $277 | | | 003067 | 0322 | 0323D | | | | | |
| $278 | | | 003240 | 0326 | 0327D | | | | | |
| $279 | | | 003375 | 0329 | 0330D | | | | | |
| $30 | | | 000331 | 0219 | 0225D | | | | | |
| $31 | | | 000411 | 0227 | 0231D | | | | | |
| $33 | | | 001471 | 0239 | 0276D | | | | | |
| $34 | | | 001520 | 0263 | 0275 | 0278D | | | | |
| $35 | | | 001127 | 0225 | 0250D | | | | | |

```
   $36                 001263   0246   0261D
   $37                 000205   0206   0208D
   $75                 002501   0217   0226   0316D
   $76                 002633   0269   0319D
   $77                 002767   0235   0236   0322D
   $78                 003140   0207   0326D
   $79                 003275   0214   0329D

 0000 ERRORS [<NAVIG >FTN-REV18.1]
```

## SUBROUTINE BASEL(XM,YM,DMG,SMG,DEX,DEY,CMG,A12,A21,SGNX,XT,YT)

```
(0333)          SUBROUTINE  BASEL (XM,YM,DMG,SMG,DEX,DEY,CMG,A12,A21,SGNX,XT,YT)
(0334)   C
(0335)   C  THIS ROUTINE COMPUTES POSITION ACROSS BASELINE (TO THE EAST )
(0336)   C
(0337)          DOUBLE PRECISION  P(50,50),PI,RAD,FLAT,FLON,R1,R2,XT(50),YT(50)
(0338)          COMMON /PMAP/ OLAT,OLON,FLAT,FLON,RAD,PI
(0339)          COMMON /POSIT/ X1,X2,Y1,Y2,R1,R2,N1,N2,TR1,TR2,GMT
(0340)          COMMON /REGRES/ X0,Y0,DMG0,CMG0,SMG0,CCFLAG,T0
(0341)          COMMON /TRANS/ B,PSI(50,50),XPDR(15,50),XLAT(50),YLON(50)
(0342)          DIMENSION  SGNX(50,50)
(0343)          LOGICAL  CCFLAG
(0344)          PHI = 360.
(0345)          CCFLAG = .TRUE.
(0346)          THETA1 = A12 + PSI(N1,N2)*SGNX(N1,N2)
(0347)          THETA2 = A21 + PSI(N2,N1)*SGNX(N2,N1)
(0348)          X1 = XT(N1) + SGNX(N2,N1)*R1*COS(THETA1)
(0349)          X2 = XT(N2) - SGNX(N2,N1)*R2*COS(THETA2)
(0350)          Y1 = YT(N1) - R1*SIN(THETA1)
(0351)          Y2 = YT(N2) - R2*SIN(THETA2)
(0352)          XM = (X1 + X2)*0.5
(0353)          YM = (Y1 + Y2)*0.5
(0354)          DMG = SQRT ((XM-X0)**2 + (YM-Y0)**2) / 1852.
(0355)          SMG = DMG/(GMT - T0)
(0356)          DEX = XM - X0
(0357)          DEY = YM - Y0
(0358)          IF (DEY.LT.0.) PHI = 0.
(0359)          CMG = PHI - (ATAN2(DEY,DEX))/RAD
(0360)          WRITE (6,300)
(0361)     300  FORMAT (1H ,17HBASELINE CROSSING)
(0362)          RETURN
(0363)          END
PROGRAM SIZE:   PROCEDURE - 000440    LINKAGE - 000114    STACK - 000120
```

SGNX.XT,Y )

(0364) X.XT,YT
(0365) I )
(0366)
(0367) ,YT(50)
(0368)
(0369)
(0370)
PROGRA )

0129

```
A12      R ARGUMENT 000071   0333S  0346
A21      R ARGUMENT 000074   0333S  0347
ATAN2    R EXTERNAL 000000   0359
B        D /TRANS/  000000   0337S  0341S
BASEL    R          000000   0333S
CCFLAG   L /REGRES/ 000012   0340S  0343S  0345M
CMG      R ARGUMENT 000066   0333S  0359M
CMGO     R /REGRES/ 000006   0340S
COS      R EXTERNAL 000000   0348   0349
COS$X    I EXTERNAL 000000   0349   0350
DEX      R ARGUMENT 000060   0333S  0356M  0359A
DEY      R ARGUMENT 000063   0333S  0357M  0358   0359A
DMG      R ARGUMENT 000052   0333S  0354M  0355
DMGO     R /REGRES/ 000004   0340S
FLAT     D /PMAP/   000004   0337S  0338S
FLON     D /PMAP/   000010   0337S  0338S
GMT      R /POSIT/  000026   0339S  0355
N1       I /POSIT/  000020   0339S  0346   0347   0348   0349   0350
N2       I /POSIT/  000021   0339S  0346   0347   0348   0349   0351
OLAT     R /PMAP/   000000   0338S
OLON     R /PMAP/   000002   0336S
PHI      R LINKAGE  000434   0344M  0358M  0359
PI       D /PMAP/   000020   0337S  0338S
PSI      R /TRANS/  023420   0341S  0346   0347
R1       D /POSIT/  000010   0337S  0339S  0348   0350
R2       D /POSIT/  000014   0337S  0339S  0349   0351
RAD      D /PMAP/   000014   0337S  0338S  0359
SGNX     R ARGUMENT 000077   0333S  0342S  0346   0347   0348   0349
SIN      R EXTERNAL 000000   0350   0351
SIN$X    I EXTERNAL 000000   0351   0352
SMG      R ARGUMENT 000055   0333S  0355M
SMGO     R /REGRES/ 000010   0340S
SQRT     R EXTERNAL 000000   0354
SQRT$X   R EXTERNAL 000000   0355
T0       R /REGRES/ 000013   0340S  0355
THETA1   R LINKAGE  000440   0346M  0348A  0350A
THETA2   R LINKAGE  000450   0347M  0349A  0351A
TR1      R /POSIT/  000022   0339S
TR2      R /POSIT/  000024   0339S
X0       R /REGRES/ 000000   0340S  0354   0356
X1       R /POSIT/  000000   0339S  0348M  0352
X2       R /POSIT/  000002   0339S  0349M  0352
XLAT     R /TRANS/  040164   0341S
XM       R ARGUMENT 000044   0333S  0352M  0354   0356
XPOR     R /TRANS/  035230   0341S
XT       D ARGUMENT 000102   0333S  0337S  0348   0349
Y0       R /REGRES/ 000002   0340S  0354   0357
Y1       R /POSIT/  000004   0339S  0350M  0353
Y2       R /POSIT/  000006   0339S  0351M  0353
YLON     R /TRANS/  040330   0341S
YM       R ARGUMENT 000047   0333S  0353M  0354   0357
YT       D ARGUMENT 000105   0333S  0337S  0350   0351

$3J0                000407   0360   0361D

0000 ERRORS [<BASEL >FTN-REV18.13
```

# FUNCTION SGN(X)

```
(0364)          FUNCTION SGN(X)
(0365)          IF (X) 1,2,2
(0366)     1    SGN = -1.
(0367)          RETURN
(0368)     2    SGN = 1.
(0369)          RETURN
(0370)          END
PROGRAM SIZE:   PROCEDURE - 000034    LINKAGE - 000022    STACK - 000046
```

```
SGN     R LINKAGE  000420   0364S   0366M   0368M
X       R ARGUMENT 000042   0364S   0365

$1                 000007   0365    0366D
$2                 000020   0365    0368D

0000 ERRORS [<SGN    >FTN-REV18.1]
```

# FUNCTION ARCOS(X)

```
(0371)        FUNCTION ARCOS (X)
(0372)        Y = SQRT (1. - X**2)
(0373)        ARCOS = ATAN2 (Y,X)
(0374)        RETURN
(0375)        END
PROGRAM SIZE:   PROCEDURE = 000040    LINKAGE = 00003C    STACK = 000050
```

```
ARCOS   R LINKAGE   000424   0371S   0373M
ATAN2   R EXTERNAL  000000   0373
SQRT    R EXTERNAL  000000   0372
SQRT$X  R EXTERNAL  000000   0373
X       R ARGUMENT  000042   0371S   0372    0373A
Y       R LINKAGE   000420   0372M   0373A

0000 ERRORS [<ARCOS >FTN-REV18.1]
```

# APPENDIX A.2

## FORTRAN Program SMFIX used to Compute Averaged Ship Positions from a Sequence of Position Fixes during One Minute Time Intervals.

```
C     PROGRAM SMFIX (INPUT,OUTPUT,TAPE5=INPUT,TAPE6=OUTPUT,TAPE1,TAPE7)
C*********************************************************************C
C                                                                     C
C     THIS PROGRAM COMPUTES SMOOTHED NAVIGATION DATA FOR PLOTTING     C
C     STANDARD OCEANOLOGICAL DATA CENTER FORMAT IS USED FOR THE OUTPUT FILE7  C
C     INPUT DATA ARE IN DECIMAL DEGREES FORMAT, SUITABLE FOR HYPERMAP C
C     INPUT FROM TTY:                                                 C
C          INPUT FILE NAME      (TAPE5=INPUT)   DECIMAL DEGREES      C
C          OUTPUT FILE NAME     (TAPE6=OUTPUT)  DECIMAL DEGREES      C
C          OUTPUT FILE NAME     (TAPE7=DATNAM)  DEGREES, DECIMAL MINUTES  C
C                  CRUISE START TIMES                                 C
C          DAY = IDAYO                                                C
C          MONTH = MONO                                               C
C          YEAR = IYEARO                                              C
C          HOUR = IHRO                                                C
C          MINUTE = MINO                                              C
C          SECOND = ISECO                                             C
C                                                                     C
C          FLAT = METERS / DEGREE LATITUDE                            C
C          FLON = METERS / DEGREE LONGITUDE                           C
C                                                                     C
C*********************************************************************C
C
      INTEGER  OUTNAM(40),DATNAM(40)
      LOGICAL  FFLAG,TFLAG
      DOUBLE PRECISION  SUMX,SUMY,SUMT,SUMXT,SUMYT,SUMX2,SUMY2,SUMT2,SMX,SMY,
     - SXM,SYM,XO,YO,DX2,DY2,DT2,XM,YM,TM,RX,RY,RAD,FLAT,FLON
      COMMON /MAP/  FLAT,FLON,RAD
      COMMON /TIMES/  GMT,TZERO,MONO,IDAYO,IYEAR,IYEARO,MONO,IDAYO,TNHRO,
     -                IHRO,TNHR1
      COMMON /SUMS/  SUMX,SUMY,SUMT,SUMXT,SUMYT,SUMX2,SUMY2,SUMT2
      COMMON /DIFF/  DELX,DELY,DELT
      COMMON /POSIT/  LATM,XOLAT,LONM,YOLON
      DIMENSION  LT(3), INNAM (40), TITLE (15)
      DATA  TO,ISECO,MINO,IHRO,BLANK /-1.,  3*0,4H    /
      DATA  GMT,GMTO,MON,IDAY,IYEAR,IYEARO,MONO,IDAYO  /2*0., 6*0/
      DATA  RAD  /1.74532925199433D-02/
      CALL GETFIL (*INPUT*,6,INNAM)
      CALL GETFIL (*OUTPUT*,6,OUTNAM)
      CALL GETFIL (*6JCOUT*,6,DATNAM)
      CALL CONTRL (1,INNAM,5)
      CALL CONTRL (2,OUTNAM,6)
      CALL CONTRL (2,DATNAM,7)
      READ (5,100) IDAYO,MONO,IYEARO,IHRO,MINO,ISECO,FLAT,FLON,IRITE
  100 FORMAT (3I2,I4,2I2,2F10.0,I5)
      SECO = ISECO/60.
      OMINO = MINO + SECO
      TZERO = IHRO + OMINO/60.
      TNHRO = 0.0
      TNHR1 = 0.0
      TFLAG = .TRUE.
      FTYPO = BLANK
      NFIX = 0
C***
C     BEGIN COMPUTING AVERAGE FIXES
C***
    1 CONTINUE
      READ (5,101) IDAY,MON,IYEAR,(LT(I),I=1,3),XLAT,YLON,FTYPE
```

BE SURE TO MOD THIS DATA AS SEPARATE FILE

```
  101  FORMAT (3I2,I4,2I2,1X,2F10.0,5X,A4)
       IF (FTYPO .EQ. BLANK) FTYPO = FTYPE
       IF (IDAY.EQ.0) GO TO 99
       IF (IRITE.EQ.1) WRITE (1,200) IDAY,MON,IYEAR,(LT(I),I=1,3),XLAT,
                YLON,FTYPE
  200  FORMAT (5X,3I2,I4,2I2,1X,2F12.5,5X,A4)
C***   COMPUTE GMT IN DECIMAL HOURS
       DECS = LT(3)/60.
       DECM = LT(2) + DECS
       GMT =  LT(1) + DECM/60.
C***   COMPUTE RELATIVE TIME SINCE CRUISE START
       CALL NTIME (MONTH,NDAY,TNHR)
       IF (IRITE.EQ.1)  WRITE (1,201) MONTH,NDAY,TNHR
  201  FORMAT (5X,'MONTH = ',I5,5X,'NDAY = ',I5,5X,'TNHR = ',F12.5)
C***   FIX AVERAGING FOLLOWS
       CALL FIXAV (LT,TNHR,FFLAG,MINT,NFIX,FTYPO,XLAT,YLON,TFLAG,MINTO,
                NDAY)
C      FFLAG IS A FLAG TO INDICATE WHEN THE FIX AVERAGE HAS BEEN COMPUTED
       FTYPO = FTYPE
       GO TO 1
   99  CONTINUE
C      LAST FIX HAS BEEN ADDED TO SUMS, NOW COMPUTE LAST AVERAGE FIX
       IF (NFIX.LE.1) GO TO 19
       CALL FIXCM (FFLAG,NFIX,XLAT,YLON,LT,IHR,MINT,FTYPO)
  199  CALL CONTRL (4,INNAM,5)
       WRITE(6,1199)
 1199  FORMAT(38X,'FINIS')
       CALL CONTRL (4,OUTNAM,6)
       WRITE (7,1099)
       CALL CONTRL (4,DATNAM,7)
 1099  FORMAT (53X,'FINIS')
       CALL EXIT
   19  CONTINUE
       IF (MINT.LT.60)  GO TO 194
       MINT = 0
       IHR = IHR + 1
  194  CONTINUE
       IF (IHR.LT.24) GO TO 195
       IHR = 0
  195  CONTINUE
       CALL FIXVL (IYR,MINT,MIN,SUMX,SUMY)
       WRITE (7,102)  IDAYO,MONO,IYR,IHRO,MIN,LATM,XOLAT,LONM,YOLON,FTYPO
  102  FORMAT (3I2,I3,I5,6X,2I2,2(I4,F6.2),12X,A4)
       WRITE (6,103)  IDAYO,MONO,IYEARO,IHRO,MIN,SUMX,SUMY,FTYPO
  103  FORMAT (1X,3I2,2X,2I2,1X,2F10.5,5X,A4,5X,'SINGLE FIX INPUT')
       GO TO 199
       END
```

| | | | | | | | | | | |
|---|---|---|---|---|---|---|---|---|---|---|
| BLANK | R | | 000006 | 0035I | 0052 | 0060 | | | | |
| CONTRL | R | EXTERNAL | 000000 | 0041 | 0042 | 0043 | 0083 | 0086 | 0088 | |
| DATNAM | I | | 000012 | 0024S | 0040A | 0043A | 0086A | | | |
| DECM | R | | 001366 | 0067M | 0068 | | | | | |
| DECS | R | | 001370 | 0065M | 0067 | | | | | |
| DELT | R | /DIFF/ | 000004 | 0032S | | | | | | |
| DELX | R | /DIFF/ | 000000 | 0032S | | | | | | |
| DELY | R | /DIFF/ | 000002 | 0032S | | | | | | |
| DMINO | R | | 001372 | 0047M | 0048 | | | | | |
| DT2 | D | | 000000 | 0026S | | | | | | |
| DX2 | D | | 000000 | 0026S | | | | | | |
| DY2 | D | | 000000 | 0026S | | | | | | |
| EXIT | R | EXTERNAL | 000000 | 0099 | | | | | | |
| FFLAG | L | | 001374 | 0025S | 0074A | 0082A | | | | |
| FIXAV | R | EXTERNAL | 000000 | 0074 | | | | | | |
| FIXCM | R | EXTERNAL | 000000 | 0082 | | | | | | |
| FIXVL | R | EXTERNAL | 000000 | 0099 | | | | | | |
| FLAT | D | /MAP/ | 000006 | 0026S | 0028S | 0044M | | | | |
| FLON | D | /MAP/ | 000004 | 0026S | 0028S | 0044M | | | | |
| FTYPO | R | | 001375 | 0052M | 0060M | 0074A | 0077M | 0082A | 0100 | 0102 |
| FTYPE | R | | 001377 | 0058M | 0060 | 0062 | 0077 | | | |
| GETFIL | R | EXTERNAL | 000000 | 0036 | 0039 | 0040 | | | | |
| GMT | R | /TIMES/ | 000000 | 0029S | 0036I | 0068M | | | | |
| GMTO | R | | 000010 | 0036I | | | | | | |
| I | I | | 001401 | 0056M | 0062M | | | | | |
| IDAY | I | /TIMES/ | 000005 | 0029S | 0036I | 0058M | 0061 | 0062 | | |
| IDAYO | I | /TIMES/ | 000011 | 0029S | 0036I | 0044M | 0100 | 0102 | | |
| IHR | I | | 001403 | 0082A | 0094M | 0096 | 0097M | | | |
| IHRO | I | /TIMES/ | 000014 | 0029S | 0036I | 0044M | 0048 | 0100 | 0102 | |
| INNAM | I | | 000062 | 0034S | 0038A | 0041A | 0083A | | | |
| IRITE | I | | 001404 | 0044M | 0062 | 0071 | | | | |
| ISECO | I | | 000004 | 0036I | 0044M | 0046 | | | | |
| IYEAR | I | /TIMES/ | 000006 | 0029S | 0036I | 0058M | 0062 | | | |
| IYEARO | I | /TIMES/ | 000007 | 0029S | 0036I | 0044M | 0102 | | | |
| IYR | I | | 001405 | 0099A | 0100 | | | | | |
| LATM | I | /POSIT/ | 000000 | 0033S | 0100 | | | | | |
| LONM | I | /POSIT/ | 000003 | 0033S | 0100 | | | | | |
| LT | I | | 000132 | 0034S | 0058M | 0062 | 0066 | 0067 | 0068 | 0074A |
| | | | | 0082A | | | | | | |
| MIN | I | | 001406 | 0099A | 0100 | 0102 | | | | |
| MINO | I | | 000005 | 0036I | 0044M | 0047 | | | | |
| MINT | I | | 001407 | 0074A | 0082A | 0092 | 0093M | 0099A | | |
| MINTO | I | | 001410 | 0074A | | | | | | |
| MOY | I | /TIMES/ | 000004 | 0029S | 0036I | 0058M | 0062 | | | |
| MONO | I | /TIMES/ | 000010 | 0029S | 0036I | 0044M | 0100 | 0102 | | |
| MONTH | I | | 001411 | 0076A | 0071 | | | | | |
| NDAY | I | | 001412 | 0076A | 0071 | 0074A | | | | |
| NFIX | I | | 001413 | 0053M | 0074A | 0081 | 0082A | | | |
| NTIME | I | EXTERNAL | 000000 | 0070 | | | | | | |
| OUTNAM | I | | 000135 | 0024S | 0034A | 0042A | 0086A | | | |
| RAD | D | /MAP/ | 000010 | 0026S | 0028S | 0037I | | | | |
| RX | D | | 000000 | 0026S | | | | | | |
| RY | D | | 000000 | 0026S | | | | | | |
| SECO | R | | 001416 | 0046M | 0047 | | | | | |
| SMXSXM | D | | 000000 | 0026S | | | | | | |
| SUMT | D | /SUMS/ | 000010 | 0026S | 0031S | | | | | |
| SUMT2 | D | /SUMS/ | 000034 | 0026S | 0031S | | | | | |
| SUMX | D | /SUMS/ | 000000 | 0026S | 0031S | 0099A | 0102 | | | |

```
SUMX2   D /SUMS/   000024   0026S   0031S
SUMXT   D /SUMS/   000014   0026S   0031S
SUMY    D /SUMS/   000024   0026S   0031S   0099A   0102
SUMY2   D /SUMS/   000030   0026S   0031S
SUMYT   D /SUMS/   000020   0026S   0031S
SYM     D          000000   0026S
T0      R          000062   0035I
TFLAG   L          001420   0025S   0051M   0074A
TITLE   R          000205   0034S
TM      D          000000   0026S
TNHR    R          001421   0074A   0071    0074A
TNHR0   R /TIMES/  000012   0029S   0049M
TNHR1   R /TIMES/  000015   0029S   0050M
TZERO   R /TIMES/  000002   0029S   0048M
X0      D          000000   0026S
X0LAT   R /POSIT/  000001   0033S   0100
XLAT    R          001423   0058M   0062    0074A   0082A
XM      D          000000   0026S
Y0      D          000000   0026S
Y0LON   R /POSIT/  000004   0033S   0100
YLON    R          001425   0058M   0062    0074A   0082A
YM      D          000000   0026S

$I                 000460   0057D   0078
$100               001340   0044    0145D
$101               000527   0058    0059D
$102               001250   0100    0101D
$103               001330   0102    0103D
$1699              001117   0087    0089D
$1199              001071   0084    0085D
$19                001130   0081    0091D
$194               001155   0092    0095D
$195               001173   0096    0098D
$199               001054   0083D   0104
$200               000637   0062    0064D
$201               000750   0071    0072D
$99                001032   0061    0079D

0000 ERRORS [<.MAIN.>FTN-REV18.1]
```

## SUBROUTINE FIXAV(LT,TNHR,FFLAG,MINT,NFIX,TR1,XLAT,YLON,TFLAG,MINT0,NDAY)

```
      SUBROUTINE FIXAV (LT,TNHR,FFLAG,MINT,NFIX,TR1,XLAT,YLON,TFLAG,
     -                  MINT0,NDAY)
C*********************************************************************C
C                                                                     C
C     MAJOR SUBPROGRAM TO COMPUTE AVERAGE FIXES FROM POSITION DATA    C
C     AVERAGE FIXES ARE COMPUTED FOR EVEN MINUTES OF TIME             C
C     NUMBER OF INPUT POSITION DATA FOR EACH AVERAGE FIX MAY VARY     C
C     AVERAGE IS DONE BETWEEN 30 SECONDS BEFORE AND 29 SECONDS AFTER  C
C     THE AVERAGING MINUTE                                            C
C                                                                     C
C*********************************************************************C
      DOUBLE PRECISION  SUMX,SUMY,SUMT,SUMXT,SUMYT,SUMX2,SUMY2,SUMT2,
     -                  RAD,FLAT,FLON
      LOGICAL  FFLAG,TFLAG
      COMMON  /MAP/  FLAT,FLON,RAD
      COMMON  /SUMS/  SUMX,SUMY,SUMT,SUMXT,SUMYT,SUMX2,SUMY2,SUMT2
      COMMON  /TIMES/  GMT,TZERO,MON,IDAY,IYEAR,IYEARO,MONO,IDAYO,TNHRO,
     -                  IHRO,TNHR1
      COMMON  /POSIT/  LATM,XOLAT,LONM,YOLON
      DIMENSION  LT(3)
      IHR = LT(1)
C***  BEGIN BY FINDING THE APPROPRIATE MINUTE TO USE FOR THE AVERAGE FIX
      IF (TFLAG)  GO TO 30
      IF (TNHR - TNHR1)  11,12,13
   13 TNHR1 = TNHR
C***  TNHR IS GREATER THAN THE PREVIOUS FIX TIME (TNHR1), RESET TNHR1
      MINT = LT(2)
      ISEC30 = LT(3) + 30
      IF (ISEC30.GT.60) MINT = LT(2) + 1
      IF (ISEC30.GT.60)  GO TO 31
C***  NEW POSITION GOES WITH NEXT MINUTE FOR FIX, SO COMPUTE AVERAGE
C***  FIX FOR PREVIOUS MINUTE
      IF (IHR.GT.IHRO)  GO TO 33
      IF (MINT.EQ.MINTO.AND.NDAY.LE.0)  GO TO 32
   33 IF (NFIX.LE.1)  GO TO 39
      CALL FIXCM (FFLAG,NFIX,XLAT,YLON,LT,IHR,MINTO,TR1)
      TNHRO = TNHR
      MINTO = MINT
      IHRO = IHR
      IYEARO = IYEAR
      IDAYO = IDAY
      MONO = MON
      TZERO = GMT
      RETURN
   31 CONTINUE
      IF (IHR.GT.IHRO)  GO TO 33
      IF (MINT.GT.MINTO)  GO TO 33
      IF (NDAY.GE.1)  GO TO 33
   32 CALL SUMIT (FFLAG,NFIX,LT,XLAT,YLON)
C***  NEW POSITION DATUM IS FOR SAME MINUTE AS LAST ONE, SO ADD TO SUMS
      IF (MINT.LT.60)  GO TO 34
      MINT = 0
      IHR = IHR + 1
   34 CONTINUE
      IF (IHR.LT.24)  GO TO 35
      IHR = 0
   35 CONTINUE
      TZERO = GMT
```

```
      RETURN
   50 ISEC30 = LT(3) + 50
C***  FOR TIMES DURING THE FIRST HOUR OF THE CRUISE
      MINT = LT(2)
      IF (ISEC30.GT.60) MINT = LT(2) + 1
      MINT0 = MINT
      IHR0 = IHR
      IYEAR0 = IYEAR
      MON0 = MON
      IDAY0 = IDAY
      TZER0 = GMT
      TNHR1 = TNHR
      IF (NFIX.LE.0) FFLAG = .TRUE.
      TFLAG = .FALSE.
      GO TO 32
   11 WRITE (6,300)  IDAY,MON,IYEAR,(LT(I),I=1,3)
      RETURN
   12 WRITE (6,301)  IDAY,MON,IYEAR,(LT(I),I=1,3)
      RETURN
   39 CONTINUE
      IF (MINT.LT.60) GO TO 394
      MINT = 0
      IHR = IHR + 1
  394 CONTINUE
      IF (IHR.LT.24) GO TO 395
      IHR = 0
  395 CONTINUE
      CALL FIXVL (IYR,MINT0,MIN,SUMX,SUMY)
      WRITE (7,302) IDAY0,MON0,IYR,IHR0,MIN,LATM,XOLAT,LONM,YOLON,TR1
  302 FORMAT(I4,I2,I3,I5,6X,2I2,2(I4,F6.2),12X,A4)
      WRITE (6,303) IDAY0,MON0,IYEAR0,IHR0,MIN,SUMX,SUMY,TR1
  303 FORMAT(1X,3I2,2X,2I2,1X,2F10.5,5X,A4,5X,'SINGLE FIX INPUT')
      FFLAG = .TRUE.
      CALL SUMIT (FFLAG,NFIX,LT,XLAT,YLON)
      TNHR0 = TNHR
      MINT0 = MINT
      IHR0 = IHR
      IDAY0 = IDAY
      IYEAR0 = IYEAR
      MON0 = MON
      TZER0 = GMT
      RETURN
  300 FORMAT (1X,'NEGATIVE TIME CHANGE',3I2,2X,3I2)
  301 FORMAT (1X,'SAME TIME',3I2,2X,3I2)
      END
```

| | | | | | | | | | | |
|---|---|---|---|---|---|---|---|---|---|---|
| [illegible]FLAG | L | ARGUMENT | [illegible] | [illegible]106S | 0119S | 0141A | 0154A | 0176M | 0196M | 0197A |
| [illegible]XAV | R | [illegible] | 000003 | 0106S | | | | | | |
| [illegible]XCM | R | EXTERNAL | 000000 | 0191 | | | | | | |
| [illegible]XVL | R | EXTERNAL | 000000 | 0191 | | | | | | |
| [illegible]LAT | D | /MAP/ | [illegible] | 0117S | 0120S | | | | | |
| [illegible] | D | /MAP/ | 000004 | 0117S | 0120S | | | | | |
| [illegible]T | R | /TIMES/ | 000000 | 0122S | 0148 | 0163 | 0174 | 0204 | | |
| [illegible] | I | | 001173 | 0179M | 0181M | | | | | |
| [illegible]AY | I | /TIMES/ | 000005 | 0122S | 0146 | 0173 | 0179 | 0181 | 0201 | |
| [illegible]AYG | I | /TIMES/ | 000011 | 0122S | 0146M | 0173M | 0192 | 0194 | 0201M | |
| [illegible] | I | | 001172 | 0125M | 0138 | 0141A | 0144 | 0151 | 0158M | 0160 |
| | | | | 0161M | 0170 | 0186M | 0188 | 0189M | 0200 | |
| [illegible] | I | /TIMES/ | 000014 | 0122S | 0138 | 0144M | 0151 | 0170M | 0192 | 0194 |
| | | | | 0200M | | | | | | |
| [illegible]C30 | I | | 001173 | 0133M | 0134 | 0135 | 0165M | 0168 | | |
| [illegible]EAR | I | /TIMES/ | 000006 | 0122S | 0145 | 0171 | 0179 | 0181 | 0202 | |
| [illegible]ERO | I | /TIMES/ | 000007 | 0122S | 0145M | 0171M | 0194 | 0202M | | |
| [illegible] | I | | 001174 | 0191A | 0192 | | | | | |
| [illegible]TM | I | /POSIT/ | 000000 | 0124S | 0192 | | | | | |
| [illegible] | I | /POSIT/ | 000003 | 0124S | 0192 | | | | | |
| [illegible] | I | ARGUMENT | 000003 | 0106S | 0125S | 0126 | 0132 | 0133 | 0134 | 0141A |
| | | | | 0154A | 0165 | 0167 | 0168 | 0179 | 0181 | 0197A |
| [illegible] | I | | 001176 | 0191A | 0192 | 0194 | | | | |
| [illegible]T | I | ARGUMENT | 000006 | 0106S | 0132M | 0134M | 0139 | 0143 | 0152 | 0156 |
| | | | | 0157M | 0167M | 0168M | 0169 | 0184 | 0185M | 0199 |
| [illegible]NTO | I | ARGUMENT | 000014 | 0106S | 0139 | 0141A | 0143M | 0152 | 0169M | 0191A |
| | | | | 0199M | | | | | | |
| [illegible] | I | /TIMES/ | 000004 | 0122S | 0147 | 0172 | 0179 | 0181 | 0203 | |
| [illegible] | I | /TIMES/ | 000010 | 0122S | 0147M | 0172M | 0192 | 0194 | 0203M | |
| [illegible]AY | I | ARGUMENT | 000015 | 0106S | 0139 | 0153 | | | | |
| [illegible]IX | I | ARGUMENT | 000007 | 0106S | 0140 | 0141A | 0154A | 0176 | 0197A | |
| [illegible] | D | /MAP/ | 000010 | 0117S | 0120S | | | | | |
| [illegible]PIT | R | EXTERNAL | 000000 | 0154 | 0197 | | | | | |
| [illegible]PT | D | /SUMS/ | 000010 | 0117S | 0121S | | | | | |
| [illegible]PT2 | D | /SUMS/ | 000034 | 0117S | 0121S | | | | | |
| [illegible]MX | D | /SUMS/ | 000000 | 0117S | 0121S | 0191A | 0194 | | | |
| [illegible]PX2 | D | /SUMS/ | 000024 | 0117S | 0121S | | | | | |
| [illegible]PXT | D | /SUMS/ | 000014 | 0117S | 0121S | | | | | |
| [illegible]MY | D | /SUMS/ | 000004 | 0117S | 0121S | 0191A | 0194 | | | |
| [illegible]PY2 | D | /SUMS/ | 000030 | 0117S | 0121S | | | | | |
| [illegible]PYT | D | /SUMS/ | 000020 | 0117S | 0121S | | | | | |
| [illegible]FLAG | L | ARGUMENT | 000013 | 0106S | 0119S | 0128 | 0177M | | | |
| [illegible]PR | R | ARGUMENT | 000004 | 0106S | 0129 | 0130 | 0142 | 0175 | 0198 | |
| [illegible]NHR0 | R | /TIMES/ | 000012 | 0122S | 0142M | 0198M | | | | |
| [illegible]NHR1 | R | /TIMES/ | 000015 | 0122S | 0129 | 0130M | 0175M | | | |
| [illegible] | R | ARGUMENT | 000010 | 0106S | 0141A | 0192 | 0194 | | | |
| [illegible]ERO | R | /TIMES/ | 000002 | 0122S | 0148M | 0163M | 0174M | 0204M | | |
| [illegible]LAT | R | /POSIT/ | 000001 | 0124S | 0192 | | | | | |
| [illegible]T | R | ARGUMENT | 000011 | 0106S | 0141A | 0154A | 0197A | | | |
| [illegible]CON | R | /POSIT/ | 000004 | 0124S | 0192 | | | | | |
| [illegible] | R | ARGUMENT | 000012 | 0106S | 0141A | 0154A | 0197A | | | |
| [illegible] | | | 000474 | 0129 | 01790 | | | | | |
| [illegible] | | | 000534 | 0129 | 01810 | | | | | |
| [illegible] | | | 000040 | 0129 | 01300 | | | | | |
| [illegible] | | | 000537 | 0128 | 01650 | | | | | |
| [illegible]0 | | | 001124 | 0179 | 02060 | | | | | |
| [illegible]1 | | | 001150 | 0181 | 02070 | | | | | |

| | | | | | | |
|---|---|---|---|---|---|---|
| 0312 | 000714 | 0192 | 0193D | | | |
| 0313 | 000774 | 0194 | 0195D | | | |
| 0311 | 000230 | 0135 | 0150D | | | |
| 0312 | 000250 | 0139 | 0154D | 0178 | | |
| 0313 | 000127 | 0138 | 0148D | 0151 | 0152 | 0153 |
| 0314 | 000304 | 0156 | 0159D | | | |
| 0315 | 000322 | 0160 | 0162D | | | |
| 0319 | 000574 | 0140 | 0183D | | | |
| 0394 | 000621 | 0184 | 0187D | | | |
| 0395 | 000637 | 0188 | 0190D | | | |

0000 ERRORS [<FIXAV >FTN-REV1A.1]

# SUBROUTINE FIXCM(FFLAG,NFIX,XLAT,YLON,LT,IHR,MINT0,TR1)

```
      SUBROUTINE FIXCM (FFLAG,NFIX,XLAT,YLON,LT,IHR,MINT0,TR1)
C*****************************************************************C
C                                                                 C
C     SUBROUTINE COMPUTES AVERAGE FIX FROM POSITION DATA USING LEAST  C
C     SQUARES METHOD                                              C
C                                                                 C
C*****************************************************************C
      DOUBLE PRECISION  SUMX,SUMY,SUMT,SUMXT,SUMYT,SUMX2,SUMY2,SUMT2,
     - SMX,SMY,SXM,SYM,X0,Y0,DX2,DY2,DT2,XM,YM,TM,RX,RY,RAD,FLAT,FLON,
     - R2X,R2Y,SXT,SYT
      LOGICAL  FFLAG
      COMMON  /MAP/  FLAT,FLON,RAD
      COMMON  /SUMS/  SUMX,SUMY,SUMT,SUMXT,SUMYT,SUMX2,SUMY2,SUMT2
      COMMON  /TIMES/  GMT,TZERO,MON,IDAY,IYEAR,IYEARO,MONO,IDAYO,TNHRO,
     -                 IHRO,TNHR1
      COMMON  /DIFF/  DELX,DELY,DELT
      COMMON  /POSIT/  LATM,XOLAT,LONM,YOLON
      DIMENSION LT(3)
      DATA  RAD  / 1.745329251994330-02 /
      ISGNX = 1
      ISGNY = 1
      TM = SUMT/NFIX
      XM = SUMX/NFIX
      YM = SUMY/NFIX
      IF (NFIX.EQ.2)  GO TO 20
      DX2 = NFIX*SUMX2 - SUMX**2
      DY2 = NFIX*SUMY2 - SUMY**2
      DT2 = NFIX*SUMT2 - SUMT**2
      SXT = NFIX*SUMXT - SUMX*SUMT
      SYT = NFIX*SUMYT - SUMY*SUMT
      SMX = SXT/DT2
      IF (SMX.EQ.0.)  GO TO 290
      SXM = DX2/SXT
      IF (SXM.EQ.0.)  GO TO 290
      R2X = SMX/SXM
      IF (R2X.LT.0.)  ISGNX = -1
      RX = ISGNX * DSQRT (R2X*ISGNX)
  209 SMY = SYT/DT2
      IF (SMY.EQ.0.)  GO TO 291
      SYM = DY2/SYT
      IF (SYM.EQ.0.)  GO TO 291
      R2Y = SMY/SYM
      IF (R2Y.LT.0.)  ISGNY = -1
      RY = ISGNY * DSQRT (R2Y*ISGNY)
  210 X0 = XM - SMX*TM
      Y0 = YM - SMY*TM
      NFACT = NFIX*(NFIX-1)
      IF (NFACT.EQ.0) GO TO 299
      FSDX = DX2/NFACT
      FSDY = DY2/NFACT
      FSDT = DT2/NFACT
      SDX = ABS (FSDX)
      SDY = ABS (FSDY)
      SDT = ABS (FSDT)
      SIGX = SQRT (SDX)
      SIGY = SQRT (SDY)
      SIGT = SQRT (SDT)
      VX = SMX*FLAT
```

```
      VY = -SMY*FLON
      SMG = SQRT (VX**2 + VY**2)
C***   COMPUTE COURSE, SPEED MADE GOOD
      IF (VX.EQ.0.0.AND.VY.EQ.0.0)  VY = 1.0E-13
      CRS = ATAN2 (VX,VY)
      CMG = CRS/RAD
      IF (CMG.LT.0.0)  CMG = 360. + CMG
      CALL FIXVL (IYR,MINTO,MIN,XO,YO)
      WRITE (7,200) IDAYO,MONO,IYR,IHRO,MIN,LATM,XOLAT,LONM,YOLON,TR1
  200 FORMAT (1X,I2,I3,I5,6X,2I2,2(I4,F6.2),12X,A4)
      WRITE (6,201) IDAYO,MONO,IYEARO,IHRO,MIN,XO,YO,TR1,RX,RY,
     - SIGX,SIGY,SIGT,SMG,CMG,NFIX
      FFLAG = .TRUE.
      CALL SUMIT (FFLAG,NFIX,LT,XLAT,YLON)
  201 FORMAT (1X,3I2,2X,2I2,1X,2F10.5,5X,A4,5F10.6,2F10.3,2X,I5)
      RETURN
   20 CONTINUE
      VX = DELX/DELT
      VY = DELY/DELT
      XO = 0.5*((SUMX+DELX) - VX*(SUMT+DELT))
      YO = 0.5*((SUMY+DELY) - VY*(SUMT+DELT))
      SMG = SQRT (VX**2 + VY**2)
      IF (VX.EQ.0.0.AND.VY.EQ.0.0)  VY = 1.0E-13
      CRS = ATAN2 (VX,VY)
      CMG = CRS/RAD
      IF (CMG.LT.0.0)  CMG = 360. + CMG
      CALL FIXVL (IYR,MINTO,MIN,XO,YO)
      WRITE(7,200) IDAYO,MONO,IYR,IHRO,MIN,LATM,XOLAT,LONM,YOLON,TR1
      WRITE(6,203) IDAYO,MONO,IYEARO,IHRO,MIN,XO,YO,TR1,SMG,CMG
  203 FORMAT(1X,3I2,2X,2I2,1X,2F10.5,5X,A4,2F10.3,5X,'TWO POINTS')
      FFLAG = .TRUE.
      CALL SUMIT (FFLAG,NFIX,LT,XLAT,YLON)
      RETURN
  299 WRITE (1,202)
  202 FORMAT (5X,'ZERO IN DENOMINATOR OF FIXGM TERM')
      RETURN
C****  SMX,SXM .EQ. 0.0, SO ALL X'S ARE THE SAME IN THIS FIX AVERAGE
  290 RX = 1.0
      GO TO 209
C****  SMY,SYM .EQ. 0.0, SO ALL Y'S ARE THE SAME IN THIS FIX AVERAGE
  291 RY = 1.0
      GO TO 219
      END
```

| | | | | | | | | | | |
|---|---|---|---|---|---|---|---|---|---|---|
| ABS | R | EXTERNAL | 000000 | 0260 | 0261 | 0262 | | | | |
| ATAN2 | R | EXTERNAL | 000000 | 0271 | 0290 | | | | | |
| CAS | R | | 001662 | 0272M | 0273M | 0277 | 0291M | 0292M | 0295 | |
| CAS | R | | 001664 | 0271M | 0272 | 0290M | 0291 | | | |
| DELT | R | /DIFF/ | 000004 | 0224S | 0284 | 0285 | 0286 | 0287 | | |
| DELX | R | /DIFF/ | 000000 | 0224S | 0284 | 0286 | | | | |
| DELY | R | /DIFF/ | 000002 | 0224S | 0285 | 0287 | | | | |
| DSQRT | D | EXTERNAL | 000000 | 0245 | 0252 | | | | | |
| DX1 | D | | 001676 | 0216S | 0236M | 0239 | 0246 | 0259 | | |
| DX2 | D | | 001702 | 0216S | 0234M | 0241 | 0257 | | | |
| DY1 | D | | 001706 | 0216S | 0235M | 0248 | 0258 | | | |
| FFLAG | L | ARGUMENT | 000003 | 0209S | 0219S | 0279M | 0280A | 0297M | 0298A | |
| FLTCH | R | | 000003 | 0209S | | | | | | |
| FLXVL | R | EXTERNAL | 000000 | 0274 | 0293 | | | | | |
| FLAT | D | /MAP/ | 000000 | 0216S | 0220S | 0266 | | | | |
| FLON | D | /MAP/ | 000004 | 0216S | 0220S | 0267 | | | | |
| FSQT | R | | 001712 | 0259M | 0262A | | | | | |
| FSQX | R | | 001714 | 0257M | 0260A | | | | | |
| FSQY | R | | 001716 | 0258M | 0261A | | | | | |
| GMT | R | /TIMES/ | 000000 | 0222S | | | | | | |
| IDAY | I | /TIMES/ | 000005 | 0222S | | | | | | |
| IDAYO | I | /TIMES/ | 000011 | 0222S | 0275 | 0277 | 0294 | 0295 | | |
| IHR | I | ARGUMENT | 000010 | 0209S | | | | | | |
| IHRO | I | /TIMES/ | 000014 | 0222S | 0275 | 0277 | 0294 | 0295 | | |
| ISGNX | I | | 001723 | 0228M | 0244M | 0245 | | | | |
| ISGNY | I | | 001721 | 0229M | 0251M | 0252 | | | | |
| IYEAR | I | /TIMES/ | 000006 | 0222S | | | | | | |
| IYEARO | I | /TIMES/ | 000007 | 0222S | 0277 | 0295 | | | | |
| JYR | I | | 001722 | 0274A | 0275 | 0293A | 0294 | | | |
| LATM | I | /POSIT/ | 000000 | 0225S | 0275 | 0294 | | | | |
| LONM | I | /POSIT/ | 000003 | 0225S | 0275 | 0294 | | | | |
| LT | I | ARGUMENT | 000007 | 0209S | 0226S | 0280A | 0298A | | | |
| MIN | I | | 001724 | 0274A | 0275 | 0277 | 0293A | 0294 | 0295 | |
| MINTO | I | ARGUMENT | 000011 | 0209S | 0274A | 0293A | | | | |
| MON | I | /TIMES/ | 000004 | 0222S | | | | | | |
| MONO | I | /TIMES/ | 000010 | 0222S | 0275 | 0277 | 0294 | 0295 | | |
| NFACT | I | | 001725 | 0255M | 0256 | 0257 | 0258 | 0259 | | |
| NFIX | I | ARGUMENT | 000004 | 0209S | 0230 | 0231 | 0232 | 0233 | 0234 | 0235 |
| | | | | 0236 | 0237 | 0238 | 0255 | 0277 | 0280A | 0298A |
| NX | D | | 001730 | 0216S | 0243M | 0244 | 0245 | | | |
| NY | D | | 001734 | 0216S | 0250M | 0251 | 0252 | | | |
| NAO | D | /MAP/ | 000010 | 0216S | 0220S | 0271 | 0272 | 0291 | | |
| NX | D | | 001740 | 0216S | 0245M | 0277 | 0304M | | | |
| NY | D | | 001744 | 0216S | 0252M | 0277 | 0307M | | | |
| SOT | R | | 001750 | 0262M | 0265A | | | | | |
| SOX | R | | 001752 | 0260M | 0263A | | | | | |
| SOY | R | | 001754 | 0261M | 0264A | | | | | |
| SIGT | R | | 001756 | 0265M | 0277 | | | | | |
| SIGX | R | | 001760 | 0263M | 0277 | | | | | |
| SIGY | R | | 001762 | 0264M | 0277 | | | | | |
| SMG | R | | 001764 | 0268M | 0277 | 0288M | 0295 | | | |
| SMX | D | | 001766 | 0216S | 0239M | 0240 | 0243 | 0253 | 0266 | |
| SMY | D | | 001772 | 0216S | 0246M | 0247 | 0250 | 0254 | 0267 | |
| SQRT | R | EXTERNAL | 000000 | 0263 | 0264 | 0265 | 0268 | 0288 | | |
| SUMIT | R | EXTERNAL | 000000 | 0280 | 0298 | | | | | |
| SUMT | D | /SUMS/ | 000010 | 0216S | 0221S | 0230 | 0236 | 0237 | 0238 | 0286 |
| | | | | 0287 | | | | | | |
| SUMT2 | D | /SUMS/ | 000034 | 0216S | 0221S | 0236 | | | | |

```
SUMX    D /SJMS/   000000   0216S  0221S  0231   0234   0237   0286
SUMX2   D /SJMS/   000024   0216S  0221S  0234
SUMXT   D /SJMS/   000014   0216S  0221S  0237
SUMY    D /SJMS/   000004   0216S  0221S  0232   0235   0238   0287
SUMY2   D /SJMS/   000030   0216S  0221S  0235
SUMYT   D /SJMS/   000020   0216S  0221S  0238
SXM     D          001776   0216S  0241M  0242   0243
SXT     D          002002   0216S  0237M  0239   0241
SYM     D          002006   0216S  0248M  0249   0250
SYT     D          002012   0216S  0238M  0246   0248
TM      D          002016   0216S  0230M  0253   0254
TWHR0   R /TIMES/  000012   0222S
TWHR1   R /TIMES/  000015   0222S
TR1     R ARGUMENT 000012   0209S  0275   0277   0294   0295
TZERO   R /TIMES/  000002   0222S
VX      R          002022   0266M  0268   0270   0271A  0284M  0286   0288
                            0289   0290A
VY      R          002024   0267M  0268   0270M  0271A  0285M  0287   0288
                            0289M  0290A
XD      D          002026   0216S  0253M  0274A  0277   0286M  0293A  0295
XDLAT   R /POSIT/  000001   0225S  0275   0294
XDLAT   R ARGUMENT 000005   0209S  0280A  0298A
XM      D          002032   0216S  0231M  0253
YD      D          002036   0216S  0254M  0274A  0277   0287M  0293A  0295
YDLON   R /POSIT/  000004   0225S  0275   0294
YDLON   R ARGUMENT 000006   0209S  0280A  0298A
YM      D          002042   0216S  0232M  0254

S20                001167   0233   0283D
S200               001006   0275   0276D  0294
S201               001133   0277   0281D
S202               001602   0300   0301D
S203               001520   0295   0296D
S209               000320   0246D  0305
S210               000420   0253D  0308
S290               001630   0240   0242   0304D
S291               001645   0247   0249   0307D
S299               001572   0256   0300D

0000 ERRORS [<FIXCM >FTN-REV18.1]
```

# SUBROUTINE SUMIT(FFLAG,NFIX,LT,XLAT,YLON)

```
      SUBROUTINE SUMIT (FFLAG,NFIX,LT,XLAT,YLON)
C*****************************************************************C
C                                                                 C
C     SUBROUTINE SUMS POSITION DATA FOR LEAST SQUARES ANALYSIS    C
C                                                                 C
C*****************************************************************C
      DOUBLE PRECISION  SUMX,SUMY,SUMT,SUMXT,SUMYT,SUMX2,SUMY2,SUMT2,
     -                  XDLAT,YDLON
      LOGICAL  FFLAG
      COMMON  /SUMS/  SUMX,SUMY,SUMT,SUMXT,SUMYT,SUMX2,SUMY2,SUMT2
      COMMON  /TIMES/ GMT,TZERO,MON,IDAY,IYEAR,IYEARO,MONO,IDAYO,TNHRO,
     -                IHRO,TNHR1
      COMMON  /DIFF/  DELX,DELY,DELT
      DIMENSION  LT(3)
      IF (FFLAG) GO TO 50
   51 NFIX = NFIX + 1
      NT = LT(3)
      IF (NT.GE.30)  NT = NT-60
      XDLAT = DBLE (XLAT)
      YDLON = DBLE (YLON)
      SUMX = SUMX + XDLAT
      SUMY = SUMY + YDLON
      SUMT = SUMT + NT
      SUMXT = SUMXT + XDLAT*NT
      SUMYT = SUMYT + YDLON*NT
      SUMX2 = SUMX2 + XDLAT**2
      SUMY2 = SUMY2 + YDLON**2
      SUMT2 = SUMT2 + NT**2
      FFLAG = .FALSE.
      IF (NFIX.EQ.2)  GO TO 52
      RETURN
   52 CONTINUE
      DELX = -(SUMX - 2.*XLAT)
      DELY = -(SUMY - 2.*YLON)
      DELT = -(SUMT - 2.*NT)
      RETURN
   50 CONTINUE
C*** INITIALIZE SUMS FOR THE NEXT LINEAR REGRESSION
      SUMX = 0.
      SUMY = 0.
      SUMT = 0.
      SUMXT= 0.
      SUMYT= 0.
      SUMX2= 0.
      SUMY2= 0.
      SUMT2= 0.
      NFIX = 0
      GO TO 51
      END
```

| | | | | | | | | | | |
|---|---|---|---|---|---|---|---|---|---|---|
| JFLE | D | EXTERNAL | 000000 | 0328 | 0329 | | | | | |
| DELT | R | /DIFF/ | 000004 | 0322S | 0344M | | | | | |
| DELX | R | /DIFF/ | 000000 | 0322S | 0342M | | | | | |
| DELY | R | /DIFF/ | 000002 | 0322S | 0343M | | | | | |
| FFLAG | L | ARGUMENT | 000003 | 0310S | 0316S | 0324 | 0330M | | | |
| GMT | R | /TIMES/ | 000000 | 0320S | | | | | | |
| IDAY | I | /TIMES/ | 000005 | 0320S | | | | | | |
| IDAYO | I | /TIMES/ | 000011 | 0320S | | | | | | |
| IHRO | I | /TIMES/ | 000014 | 0320S | | | | | | |
| IYEAR | I | /TIMES/ | 000006 | 0320S | | | | | | |
| IYEARO | I | /TIMES/ | 000007 | 0320S | | | | | | |
| LT | I | ARGUMENT | 000005 | 0310S | 0323S | 0326 | | | | |
| MON | I | /TIMES/ | 000004 | 0320S | | | | | | |
| MONO | I | /TIMES/ | 000013 | 0320S | | | | | | |
| NFIX | I | ARGUMENT | 000004 | 0310S | 0325M | 0339 | 0356M | | | |
| NT | I | | 000413 | 0326M | 0327M | 0332 | 0333 | 0334 | 0337 | 0344 |
| SUMIT | R | | 000000 | 0310S | | | | | | |
| SUMT | D | /SUMS/ | 000010 | 0316S | 0319S | 0332M | 0344 | 0350M | | |
| SUMT2 | D | /SUMS/ | 000034 | 0316S | 0319S | 0337M | 0355M | | | |
| SUMX | D | /SUMS/ | 000000 | 0316S | 0319S | 0330M | 0342 | 0348M | | |
| SUMX2 | D | /SUMS/ | 000024 | 0316S | 0319S | 0335M | 0353M | | | |
| SUMXT | D | /SUMS/ | 000014 | 0316S | 0319S | 0333M | 0351M | | | |
| SUMY | D | /SUMS/ | 000004 | 0316S | 0319S | 0331M | 0343 | 0349M | | |
| SUMY2 | D | /SUMS/ | 000030 | 0316S | 0319S | 0336M | 0354M | | | |
| SUMYT | D | /SUMS/ | 000020 | 0316S | 0319S | 0334M | 0352M | | | |
| TNHRO | R | /TIMES/ | 000012 | 0320S | | | | | | |
| TNHR1 | R | /TIMES/ | 000015 | 0320S | | | | | | |
| TZERO | R | /TIMES/ | 000002 | 0320S | | | | | | |
| XDLAT | D | | 000414 | 0316S | 0328M | 0330 | 0333 | 0335 | | |
| XLAT | R | ARGUMENT | 000006 | 0310S | 0328A | 0342 | | | | |
| YDLON | D | | 000420 | 0316S | 0329M | 0331 | 0334 | 0336 | | |
| YLON | R | ARGUMENT | 000007 | 0310S | 0329A | 0343 | | | | |
| $50 | | | 000312 | 0324 | 0346D | | | | | |
| $51 | | | 000613 | 0325D | 0357 | | | | | |
| $52 | | | 000236 | 0339 | 0341D | | | | | |

0000 ERRORS [<SUMIT>FTN-KLV10.1]

## SUBROUTINE NTIME(MONTH,NDAY,TNHR)

```
      SUBROUTINE NTIME (MONTH,NDAY,TNHR)
C*****************************************************************C
C     SUBROUTINE COMPUTES THE TOTAL NUMBER OF HOURS (TNHR) SINCE THE   C
C     START OF CRUISE                                                  C
C*****************************************************************C
      COMMON  /TIMES/  GMT,TZERO,MON,IDAY,IYEAR,IYEARO,MONO,IDAYO,TNHRO,
     -                 IHRO,TNHR1
      DIMENSION LMON (12)
      DATA  LMON / 31, 31, 28, 31, 30, 31, 30, 31, 31, 30, 31, 30 /
      LMON(3) = 28
      TLEAP = (IYEAR)/4.
      ILEAP = IFIX (TLEAP)
      IF (TLEAP - ILEAP .EQ. 0.0)  LMON(3) = 29
      MONTH = (IYEAR-IYEARO)*12 + MON-MONO
      NDAY = MONTH*LMON(MON) + IDAY-IDAYO
      TNHR = NDAY*24 + GMT-TZERO + TNHR1
      RETURN
      END
```

```
GMT     R /TIMES/  000000   0364S  0374
IDAY    I /TIMES/  000005   0364S  0373
IDAYO   I /TIMES/  000011   0364S  0373
IFIX    I EXTERNAL 000000   0370
IHRO    I /TIMES/  000014   0364S
ILEAP   I          000132   0370M  0371
IYEAR   I /TIMES/  000006   0364S  0369   0372
IYEARO  I /TIMES/  000007   0364S  0372
LMON    I          000007   0366S  0367I  0368M  0371M  0373
MON     I /TIMES/  000004   0364S  0372   0373
MONO    I /TIMES/  000010   0364S  0372
MONTH   I ARGUMENT 000003   0359S  0372M  0373
NDAY    I ARGUMENT 000004   0359S  0373M  0374
NTIME   I          000000   0359S
TLEAP   R          000133   0369M  0370   0371
TNHR    R ARGUMENT 000005   0359S  0374M
TNHRO   R /TIMES/  000012   0364S
TNHR1   R /TIMES/  000015   0364S  0374
TZERO   R /TIMES/  000002   0364S  0374

0000 ERRORS [<NTIME >FTN-REV18.13
```

## SUBROUTINE FIXVL(IYR,MINT0,MIN,X0,Y0)

```
      SUBROUTINE  FIXVL (IYR,MINT0,MIN,X0,Y0)
C*****************************************************************************C
C
C     COMPUTES THE LAT AND LONG IN GDC FORMAT
C
C*****************************************************************************C
      DOUBLE PRECISION  X0,Y0
      COMMON  /TIMES/  GMT,TZERO,MON,IDAY,IYEAR,IYEAR0,MON0,IDAY0,TNHR0,
     -                 IHR0,TNHR1
      COMMON  /POSIT/  LATM,X0LAT,LONM,Y0LON
C
      IYR = IYEAR0 + 1900
      MIN = MINT0
      LATM = IFIX (X0)
      X0LAT = (X0 - LATM)*60.
      LONM = -IFIX (Y0)
      Y0LON = -(Y0 + LONM)*60.
      RETURN
      END
```

```
FIXVL   R           000000   0377S
GMT     R /TIMES/   000000   0384S
IDAY    I /TIMES/   000005   0384S
IDAYO   I /TIMES/   000011   0384S
IFIX    I EXTERNAL  000000   0390    0392
IHRO    I /TIMES/   000014   0384S
IYEAR   I /TIMES/   000006   0384S
IYEARO  I /TIMES/   000007   0384S   0388
IYR     I ARGUMENT  000003   0377S   0388M
LATM    I /POSIT/   000000   0386S   0390M   0391
LONM    I /POSIT/   000003   0386S   0392M   0393
MIN     I ARGUMENT  000005   0377S   0389M
MINTO   I ARGUMENT  000004   0377S   0389
MON     I /TIMES/   000004   0384S
MONO    I /TIMES/   000010   0384S
TNHRO   R /TIMES/   000012   0384S
TNHR1   R /TIMES/   000015   0384S
TZERO   R /TIMES/   000002   0384S
X0      D ARGUMENT  000006   0377S   0383S   0390    0391
XOLAT   R /POSIT/   000001   0386S   0391M
Y0      D ARGUMENT  000007   0377S   0383S   0392    0393
YOLON   R /POSIT/   000004   0386S   0393M

0000 ERRORS [<FIXVL >FTN-REV18.1]
```

# APPENDIX A.3

## FORTRAN Subroutine GETFIL to Input Filenames Interactively.

```
      SUBROUTINE GETFIL (JMES,N,INNAM)
C.... SUBROUTINE GETFIL.  GETS TRFNAM (UP TO 80 CHARS) FROM USER.  RESULTS
C.... STORED IN COMMON.  NAMLEN IS NAME LENGTH IN CHARACTERS
C.... DON ALTMAN
C.... 28 MAY 82

      COMMON /FILES/ NAMLEN
      DIMENSION IMES(8),JMES(1),INNAM(40)
      LOGICAL GOODNM,RNAMSA

      NAMLEN = 8.
      NLIM = N/2

      DO 5 I = 1,NLIM
    5 IMES(I) = JMES(I)

      IF (NLIM .GE. 8) GO TO 20
      NLIM = NLIM + 1

      DO 10 I = NLIM,8
   10 IMES(I) = '  '

   20 WRITE (1,100) (IMES(J),J=1,8)
      GOODNM = RNAMSA(0,0,1,INNAM,NAMLEN)
      IF (.NOT. GOODNM) GO TO 20
      RETURN

  100 FORMAT (5X,'ENTER ',8A2,' FILE (.LE. 80 CHARS)')

      END                                                          GETFIL
```

```
GETFIL R              00000   0001S
GOODNM L              00146   0009S   0024M   0025
I      I              00147   0014M   0015    0020M   0021
IMES   I              000007   0008S   0015M   0021M   0023
INNAM  I ARGUMENT     00005   0001S   0008S   0024A
J      I              00151   0023M
JMES   I ARGUMENT     000003   0001S   0008S   0015
N      I ARGUMENT     00004   0001S   0012
NAMLEN I /FILES/      000000   0007S   0011M   0024A
NLIM   I              00152   0012M   0014    0017    0018M   0020
RNAM$A L EXTERNAL     000000   0009S   0024

$1                    000052   0020    0021D
$1 J                  00117   0023    0028D
$2                    000063   0017    0023D   0025
$5                    000027   0014    0015D

0000 ERRORS [<GETFIL>FTN-REV18.1]
```

# APPENDIX A.4

## FORTRAN Program HYPRIN to Convert GDC Format Data to SMFIX Input Format

```
C      PROGRAM  HYPRIN (INPUT,OUTPUT,TAPE5=INPUT,TAPE6=OUTPUT)
C
C      CONVERTS GDCOUT DATA TO HYPERMAP INPUT DATA FORMAT                C
C      DEGREES MINUTES TO DECIMAL DEGREES                                C
C                                                                        C
       INTEGER  OUTNAM (40)
       DIMENSION  INNAM (40)
       CALL GETFIL ('INPUT ',6,INNAM)
       CALL GETFIL ('OUTPUT',6,OUTNAM)
       CALL CONTRL (1,INNAM,5)
       CALL CONTRL (2,OUTNAM,6)
C
    1  READ (5,101) IDAY,MONTH,IYR,LHR,MIN,LATM,PAMNM,NLON,
     *POMNM,TR1
  101  FORMAT (I3,I3,I5,I8,I2,2(I4,F6.2),12X,A4)
C
       IF (IDAY.LE.0) GO TO 99
C
       IYEAR = IYR - 1900
       XLAT = LATM - PAMNM/60.
       YLON = NLON - POMNM/60.
C
       WRITE (6,102) IDAY,MONTH,IYEAR,LHR,MIN,XLAT,YLON,TR1
  102  FORMAT (3I2,2X,2I2,3X,2F10.4,5X,A4)
       GO TO 1
C
   99  CALL CONTRL (4,INNAM,5)
       WRITE (6,109)
  109  FORMAT (39X,'FINIS')
       CALL CONTRL (4,OUTNAM,6)
       CALL EXIT
       END
```

```
CONTRL  R EXTERNAL 000000   0010   0011   0027   0030
EXIT    R EXTERNAL 000001   0031
GETFIL  R EXTERNAL 000000   0008   0009
IDAY    I          000373   0013M  0017   0023
INNAM   I          000002   0007S  0008A  0010A  0027A
IYEAR   I          000374   0019M  0023
IYR     I          000375   0013M  0019
LATM    I          000376   0013M  0020
LHR     I          000377   0013M  0023
MIN     I          000400   0013M  0023
MONTH   I          000401   0013M  0023
NLON    I          000402   0013M  0021
OUTNAM  I          000052   0006S  0009A  0011A  0030A
PAMNM   R          000403   0013M  0022
POMNM   R          000405   0013M  0021
TR1     R          000411   0013M  0023
XLAT    R          000413   0023M  0023
YLON    R          000415   0021M  0023

$1                 000146   0013D  0025
$101               000210   0013   0015D
$102               000324   0023   0024D
$109               000355   0028   0029D
$99                000344   0017   0027D

0000 ERRORS [<,MAIN,>FTN-REV18.13
```

# NOTES

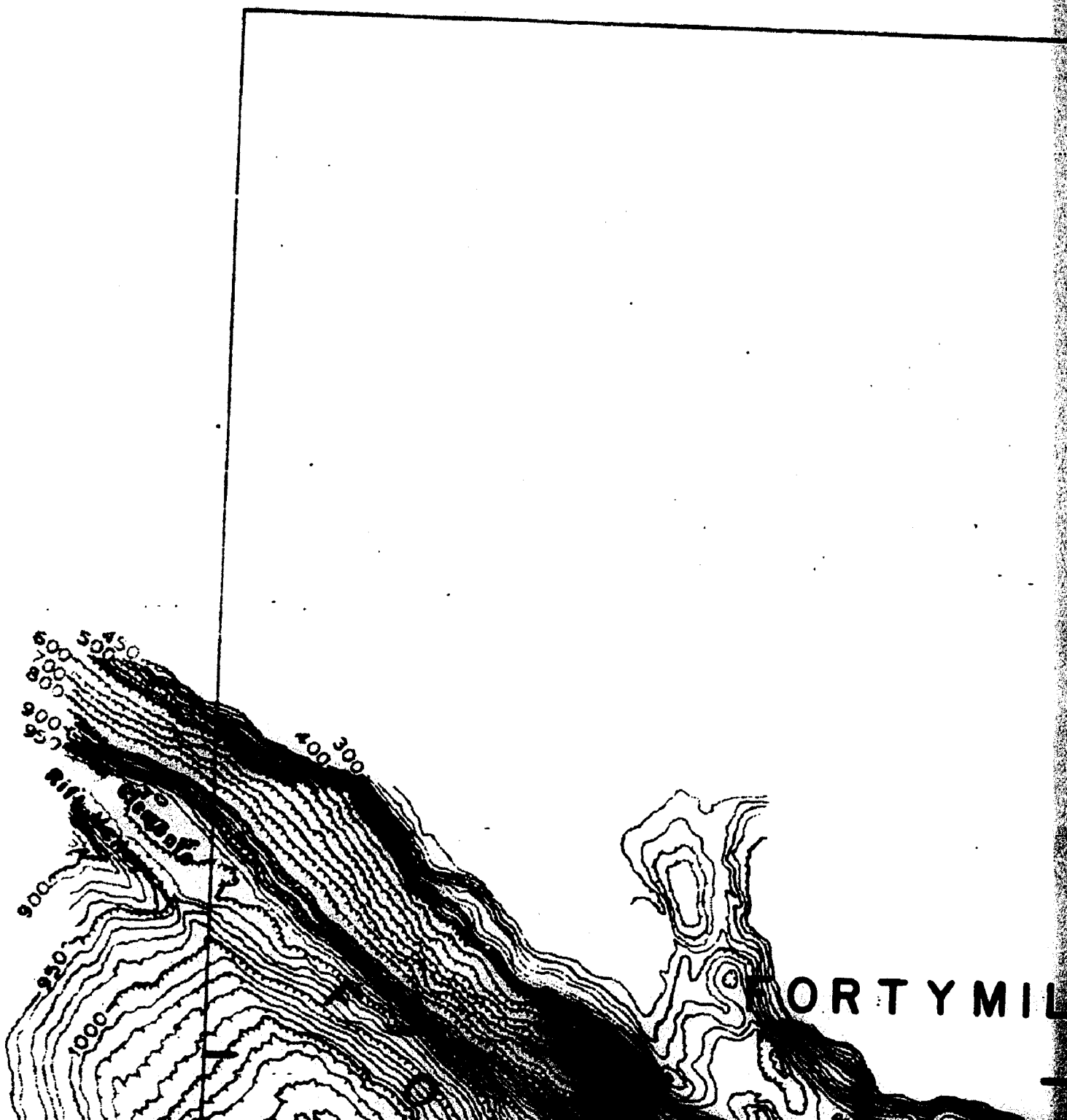
600
500
450
700
800
900
950
400
300
900
950
1000
FORTYMIL

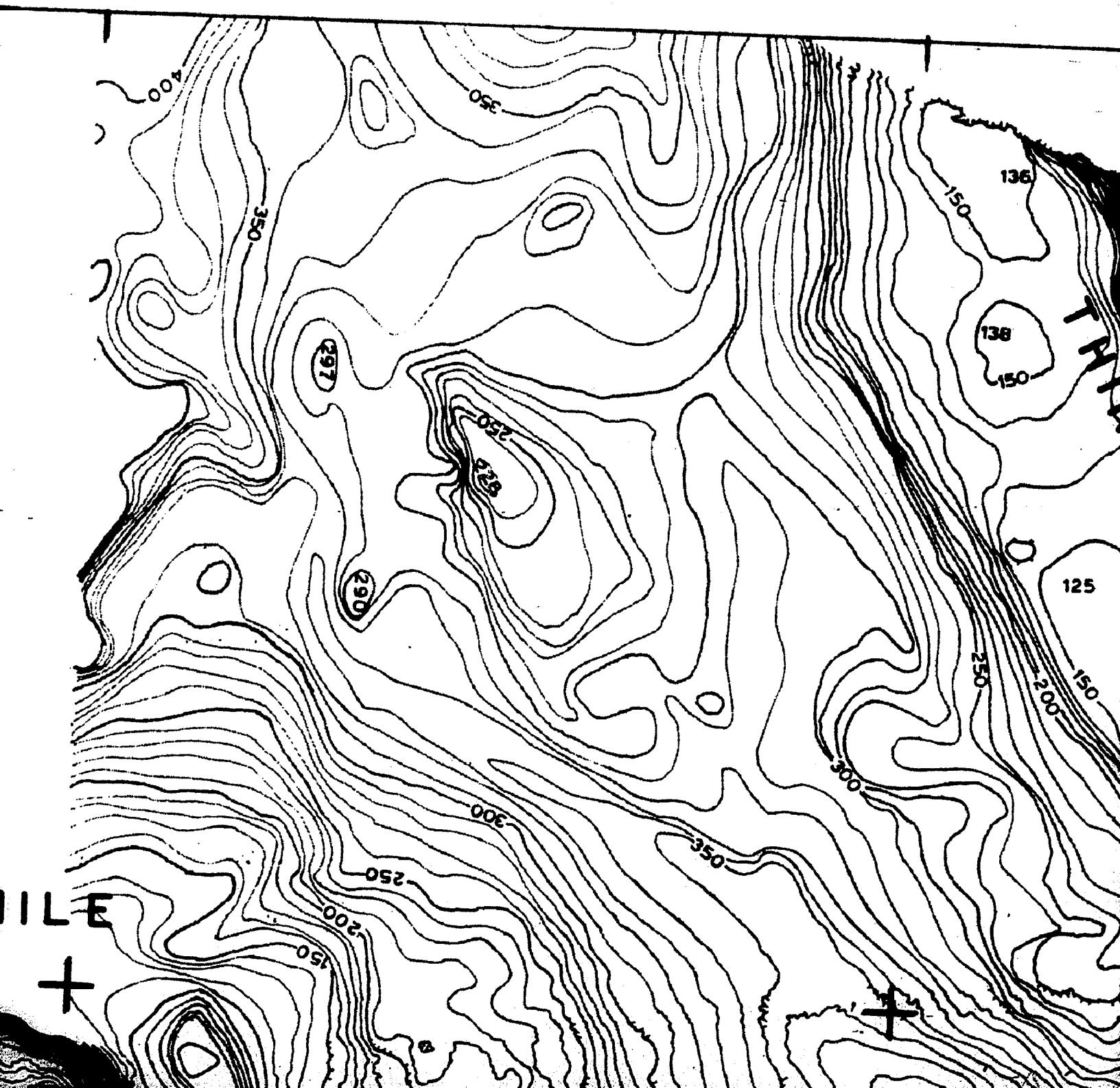

400
350
350
136
150
138
150
297
250
228
290
125
250
200
150
300
300
350
250
200
150
ILE

# INNER CALIFORN

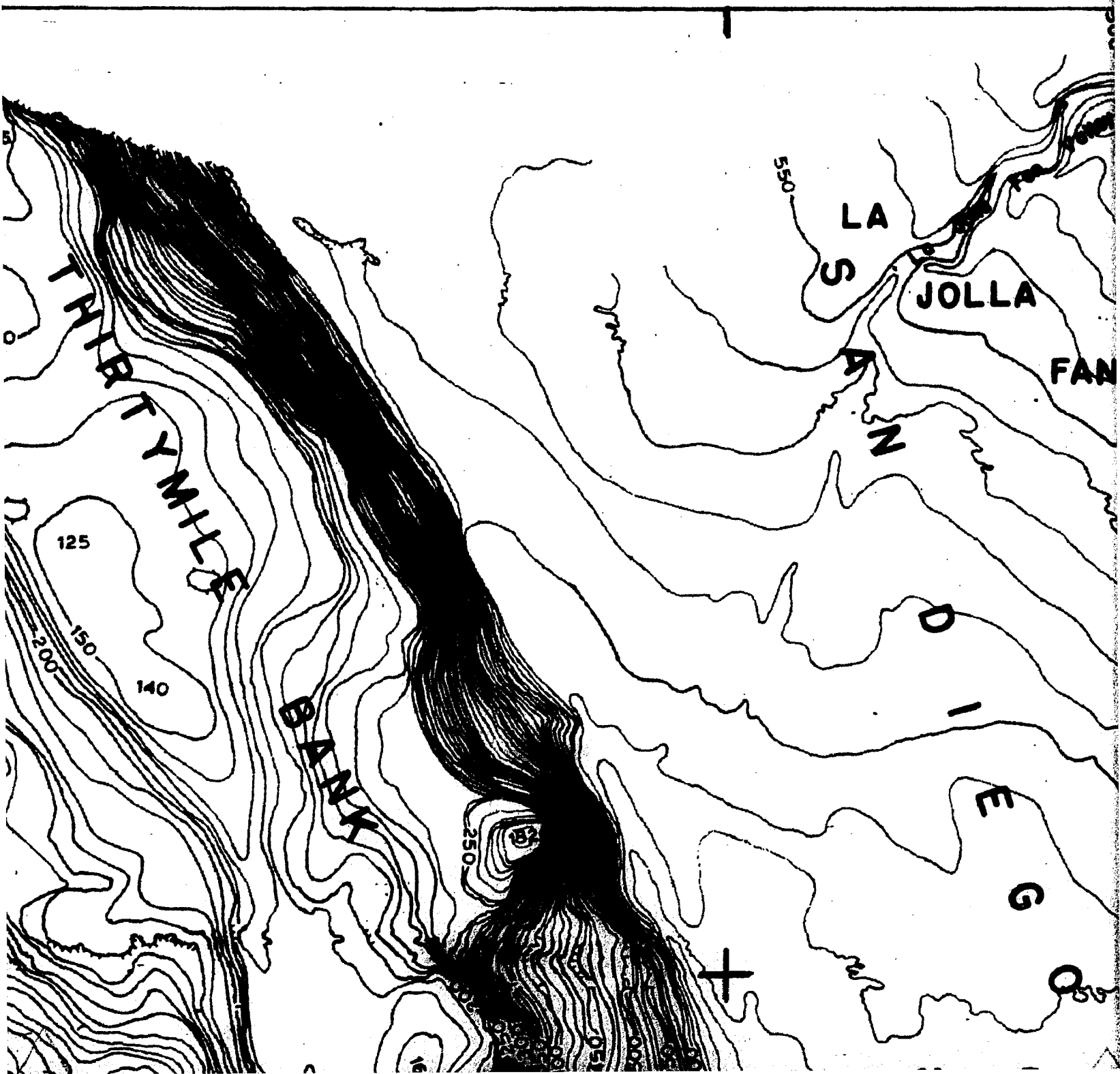

# NIA CONTINENTAL BO

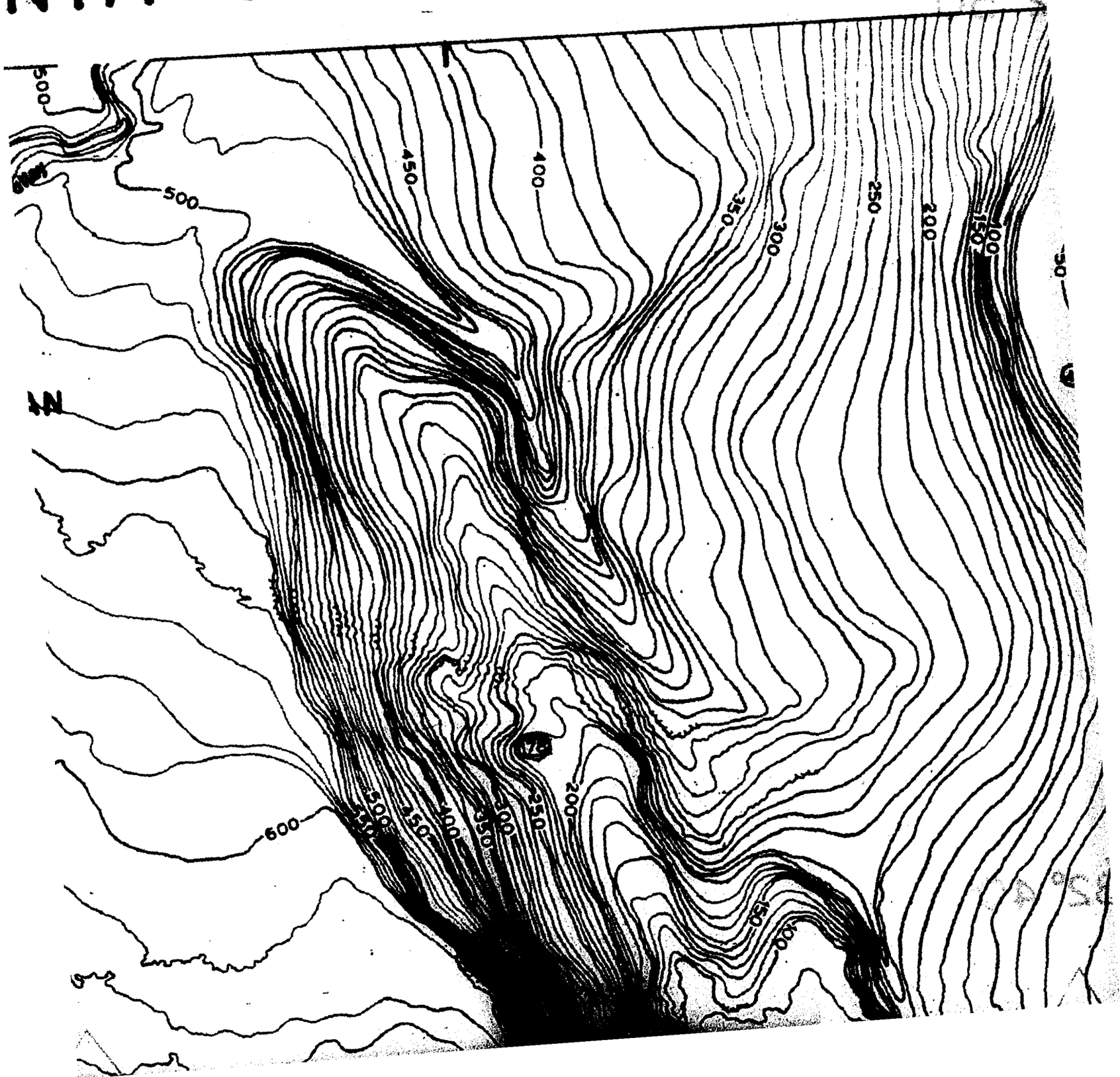

# ORDERLAND

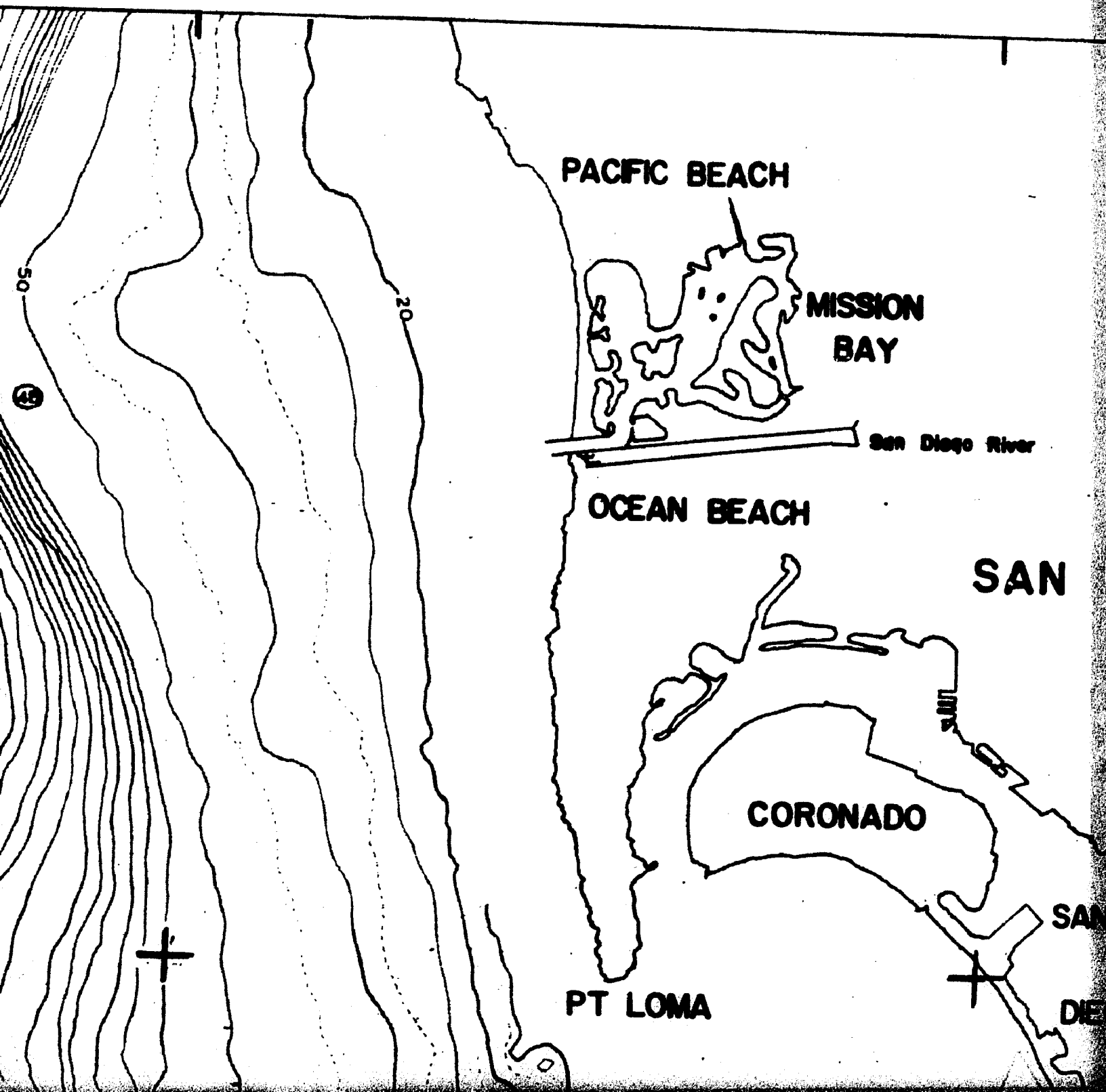
PACIFIC BEACH
MISSION
BAY
San Diego River
OCEAN BEACH
SAN
CORONADO
PT LOMA
50
20
45

# PLATE 1A
# BATHYMETRY

N DIEGO

0 5

STATUTE MILES

0 1 2 3 4 5

NAUTICAL MILES

0 5 10

KILOMETERS

## MERCATOR PROJECTION

CONTOUR INTERVAL 10 FATHOMS
(UNCORRECTED)

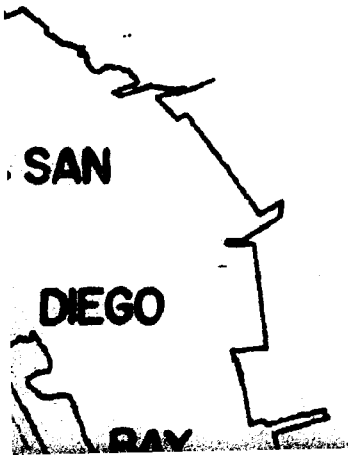

32° 50'

E 1A

METRY

10

MILES

10

. MILES

10

ETERS

PROJECTION

AL 10 FATHOMS
ECTED)

32° 40'

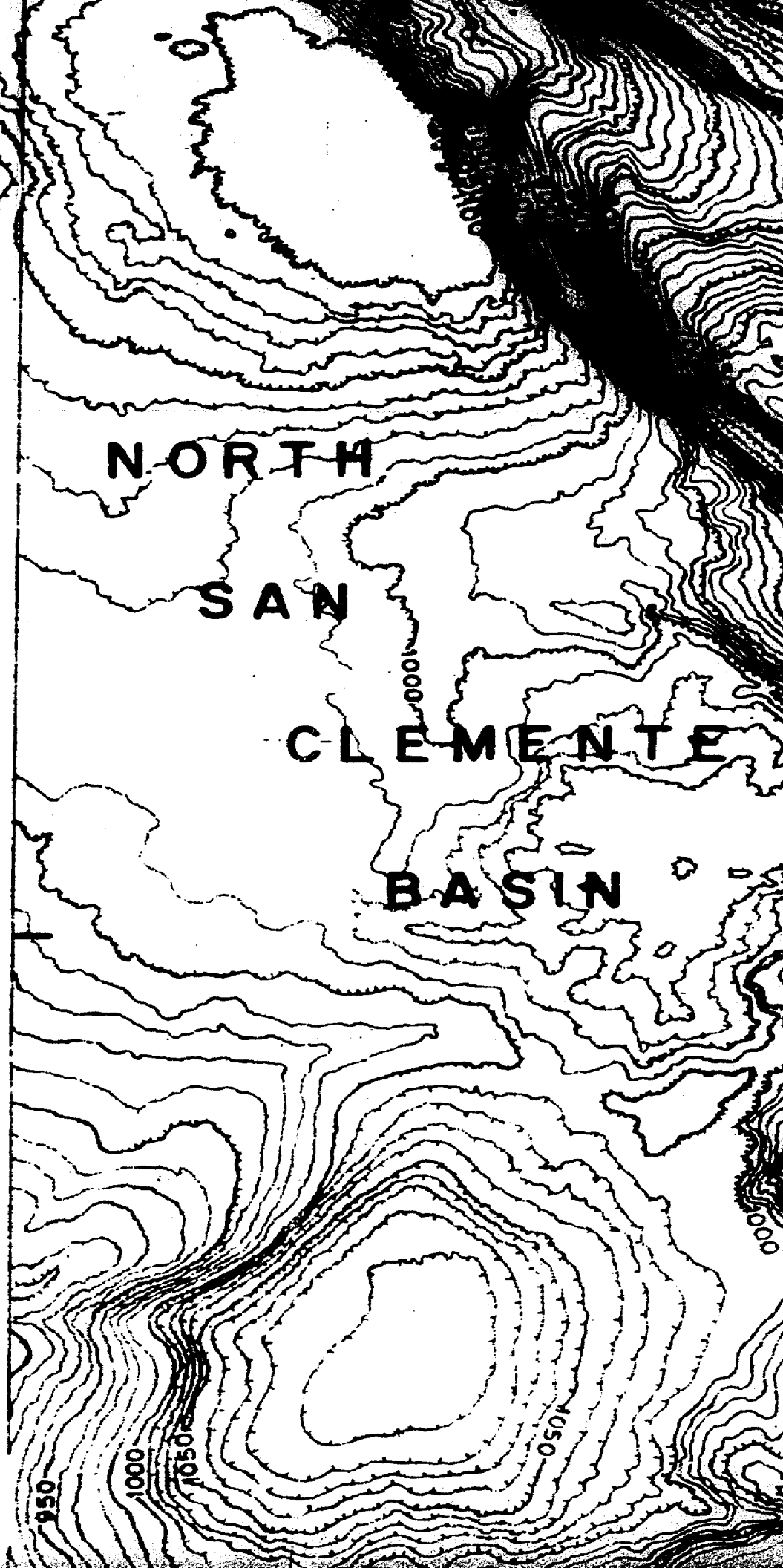
NORTH
SAN
CLEMENTE
BASIN
1000
1000
1050
1050
1000
950

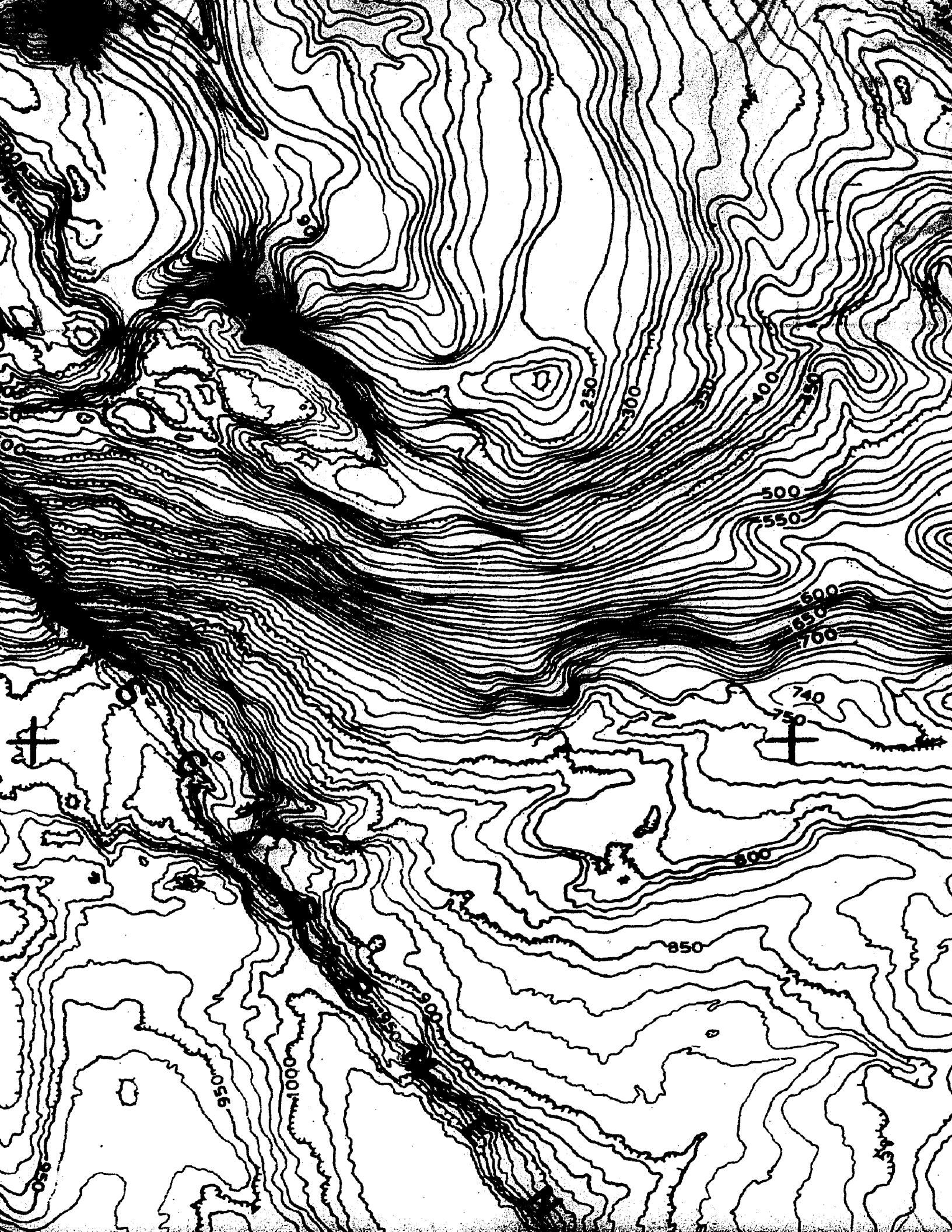
250
300
350
400
450
500
550
600
650
700
740
750
800
850
900
950
1000
950

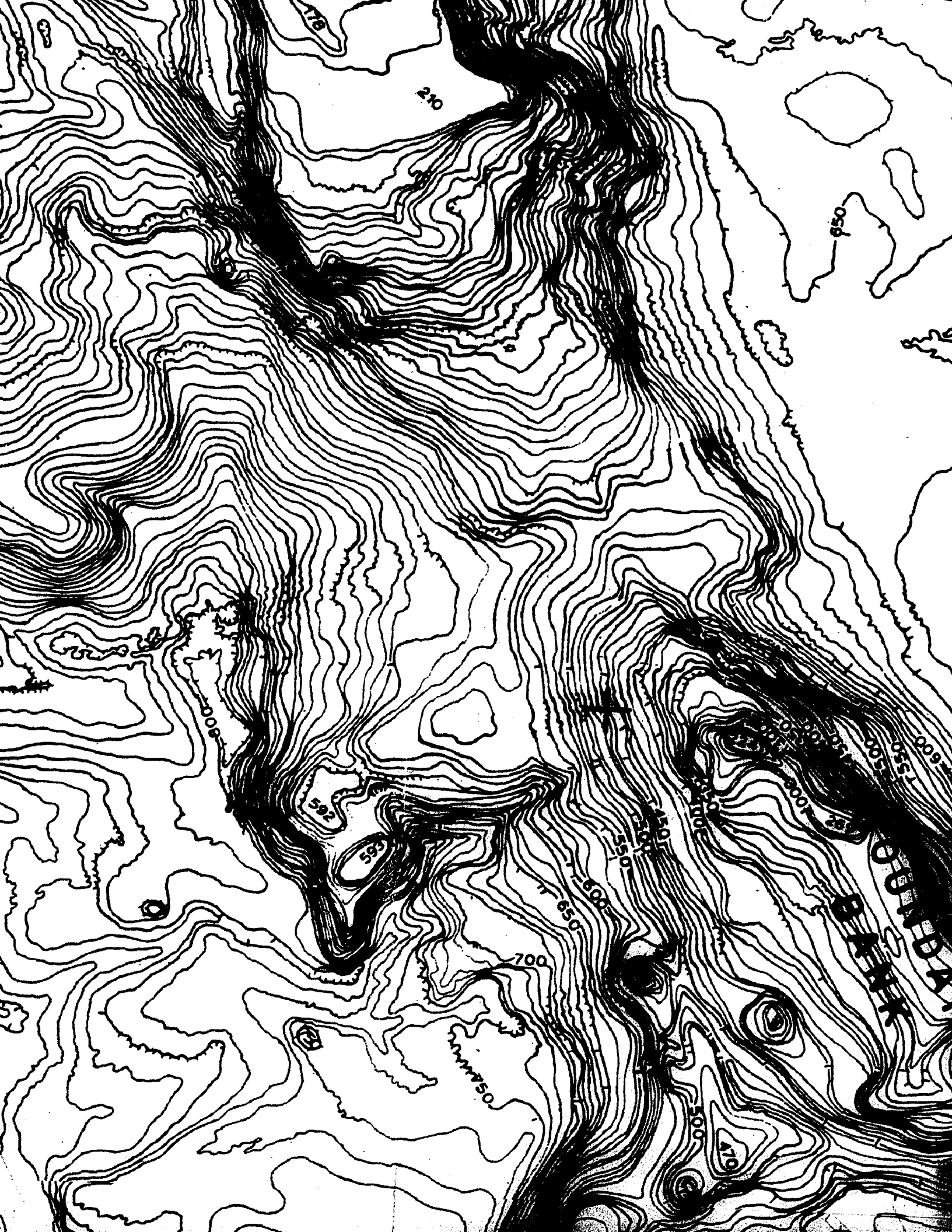

178
210
650
800
592
593
700
650
600
550
500
450
470

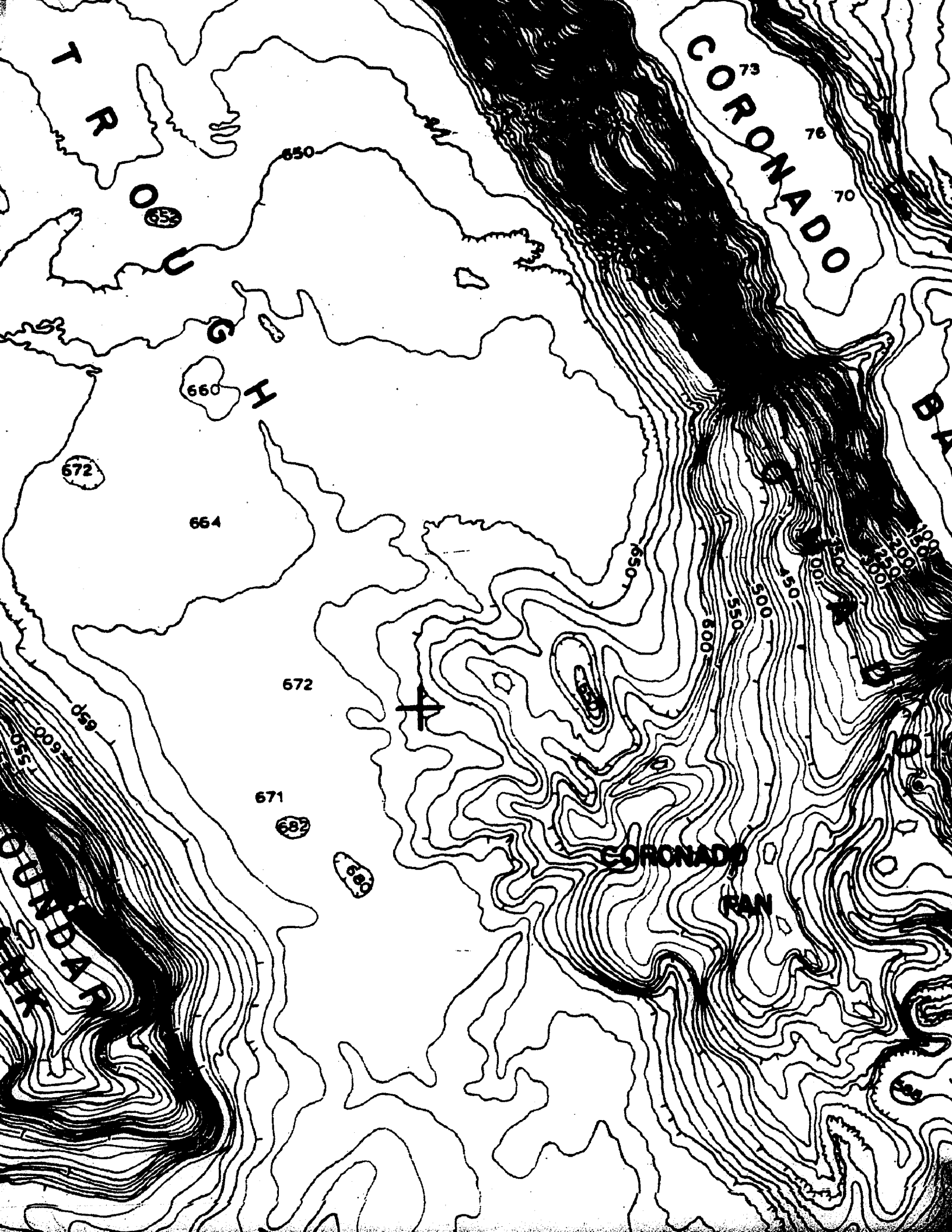

TROUGH
CORONADO
73
76
70
650
652
660
672
664
672
671
682
680
650
600
550
500
450
CORONADO
FAN

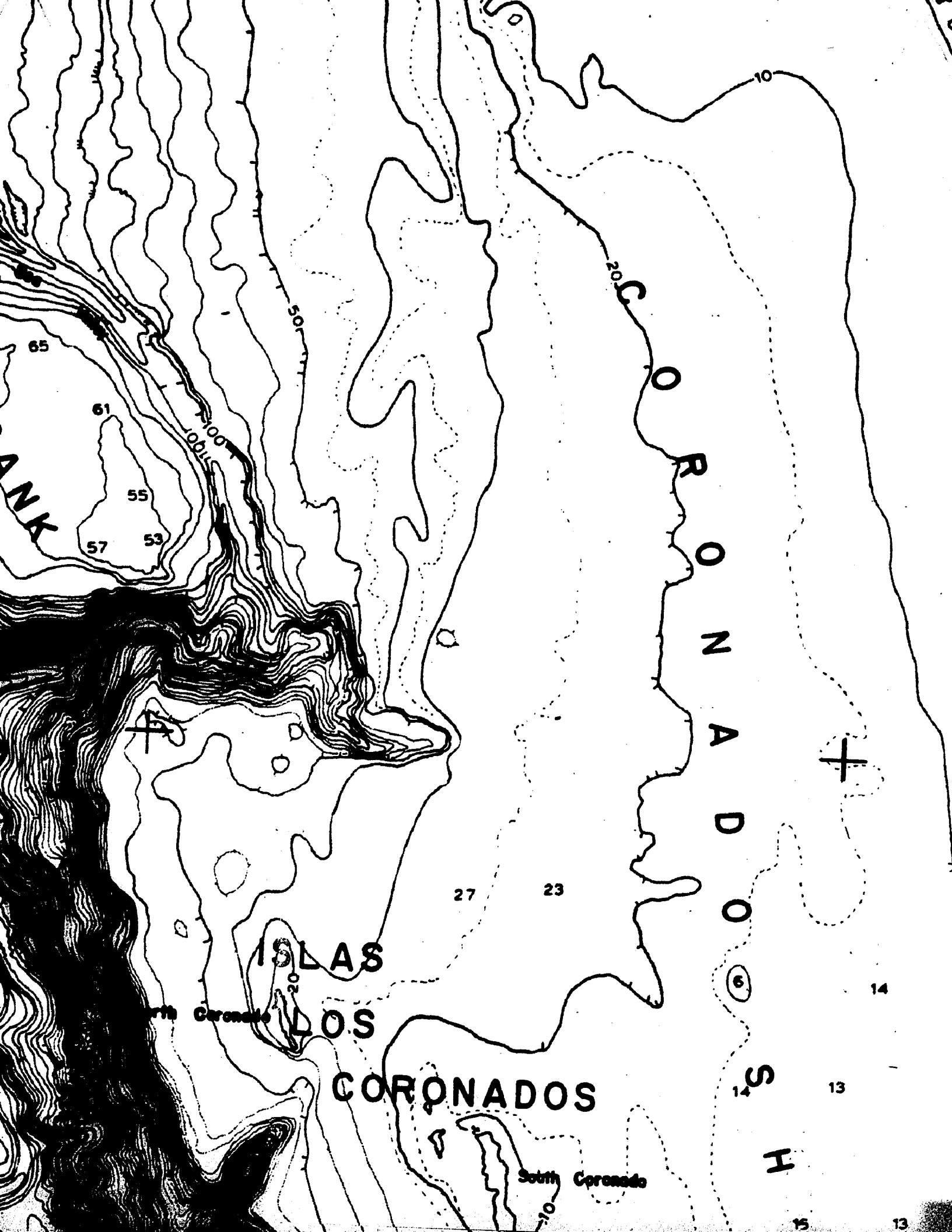

CORONADO
ISLAS
LOS
CORONADOS
South Coronado
ANK
65
61
55
57
53
27
23
6
14
13
15
10
20
50
100

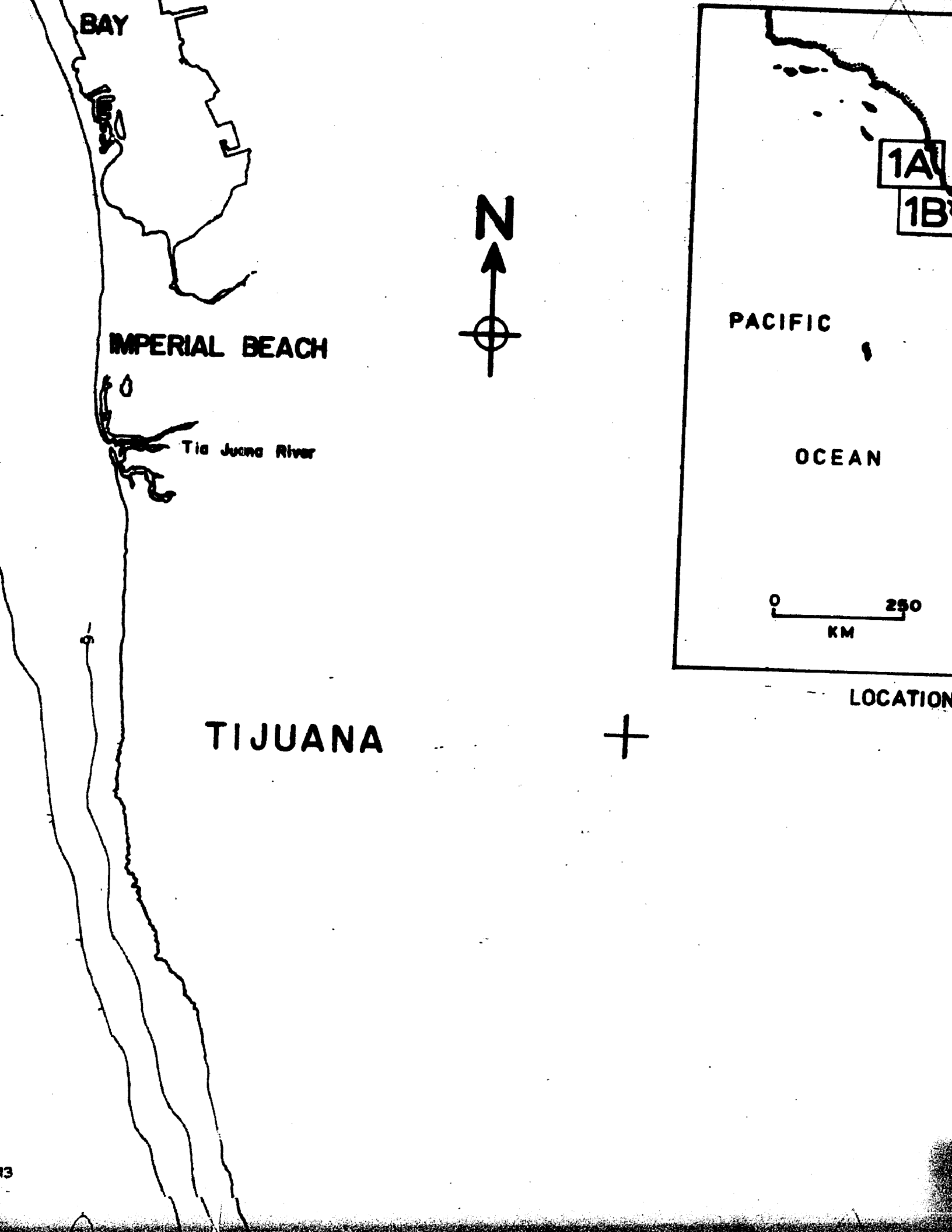
BAY
IMPERIAL BEACH
Tia Juana River
TIJUANA
N
1A
1B
PACIFIC
OCEAN
0
250
KM
LOCATION

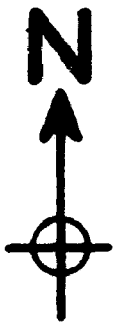


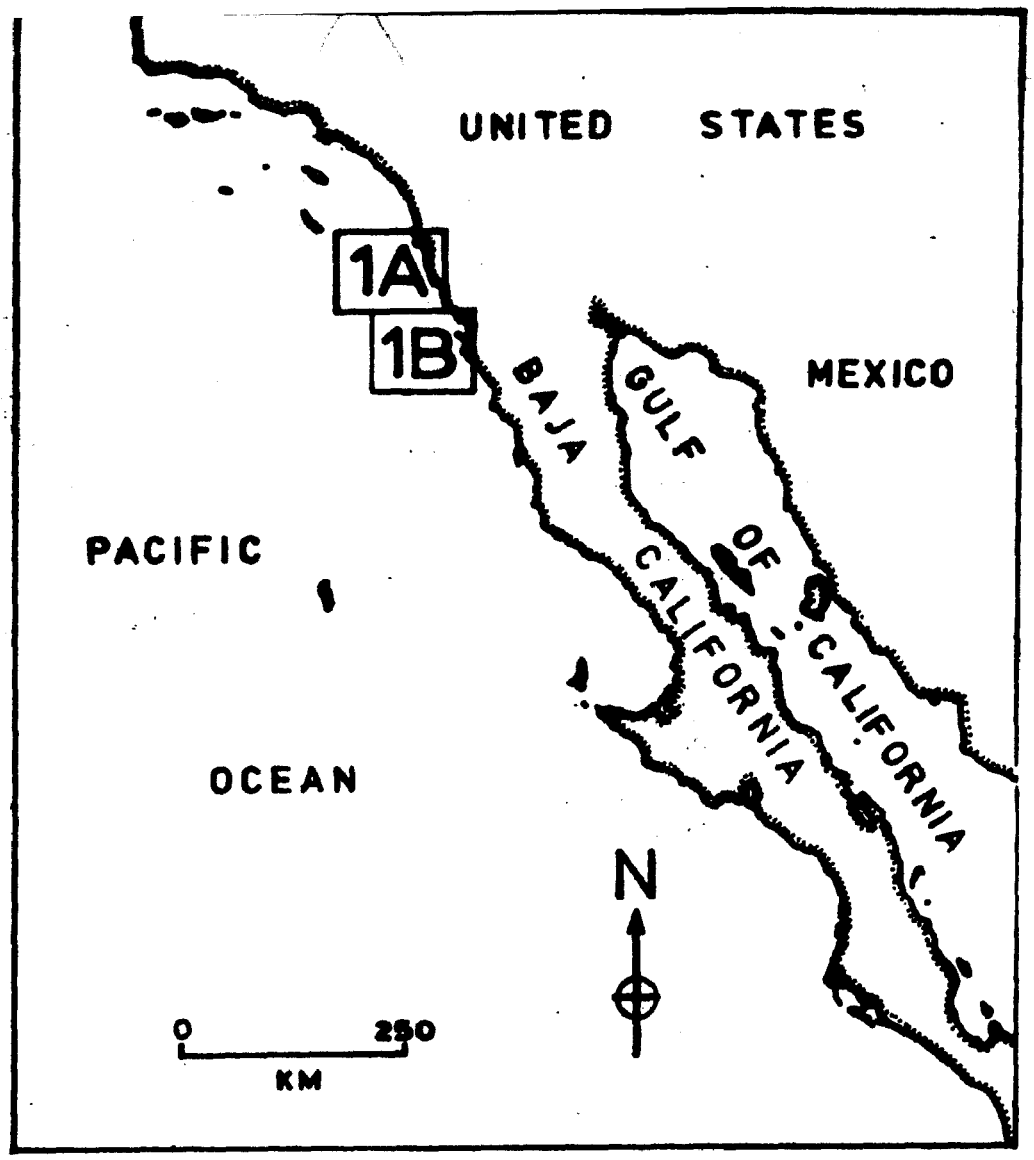


LOCATION OF PLATES

32'

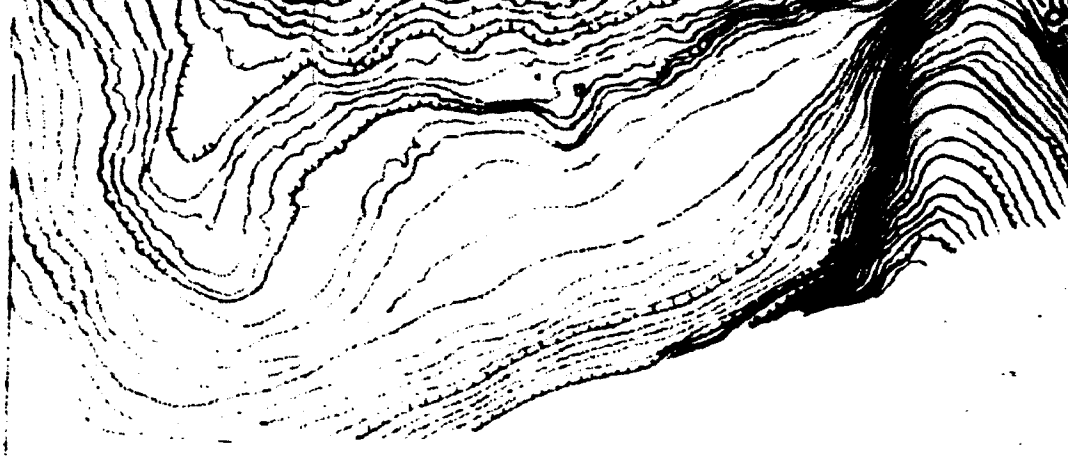

# BLAKE KNOLLS

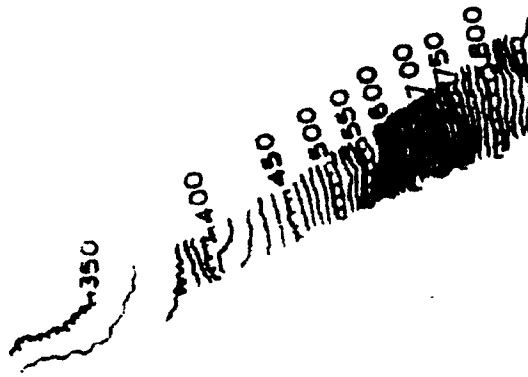

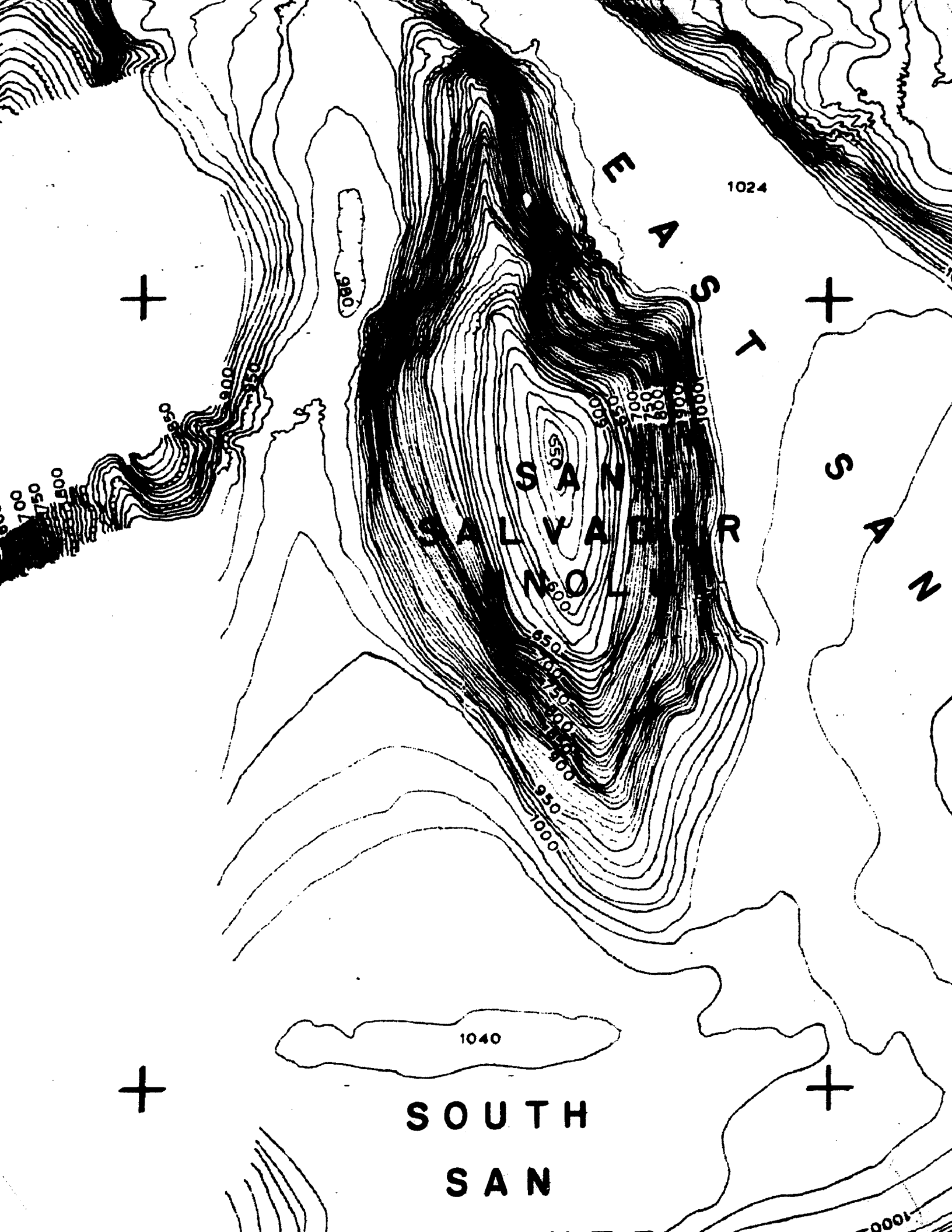

EAST SAN
SAN SALVADOR
1024
980
1040
SOUTH SAN

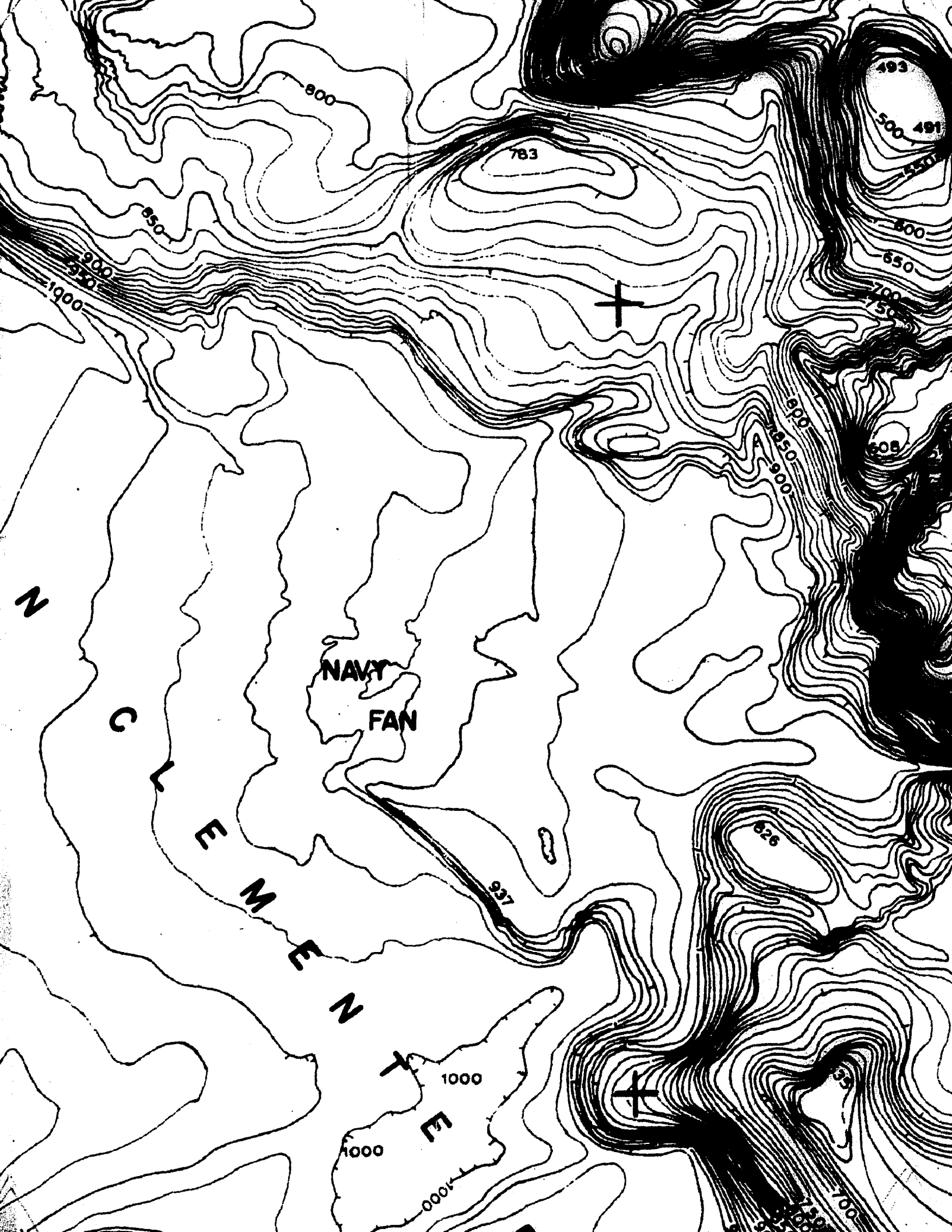

493
500
491
800
783
850
900
950
1000
600
650
700
750
800
850
900
608
NAVY
FAN
N
C
L
E
M
E
N
T
E
937
826
1000
1000
1000
700

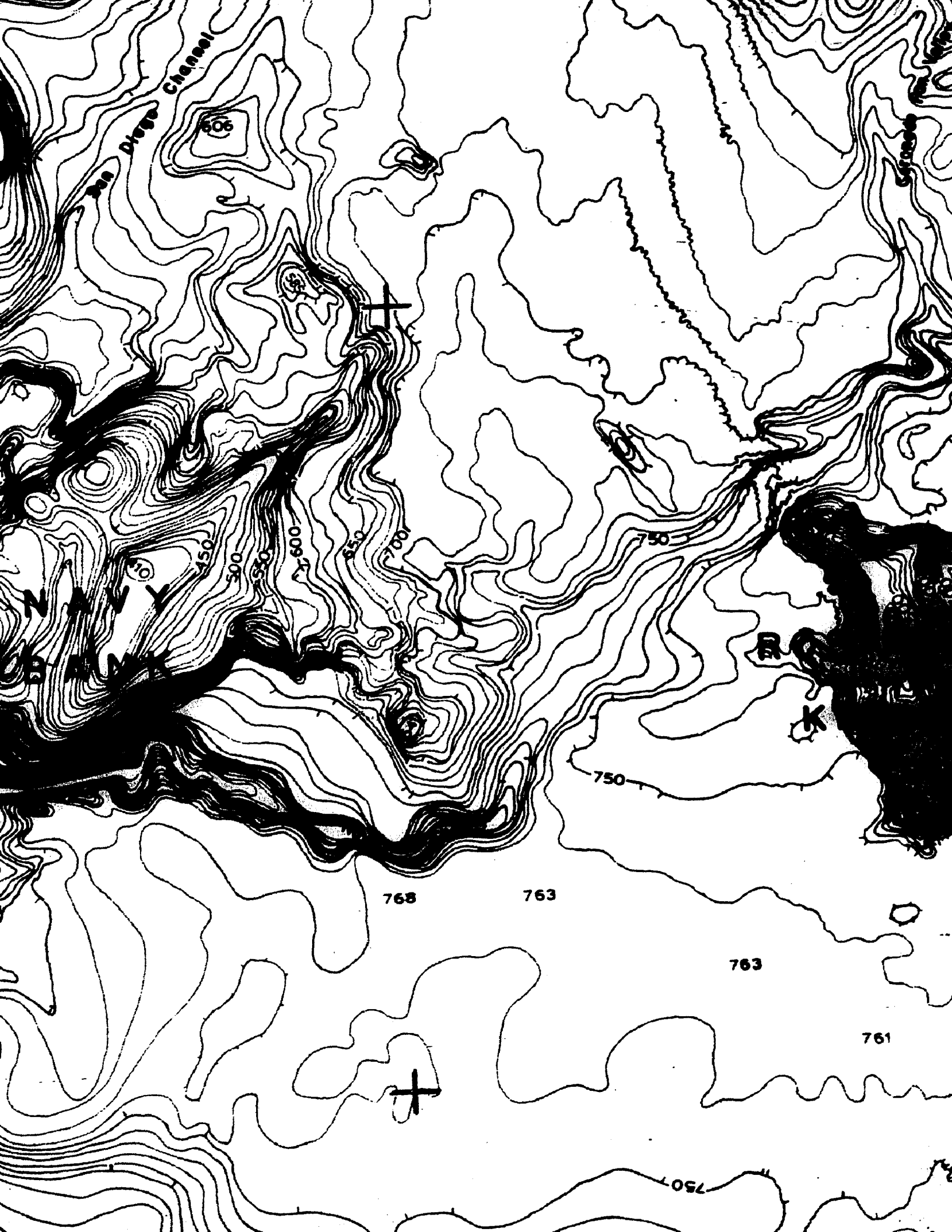
San Diego Channel
606
450
500
550
600
650
700
750
768
763
763
761
750

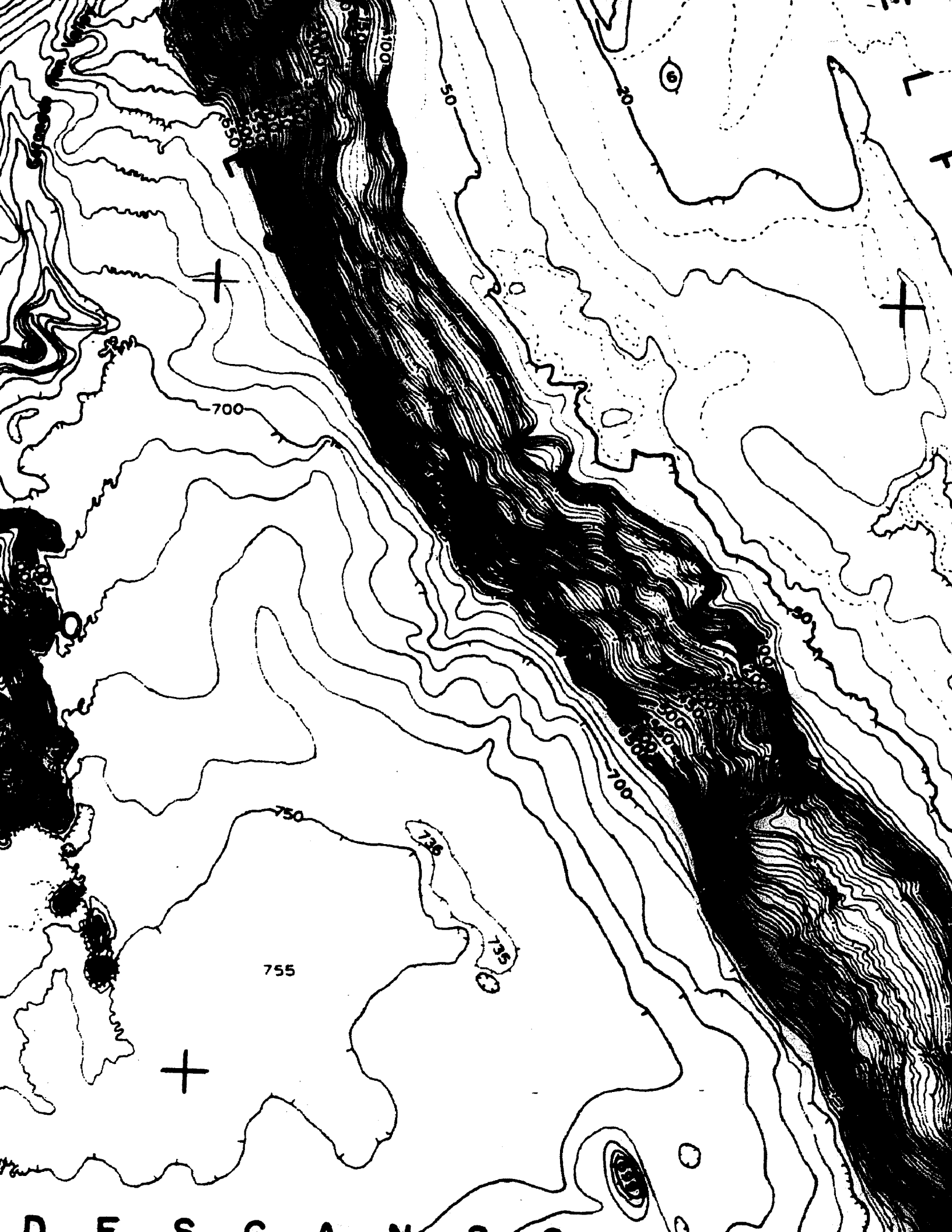

700
750
736
735
755
50
20
6

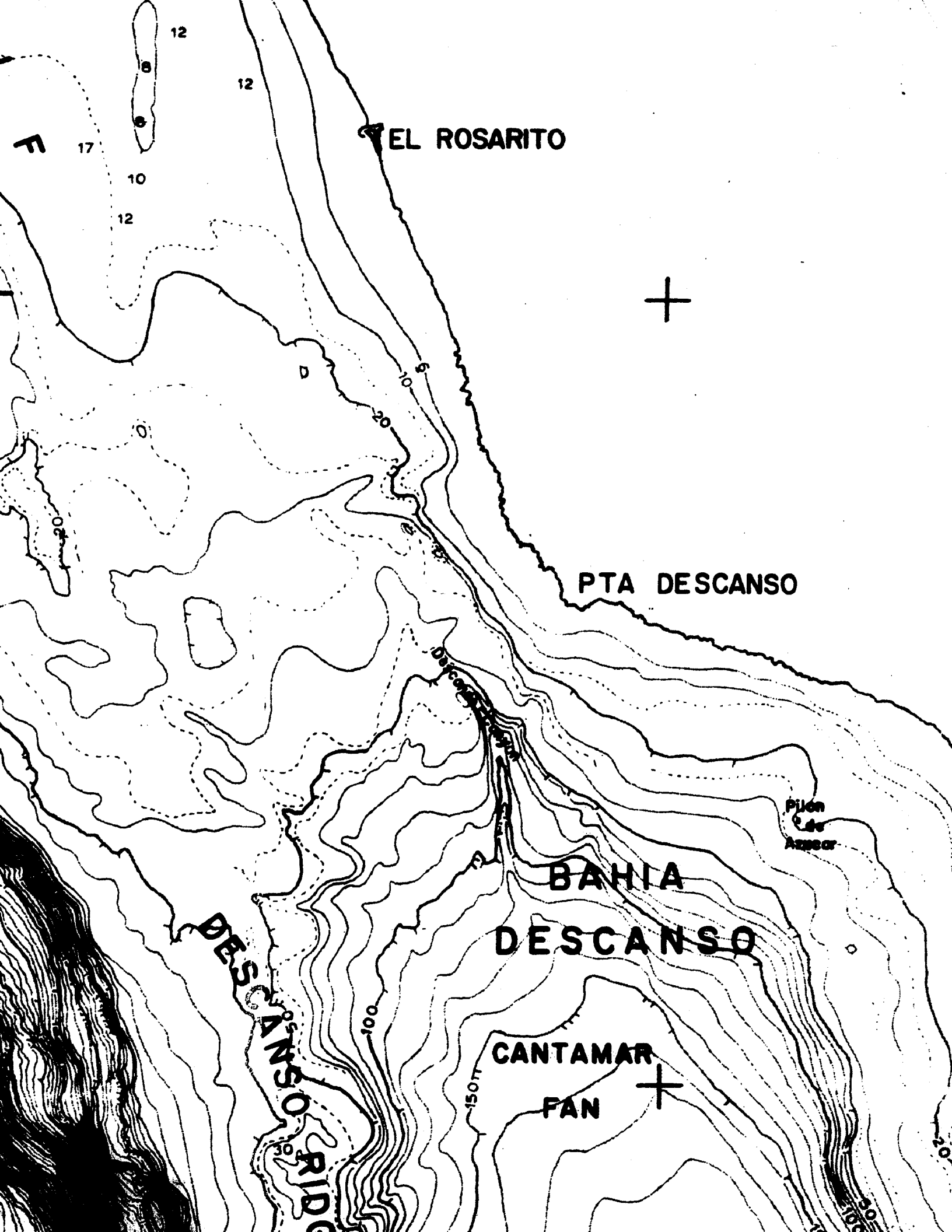
EL ROSARITO
PTA DESCANSO
BAHIA
DESCANSO
CANTAMAR
FAN
DESCANSO RIDG
Pilón
de
Azucar
12
8
12
17
10
12
6
10
20
20
100
150
30
20

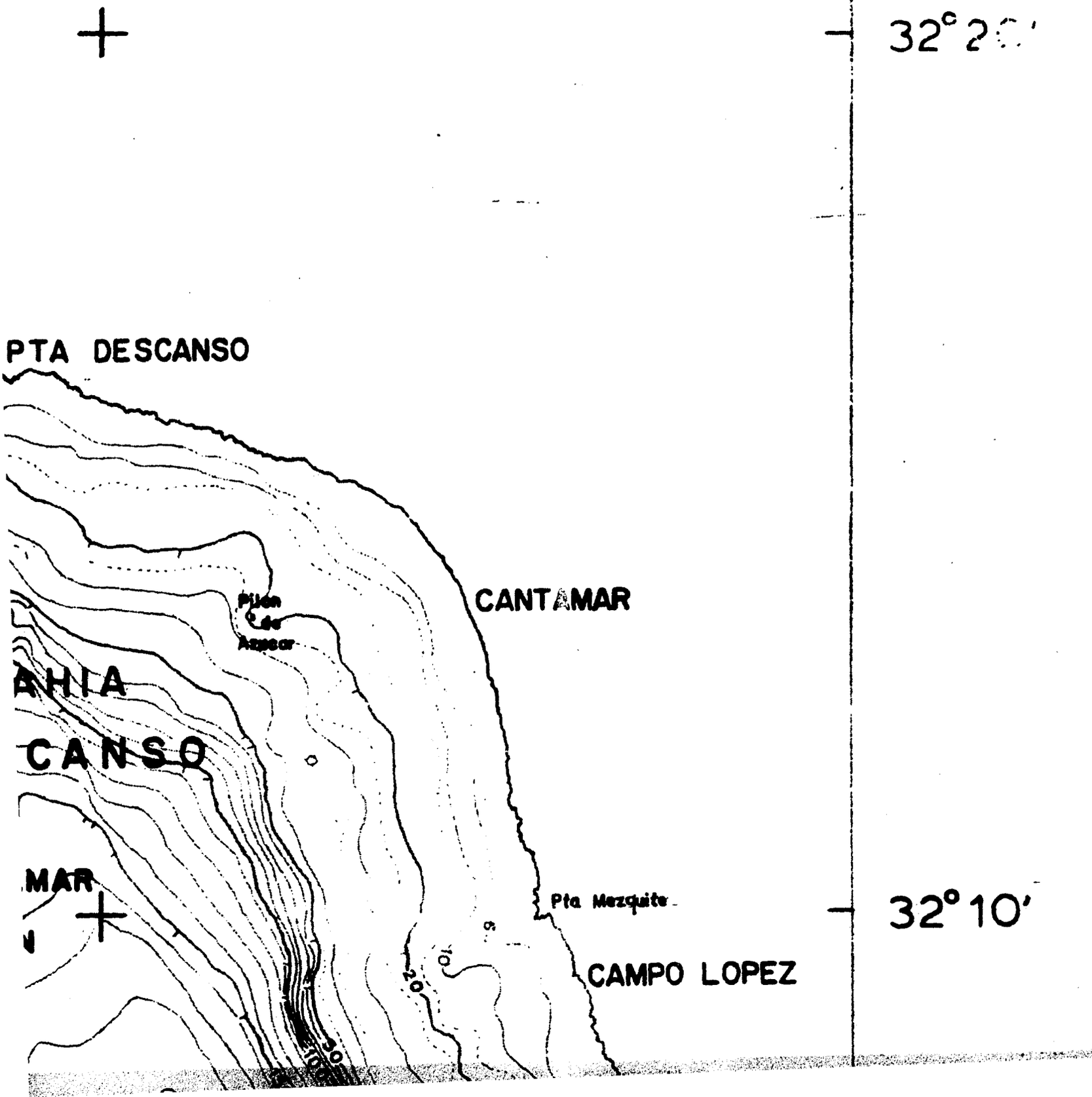
32° 20'
PTA DESCANSO
CANTAMAR
Pilón de Azúcar
AHIA
CANSO
MAR
Pta Mezquite
32° 10'
CAMPO LOPEZ
10
20
30

Compiled & Drafted by Mark R. Legg (198

118°10'

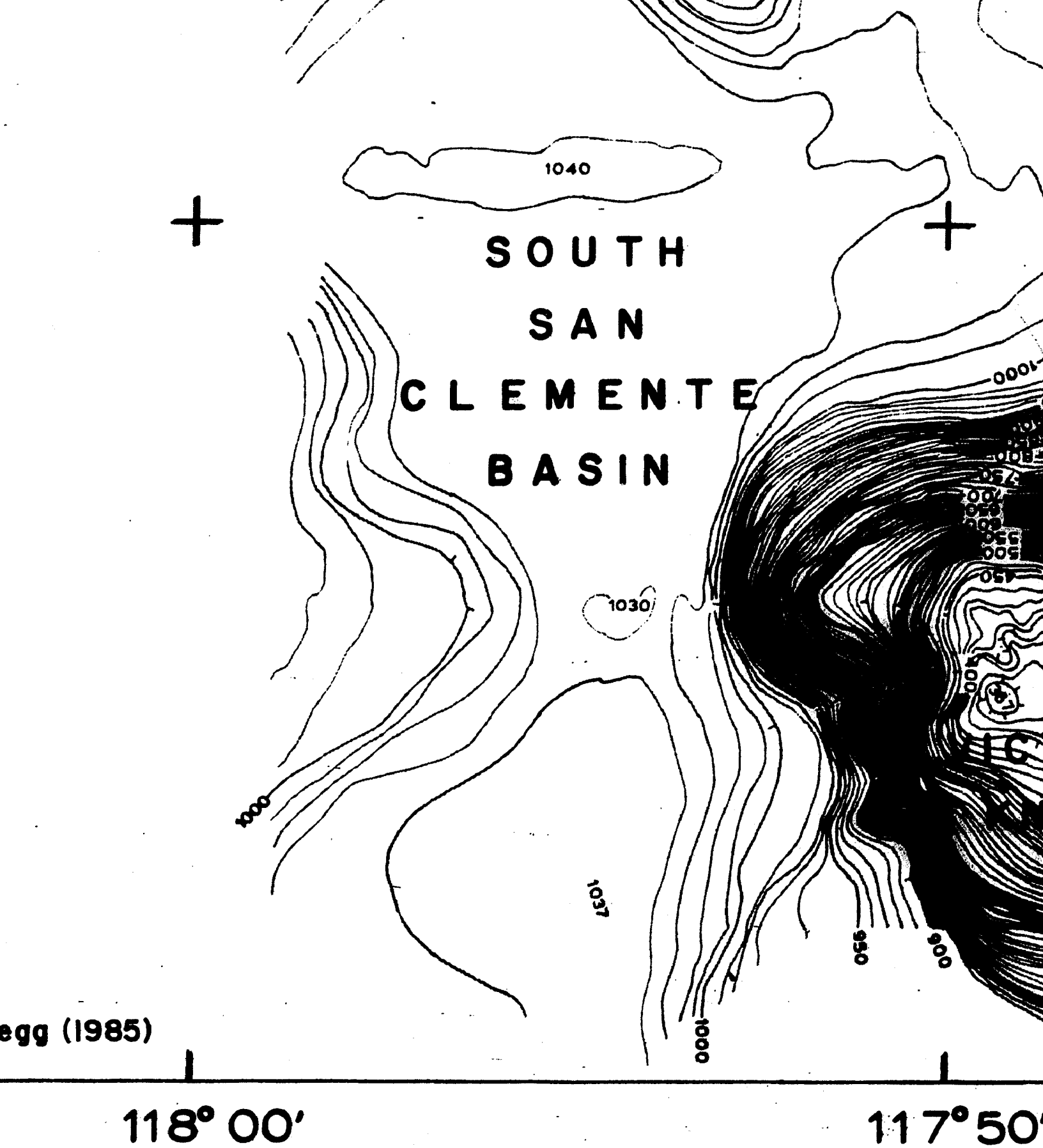

1040
SOUTH
SAN
CLEMENTE
BASIN
1030
1000
1037
950
900
1000
1000
egg (1985)
118° 00'
117° 50'

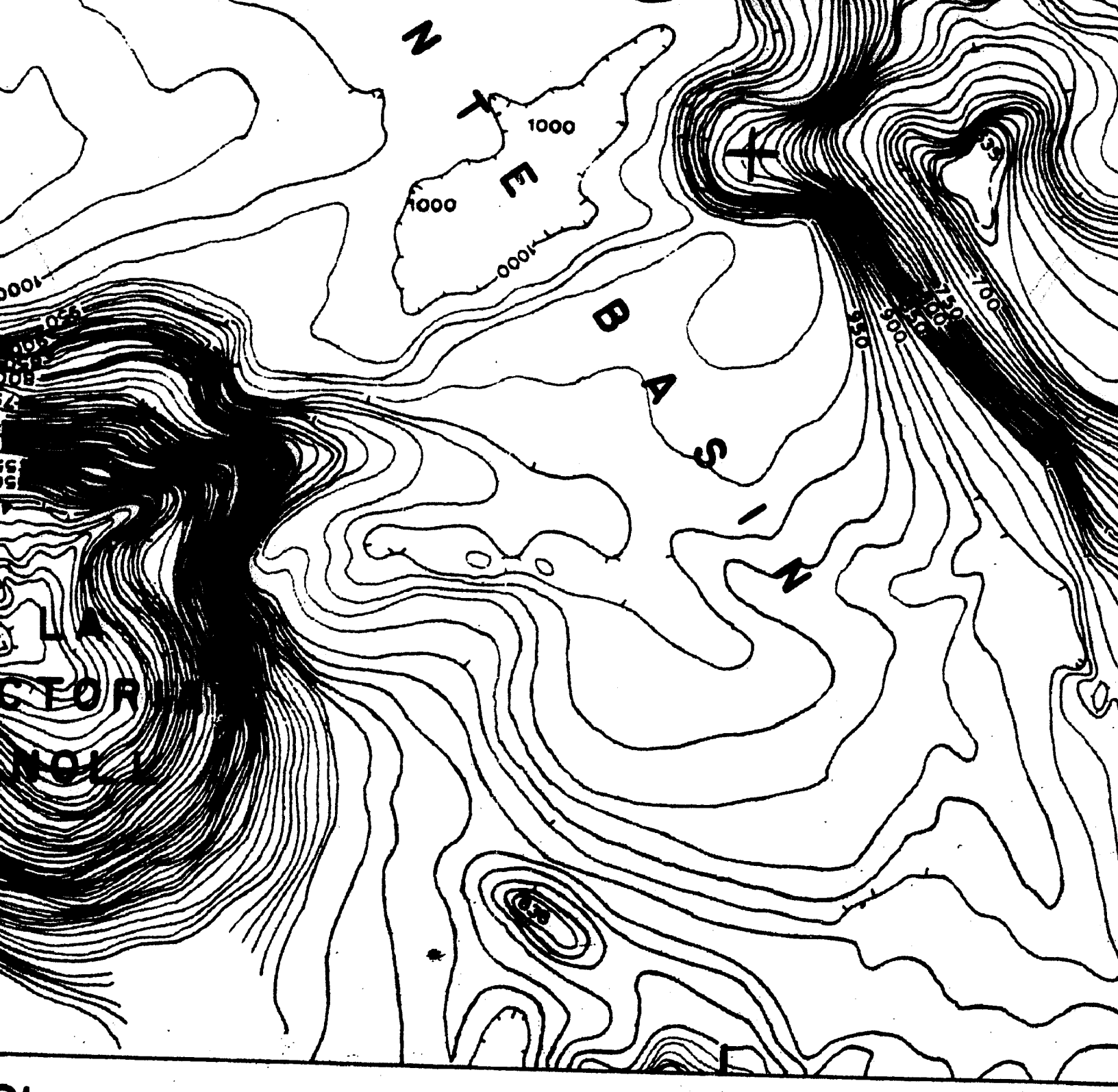


D'

117°40'

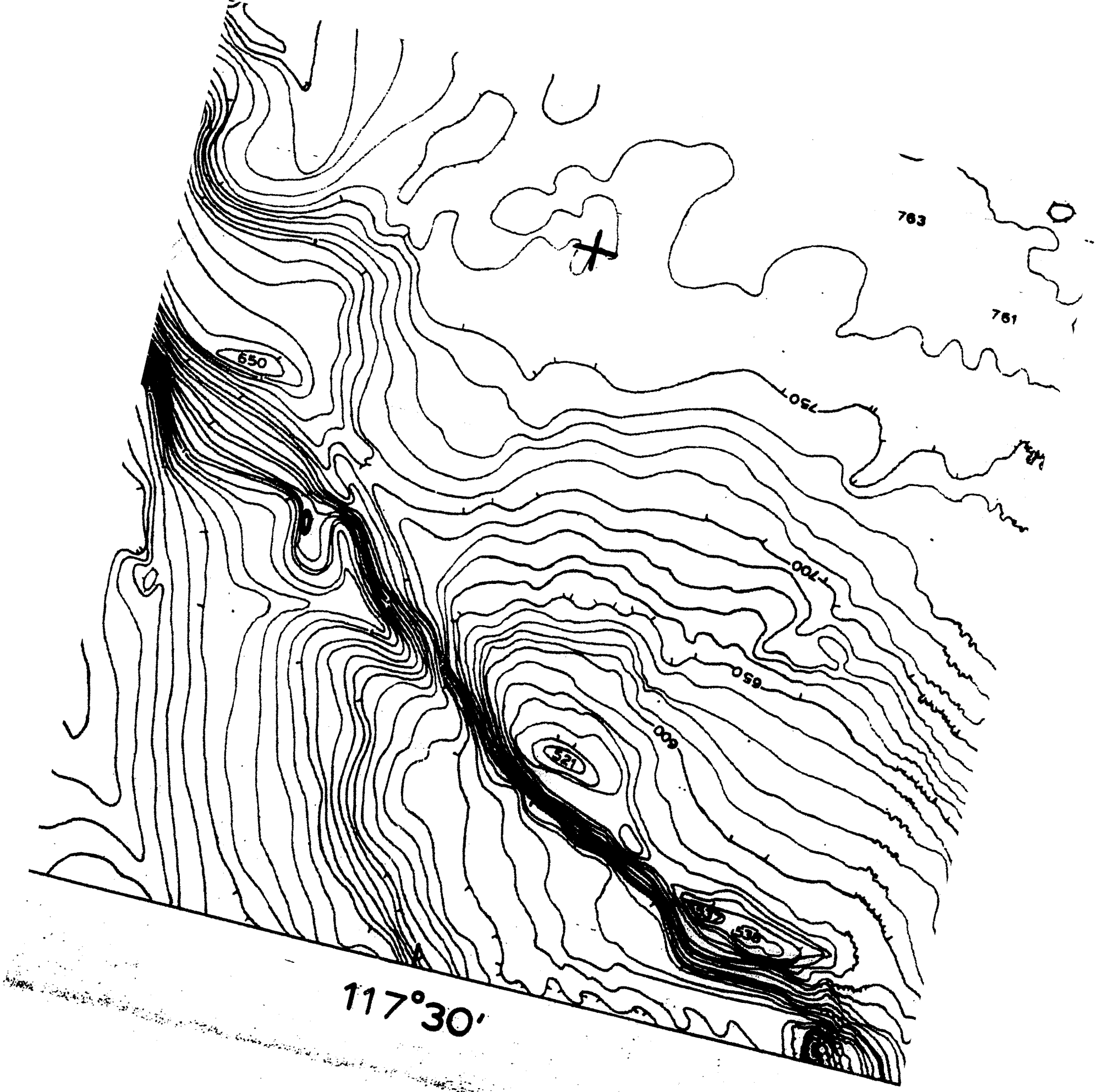
763
761
650
750
700
650
600
521
536
117°30'

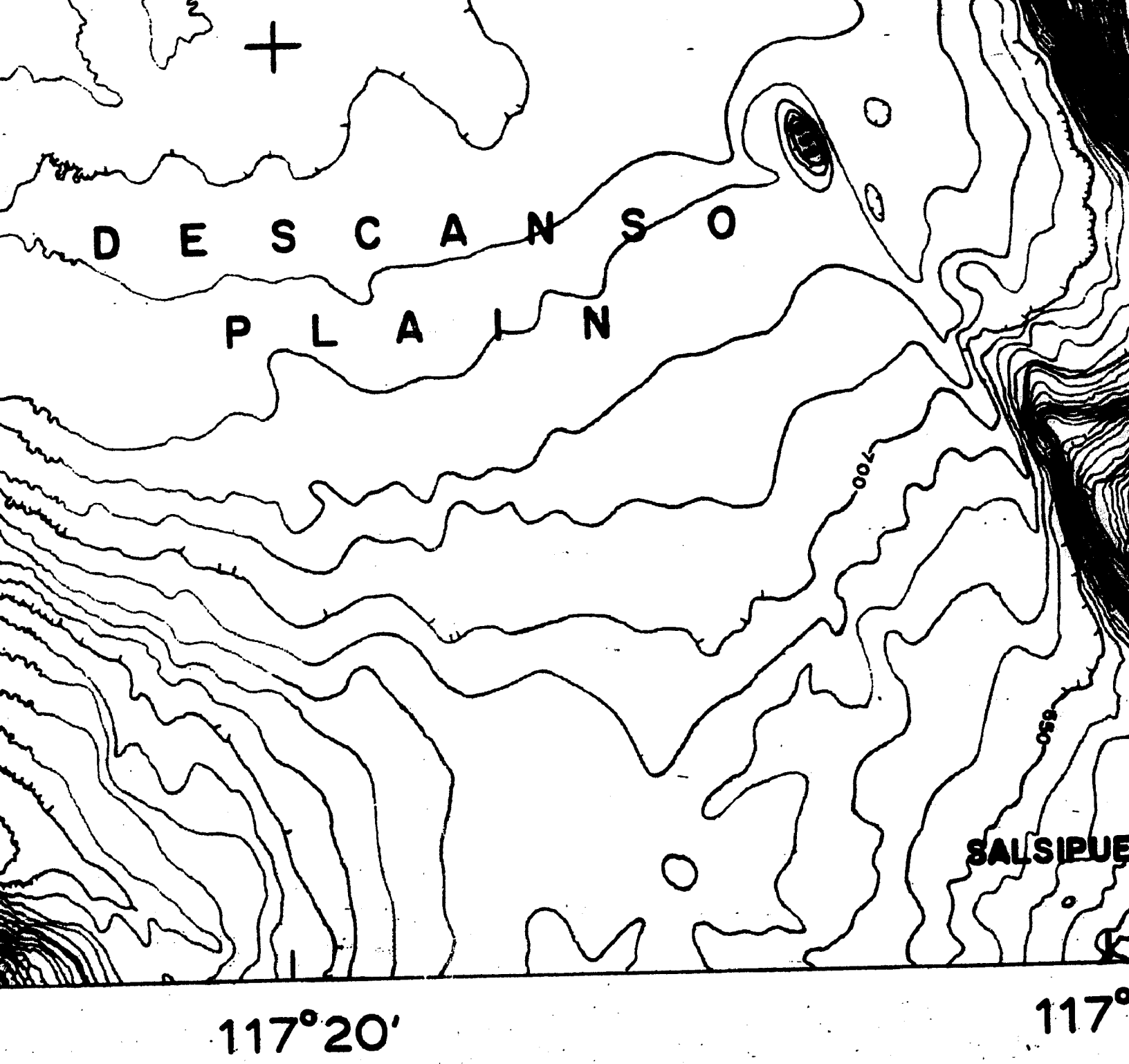
DESCANSO
PLAIN
700
650
SALSIPUE
117°20'
117°

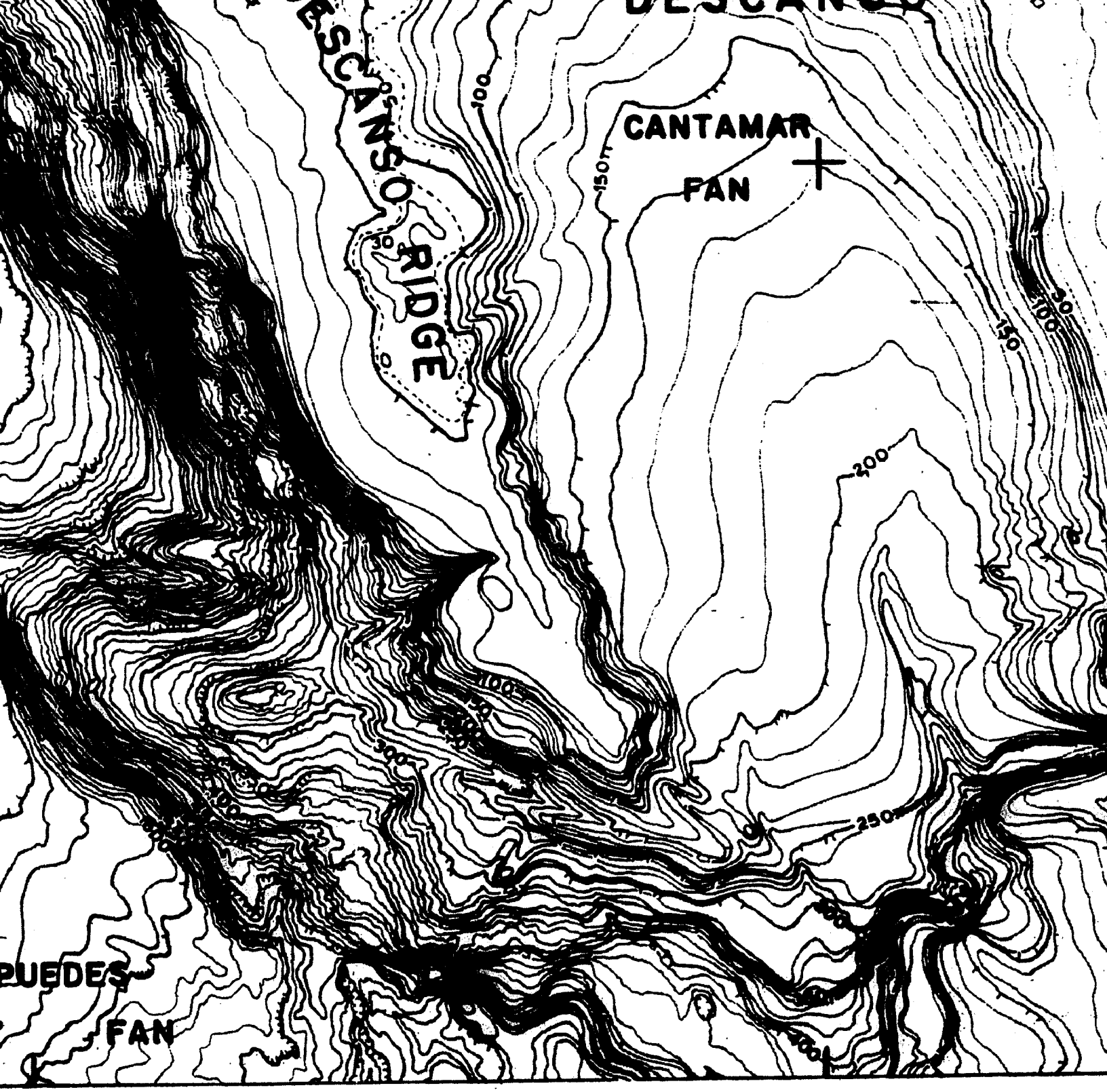
DESCANSO
DESCANSO RIDGE
CANTAMAR
FAN
PUEDES
FAN
100
150
200
250
300
30
7°10'
117° 00'

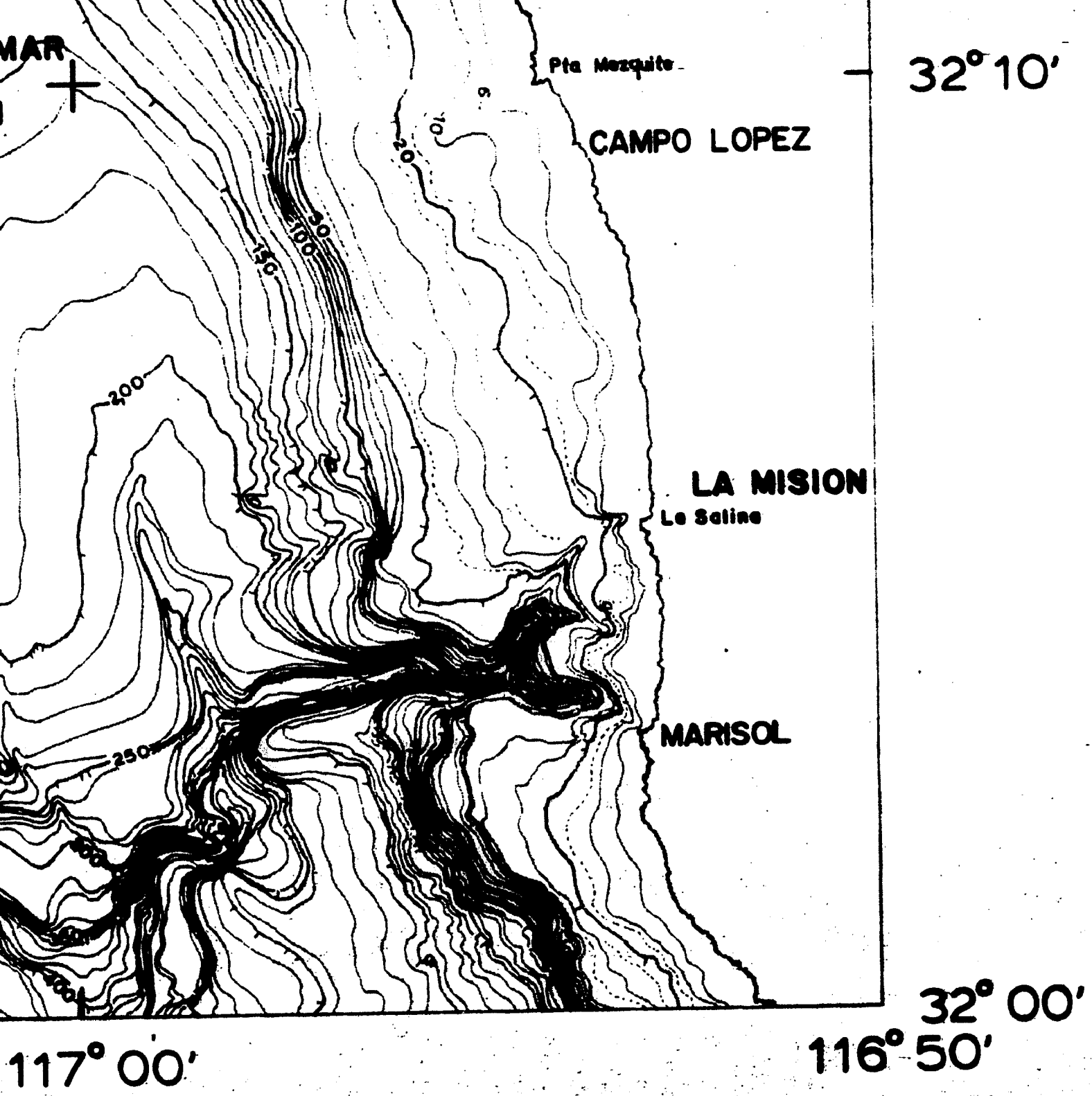
MAR
Pta Mezquite
32° 10'
CAMPO LOPEZ
20
10
50
100
150
200
LA MISION
La Saline
MARISOL
250
32° 00'
117° 00'
116° 50'

EAST
SAN
CLEMENTE
BASIN
?
?
?

INNE

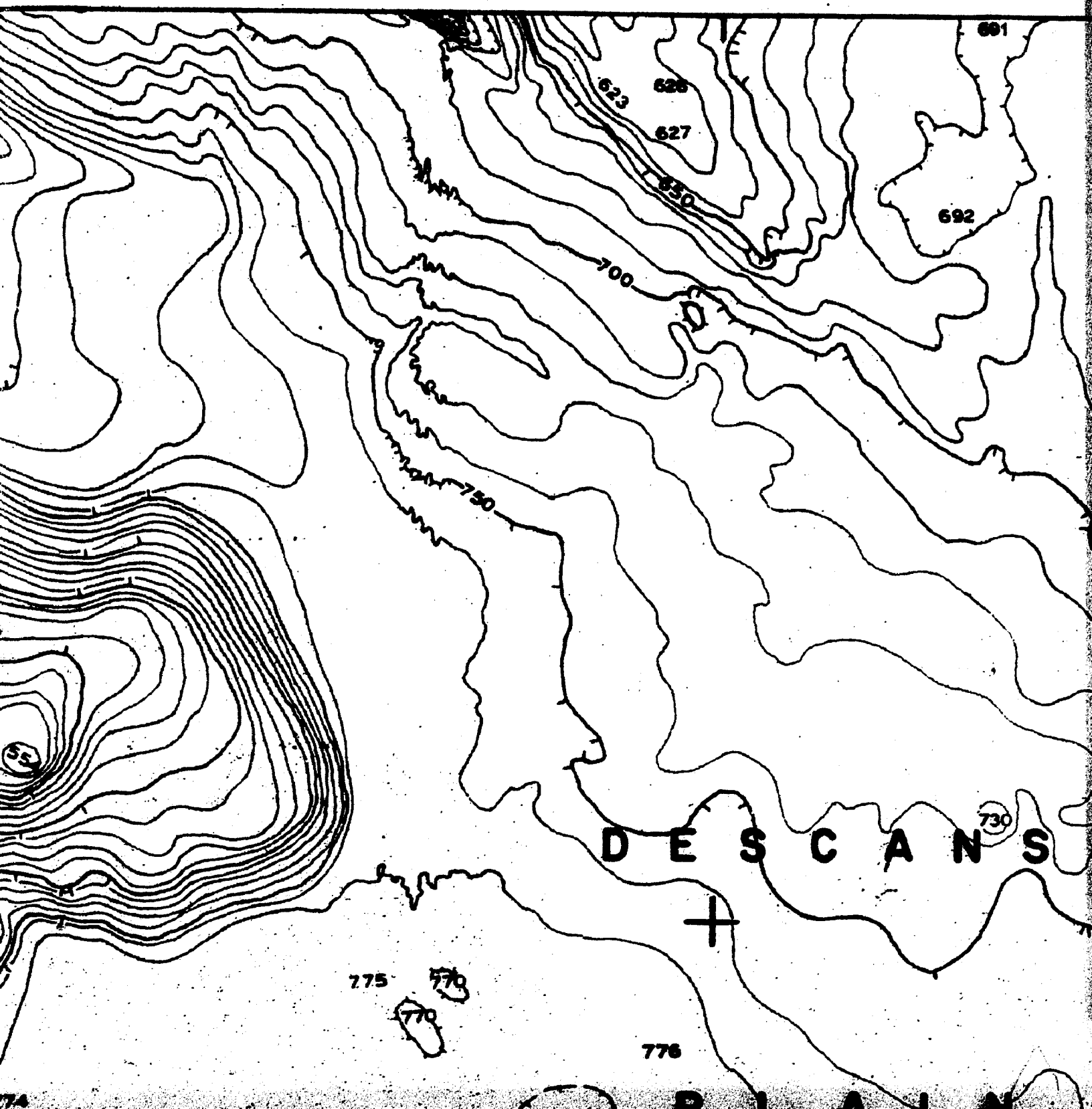

ER CALIFORNIA CONTINEN

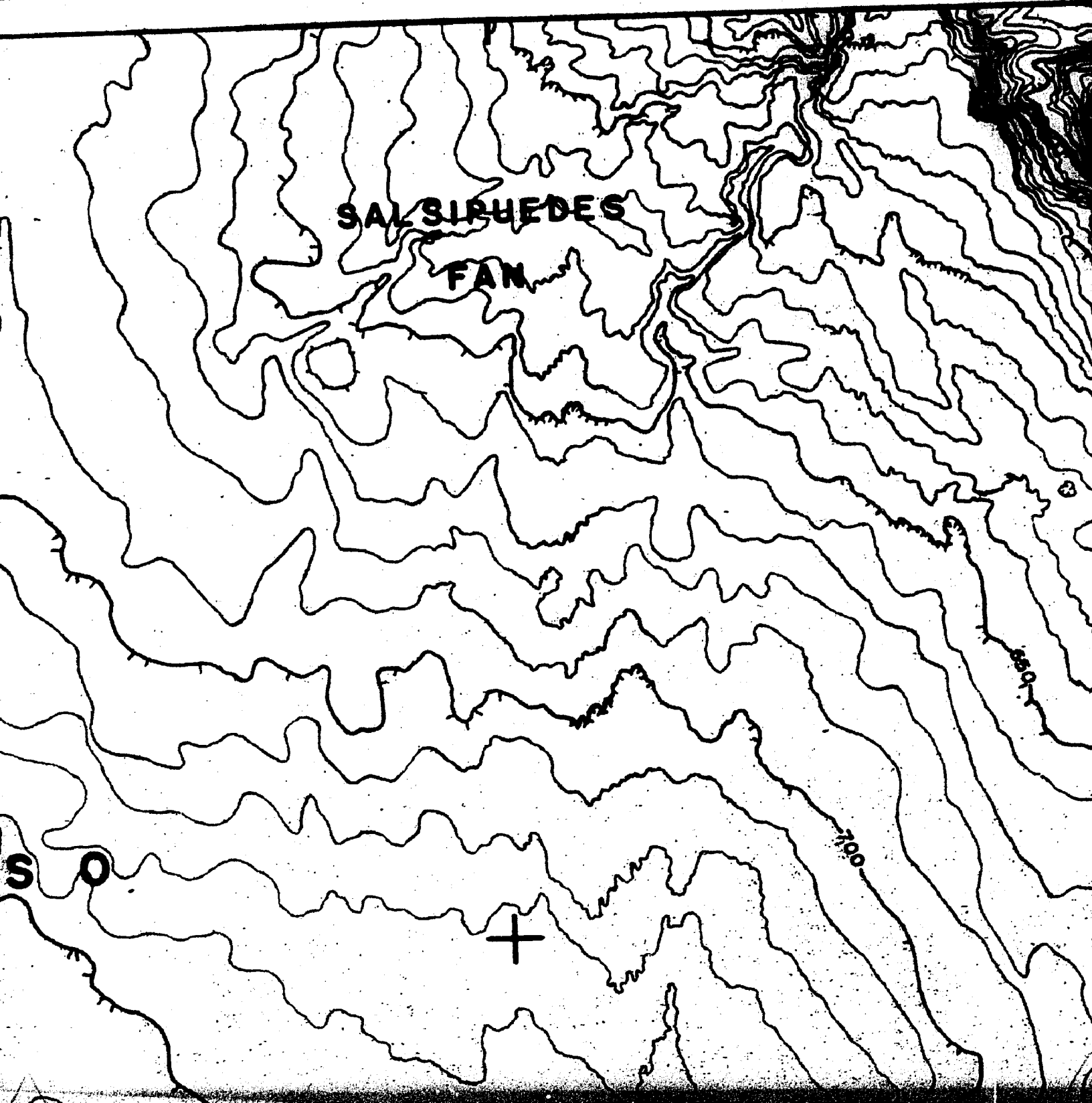

# NTAL BORDERLAND

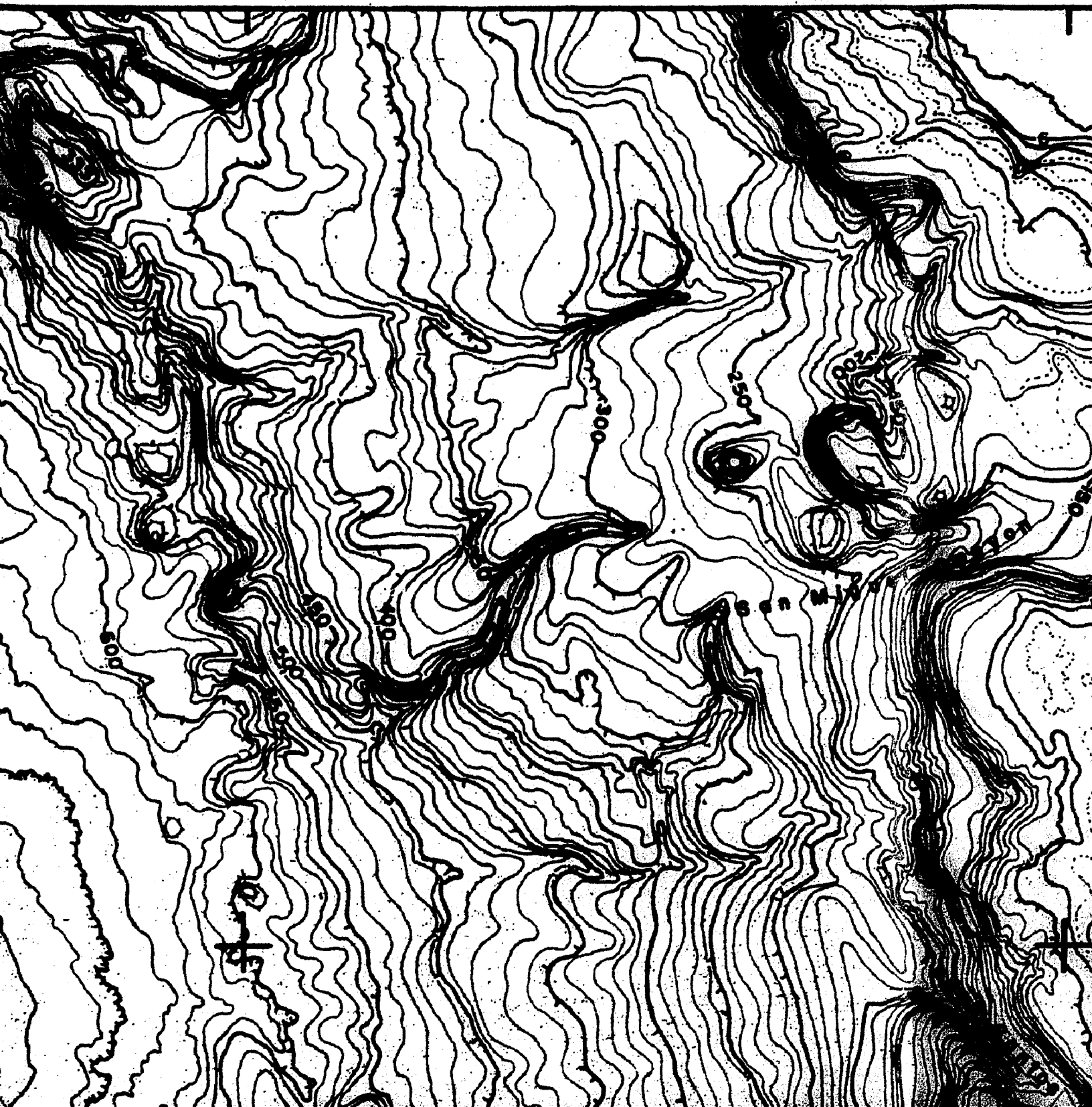

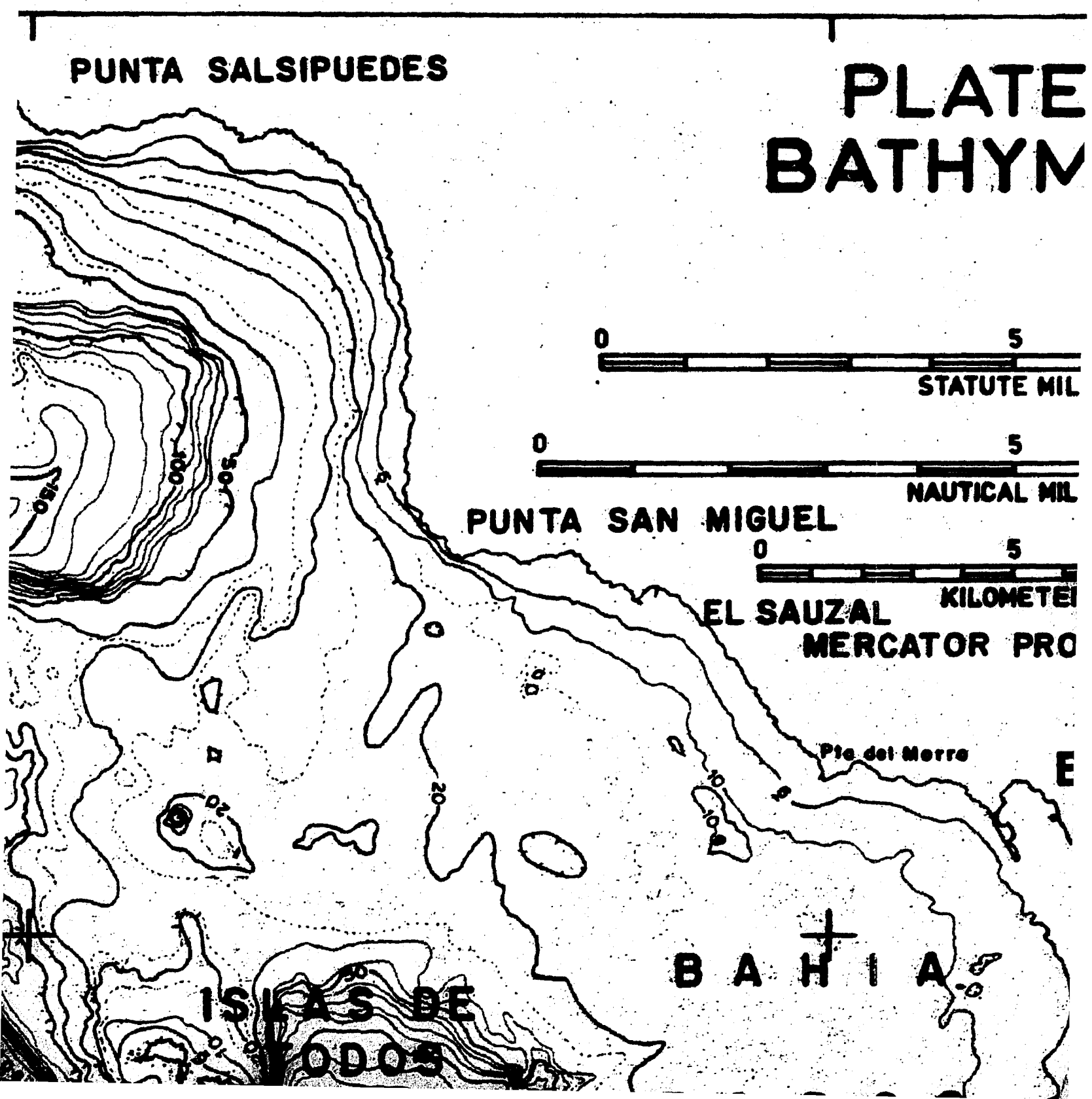
PUNTA SALSIPUEDES
PLATE
BATHYM
0
5
STATUTE MIL
0
5
NAUTICAL MIL
PUNTA SAN MIGUEL
0
5
KILOMETE
EL SAUZAL
MERCATOR PRO
Pta del Morro
BAHIA
ISLAS DE
TODOS
150
100
50
20
10

32° 00'

E 1B
METRY

10
ES

10
ES

10
S

JECTION

N SENADA

31° 50'

N

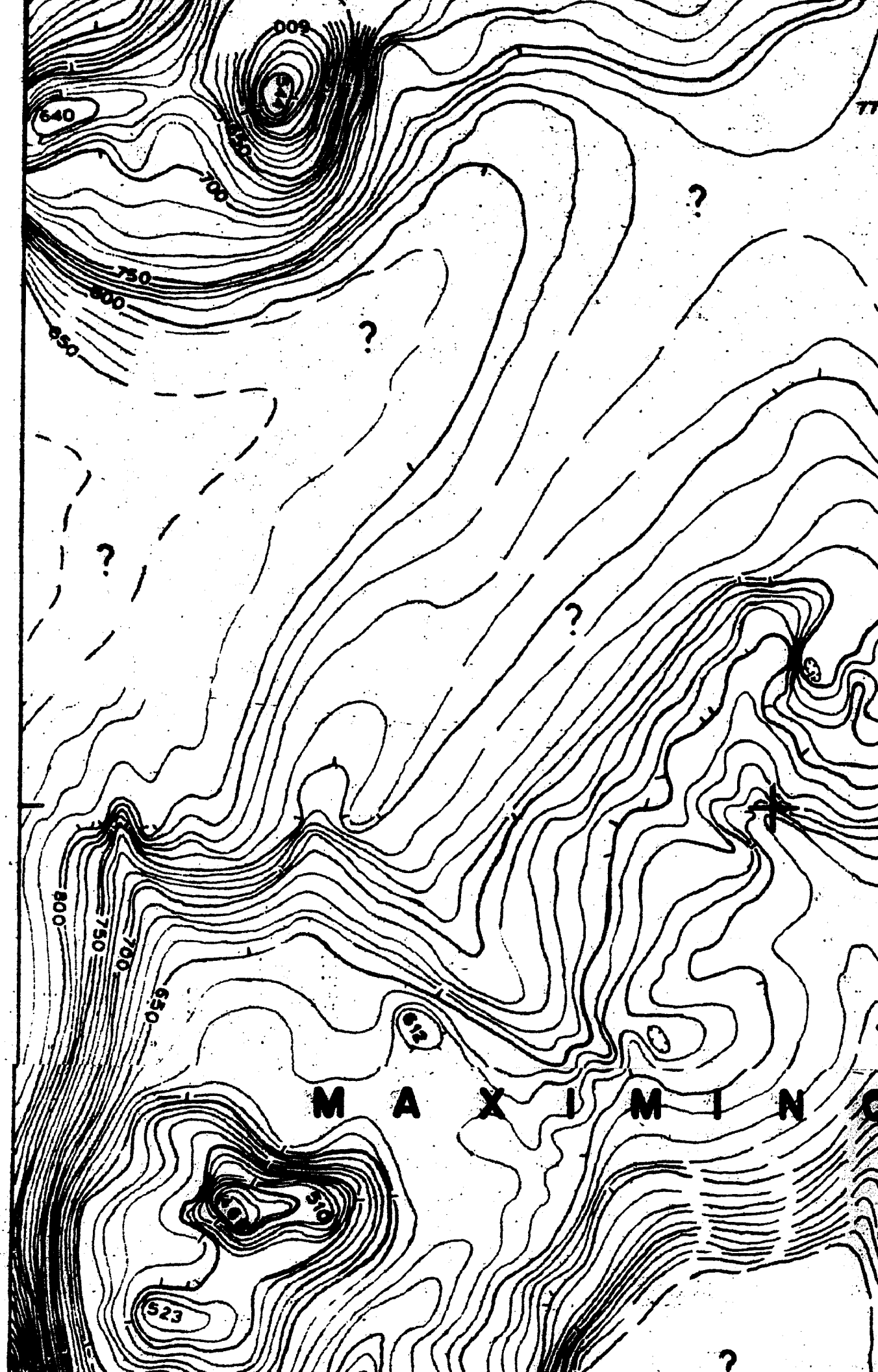

640
700
750
800
850
?
?
?
?
800
750
700
650
612
M A X I M I N
510
523
?

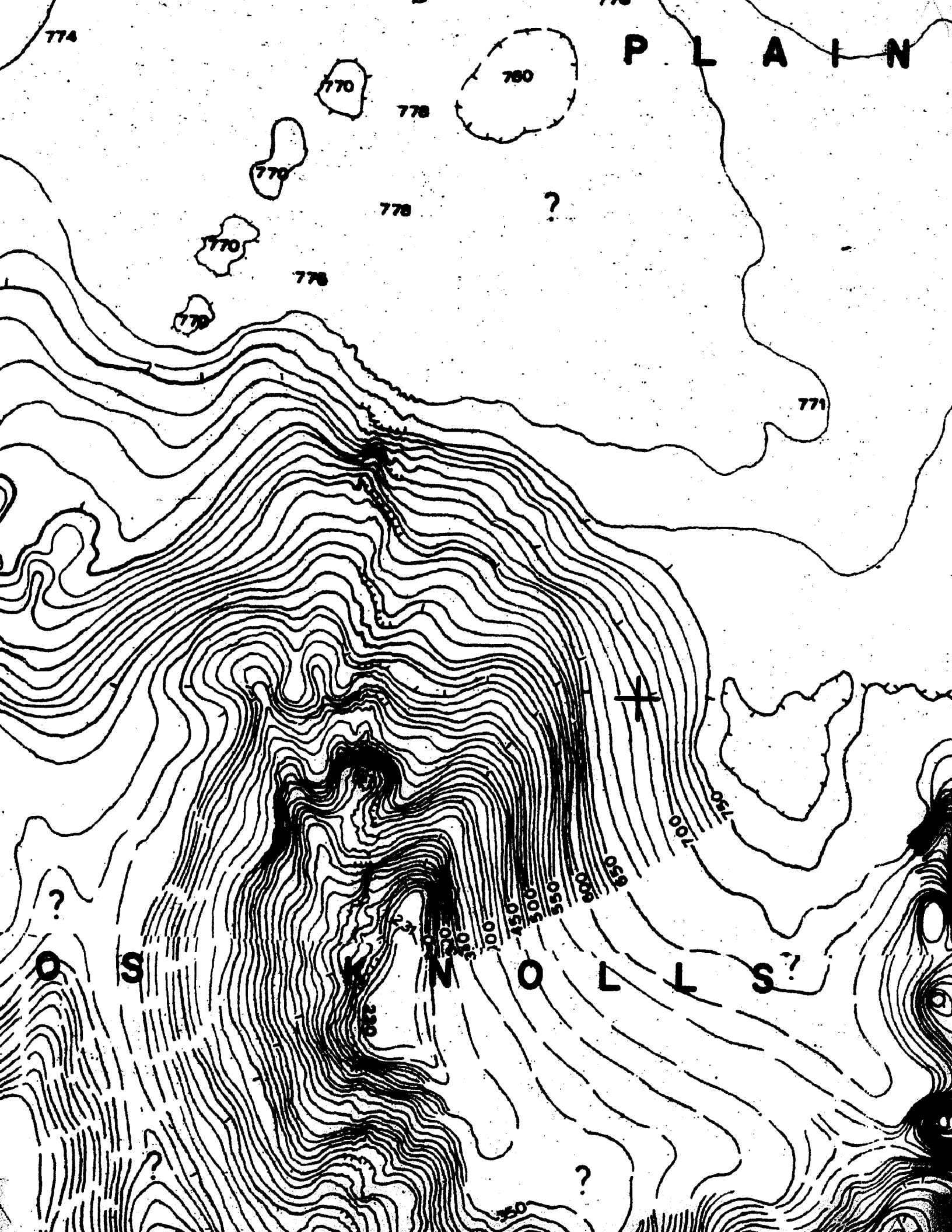

PLAIN
774
770
780
778
770
778
?
770
776
770
771
750
700
650
600
550
500
450
400
350
300
250
230
?
OS
KNOLLS
?
?
?
350

750
700
650
600
550
E
N
S

BANDA
FAN
RIDGE
ENSENAD
300
350
400
450
500
550
600
650

TODOS SANTOS
TODOS SANTOS
PUNTA BANDA
VALLE
Estero Banda
Valley
SANTO TOMAS SHELF
BAHIA SOLEDAD
PUNTA LOS MAXIMINOS
PUNTA SANTO TOMAS
47
150
200
250
100

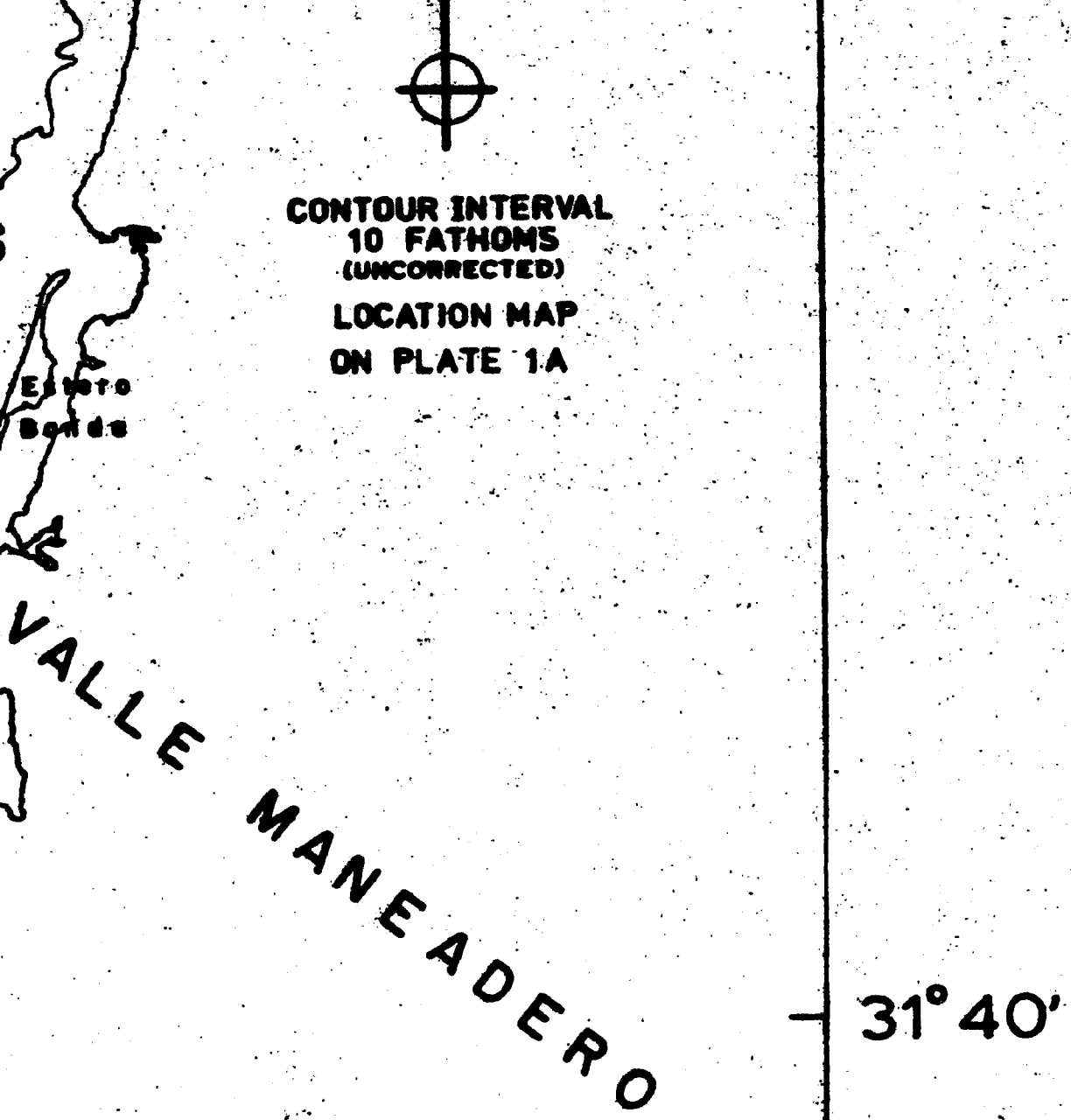


OS MAXIMINOS

TO TOMAS

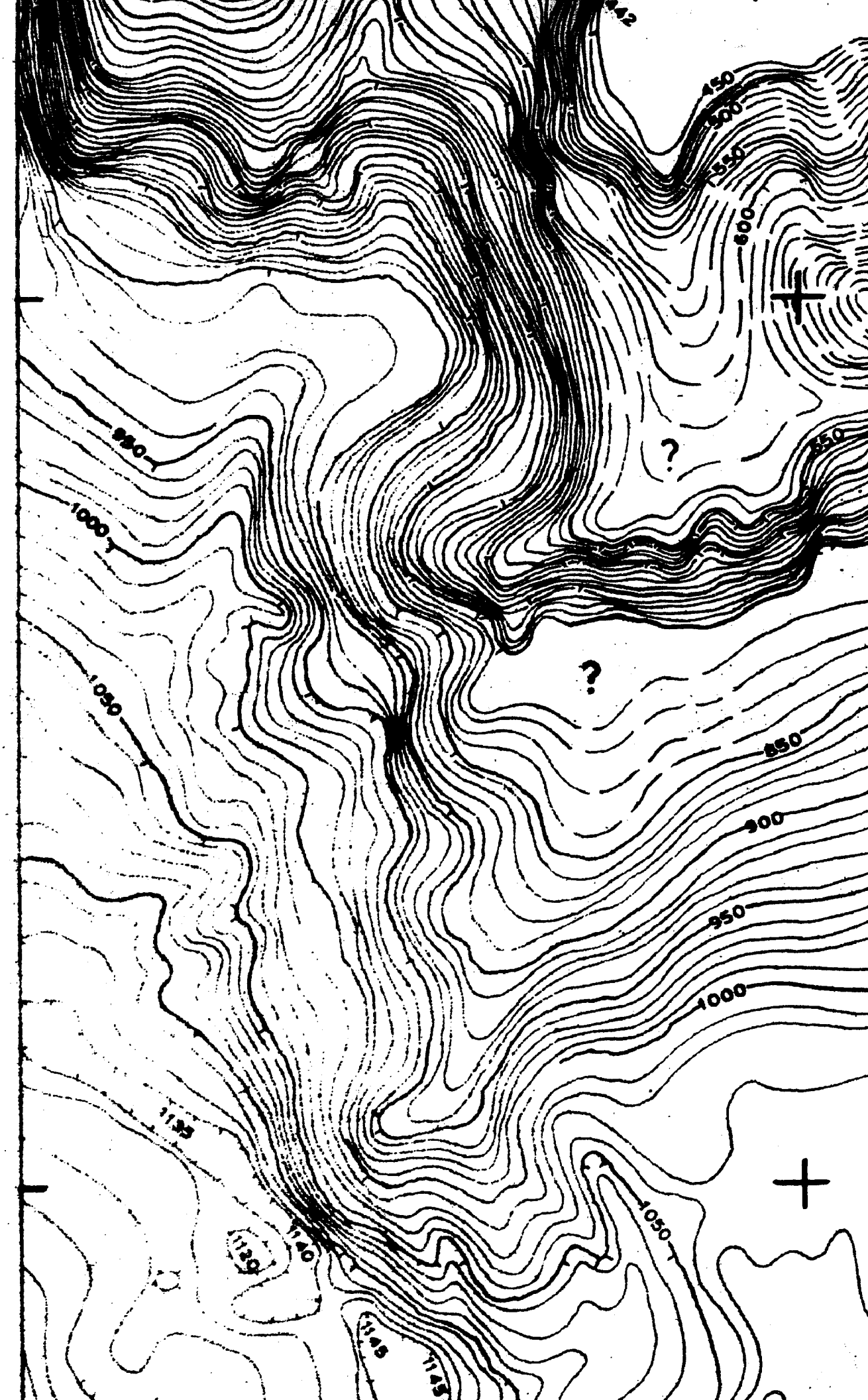

450
500
550
600
?
550
950
1000
?
1050
850
900
950
1000
1135
1120
1140
1145
1145
1050

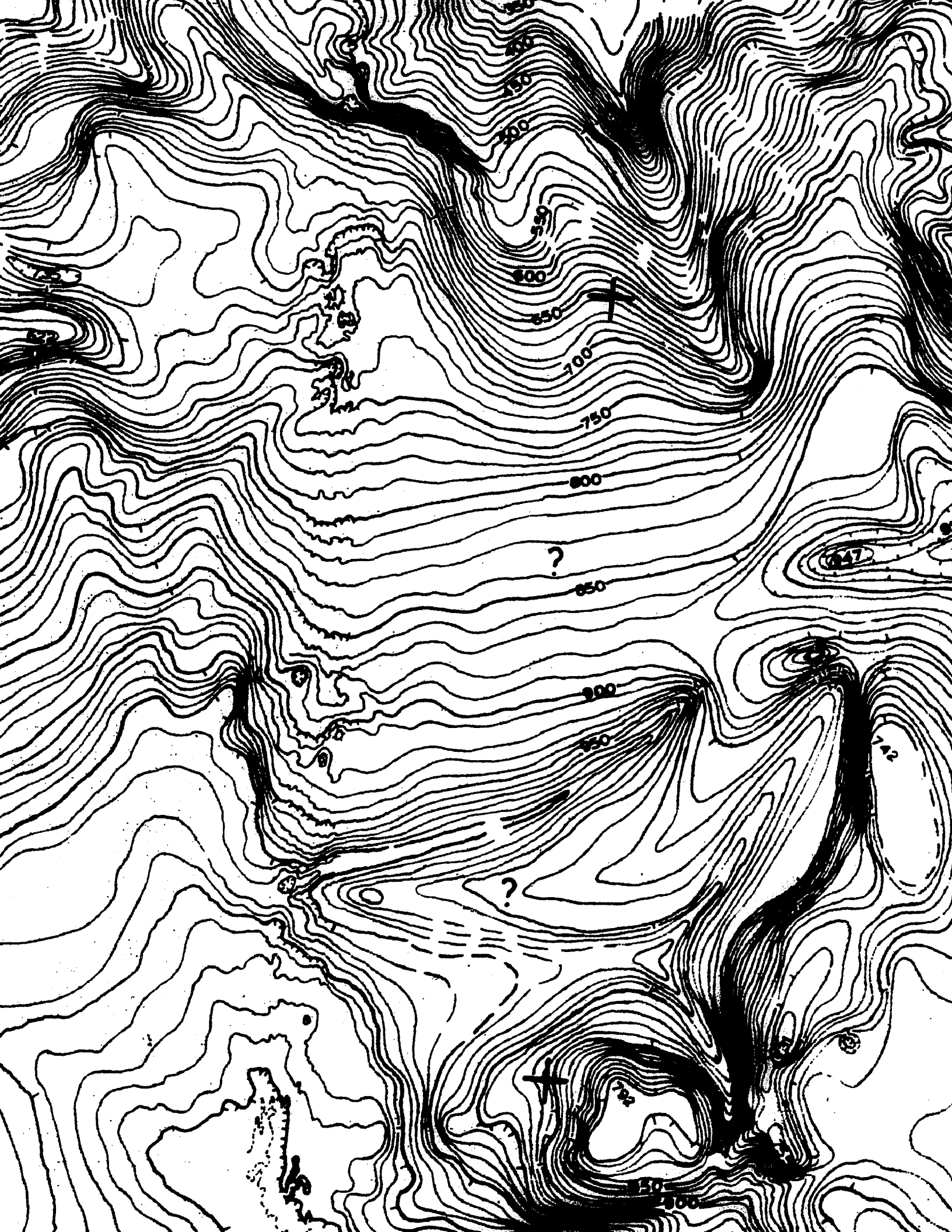

350
400
450
500
550
600
650
700
750
800
?
850
900
950
742
?
792
850
900

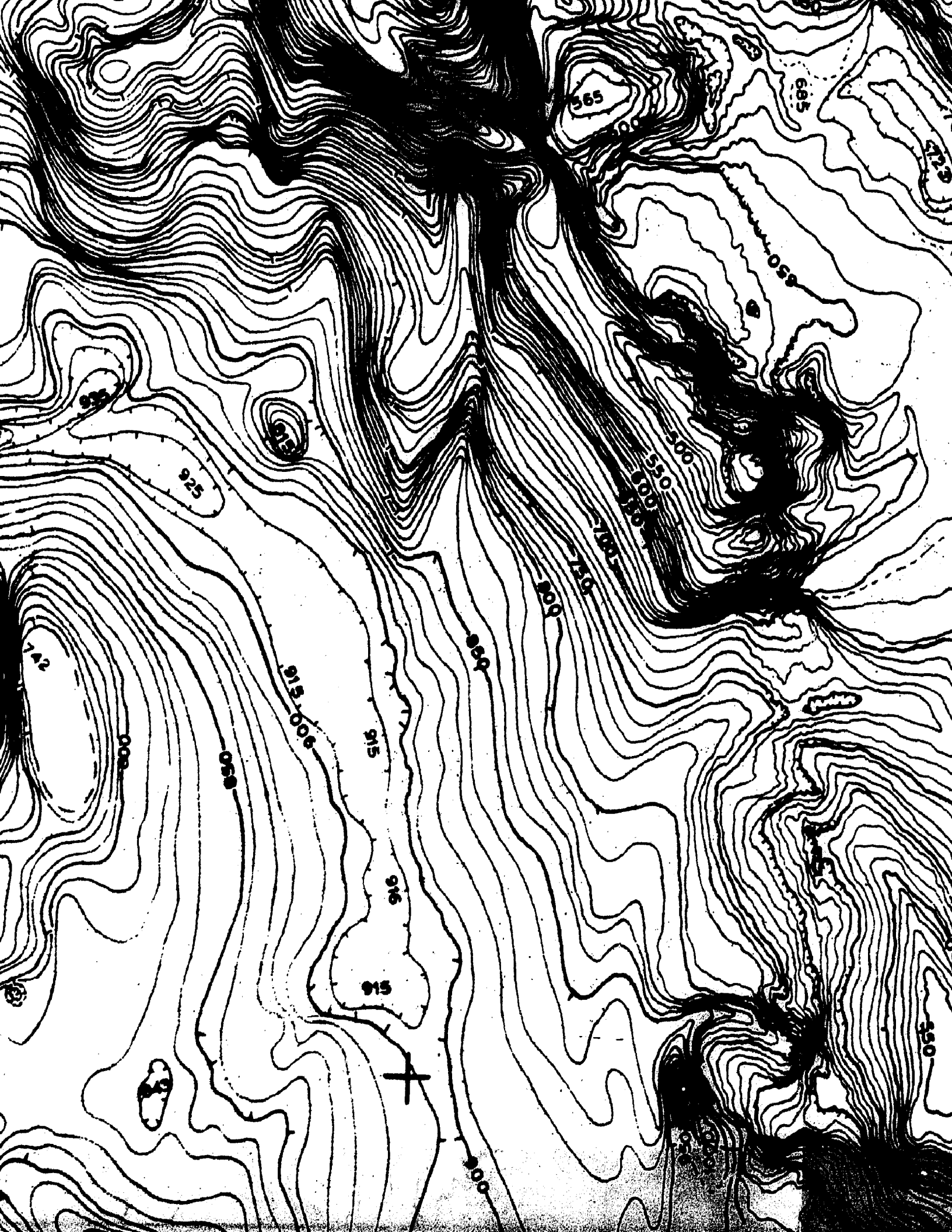
565
685
650
500
550
600
700
750
800
850
925
915
916
742

TROUGH
SANTO
TOMAS
FAN
681
684
682
683
685
700
650
600
550
500
450

Isolote
?
SAN IS
CABRAS
BANK
33
58
58
135
150
150
100
200
150
100
200
250
300
350
400

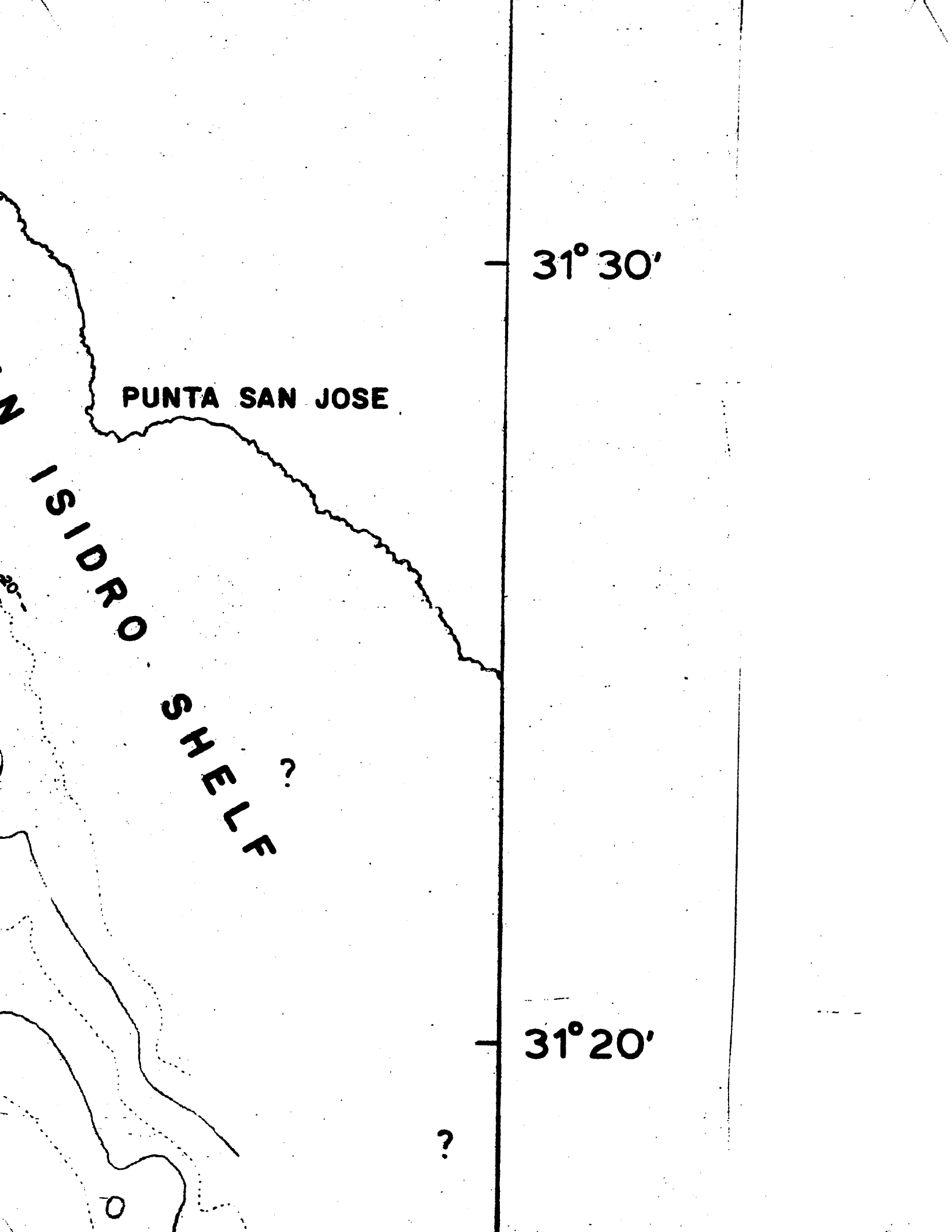
31° 30'
PUNTA SAN JOSE
N ISIDRO SHELF
?
31° 20'
?

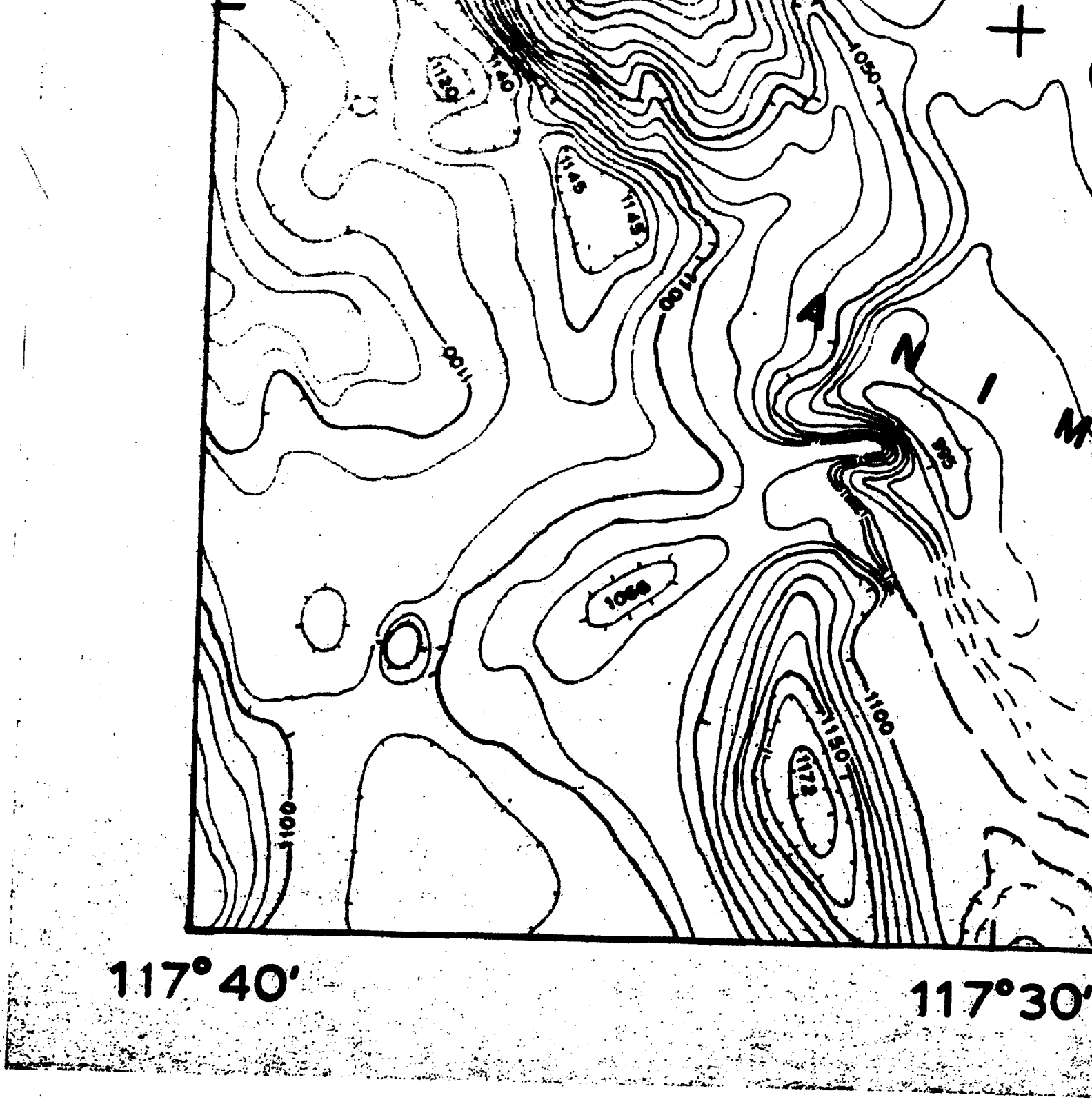
1050
1120
1140
1145
1145
1100
1100
1100
1100
1150
1172
117°40'
117°30'

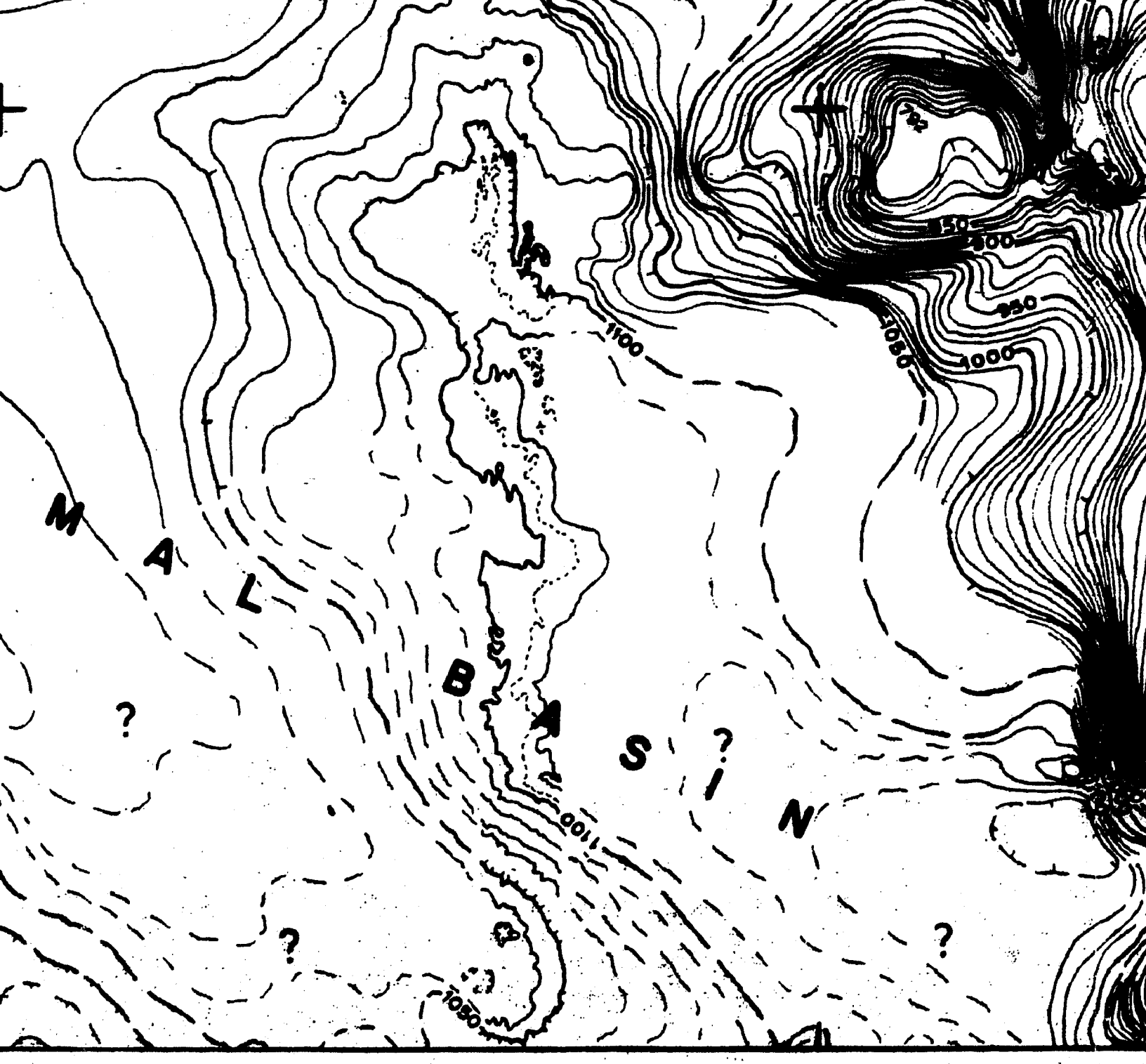


°30′ 117°20′

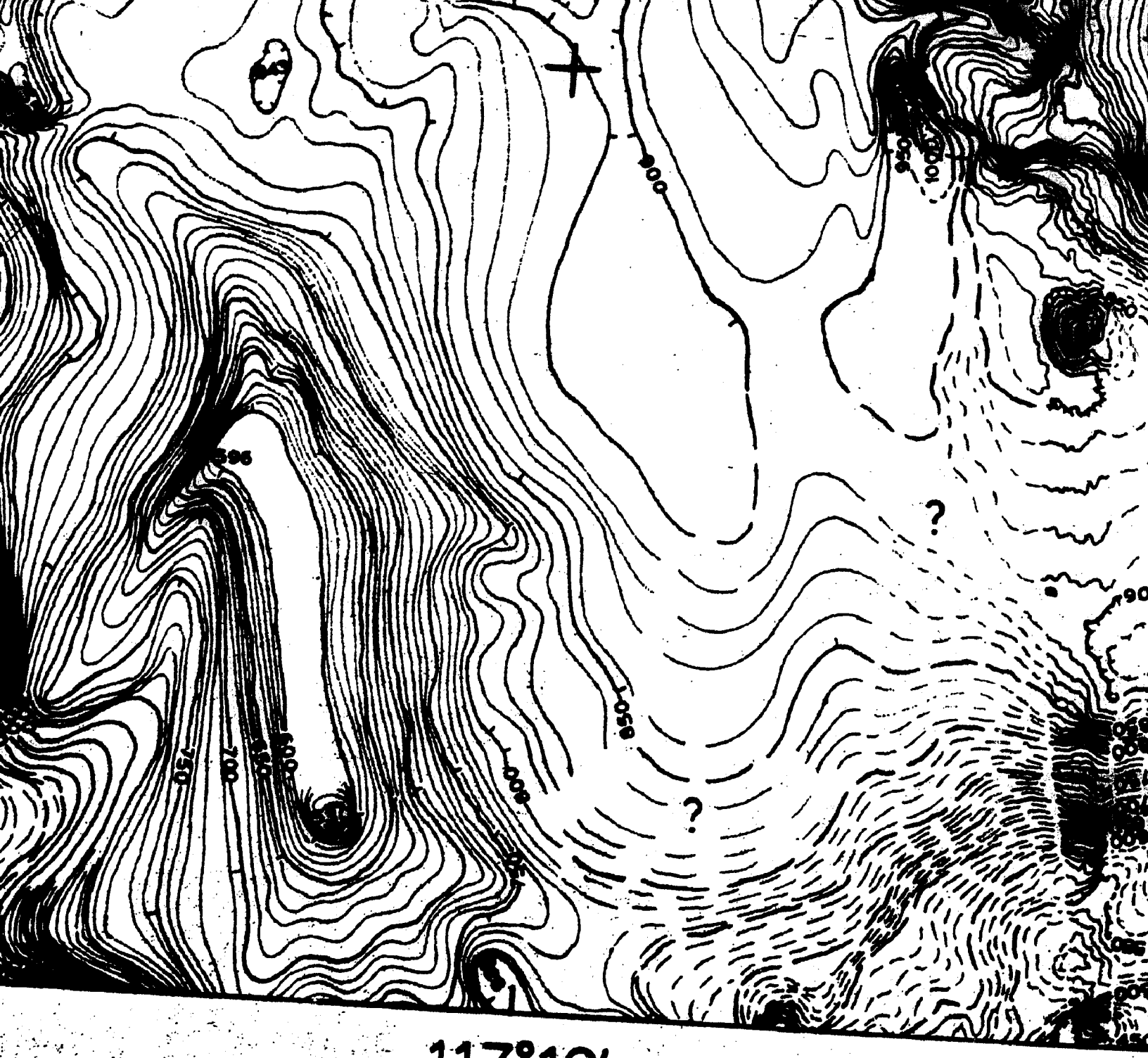


117°10′

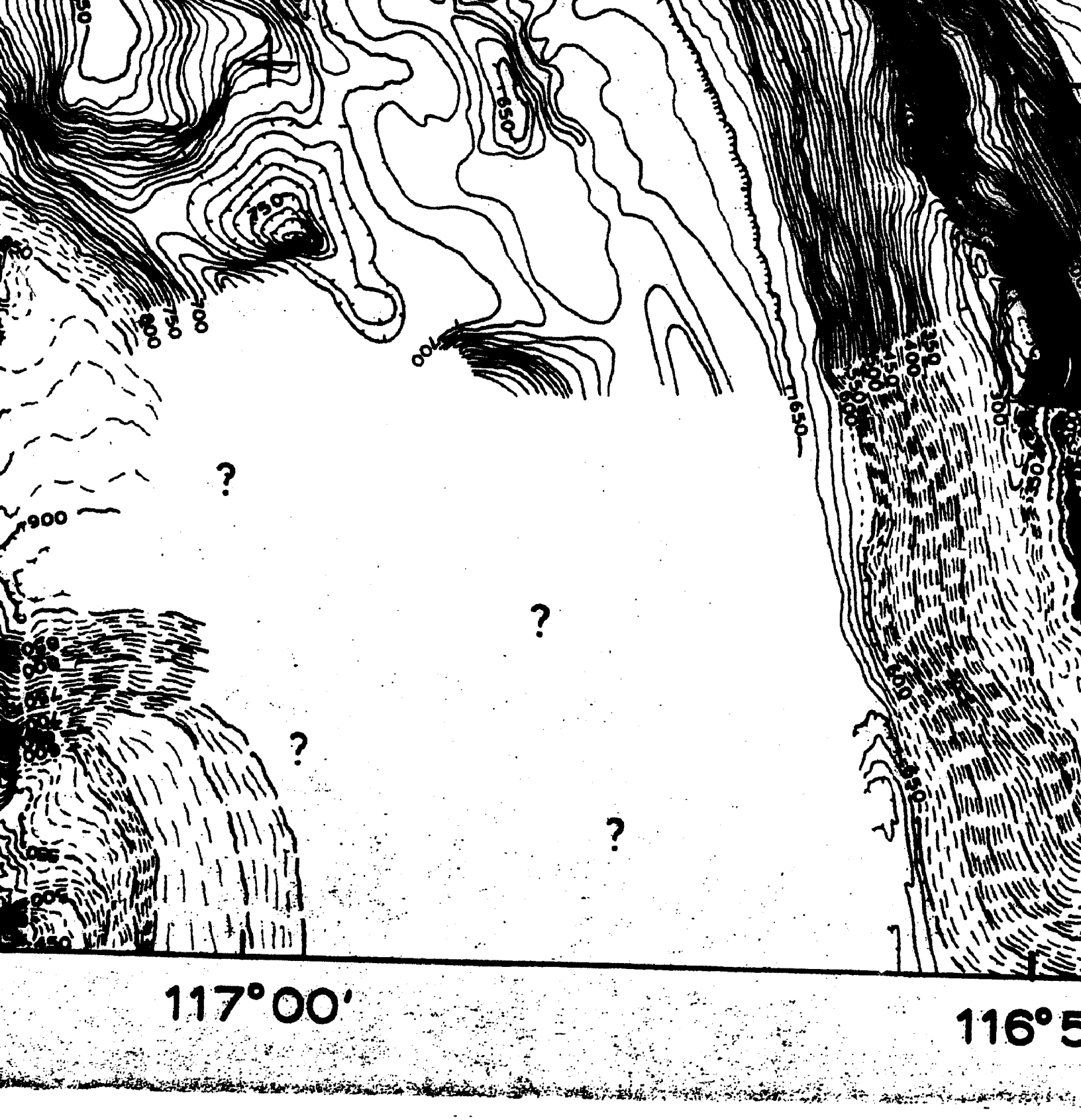

650
750
700
800
900
?
?
?
?
117°00'
116°5

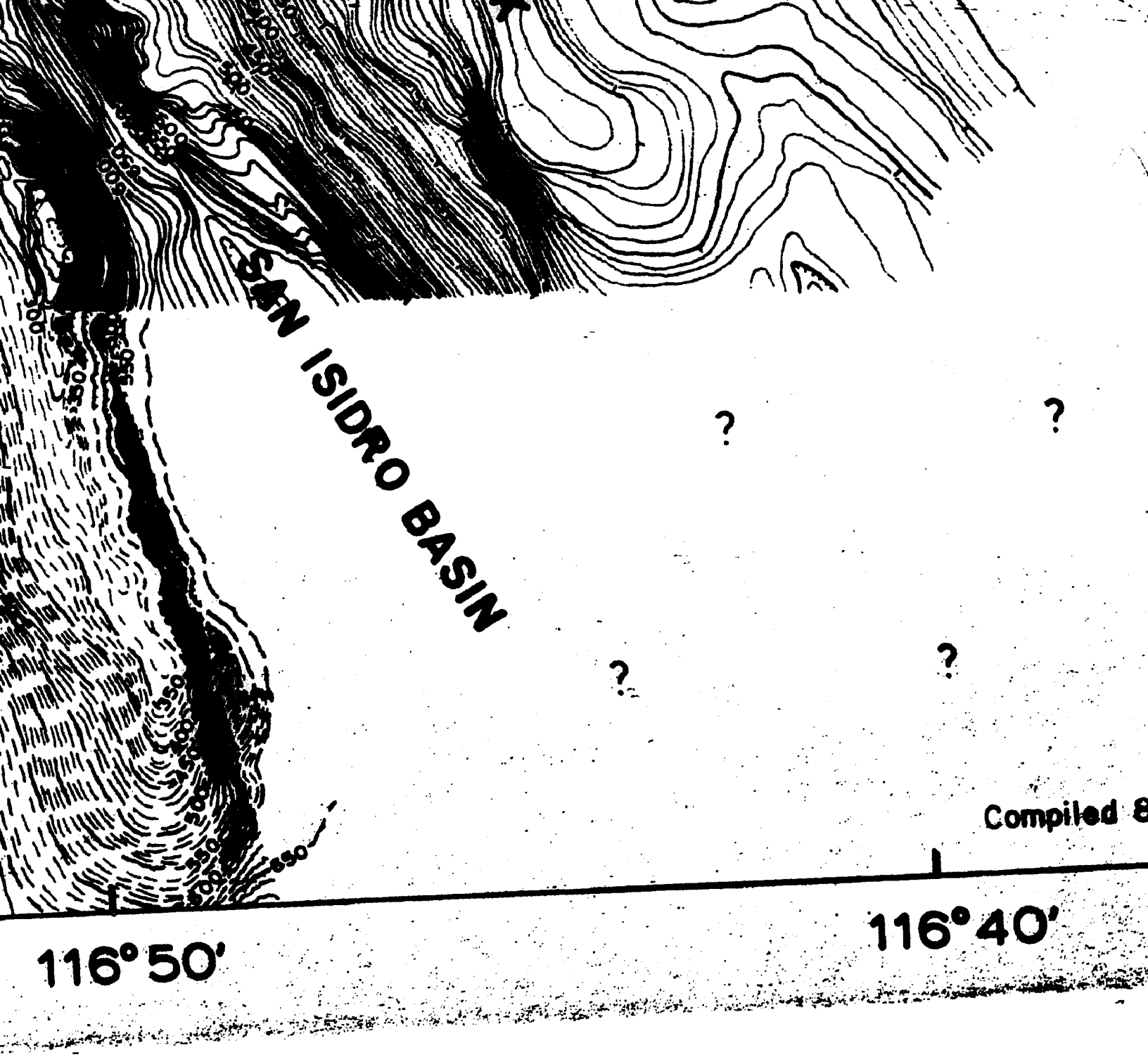
SAN ISIDRO BASIN
?
?
?
?
Compiled 8
116°50'
116°40'

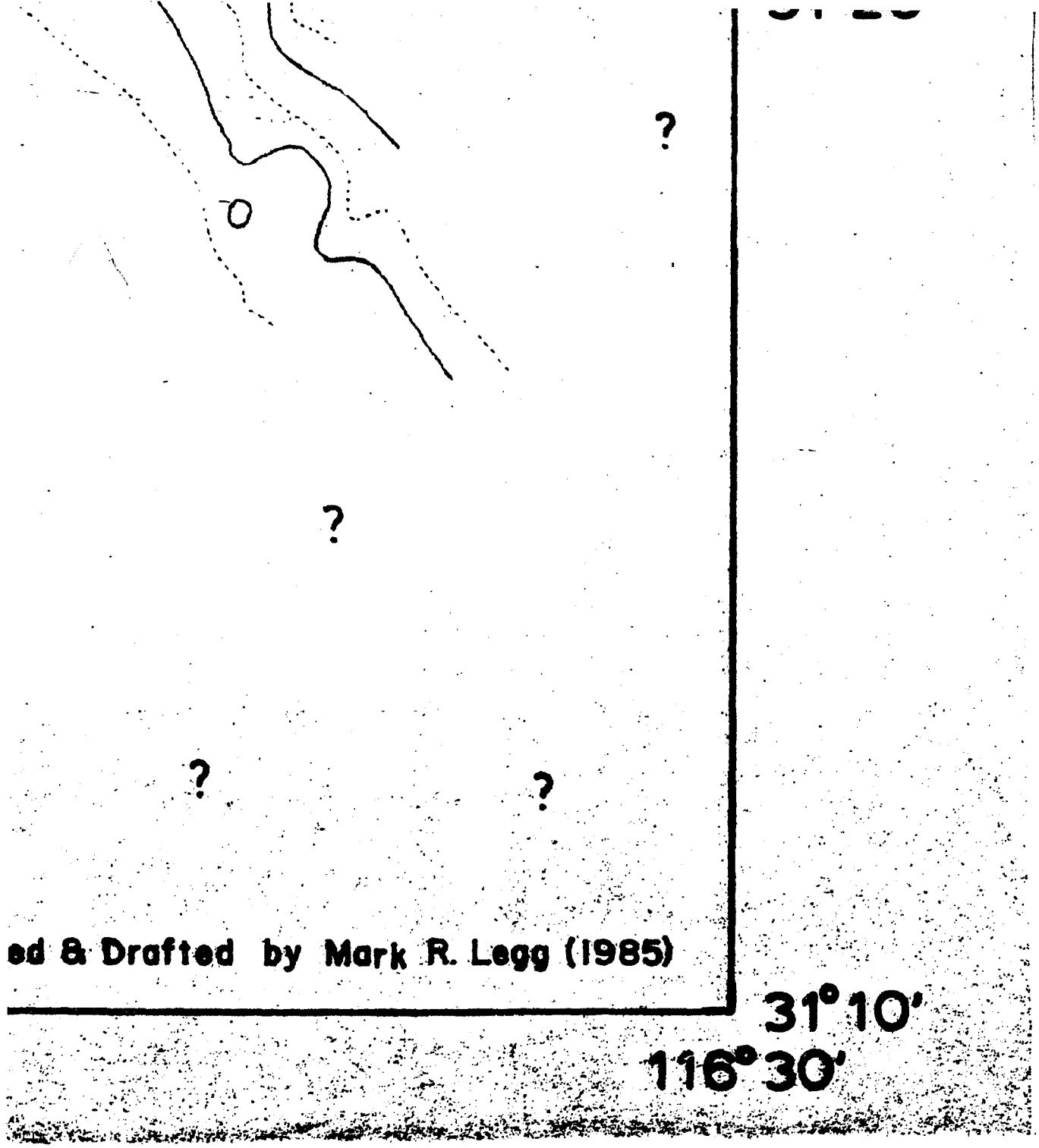
?
?
?
?
ed & Drafted by Mark R. Legg (1985)
31°10'
116°30'

118°00′

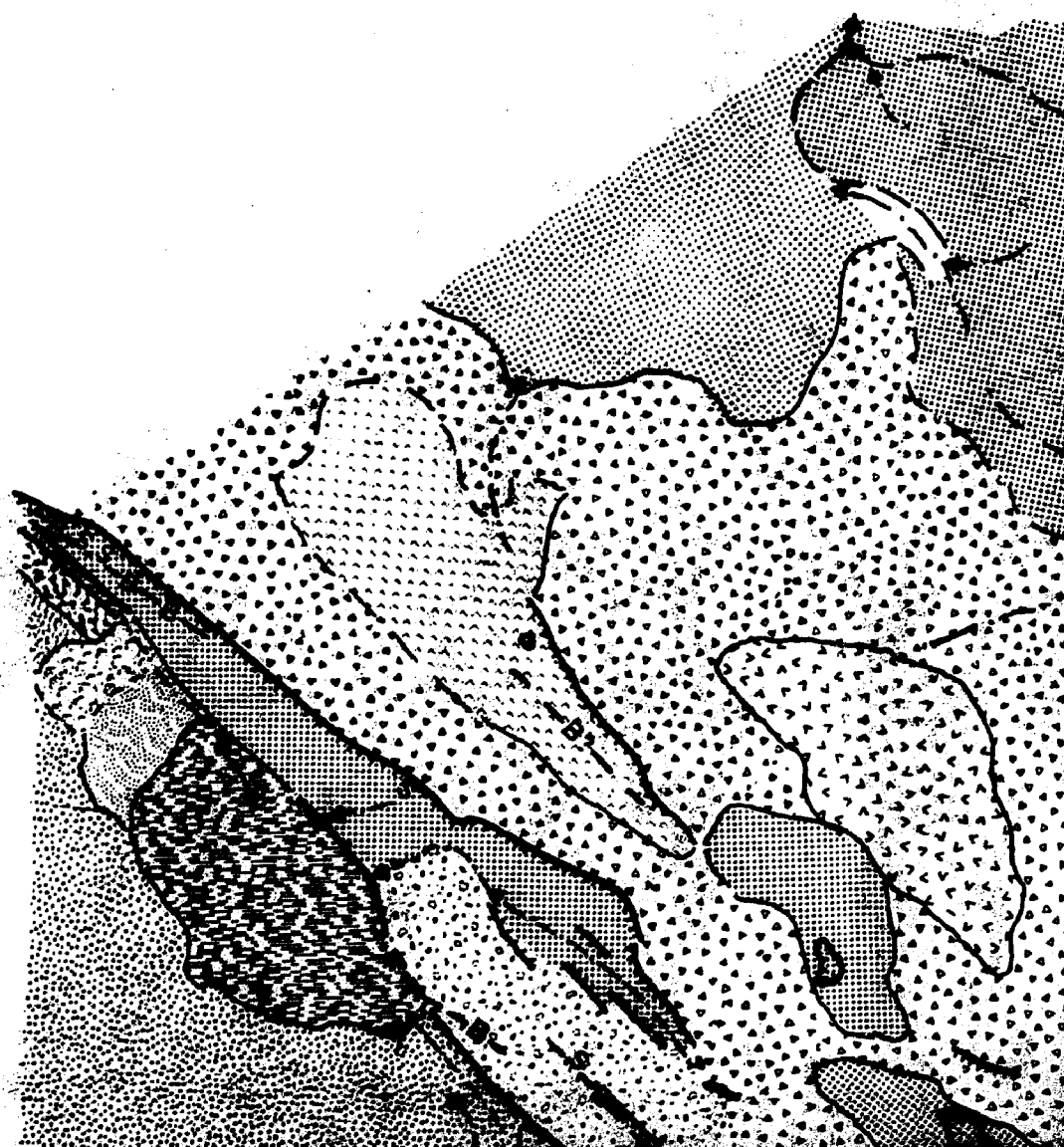

# INNER CALIF

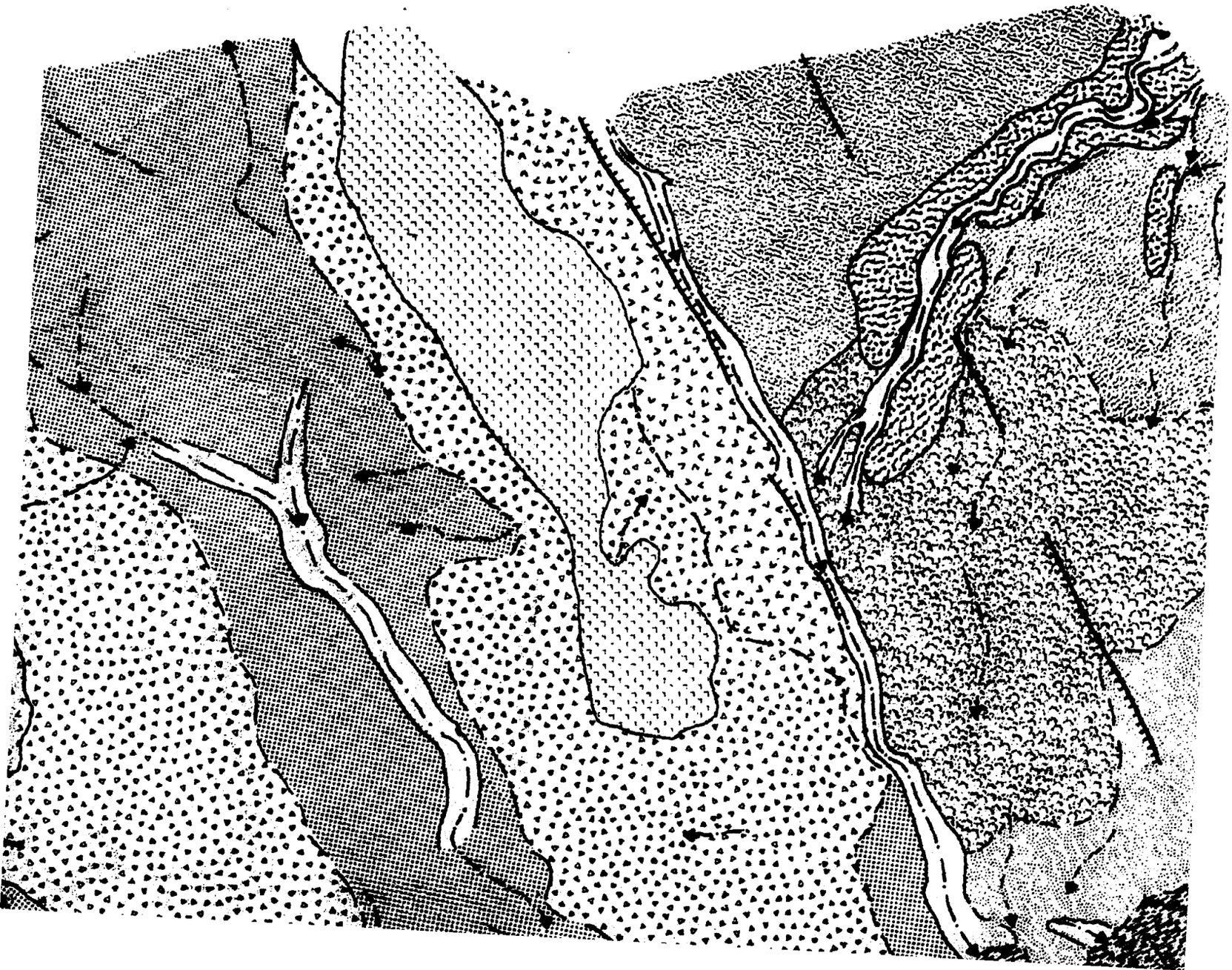

# FORNIA CONTINENTAL BOR

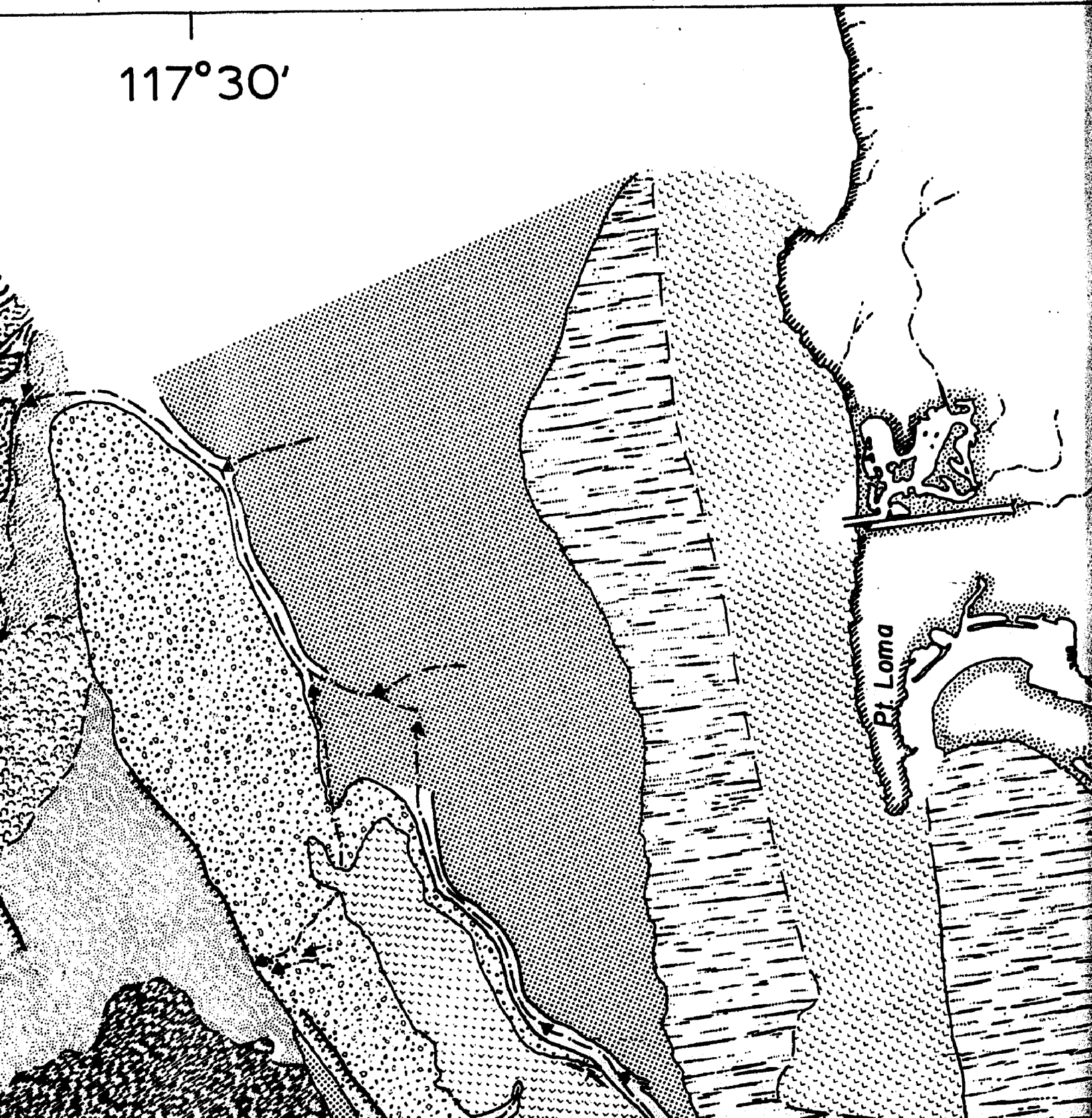

RDERLAND

117°00'

PL

GEOMO

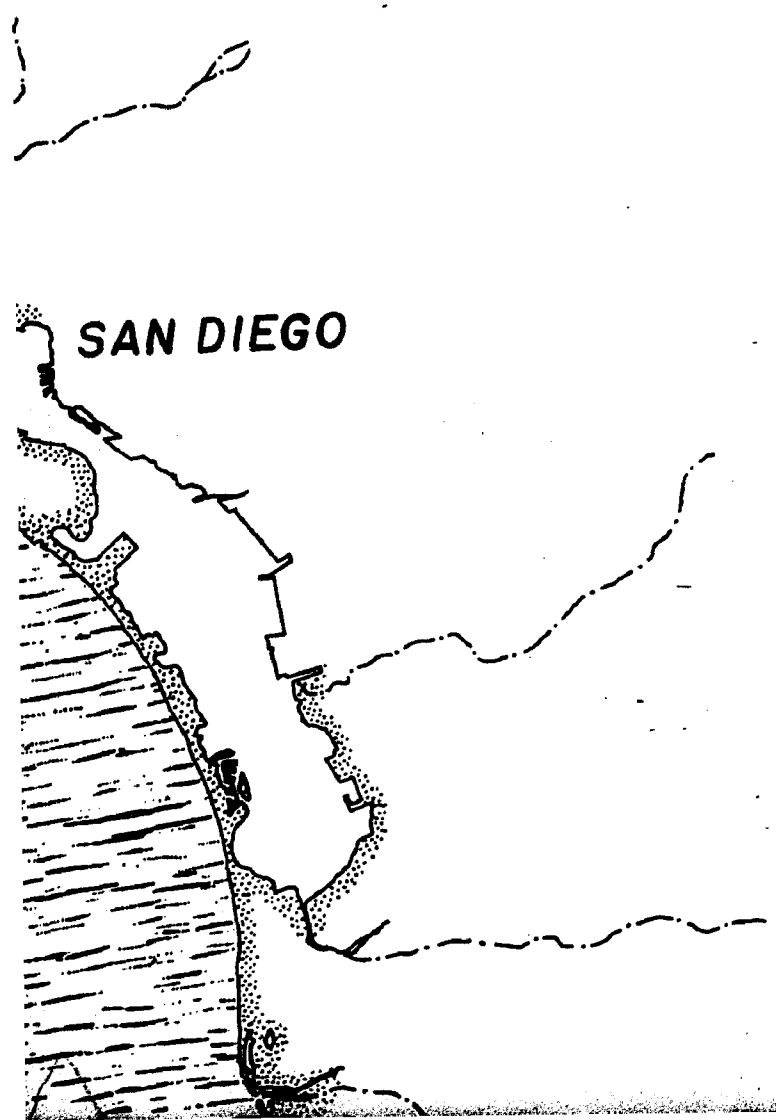


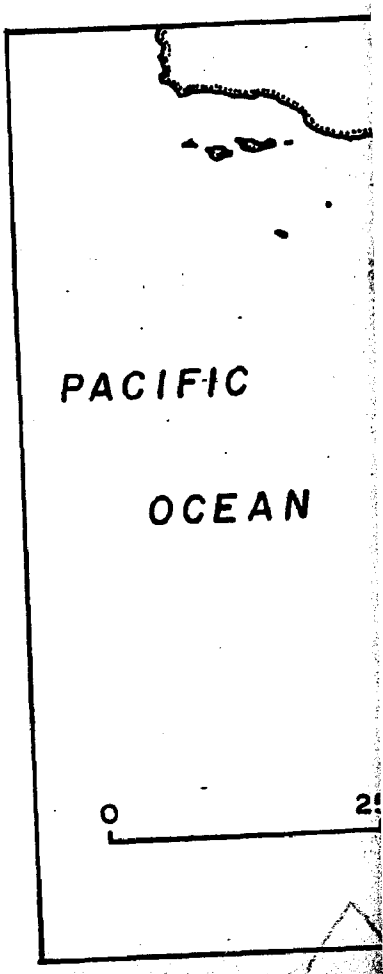

# ATE 2

# RPHOLOGY

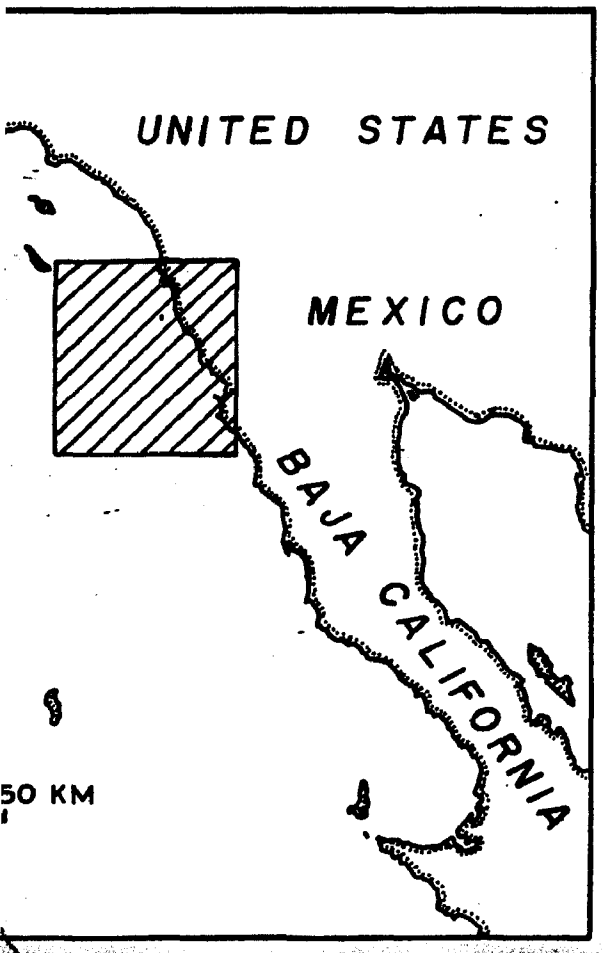

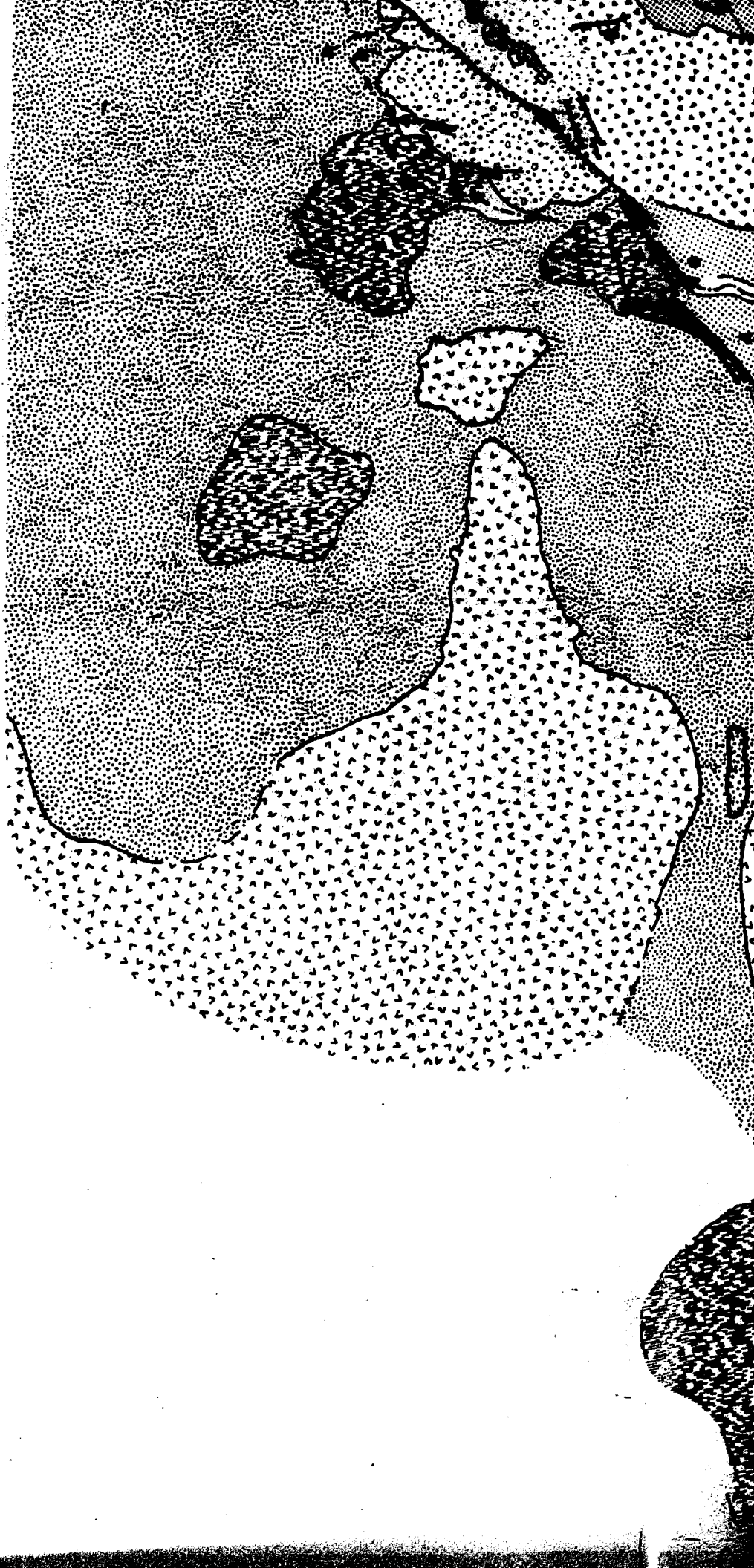

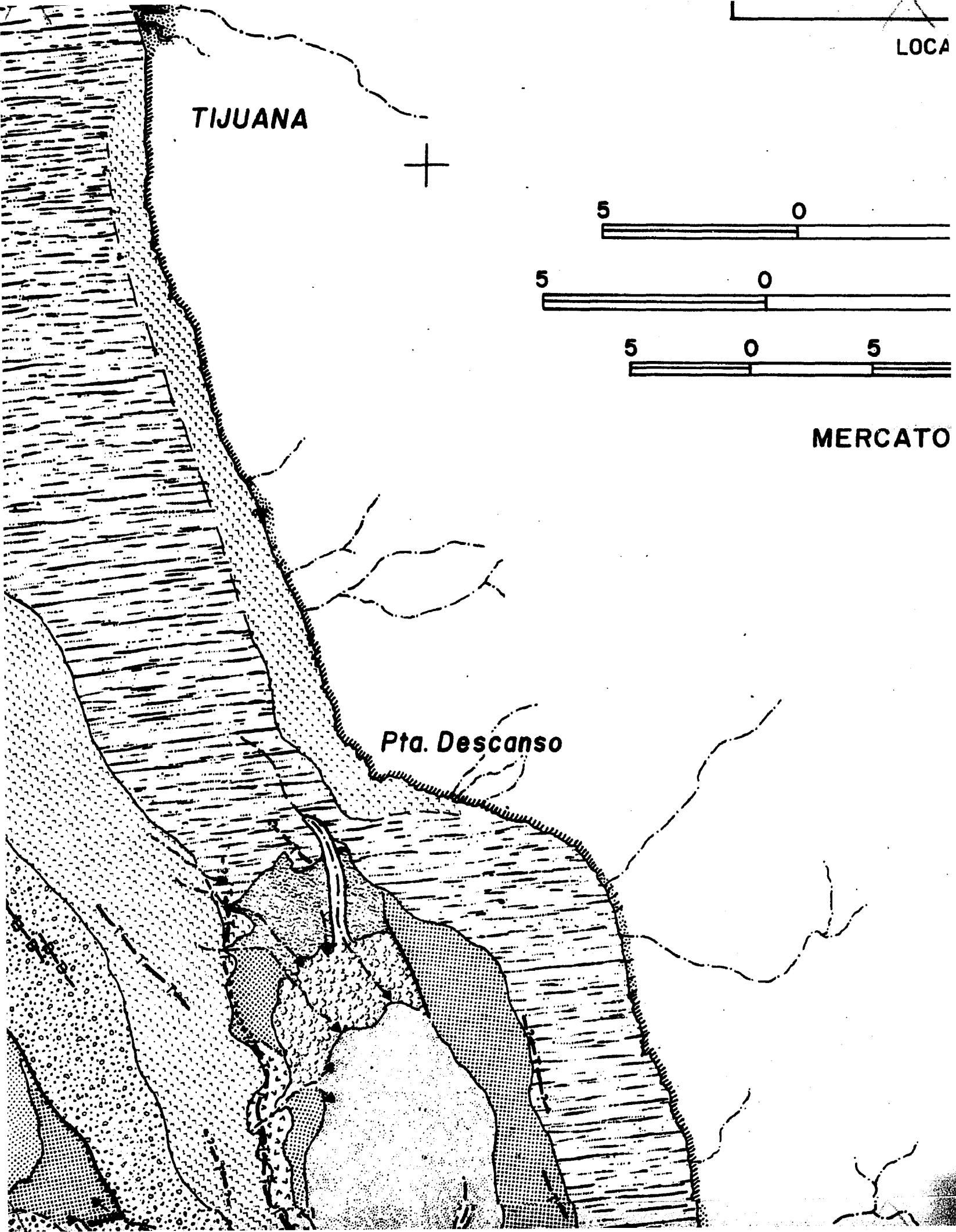
LOCA
TIJUANA
5
0
5
0
5
0
5
MERCATO
Pta. Descanso

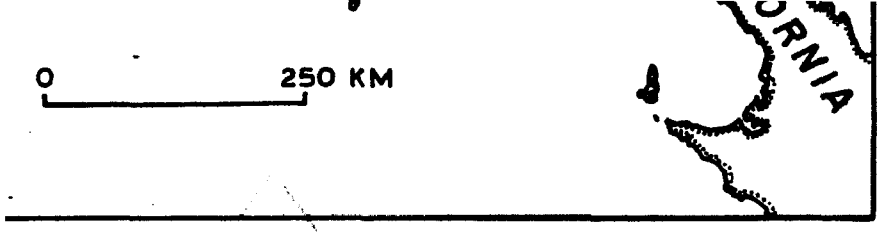


LOCATION OF MAP

32° 30′

0 5 10 15 ST. MILES

0 5 10 15 N. MILES

0 5 10 15 20 25 KILOMETERS

MERCATOR PROJECTION

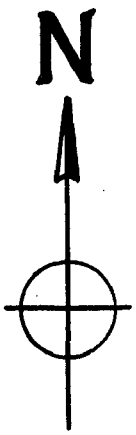

# EXPLANATIO

COASTLINES

Erosional

Depositional

SHELVES, BANKS, RIDGES AN

Ponded or Prograding Shelf S

Bedrock Shelves or Flat-Top

Bedrock Ridges and Peaks, Volcanic o

" " " " , Sedimento

" " " " , Undifferen

BASIN AND TROUGH SLOP

Bedrock (Same as Ridges and

Sediment Covered

T T T Terraces

B B B Benches

Escarpments

Slides, Slumps, and Debris Fl

SUBMARINE CANYONS, FAN VALLEYS, GULL

Major Channels (Dashed Where

Minor Channels and Gullie

Rift Valleys or Fault Trougl

BASINS

s Small, Closed Depressions or S

Flat, Ponded Sediments

Gently Sloping Basin Plain or L

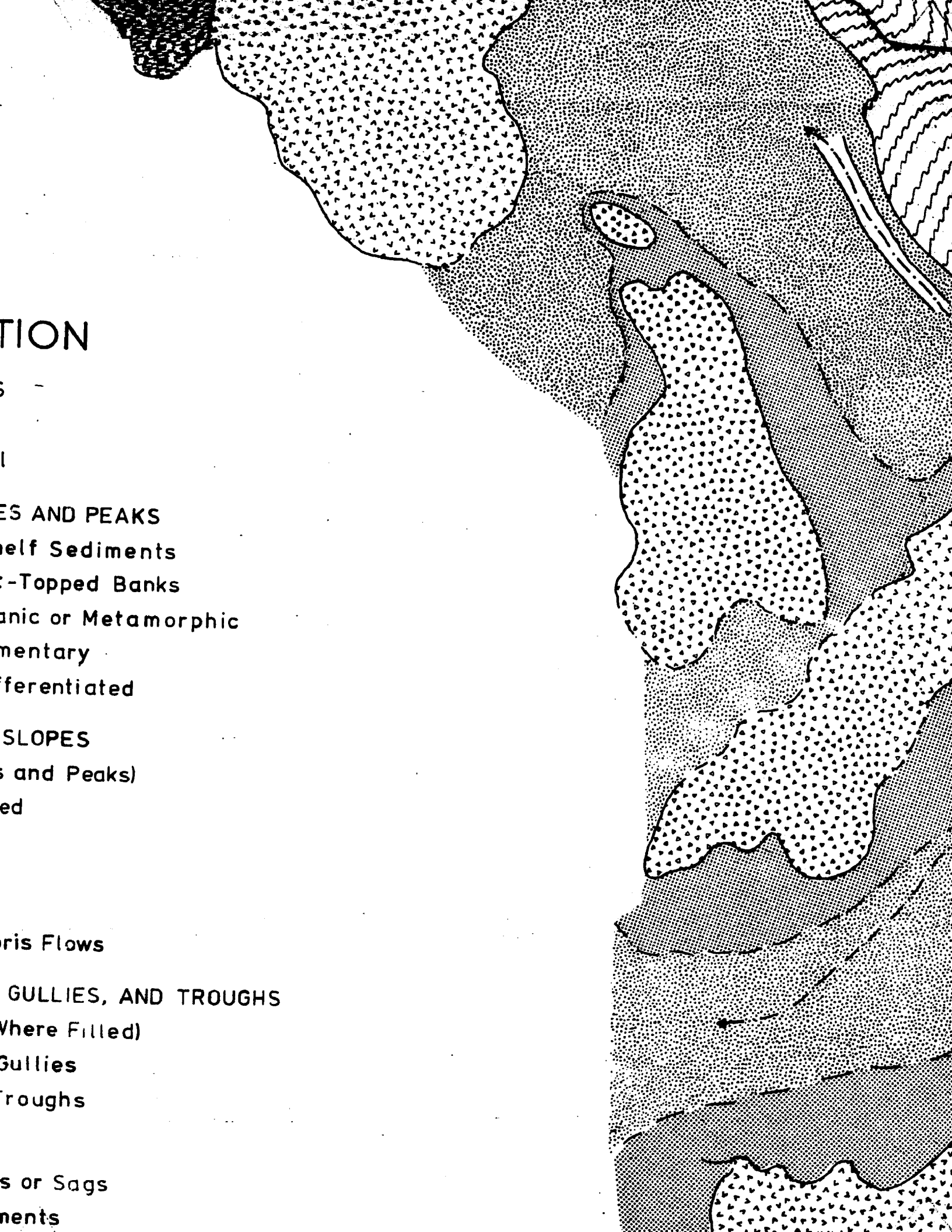
TION
S
l
ES AND PEAKS
helf Sediments
C-Topped Banks
anic or Metamorphic
mentary
fferentiated
SLOPES
s and Peaks)
ed
bris Flows
GULLIES, AND TROUGHS
Where Filled)
Gullies
Troughs
s or Sags
ments

Pta. Sals

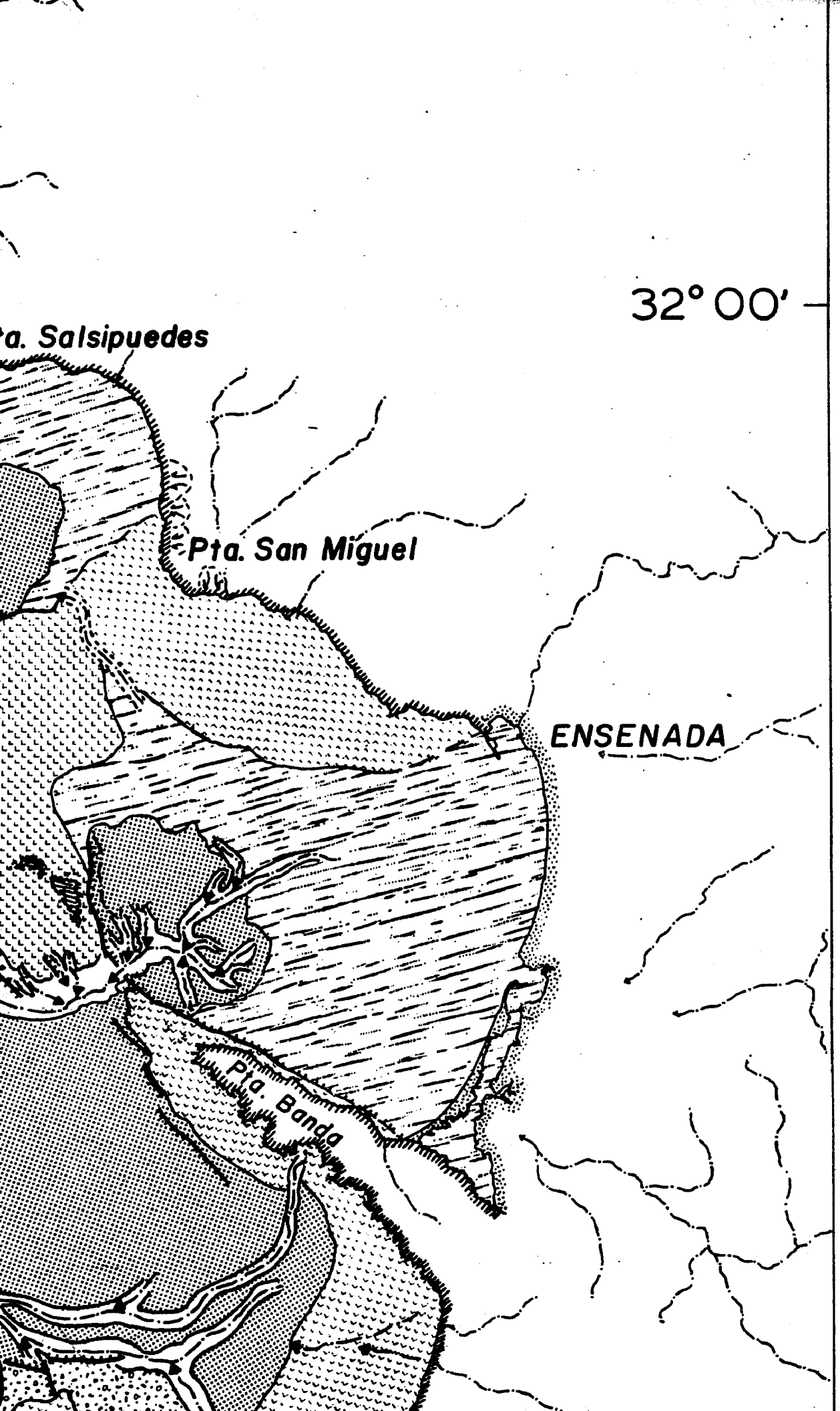
32° 00'
Pta. Salsipuedes
Pta. San Miguel
ENSENADA
Pta. Banda

s Small, Closed Depressions or Sa

Flat, Ponded Sediments

Gently Sloping Basin Plain or Lowe

Moderately Warped and Folde

Outer Basin Fills

SUBMARINE FANS AND SLOPE A

Levees

Overbank or Interchannel

Hummocky Topography

Large Sediment Waves

Slope Aprons

Compiled & Drafted by Mark R. l

, or Sags
ents
: Lower Fan
l Folded
s

OPE APRONS

nannel
phy
ves

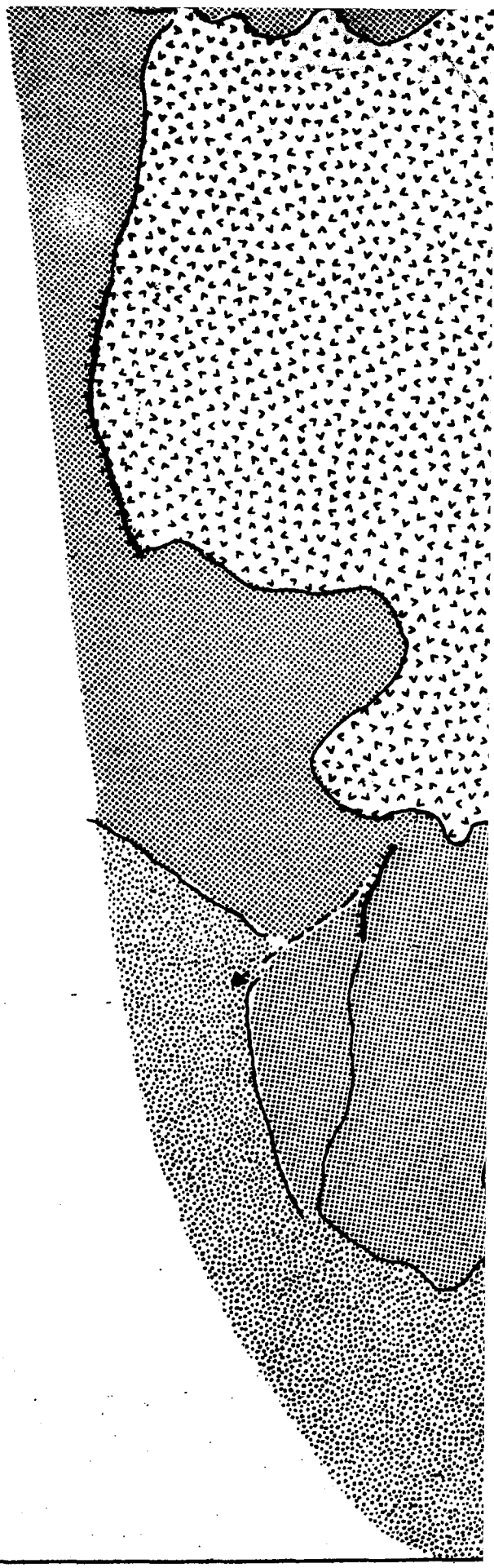

R. Legg (1985)

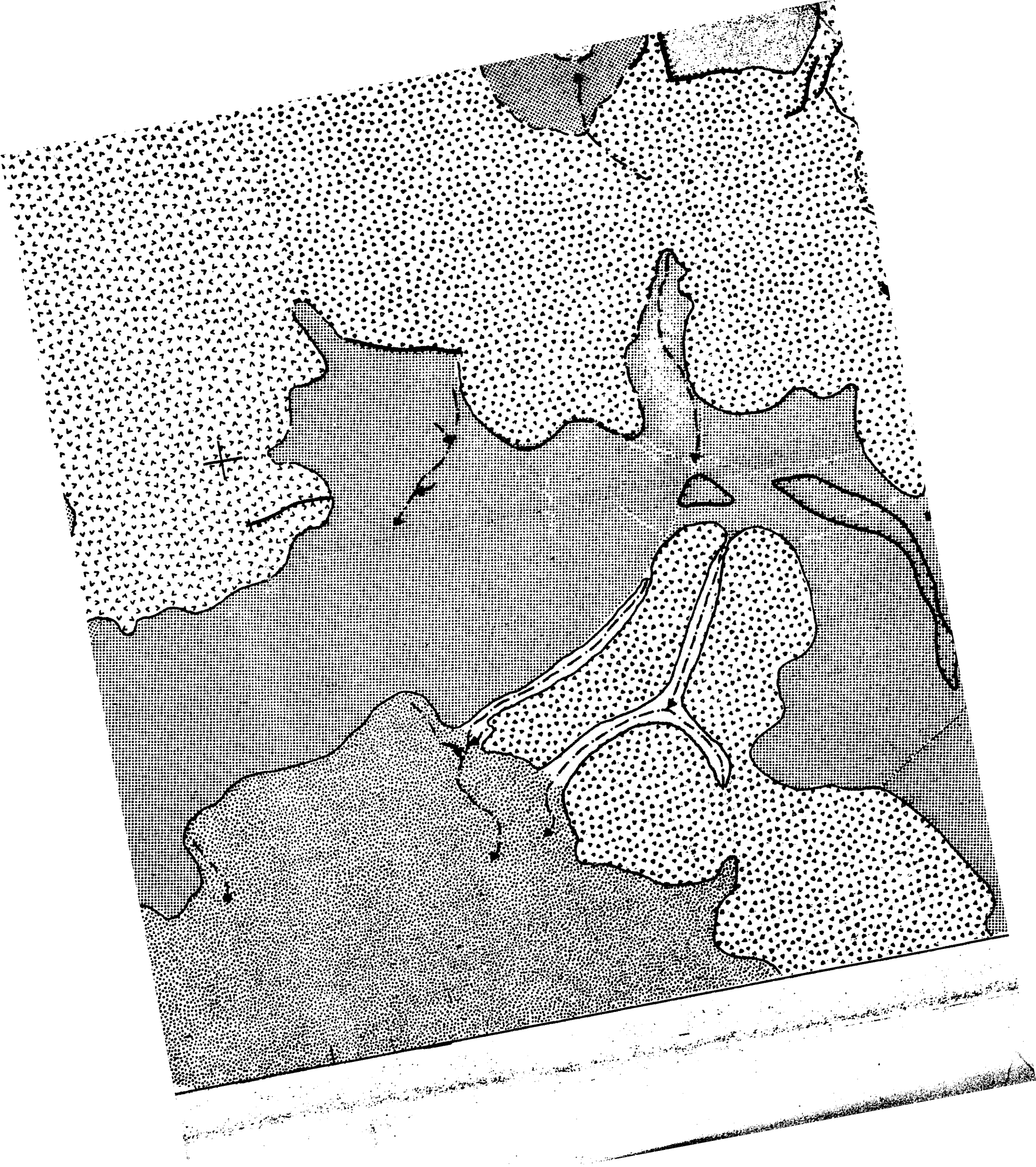

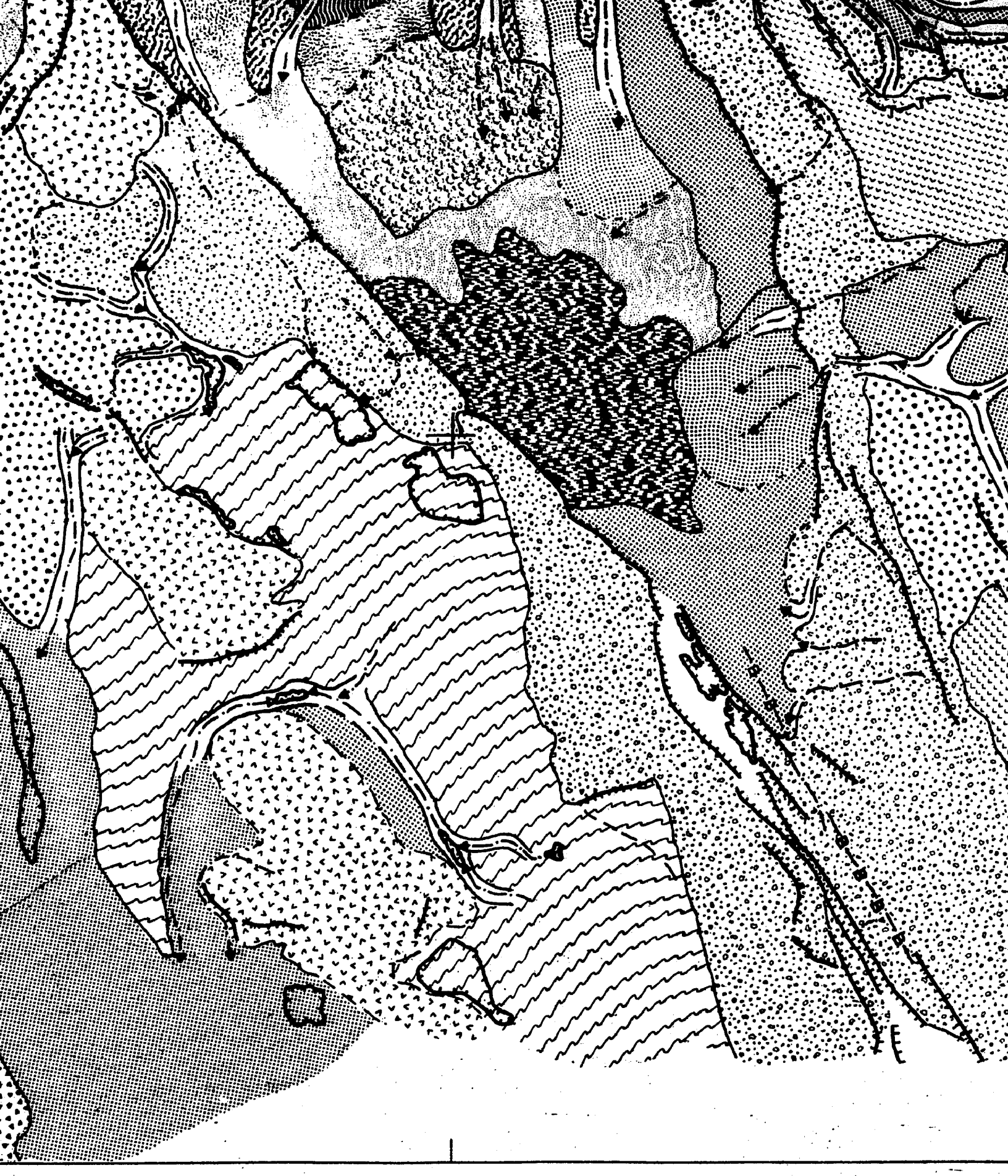

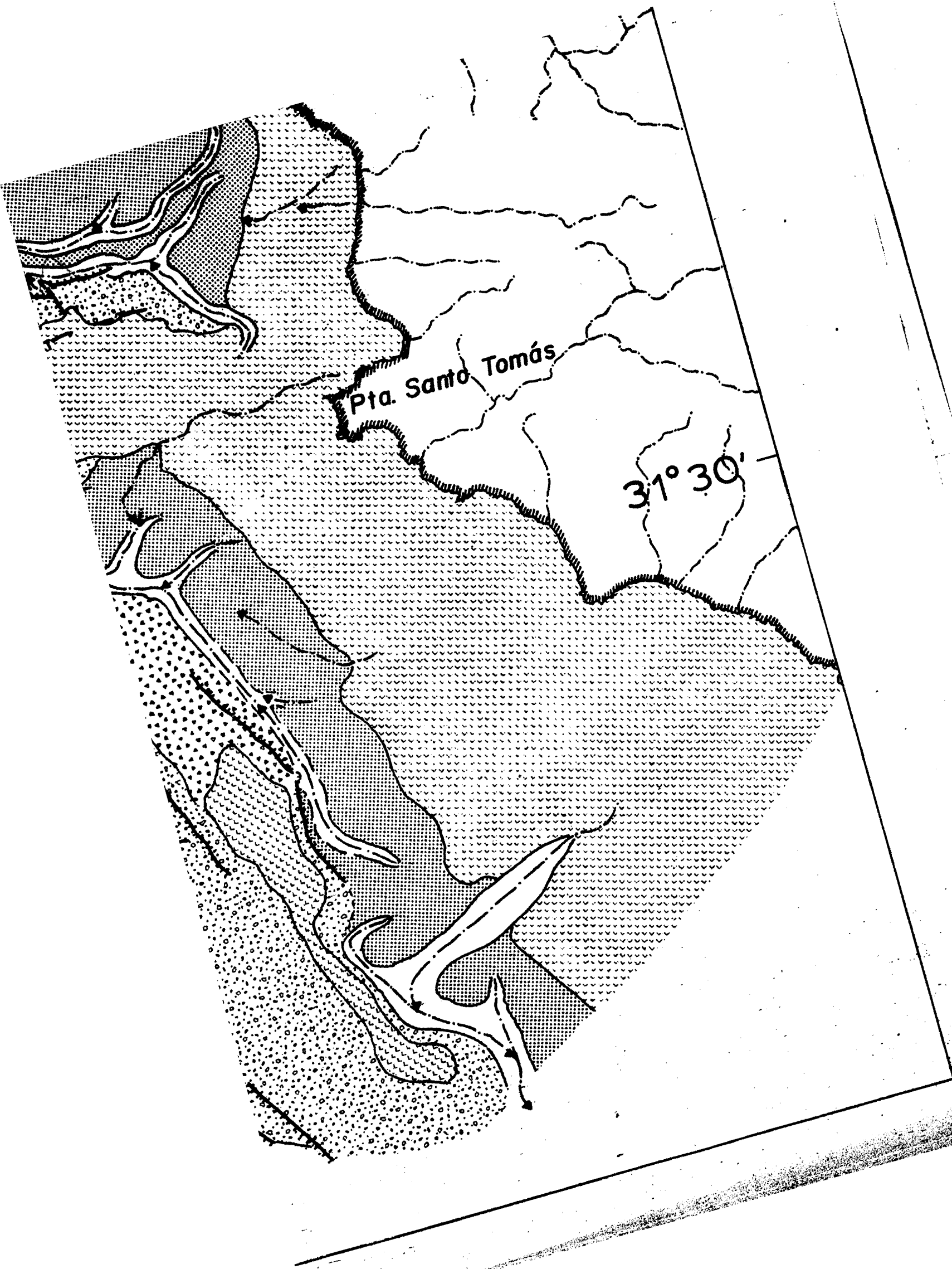
Pta. Santo Tomás
31° 30'

NO DATA

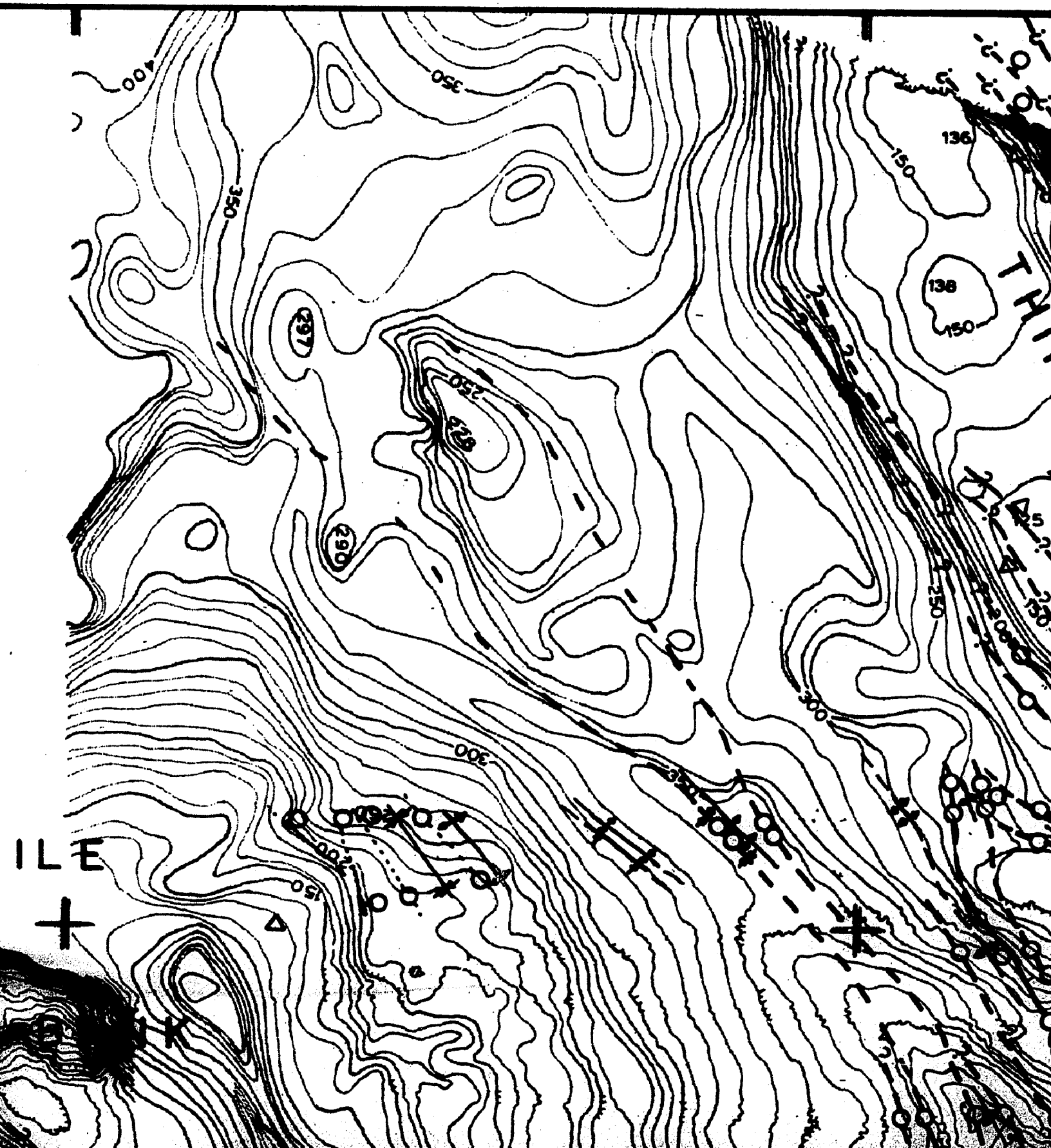

400
350
350
136
150
138
150
297
250
290
250
300
300
150
ILE

# INNER CALIFORN

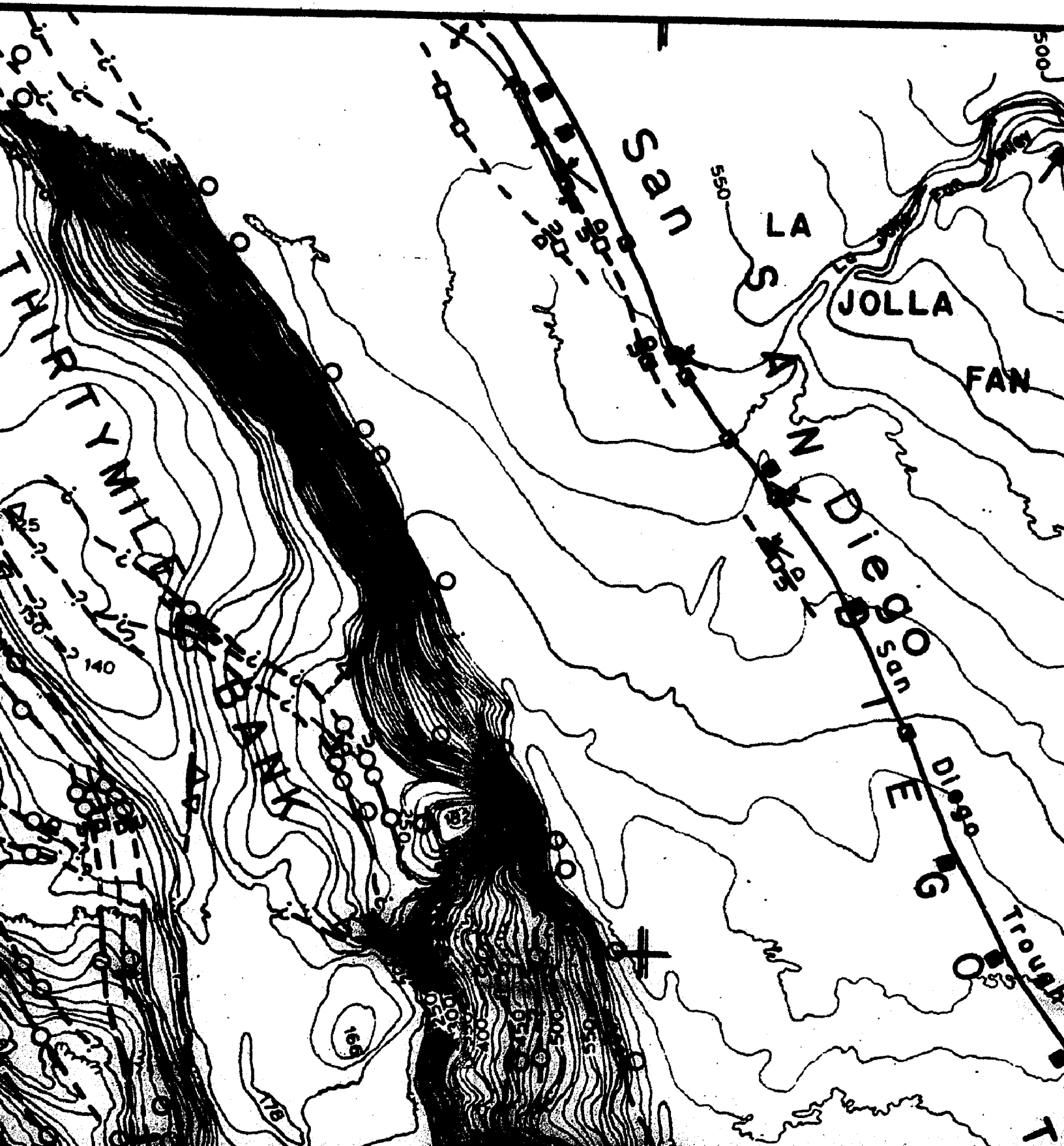

# IIA CONTINENTAL BO

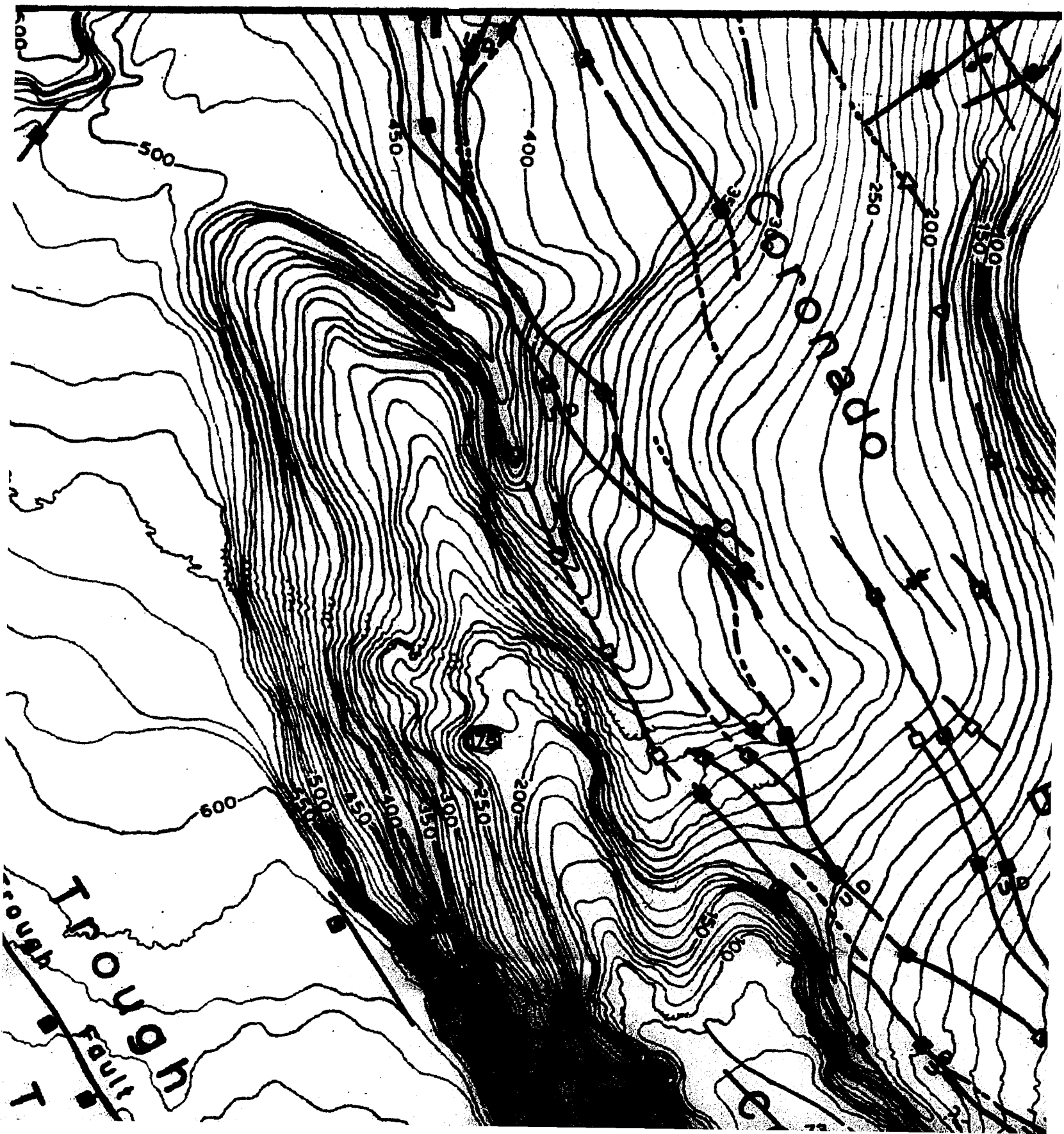

RDERLAND

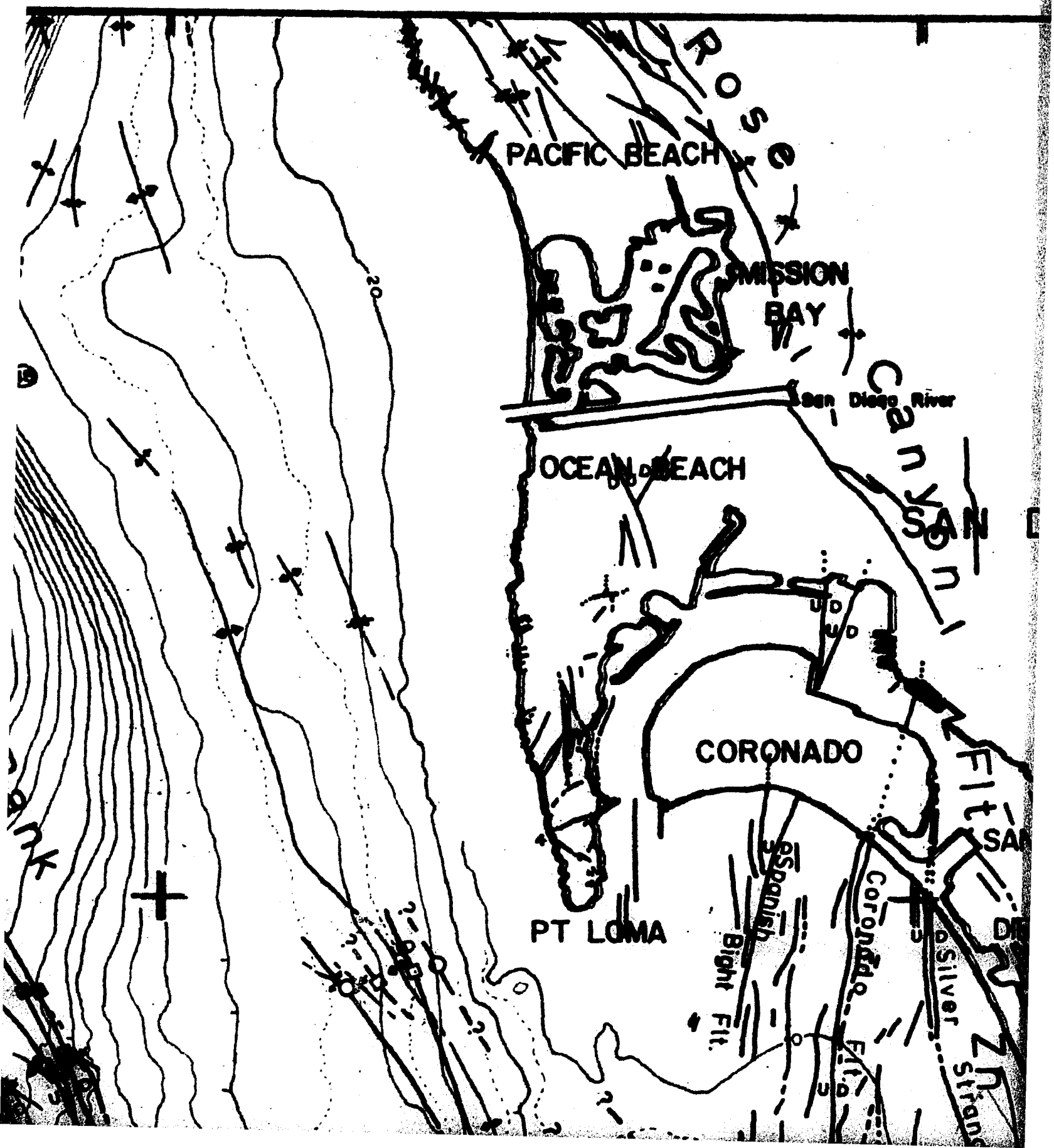

Rose
PACIFIC BEACH
MISSION
BAY
San Diego River
Canyon
OCEAN BEACH
SAN
CORONADO
Flt
PT LOMA
Spanish
Bight
Flt.
Coronado
Flt.
Silver
Strand

# PLATE 3A

# RECENCY AND CHARA
# OF FAULTING

N DIEGO

0 5

STATUTE MILES

0 1 2 3 4 5

NAUTICAL MILES

0 5 10

KILOMETERS

MERCATOR PROJECTION

CONTOUR INTERVAL 10 FATHOMS
(UNCORRECTED)

# E 3A
# ) CHARACTER
# ULTING

10

MILES

10

MILES

10

ETERS

PROJECTION

AL 10 FATHOMS
ECTED)

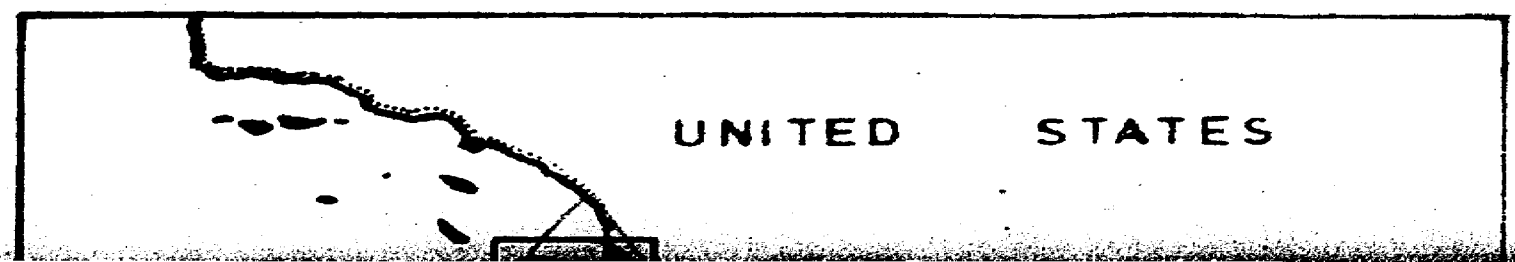

32° 50′

32° 40′

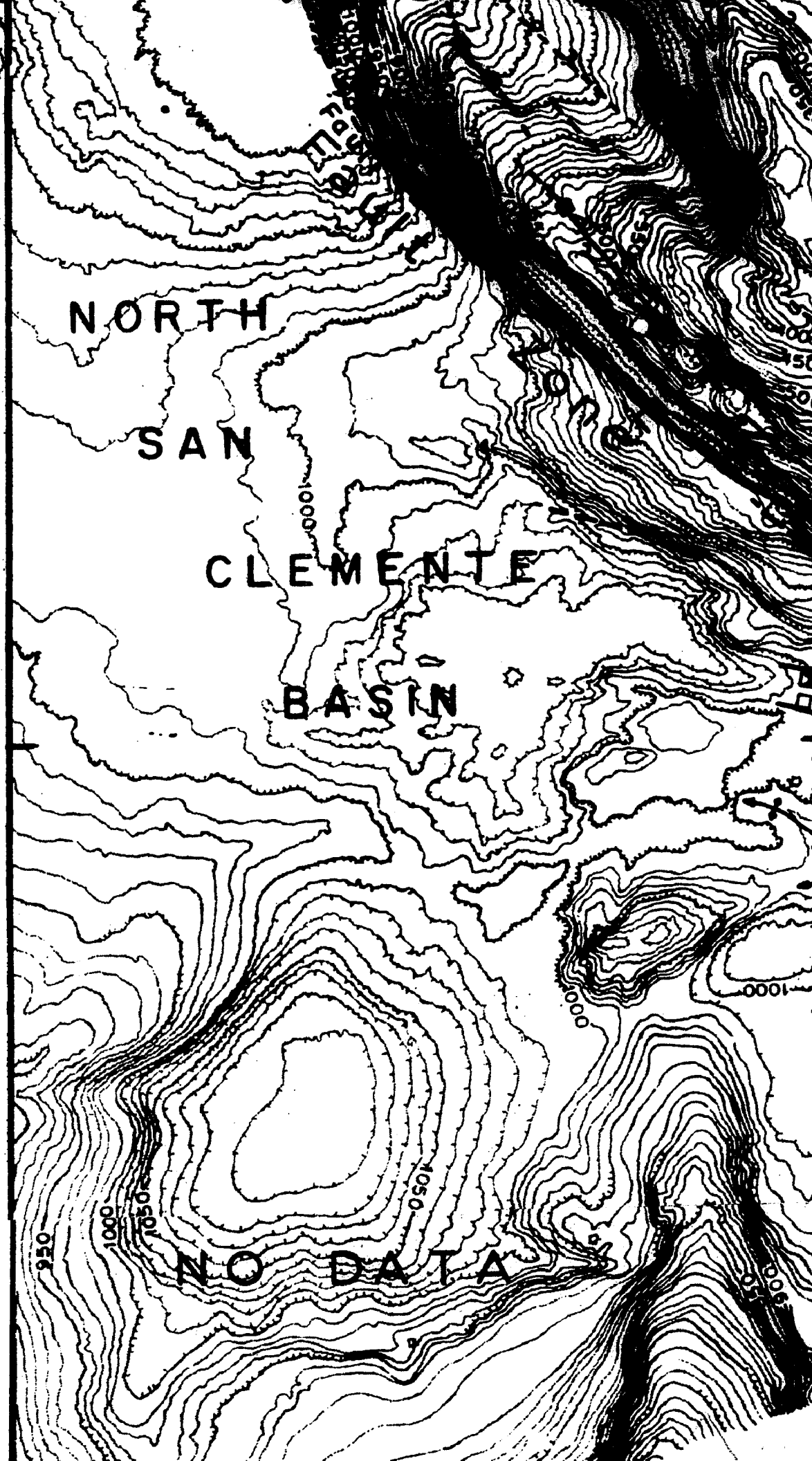
NORTH
SAN
CLEMENTE
BASIN
Zone
NO DATA
1000
1050
950

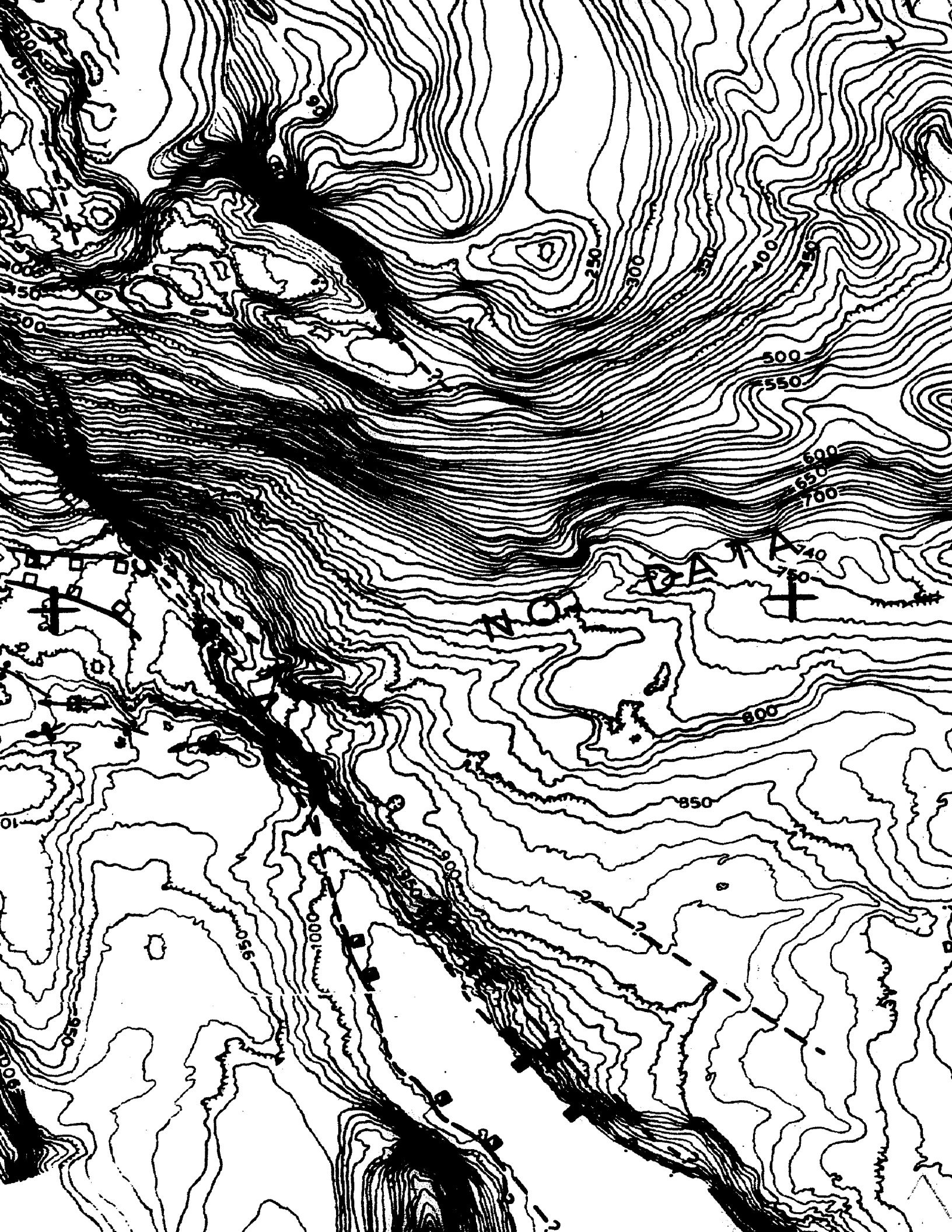
250
300
350
400
450
500
550
600
650
700
750
800
850
900
950
1000
NO DATA

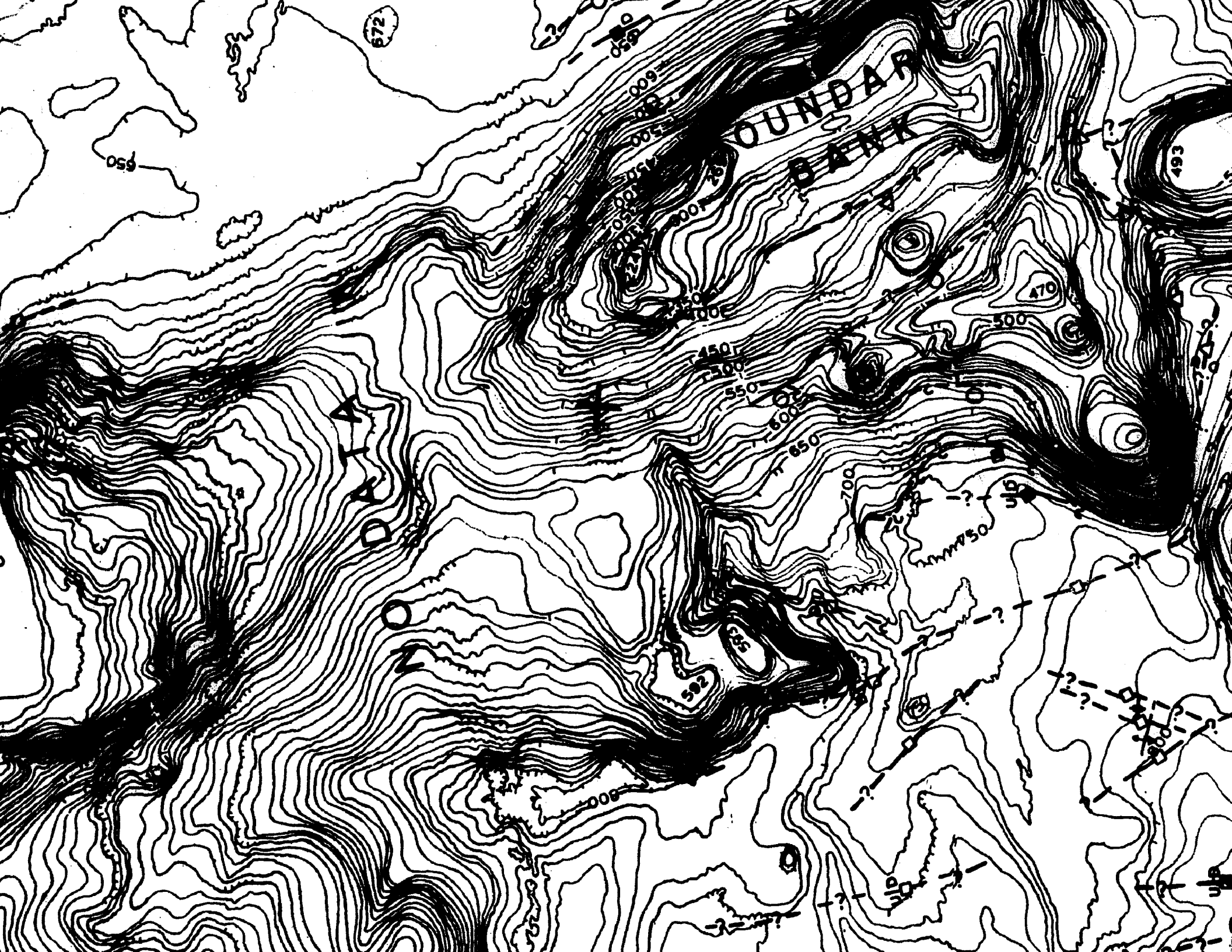

OUNDAR
BANK
672
650
493
470
500
450
500
550
600
650
700
750
592

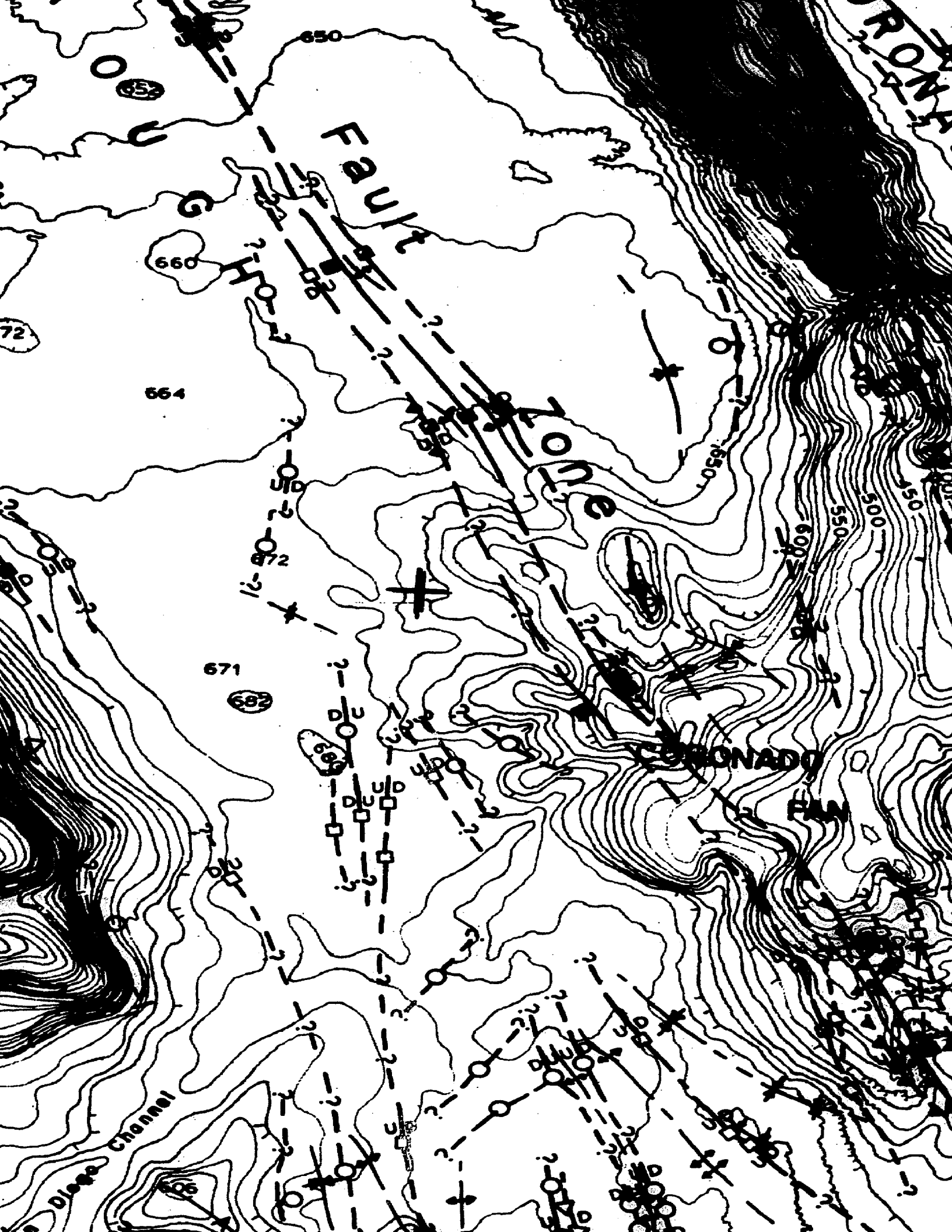

Fault Zone
CORONADO FAN
Diego Channel
650
652
660
664
672
671
682
606
550
500
450

Fault
and
CORONADO SHELF
Coro
Zone
CORONADOS
South Coronado
Coronado
Fault

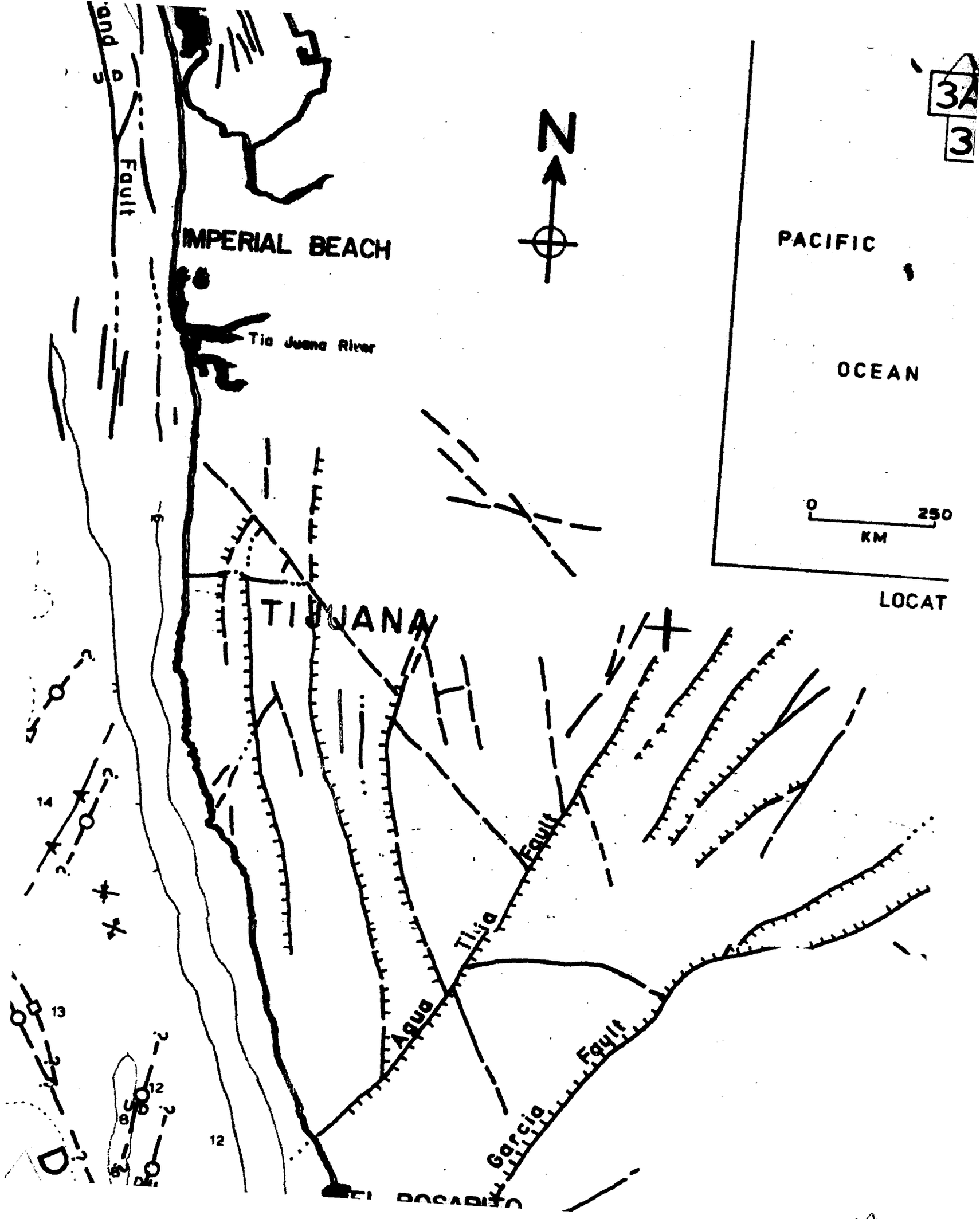
3A
3
N
PACIFIC
OCEAN
0
250
KM
LOCAT
IMPERIAL BEACH
Tia Juana River
TIJUANA
Fault
Agua Tijia Fault
Garcia Fault
14
13
12
12

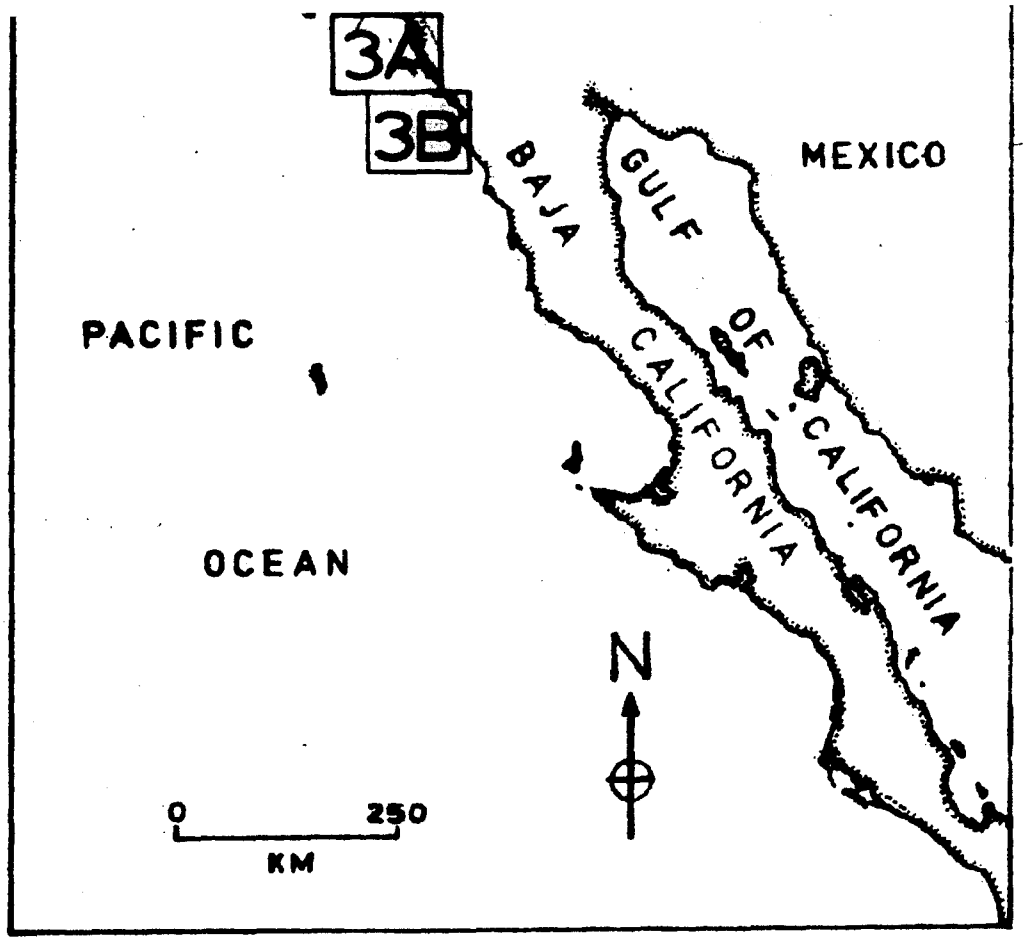


LOCATION OF PLATES

32° 30'

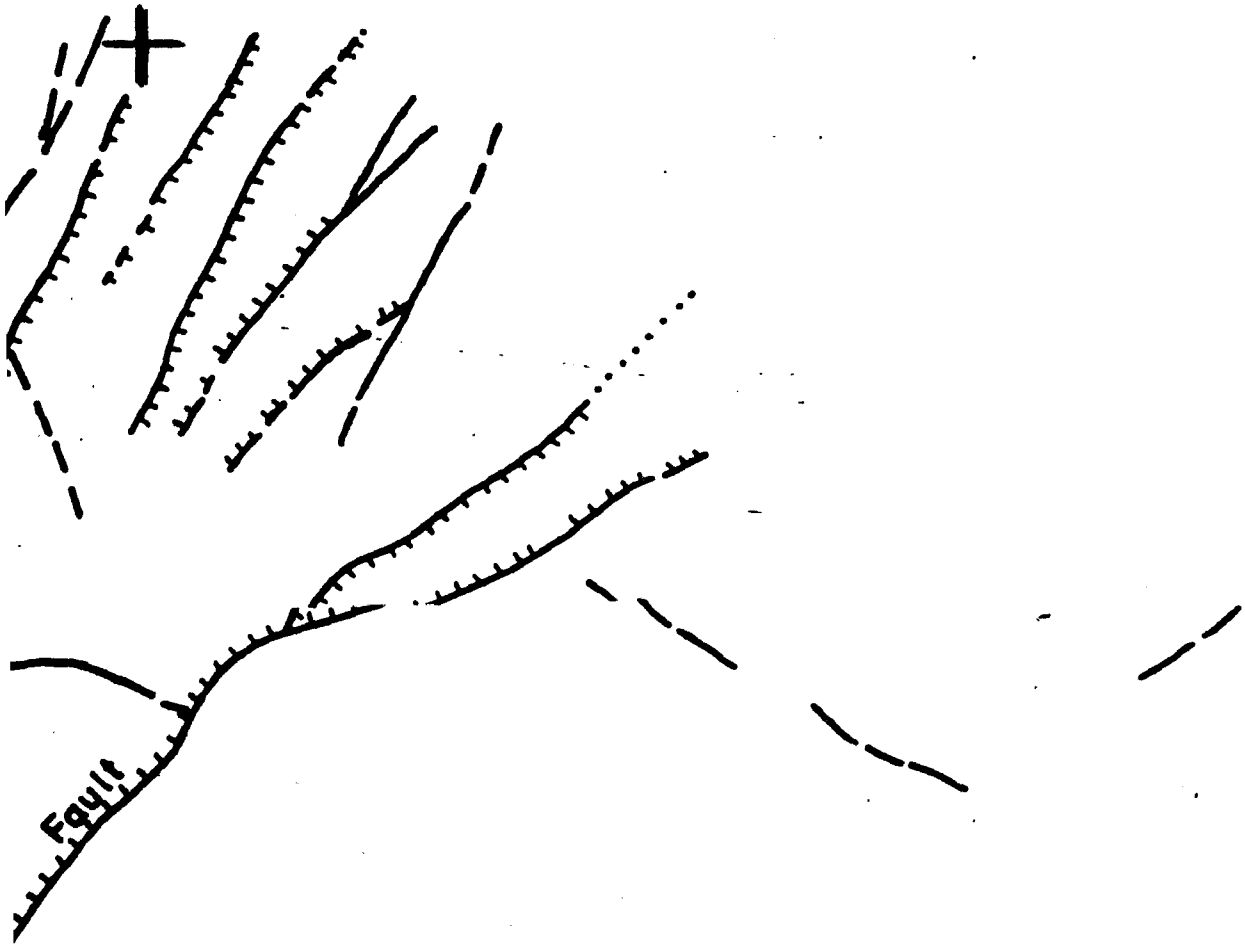

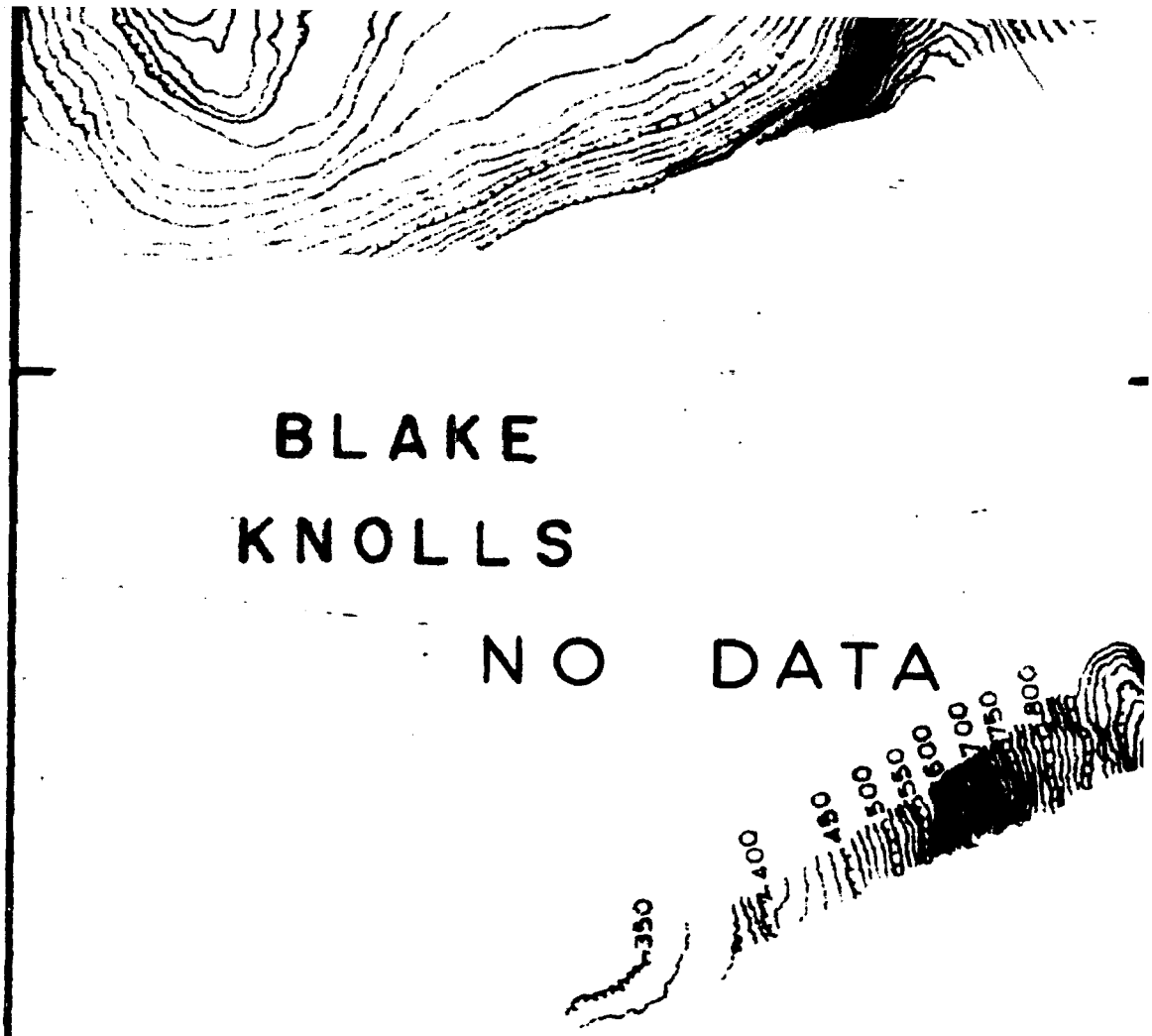


Compiled & Drafted by Mark R. Legg (1985)

# EXPLANATION

REVERSE FAULT

FAULTS: SOLID WHERE WELL-DEFINED;
WHERE APPROXIMATELY LOCATED OR
QUERIED WHERE EXISTENCE IS UNCER
WHERE FAULT OFFSETS SEA FLOOR,
BOL IS SHOWN ON BAR ON DOWNTH
OTHERWISE, WHERE AGE WAS DETE
SYMBOL IS SHOWN ASTRIDE FAULT
OFFSET IS SHOWN BY "D" AND "U"
THROWN AND UPTHROWN SIDES.

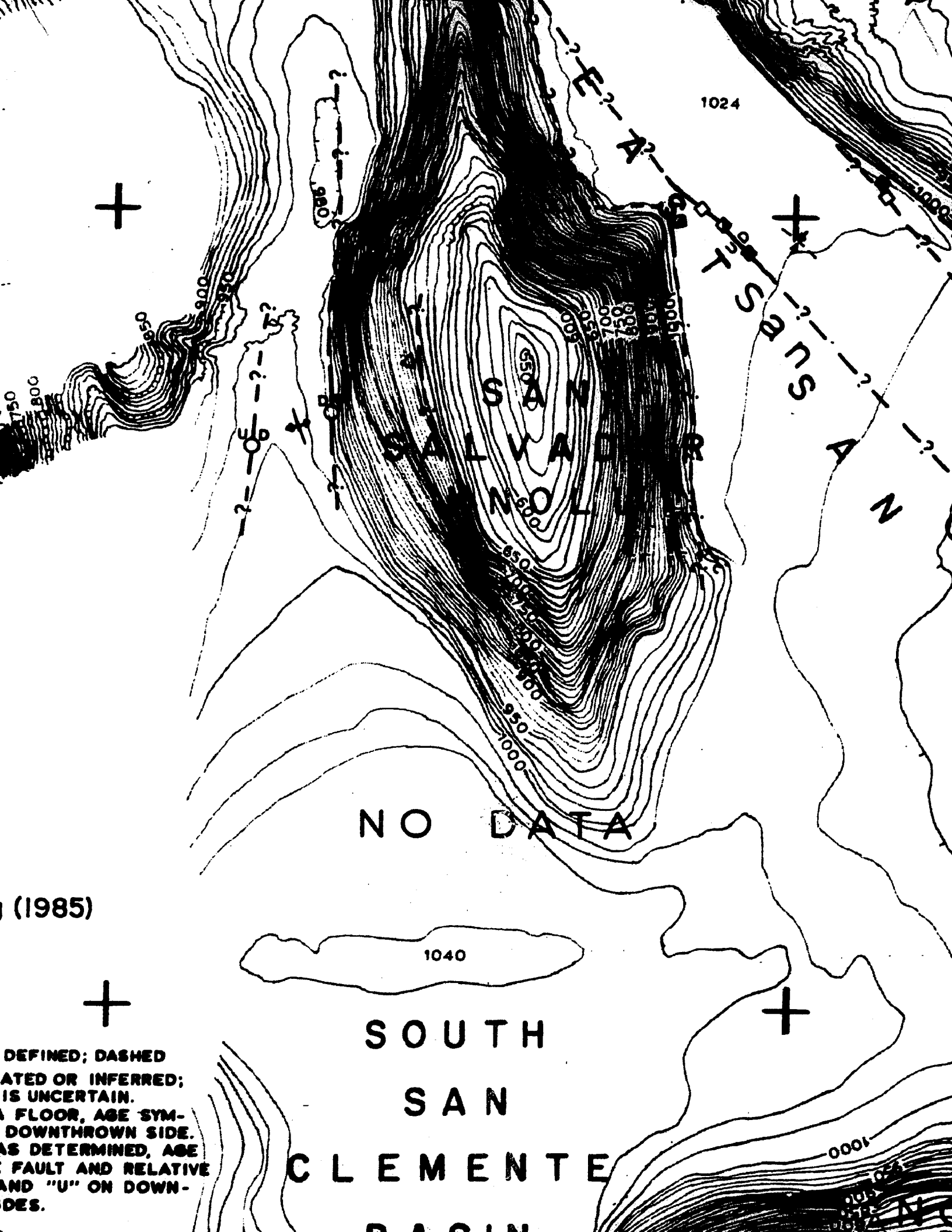

1024
SAN
SALVADOR
NO DATA
1040
SOUTH
SAN
CLEMENTE
(1985)
DEFINED; DASHED
ATED OR INFERRED;
IS UNCERTAIN.
FLOOR, AGE SYM-
DOWNTHROWN SIDE.
AS DETERMINED, AGE
FAULT AND RELATIVE
AND "U" ON DOWN-
DES.

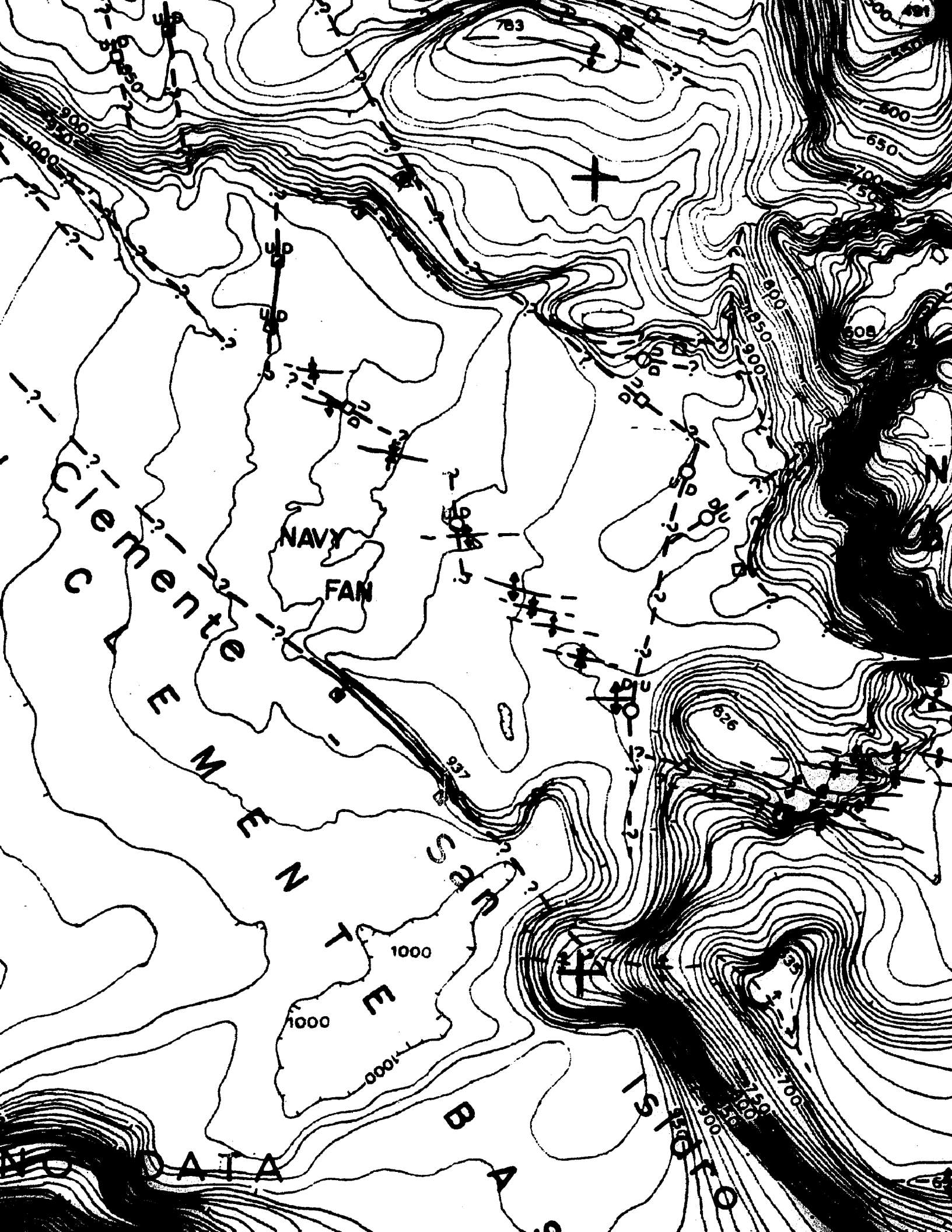

NAVY
FAN
Clemente
CLEMENTE
San
Isidro
BA
NO DATA
783
491
600
650
700
750
800
850
900
950
1000
937
826
1000
1000
1000

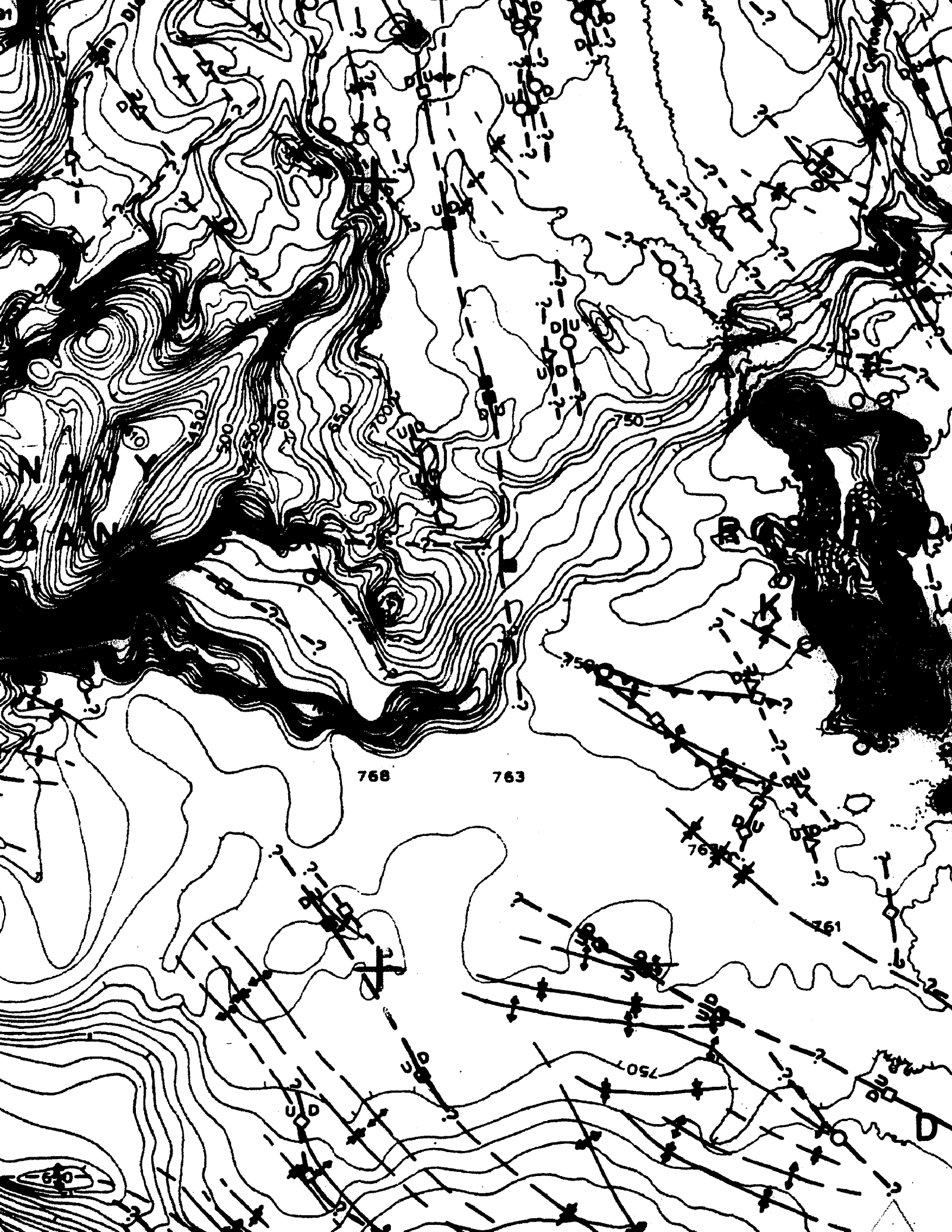

NAVY
BAN
450
500
550
600
650
700
750
768
763
761
750
D

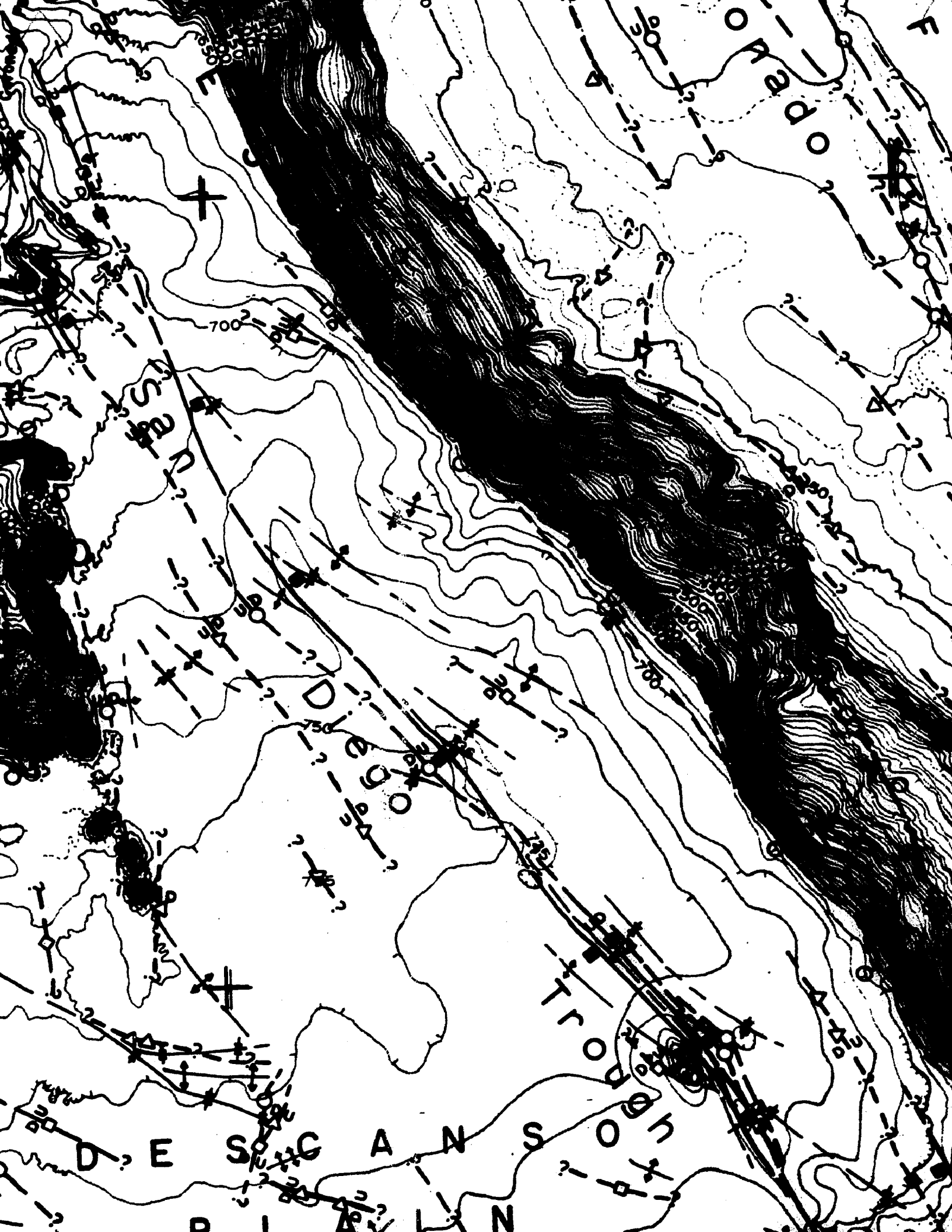

San Diego Trough
DESCANSO
700
750

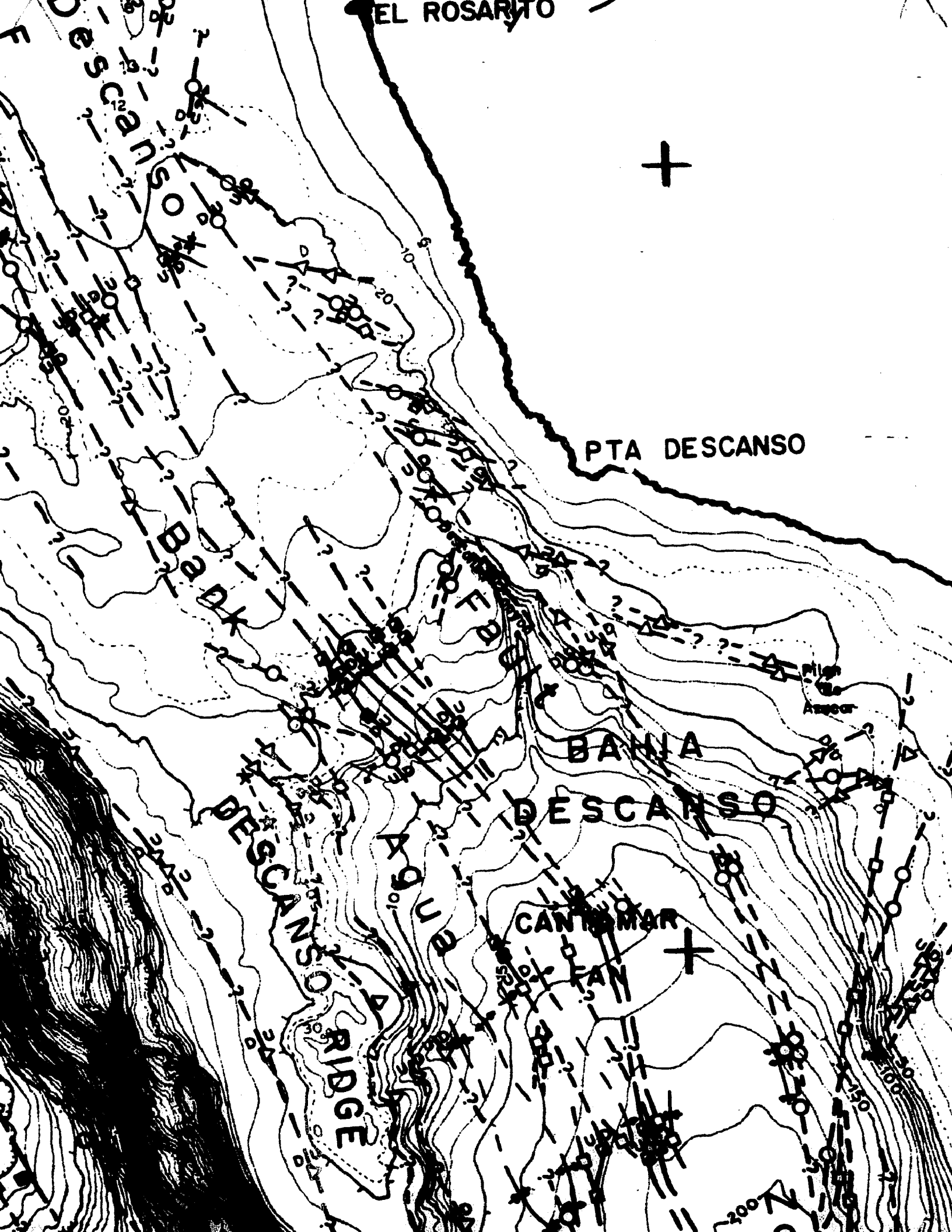
EL ROSARITO
PTA DESCANSO
Descanso
Bank
Fault
BAHIA
DESCANSO
Agua
DESCANSO
RIDGE
CANTAMAR
FAN
Pilon
de
Azucar

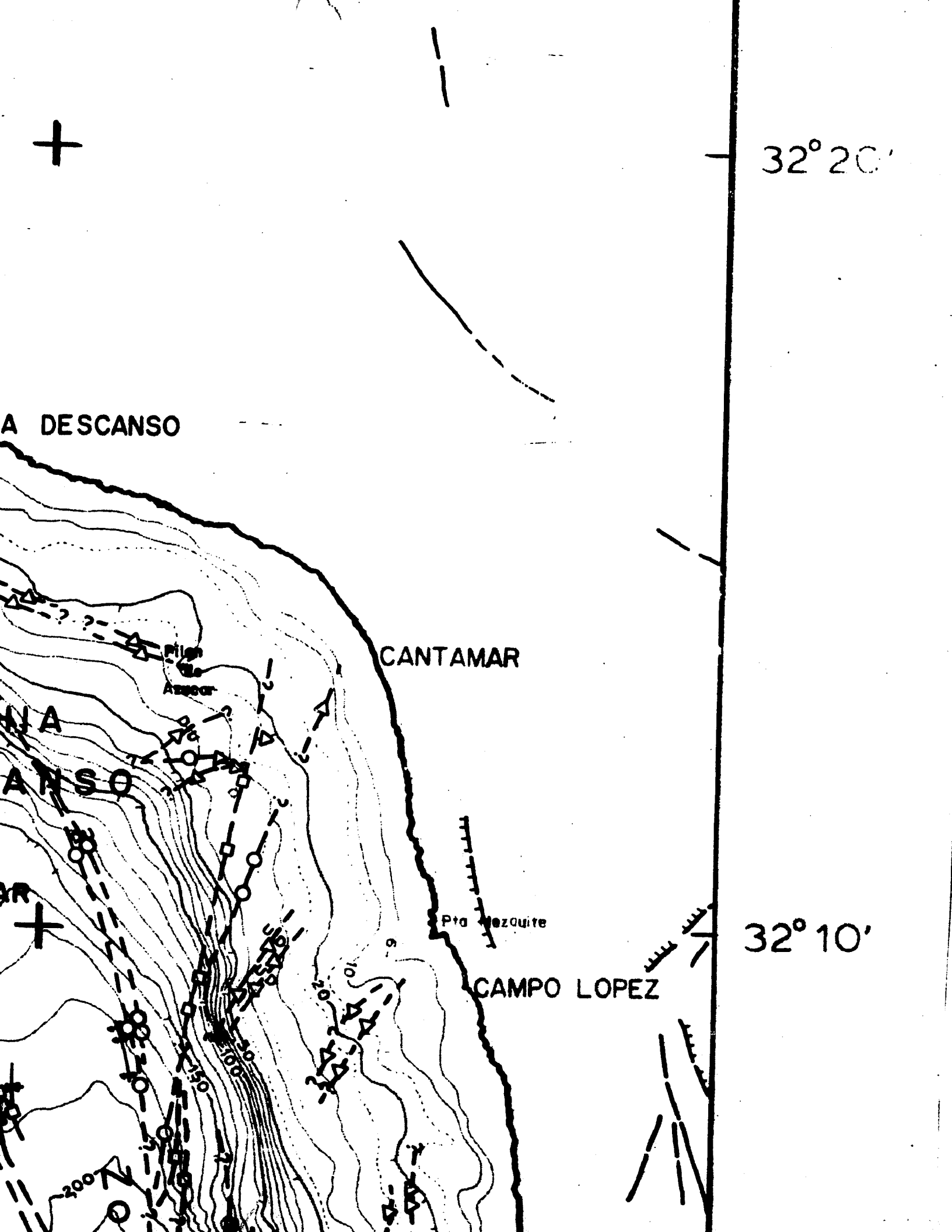
32°20'
A DESCANSO
CANTAMAR
NA
ANSO
Pta Mezquite
32°10'
CAMPO LOPEZ
-100
-150
-200

# EXPLANATION

REVERSE FAULT

FAULTS: SOLID WHERE WELL-DEFINED; DASHE
WHERE APPROXIMATELY LOCATED OR INFERR
QUERIED WHERE EXISTENCE IS UNCERTAIN.
WHERE FAULT OFFSETS SEA FLOOR, AGE SY
BOL IS SHOWN ON BAR ON DOWNTHROWN S
OTHERWISE, WHERE AGE WAS DETERMINED,
SYMBOL IS SHOWN ASTRIDE FAULT AND REL
OFFSET IS SHOWN BY "D" AND "U" ON DOW
THROWN AND UPTHROWN SIDES.

AGES OF FAULTS ARE INDICATED AS FOLLOW

- ■ CUTS STRATA OF HOLOCENE AGE.
- ■ CUTS STRATA OF LATE QUATERNARY AGE, UNDIFFERENTIATED.
- □ CUTS STRATA OF PLEISTOCENE AGE.
- ○ CUTS STRATA OF LATE TERTIARY-QUATERN AGE, UNDIFFERENTIATED.
- △ CUTS STRATA OF MIOCENE AGE OR OLDER.

FOLDS: SOLID WHERE WELL-DEFINED; DASHED WHERE INFERRED; QUERIED WHERE UNCERTA

ANTICLINE.

SYNCLINE.

ANTICLINE IN OLDER SEDIMENTS OR ACOU BASEMENT.

SYNCLINE IN OLDER SEDIMENTS OR ACOUST BASEMENT.

NOTE: ONSHORE FAULTS FROM GASTIL & OTHERS (1975) AND KENNEDY &

118°10′ 118° C

egg (1985)

'ELL-DEFINED; DASHED
' LOCATED OR INFERRED;
ENCE IS UNCERTAIN.
E SEA FLOOR, AGE SYM-
E ON DOWNTHROWN SIDE.
IE WAS DETERMINED, AGE
TRIDE FAULT AND RELATIVE
"D" AND "U" ON DOWN-
WN SIDES.

NDICATED AS FOLLOWS:

ICENE AGE.

QUATERNARY AGE,

STOCENE AGE.

TERTIARY-QUATERNARY
ED.

CENE AGE OR OLDER.

LL-DEFINED; DASHED
RIED WHERE UNCERTAIN

SEDIMENTS OR ACOUSTIC

EDIMENTS OR ACOUSTIC

975) AND KENNEDY & OTHERS (1980)

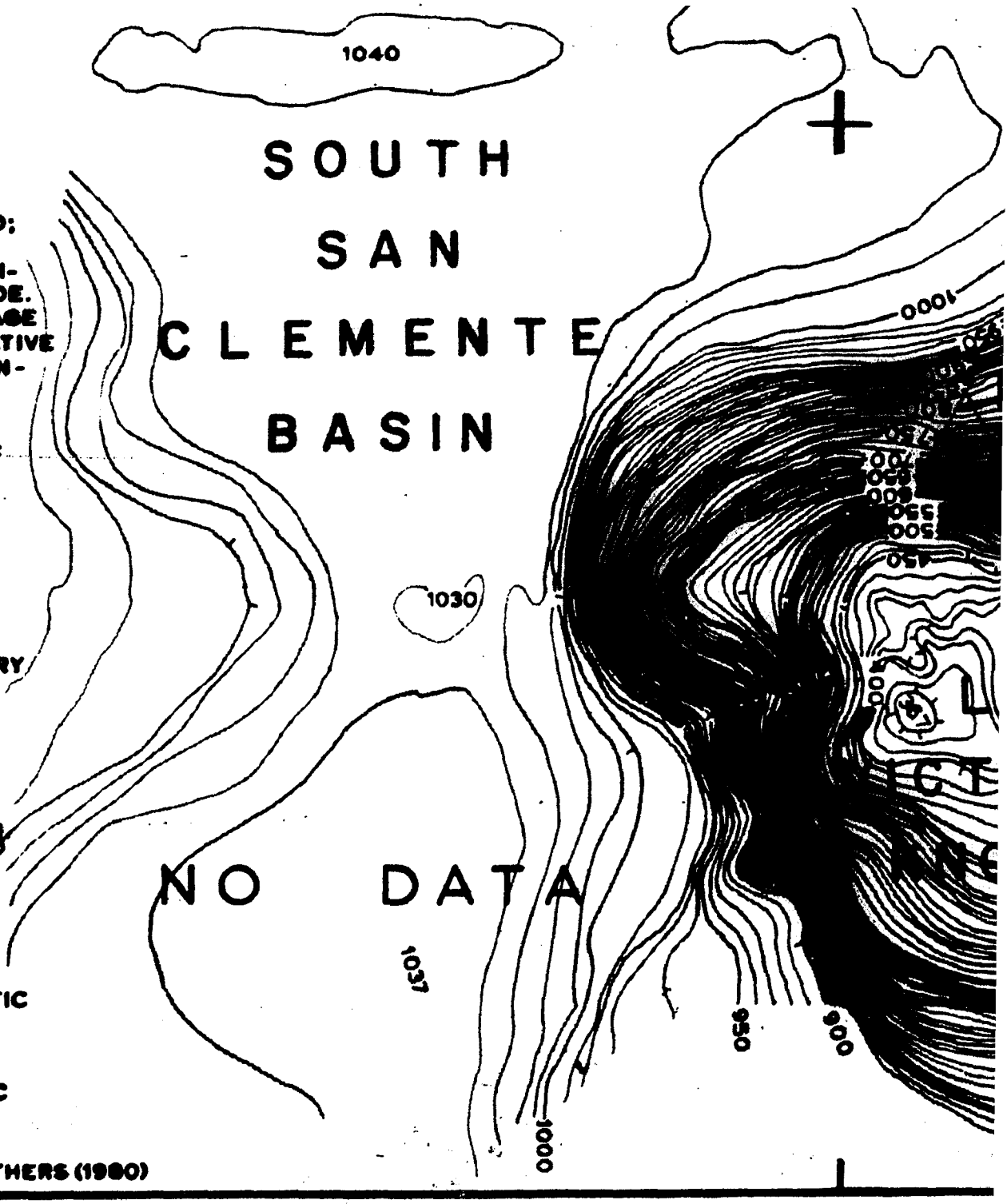


118° 00'

117° 50'

0'

117°40'

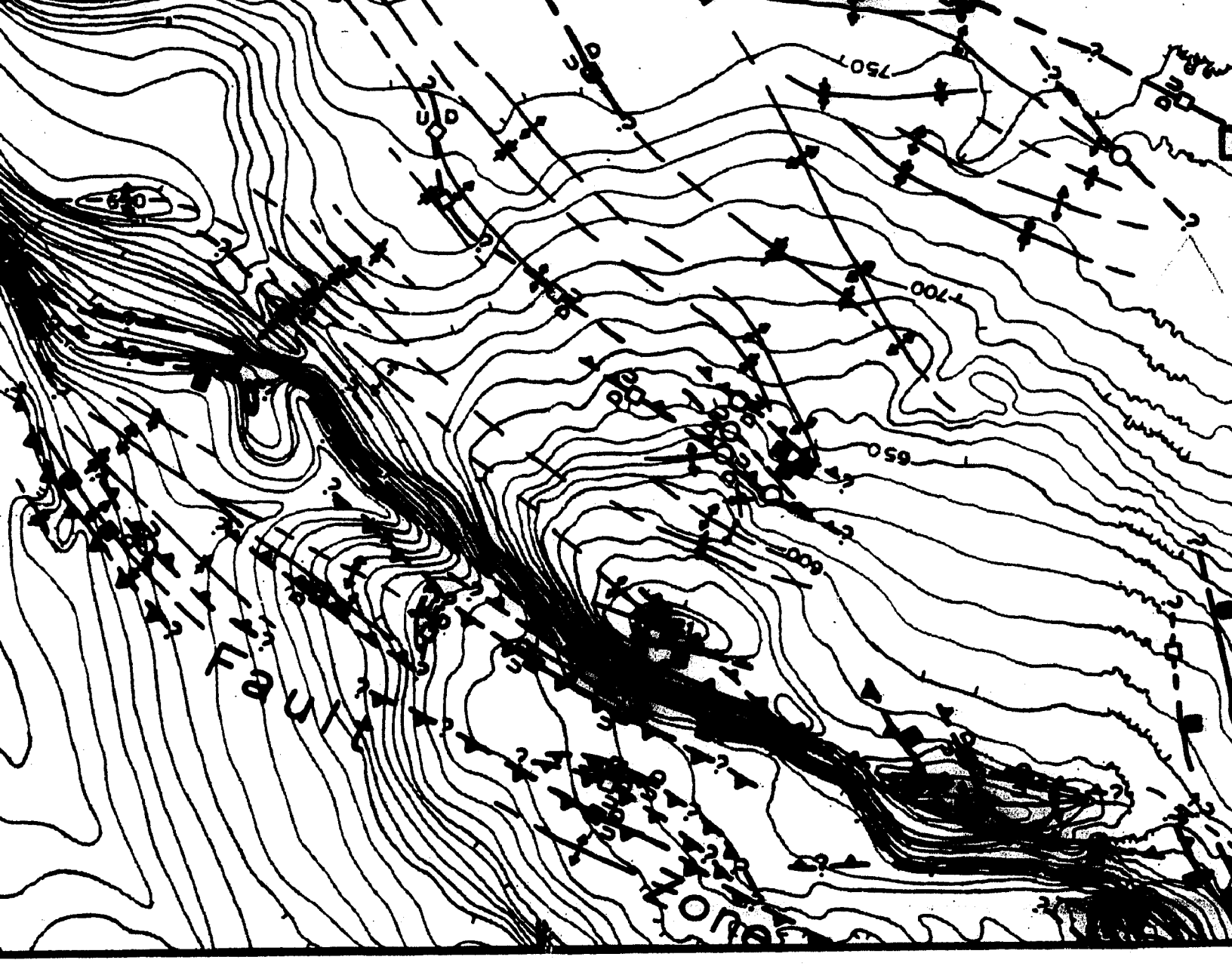


117°30'

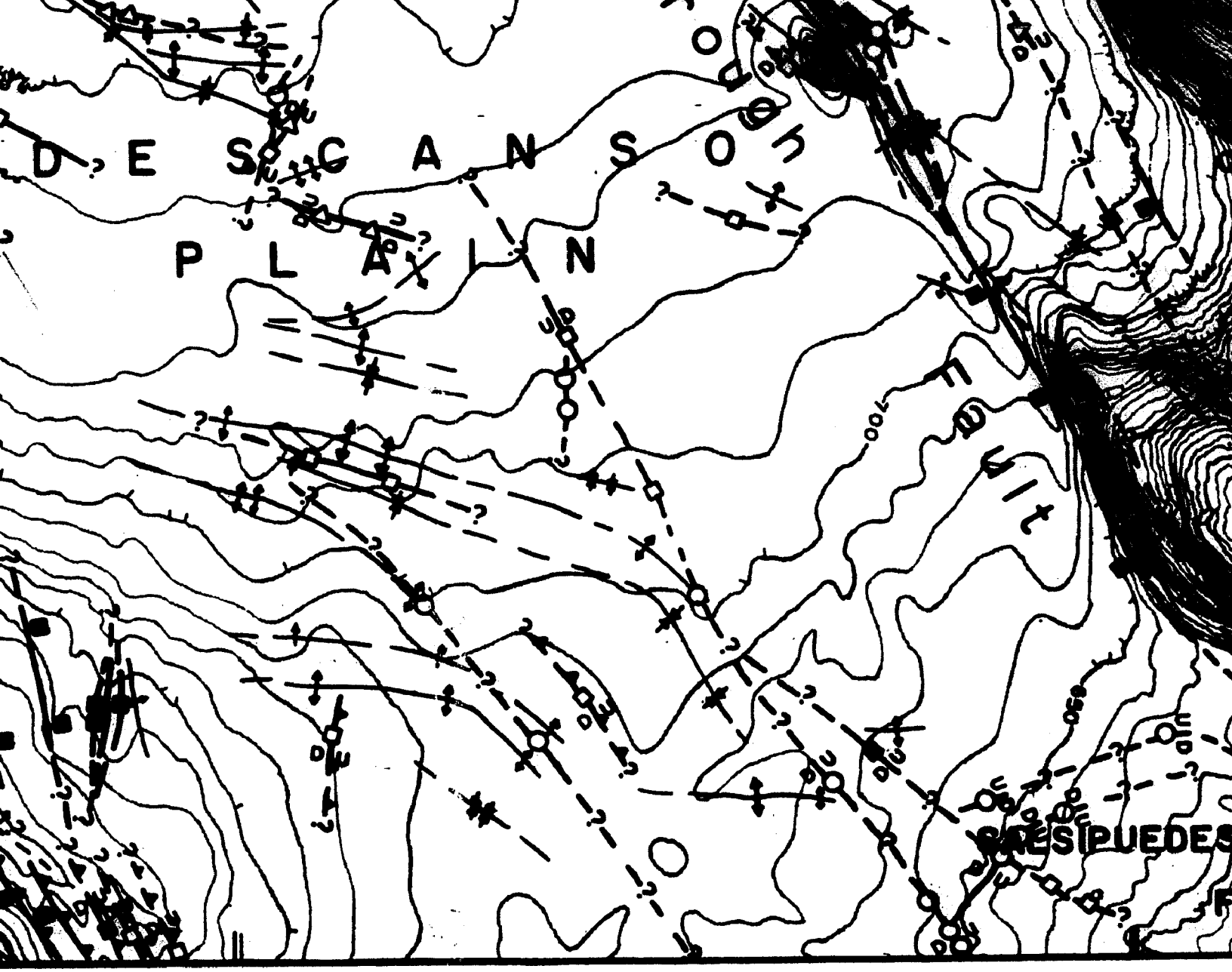


117°20′ 117°10′

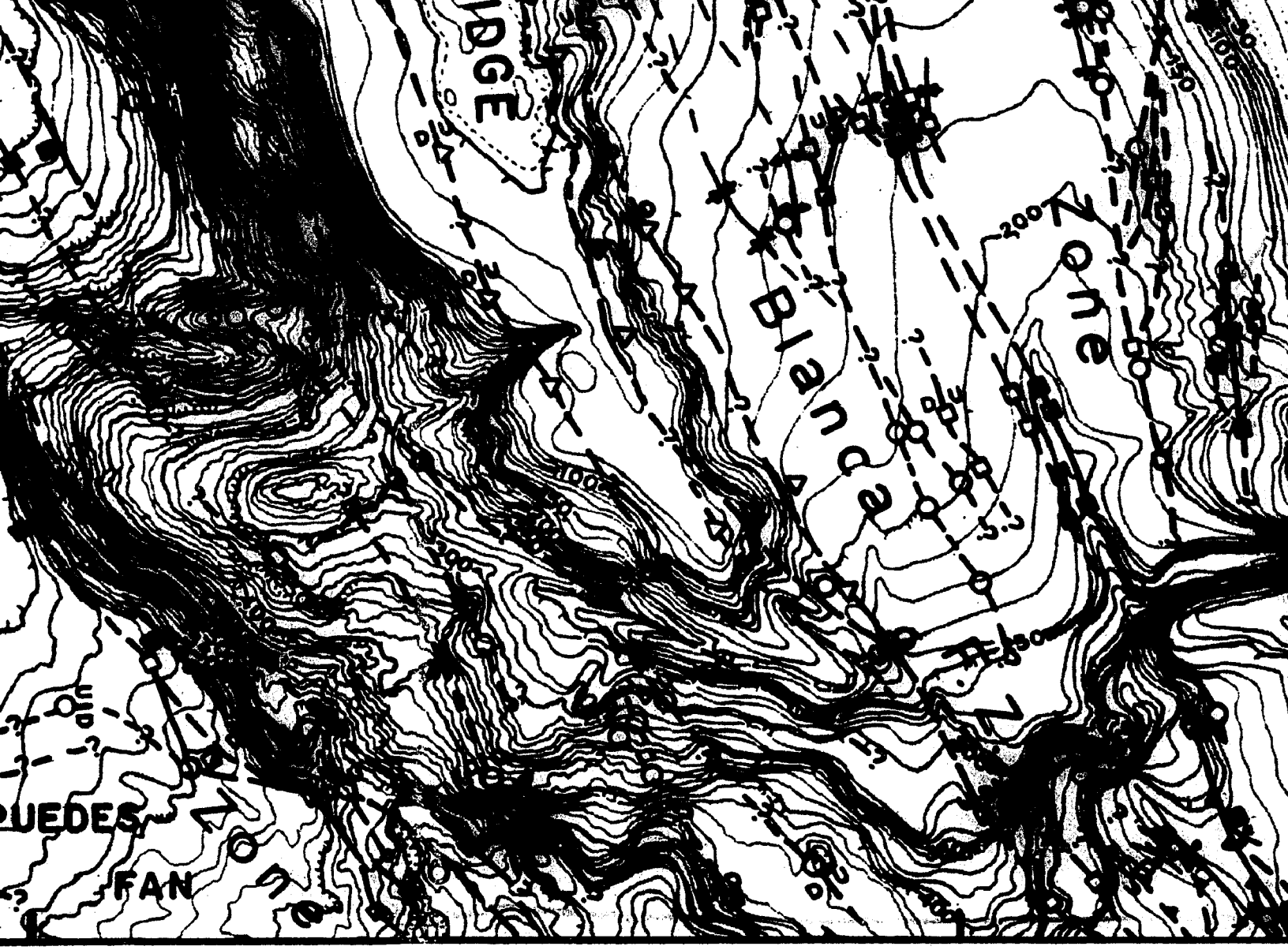


7°10′ 117°00′

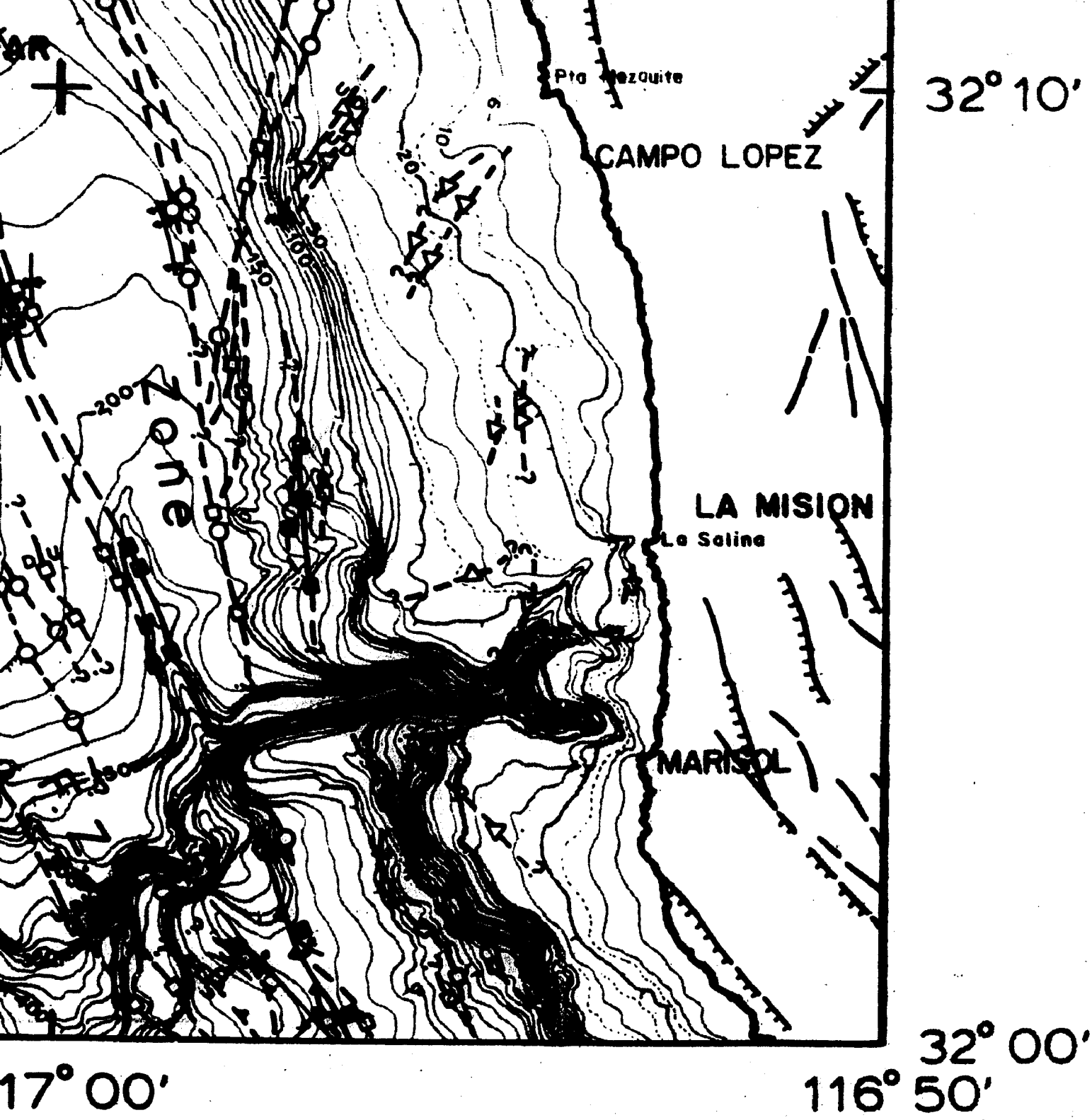
Pta Mezquite
CAMPO LOPEZ
LA MISION
La Salina
MARISOL
32° 10'
32° 00'
117° 00'
116° 50'
100
150
200

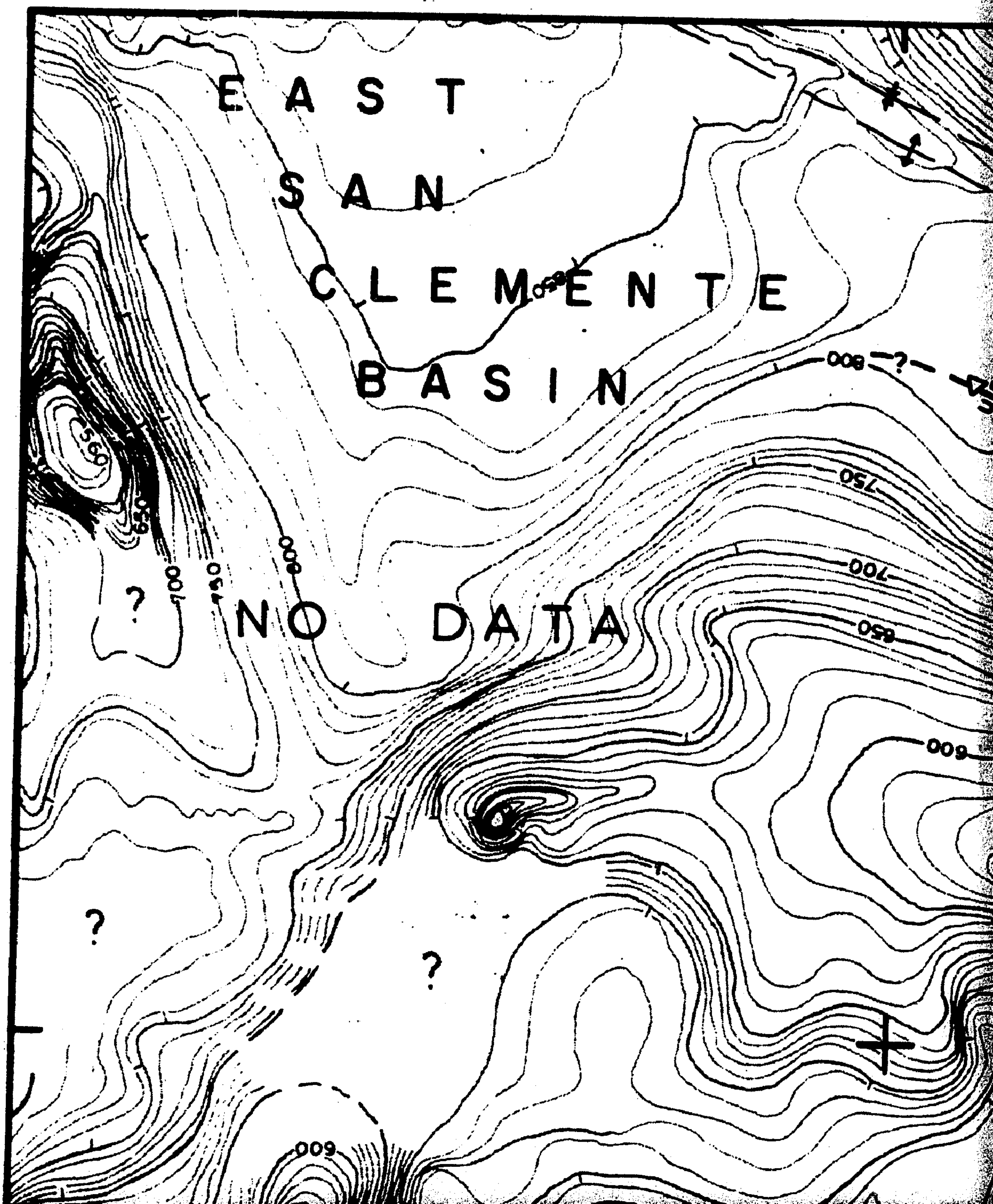
EAST
SAN
CLEMENTE
BASIN
NO DATA
560
650
700
750
800
600

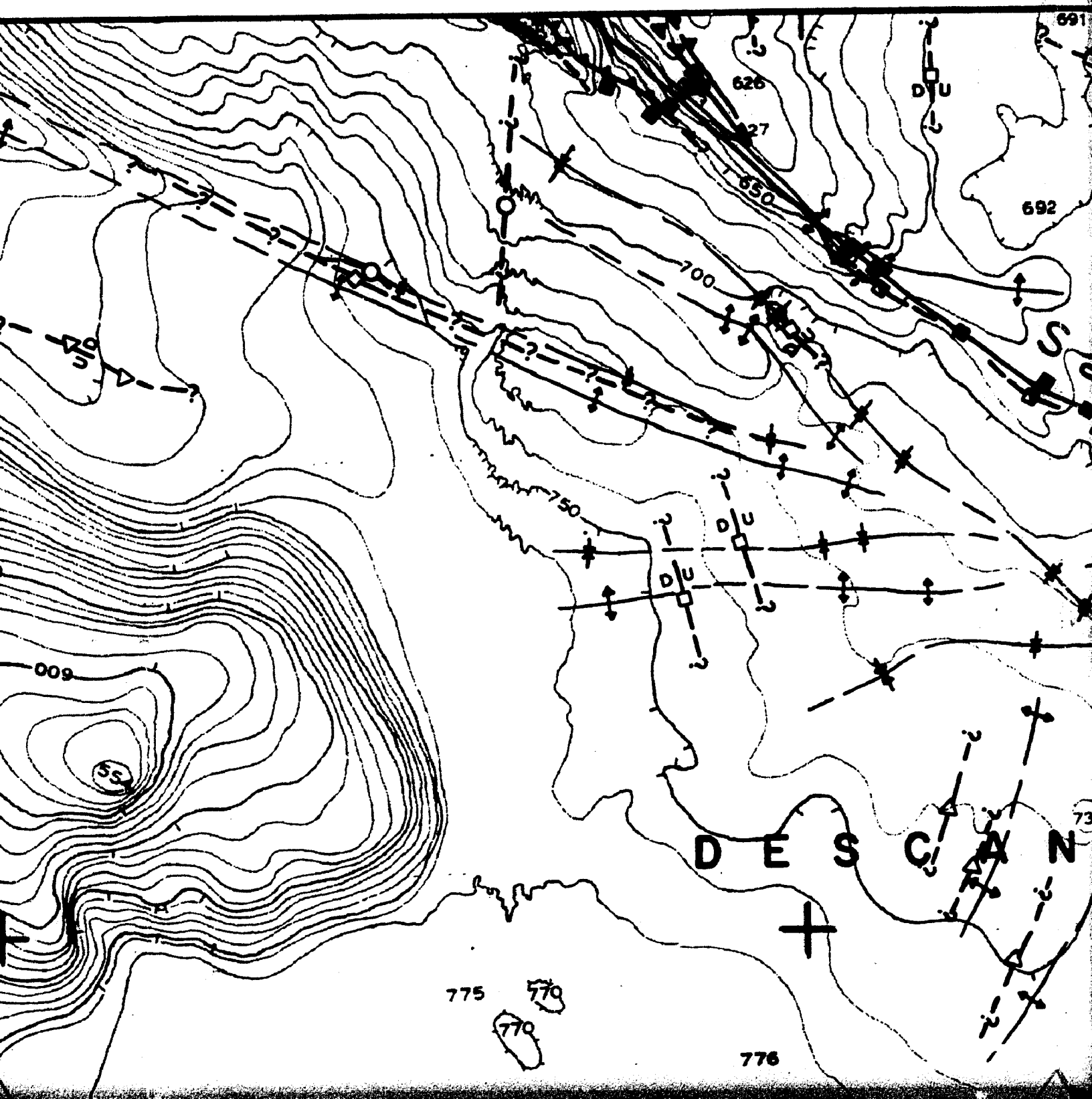
INN
691
626
D U
27
650
692
700
750
D U
D U
600
55
DESCAN
775
770
770
776

# NER CALIFORNIA CONTINE

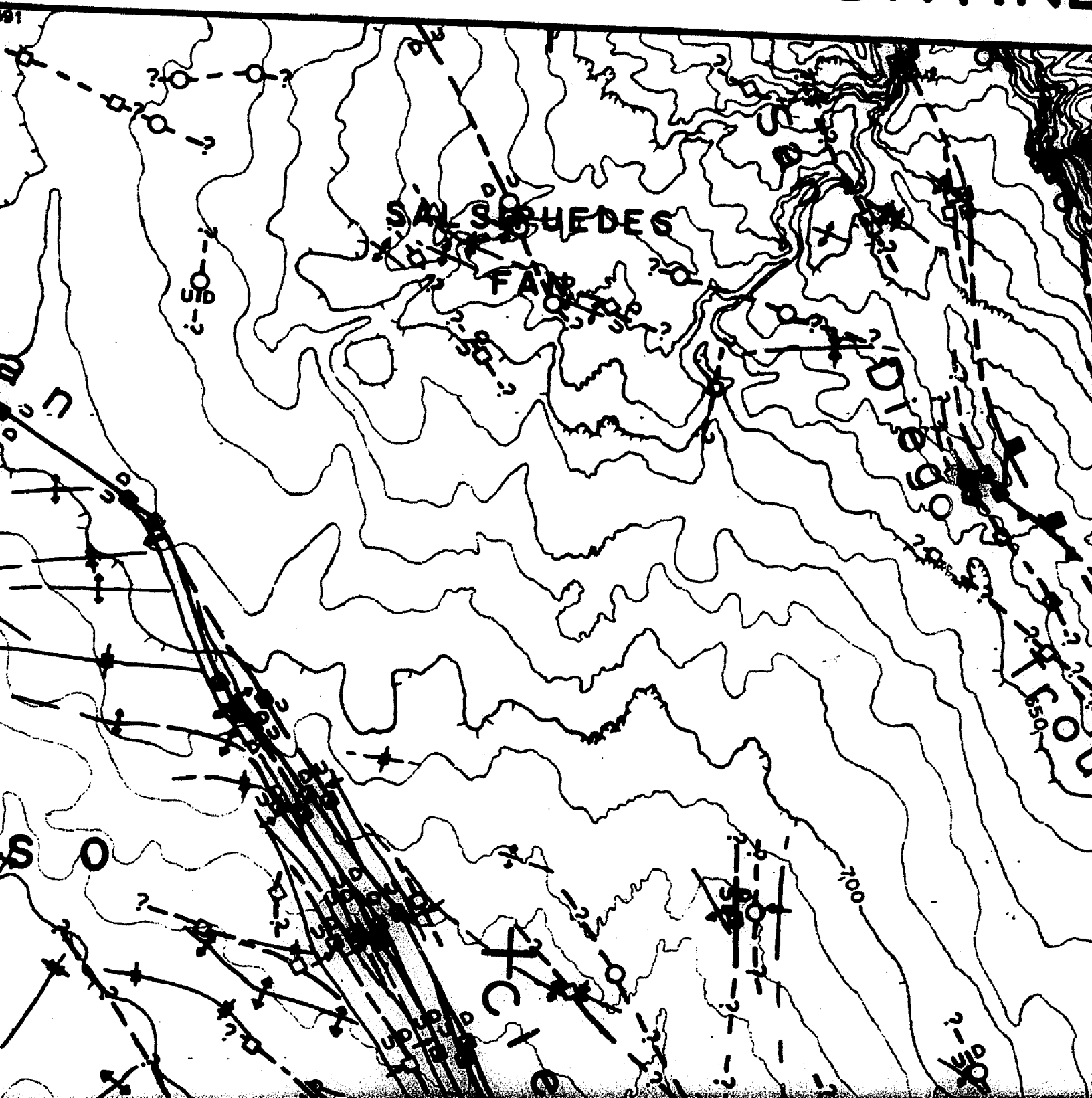

# ENTAL BORDERLAND

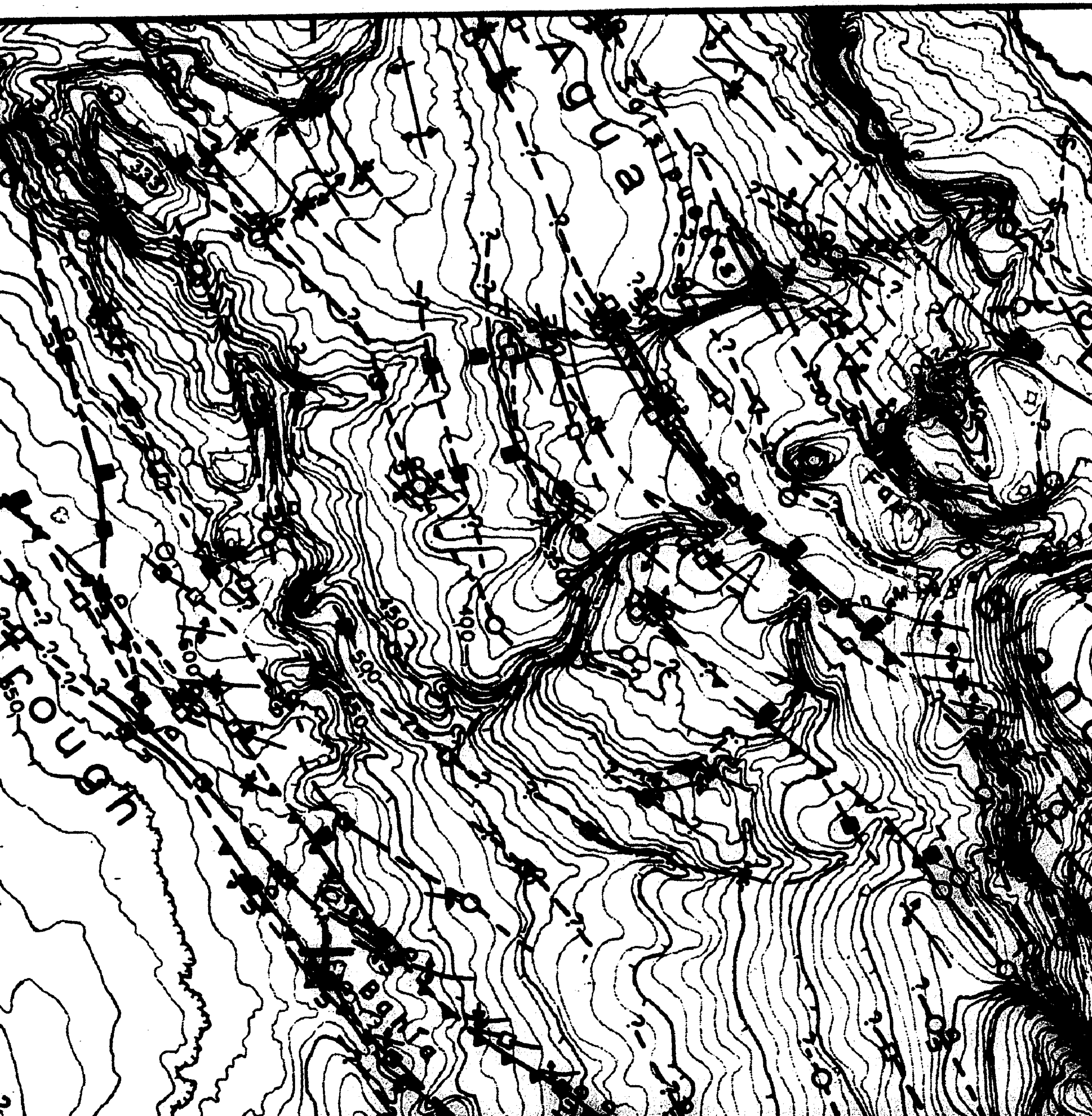

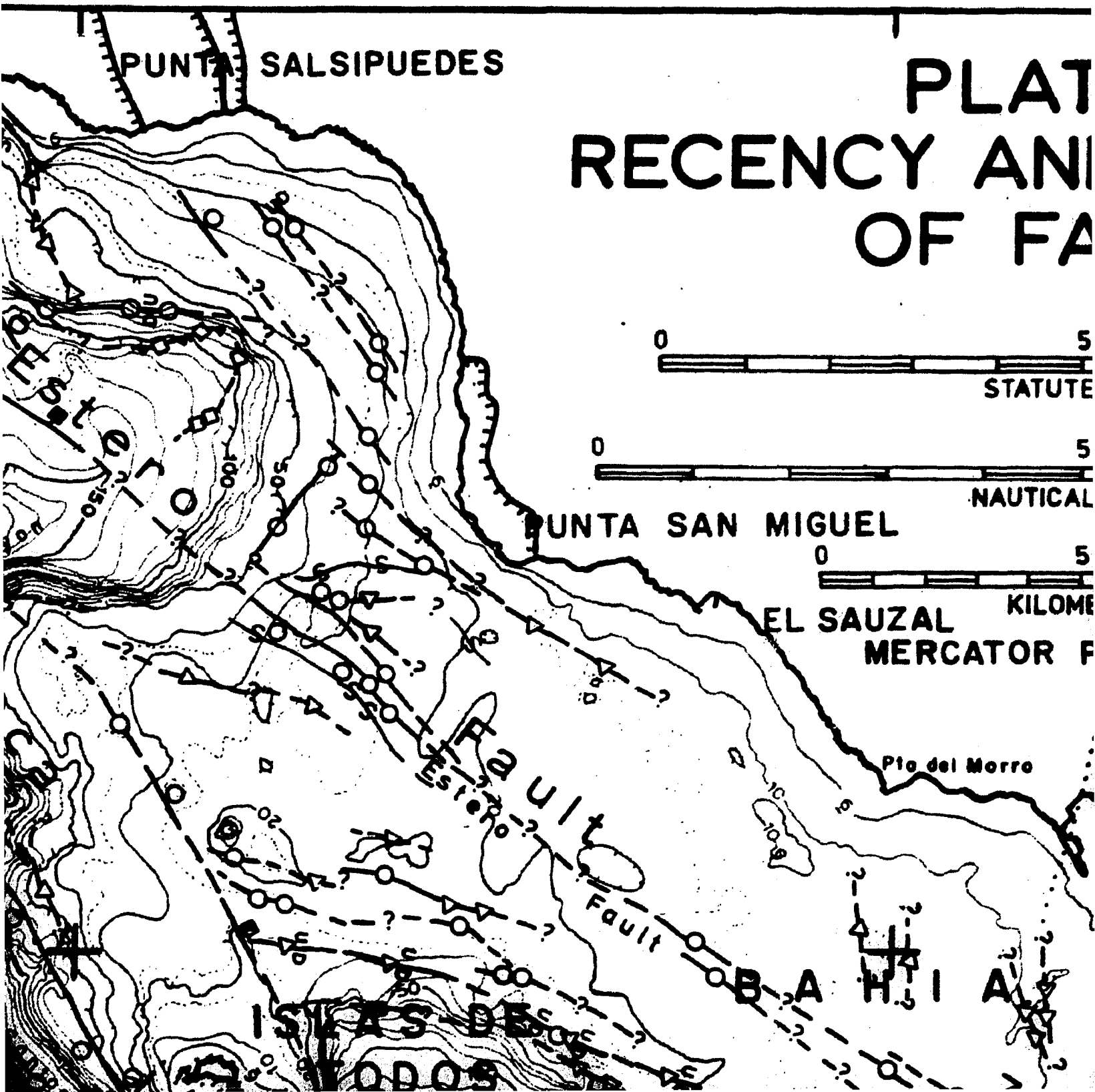
PUNTA SALSIPUEDES
PLAT
RECENCY AN
OF FA
0
5
STATUTE
0
5
NAUTICAL
PUNTA SAN MIGUEL
0
5
KILOME
EL SAUZAL
MERCATOR P
Pto del Morro
Estero
Fault
Fault
B A H I A
ISLAS DE
TODOS

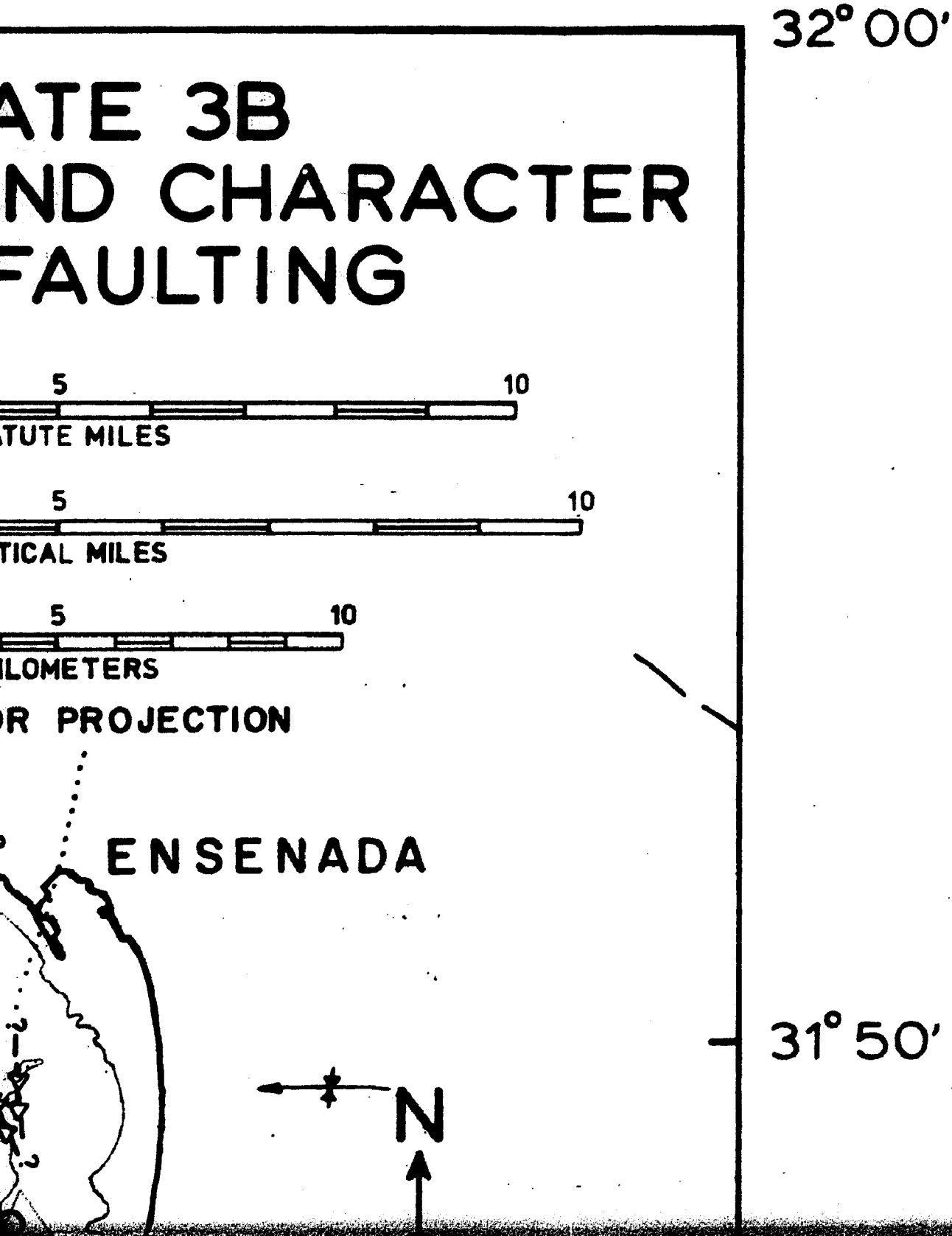
32° 00'
ATE 3B
ND CHARACTER
FAULTING
5
10
TUTE MILES
5
10
TICAL MILES
5
10
LOMETERS
R PROJECTION
ENSENADA
31° 50'
N

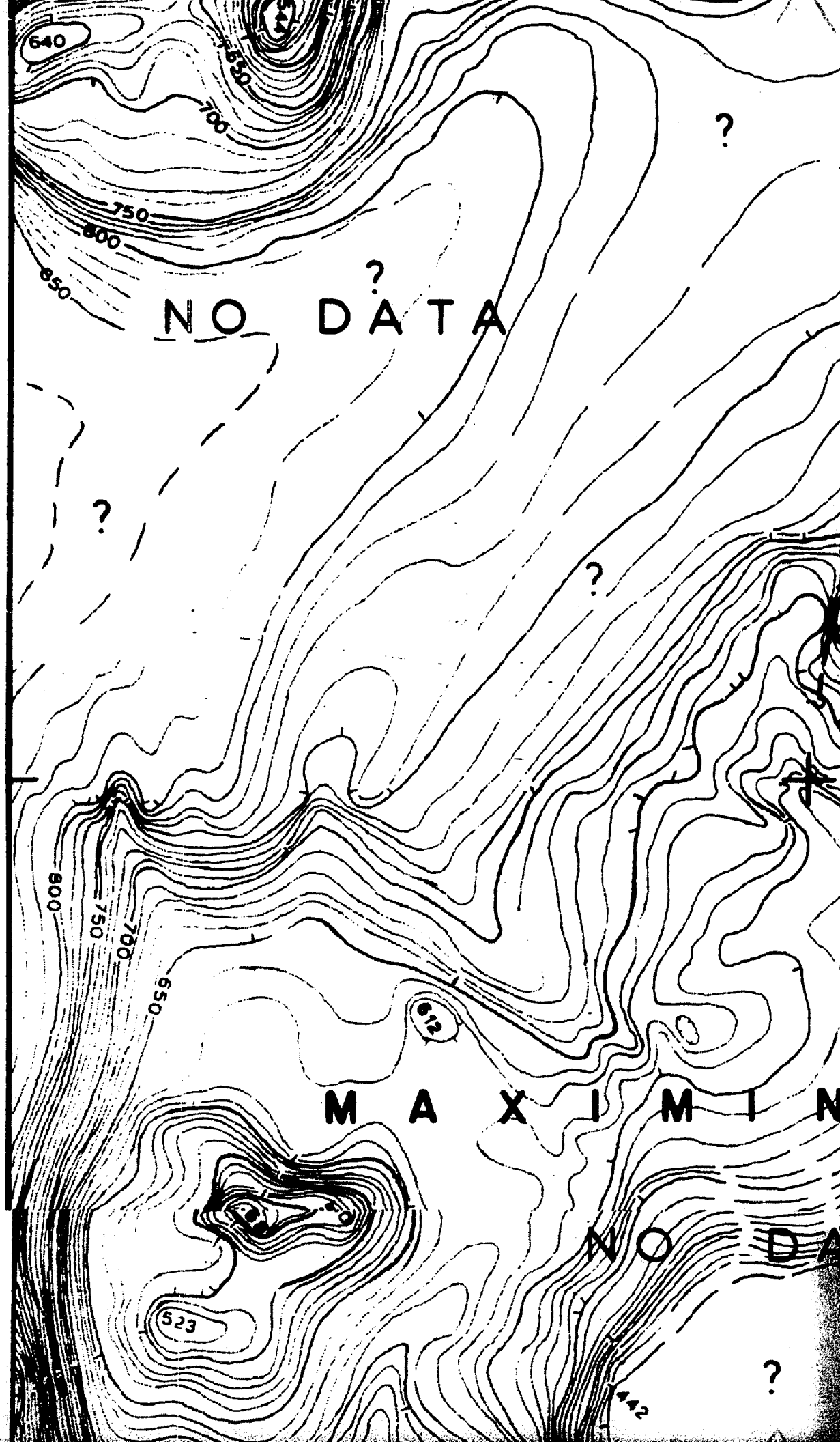
640
650
700
750
800
850
NO DATA
?
?
?
?
800
750
700
650
612
M A X I M I N
NO DA
523
442
?

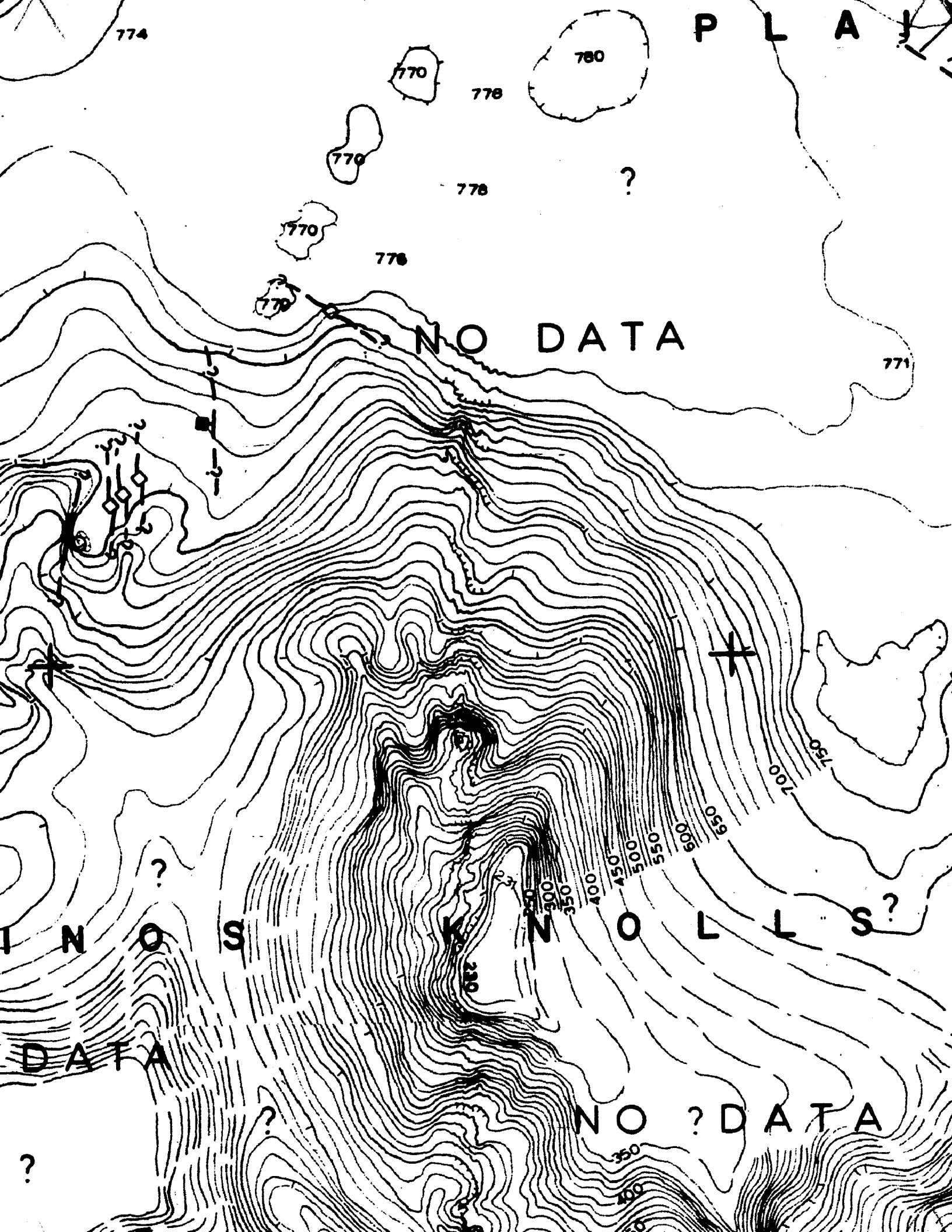

PLA
774
770
780
778
770
778
?
770
778
770
NO DATA
771
750
700
650
600
550
500
450
400
350
300
250
230
?
?
INOS KNOLLS
DATA
?
NO ?DATA
?
350
400

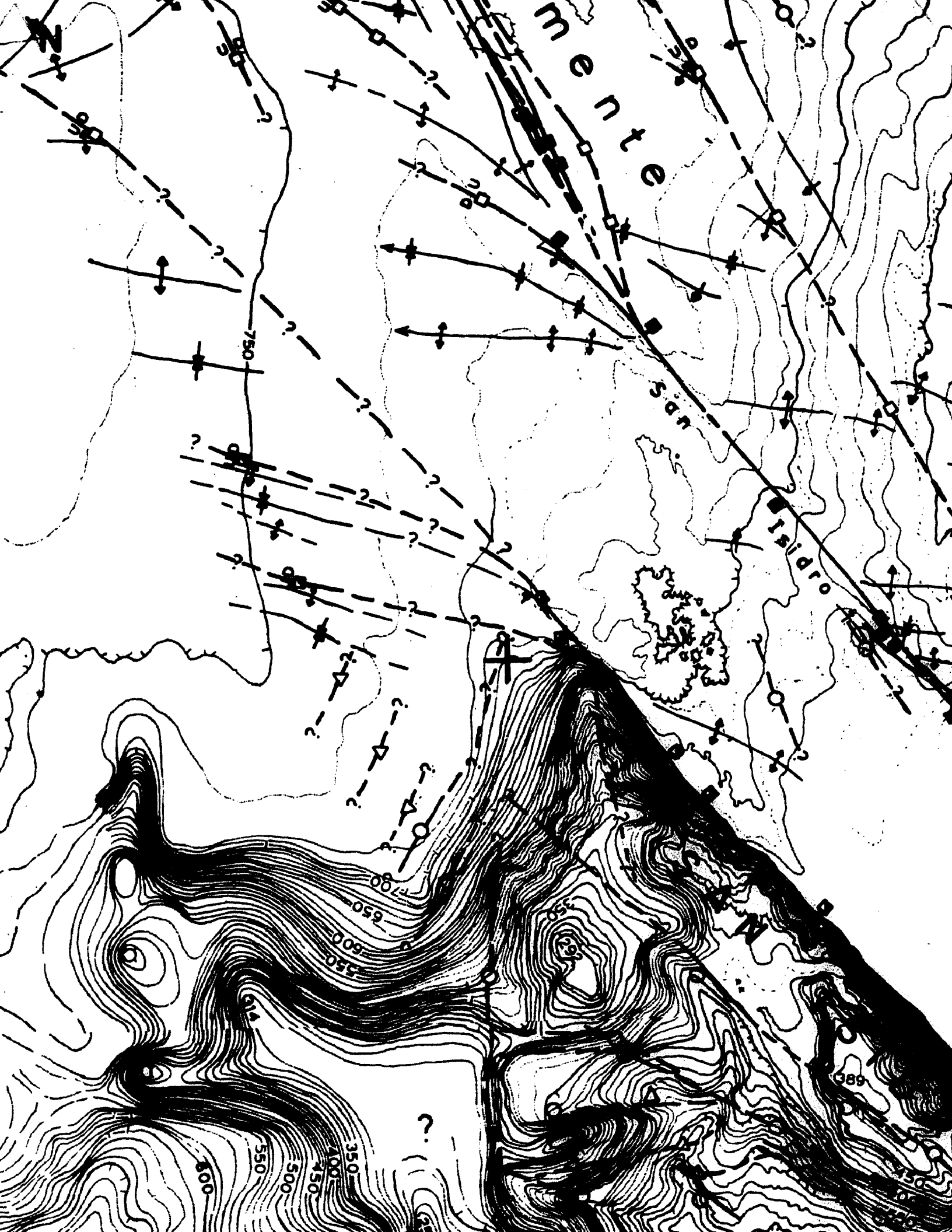

mente
San
Isidro
750
700
650
600
550
500
450
400
350
389

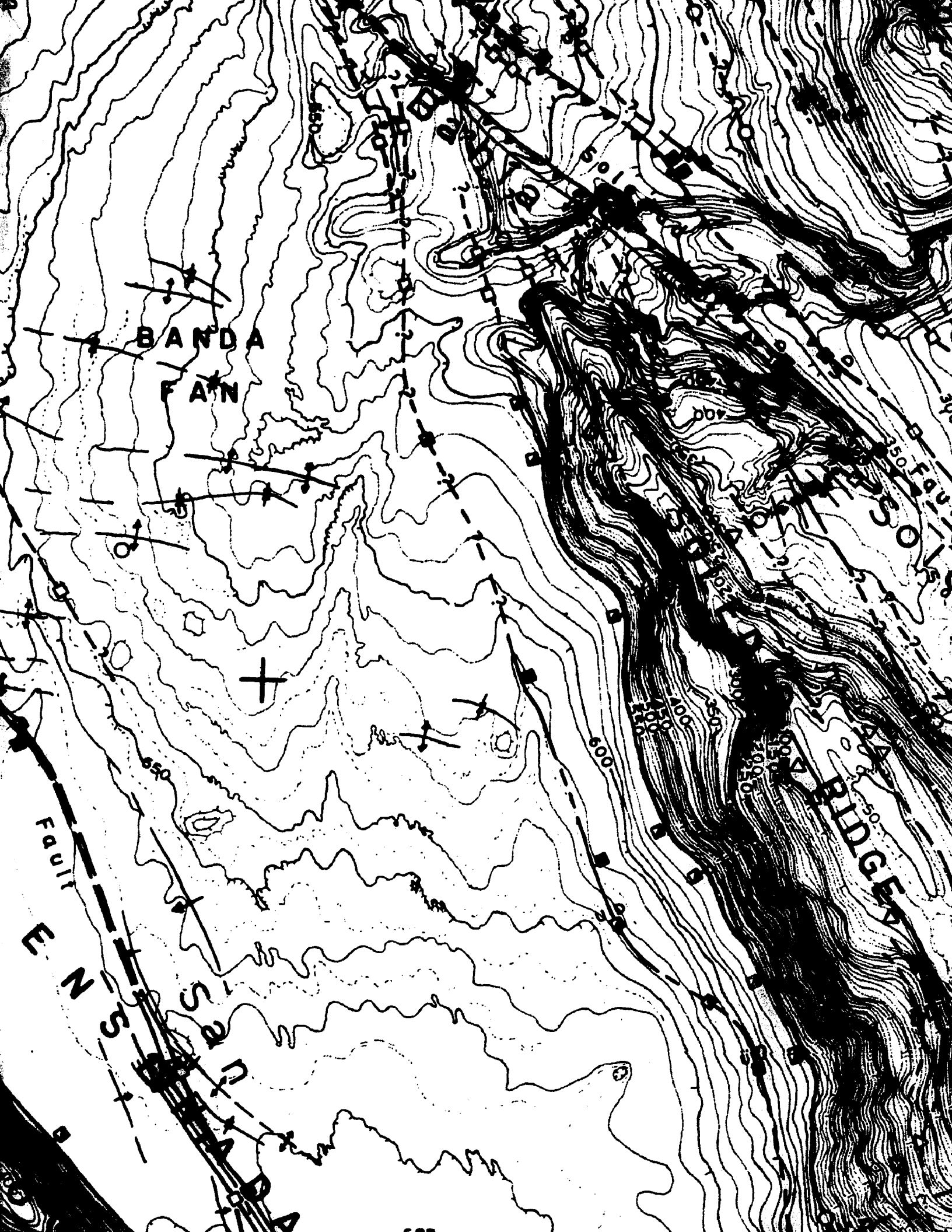
BANDA
FAN
Fault
RIDGE
600
650
400
350
300
250
200
150
100
50

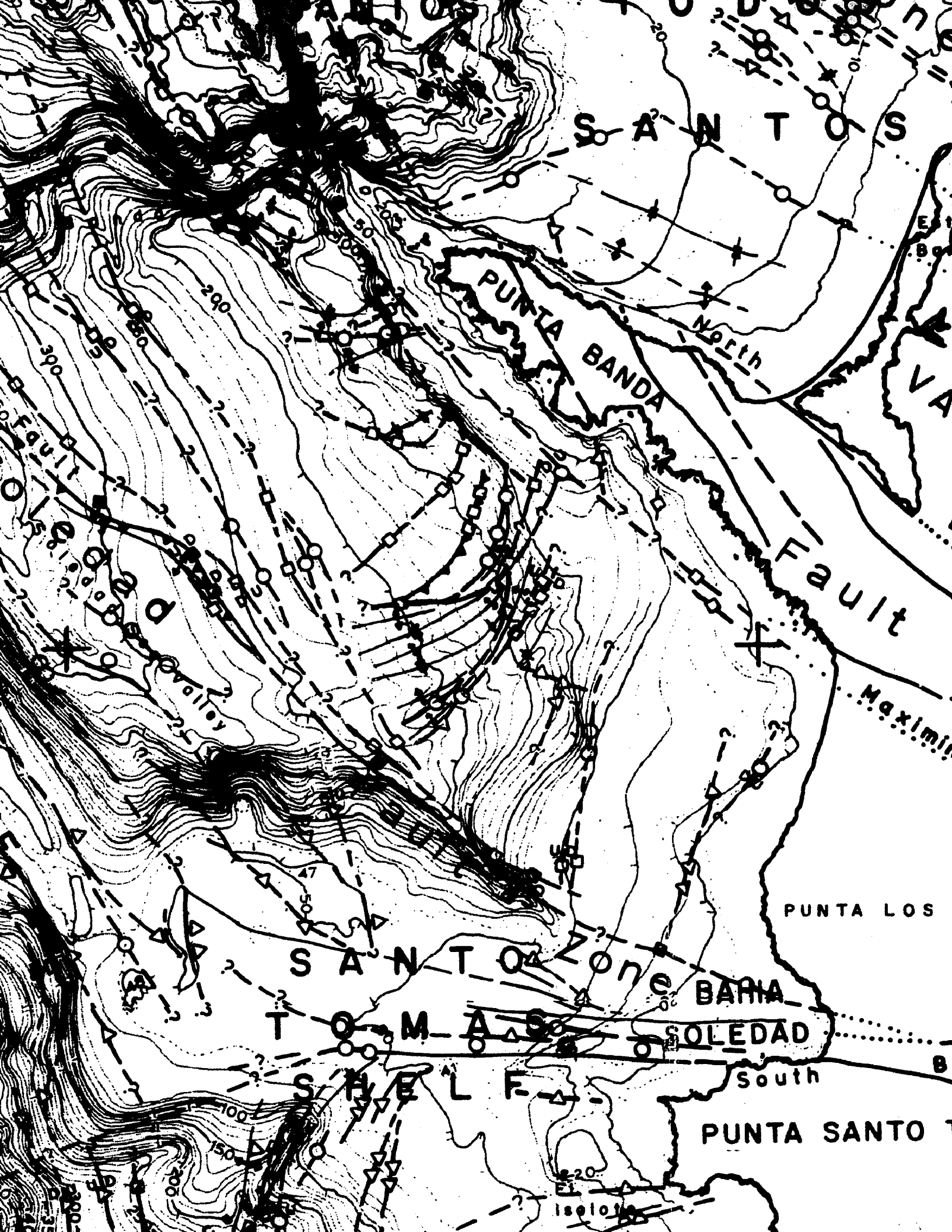
SANTOS
PUNTA BANDA
North
Fault
Maximi
Fault
Valley
Fault
SANTO
Zone
TOMAS
SHELF
BAHIA
SOLEDAD
South
PUNTA LOS
PUNTA SANTO
Isolote
200
300
50
100
150
47

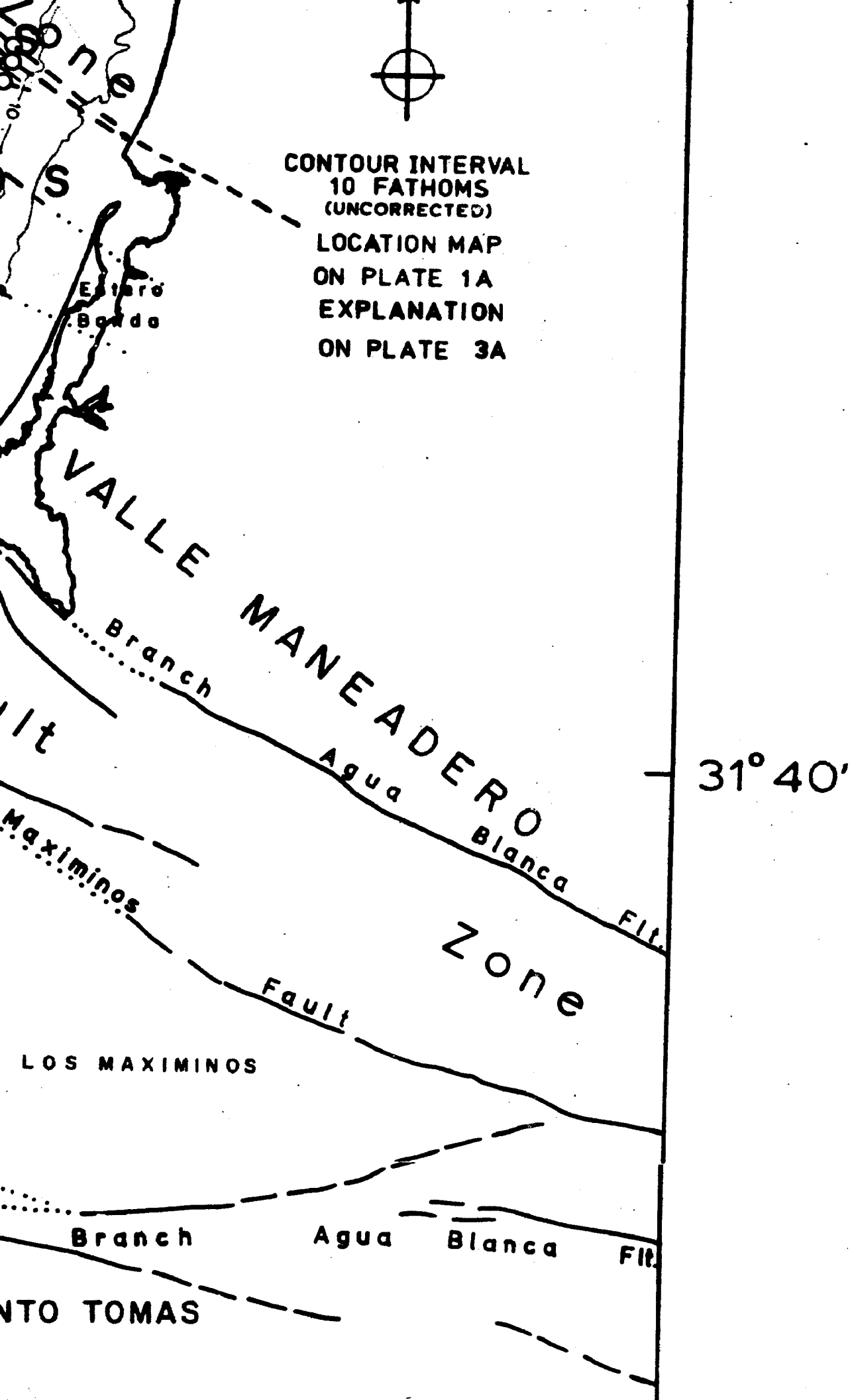
CONTOUR INTERVAL
10 FATHOMS
(UNCORRECTED)
LOCATION MAP
ON PLATE 1A
EXPLANATION
ON PLATE 3A
Estero
Bonda
VALLE MANEADERO
Branch
Agua
Blanca
Flt.
31° 40'
Maximinos
Fault
Zone
LOS MAXIMINOS
Branch
Agua
Blanca
Flt.
NTO TOMAS

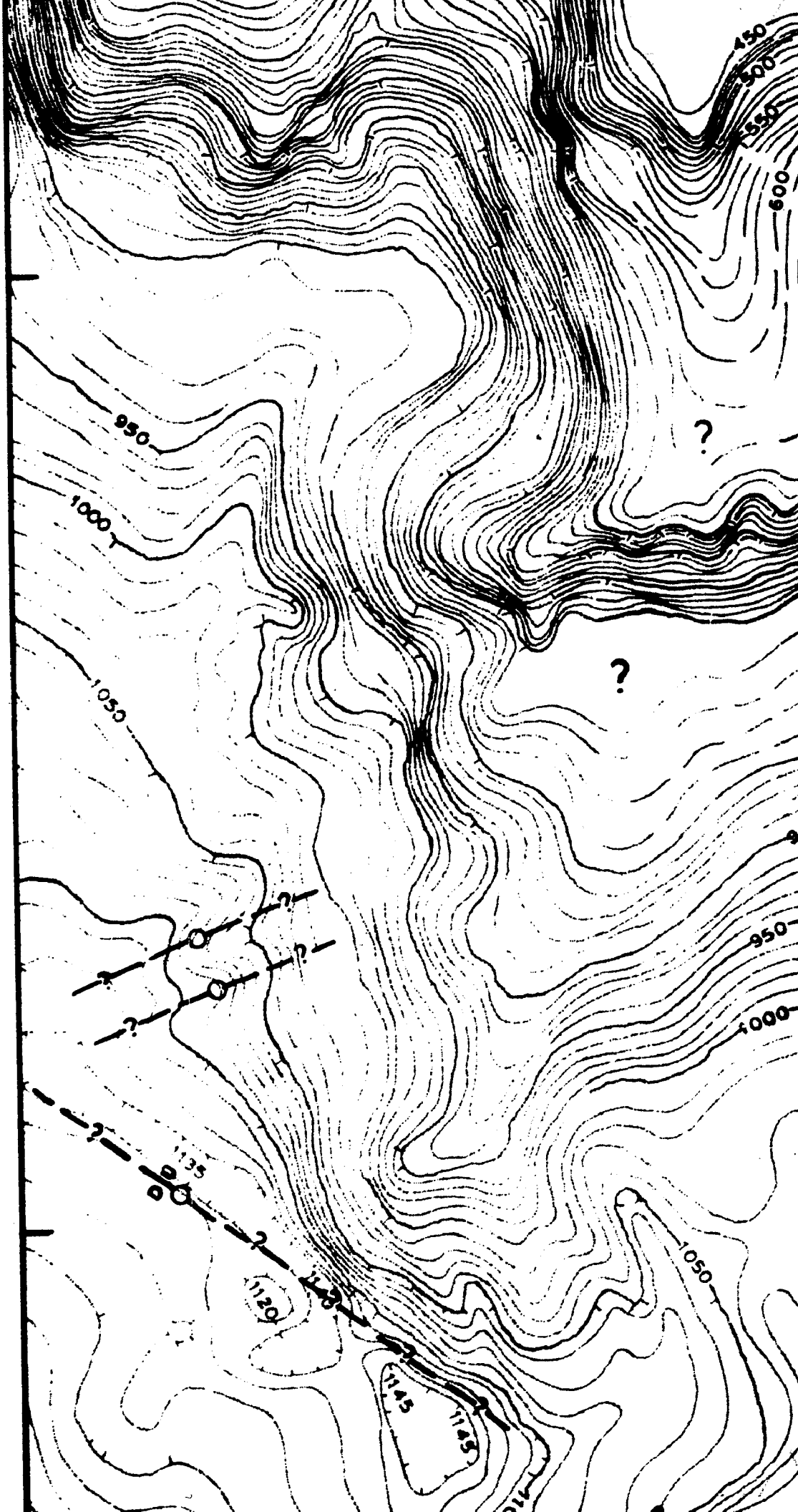
450
500
550
600
950
1000
1050
?
?
950
1000
1050
1135
1120
1145
1145

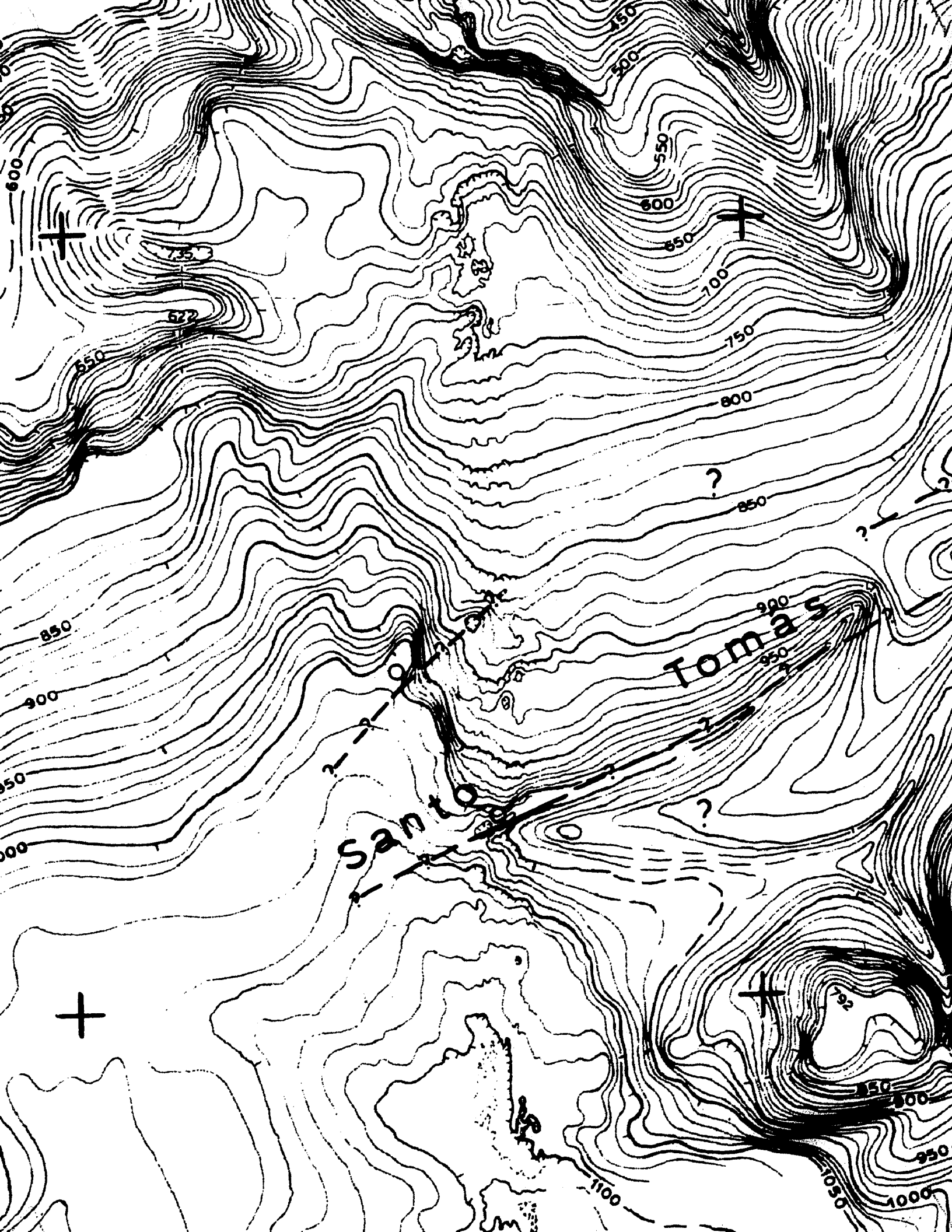
Santo
Tomas
450
500
550
600
650
700
750
800
850
900
950
1000
1050
1100
735
622
792

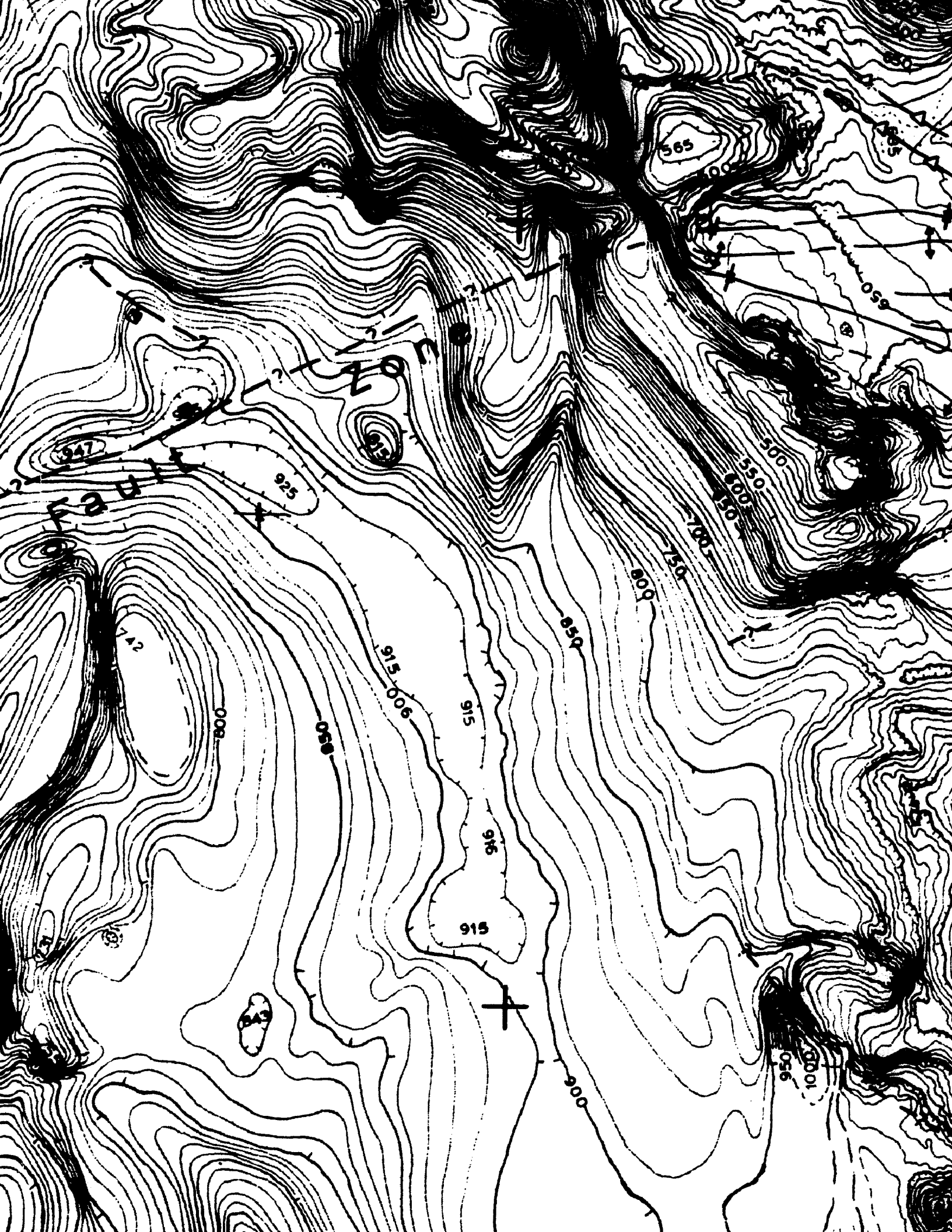
Fault
Zone
947
925
742
915
915
916
915
843
800
850
900
850
800
750
700
650
600
550
500
565
650
950
1000

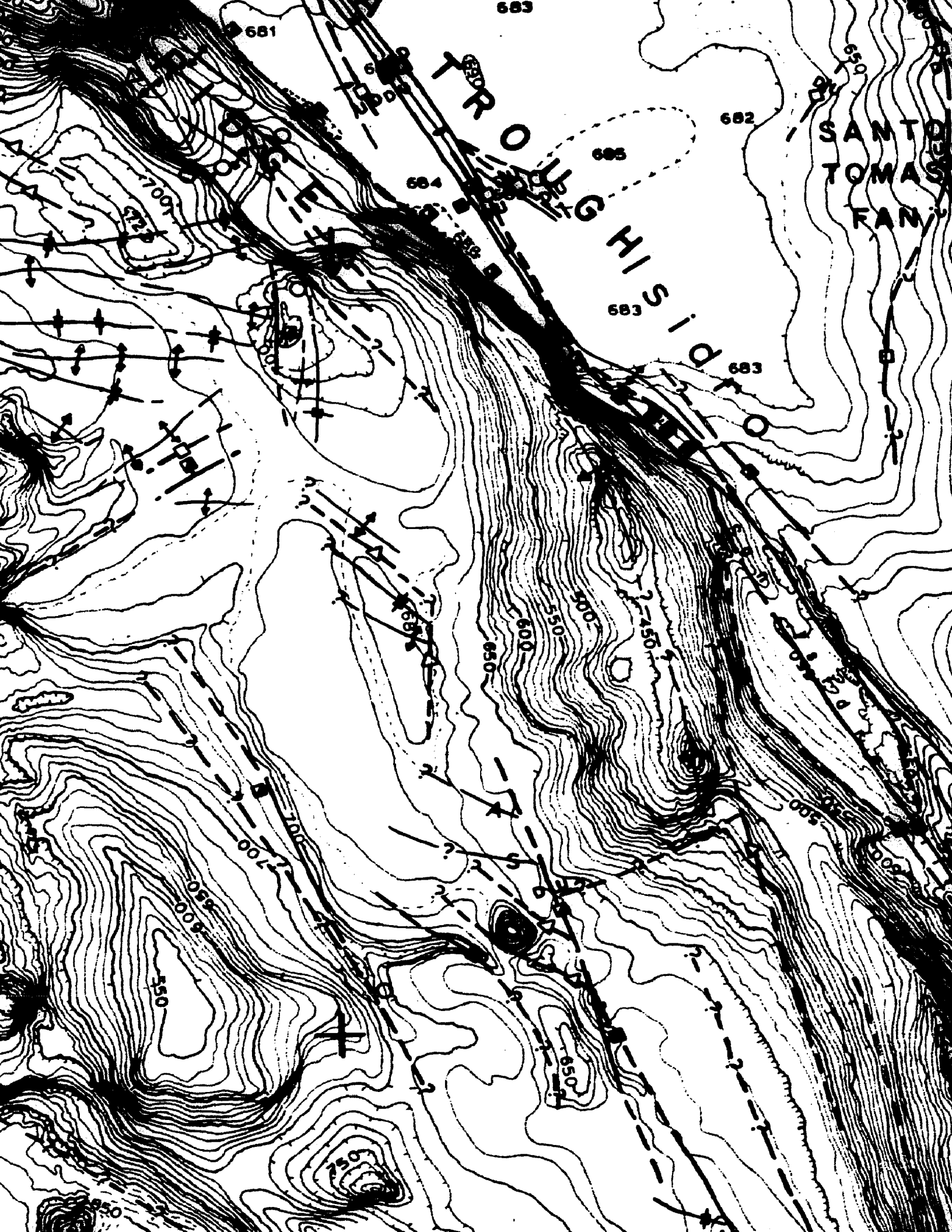
683
681
682
685
684
683
683
TROUGH Hisidro
SANTO
TOMAS
FAN
700
650
600
550
500
450
700
650
600
550
650
750
850

SAN
CABRAS
BANK
BUT
750
100
150
200
250
300
350
400
450
500
600

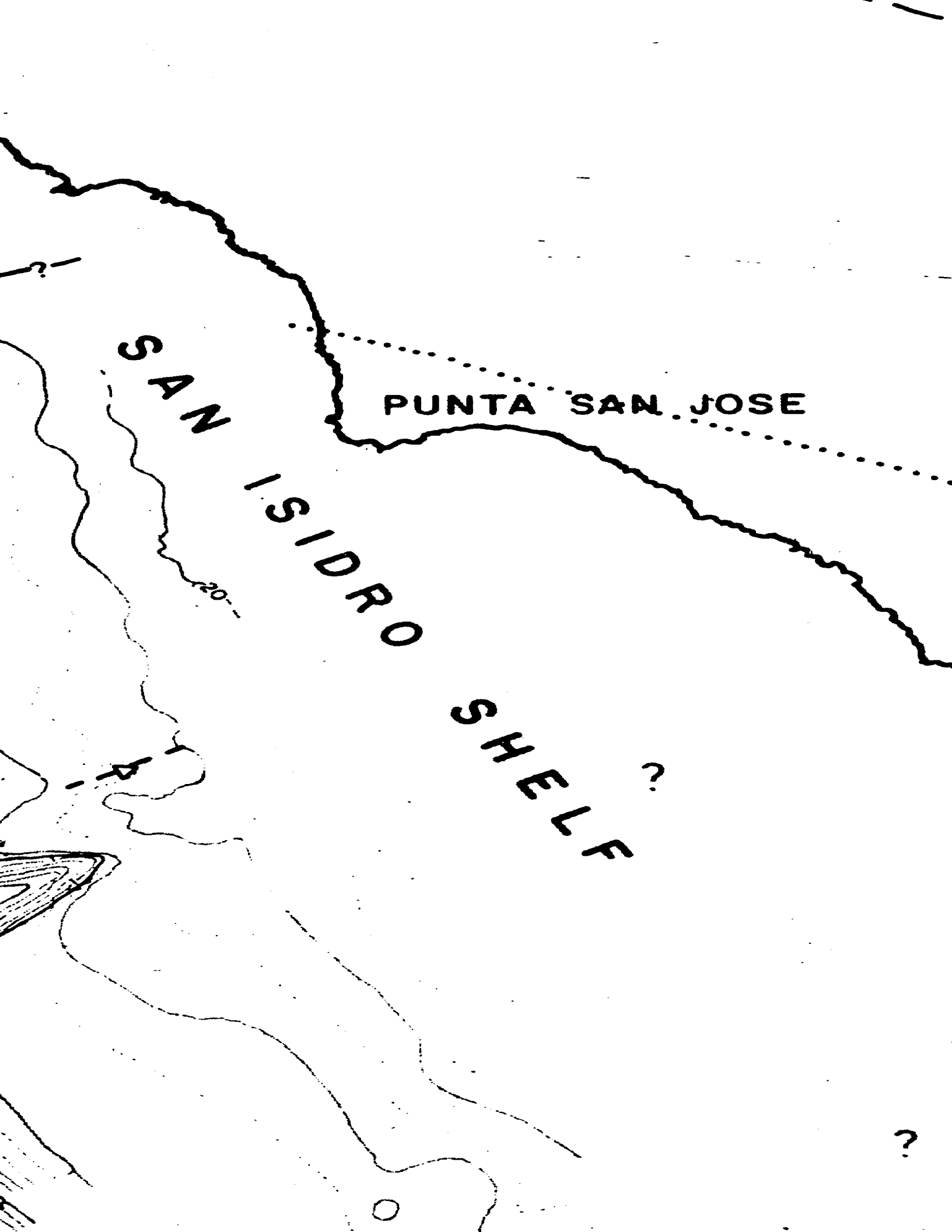
SAN ISIDRO SHELF
PUNTA SAN JOSE
20
?
?

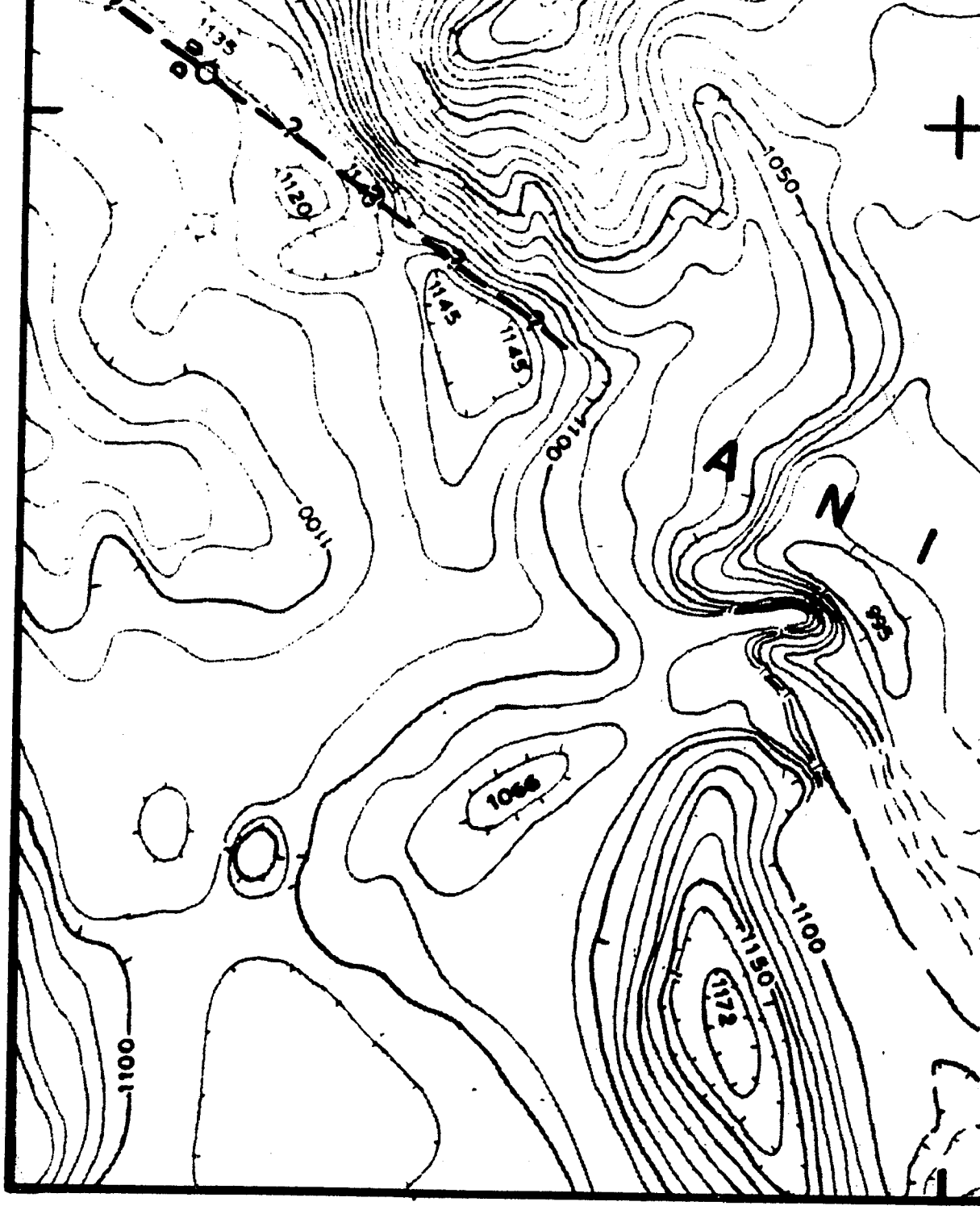
1135
1120
1145
1145
1100
1100
1050
A
N
I
995
1066
1100
1150
1172
1100

117°40′

117°

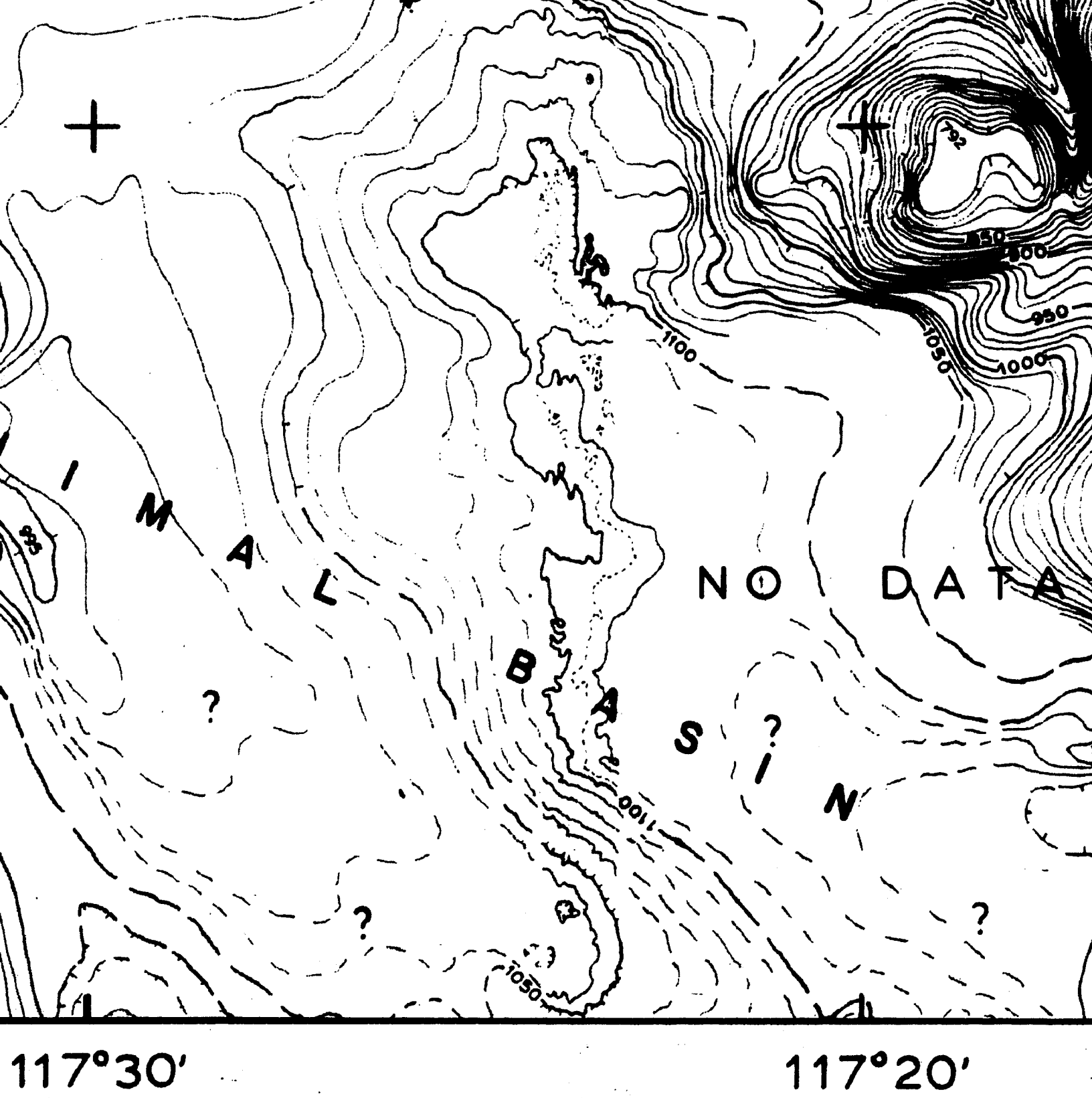


117°30′ 117°20′

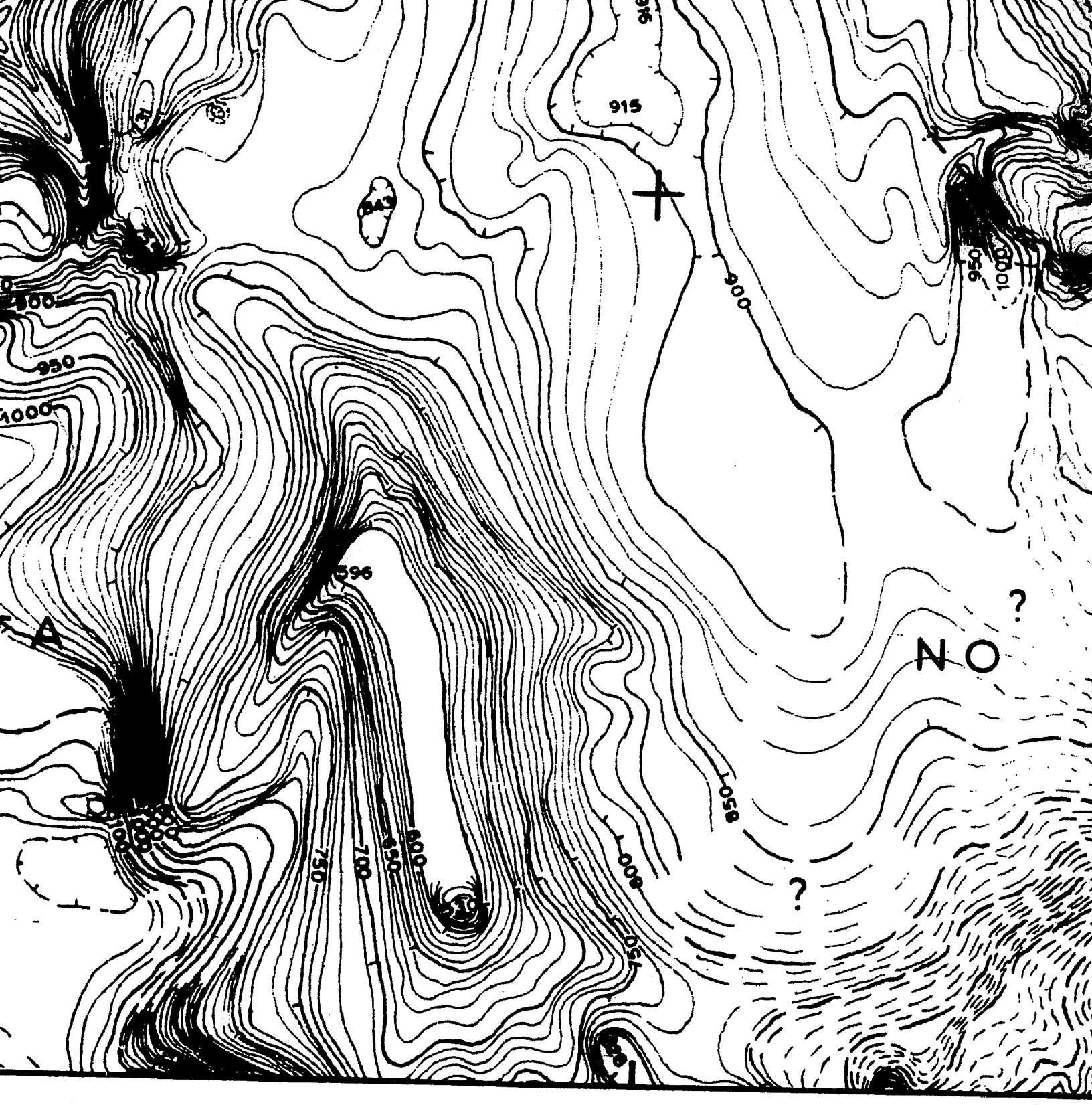


117°10′

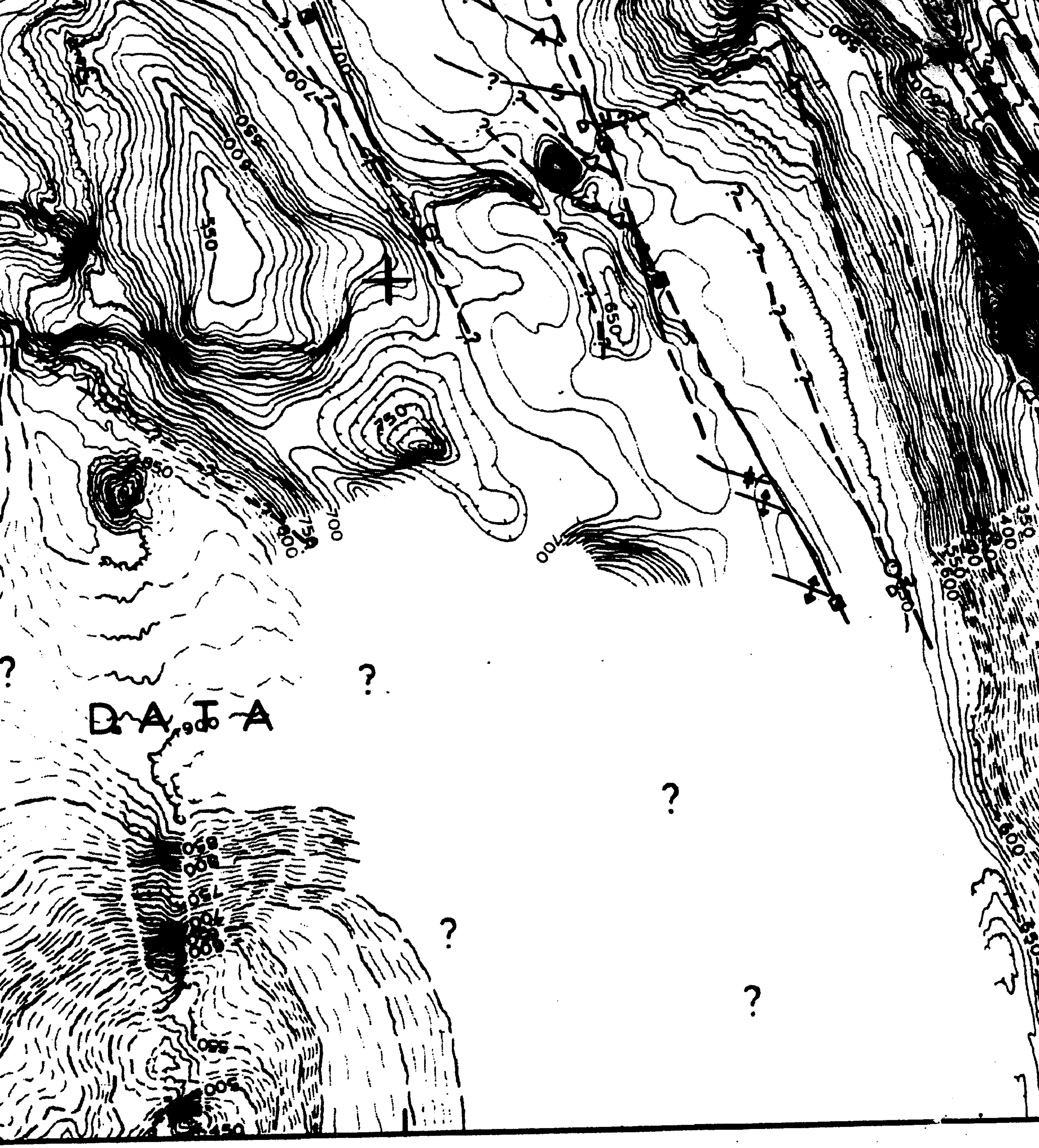


117°00′

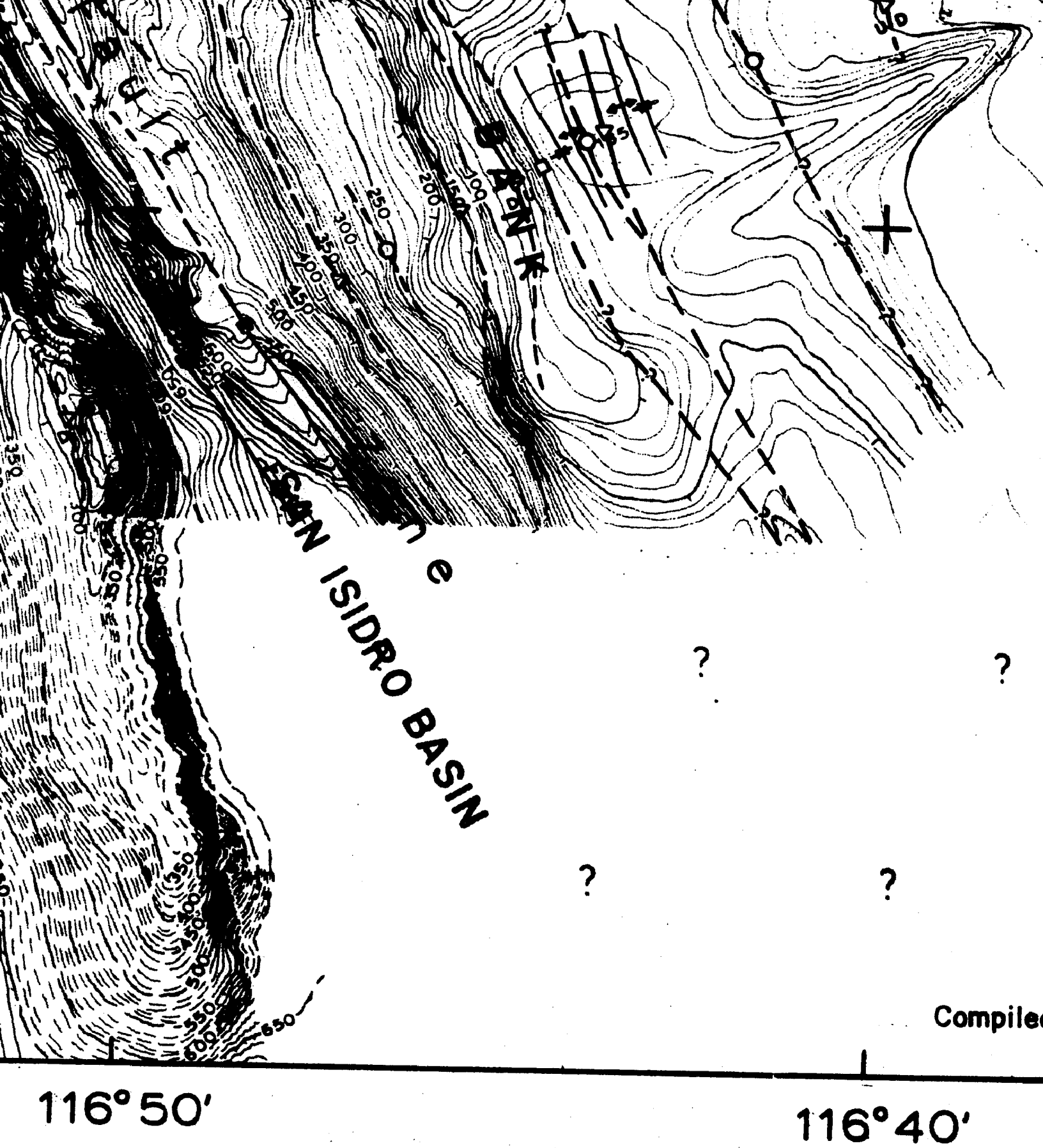
SAN ISIDRO BASIN
Compile
116°50'
116°40'

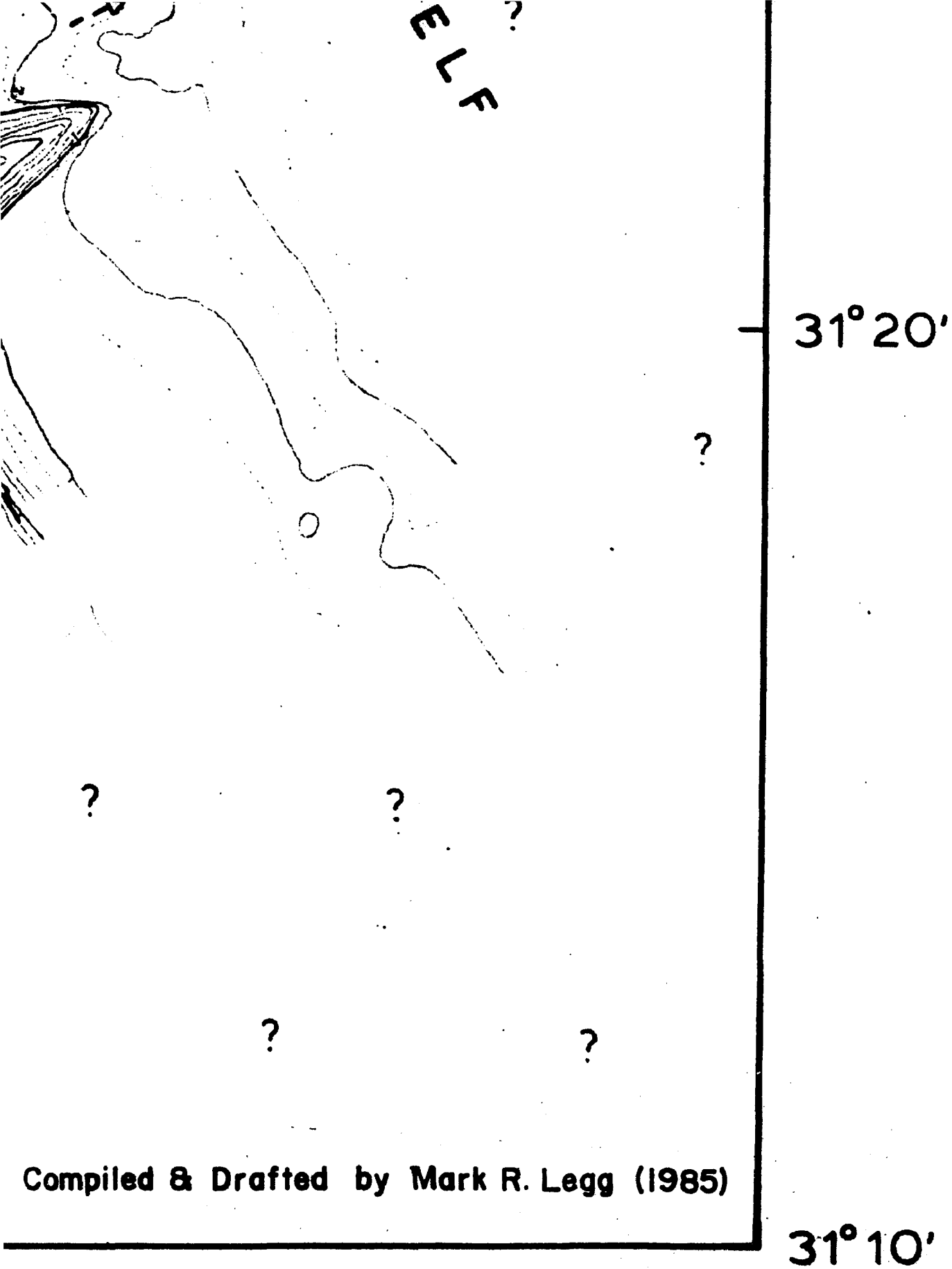
ELF
31°20'
31°10'
116°30'
Compiled & Drafted by Mark R. Legg (1985)

1000
1100
1200
1300
1400
1500
1600
1700
1800
1800
1700
San Clemente
Rift Valley

118°10'
900
1100
1000
900
800
700
600
500
600
700
nente
ey
N

118° 05'

NORTH SAN CLEM

SAN CLEMENTE F

118°00'

NENTE BASIN

FAULT ZONE

Sea Beam

117° 55'

# Plate 4

# Sea Beam Bathymetry

Sea Beam

+ 32° 45'

117° 50'

# Plate 4

# Sea Beam

# Bathymetry

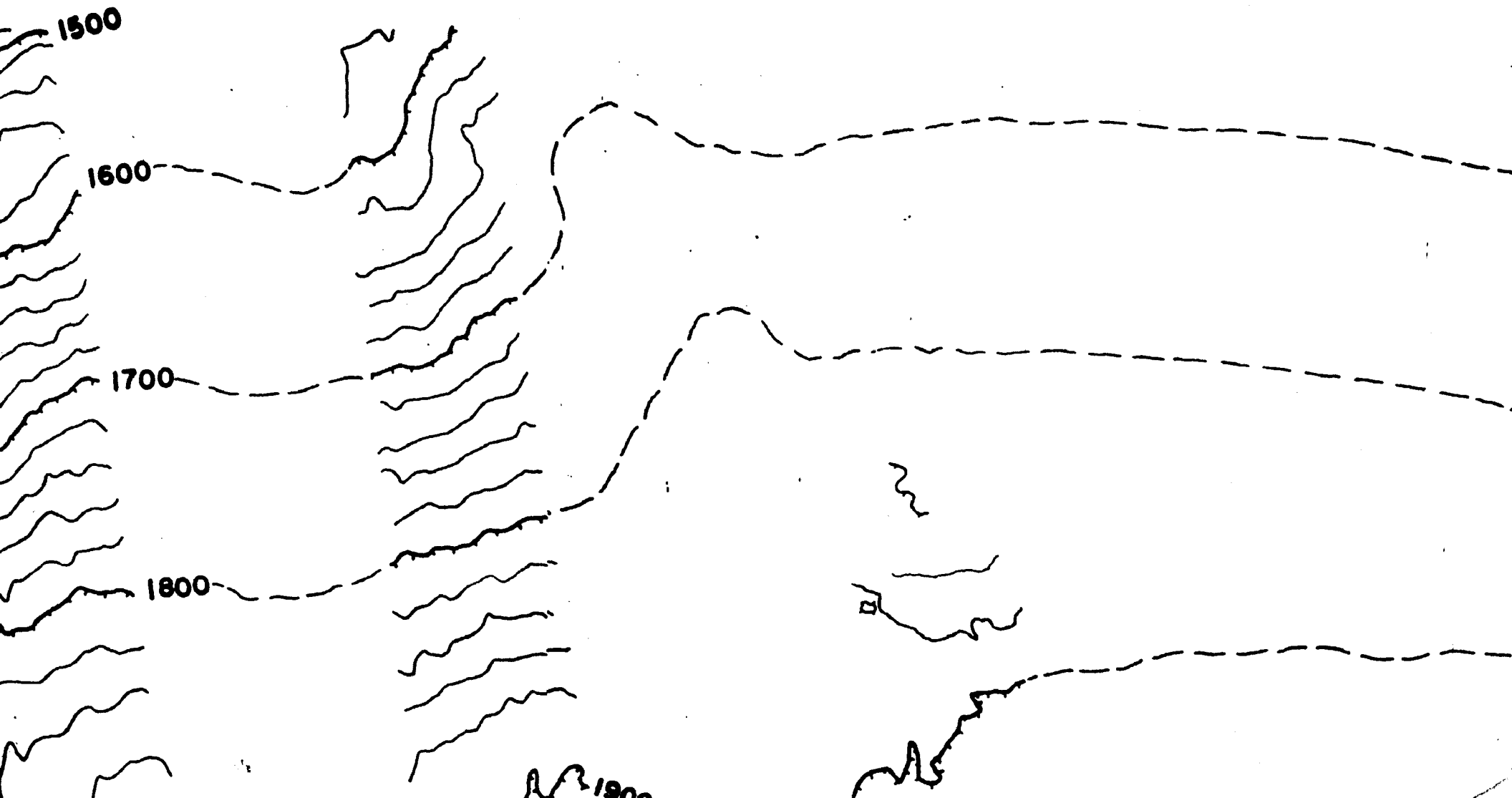
1500
1600
1700
1800

2000
Bound
Fan/Slope
1900
1900
1900

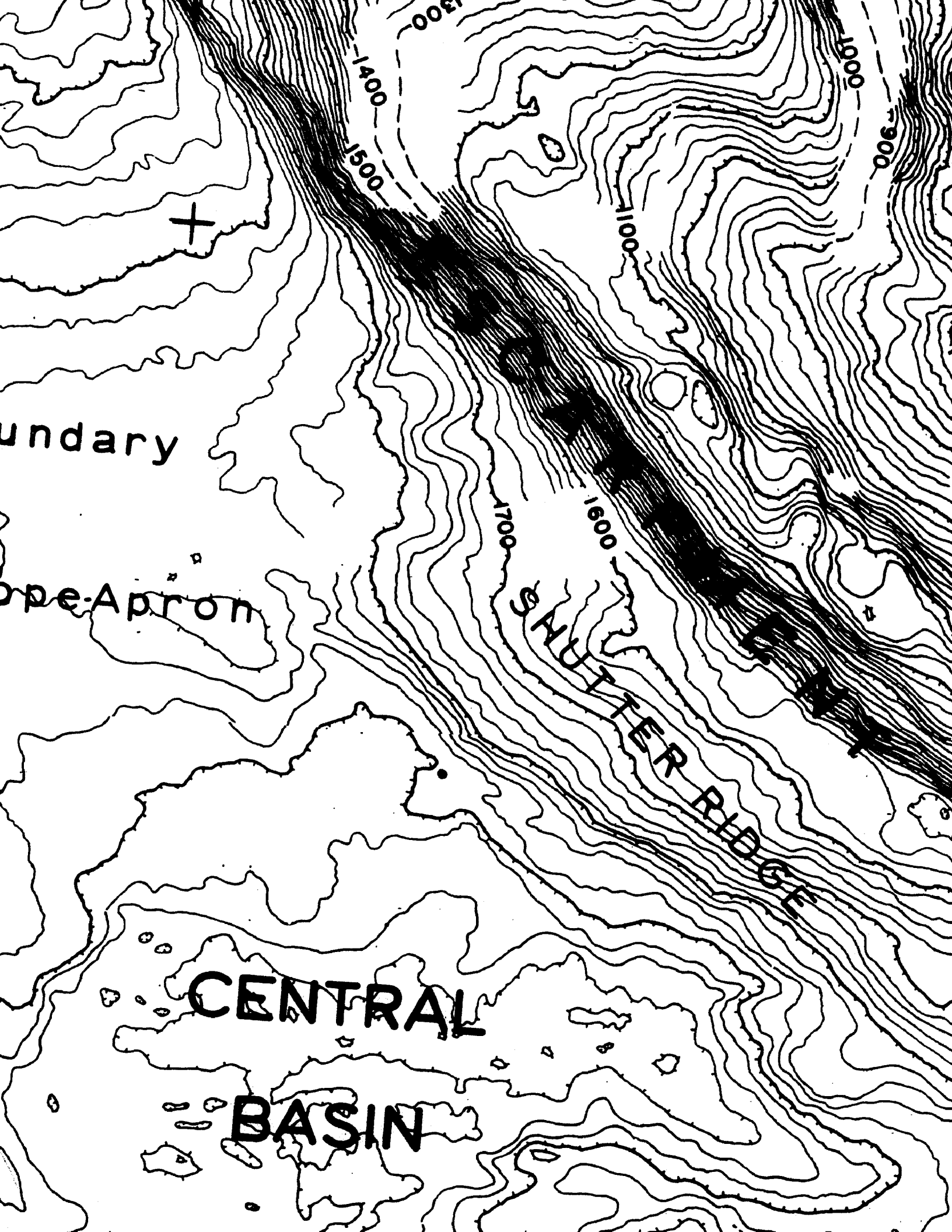
1300
1400
1500
1100
1000
900
1700
1600
undary
ope Apron
SHUTTER RIDGE
CENTRAL
BASIN

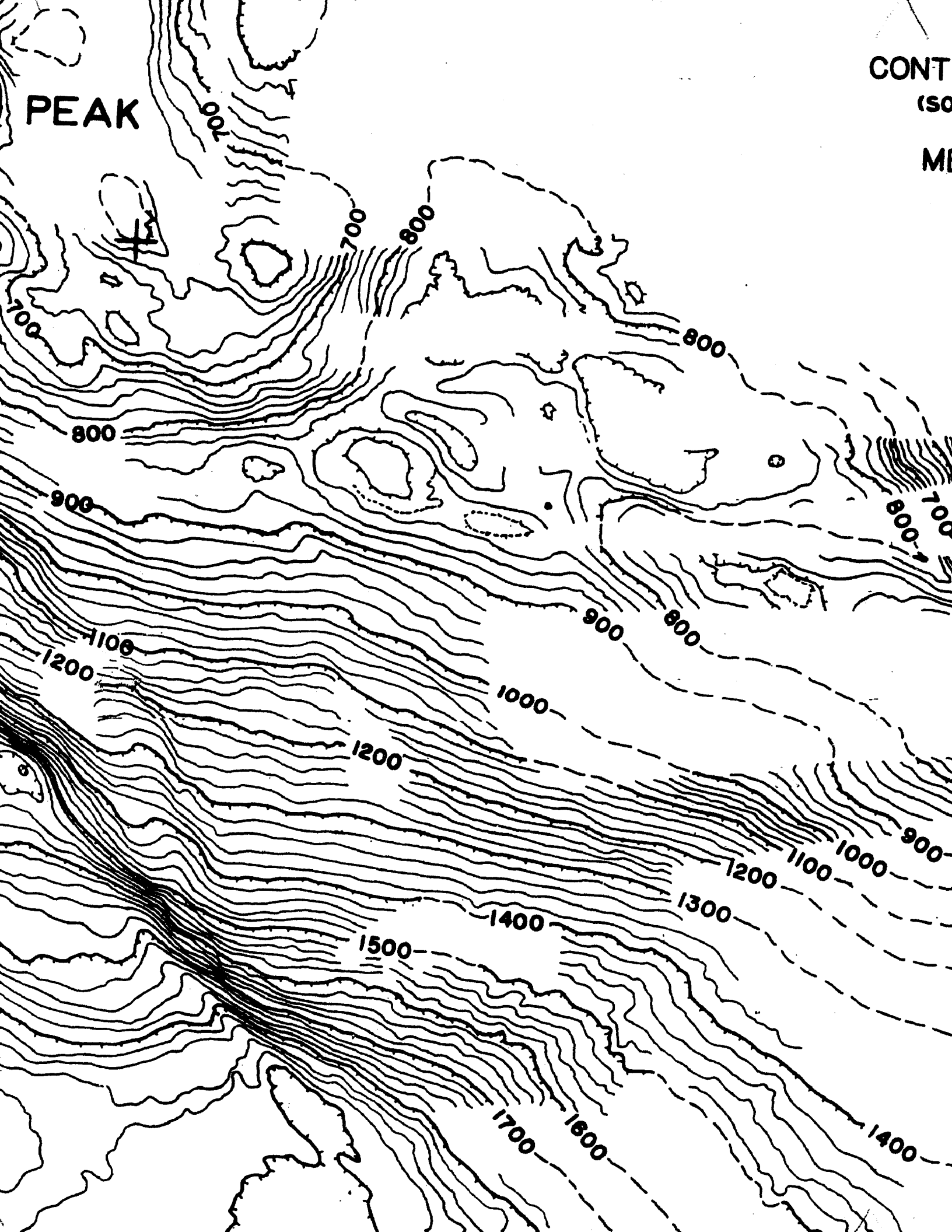
PEAK
CONT
(SO
ME
700
800
900
1000
1100
1200
1300
1400
1500
1600
1700

ONTOUR INTERVAL 20 METERS
(SOUNDING VELOCITY 1500 M/SEC)

MERCATOR PROJECTION

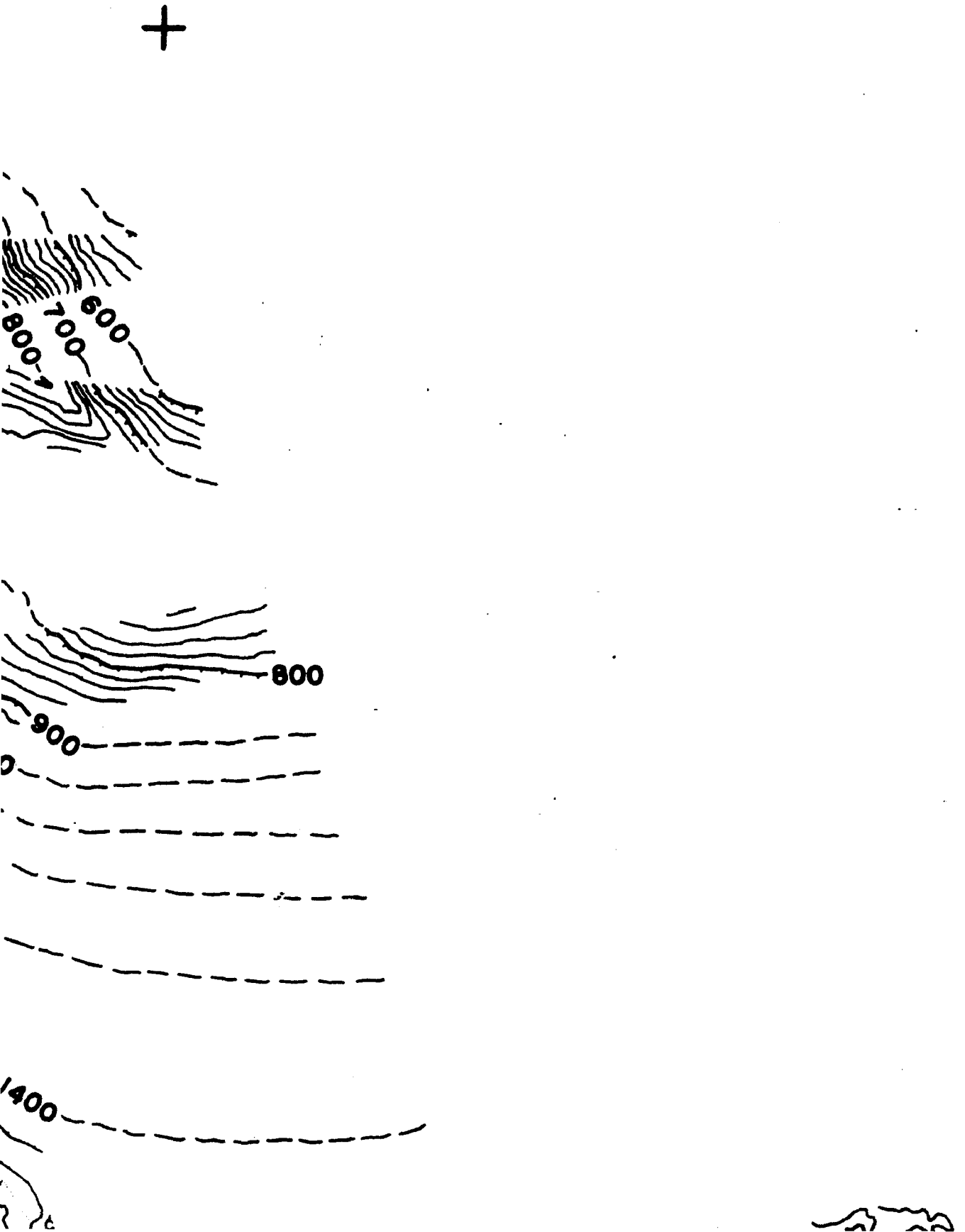

RS

+ 32° 35'

+ 32° 30'

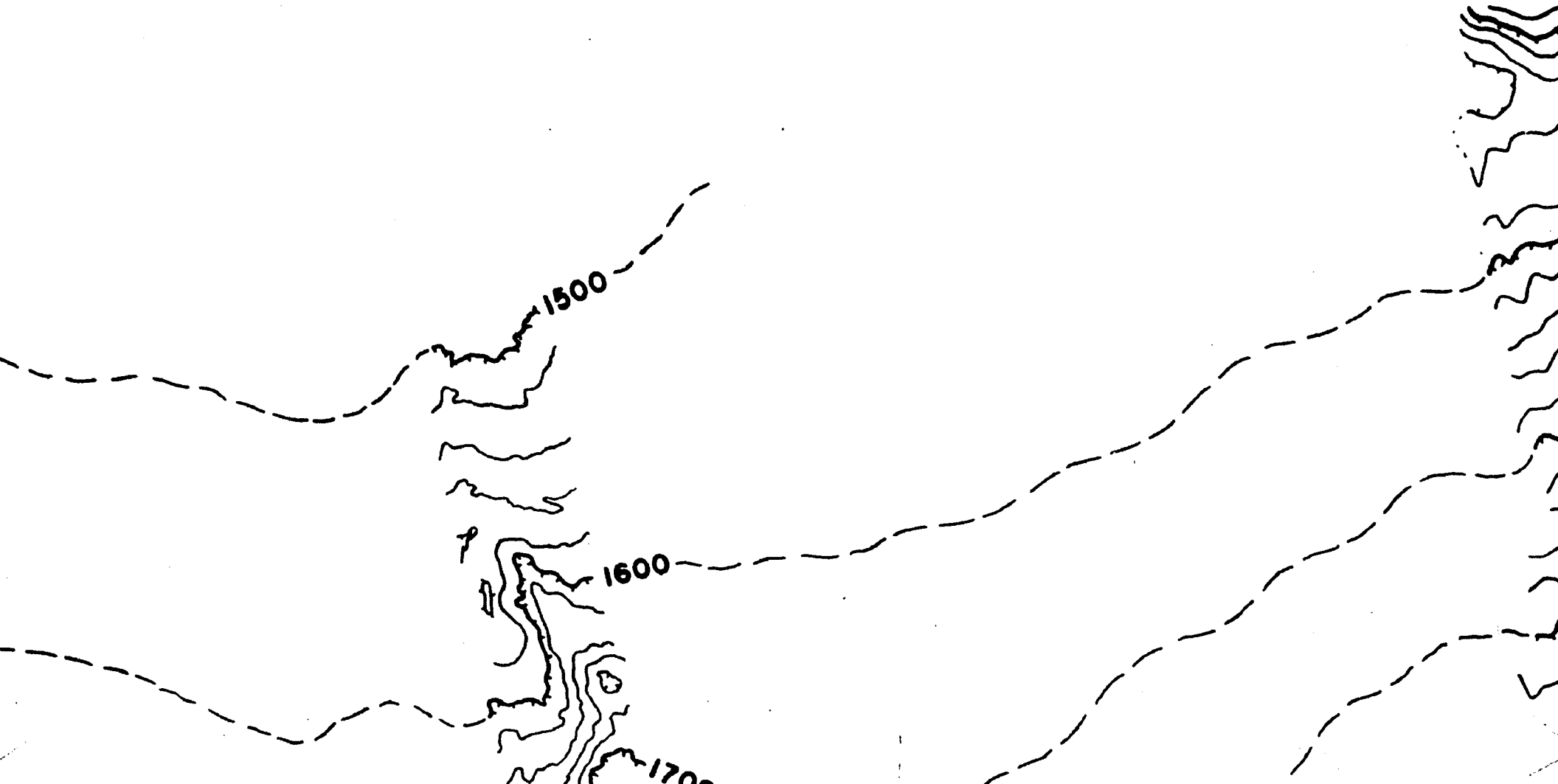
1500
1600
1700

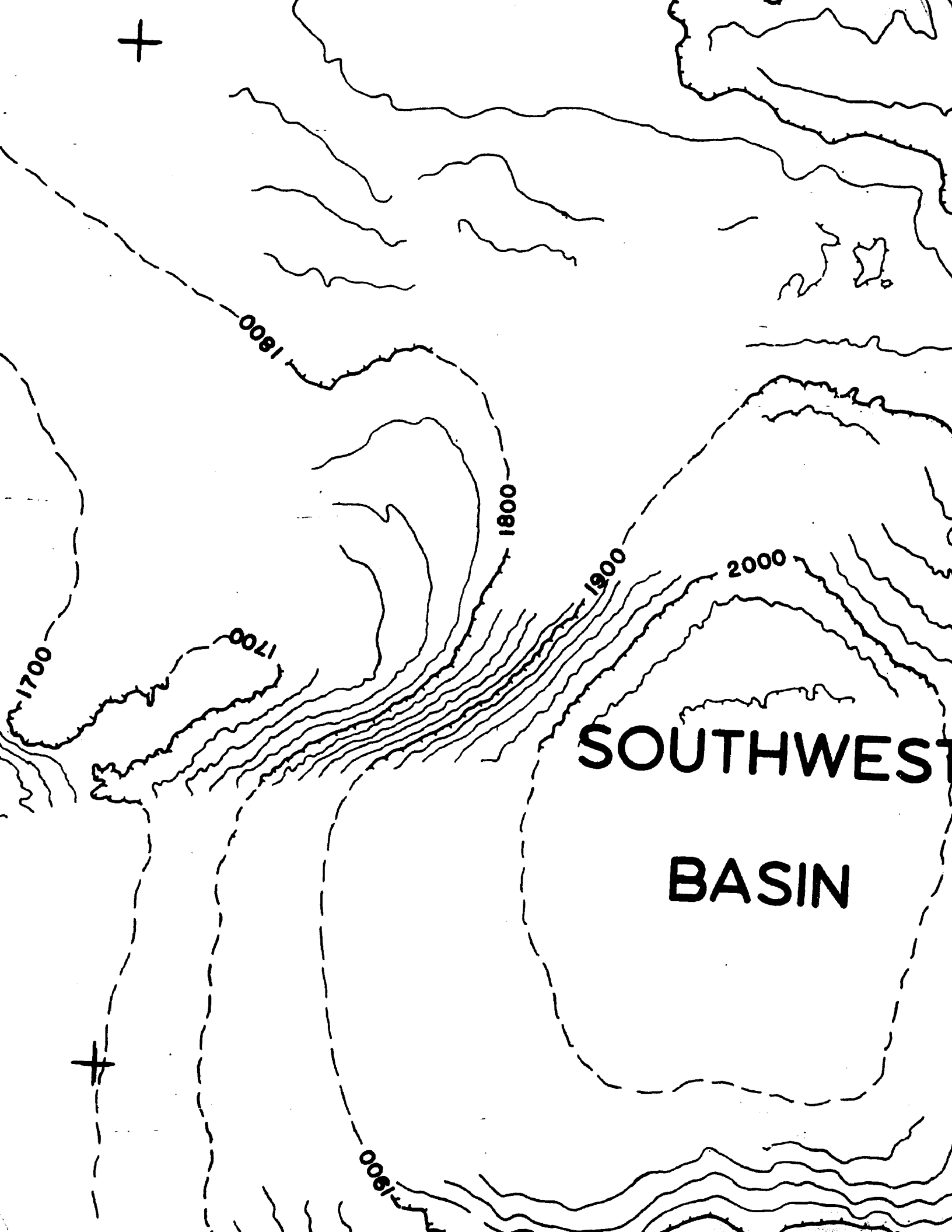
1800
1800
1900
2000
1700
1700
SOUTHWEST
BASIN
1900

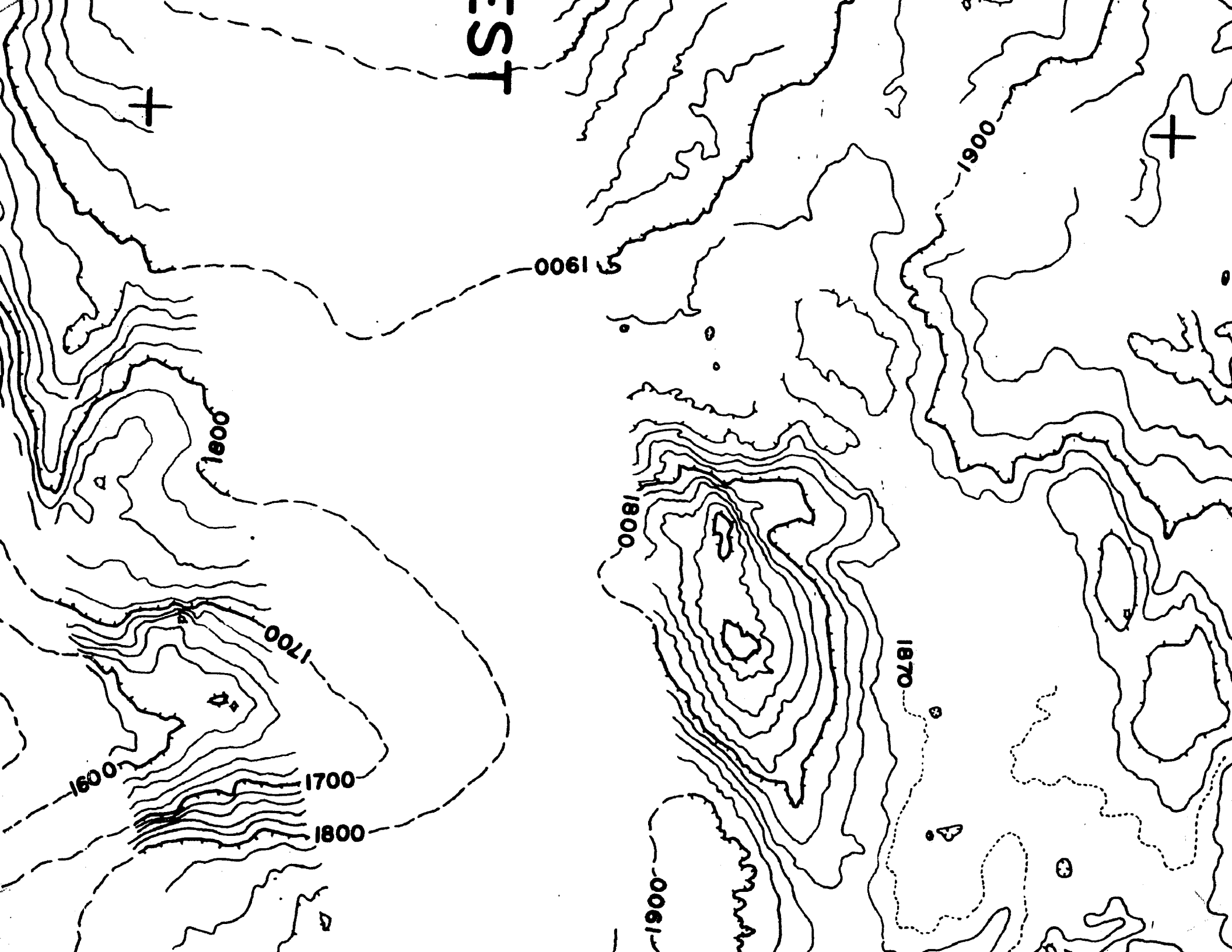

1900
1900
1800
1800
1700
1600
1700
1800
1870
1900

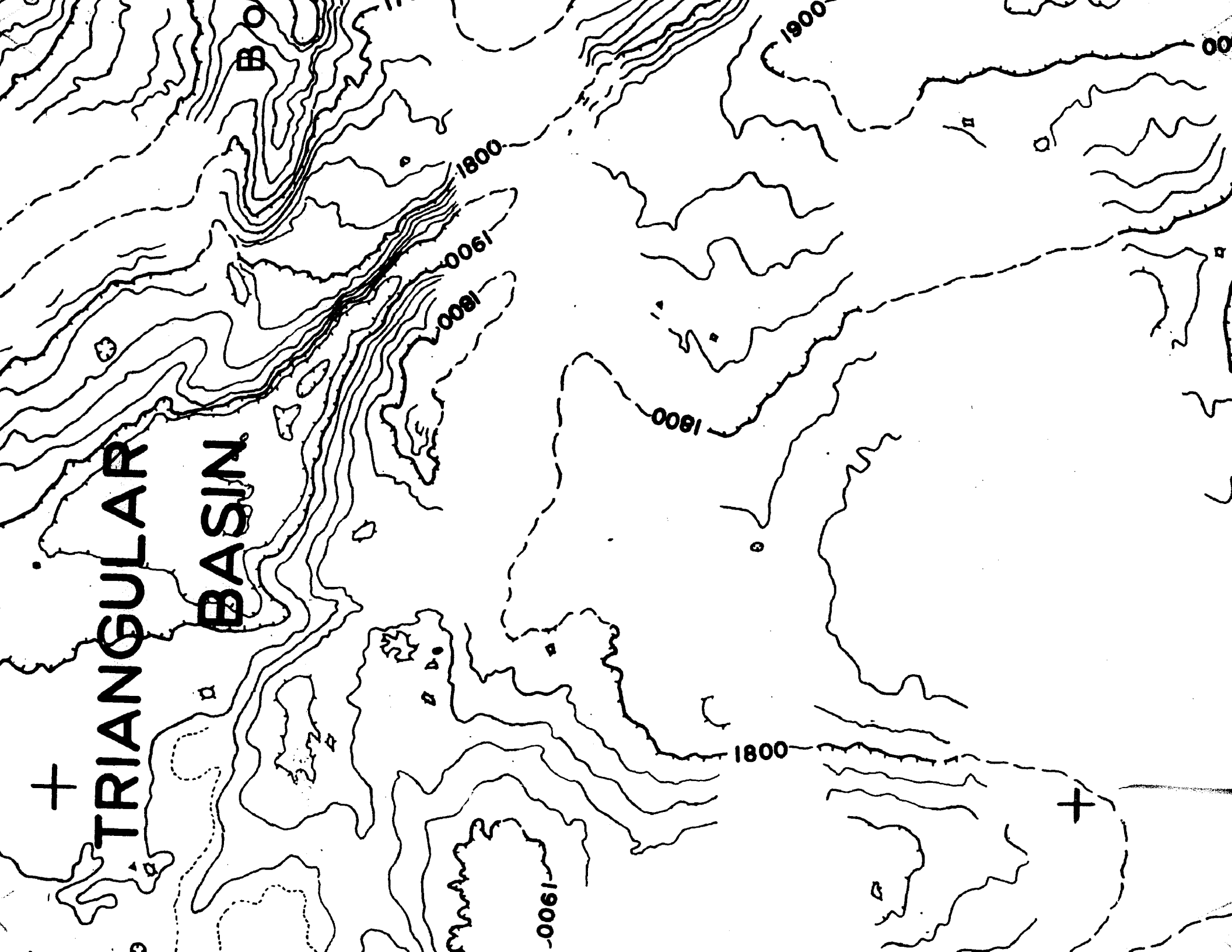
TRIANGULAR
BASIN
1800
1900
1800
1900
1800
1800
1900

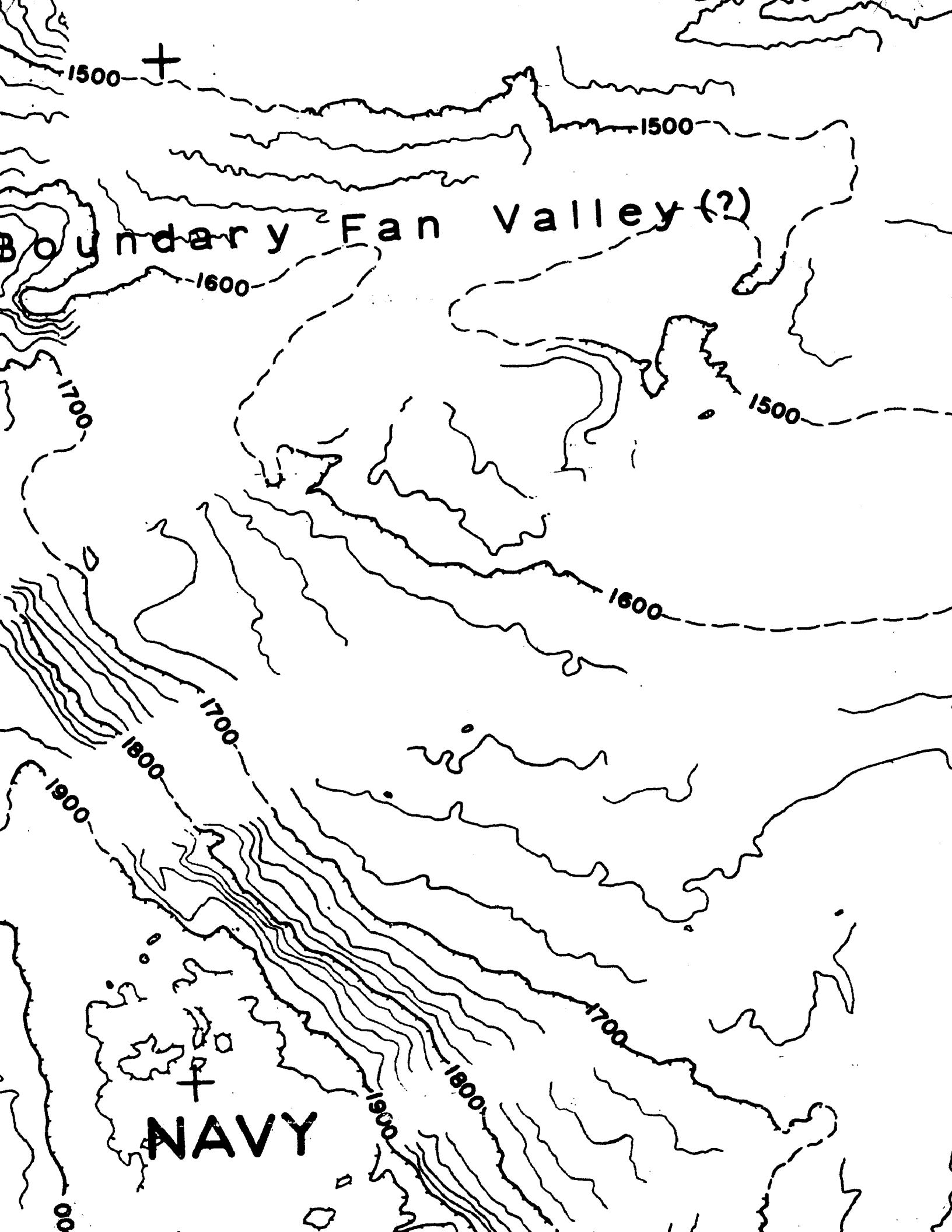
1500
1500
Boundary Fan Valley (?)
1600
1700
1500
1600
1700
1800
1900
1700
1800
1900
NAVY

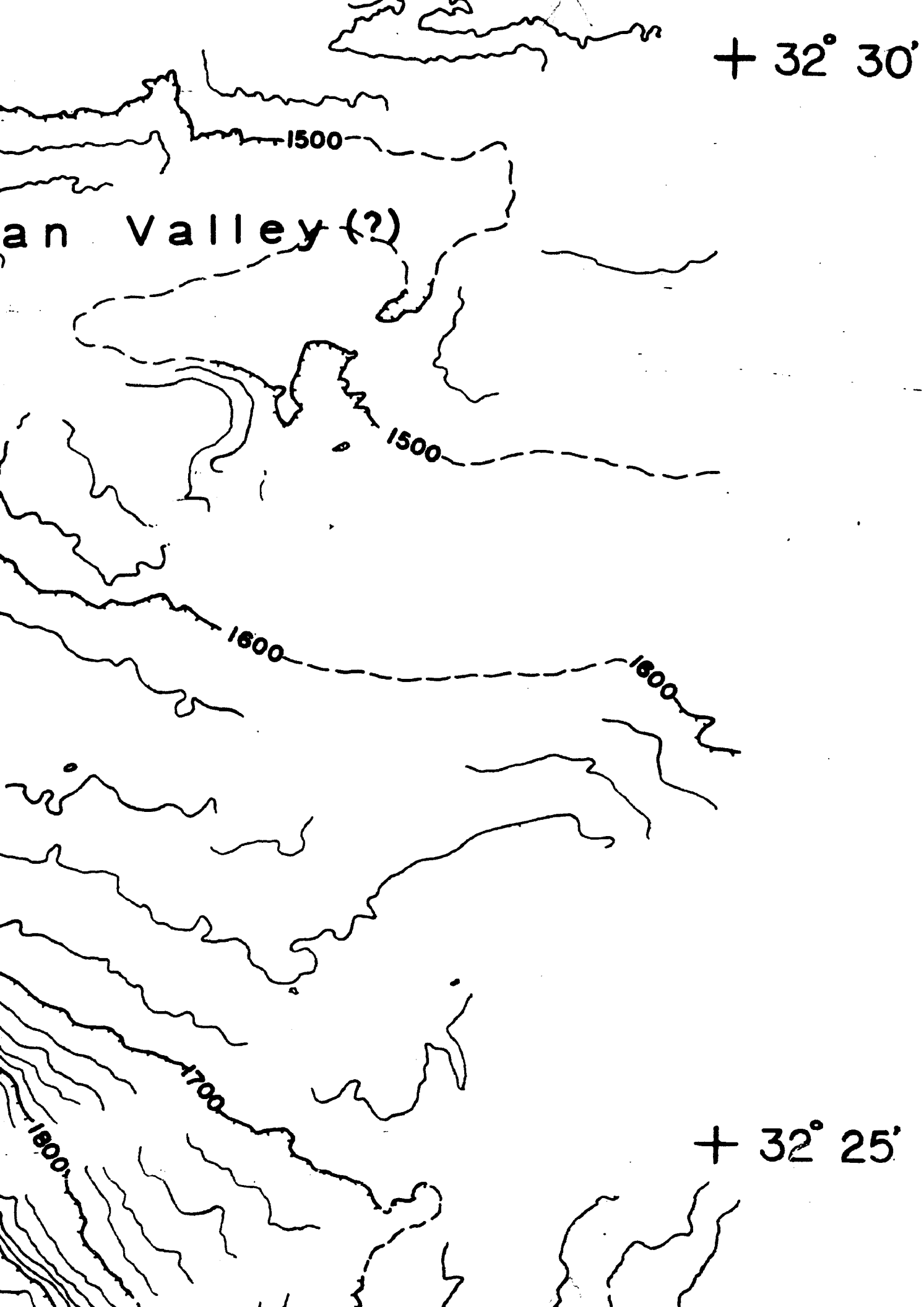
+ 32° 30'
1500
an Valley (?)
1500
1600
1600
1700
1800
+ 32° 25'

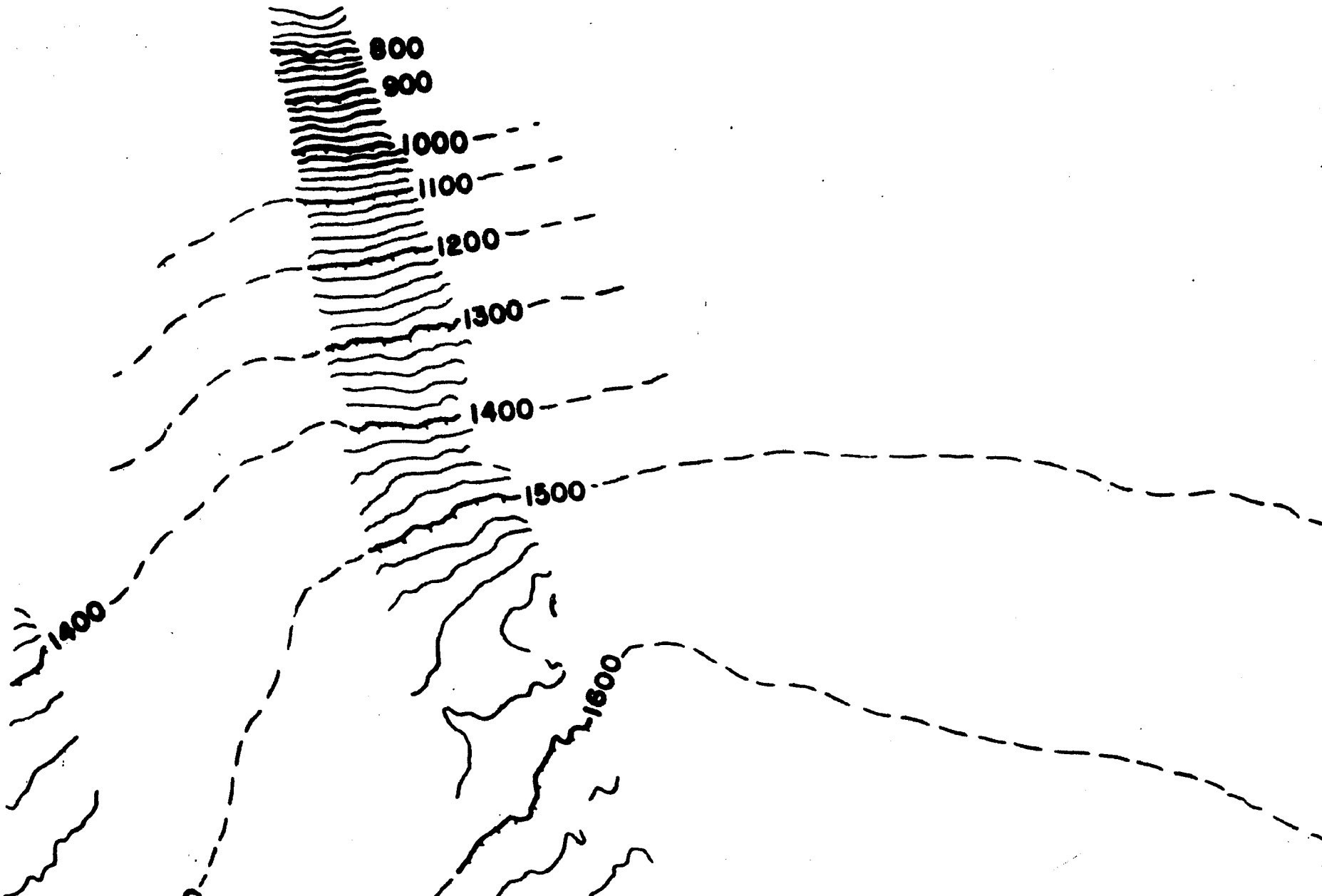
800
900
1000
1100
1200
1300
1400
1500
1400
1600

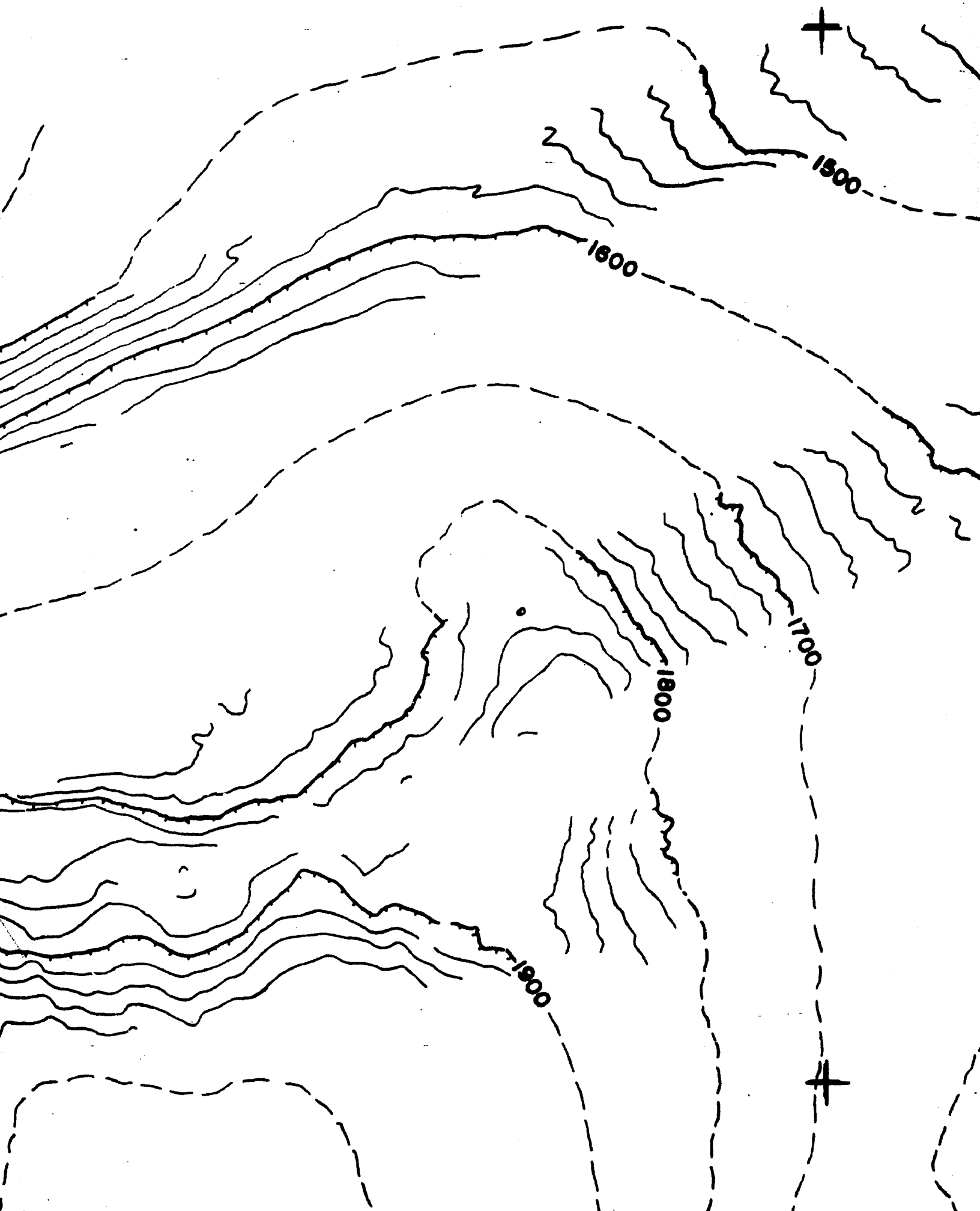
1500
1600
1700
1800
1900

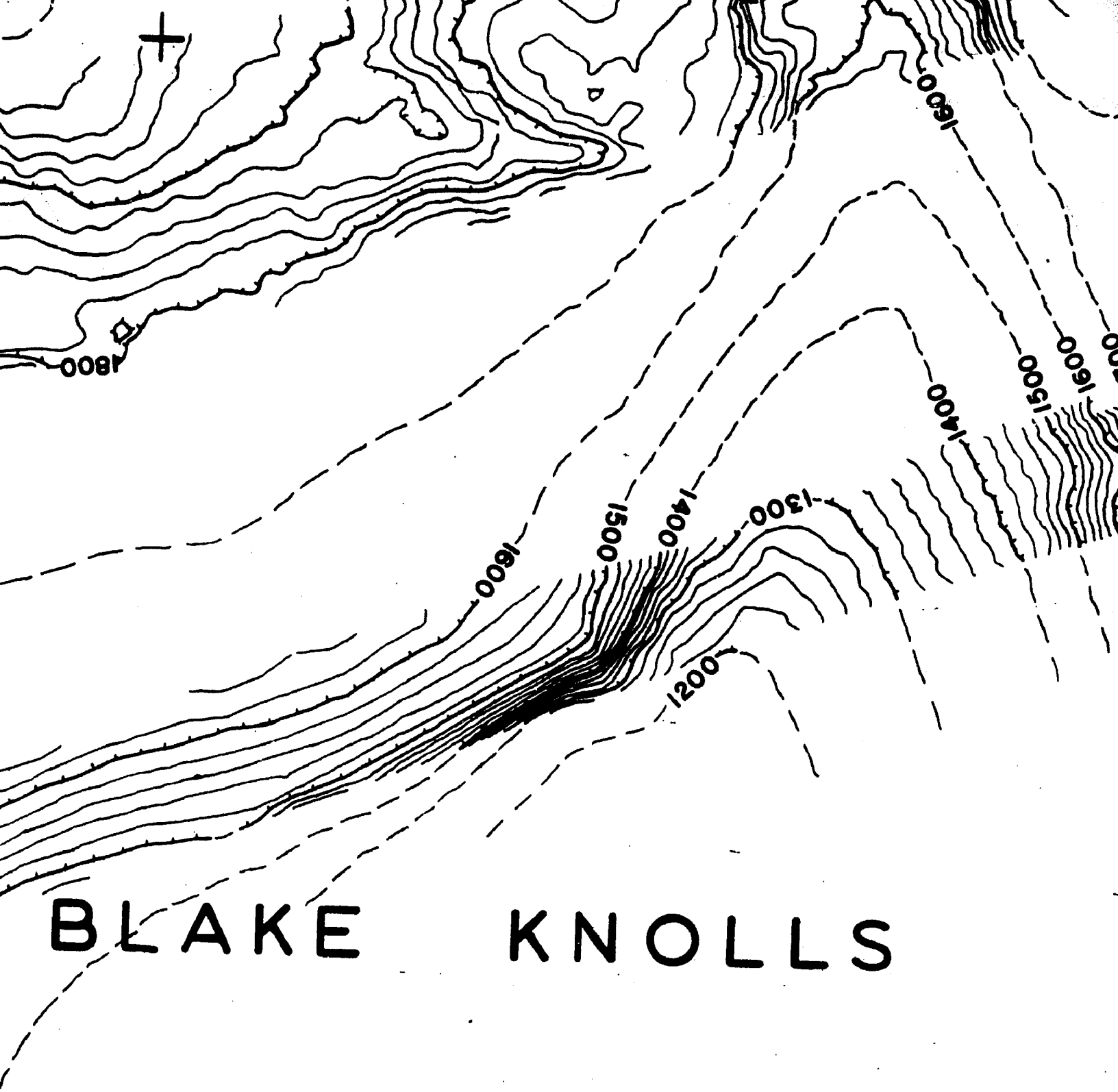


# BLAKE KNOLLS

Compiled & Drafted by Mark R. Legg (1985)

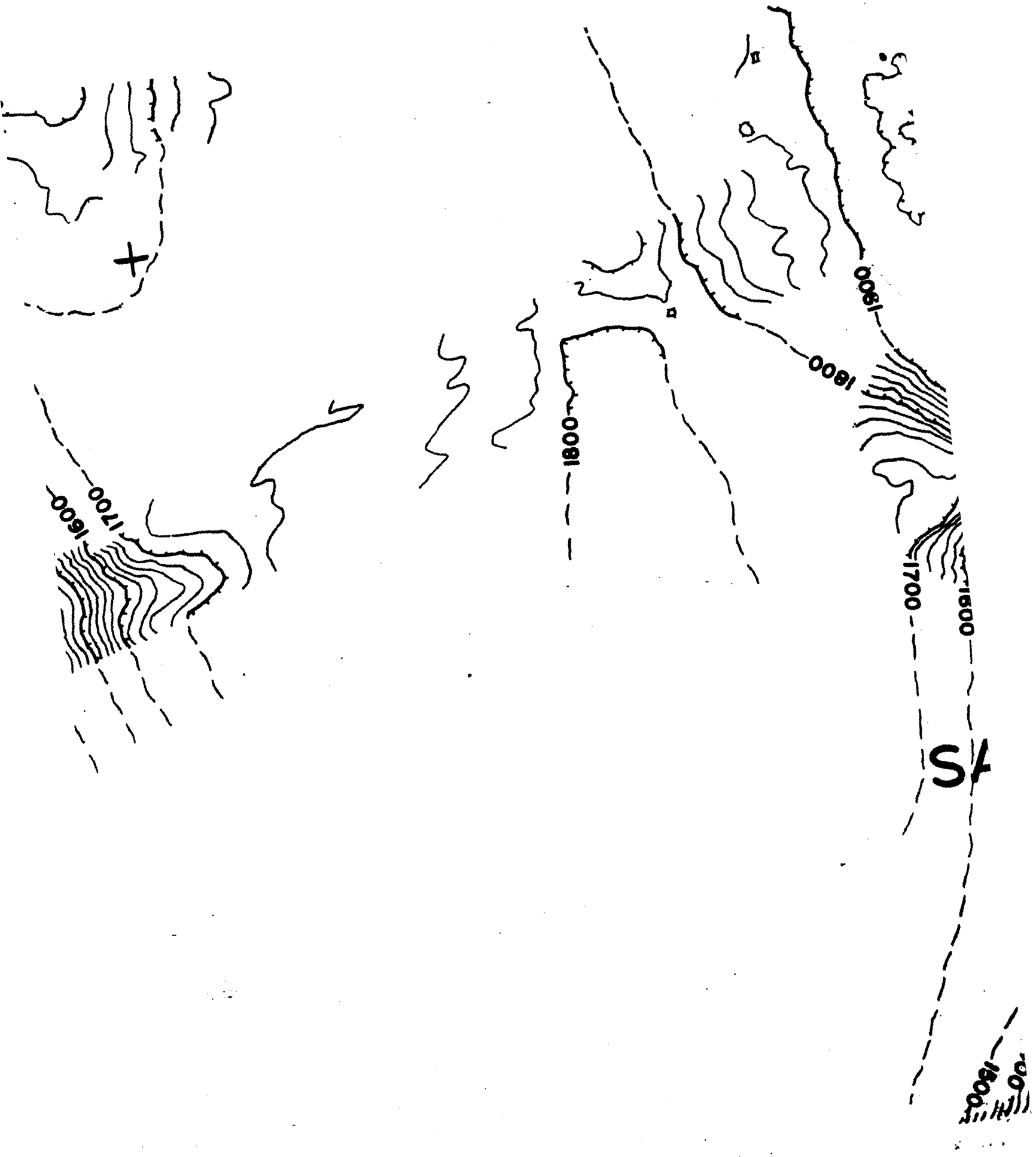


5)

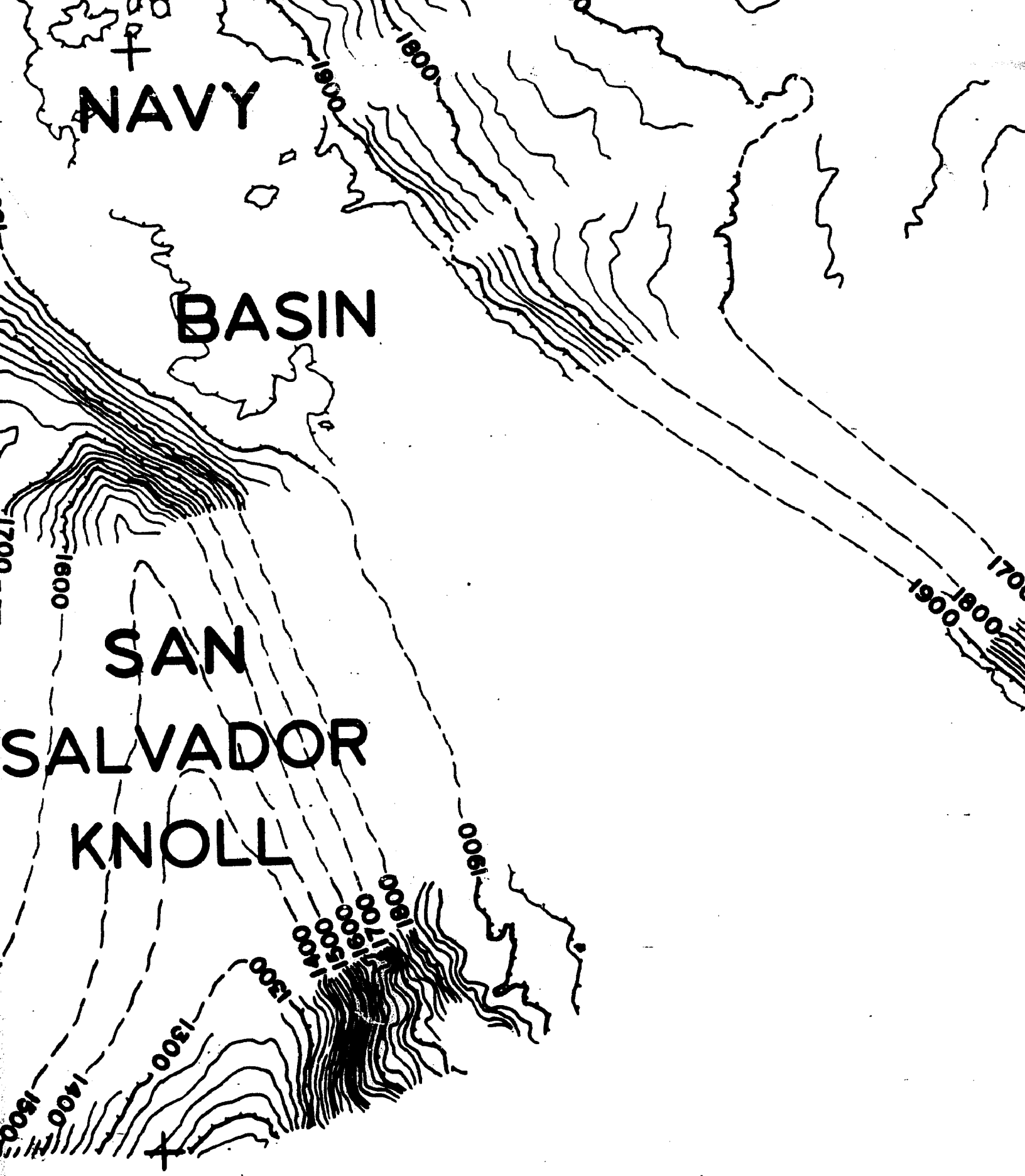
NAVY
BASIN
SAN
SALVADOR
KNOLL
1800
1900
1700
1600
1500
1400
1300

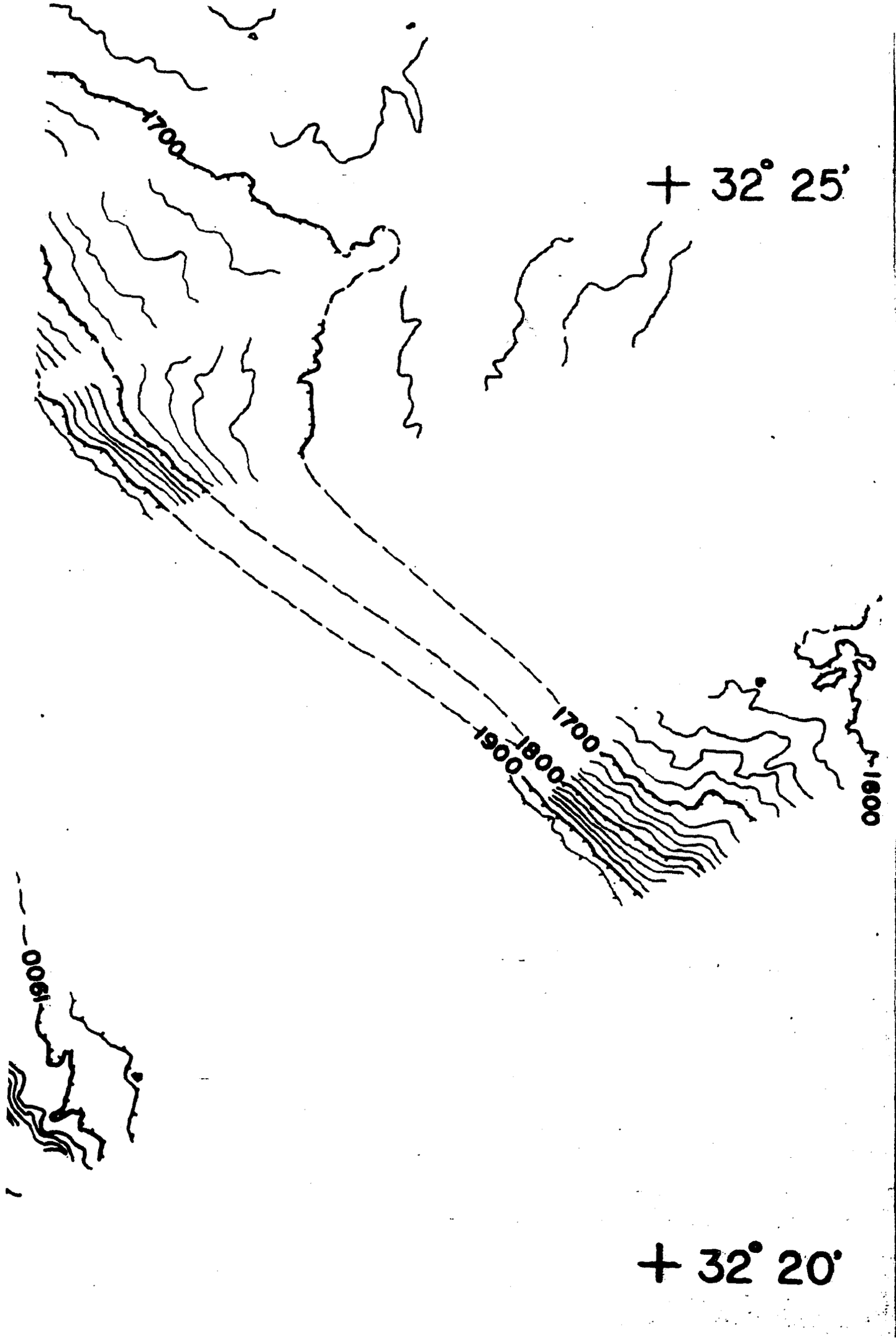
+ 32° 25'
1700
1700
1800
1900
1800
1900
+ 32° 20'

118°10'
1000?
1100
1200
1300
1400
1500
1600?
1700
1800?
900
?
?
?
1800
1700
San Clemente
Bluff Valley

118° 10'
118° 05'
N O
S A
1100
1000
900
800
700
600
500

118° 05'

118° 00'

ORTH SAN CLEME

SAN CLEMENTE FA

118°00'

NTE BASIN

ULT ZONE

Sea Beam

117° 55'

117° 50'

# Plate 5

# Sea Beam Bathymetry

117° 50′

e 5

eam

netry

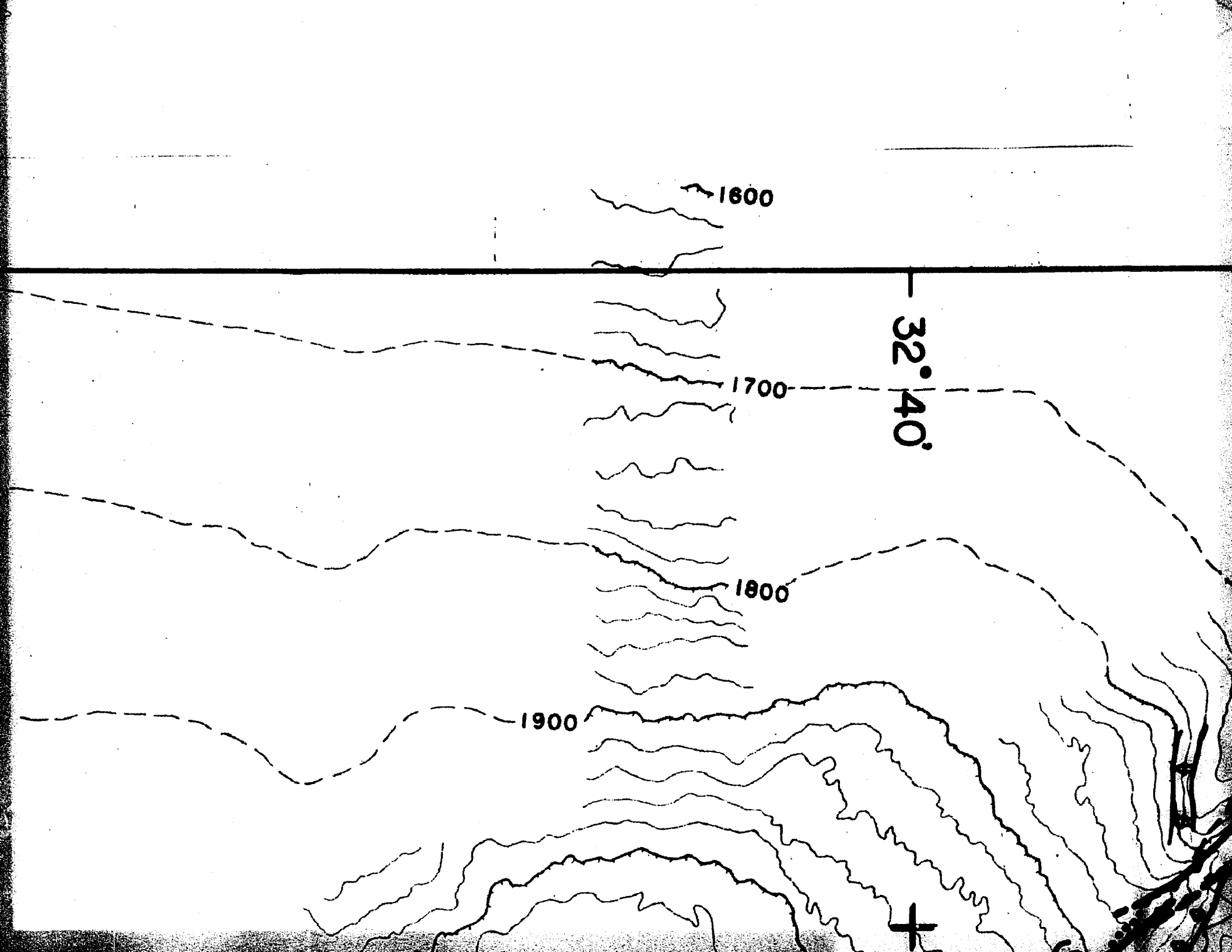
1600
1700
1800
1900
32° 40'

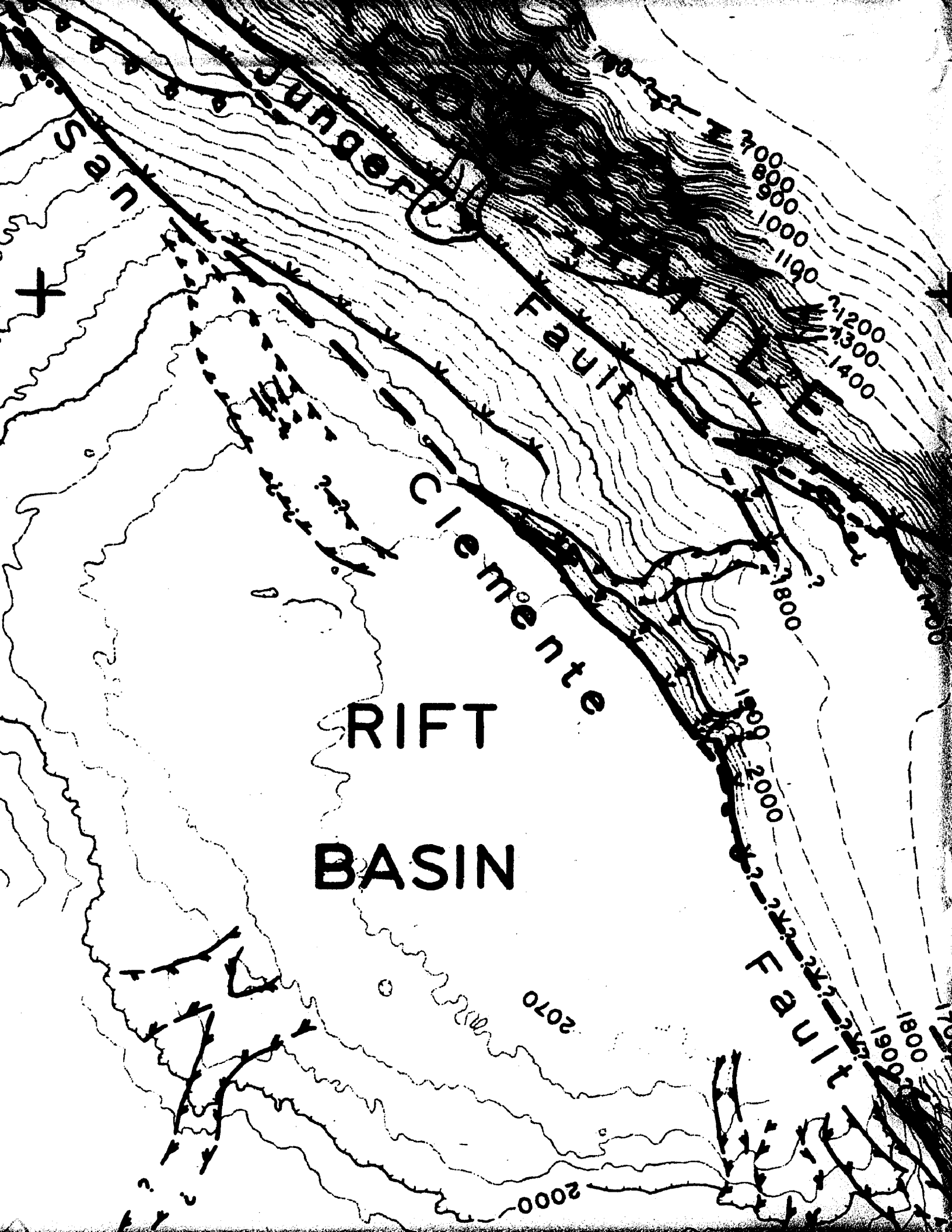
San Jacinto Fault
San Clemente Fault
RIFT
BASIN
700
800
900
1000
1190
1200
1300
1400
1800
1900
2000
2070
2000
1800
1900

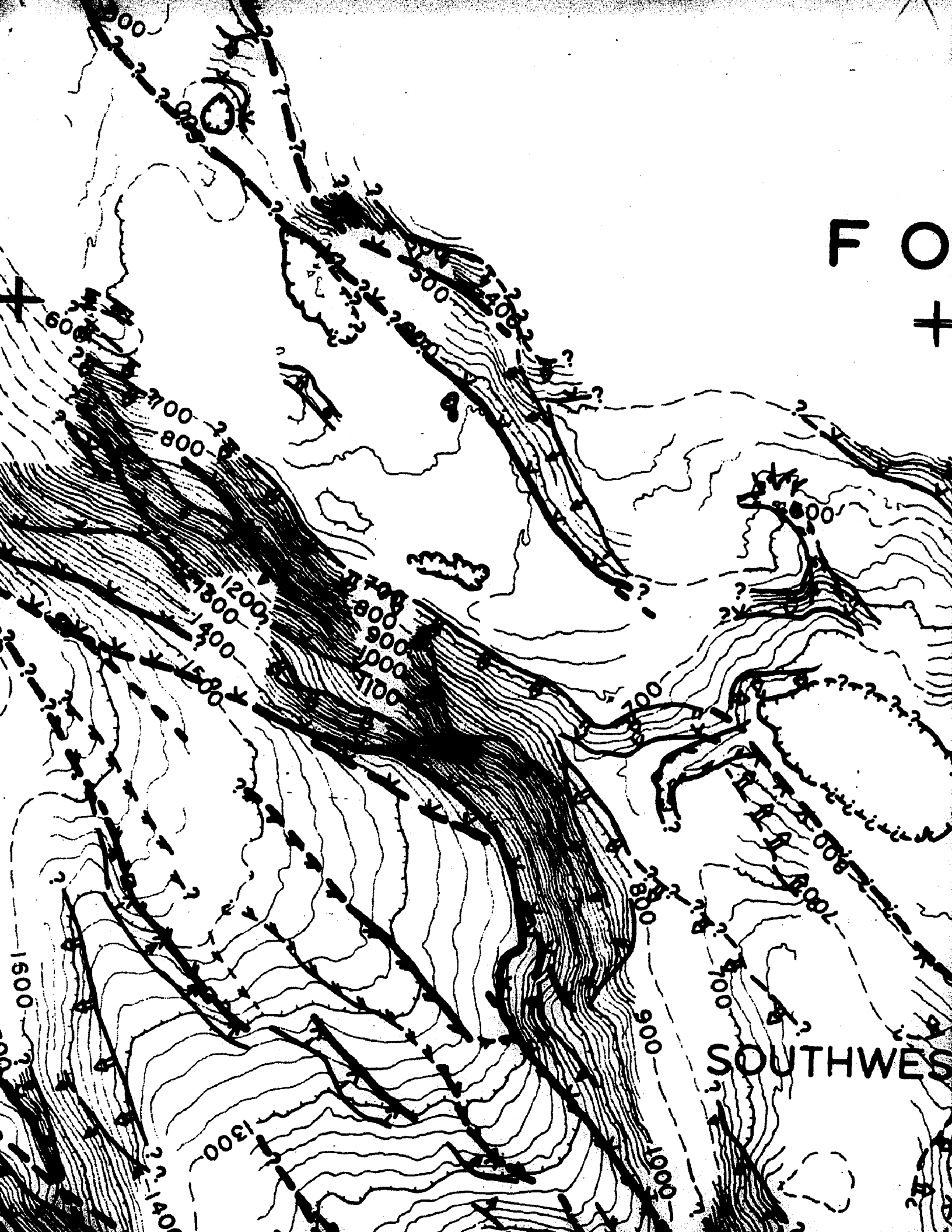
FO
SOUTHWES
500
600
700
800
900
1000
1100
1200
1300
1400
1500
1600

ORTYMILE

BANK

AGE OF FAULTING

- CUTS STRATA OF HOLOCENE
- CUTS STRATA OF LATE QUATER
- CUTS STRATA OF PLEISTOCENE

WHERE FAULT OFFSETS SEAFL
SYMBOL IS SHOWN ON BAR ON
THROWN SIDE.

0 1

CONTOUR I
(SOUNDING

# Geomorphology

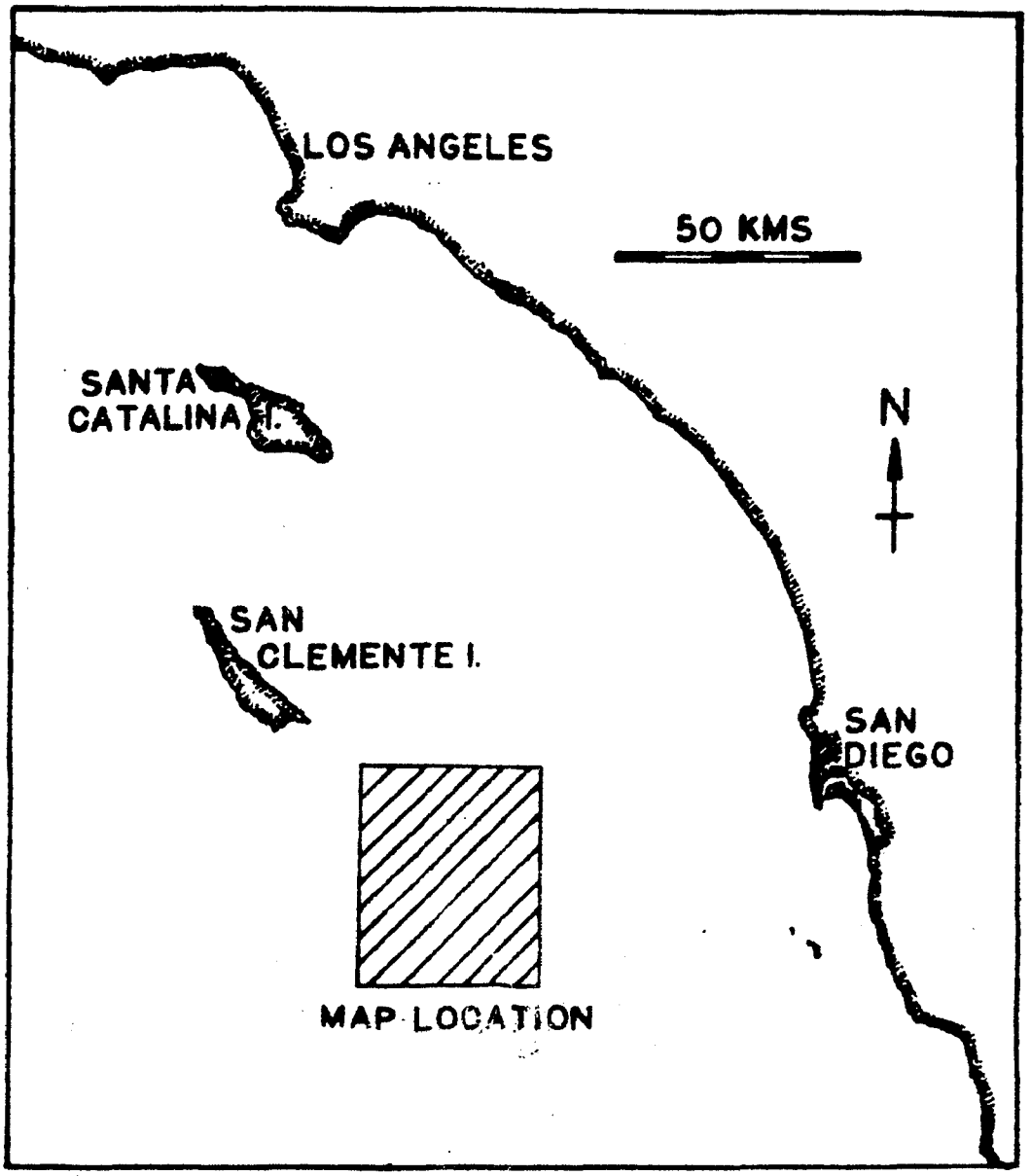


ING

NE AGE.

ATERNARY AGE.

ENE AGE.

AFLOOR, AGE
R ON DOWN-

2 3 4 5

KILOMETERS

R INTERVAL 20 METERS
ING VELOCITY (1500 M/SEC)

CATOR PROJECTION

# hology

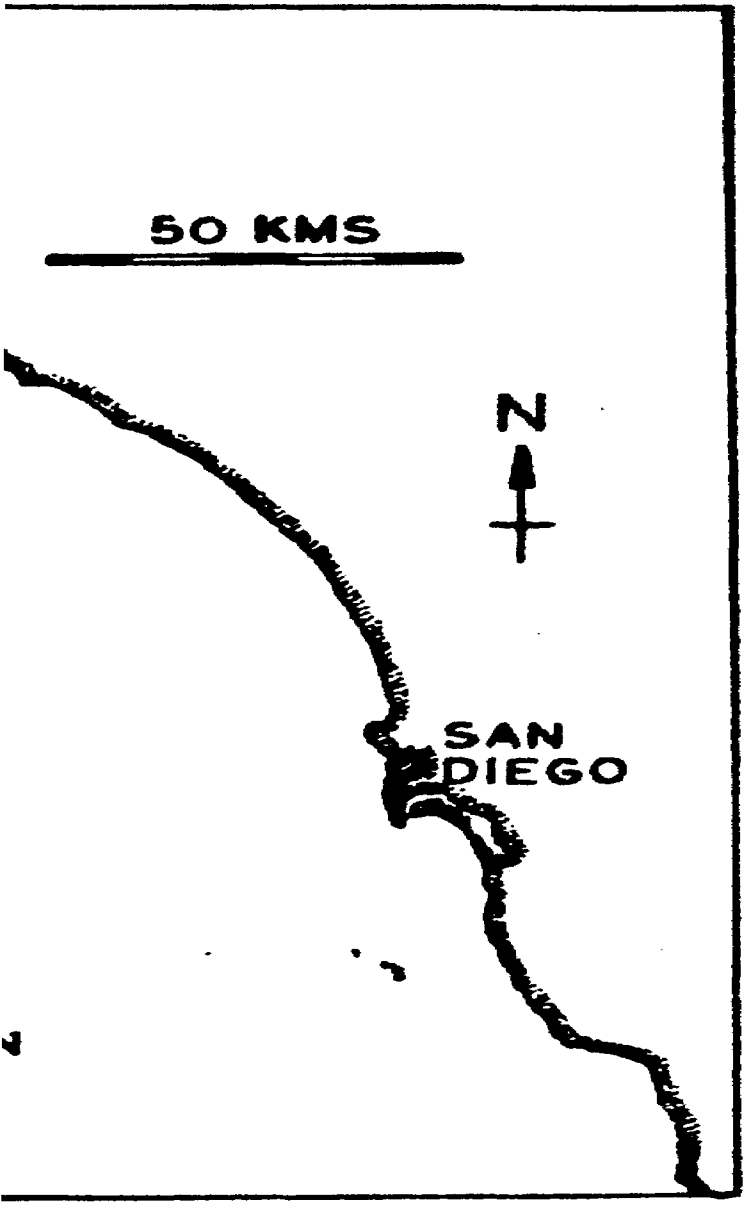


32° 40'

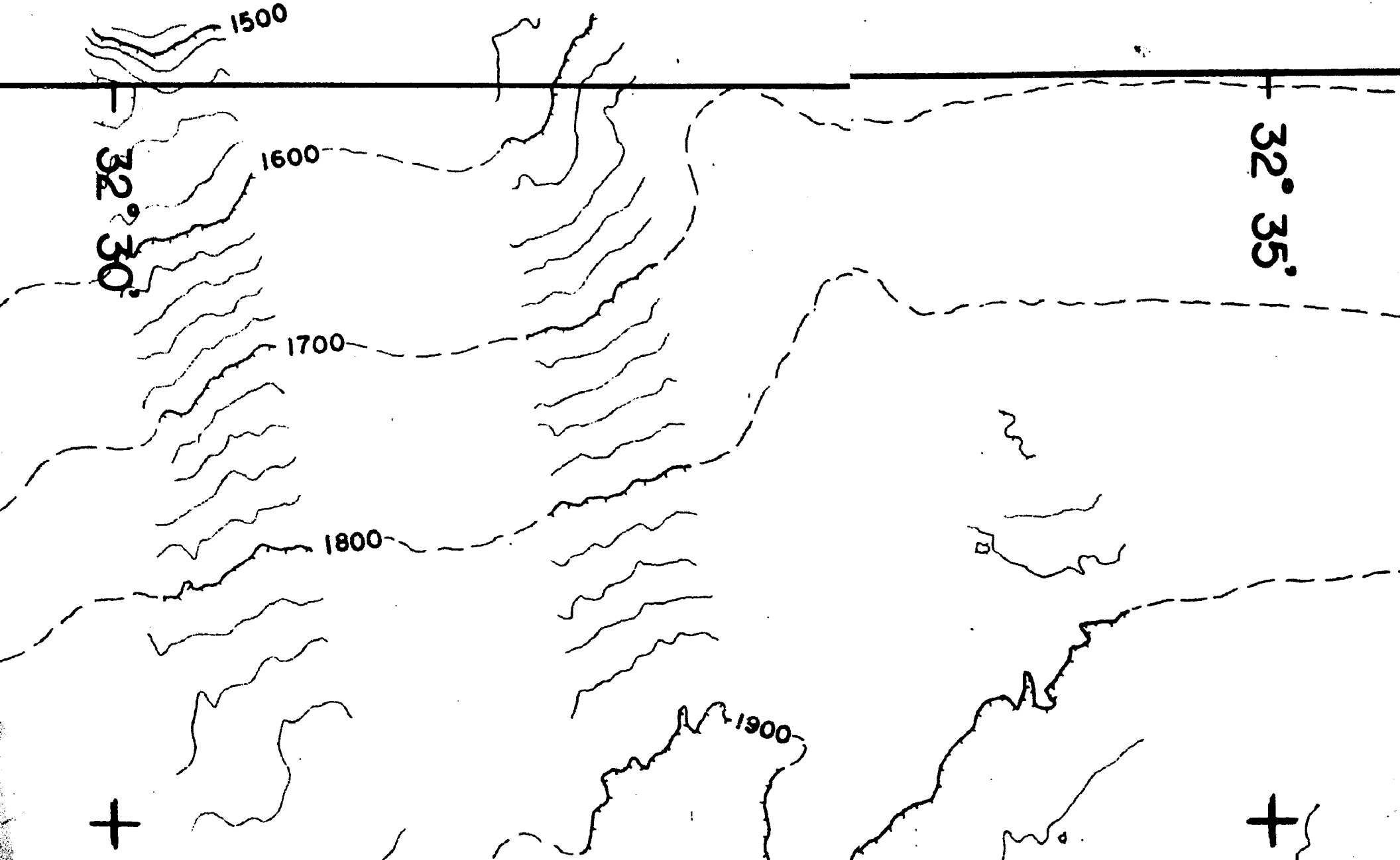
1500
1600
1700
1800
1900
32° 30'
32° 35'

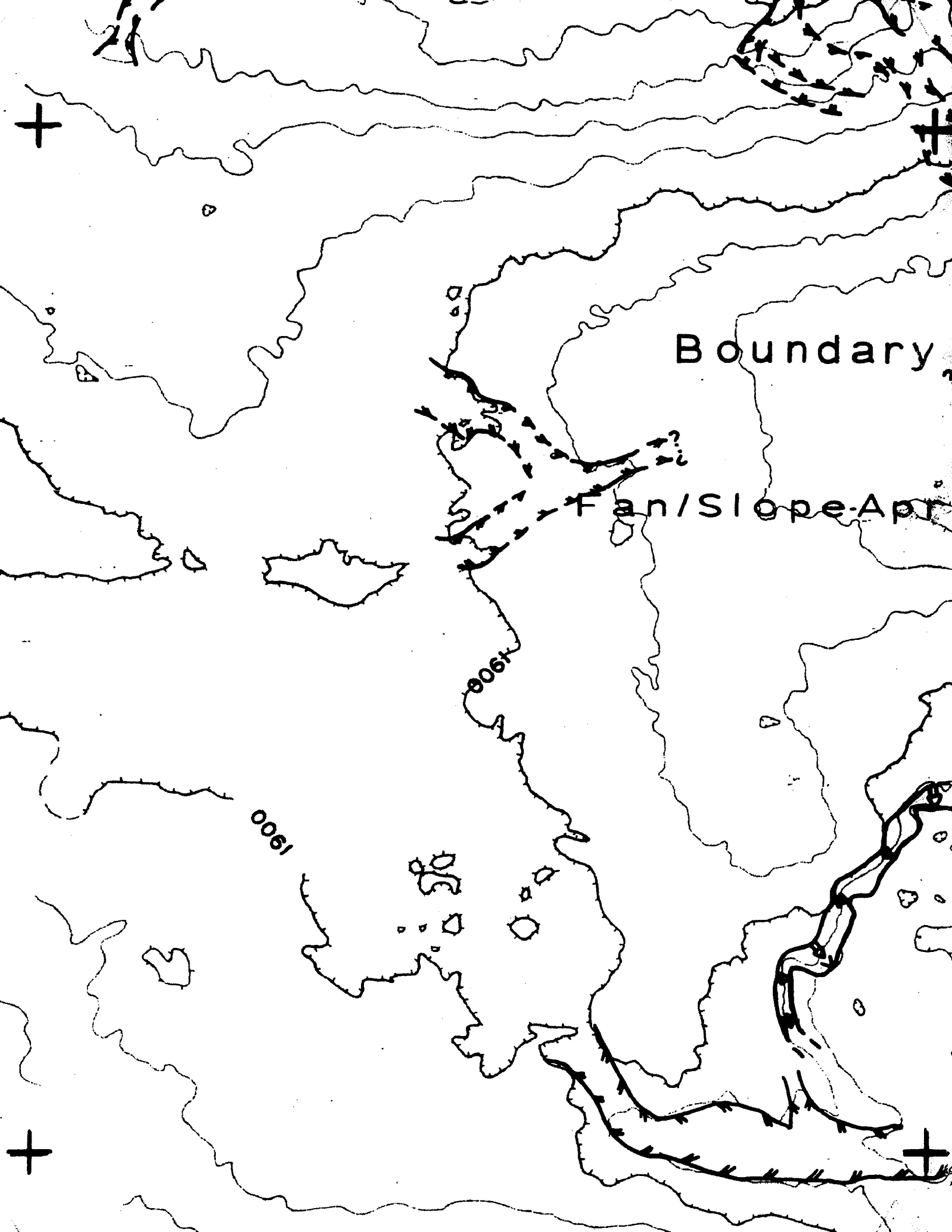
Boundary
Fan/Slope-Apr
1900
1900

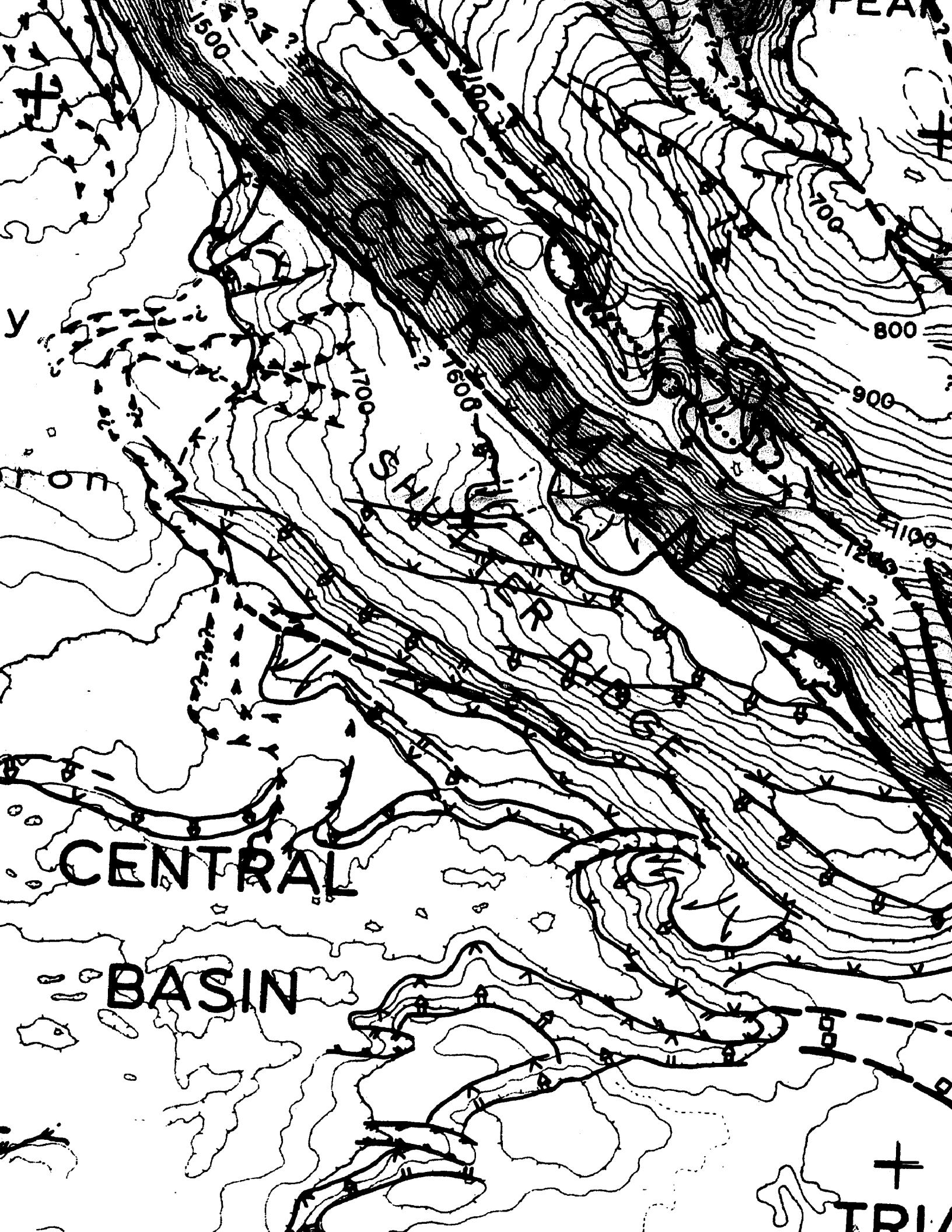

1500
1700
1600
700
800
900
1100
CENTRAL
BASIN

(SOUNDING VE

MERCATO

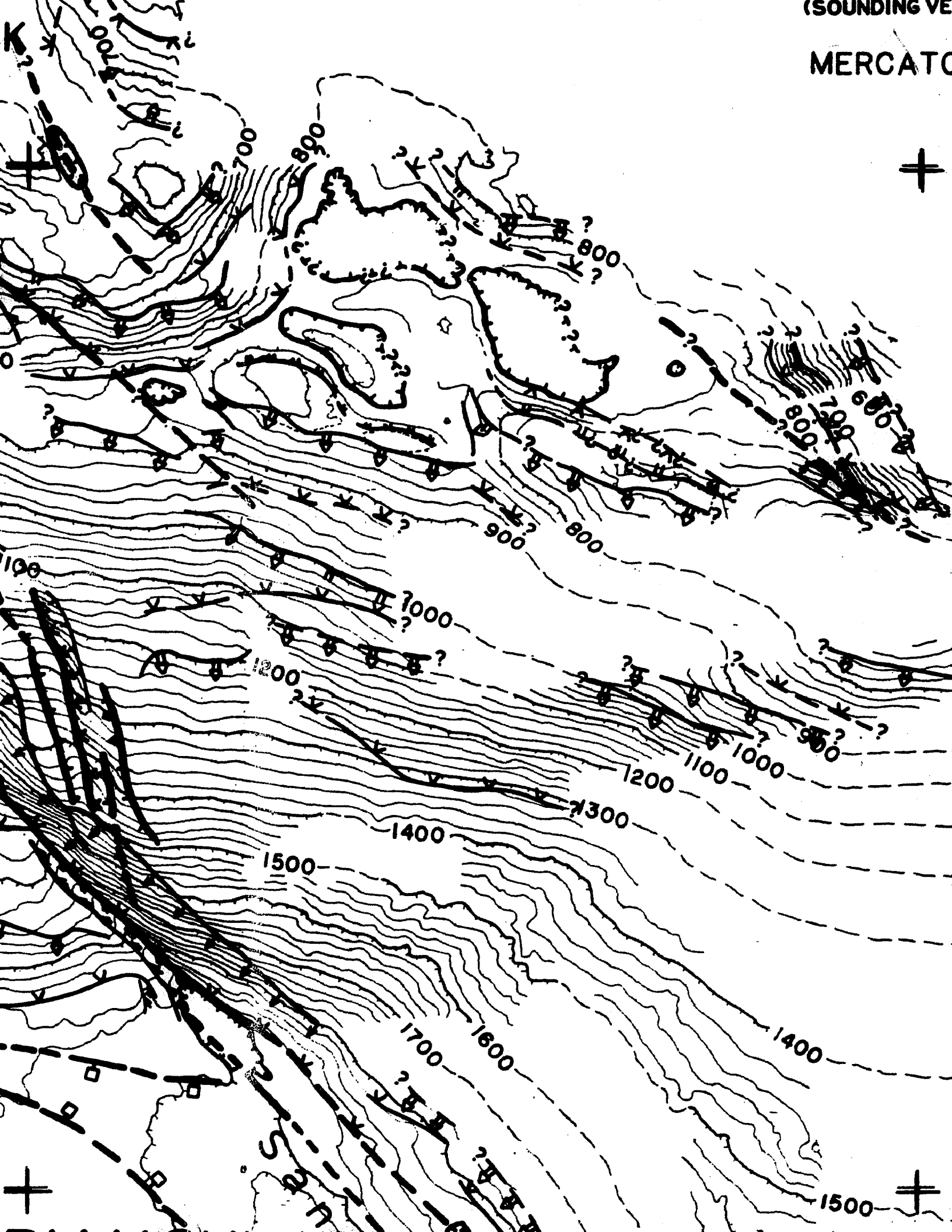

RCATOR PROJECTION

# Explanation of Symbols

FAULTS

AGE SYMBOL SHOWN WI
PROFILE CROSSES FAUL

SAGS OR OTHER SMALL, CLOSED DEPRESSIONS

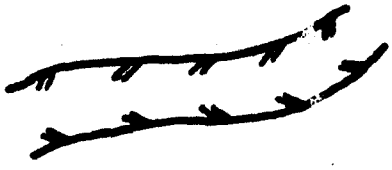

CHANNEL-LIKE FEATURES

SLIDES OR SLUMPS

ESCARPMENTS

TECTONIC

NON-TECTONIC(?)

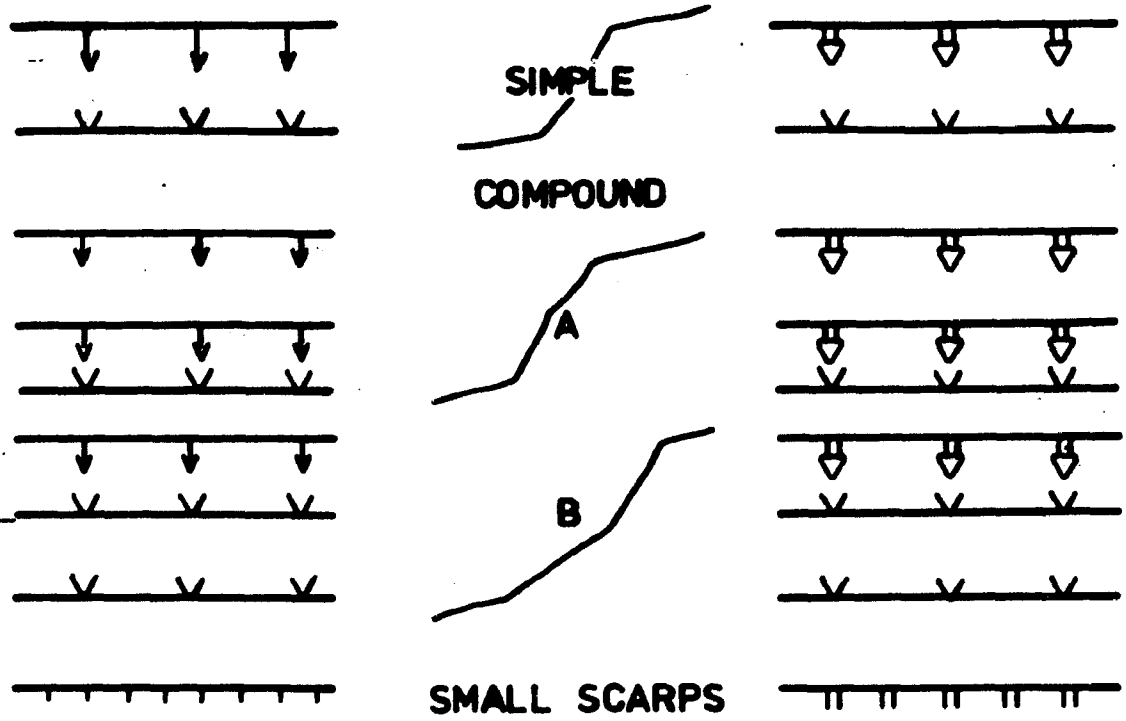


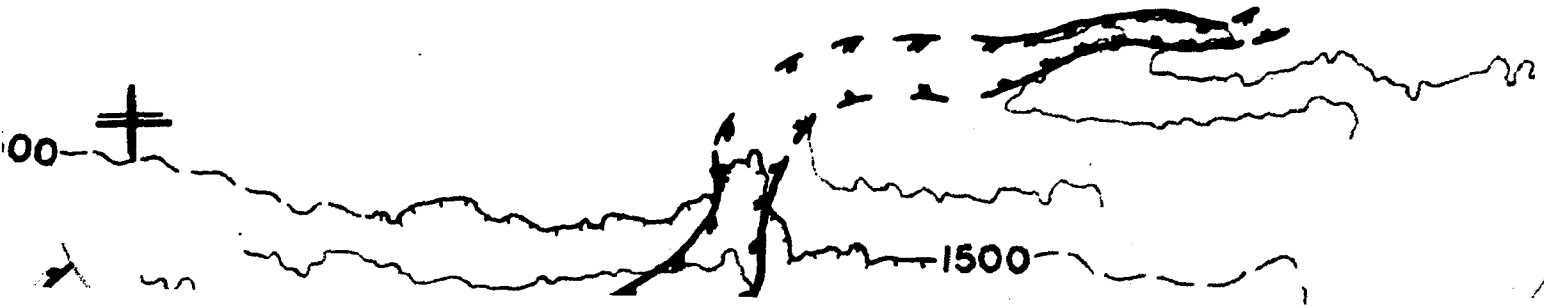

# ion of Symbols

32° 35'

—?—?—

D UNCERTAIN

FAULTS

AGE SYMBOL SHOWN WHERE SEISMIC PROFILE CROSSES FAULT.

SAGS OR OTHER SMALL, CLOSED DEPRESSIONS

CHANNEL-LIKE FEATURES

SLIDES OR SLUMPS

CARPMENTS

NON-TECTONIC(?)

SIMPLE

COMPOUND

A

B

ALL SCARPS

32° 30'

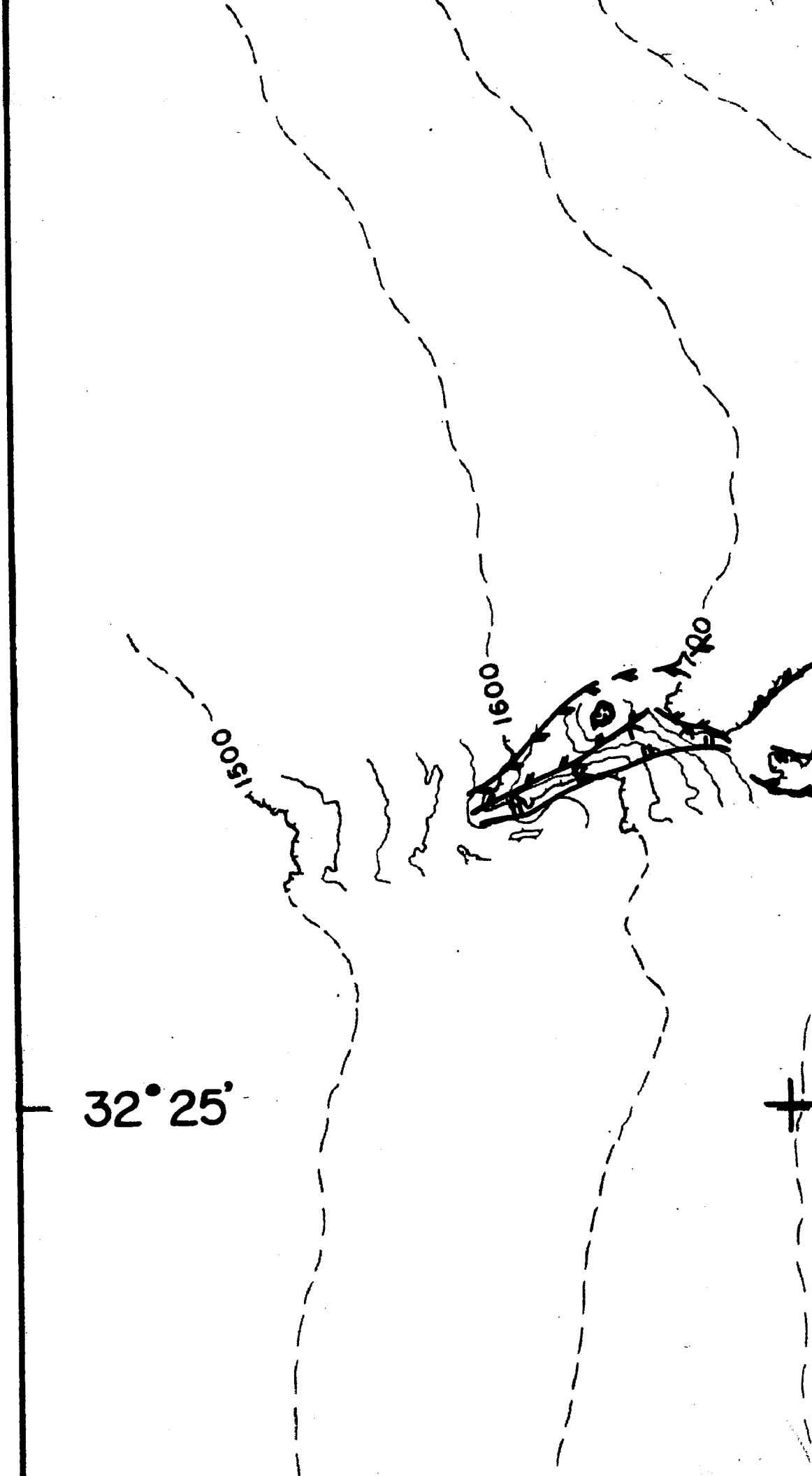
1500
1600
1700
32°25'

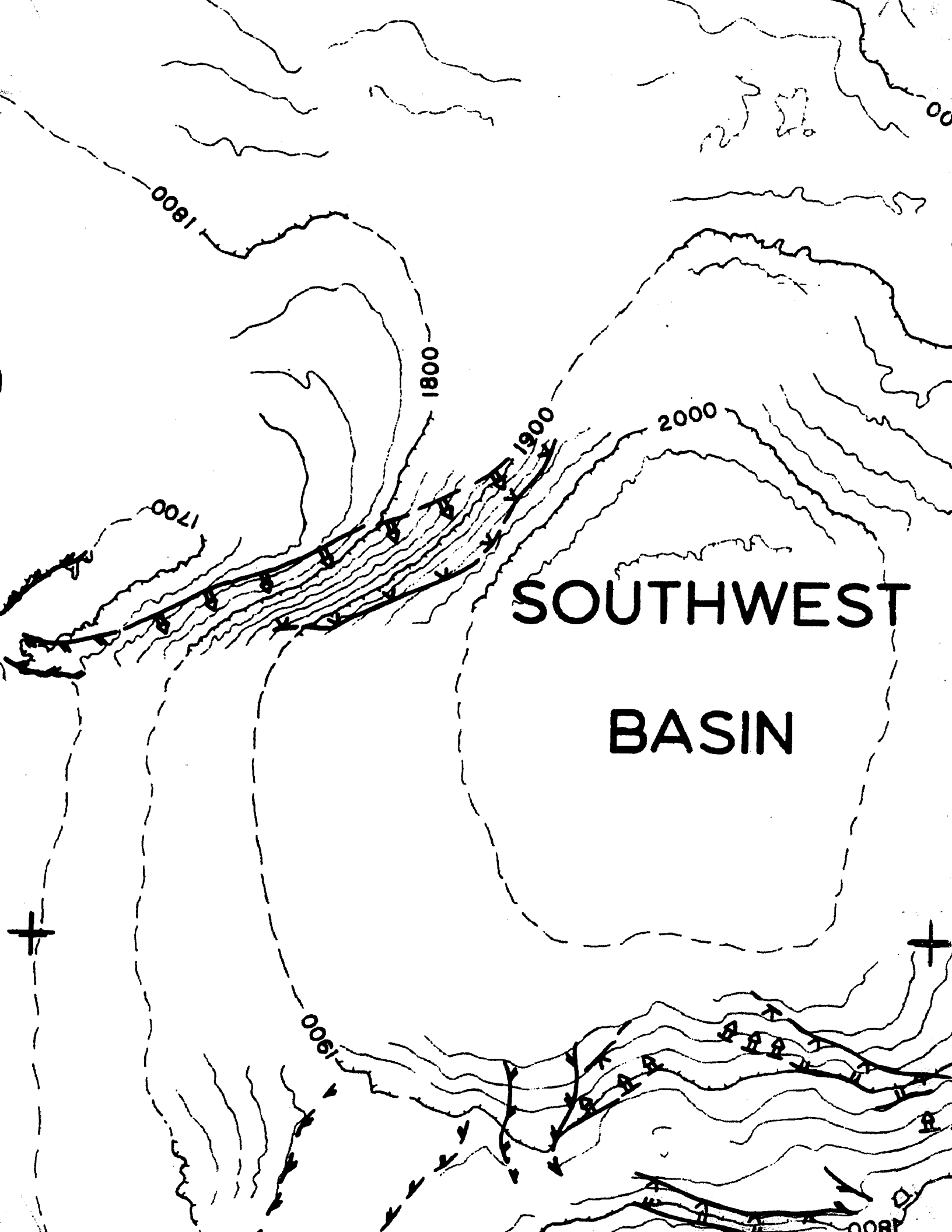
SOUTHWEST
BASIN
1800
1800
1900
2000
1700
1900

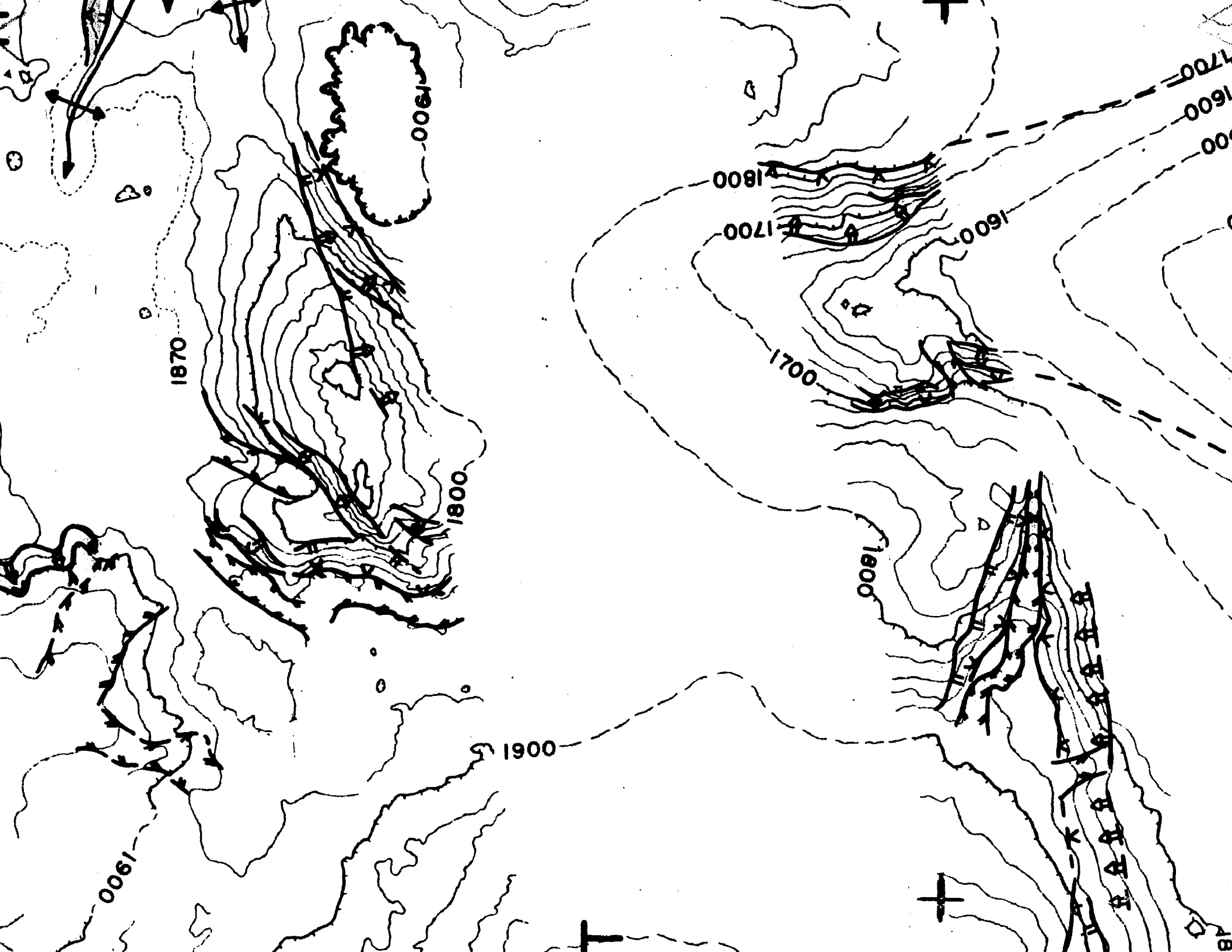
1900
1870
1800
1700
1600
1900
1900
1800
1700
1600
1700
1800
1900

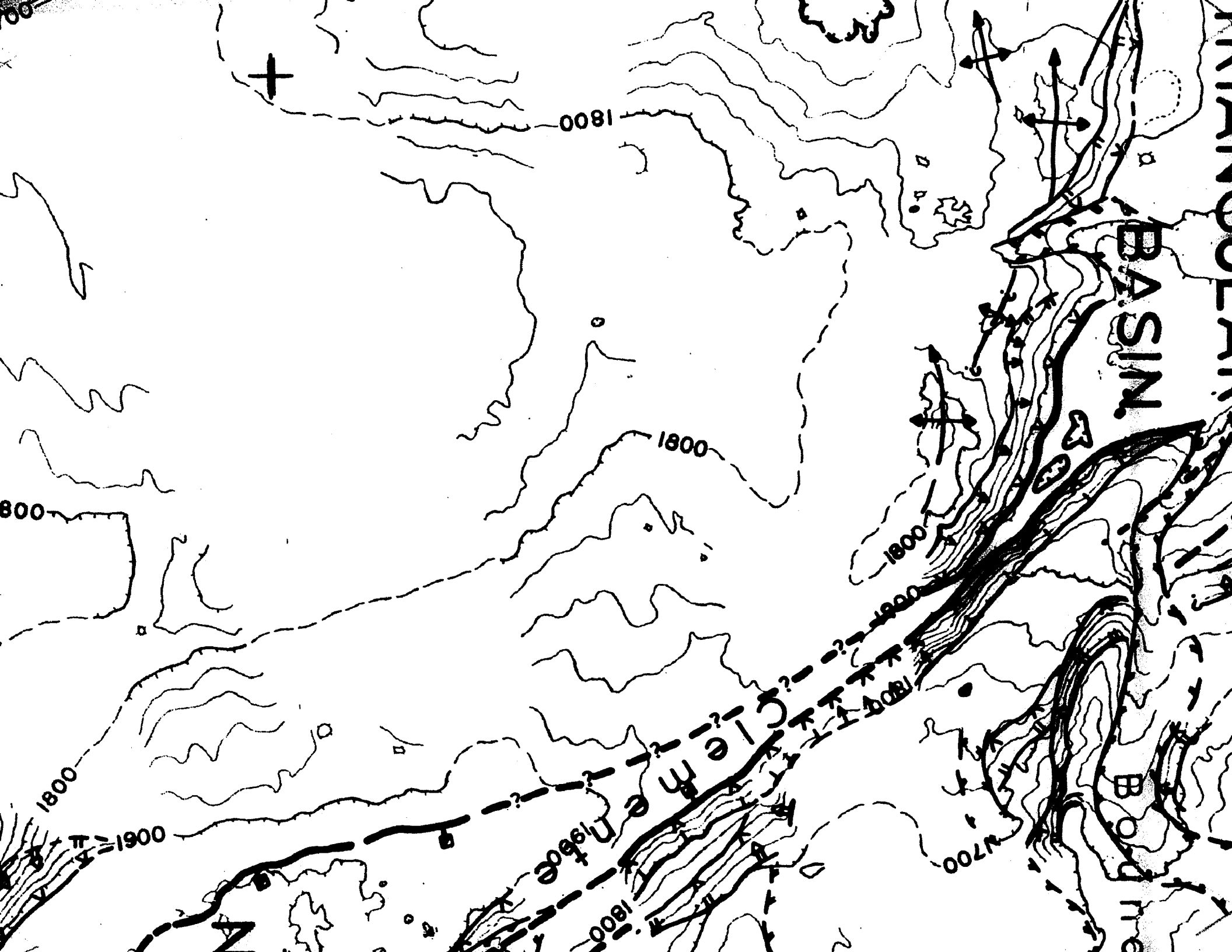

1800
1800
1800
1800
1800
1800
1900
1900
1900
1800
1800
1700
BASIN

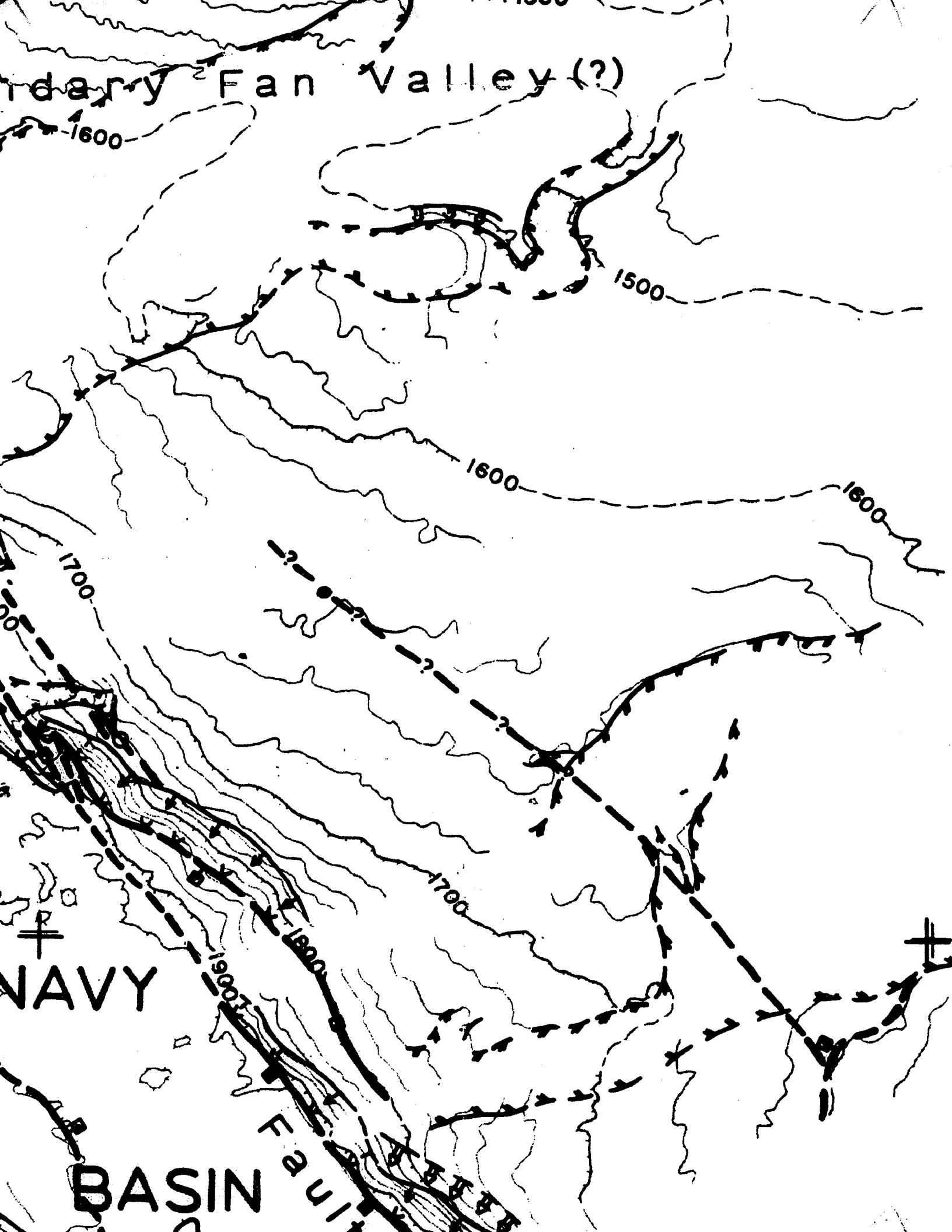
rdary Fan Valley (?)
1600
1500
1600
1600
1700
1700
1800
1900
NAVY
BASIN
Fault

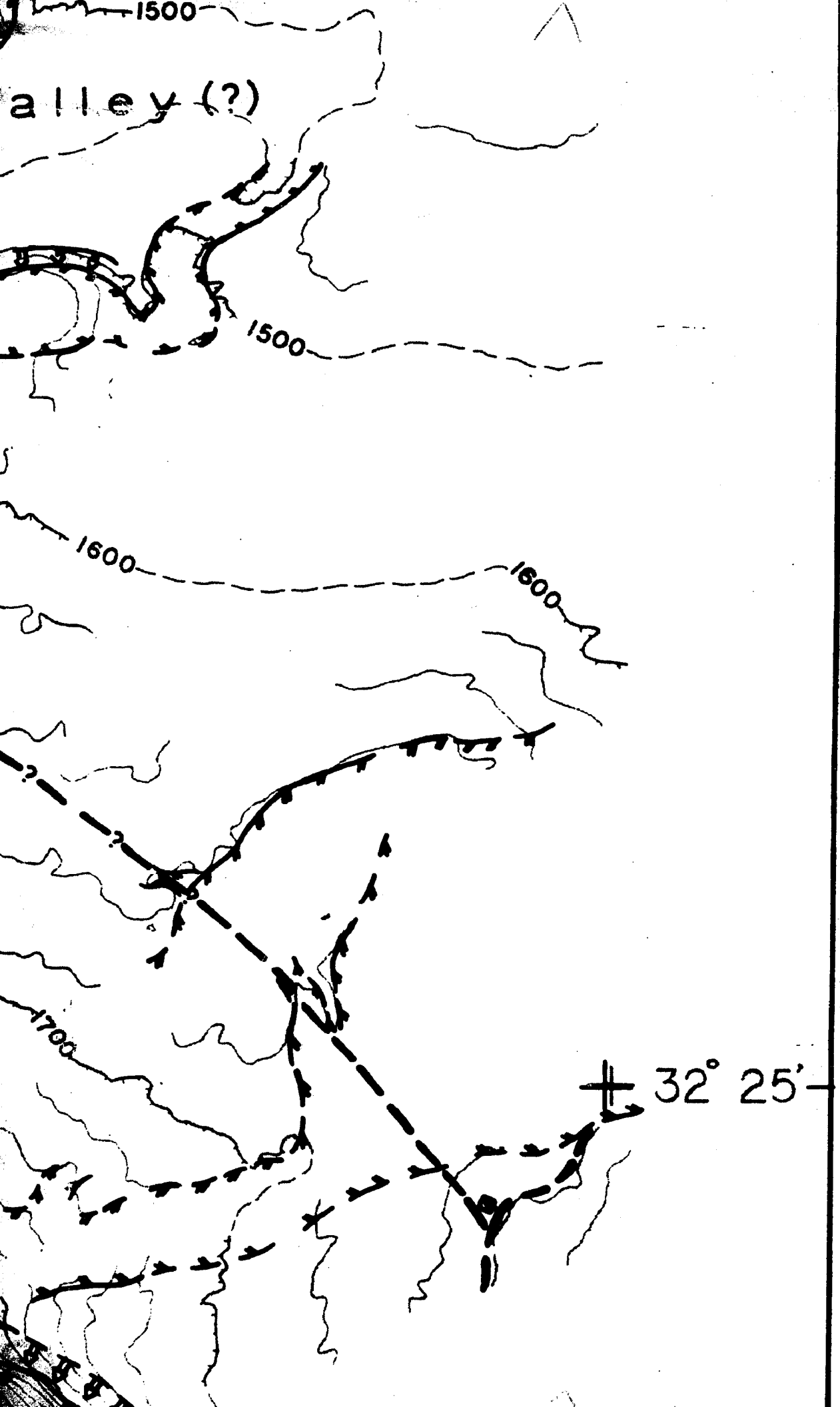
1500
alley (?)
1500
1600
1600
1700
32° 25'

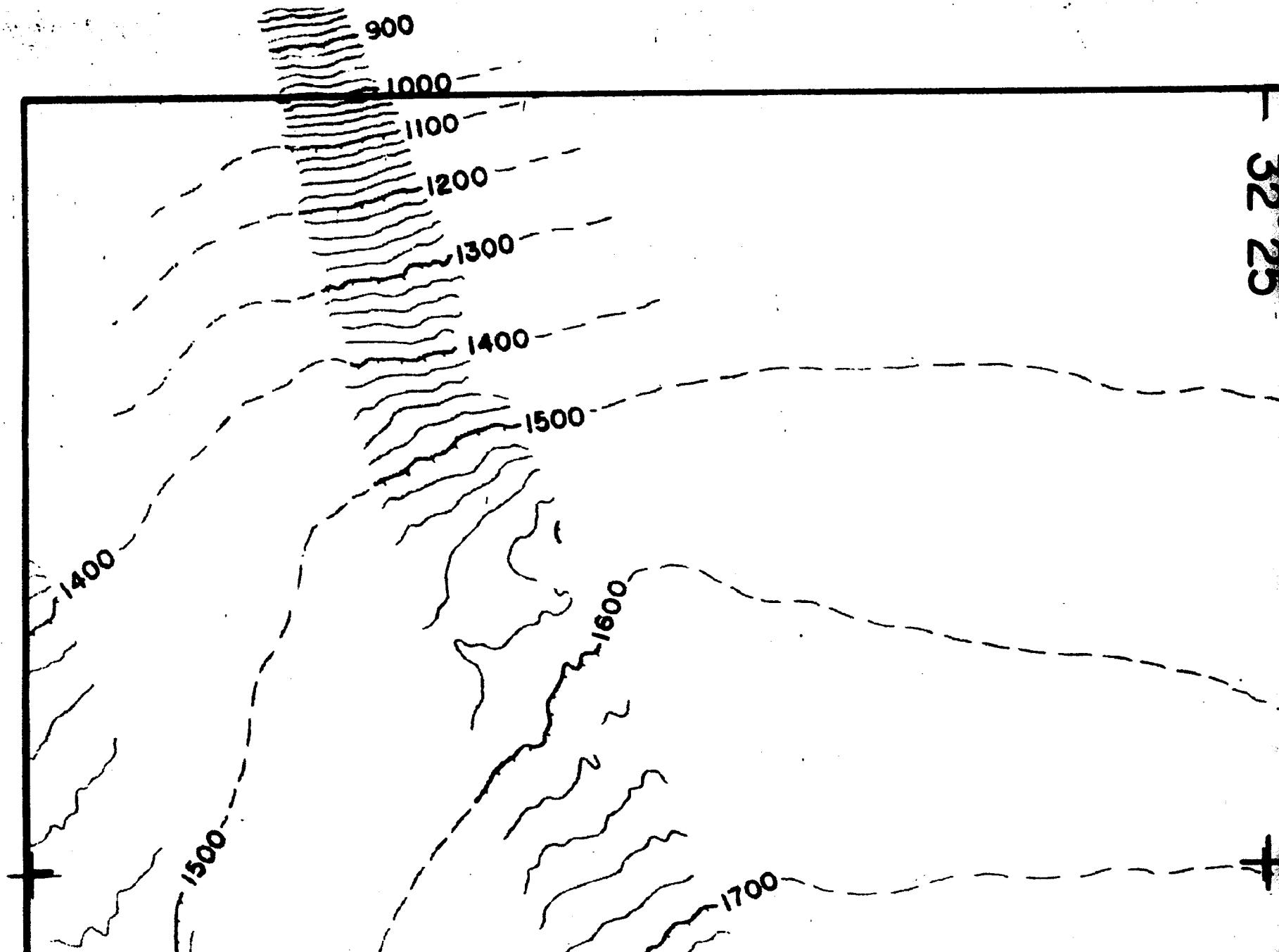
900
1000
1100
1200
1300
1400
1500
1400
1600
1500
1700
32 25

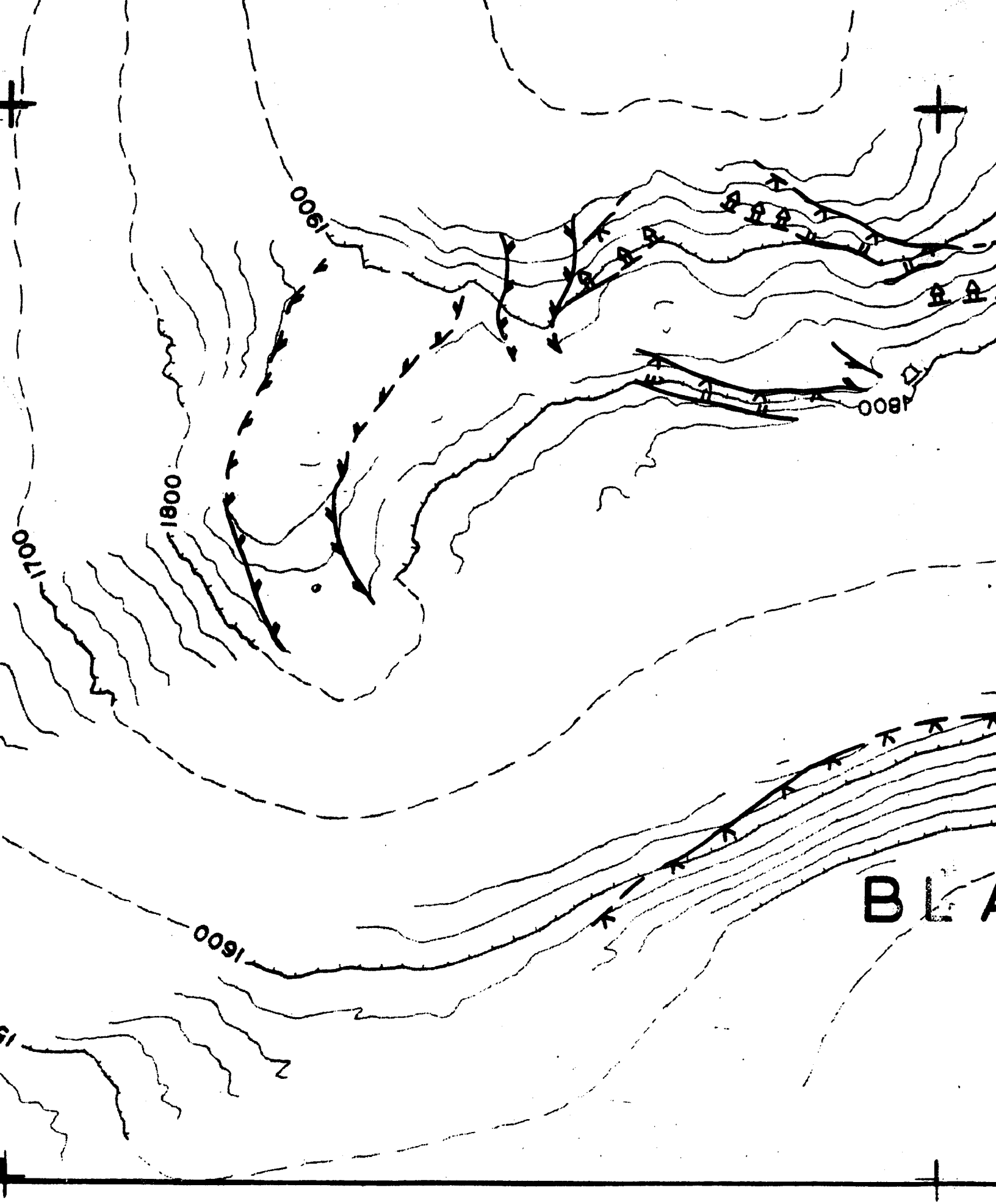
1900
1800
1700
1600
BL

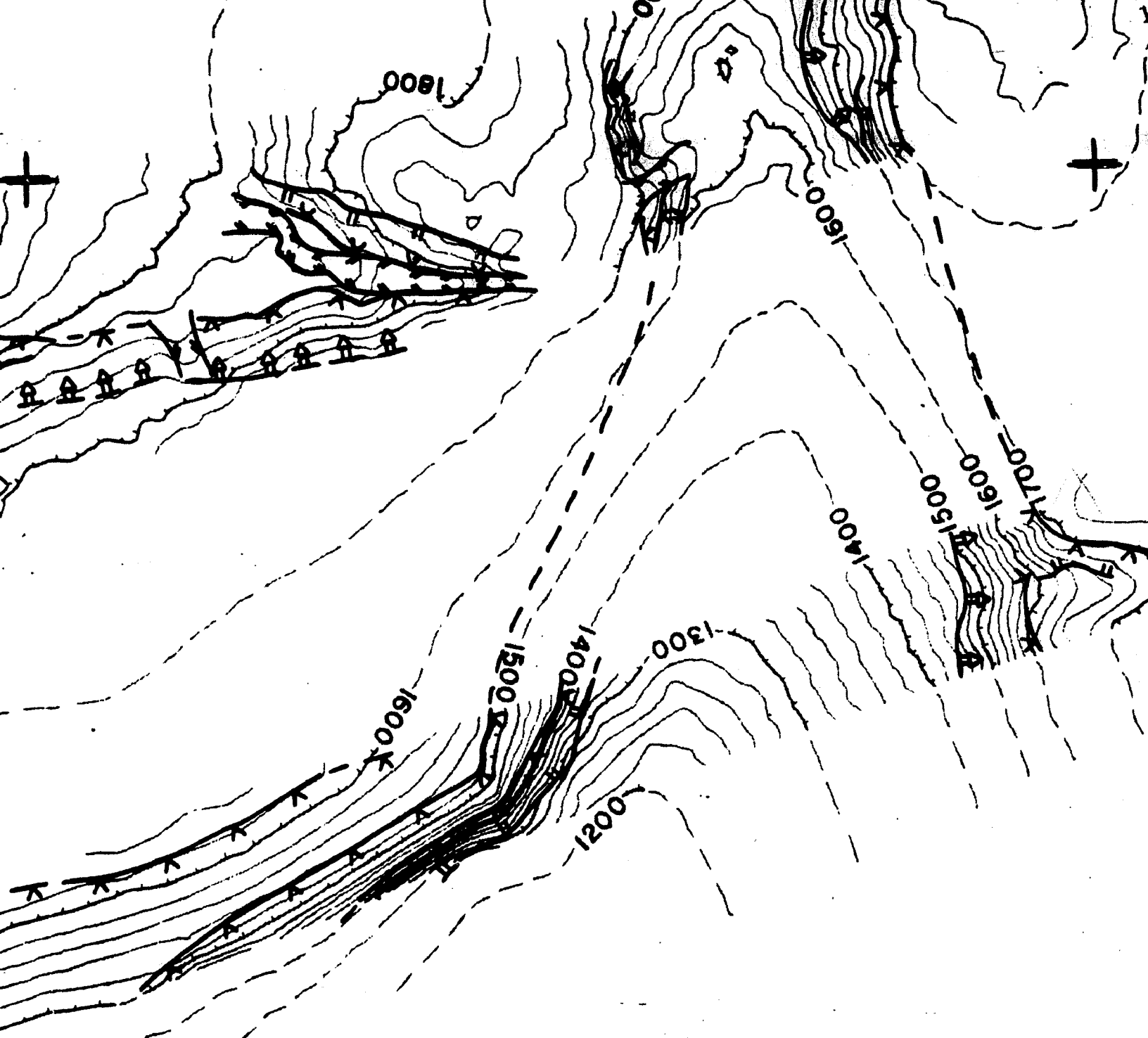


# LAKE KNOLLS

Compiled & Drafted by Mark R. Legg (1985)

1800
1800
1700
1600
1900
1500
1400
1300
SALV
SA
KNO
NA

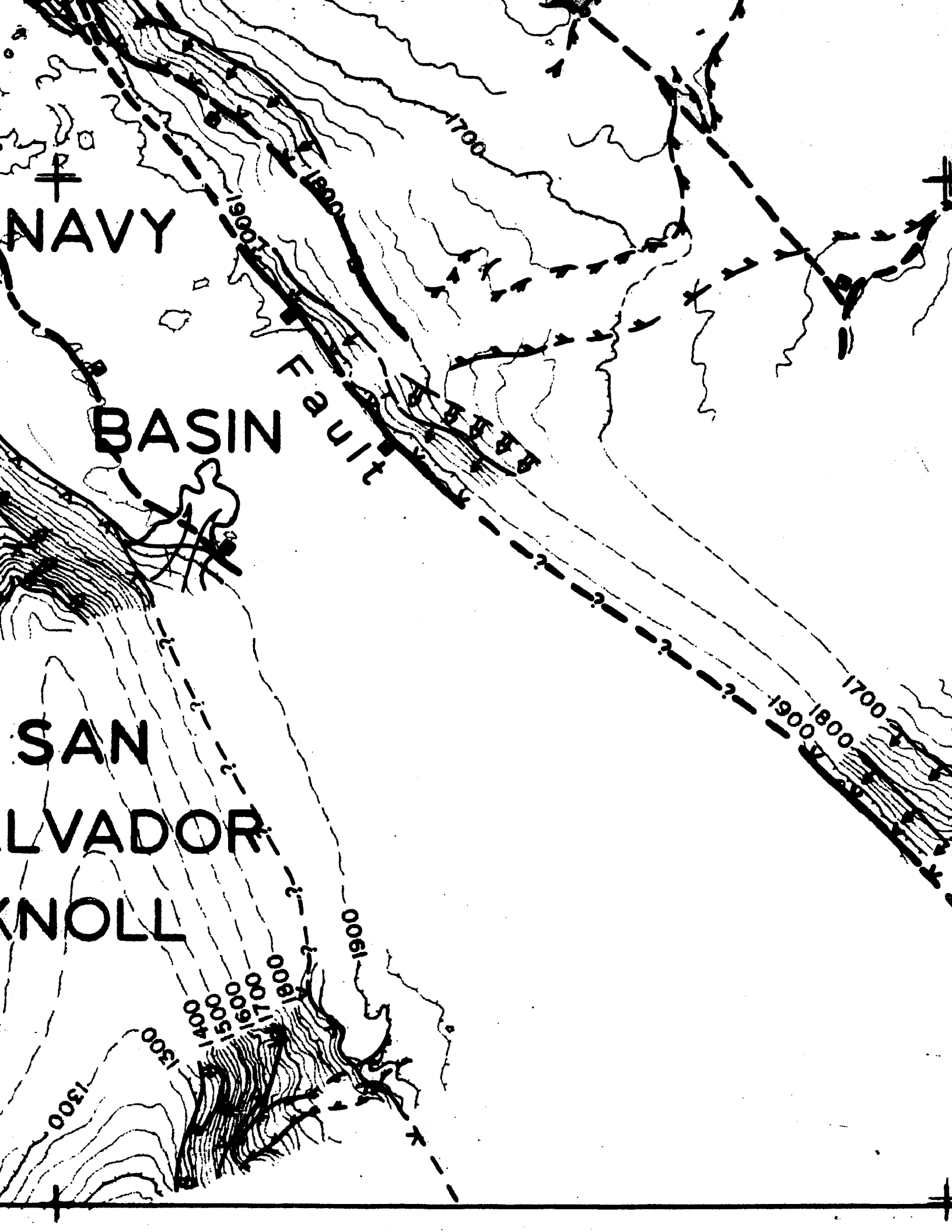
NAVY
BASIN
Fault
SAN
LVADOR
NOLL
1700
1800
1900
1300
1400
1500
1600
1700
1800
1900

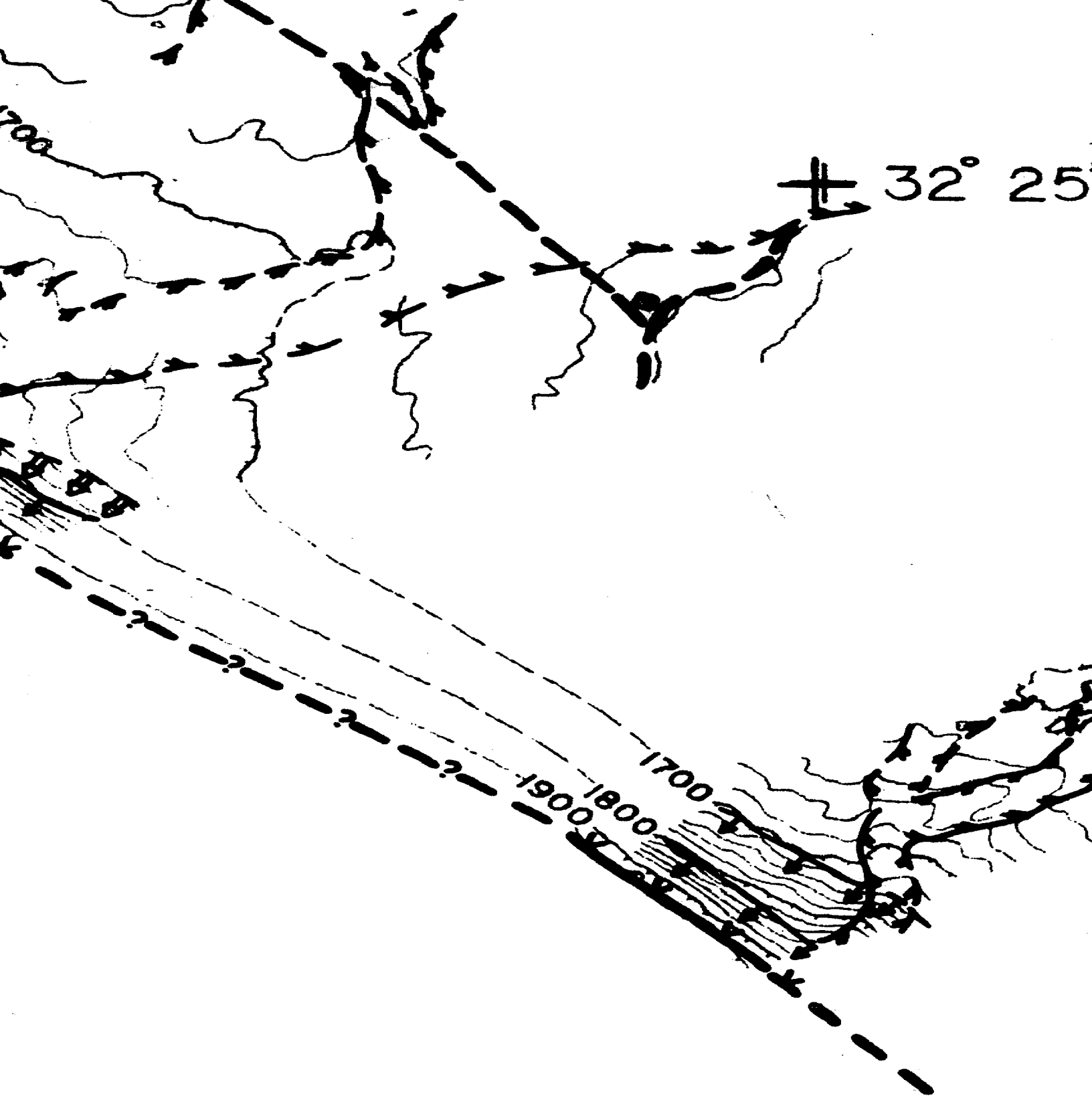
32° 25
1700
1800
1900